

IHDP/Future Earth-Integrated Risk Governance Project Series

Peijun Shi · Roger Kasperson  
*Editors in Chief*

# World Atlas of Natural Disaster Risk

---

# **IHDP/Future Earth—Integrated Risk Governance Project Series**

*Series editors*

Carlo C. Jaeger, Global Climate Change Forum, Berlin, Germany  
Peijun Shi, Beijing Normal University, Beijing, People's Republic of China

*Editors-in-Chief*

Peijun Shi, Beijing Normal University, Beijing, People's Republic of China  
Roger Kaspersen, Clark University, Worcester, MA, USA

For further volumes:  
<http://www.springer.com/series/13536>

## **About this Series**

This book series, entitled “IHDP/Future Earth—Integrated Risk Governance Project Series” for the International Human Dimensions Programme on Global Environmental Change—Integrated Risk Governance Project (IHDP/Future Earth—IRG Project), is intended to present in monograph form the most recent scientific achievements in the identification, evaluation and management of emerging global large-scale risks. Future Earth is a flagship initiative of the Science and Technology Alliance for Global Sustainability. It aims to provide critical knowledge required for societies to understand and address challenges posed by global environmental change (GEC) and to seize opportunities for transitions to global sustainability. Future Earth identifies three research themes, i.e., Dynamic Planet, Global Development and Transition toward Sustainability in its plan and adopts a new approach of “Co-designing and co-producing” to incorporate GEC researchers with stakeholders in governments, industry and business, international or intergovernmental organizations, and civil society.

Books published in this series are mainly collected research works on theories, methods, models and modeling, and case analyses conducted by scientists from various disciplines and practitioners from various sectors under the IHDP/Future Earth—IRG Project. It includes the IRG Project Science Plan, research on social-ecological system responses, “Entry and Exit Transition” mechanisms, models and modeling, early warning systems, understanding regional dynamics of vulnerability, as well as case comparison studies of large-scale disasters and paradigms for integrated risk governance around the world. This book series, therefore, will be of interest not only to researchers, educators and students working in this field but also to policy-makers and decision-makers in government, industry and civil society around the world.

The series will be contributed by the international research teams working on the six scientific themes identified by the IHDP/Future Earth—IRG Project science plan, i.e., Social-Ecological Systems, Entry and Exit Transitions, Early Warning Systems, Models and Modeling, Comparative Case Studies, and Governance and Paradigms, and by six regional offices of the IRG Project around the world.

---

Peijun Shi • Roger Kasperson  
Editors-in-Chief

# World Atlas of Natural Disaster Risk

 BNUP

 Springer

*Editors-in-Chief*  
Peijun Shi  
Beijing Normal University  
Beijing  
People's Republic of China

Roger Kasperson  
Clark University  
Worcester, MA  
USA

ISSN 2363-4979 ISSN 2363-4987 (electronic)  
IHDP/Future Earth—Integrated Risk Governance Project Series  
ISBN 978-3-662-45429-9 ISBN 978-3-662-45430-5 (eBook)  
DOI 10.1007/978-3-662-45430-5

Jointly published with Beijing Normal University Press  
ISBN: 978-7-303-18117-9 Beijing Normal University Press

Library of Congress Control Number: 2014956198

Springer Heidelberg New York Dordrecht London

© Springer-Verlag Berlin Heidelberg and Beijing Normal University Press 2015

This work is subject to copyright. All rights are reserved by the Publishers, whether the whole or part of the material is concerned, specifically the rights of translation, reprinting, reuse of illustrations, recitation, broadcasting, reproduction on microfilms or in any other physical way, and transmission or information storage and retrieval, electronic adaptation, computer software, or by similar or dissimilar methodology now known or hereafter developed.

The use of general descriptive names, registered names, trademarks, service marks, etc. in this publication does not imply, even in the absence of a specific statement, that such names are exempt from the relevant protective laws and regulations and therefore free for general use.

The publishers, the authors and the editors are safe to assume that the advice and information in this book are believed to be true and accurate at the date of publication. Neither the publishers nor the authors or the editors give a warranty, express or implied, with respect to the material contained herein or for any errors or omissions that may have been made.

No. of licenced maps: JS (2015) 01-052

Printed on acid-free paper

Springer-Verlag GmbH Berlin Heidelberg is part of Springer Science+Business Media (www.springer.com)

---

## Foreword I

Economic losses as a result of disasters continue to escalate. In each of the past 3 years direct economic losses from disasters have surpassed \$100 billion in the world. This trend is set to worsen unless more private and public investment strategies start to reduce the vulnerability and exposure of people and assets to natural hazards. This will require a shift from reactive approaches that manage disasters to proactive ones that, instead, manage disaster risk.

I am pleased to say that this change is underway, and in many parts of the world is gathering pace. Several countries have come a long way in reducing their disaster risk. Substantial progress has been recorded in the implementation of the Hyogo Framework for Action 2005–2015 (HFA) in all regions. Yet despite this good news, effectively addressing the underlying drivers of disaster risk, such as poverty, poor urban planning and enforcement of regulations, and the destruction of natural protective eco-systems, remains a stubbornly difficult challenge.

Understanding disaster risk and its potential impact on human lives and livelihoods as well as social, economic, and environmental assets has been shown to be crucial to strengthening resilience. Accurate, timely, and understandable information on disaster risk and losses should be integral to both private and public investment planning decisions.

This “World Atlas of Natural Disaster Risk” is one major step forward in this effort to increase understanding of hazard, vulnerability, exposure, and risk. The Atlas presents in detail the distribution of disaster risk, which, if not addressed, will undermine sustainable development in many parts of the world. The analysis of hazards such as earthquake, volcanic eruption, landslide, typhoon, flood, drought, sand-dust storm, storm surge, wildfire, heat wave, and cold wave provides countries with a greater understanding of prevailing risks.

The publication of this Atlas is timely. The world is moving towards a post-2015 international framework for disaster risk reduction that is set to highlight the importance of policies, investment planning, and local actions that are all disaster risk-informed.

The result is a truly remarkable effort of Beijing Normal University and all other associated institutions that will be very useful for disaster risk policymakers and practitioners at the national and city level. Indeed, the subsequent development of more in-depth National Atlases of Natural Disaster Risk could be appropriate for many countries.

I would like to express my sincere appreciation to all the international and Chinese experts who are represented by the Disaster Risk Scientific Research Team of Beijing Normal University, and extend my congratulation for their achievement in developing this publication.



Margareta Wahlström  
United Nations Special Representative  
of the Secretary-General for Disaster Risk Reduction

---

## Foreword II

Nearly 25 years have elapsed since the initiation of International Natural Disasters Reduction Activity proposed by the United Nations in the late 1980s. Though significant achievements have been attained and this activity has received wide acclaim from countries and regions all over the world, according to reports by related organizations of United Nations, the losses and damages caused by various natural disasters still increase with fluctuation, especially those caused by catastrophes. This has been witnessed by severe natural hazards happened during recent years, such as the 2003 European heat wave, the 2004 Indian Ocean earthquake and tsunami, the 2005 Hurricane Katrina in the United States, the 2008 typhoon disaster in Burma, the 2008 Wenchuan earthquake in China, 2011 Tohoku earthquake and tsunami in Japan, as well as 2013 typhoon and tsunami in Philippines, etc. Undoubtedly, the mission of reducing worldwide natural disaster risk has been arduous.

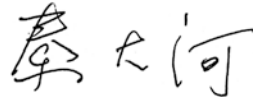
Disasters risk reduction and adaptations to global climate change play an essential role in enhancing global sustainable development. According to the IPCC-SREX report, the future impacts on many countries and regions due to global climate change will continue unabated, and weather extremes such as torrential rain, drought, typhoon, as well as heat wave will apparently mount their damages on the world. Thus, enhancing the adaptation to global climate change and improving the capacity building of comprehensive disaster prevention and reduction remain the main tasks for every country and region in the process of sustainable development.

Raising our awareness of the formation mechanism, changing pattern, and distribution of worldwide natural disaster risk is not only crucial to improve related scientific research, but also props up the implementation of natural disaster prevention and mitigation in every country. By means of systemically collating existing relevant data and compiling disasters–disaster risk atlases, we can demonstrate the regional distribution of main natural hazards and disaster risks. This job will not only be beneficial for countries and regions all over the world to plan scientific programs and schematize various projects on disaster prevention and reduction, but will also facilitate increasing public awareness of both disaster prevention and mitigation and disaster risk governance.

On the basis of systematic study of natural disaster risks in China, Beijing Normal University has organized multiple domestic and international scientific research institutions to compile the “World Atlas of Natural Disaster Risk.” This atlas is aimed to illustrate the spatial distribution of the main natural disasters in the world, which is especially commendable. Employing cartographic language in geography, this World Atlas of Natural Disaster Risk systemically depicts the global distribution of natural disasters such as earthquake, volcano eruption, landslide, typhoon, flood, drought, sandstorm, storm surge, wildfire, heat wave, and cold wave, and it clearly highlights the hot zones for these disaster risks, and thus provides important information for both global disaster prevention and reduction and integrated risk governance.

We hereby appeal to geoscience personnel, especially geographic scholars, to pay high attention to the impacts of global environmental change on mankind’s social-economical

system, to scientifically and objectively assess the risks to our social-economical systems resulting from the global change, to attach great emphasis on the worldwide undertaking science project “Future Earth,” to intensify the research on Earth System Science, Global Development and Sustainable Development, to provide scientific and technological supports for comprehensive disaster prevention and reduction, and eventually to make contribution to global sustainable development. Let us advance the enhancement of capacity building for global integrated risk governance, and meanwhile accelerate the development of related subjects on disaster risk science, promote the further expansion of Earth System Science, and strive together for the betterment of mankind and realization of the global sustainable development.

The image shows a handwritten signature in Chinese characters, which reads '秦大河' (Qin Dahe). The characters are written in a fluid, cursive style.

Dahe Qin  
Academician of Chinese Science Academy  
Former Director of China Meteorological Administration  
Director of State Commission of Future Earth in China  
Vice President of China Science and Technology Association  
Vice President of International Geographical Union  
Co-Chair of Working Group I, IPCC

---

## Preface

The year 2015 will be the 25th year of the implementation of the International Decade for Natural Disaster Reduction (IDNDR) and International Strategy for Disaster risk Reduction (ISDR) proposed by the United Nations. Great achievements have been attained in the field of global integrated disaster reduction. Disaster risk reduction, global climate adaptation, and sustainable development have become the joint responsibilities of every country in economical, social, cultural, political, and ecological construction. During these 25 years, UNIDNDR or UNISDR has worked together with governments around the world, scientific and technological groups, nongovernmental organizations, entrepreneur groups, media groups, and various relevant regional organizations, gaining effective results in alleviating human casualties, property loss, damage to resources and environment caused by natural hazards in the world, and earning a great reputation at every stratum of society as well. However, the data released by UN organizations demonstrate that the number of natural disasters is ascending in fluctuation. Though some countries and regions have obtained remarkable results in natural disaster reduction, and have reduced the impacts brought by natural hazards, the ability to cope with large-scale disaster remains insufficient. The task of natural disaster risk reduction is still arduous.

The decade-long IHDP/Future Earth—IRG international program proposed by CNC-IHDP/Future Earth and organized by scientists around the world has been implemented for nearly 5 years. Meanwhile, the “Hazard and Risk Science Base” at Beijing Normal University supported by the Ministry of Education and the State Administration of Foreign Experts Affairs of China (111 Project, No. B08008), which is sponsored by Chinese government has also been carried out for nearly 7 years since 2008. Funded by the Chinese government, a series of scientific projects have attained enormous results and valuable references which laid a solid foundation for the compilation of this atlas, including the phrasal results and findings from the following ongoing projects: the “Relationship Between Global Change and Environmental Risks and its Adaptation Paradigm” (No. 2012CB955400)—a project supported by the special research plan of global change of the Ministry of Science and Technology of China (MOST), the creative research group “Model and Simulation of Earth Surface Process” (No. 41321001), the “Research on the Regional Agriculture Drought Adaptation Assessment Model and Risk Reduction Paradigm” (No. 41171402), and the project “the Land-use and Integrated Erosion of Soil by Wind and Water in the Eastern Ecotone of Agriculture and Animal Husbandry in North China” (No. 41271286) sponsored by the National Natural Science Foundation of China (NSFC). The atlas has also received help and data from the following completed projects: the “Geographic Transaction Zone Study on Interaction Mechanism of Human-earth System on Earth Surface” (No. 40425008)—distinguished young scientists projects, the “Integrated Natural Disaster Risk Evaluation and Disaster Reduction Paradigm Study in Rapid Urbanization Regions” (No. 40535024)—a key project of National Nature Science Foundation of China, the major international joint research program “Integrated Risk Governance—case study of IHDP—IRG Core Science Plan” (No. 40821140354), a key project of NSFC, “Global Climate Change and Large-scale Disaster Governance” (No. 2008DFA20640)—an international joint project of MOST, “the Key Technology Study and Demonstration of Integrated

Risk Prevention” (No. 2006BAD20B00)—a key science and technology pillar project of MOST, and the “Technology for Evaluating Natural Disaster Risk in the Yangtze River Delta” (No. 2008BAK50B07).

We organized all faculties and students of Beijing Normal University in the disaster risk science, and international experts who participated in the IHDP/Future Earth—IRG and “111 Project”, as well as all the personnel involved in these two projects, throughout 10 years of preparation, planning, and execution, to compile this atlas, aiming to reflect the spatial patterns of major natural disaster risk all around the world. This atlas provides scientific evidence for taking effective measures of world natural disaster risk reduction by demonstrating the spatial variation from the following three spatial scales for the main natural disaster risk on the world: the grid ( $1\text{km} \times 1\text{km}$ ,  $0.1^\circ \times 0.1^\circ$ ,  $0.25^\circ \times 0.25^\circ$ ,  $0.5^\circ \times 0.5^\circ$ ,  $0.75^\circ \times 0.75^\circ$  and  $1^\circ \times 1^\circ$ ), the comparable-geographic unit (about  $448334 \text{ km}^2/\text{region}$ ), and the national or regional unit (245 nations and regions).

The “Natural Disaster Hotspots” program, jointly completed by the World Bank and Columbia University (USA), has for the first time provided the major global natural disaster risk maps in small scale, which enormously inspires us in compiling this atlas. Our job has obtained desirable improvement in aspects like sorting natural disaster types, assessment method and accuracy, data upgrading, spatial comparability, temporal and spatial resolution, and results verification. Moreover, these improvements have wider and more effective applicability.

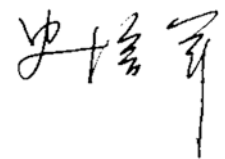
The providers of the shared data online has made great scientific contribution to world natural disaster risk reduction, which not only inspires us to make joint efforts to develop disaster risk science and compile this atlas, but will also save numerous lives, property, and the service capacity of the earth’s ecological system from damage by disasters. Hence, we express our heartfelt appreciation and respect to those institutions and websites which provide related shared global data, and to those scientific personnel who devoted themselves to this grand cause.

Since 1989, BNU’s integrated disaster research efforts by all its involved faculty and students have evolved in synchronization with the disaster reduction activities of the United Nations. Initiated by the establishment of “China Natural Disaster Monitoring and Prevention Research Laboratory” in 1989, a number of academic institutions and subjects have been set up, such as the “Disaster Insurance Technology Center at BNU” in 1992, “Open Laboratory for Environmental Change and Natural Disaster of Ministry of Education of China (MOE)” in 1994, “Catastrophe Insurance Technology Center at BNU” in 1998, “Key Laboratory of Environmental Change and Natural Disaster, MOE, BNU” in 1998, “Beijing Desertification and Blown-sand Control Technology Center” in 2002, the master and doctor programs of “Natural Disaster Science” which has been granted to admit students in 2003, the “Desertification and Blown-sand Control Engineering Center of MOE” in 2006, “Academy of Disaster Reduction and Emergency Management, Ministry of Civil Affairs of China (MOCA) and MOE” in 2006, and the “State Key Laboratory of Earth Surface Processes and Resource Ecology” in 2007. The BNU disaster and risk study group has enlarged from three faculties at the very beginning to nearly 100 faculties, more than 100 master students, and over 200 doctoral students today, making itself a national professional team focusing on R&D projects of natural disaster risk. Furthermore, it keeps close and excellent collaborative relationships with many top research institutions all over the world, such as Disaster Prevention Research Institute of Kyoto University in Japan, International Institute for Applied Systems Analysis in Austria, Stockholm Environment Institute in Sweden, Hazard Research Center of Clark University in the U.S., School of Sustainability Science at Arizona State University in the U.S., as well as Potsdam Institute for Climate Impact Research in the Germany, etc. Now this group is playing a significant role in integrated natural disaster risk research in the world.

In the process of compiling and publishing this atlas, as well as in the evolution of Disaster Risk Science of BNU, we received strong support and help from many institutions at home and abroad. We would like to express our gratitude to the following centers, academic

institutions, and state-owned enterprises for their help in related references, data, and technological guidance and guarantee: National Climate Center of China Meteorological Administration, National Remote Sensing Center of China Ministry of Science and Technology of the People's Republic of China, National Disaster Reduction Center of China, Ministry of Civil Affairs, Institute of Geographic Sciences and Natural Resources Research, Chinese Academy of Science (CAS), Cold and Arid Regions Environmental and Engineering Research Institute, CAS, Research Center for Eco-Environmental Sciences, CAS, Institute of Tibetan Plateau Research, CAS, Institute of Earth Environment, CAS, Institute of Mountain Hazards and Environment, CAS, Institute of Atmospheric Physics, CAS, Institute of Geology and Geophysics, CAS, College of Urban and Environmental Sciences of Beijing University, School of Geography and Ocean Sciences of Nanjing University, College for Global Change Studies of Tsinghua University, School of Geography and Planning of Sun Yat-Sen University, Faculty of Geo-Science of East China Normal University, College of Earth and Environmental Sciences of Lanzhou University, School of Resource and Environmental Sciences of Wuhan University, People's Insurance Company of China, and China Reinsurance Company. Many world-recognized universities and academic institutions, who keep close academic collaborative relationship with us, have also supplied us with substantial data and references, as well as the theoretical support regarding assessing methodology. They are University of Maryland in the USA, Nanyang Technological University in Singapore, University Wien in Austria, Oxford University in the UK, University of Stuttgart in Germany, University of California-Berkeley in the USA, Risk Management Solution (RMS), Swiss Re, Munich Re, and Aon Benfield. UNISDR, UNISDR Asia-Pacific Office and UNISDR-Global Assessment Report on Disaster Risk Reduction (GAR) have also offered us great supports and detailed guidance. Star Map Press (Beijing) has provided great supports in editing the maps, and Beijing Normal University Press and Springer-Verlag have jointly provided the ideal conditions for the publishing of this atlas.

We also owe an incalculable debt of gratitude to the following notable scientists and experts for their guidance to this atlas: Academician Guanhua Xu, Dahe Qin, Zhisheng An, Changming Liu, Xueyu Lin, Xiaowen Li, Yong Chen, Zongjin Ma, Xinshi Zhang, Rixiang Zhu, Tandong Yao, Bojie Fu, Prof. Yanhua Liu, Jun Chen, Ms. Margareta Wahlström, Dr. Fenmin Kan, Sujit Mohanty and Pedro Basabe. Ms. Margareta Wahlström and Academician Dahe Qin also wrote prefaces for this atlas. Here, we would like to express our sincere appreciation to all of the leaders and experts. At the same time, we are looking forward to a greater achievement in worldwide disaster prevention and reduction, and a significant improvement of integrated disaster risk governance capability in the near future. Restricted from limited references and data, it is regrettable to give an incomplete evaluation to some countries and regions. We wish that the insufficiency will be revised and perfected in our further work. Comments and suggestions from peers and readers will be highly welcome and appreciated.



Professor Peijun Shi  
State Key Laboratory of Earth Surface Processes and Resource Ecology  
Key Laboratory of Environmental Change and Natural Disaster, MOE  
Academy of Disaster Reduction and Emergency Management, MOCA and MOE  
Beijing Normal University

---

## Editorial Committee

### Academic Advisors

#### *Domestic Advisors*

Bojie Fu	Changming Liu	Changqing Song	Chenghu Zhou	Dadao Lu
Dahe Qin	Deren Li	Du Zheng	Guanhua Xu	Guoyi Han
Hai Lin	Hao Wang	Honglie Sun	Huadong Guo	Huijun Wang
Ji Zhao	Jianguo Wu	Jianya Gong	Jiyuan Liu	Jun Chen
Jun Gao	Lansheng Zhang	Peng Cui	Qian Ye	Qiming Zhou
Quansheng Ge	Rixiang Zhu	Shangyu Gao	Shaohong Wu	Shu Tao
Shunlin Liang	Shuying Leng	Tandong Yao	Wenjie Dong	Xiaofeng Xu
Xiaowen Li	Xiaoxi Li	Xinshi Zhang	Xiubin Li	Xueyu Lin
Yanhe Ma	Yanhua Liu	Yaning Chen	Yida Fan	Yong Chen
Yongqi Gao	Zhanqing Li	Zhengtang Guo	Zongjin Ma	

#### *International Advisors*

Ananth Darsiappah	Andreas Reckemmer	Armin Haas
Benjamin Wisner	Carlo C. Jaeger	Cathy Roth
David Johnston	Dennis Wenger	Fengmin Kan
Gopalakrishnan Chennal	Jim Hall	Joanne Linnerooth-Bayer
Laban Ogallo	Margareta Wahlstrom	Norio Okada
Oran Young	Ortwin Renn	Pedro Basabe
Salvano Briceno	Sander van der Leeuw	Sujit Mohanty
Susan Cutter	Takashi Onishi	Thomas Glade
Virginia Murray	Walter Ammann	

### Academic Leaders

Peijun Shi                      Roger Kasperson

### Academic Members

Chunyang He	Deyong Yu	Guoyi Han	Jianjun Wu	Jianqi Sun
Jin Chen	Jing'ai Wang	Kai Liu	Lianyou Liu	Ming Wang
Ning Li	Qian Ye	Qihong Tang	Saini Yang	Tao Ye
Wei Xu	Weihua Fang	Yi Yuan		

## Editors in Chief

Peijun Shi                      Roger Kasperson

## Associate Editors in Chief

Jing'ai Wang                      Wei Xu                      Tao Ye

## Leaders of Mapping Major Natural Disaster Risk

Peijun Shi                      Jing'ai Wang                      Lianyou Liu                      Weihua Fang

### Earthquake Disaster Risk

Man Li                      Zhenhua Zou                      Wei Xu                      Guodong Xu                      Peijun Shi

### Volcano Disaster Risk

Hongmei Pan                      Tao Ye                      Peijun Shi

### Landslide Disaster Risk

Wentao Yang                      Lingling Shen                      Ming Wang                      Peijun Shi

### Flood Disaster Risk

Jian Fang                      Mengjie Li                      Bo Chen                      Guoyi Han                      Peijun Shi

### Storm Surge Disaster Risk

Shao Sun                      Jiayi Fang                      Wei Gu                      Peijun Shi

### Sand-Dust Storm Disaster Risk

Huimin Yang                      Xingming Zhang                      Fangyuan Zhao                      Mengmeng Qiu                      Ya'nan Shen  
Yaojie Yue                      Kun Gao                      Jing'ai Wang                      Peijun Shi                      Lianyou Liu

### Tropical Cyclone Disaster Risk

Weihua Fang                      Chenyan Tan                      Wei Lin                      Xiaoning Wu                      Yanting Ye                      Shijia Cao  
Wanmei Mo                      Ying Li                      Yi Li                      Yuping Wu                      Guobin Lin                      Yang Yang

### Heat Wave Disaster Risk

Mengyang Li                      Zhao Liu                      Xian'en Li                      Weihua Dong                      Jing'ai Wang  
Jun Wang                      Peijun Shi

### Cold Wave Disaster Risk

Lili Lu                      Zhu Wang                      Ying Wang                      Peijun Shi

**Drought Disaster Risk (Maize)**

Yuanyuan Yin YaojieYue	Xingming Zhang	Han Yu	Degen Lin	Jing'ai Wang
---------------------------	----------------	--------	-----------	--------------

**Drought Disaster Risk (Wheat)**

Xingming Zhang YaojieYue	Hao Guo Jing'ai Wang	Weixia Yin	Ran Wang	Jian Li
-----------------------------	-------------------------	------------	----------	---------

**Drought Disaster Risk (Rice)**

Xingming Zhang	Degen Lin	Hao Guo	Yaoyao Wu	Jing'ai Wang
----------------	-----------	---------	-----------	--------------

**Forest Wildfire Disaster Risk**

Yongchang Meng	Ying Deng	Ying Wang	Ming Wang	Peijun Shi
----------------	-----------	-----------	-----------	------------

**Grassland Wildfire Disaster Risk**

Xin Cao	Yongchang Meng	Jin Chen
---------	----------------	----------

**Leaders of Mapping Multi-hazard Risk**

Peijun Shi Kai Liu	Wei Xu Jing'ai Wang	Tao Ye	Ming Wang	Saini Yang
-----------------------	------------------------	--------	-----------	------------

**Population Risk**

Xu Yang Jing'ai Wang	Jiayi Fang Kai Liu	Fan Liu Peijun Shi	Wei Xu	Tao Ye
-------------------------	-----------------------	-----------------------	--------	--------

**Property Risk**

Xu Yang Ming Wang	Wenfang Chen Peijun Shi	Feng Kong	Lili Lu	Saini Yang
----------------------	----------------------------	-----------	---------	------------

**Chief Map Designers**

Jing'ai Wang, Wei Xu

**Map Designer**

Chunqin Zhang Xingming Zhang Shao Sun Yin Zhou	Fang Lian Huimin Yang Yongchang Meng Shujuan Cui	Hongmei Pan Lili Lu Man Li Fang Chen	Weihua Fang Jian Fang Mengyang Li	Yuanyuan Yin Wentao Yang Xu Yang
---	---	---	---	--

**Chief Text Editors and Secretariat Members**

Peijun Shi  
Ning Li

Jing'ai Wang  
Wei Xu

Tao Ye

Saini Yang

Kai Liu

**Text Members**

Ming Wang  
Fang Lian

Zhao Zhang  
Hongmei Pan

Xiaobing Hu

Weihua Fang

Ying Li

**Secretariat Members**

Hongmei Pan  
Xu Yang

Chunqin Zhang  
Fan Liu

Fang Lian  
Zhao Liu

Fangyuan Zhao  
Feng Kong

Jiayi Fang

---

## Editorial Institutions

### Leading Institutions

State Key Laboratory of Earth Surface Processes and Resource Ecology, Beijing Normal University (BNU)  
Key Laboratory of Environmental Change and Natural Disaster, Ministry of Education of China, BNU  
Key Laboratory of Regional Geography, School of Geography, BNU  
Academy of Disaster Reduction and Emergency Management, Ministry of Civil Affairs (MOCA) and Ministry of Education (MOE)

### Participating Institutions

Institute of Geographical Sciences and Natural Resources Research, Chinese Academy of Science (CAS), China  
Institute of Atmospheric Physics, CAS, China  
Cold and Arid Regions Environmental and Engineering Research Institute, CAS, China  
National Disaster Reduction Center of China, MOCA, China  
Global Climate Forum/University of Potsdam/Potsdam Institute for Climate Impact Research (PIK), Germany  
George Perkins Marsh Institute at Clark University, USA  
Research Center for Interdisciplinary Risk and Innovation Studies at Stuttgart University, Germany  
School of Sustainability at Arizona State University, USA  
Disaster Prevention Research Institute of Kyoto University, Japan

### Data Providers

Ministry of Civil Affairs of China (MOCA)  
National Bureau of Statistics of China  
China Meteorological Administration (CMA)  
China Earthquake Administration  
Ministry of Water Resources of China  
Ministry of Land and Resources of China  
National Geomatics Center of China  
Institute of Geographical Sciences and Natural Resources Research, CAS, China  
Institute of Atmospheric Physics, CAS, China  
Cold and Arid Regions Environmental and Engineering Research Institute, CAS, China  
Chinese Academy of Forestry of China, National Forestry Bureau of China  
Science Press, Beijing, China  
Star Map Press, Beijing, China

## Data Sources

Food and Agriculture Organization (FAO), UN  
 United Nations Environment Programme (UNEP), UN  
 International Lithosphere Program (ILP), UN  
 International Institute for Applied Systems Analysis (IIASA), Austria  
 International Union of Geological Sciences (IUGS), China  
 International Union of Geodesy and Geophysics (IUGG), Germany  
 Asian Disaster Reduction Centre (ADRC), Japan  
 United States Geological Survey (USGS), USA  
 United States Department of Agriculture (USDA), USA  
 National Aeronautics and Space Administration (NASA), USA  
 National Oceanic and Atmospheric Administration (NOAA), USA  
 Oak Ridge National Laboratory (ORNL), USA  
 Dartmouth Flood Observatory (DFO), USA  
 International Soil Reference and Information Centre (ISRIC), the Netherlands  
 The international Disaster Database Centre for Research on the Epidemiology of Disasters  
 CRED (EM-DAT), Belgium  
 National Snow and Ice Data Center (NSIDC), USA  
 Earthquake Engineering Research Institute (EERI), USA  
 The International Association for Earthquake Engineering (IAEE), Japan  
 Australian Bureau of Statistics (ABS), Australian  
 Global Volcanism Program (GVP), USA  
 British Geological Survey (BGS), UK  
 Consultative Group on International Agricultural Research (CGIAR), USA  
 World Bank  
 Swiss Seismological Service (SED), Switzerland  
 British Geological Survey, UK  
 European Centre for Medium-Range Weather Forecasts (ECMWF), UK  
 German Federal Ministry of Education and Research (BMBF), Germany  
 McGill University, Canada  
 Columbia University, USA  
 University of Maryland, USA  
 Texas A&M University (A&M), USA  
 University of Montana, USA  
 The University of Hawaii, USA  
 University of Wisconsin-Madison Sustainability and the Global Environment (SAGE), USA  
 The University of Tokyo, Japan  
 Directorate of Economics and Statistics (DES), India

## Sponsors

Ministry of Science and Technology of China  
 Ministry of Education of China  
 Ministry of Civil Affairs of China  
 National Natural Science Foundation of China  
 State Administration of Foreign Experts Affairs of China  
 National Disaster Reduction Commission of China  
 United Nations International Strategy for Disaster Reduction (UNISDR)  
 UNISDR Asia-Pacific Office  
 Integrated Risk Governance Project (IRG), IHDP/Future Earth (FE), ICSU  
 International Disaster and Risk Conference, IDRC DAVOS, Switzerland  
 Scientific and Technical Advisory Group (STAG), UNISDR

---

# Contents

## **Part I Environments and Exposures**

<b>Mapping Environments and Exposures of the World</b> . . . . .	3
Fang Lian, Chunqin Zhang, Hongmei Pan, Man Li, Wentao Yang, Yongchang Meng, Jian Fang, Weihua Fang, Jing'ai Wang, and Peijun Shi	

## **Part II Earthquake, Volcano and Landslide Disasters**

<b>Mapping Earthquake Risk of the World</b> . . . . .	25
Man Li, Zhenhua Zou, Guodong Xu, and Peijun Shi	

<b>Mapping Volcano Risk of the World</b> . . . . .	41
Hongmei Pan and Peijun Shi	

<b>Mapping Landslide Risk of the World</b> . . . . .	57
Wentao Yang, Lingling Shen, and Peijun Shi	

## **Part III Flood and Storm Surge Disasters**

<b>Mapping Flood Risk of the World</b> . . . . .	69
Jian Fang, Mengjie Li, and Peijun Shi	

<b>Mapping Storm Surge Risk of the World</b> . . . . .	103
Shao Sun, Jiayi Fang, and Peijun Shi	

## **Part IV Sand-dust Storm and Tropical Cyclone Disasters**

<b>Mapping Sand-dust Storm Risk of the World</b> . . . . .	115
Huimin Yang, Xingming Zhang, Fangyuan Zhao, Jing'ai Wang, Peijun Shi, and Lianyou Liu	

<b>Mapping Tropical Cyclone Wind Risk of the World</b> . . . . .	151
Weihua Fang, Chenyan Tan, Wei Lin, Xiaoning Wu, Yanting Ye, Shijia Cao, Wanmei Mo, Ying Li, Yi Li, Yuping Wu, Guobin Lin, and Yang Yang	

## **Part V Heat Wave and Cold Wave Disasters**

**Mapping Heat Wave Risk of the World** . . . . . 169  
Mengyang Li, Zhao Liu, Weihua Dong, and Peijun Shi

**Mapping Cold Wave Risk of the World** . . . . . 189  
Lili Lu, Zhu Wang, and Peijun Shi

## **Part VI Drought Disasters**

**Mapping Drought Risk (Maize) of the World** . . . . . 211  
Yuanyuan Yin, Xingming Zhang, Han Yu, Degen Lin,  
Yaoyao Wu, and Jing'ai Wang

**Mapping Drought Risk (Wheat) of the World** . . . . . 227  
Xingming Zhang, Hao Guo, Weixia Yin, Ran Wang, Jian Li,  
Yaojie Yue, and Jing'ai Wang

**Mapping Drought Risk (Rice) of the World** . . . . . 243  
Xingming Zhang, Degen Lin, Hao Guo, Yaoyao Wu, and Jing'ai Wang

## **Part VII Wildfire Disasters**

**Mapping Forest Wildfire Risk of the World** . . . . . 261  
Yongchang Meng, Ying Deng, and Peijun Shi

**Mapping Grassland Wildfire Risk of the World** . . . . . 277  
Xin Cao, Yongchang Meng, and Jin Chen

## **Part VIII Multi-natural Disasters**

**Mapping Multi-hazard Risk of the World** . . . . . 287  
Peijun Shi, Xu Yang, Fan Liu, Man Li, Hongmei Pan, Wentao Yang,  
Jian Fang, Shao Sun, Chenyan Tan, Huimin Yang, Yuanyuan Yin,  
Xingming Zhang, Lili Lu, Mengyang Li, Xin Cao, and Yongchang Meng

## **Part IX Understanding the Spatial Patterns of Global Natural Disaster Risk**

**World Atlas of Natural Disaster Risk** . . . . . 309  
Peijun Shi, Jing'ai Wang, Wei Xu, Tao Ye, Saini Yang, Lianyou Liu,  
Weihua Fang, Kai Liu, Ning Li, and Ming Wang

**Appendix I: Name and Abbreviation of Countries and Regions** . . . . . 325

**Appendix II: Name and Coding System of the Comparable-Geographic  
Unit in the Atlas (Alphabetical Order of the Initial  
of the Country Name)** . . . . . 329

---

<b>Appendix III: Data Source and Database for World Atlas of Natural Disaster Risk. . . . .</b>	<b>335</b>
<b>Appendix IV: Validation . . . . .</b>	<b>345</b>
<b>Appendix V: Ranks of Multi-hazard Risk of the World. . . . .</b>	<b>351</b>

---

## Maps

Political Map of the World (2014) . . . . .	xxxiv
Global Satellite Image (2012) . . . . .	xxxv
<b>Environments and Exposures</b>	
Global Lithology (2012) ( $0.5^\circ \times 0.5^\circ$ ) . . . . .	5
Global Tectonic Faults (2010) ( $10\text{km} \times 10\text{km}$ ) . . . . .	6
Global Land Elevation (1997) ( $1\text{km} \times 1\text{km}$ ) . . . . .	7
Global Terrain Slope (2006) ( $10\text{km} \times 10\text{km}$ ) . . . . .	8
Global Permafrost Zones (1997) . . . . .	9
Global Land Cover (2010) ( $1\text{km} \times 1\text{km}$ ) . . . . .	10
Global Soil (2010) ( $1\text{km} \times 1\text{km}$ ) . . . . .	11
Global Climate Zones (2010) ( $10\text{km} \times 10\text{km}$ ) . . . . .	12
Global River Systems (2010) . . . . .	13
Global Annual Average Net Primary Production (NPP) (2001–2012) ( $1\text{km} \times 1\text{km}$ ) . . . . .	14
Land Use Systems of the World (2010) ( $10\text{km} \times 10\text{km}$ ) . . . . .	15
Population Density of the World (2010) ( $1\text{km} \times 1\text{km}$ ) . . . . .	16
Economic-social Wealth of the World (2013) ( $0.5^\circ \times 0.5^\circ$ ) . . . . .	17
Gross Domestic Product (GDP) of the World (2010) ( $0.5^\circ \times 0.5^\circ$ ) . . . . .	18
Livestock Density of the World (2010) ( $10\text{km} \times 10\text{km}$ ) . . . . .	19
Night Light Index of the World (2012) ( $1\text{km} \times 1\text{km}$ ) . . . . .	20
<b>Earthquake, Volcano and Landslide Disasters</b>	
<b>Earthquake</b>	
Historical Event Locations of Global Earthquake (1900–2009, $5.50 \leq M_s < 6.00$ ) . . . . .	30
Historical Event Locations of Global Earthquake (1900–2009, $6.00 \leq M_s < 6.50$ ) . . . . .	30
Historical Event Locations of Global Earthquake (1900–2009, $6.50 \leq M_s < 7.00$ ) . . . . .	31
Historical Event Locations of Global Earthquake (1900–2009, $M_s \geq 7.00$ ) . . . . .	31
Global Peak Ground Acceleration (PGA) ( $0.5^\circ \times 0.5^\circ$ ) . . . . .	32
Mortality Rate of Earthquake Disaster (Intensity = VI) of the World . . . . .	33
Mortality Rate of Earthquake Disaster (Intensity = VII) of the World . . . . .	33
Mortality Rate of Earthquake Disaster (Intensity = VIII) of the World . . . . .	34
Mortality Rate of Earthquake Disaster (Intensity $\geq$ IX) of the World . . . . .	34
Expected Annual Mortality Risk of Earthquake of the World ( $0.5^\circ \times 0.5^\circ$ ) . . . . .	35
Expected Annual Mortality Risk of Earthquake of the World (Comparable-geographic Unit) . . . . .	36
Expected Annual Mortality Risk of Earthquake of the World (Country and Region Unit) . . . . .	36

Expected Annual Economic-social Wealth (ESW) Loss Risk of Earthquake of the World ( $0.1^\circ \times 0.1^\circ$ ) . . . . .	37
Expected Annual Economic-social Wealth (ESW) Loss Risk of Earthquake of the World (Comparable-geographic Unit). . . . .	38
Expected Annual Economic-social Wealth (ESW) Loss Risk of Earthquake of the World (Country and Region Unit) . . . . .	38

### **Volcano**

Historical Eruption Locations of Global Volcano (4360 B.C.–2012 A.D.) . . . . .	44
Historical Eruption Frequency of Global Volcano (4360 B.C.–2012 A.D.) . . . . .	45
Historical Mortality Record of Global Volcano (1900–2009) . . . . .	45
Expected Annual Intensity of Global Volcano. . . . .	46
Global Volcano Intensity by Return Period (10a) . . . . .	47
Global Volcano Intensity by Return Period (20a) . . . . .	47
Global Volcano Intensity by Return Period (50a) . . . . .	48
Global Volcano Intensity by Return Period (100a). . . . .	48
Expected Annual Mortality Risk of Volcano of the World (Comparable-geographic Unit) . . . . .	49
Mortality Risk of Volcano of the World by Return Period (10a) (Comparable-geographic Unit) . . . . .	50
Mortality Risk of Volcano of the World by Return Period (20a) (Comparable-geographic Unit) . . . . .	50
Mortality Risk of Volcano of the World by Return Period (50a) (Comparable-geographic Unit) . . . . .	51
Mortality Risk of Volcano of the World by Return Period (100a) (Comparable-geographic Unit) . . . . .	51
Expected Annual Mortality Risk of Volcano of the World (Country and Region Unit). . . . .	52
Mortality Risk of Volcano of the World by Return Period (10a) (Country and Region Unit). . . . .	53
Mortality Risk of Volcano of the World by Return Period (20a) (Country and Region Unit). . . . .	53
Mortality Risk of Volcano of the World by Return Period (50a) (Country and Region Unit). . . . .	54
Mortality Risk of Volcano of the World by Return Period (100a) (Country and Region Unit). . . . .	54

### **Landslide**

Historical Event Locations of Global Landslide (2003 and 2007–2011) . . . . .	61
Global Landslide Susceptibility ( $0.1^\circ \times 0.1^\circ$ ) . . . . .	62
Global Rainfall-induced Landslide Intensity ( $0.25^\circ \times 0.25^\circ$ ) . . . . .	63
Expected Annual Mortality Risk of Landslide of the World ( $0.25^\circ \times 0.25^\circ$ ) . . . . .	64
Expected Annual Mortality Risk of Landslide of the World (Comparable-geographic Unit) . . . . .	65
Expected Annual Mortality Risk of Landslide of the World (Country and Region Unit). . . . .	65

### **Flood and Storm Surge Disasters**

#### **Flood**

Global Expected Annual Accumulated 3-day Extreme Precipitation ( $1^\circ \times 1^\circ$ ) . . . . .	74
Expected Annual Extreme Discharge of Global Main Watersheds . . . . .	74
Global Accumulated 3-day Extreme Precipitation by Return Period (10a) ( $1^\circ \times 1^\circ$ ) . . . . .	75
Global Accumulated 3-day Extreme Precipitation by Return Period (20a) ( $1^\circ \times 1^\circ$ ) . . . . .	75

Global Accumulated 3-day Extreme Precipitation by Return Period (50a) (1° × 1°) . . . . .	76
Global Accumulated 3-day Extreme Precipitation by Return Period (100a) (1° × 1°) . . . . .	76
Extreme Discharge of Global Main Watersheds by Return Period (10a) . . . . .	77
Extreme Discharge of Global Main Watersheds by Return Period (20a) . . . . .	77
Extreme Discharge of Global Main Watersheds by Return Period (50a) . . . . .	78
Extreme Discharge of Global Main Watersheds by Return Period (100a) . . . . .	78
Global Flood Inundation Area by Return Period (100a) . . . . .	79
Population of Main Watersheds of the World (2010) . . . . .	80
GDP of Main Watersheds of the World (2010) . . . . .	80
Annual Mortality in Historical Flood Disaster of the World (1950–2012) . . . . .	81
Annual GDP Loss in Historical Flood Disaster of the World (1950–2012) . . . . .	81
Expected Annual Affected Population Risk of Flood of the World (1° × 1°) . . . . .	82
Affected Population Risk of Flood of the World by Return Period (10a) (1° × 1°) . . . . .	83
Affected Population Risk of Flood of the World by Return Period (20a) (1° × 1°) . . . . .	83
Affected Population Risk of Flood of the World by Return Period (50a) (1° × 1°) . . . . .	84
Affected Population Risk of Flood of the World by Return Period (100a) (1° × 1°) . . . . .	84
Expected Annual Affected GDP Risk of Flood of the World (1° × 1°) . . . . .	85
Affected GDP Risk of Flood of the World by Return Period (10a) (1° × 1°) . . . . .	86
Affected GDP Risk of Flood of the World by Return Period (20a) (1° × 1°) . . . . .	86
Affected GDP Risk of Flood of the World by Return Period (50a) (1° × 1°) . . . . .	87
Affected GDP Risk of Flood of the World by Return Period (100a) (1° × 1°) . . . . .	87
Expected Annual Affected Population Risk of Flood of the World (Comparable-geographic Unit) . . . . .	88
Affected Population Risk of Flood of the World by Return Period (10a) (Comparable-geographic Unit) . . . . .	89
Affected Population Risk of Flood of the World by Return Period (20a) (Comparable-geographic Unit) . . . . .	89
Affected Population Risk of Flood of the World by Return Period (50a) (Comparable-geographic Unit) . . . . .	90
Affected Population Risk of Flood of the World by Return Period (100a) (Comparable-geographic Unit) . . . . .	90
Expected Annual Affected GDP Risk of Flood of the World (Comparable-geographic Unit) . . . . .	91
Affected GDP Risk of Flood of the World by Return Period (10a) (Comparable-geographic Unit) . . . . .	92
Affected GDP Risk of Flood of the World by Return Period (20a) (Comparable-geographic Unit) . . . . .	92
Affected GDP Risk of Flood of the World by Return Period (50a) (Comparable-geographic Unit) . . . . .	93
Affected GDP Risk of Flood of the World by Return Period (100a) (Comparable-geographic Unit) . . . . .	93
Expected Annual Affected Population Risk of Flood of the World (Watershed Unit) . . . . .	94
Affected Population Risk of Flood of the World by Return Period (10a) (Watershed Unit) . . . . .	95
Affected Population Risk of Flood of the World by Return Period (20a) (Watershed Unit) . . . . .	95
Affected Population Risk of Flood of the World by Return Period (50a) (Watershed Unit) . . . . .	96

Affected Population Risk of Flood of the World by Return Period (100a) (Watershed Unit) . . . . .	96
Expected Annual Affected GDP Risk of Flood the World (Watershed Unit) . . . . .	97
Affected GDP Risk of Flood of the World by Return Period (10a) (Watershed Unit) . . . . .	98
Affected GDP Risk of Flood of the World by Return Period (20a) (Watershed Unit) . . . . .	98
Affected GDP Risk of Flood of the World by Return Period (50a) (Watershed Unit) . . . . .	99
Affected GDP Risk of Flood of the World by Return Period (100a) (Watershed Unit) . . . . .	99
Mortality Risk of Flood of the World by Return Period (100a) (Country and Region Unit) . . . . .	100
GDP Loss Risk of Flood of the World by Return Period (100a) (Country and Region Unit) . . . . .	101
<b>Storm Surge</b>	
Historical Event Locations of Global Storm Surge (1975–2007) . . . . .	106
Global Coastal Geomorphology . . . . .	106
Expected Annual Relative Maximum Value of Water-level Rise of Global Coastal Zones. . . . .	107
Expected Annual Inundation Area of Global Coastal Zones . . . . .	108
Expected Annual Affected Population Risk of Storm Surge of the World. . . . .	109
Expected Annual Affected GDP Risk of Storm Surge of the World. . . . .	110
<b>Sand-dust Storm and Tropical Cyclone Disasters</b>	
<b>Sand-dust Storm</b>	
Susceptibility of Global Sand-dust Storm ( $0.5^\circ \times 0.5^\circ$ ) . . . . .	119
Expected Annual Kinetic Energy of Global Sand-dust Storm ( $PM_{10}$ ) ( $0.5^\circ \times 0.5^\circ$ ). . . . .	120
Kinetic Energy of Global Sand-dust Storm ( $PM_{10}$ ) by Return Period (10a) ( $0.5^\circ \times 0.5^\circ$ ). . . . .	121
Kinetic Energy of Global Sand-dust Storm ( $PM_{10}$ ) by Return Period (20a) ( $0.5^\circ \times 0.5^\circ$ ). . . . .	121
Kinetic Energy of Global Sand-dust Storm ( $PM_{10}$ ) by Return Period (50a) ( $0.5^\circ \times 0.5^\circ$ ). . . . .	122
Kinetic Energy of Global Sand-dust Storm ( $PM_{10}$ ) by Return Period (100a) ( $0.5^\circ \times 0.5^\circ$ ). . . . .	122
Expected Annual Affected Population Risk of Sand-dust Storm of the World ( $0.5^\circ \times 0.5^\circ$ ). . . . .	123
Affected Population Risk of Sand-dust Storm of the World by Return Period (10a) ( $0.5^\circ \times 0.5^\circ$ ). . . . .	124
Affected Population Risk of Sand-dust Storm of the World by Return Period (20a) ( $0.5^\circ \times 0.5^\circ$ ). . . . .	124
Affected Population Risk of Sand-dust Storm of the World by Return Period (50a) ( $0.5^\circ \times 0.5^\circ$ ). . . . .	125
Affected Population Risk of Sand-dust Storm of the World by Return Period (100a) ( $0.5^\circ \times 0.5^\circ$ ). . . . .	125
Expected Annual Affected Population Risk of Sand-dust Storm of the World (Comparable-geographic Unit). . . . .	126
Affected Population Risk of Sand-dust Storm of the World by Return Period (10a) (Comparable-geographic Unit) . . . . .	127
Affected Population Risk of Sand-dust Storm of the World by Return Period (20a) (Comparable-geographic Unit) . . . . .	127

Affected Population Risk of Sand-dust Storm of the World by Return Period (50a) (Comparable-geographic Unit) . . . . .	128
Affected Population Risk of Sand-dust Storm of the World by Return Period (100a) (Comparable-geographic Unit) . . . . .	128
Expected Annual Affected Population Risk of Sand-dust Storm of the World (Country and Region Unit) . . . . .	129
Affected Population Risk of Sand-dust Storm of the World by Return Period (10a) (Country and Region Unit) . . . . .	130
Affected Population Risk of Sand-dust Storm of the World by Return Period (20a) (Country and Region Unit) . . . . .	130
Affected Population Risk of Sand-dust Storm of the World by Return Period (50a) (Country and Region Unit) . . . . .	131
Affected Population Risk of Sand-dust Storm of the World by Return Period (100a) (Country and Region Unit) . . . . .	131
Expected Annual Affected GDP Risk of Sand-dust Storm of the World (0.5° × 0.5°) . . . . .	132
Affected GDP Risk of Sand-dust Storm of the World by Return Period (10a) (0.5° × 0.5°) . . . . .	133
Affected GDP Risk of Sand-dust Storm of the World by Return Period (20a) (0.5° × 0.5°) . . . . .	133
Affected GDP Risk of Sand-dust Storm of the World by Return Period (50a) (0.5° × 0.5°) . . . . .	134
Affected GDP Risk of Sand-dust Storm of the World by Return Period (100a) (0.5° × 0.5°) . . . . .	134
Expected Annual Affected GDP Risk of Sand-dust Storm of the World (Comparable-geographic Unit) . . . . .	135
Affected GDP Risk of Sand-Dust Storm of the World by Return Period (10a) (Comparable-geographic Unit) . . . . .	136
Affected GDP Risk of Sand-Dust Storm of the World by Return Period (20a) (Comparable-geographic Unit) . . . . .	136
Affected GDP Risk of Sand-dust Storm of the World by Return Period (50a) (Comparable-geographic Unit) . . . . .	137
Affected GDP Risk of Sand-dust Storm of the World by Return Period (100a) (Comparable-geographic Unit) . . . . .	137
Expected Annual Affected GDP Risk of Sand-dust Storm of the World (Country and Region Unit) . . . . .	138
Affected GDP Risk of Sand-dust Storm of the World by Return Period (10a) (Country and Region Unit) . . . . .	139
Affected GDP Risk of Sand-dust Storm of the World by Return Period (20a) (Country and Region Unit) . . . . .	139
Affected GDP Risk of Sand-dust Storm of the World by Return Period (50a) (Country and Region Unit) . . . . .	140
Affected GDP Risk of Sand-dust Storm of the World by Return Period (100a) (Country and Region Unit) . . . . .	140
Expected Annual Affected Livestock Risk of Sand-dust Storm of the World (0.5° × 0.5°) . . . . .	141
Affected Livestock Risk of Sand-dust Storm of the World by Return Period (10a) (0.5° × 0.5°) . . . . .	142
Affected Livestock Risk of Sand-dust Storm of the World by Return Period (20a) (0.5° × 0.5°) . . . . .	142
Affected Livestock Risk of Sand-dust Storm of the World by Return Period (50a) (0.5° × 0.5°) . . . . .	143
Affected Livestock Risk of Sand-dust Storm of the World by Return Period (100a) (0.5° × 0.5°) . . . . .	143

Expected Annual Affected Livestock Risk of Sand-dust Storm of the World (Comparable-geographic Unit) . . . . .	144
Affected Livestock Risk of Sand-dust Storm of the World by Return Period (10a) (Comparable-geographic Unit) . . . . .	145
Affected Livestock Risk of Sand-dust Storm of the World by Return Period (20a) (Comparable-geographic Unit) . . . . .	145
Affected Livestock Risk of Sand-dust Storm of the World by Return Period (50a) (Comparable-geographic Unit) . . . . .	146
Affected Livestock Risk of Sand-dust Storm of the World by Return Period (100a) (Comparable-geographic Unit) . . . . .	146
Expected Annual Affected Livestock Risk of Sand-dust Storm of the World (Country and Region Unit) . . . . .	147
Affected Livestock Risk of Sand-dust Storm of the World by Return Period (10a) (Country and Region Unit) . . . . .	148
Affected Livestock Risk of Sand-dust Storm of the World by Return Period (20a) (Country and Region Unit) . . . . .	148
Affected Livestock Risk of Sand-dust Storm of the World by Return Period (50a) (Country and Region Unit) . . . . .	149
Affected Livestock Risk of Sand-dust Storm of the World by Return Period (100a) (Country and Region Unit) . . . . .	149
<b>Tropical Cyclone</b>	
Global Tropical Cyclone Tracks . . . . .	155
Global Expected Annual 10-minute Maximum Sustained Wind of Tropical Cyclone (1km × 1km) . . . . .	156
Global 10-minute Maximum Sustained Wind of Tropical Cyclone by Return Period (10a) (1km × 1km) . . . . .	157
Global 10-minute Maximum Sustained Wind of Tropical Cyclone by Return Period (20a) (1km × 1km) . . . . .	157
Global 10-minute Maximum Sustained Wind of Tropical Cyclone by Return Period (50a) (1km × 1km) . . . . .	158
Global 10-minute Maximum Sustained Wind of Tropical Cyclone by Return Period (100a) (1km × 1km) . . . . .	158
Global Expected Annual 3-second Gust Wind of Tropical Cyclone (1km x 1km) . . . . .	159
Global 3-second Gust Wind of Tropical Cyclone by Return Period (10a) (1km × 1km) . . . . .	160
Global 3-second Gust Wind of Tropical Cyclone by Return Period (20a) (1km × 1km) . . . . .	160
Global 3-second Gust Wind of Tropical Cyclone by Return Period (50a) (1km × 1km) . . . . .	161
Global 3-second Gust Wind of Tropical Cyclone by Return Period (100a) (1km × 1km) . . . . .	161
Expected Annual Affected Population Risk of Tropical Cyclone of the World (Country and Region Unit) . . . . .	162
Affected Population Risk of Tropical Cyclone of the World by Return Period (10a) (Country and Region Unit) . . . . .	163
Affected Population Risk of Tropical Cyclone of the World by Return Period (20a) (Country and Region Unit) . . . . .	163
Affected Population Risk of Tropical Cyclone of the World by Return Period (50a) (Country and Region Unit) . . . . .	164
Affected Population Risk of Tropical Cyclone of the World by Return Period (100a) (Country and Region Unit) . . . . .	164
Expected Annual Affected GDP Risk of Tropical Cyclone of the World (0.1° × 0.1°) . . . . .	165

**Heat Wave and Cold Wave Disasters**

**Heat Wave**

Temperature Threshold and Historical Event Locations of Global Heat Wave (1950–2013) (0.75° × 0.75°) . . . . . 172

Expected Annual Duration of Global Heat Wave (0.75° × 0.75°) . . . . . 173

Duration of Global Heat Wave by Return Period (10a) (0.75° × 0.75°) . . . . . 174

Duration of Global Heat Wave by Return Period (20a) (0.75° × 0.75°) . . . . . 174

Duration of Global Heat Wave by Return Period (50a) (0.75° × 0.75°) . . . . . 175

Duration of Global Heat Wave by Return Period (100a) (0.75° × 0.75°) . . . . . 175

Expected Annual Maximum Temperature of Global Heat Wave (0.75° × 0.75°) . . . . . 176

Maximum Temperature of Global Heat Wave by Return Period (10a) (0.75° × 0.75°) . . . . . 177

Maximum Temperature of Global Heat Wave by Return Period (20a) (0.75° × 0.75°) . . . . . 177

Maximum Temperature of Global Heat Wave by Return Period (50a) (0.75° × 0.75°) . . . . . 178

Maximum Temperature of Global Heat Wave by Return Period (100a) (0.75° × 0.75°) . . . . . 178

Expected Annual Mortality Risk of Heat Wave of the World (0.75° × 0.75°) . . . . . 179

Mortality Risk of Heat Wave of the World by Return Period (10a) (0.75° × 0.75°) . . . . . 180

Mortality Risk of Heat Wave of the World by Return Period (20a) (0.75° × 0.75°) . . . . . 180

Mortality Risk of Heat Wave of the World by Return Period (50a) (0.75° × 0.75°) . . . . . 181

Mortality Risk of Heat Wave of the World by Return Period (100a) (0.75° × 0.75°) . . . . . 181

Expected Annual Mortality Risk of Heat Wave of the World (Comparable-geographic Unit) . . . . . 182

Mortality Risk of Heat Wave of the World by Return Period (10a) (Comparable-geographic Unit) . . . . . 183

Mortality Risk of Heat Wave of the World by Return Period (20a) (Comparable-geographic Unit) . . . . . 183

Mortality Risk of Heat Wave of the World by Return Period (50a) (Comparable-geographic Unit) . . . . . 184

Mortality Risk of Heat Wave of the World by Return Period (100a) (Comparable-geographic Unit) . . . . . 184

Expected Annual Mortality Risk of Heat Wave of the World (Country and Region Unit) . . . . . 185

Mortality Risk of Heat Wave of the World by Return Period (10a) (Country and Region Unit) . . . . . 186

Mortality Risk of Heat Wave of the World by Return Period (20a) (Country and Region Unit) . . . . . 186

Mortality Risk of Heat Wave of the World by Return Period (50a) (Country and Region Unit) . . . . . 187

Mortality Risk of Heat Wave of the World by Return Period (100a) (Country and Region Unit) . . . . . 187

**Cold Wave**

Temperature Threshold and Historical Event Locations of Global Cold Wave (1950–2013) (0.75° × 0.75°) . . . . . 193

Occurrence Concentration Degree (CCD) of Global Cold Wave (0.75° × 0.75°) . . . . . 194

Occurrence Concentrated Period (CCP) of Global Cold Wave (0.75° × 0.75°) . . . . . 194

Expected Annual Global Temperature Drop (0.75° × 0.75°) . . . . . 195

Global Temperature Drop by Return Period (10a) ( $0.75^\circ \times 0.75^\circ$ ) . . . . .	196
Global Temperature Drop by Return Period (20a) ( $0.75^\circ \times 0.75^\circ$ ) . . . . .	196
Global Temperature Drop by Return Period (50a) ( $0.75^\circ \times 0.75^\circ$ ) . . . . .	197
Global Temperature Drop by Return Period (100a) ( $0.75^\circ \times 0.75^\circ$ ) . . . . .	197
Expected Annual Affected Population Risk of Cold Wave of the World ( $0.75^\circ \times 0.75^\circ$ ) . . . . .	198
Affected Population Risk of Cold Wave of the World by Return Period (10a) ( $0.75^\circ \times 0.75^\circ$ ) . . . . .	199
Affected Population Risk of Cold Wave of the World by Return Period (20a) ( $0.75^\circ \times 0.75^\circ$ ) . . . . .	199
Affected Population Risk of Cold Wave of the World by Return Period (50a) ( $0.75^\circ \times 0.75^\circ$ ) . . . . .	200
Affected Population Risk of Cold Wave of the World by Return Period (100a) ( $0.75^\circ \times 0.75^\circ$ ) . . . . .	200
Expected Annual Affected Population Risk of Cold Wave of the World (Comparable-geographic Unit) . . . . .	201
Affected Population Risk of Cold Wave of the World by Return Period (10a) (Comparable-geographic Unit) . . . . .	202
Affected Population Risk of Cold Wave of the World by Return Period (20a) (Comparable-geographic Unit) . . . . .	202
Affected Population Risk of Cold Wave of the World by Return Period (50a) (Comparable-geographic Unit) . . . . .	203
Affected Population Risk of Cold Wave of the World by Return Period (100a) (Comparable-geographic Unit) . . . . .	203
Expected Annual Affected Population Risk of Cold Wave of the World (Country and Region Unit) . . . . .	204
Affected Population Risk of Cold Wave of the World by Return Period (10a) (Country and Region Unit) . . . . .	205
Affected Population Risk of Cold Wave of the World by Return Period (20a) (Country and Region Unit) . . . . .	205
Affected Population Risk of Cold Wave of the World by Return Period (50a) (Country and Region Unit) . . . . .	206
Affected Population Risk of Cold Wave of the World by Return Period (100a) (Country and Region Unit) . . . . .	206

## Drought Disasters

### Drought Risk (Maize)

Global Expected Annual Drought Intensity for Maize ( $0.5^\circ \times 0.5^\circ$ ) . . . . .	214
Global Drought Intensity for Maize by Return Period (10a) ( $0.5^\circ \times 0.5^\circ$ ) . . . . .	215
Global Drought Intensity for Maize by Return Period (20a) ( $0.5^\circ \times 0.5^\circ$ ) . . . . .	215
Global Drought Intensity for Maize by Return Period (50a) ( $0.5^\circ \times 0.5^\circ$ ) . . . . .	216
Global Drought Intensity for Maize by Return Period (100a) ( $0.5^\circ \times 0.5^\circ$ ) . . . . .	216
Expected Annual Maize Yield Loss Risk of Drought of the World ( $0.5^\circ$ $\times 0.5^\circ$ ) . . . . .	217
Maize Yield Loss Risk of Drought of the World by Return Period (10a) ( $0.5^\circ \times 0.5^\circ$ ) . . . . .	218
Maize Yield Loss Risk of Drought of the World by Return Period (20a) ( $0.5^\circ \times 0.5^\circ$ ) . . . . .	218
Maize Yield Loss Risk of Drought of the World by Return Period (50a) ( $0.5^\circ \times 0.5^\circ$ ) . . . . .	219
Maize Yield Loss Risk of Drought of the World by Return Period (100a) ( $0.5^\circ \times 0.5^\circ$ ) . . . . .	219
Expected Annual Maize Yield Loss Risk of Drought of the World (Comparable-geographic Unit) . . . . .	220

Maize Yield Loss Risk of Drought of the World by Return Period (10a) (Comparable-geographic Unit) . . . . .	221
Maize Yield Loss Risk of Drought of the World by Return Period (20a) (Comparable-geographic Unit) . . . . .	221
Maize Yield Loss Risk of Drought of the World by Return Period (50a) (Comparable-geographic Unit) . . . . .	222
Maize Yield Loss Risk of Drought of the World by Return Period (100a) (Comparable-geographic Unit) . . . . .	222
Expected Annual Maize Yield Loss Risk of Drought of the World (Country and Region Unit). . . . .	223
Maize Yield Loss Risk of Drought of the World by Return Period (10a) (Country and Region Unit). . . . .	224
Maize Yield Loss Risk of Drought of the World by Return Period (20a) (Country and Region Unit). . . . .	224
Maize Yield Loss Risk of Drought of the World by Return Period (50a) (Country and Region Unit). . . . .	225
Maize Yield Loss Risk of Drought of the World by Return Period (100a) (Country and Region Unit). . . . .	225

**Drought Risk (Wheat)**

Global Expected Annual Drought Intensity for Wheat (0.5° × 0.5°). . . . .	230
Global Drought Intensity for Wheat by Return Period (10a) (0.5° × 0.5°) . . . . .	231
Global Drought Intensity for Wheat by Return Period (20a) (0.5° × 0.5°) . . . . .	231
Global Drought Intensity for Wheat by Return Period (50a) (0.5° × 0.5°) . . . . .	232
Global Drought Intensity for Wheat by Return Period (100a) (0.5° × 0.5°). . . . .	232
Expected Annual Wheat Yield Loss Risk of Drought of the World (0.5° × 0.5°). . . . .	233
Wheat Yield Loss Risk of Drought of the World by Return Period (10a) (0.5° × 0.5°). . . . .	234
Wheat Yield Loss Risk of Drought of the World by Return Period (20a) (0.5° × 0.5°). . . . .	234
Wheat Yield Loss Risk of Drought of the World by Return Period (50a) (0.5° × 0.5°). . . . .	235
Wheat Yield Loss Risk of Drought of the World by Return Period (100a) (0.5° × 0.5°). . . . .	235
Expected Annual Wheat Yield Loss Risk of Drought of the World (Comparable-geographic Unit) . . . . .	236
Wheat Yield Loss Risk of Drought of the World by Return Period (10a) (Comparable-geographic Unit) . . . . .	237
Wheat Yield Loss Risk of Drought of the World by Return Period (20a) (Comparable-geographic Unit) . . . . .	237
Wheat Yield Loss Risk of Drought of the World by Return Period (50a) (Comparable-geographic Unit) . . . . .	238
Wheat Yield Loss Risk of Drought of the World by Return Period (100a) (Comparable-geographic Unit) . . . . .	238
Expected Annual Wheat Yield Loss Risk of Drought of the World (Country and Region Unit). . . . .	239
Wheat Yield Loss Risk of Drought of the World by Return Period (10a) (Country and Region Unit). . . . .	240
Wheat Yield Loss Risk of Drought of the World by Return Period (20a) (Country and Region Unit). . . . .	240
Wheat Yield Loss Risk of Drought of the World by Return Period (50a) (Country and Region Unit). . . . .	241
Wheat Yield Loss Risk of Drought of the World by Return Period (100a) (Country and Region Unit). . . . .	241

**Drought Risk (Rice)**

Global Expected Annual Drought Intensity for Rice ( $0.5^\circ \times 0.5^\circ$ ) . . . . .	246
Global Drought Intensity for Rice by Return Period (10a) ( $0.5^\circ \times 0.5^\circ$ ) . . . . .	247
Global Drought Intensity for Rice by Return Period (20a) ( $0.5^\circ \times 0.5^\circ$ ) . . . . .	247
Global Drought Intensity for Rice by Return Period (50a) ( $0.5^\circ \times 0.5^\circ$ ) . . . . .	248
Global Drought Intensity for Rice by Return Period (100a) ( $0.5^\circ \times 0.5^\circ$ ) . . . . .	248
Expected Annual Rice Yield Loss Risk of Drought of the World ( $0.5^\circ \times 0.5^\circ$ ) . . . . .	249
Rice Yield Loss Risk of Drought of the World by Return Period (10a) ( $0.5^\circ \times 0.5^\circ$ ) . . . . .	250
Rice Yield Loss Risk of Drought of the World by Return Period (20a) ( $0.5^\circ \times 0.5^\circ$ ) . . . . .	250
Rice Yield Loss Risk of Drought of the World by Return Period (50a) ( $0.5^\circ \times 0.5^\circ$ ) . . . . .	251
Rice Yield Loss Risk of Drought of the World by Return Period (100a) ( $0.5^\circ \times 0.5^\circ$ ) . . . . .	251
Expected Annual Rice Yield Loss Risk of Drought of the World (Comparable-geographic Unit) . . . . .	252
Rice Yield Loss Risk of Drought of the World by Return Period (10a) (Comparable-geographic Unit) . . . . .	253
Rice Yield Loss Risk of Drought of the World by Return Period (20a) (Comparable-geographic Unit) . . . . .	253
Rice Yield Loss Risk of Drought of the World by Return Period (50a) (Comparable-geographic Unit) . . . . .	254
Rice Yield Loss Risk of Drought of the World by Return Period (100a) (Comparable-geographic Unit) . . . . .	254
Expected Annual Rice Yield Loss Risk of Drought of the World (Country and Region Unit) . . . . .	255
Rice Yield Loss Risk of Drought of the World by Return Period (10a) (Country and Region Unit) . . . . .	256
Rice Yield Loss Risk of Drought of the World by Return Period (20a) (Country and Region Unit) . . . . .	256
Rice Yield Loss Risk of Drought of the World by Return Period (50a) (Country and Region Unit) . . . . .	257
Rice Yield Loss Risk of Drought of the World by Return Period (100a) (Country and Region Unit) . . . . .	257

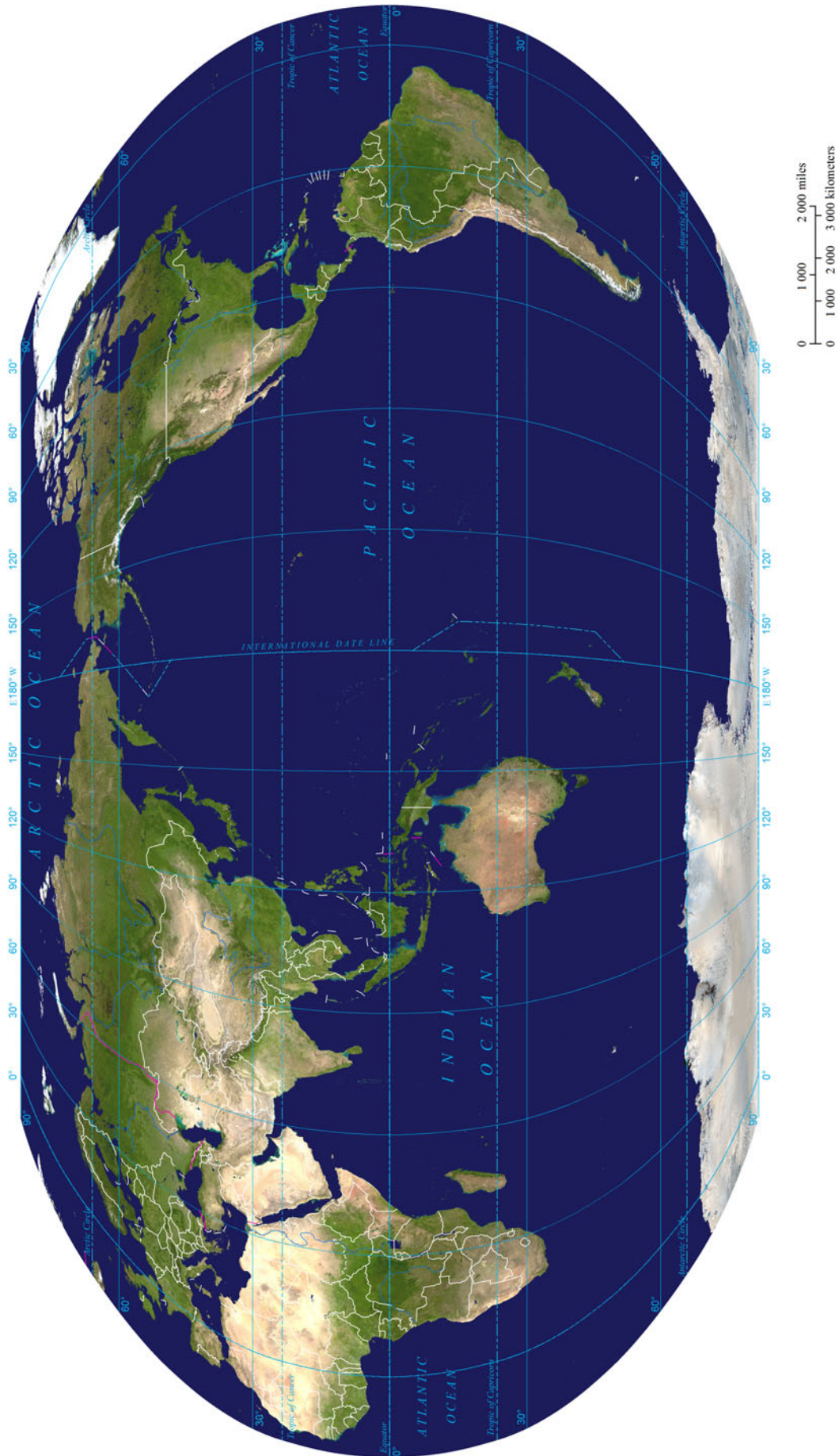
**Wildfire Disasters****Forest Wildfire**

Expected Annual Intensity of Global Forest Wildfire ( $0.1^\circ \times 0.1^\circ$ ) . . . . .	265
Global Intensity of Forest Wildfire by Return Period (10a) ( $0.1^\circ \times 0.1^\circ$ ) . . . . .	266
Global Intensity of Forest Wildfire by Return Period (20a) ( $0.1^\circ \times 0.1^\circ$ ) . . . . .	266
Global Intensity of Forest Wildfire by Return Period (50a) ( $0.1^\circ \times 0.1^\circ$ ) . . . . .	267
Global Intensity of Forest Wildfire by Return Period (100a) ( $0.1^\circ \times 0.1^\circ$ ) . . . . .	267
Average Annual Burned Area of Global Forest Wildfire (2001–2012) ( $0.1^\circ \times 0.1^\circ$ ) . . . . .	268
Expected Annual Burned Area Risk of Forest Wildfire of the World ( $0.1^\circ \times 0.1^\circ$ ) . . . . .	269
Burned Area Risk of Forest Wildfire of the World by Return Period (10a) ( $0.1^\circ \times 0.1^\circ$ ) . . . . .	270
Burned Area Risk of Forest Wildfire of the World by Return Period (20a) ( $0.1^\circ \times 0.1^\circ$ ) . . . . .	271
Burned Area Risk of Forest Wildfire of the World by Return Period (50a) ( $0.1^\circ \times 0.1^\circ$ ) . . . . .	272

Burned Area Risk of Forest Wildfire of the World by Return Period (100a) (0.1° × 0.1°) . . . . .	273
Expected Annual Burned Area Risk of Forest Wildfire of the World (Comparable-geographic Unit) . . . . .	274
Expected Annual Burned Area Risk of Forest Wildfire of the World (Country and Region Unit) . . . . .	274
<b>Grassland Wildfire</b>	
Average Annual Burning Probability of Global Grassland Wildfire (2000–2010) (1km × 1km) . . . . .	280
Expected Annual NPP Loss Risk of Grassland Wildfire of the World (1km × 1km) . . . . .	281
Expected Annual NPP Loss Risk of Grassland Wildfire of the World (Comparable-geographic Unit) . . . . .	282
Expected Annual NPP Loss Risk of Grassland Wildfire of the World (Country and Region Unit) . . . . .	282
<b>Multi-natural Disasters</b>	
<b>Multi-hazard</b>	
Expected Annual Multi-hazard Risk Level of Mortality and Affected Population of the World (Measured by TRI) (0.5° × 0.5°) . . . . .	293
Expected Annual Multi-hazard Risk Level of Mortality and Affected Population of the World (Measured by TRI) (Comparable-geographic Unit) . . . . .	294
Expected Annual Multi-hazard Risk Level of Mortality and Affected Population of the World (Measured by TRI) (Country and Region Unit) . . . . .	295
Expected Annual Multi-hazard Risk Level of Economic Loss and Affected Property of the World (Measured by TRI) (0.5° × 0.5°) . . . . .	296
Expected Annual Multi-hazard Risk Level of Economic Loss and Affected Property of the World (Measured by TRI) (Comparable-geographic Unit) . . . . .	297
Expected Annual Multi-hazard Risk Level of Economic Loss and Affected Property of the World (Measured by TRI) (Country and Region Unit) . . . . .	298
Global Expected Annual Multi-hazard Intensity (0.5° × 0.5°) . . . . .	299
Expected Annual Multi-hazard Risk Level of Affected Population of the World (Measured by MhRI) (0.5° × 0.5°) . . . . .	300
Expected Annual Multi-hazard Risk Level of Affected Population of the World (Measured by MhRI) (Comparable-geographic Unit) . . . . .	301
Expected Annual Multi-hazard Risk Level of Affected Population of the World (Measured by MhRI) (Country and Region Unit) . . . . .	302
Expected Annual Multi-hazard Risk Level of Affected Property of the World (Measured by MhRI) (0.5° × 0.5°) . . . . .	303
Expected Annual Multi-hazard Risk Level of Affected Property of the World (Measured by MhRI) (Comparable-geographic Unit) . . . . .	304
Expected Annual Multi-hazard Risk Level of Affected Property of the World (Measured by MhRI) (Country and Region Unit) . . . . .	305



Global Satellite Image (2012)



Data Source: National Aeronautics and Space Administration(NASA) <http://visibleearth.nasa.gov/view.php?id=57752>

---

**Part I**

**Environments and Exposures**

---

# Mapping Environments and Exposures of the World

Fang Lian, Chunqin Zhang, Hongmei Pan, Man Li, Wentao Yang, Yongchang Meng, Jian Fang, Weihua Fang, Jing'ai Wang, and Peijun Shi

---

## 1 Introduction

Disaster system, a dynamic system on the earth surface with complex characteristics, is composed of natural hazards (H), exposures (S), environments (E), and disaster losses (D) (Fig. 1).

Disaster system is a type of social–ecological system and also an important part of the earth surface system. Since hazards can be classified into three types by origin—natural, natural–human (environmental or ecological), and human, a disaster system can also be classified into three subsystems—natural disaster system, environmental (ecological) disaster system, and human ecological system. Disaster losses and damages are consequences of the interactions of hazards (H),

---

**Cartographic Editors:** Jing'ai Wang (Key Laboratory of Regional Geography, Beijing Normal University, Beijing 100875, China) and Fang Lian (School of Geography, Beijing Normal University, Beijing 100875, China).

**Language Editor:** Saini Yang (State Key Laboratory of Earth Surface Processes and Resource Ecology, Beijing Normal University, Beijing 100875, China).

---

F. Lian · C. Zhang  
School of Geography, Beijing Normal University,  
Beijing 100875, China

H. Pan · M. Li · W. Yang · Y. Meng · J. Fang  
Academy of Disaster Reduction and Emergency Management,  
Ministry of Civil Affairs and Ministry of Education, Beijing  
Normal University, Beijing 100875, China

W. Fang  
Key Laboratory of Environmental Change and Natural Disaster,  
Ministry of Education, Beijing Normal University, Beijing  
100875, China

J. Wang  
Key Laboratory of Regional Geography, Beijing Normal  
University, Beijing 100875, China

P. Shi (✉)  
State Key Laboratory of Earth Surface Processes and Resource  
Ecology, Beijing Normal University, Beijing 100875, China  
e-mail: spj@bnu.edu.cn

exposures (S), and the environmental system (E) in which disasters occur (Shi 1991, 1996, 2002, 2005, 2009).

---

## 2 Environments

Environments (E) mainly refer to physical environments that are cradles for physical hazards, namely geology, landform, climate, hydrology, vegetation, and soil.

Land elevation, terrain slope and lithology have an impact on the occurrence, development, and spatial distribution of geological hazards, such as landslide, collapse, and debris flow. Tectonic faults have an impact on the occurrence, development, and spatial distribution of earthquakes and volcanic eruptions. Climate zones directly or indirectly reflect the distribution of extreme climatic events. Soil, land cover, and net primary products (NPP) directly or indirectly influence floods, droughts, and geological hazards. River systems determine the spatial pattern of floods.

---

## 3 Exposures

Exposures (S) mainly include social and economic elements. Population and livestock density exposed to hazards may influence the loss and damage of population and livestock. Land use decides the total loss and loss structures of property caused by natural disasters. Social wealth and gross domestic products (GDP) influence the direct and indirect economic losses. Urbanization level represented by night light index (NLI) directly or indirectly influences the total loss and loss structures of properties.

---

## 4 Mapping Environments and Exposures of the World

There are two major data sources for these maps: reference data and generated data.

#### 4.1 Maps Based on Reference Data

Maps based on reference data include Global Lithology (2012), Global Tectonic Fault Density (2010), Global Land Elevation (1997), Global Terrain Slope (2006), Global Permafrost Zones (1997), Global Land Cover (2010), Global Soil (2010), Global Climate Zone (2010), Global River Systems (2010), Global Annual Average Net Primary Production (NPP) (2001–2012), Land Use System of the World (2010), Population of the World (2010), Social Wealth of the World (2013), Gross Domestic Product (GDP) of the World (2010), Livestock Density of the World (2010), and Night Light Index of the World (2012). The data sources of these maps have been noted in the right corner under each map. In addition, the data of Global Lithology and Fault Density can be purchased with downloaded data from given URLs noted in the maps.

#### 4.2 Maps Based on Generated Data

These maps include the maps of Global Average Net Primary Production and Economic-social Wealth of the World.

**Fig. 1** Disaster system

#### 4.2.1 Global Average Net Primary Production

The average NPP ( $\overline{\text{NPP}}$ ), which is an average of the annual values from 2001 to 2012, is calculated by Eq. (1):

$$\overline{\text{NPP}} = \frac{\sum_{i=1}^n \text{NPP}_i}{n} \quad (1)$$

where  $\text{NPP}_i$  is the annual NPP of the  $i$ th year;  $n = 12$ .

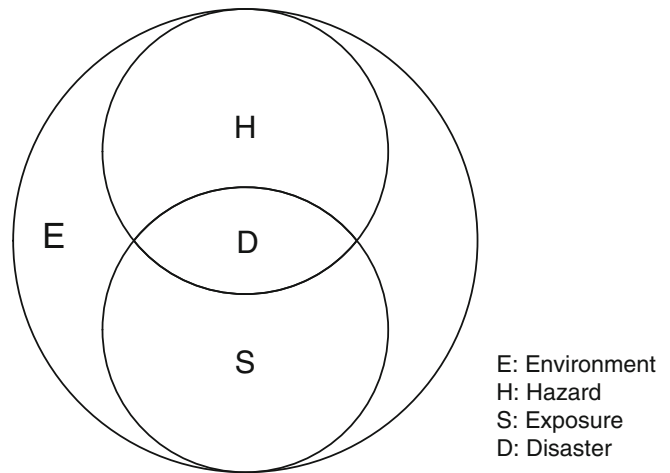
#### 4.2.2 Economic–Social Wealth of the World

Economic–social wealth (ESW) is the ratio of GDP and the investment ratio of one country (Badal et al. 2005). Social wealth per grid cell can be calculated by Eq. (2):

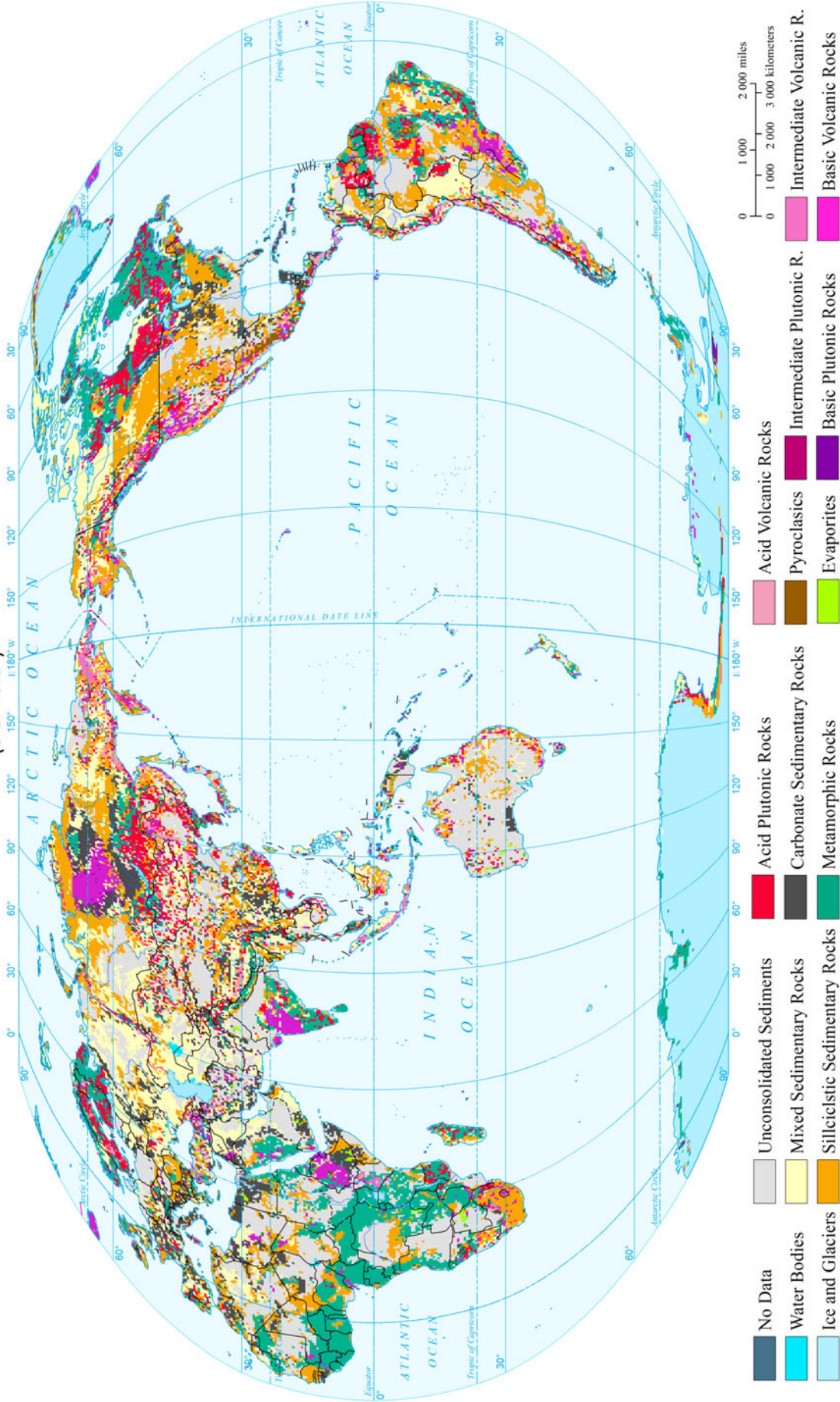
$$\text{ESW}_{\text{cell}} = \frac{\text{GDP}_{\text{cell}}}{\text{INV}_r} \times 100 \% \quad (2)$$

where  $\text{ESW}_{\text{cell}}$  is the economic–social wealth per grid cell;  $\text{GDP}_{\text{cell}}$  is the GDP per grid cell;  $\text{INV}_r$  is the investment ratio of a country, which is the ratio of total investment to GDP. The value of total investment is based on the national accounting statistics from International Monetary Fund (IMF).

## 5 Maps



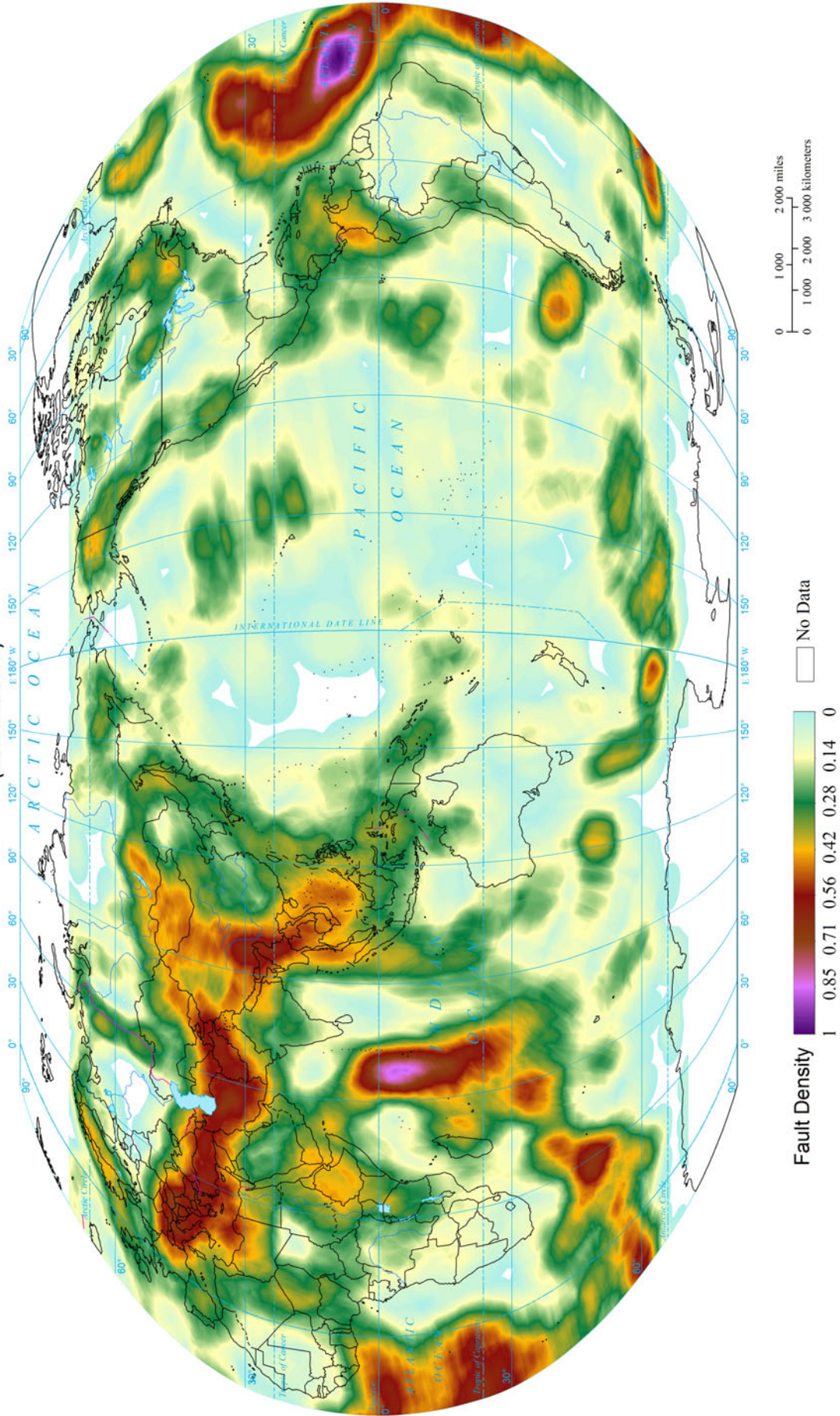
Global Lithology (2012)  
(0.5°x0.5°)



Data Source: Hartmann, J., and N. Moosdorf (2012) <http://doi.pangaea.de/10.1594/PANGAEA.788537>

Global Tectonic Faults (2010)

(10kmx10km)



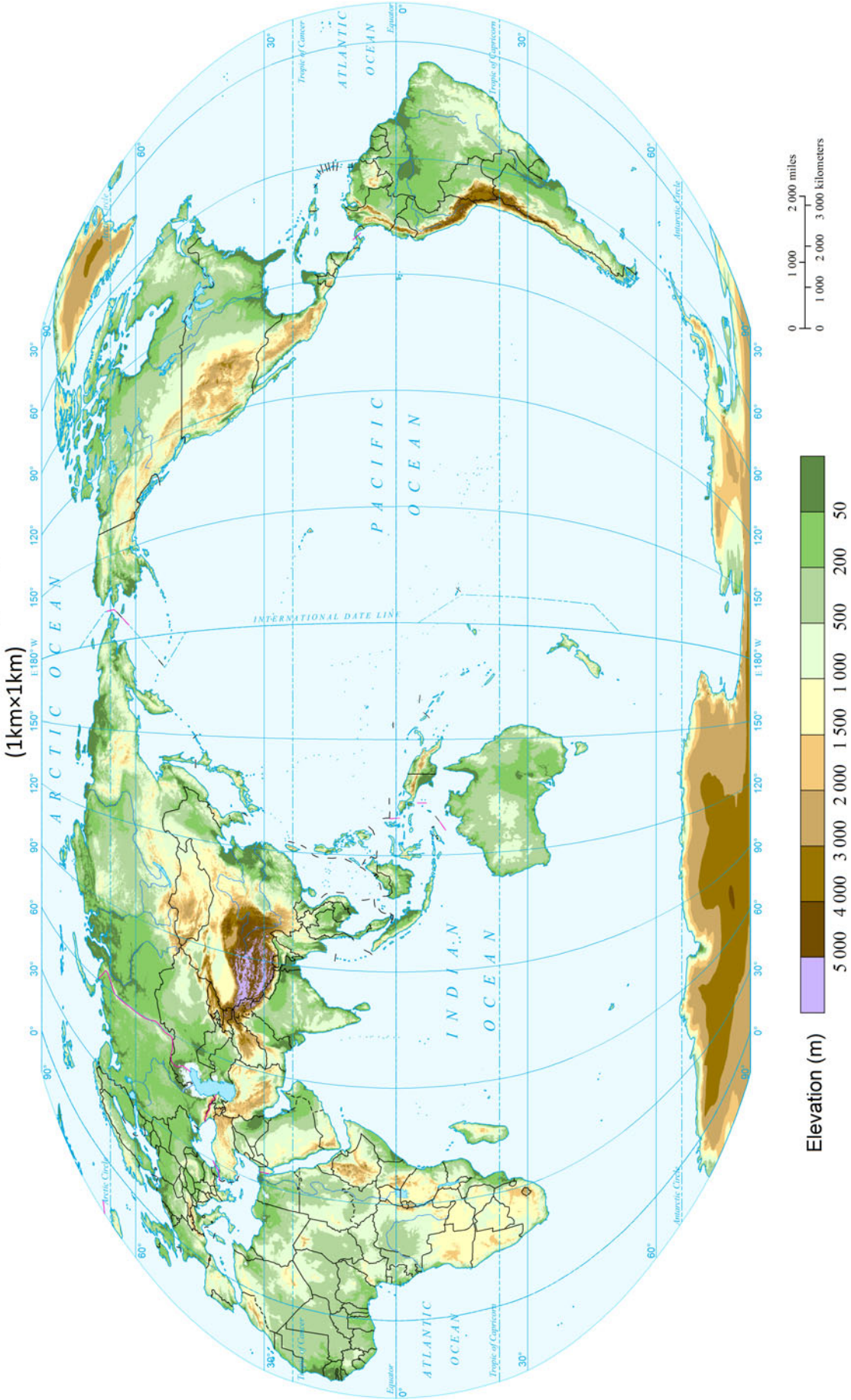
Data Source: Commission for the Geological Map of the World (CGMW) <http://cegm.org/img/cms/Exp!%20Notes%20Geol%20Map%20World.pdf>



Land Elevation

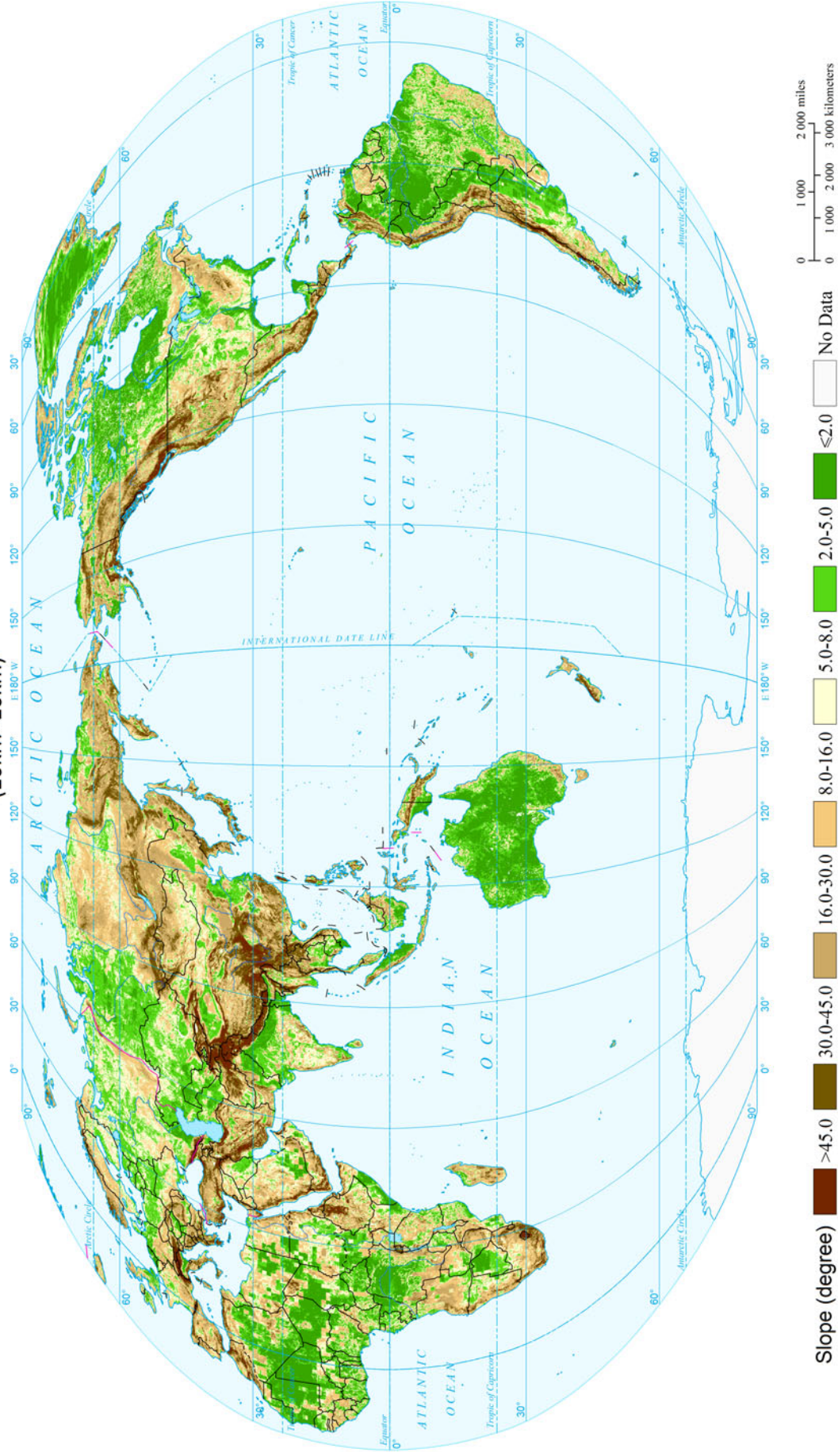
Environments and Exposures

Global Land Elevation (1997)  
(1kmx1km)



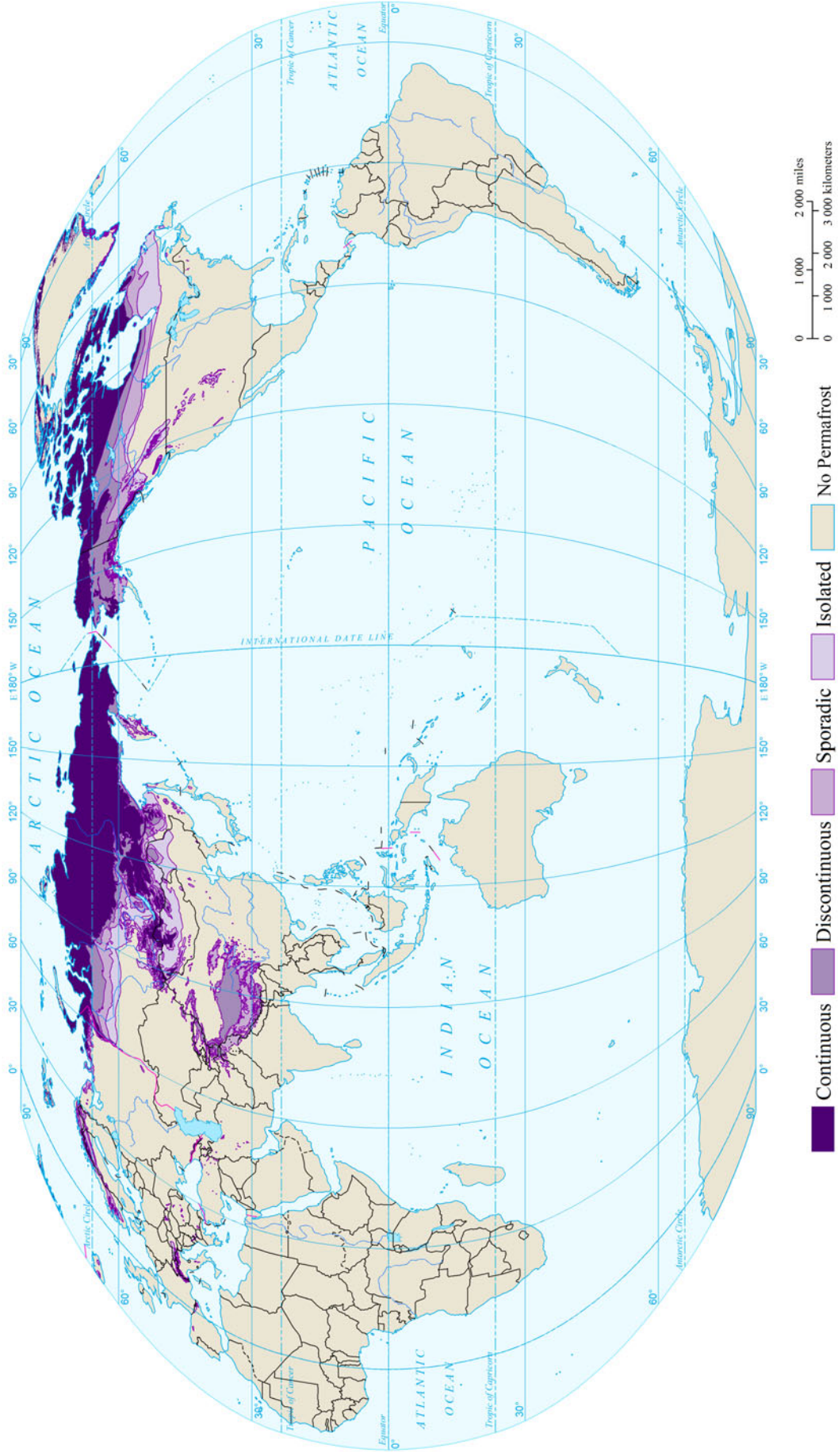
Data Source: United States Geological Survey(USGS),1997 <ftp://edftp.cr.usgs.gov/data/gtopo30/global/>

Global Terrain Slope (2006)  
(10km×10km)



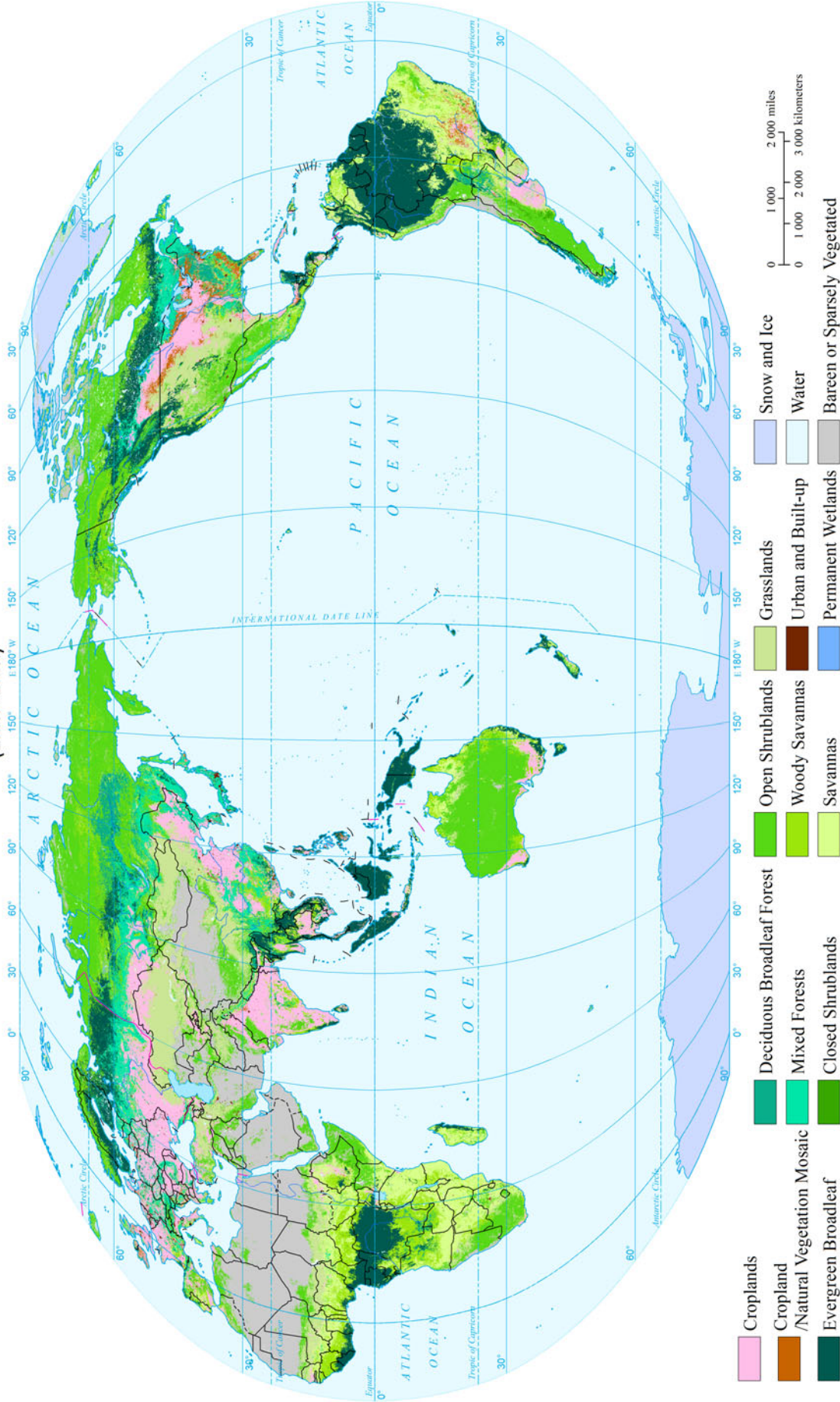
Data Source: International Institute for Applied Systems Analysis-Global Agro-ecological Zones (GAEZ)  
[http://www.gaez.iiasa.ac.at/w/ctrl?\\_flow=Vwr&\\_view=Vwr&idAS=0&idFS=0&fieldmain=main\\_lr\\_slpm&idPS=1e1d6e7d7ec3368cf13a681c523d1ed44870e8b45](http://www.gaez.iiasa.ac.at/w/ctrl?_flow=Vwr&_view=Vwr&idAS=0&idFS=0&fieldmain=main_lr_slpm&idPS=1e1d6e7d7ec3368cf13a681c523d1ed44870e8b45)

Global Permafrost Zones (1997)



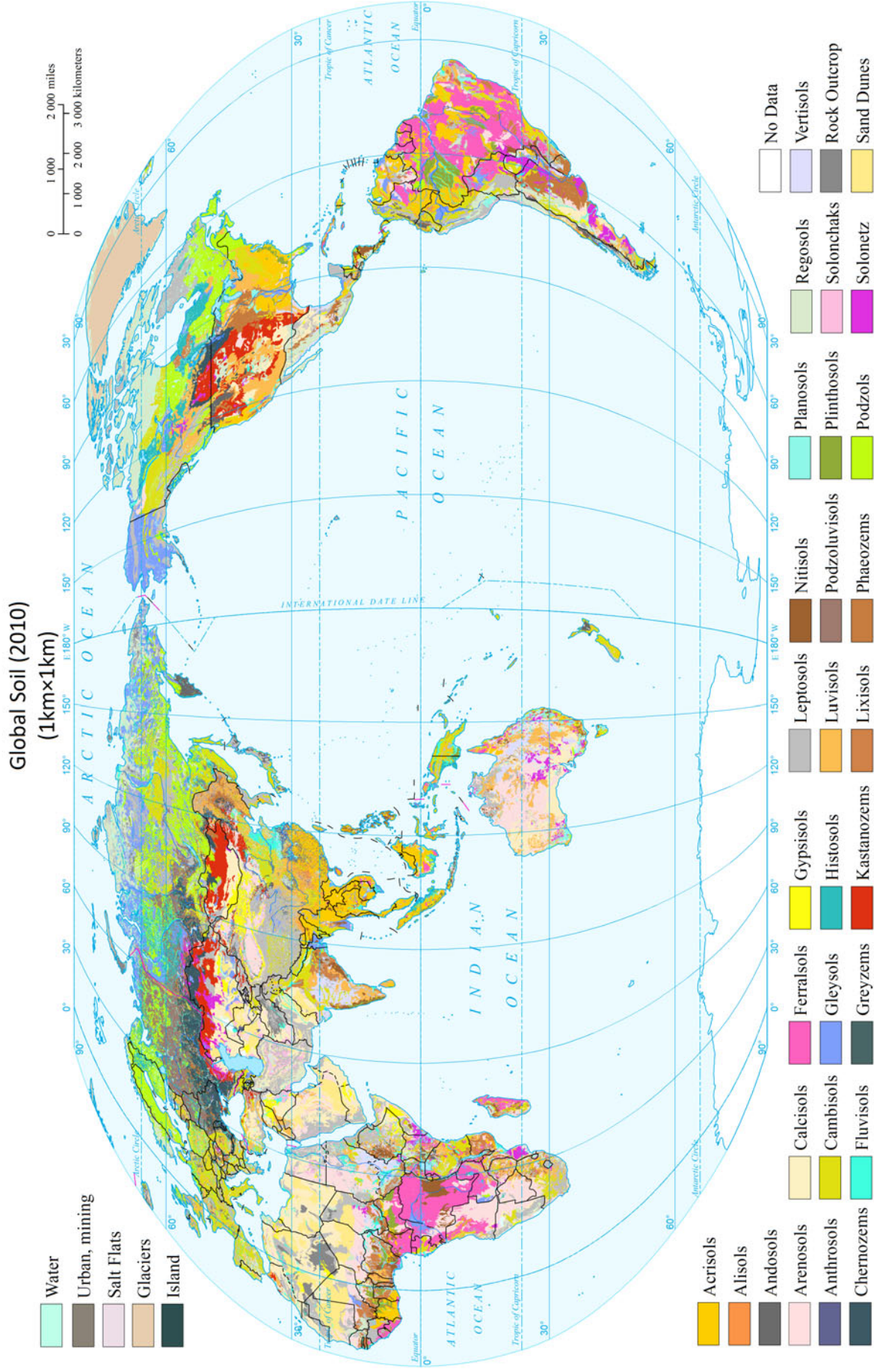
Data Source: Brown, J., O. Ferrians, J. A. Heginbottom, and E. Melnikov. 2014. Circum-Arctic Map of Permafrost and Ground-Ice Conditions. Boulder, Colorado, USA: National Snow and Ice Data Center <http://nsidc.org/data/ggd318>

Global Land Cover (2010)  
(1kmx1km)



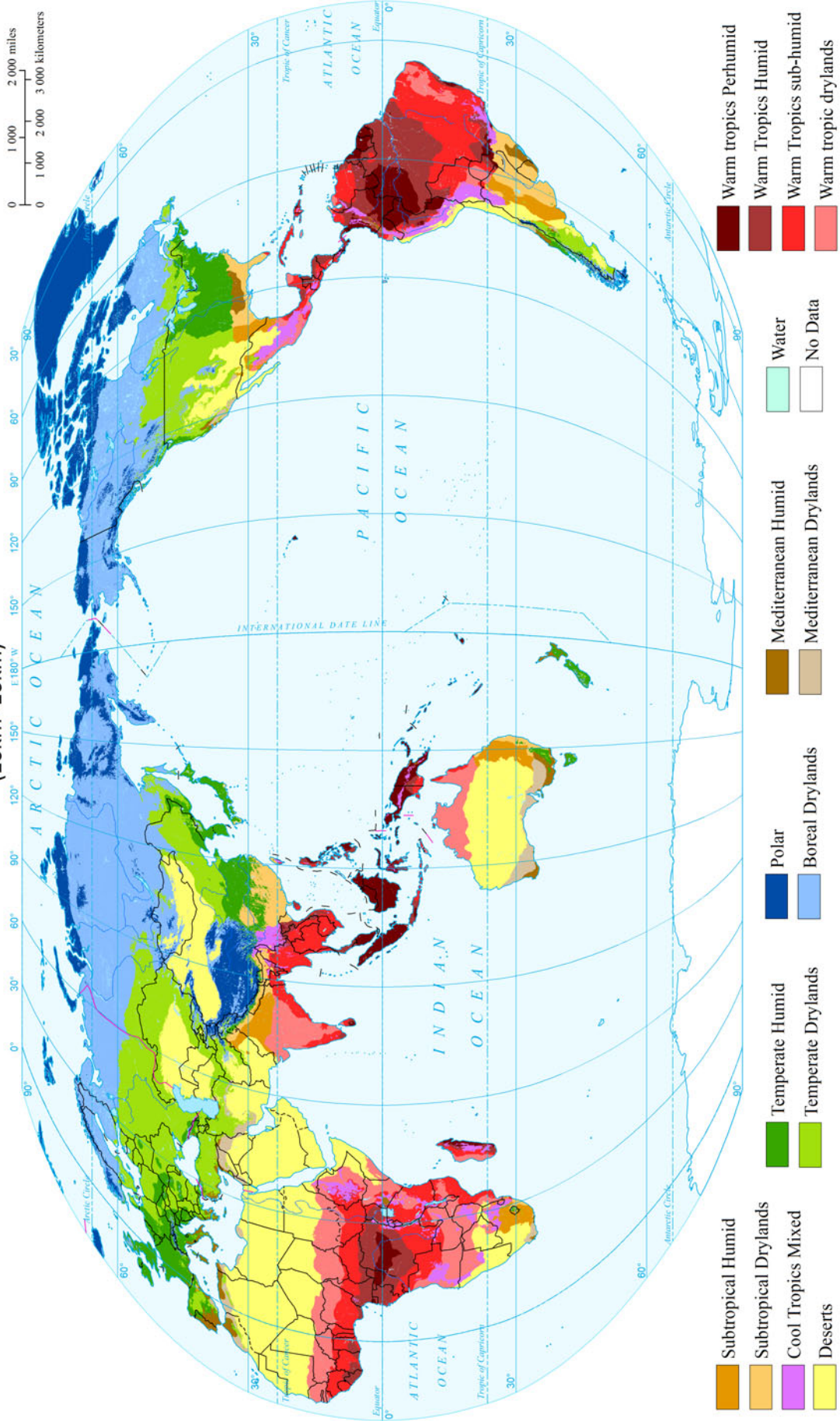
Soil

Environments and Exposures



Data Source: Food and Agriculture Organization (FAO) United Nations Environment Programme (UNEP) Land Degradation Assessment in Drylands (LDAD) Project  
<http://www.fao.org/geonetwork/srv/en/metadata.show?id=37139&currTab=distribution>

Global Climate Zones (2010)  
(10kmx10km)



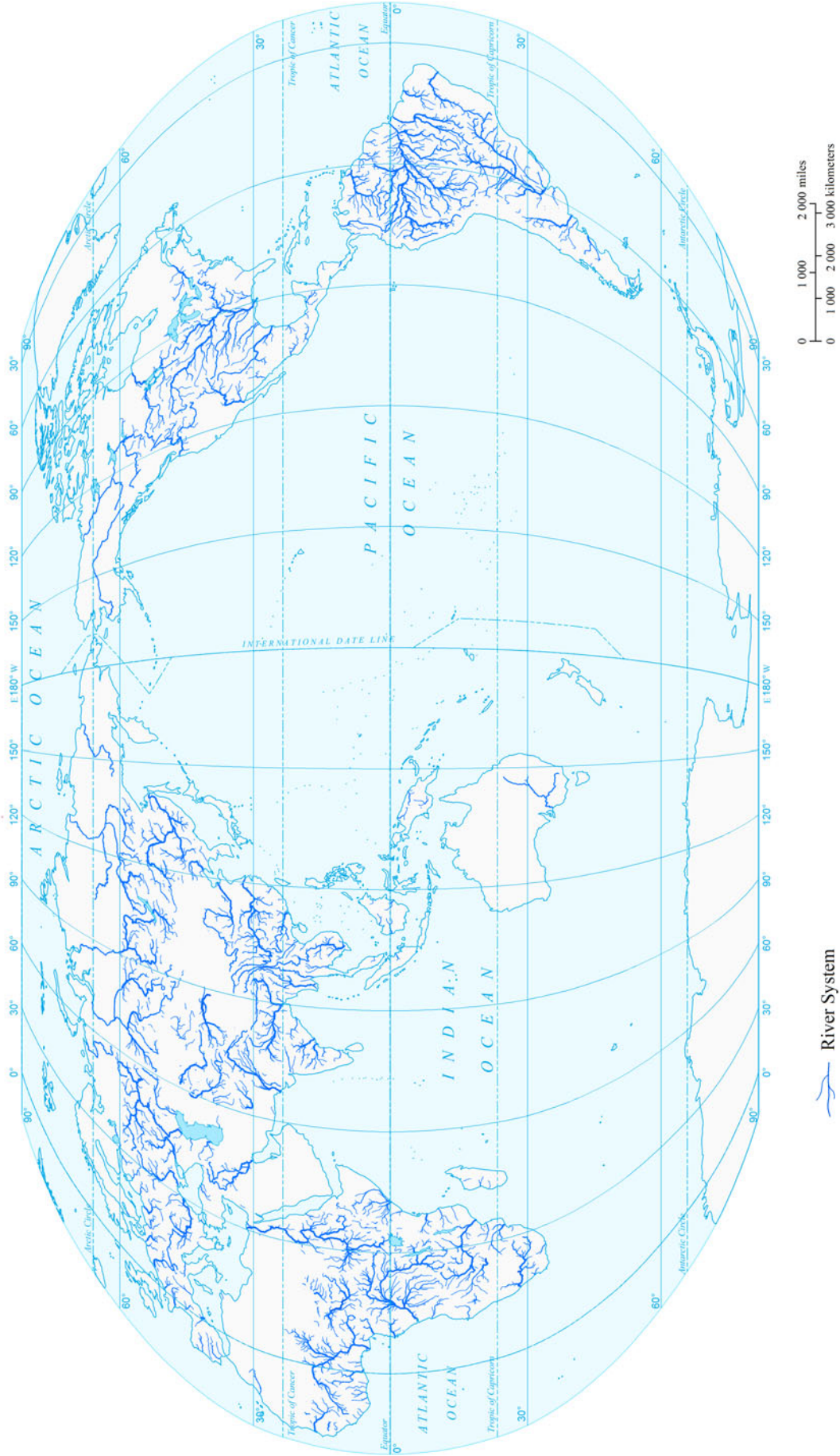
Data Source: Food and Agriculture Organization(FAO) United Nations Environment Programme(UNEP) Land Degradation Assessment in Drylands(LDAD) Project  
<http://www.fao.org/geonetwork/srv/en/metadata.show?id=37139&currTab=distribution>



River System

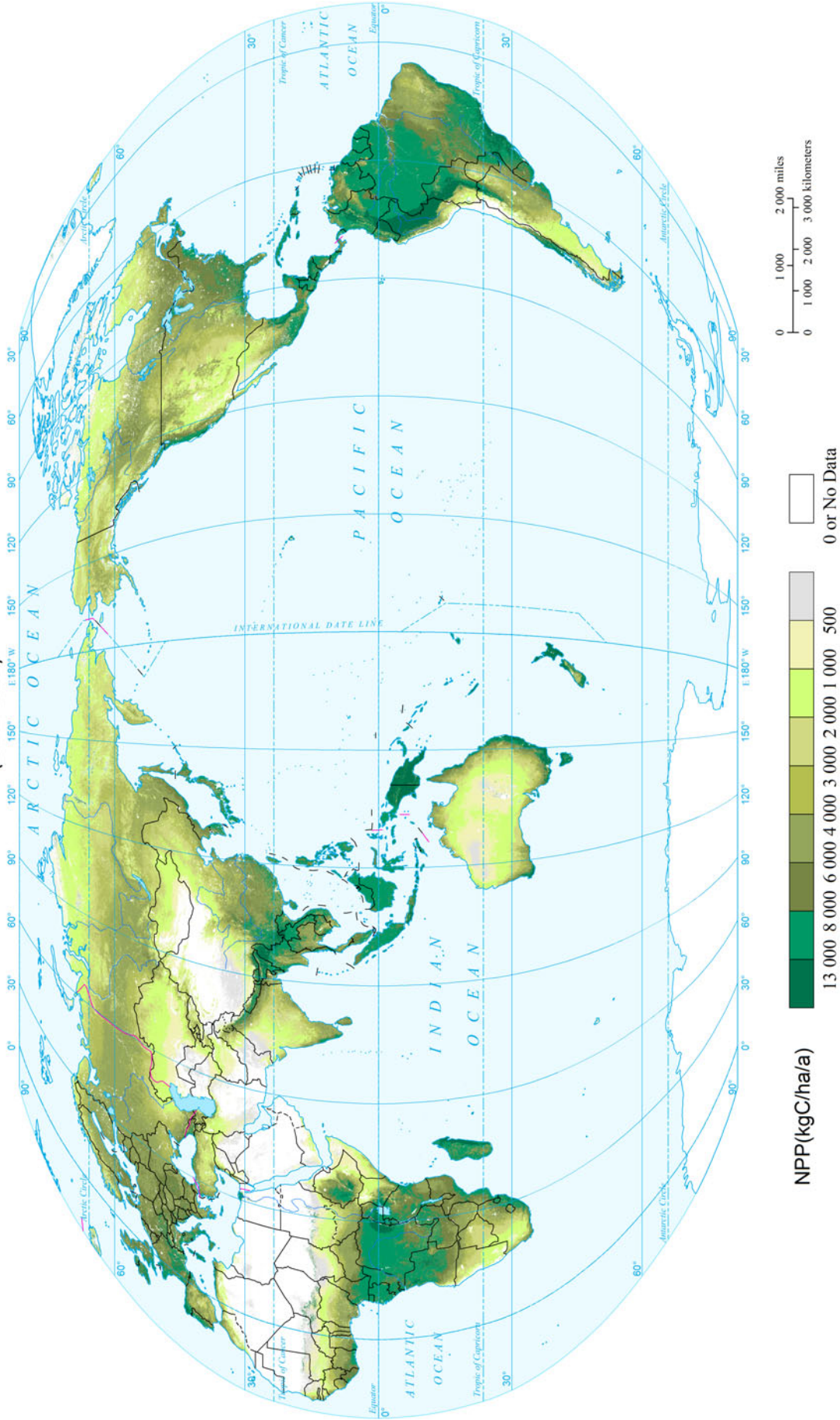
Environments and Exposures

### Global River Systems (2010)



Data Source: Food and Agriculture Organization(FAO) AQUASTAT - programme of the Land and Water Division Montana  
<http://www.fao.org/geonetwork/?uid=7538cb25-7b2e-4030-8454-7197a495a48a>

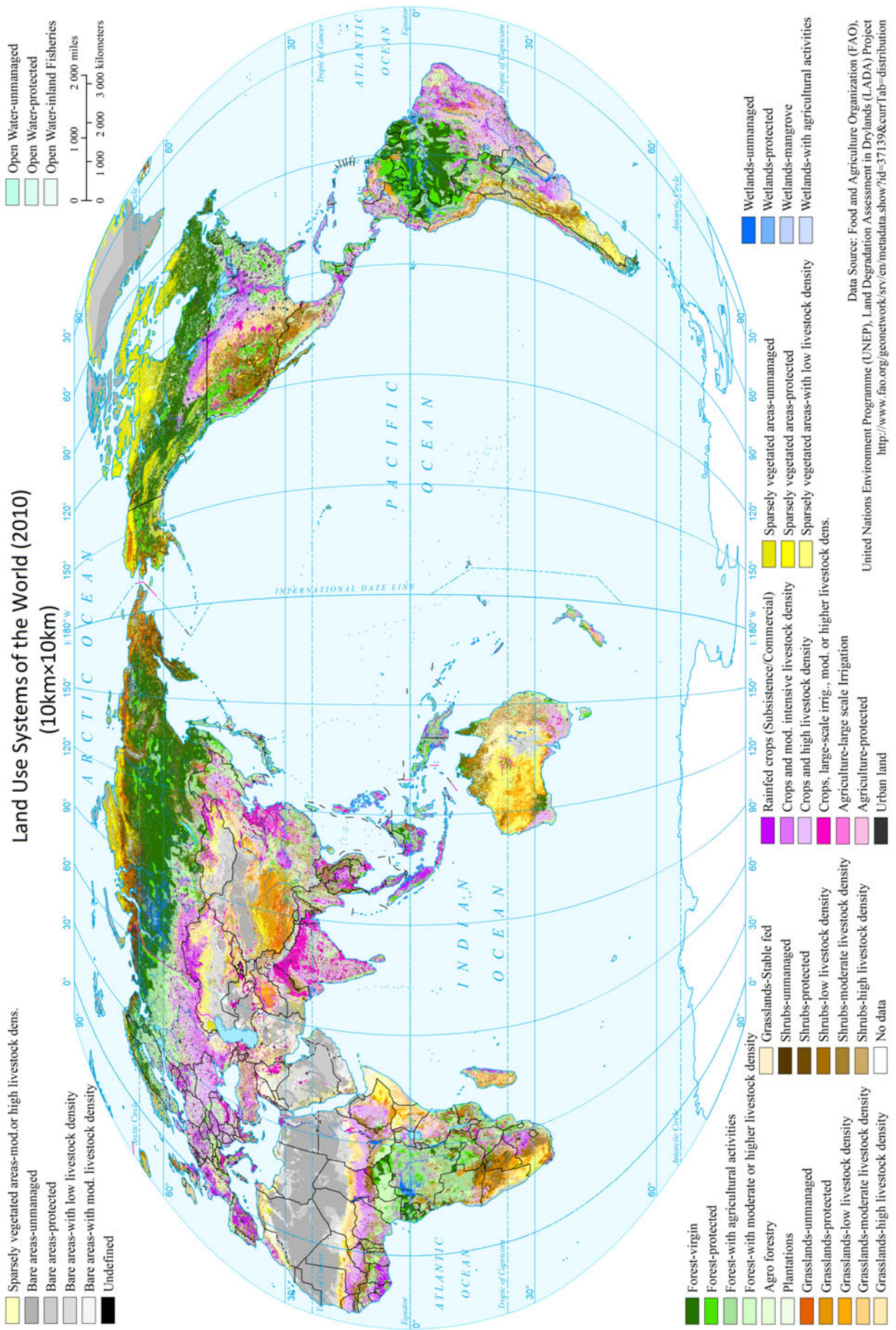
Global Annual Average Net Primary Production (NPP) (2001-2012)  
(1kmx1km)



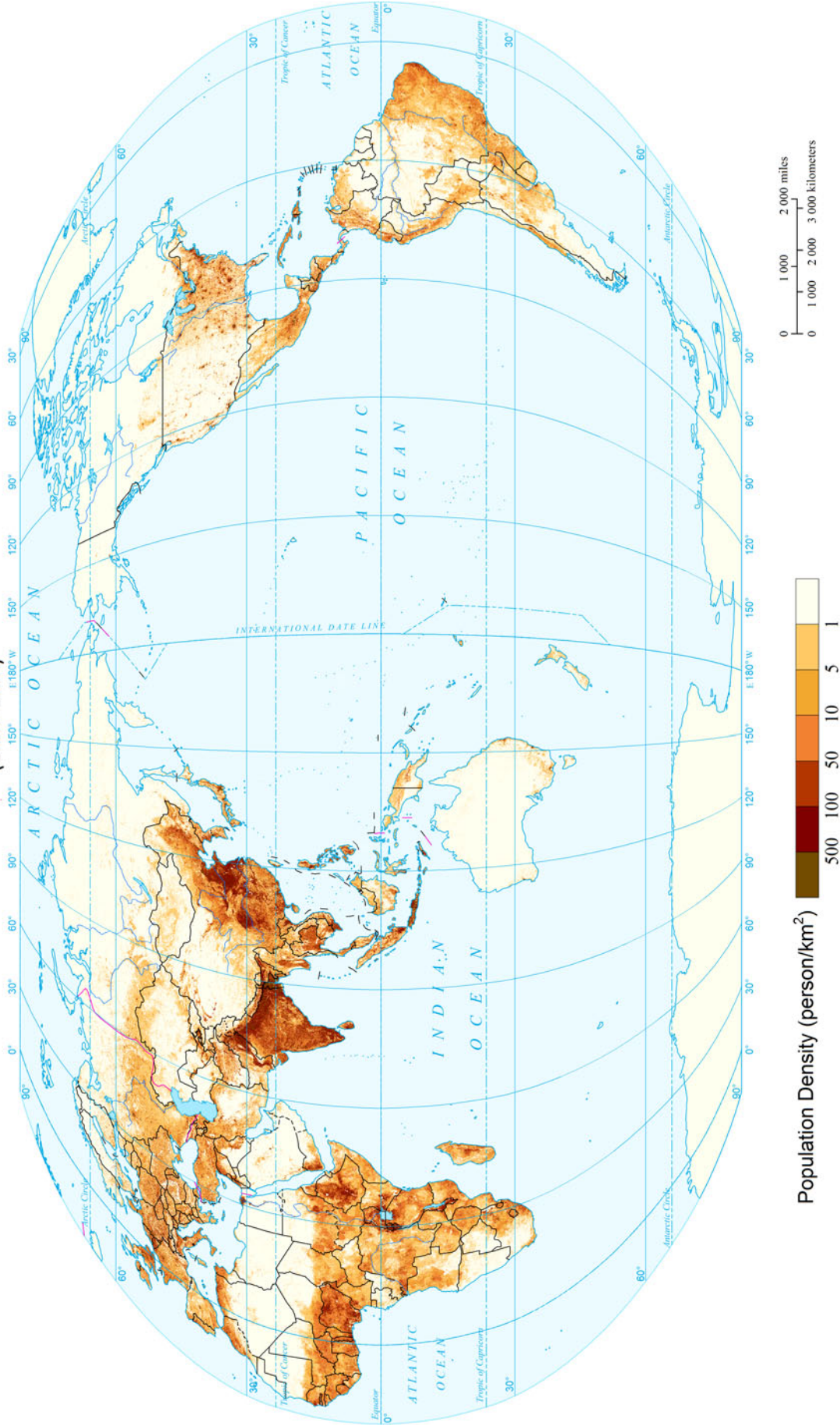
Data Source: MODIS GPP/NPP Project (MOD17) of The University of Montana <http://www.mtsi.umt.edu/project/mod17>

Environments and Exposures

Land Use System



Population Density of the World (2010)  
(1kmx1km)



Data Source: Food and Agriculture Organization (FAO) AQUASTAT - programme of the Land and Water Division Montana  
<http://www.fao.org/geonetwork/tuid-7538cb25-7b2e-4030-8454-7197a49af48a>

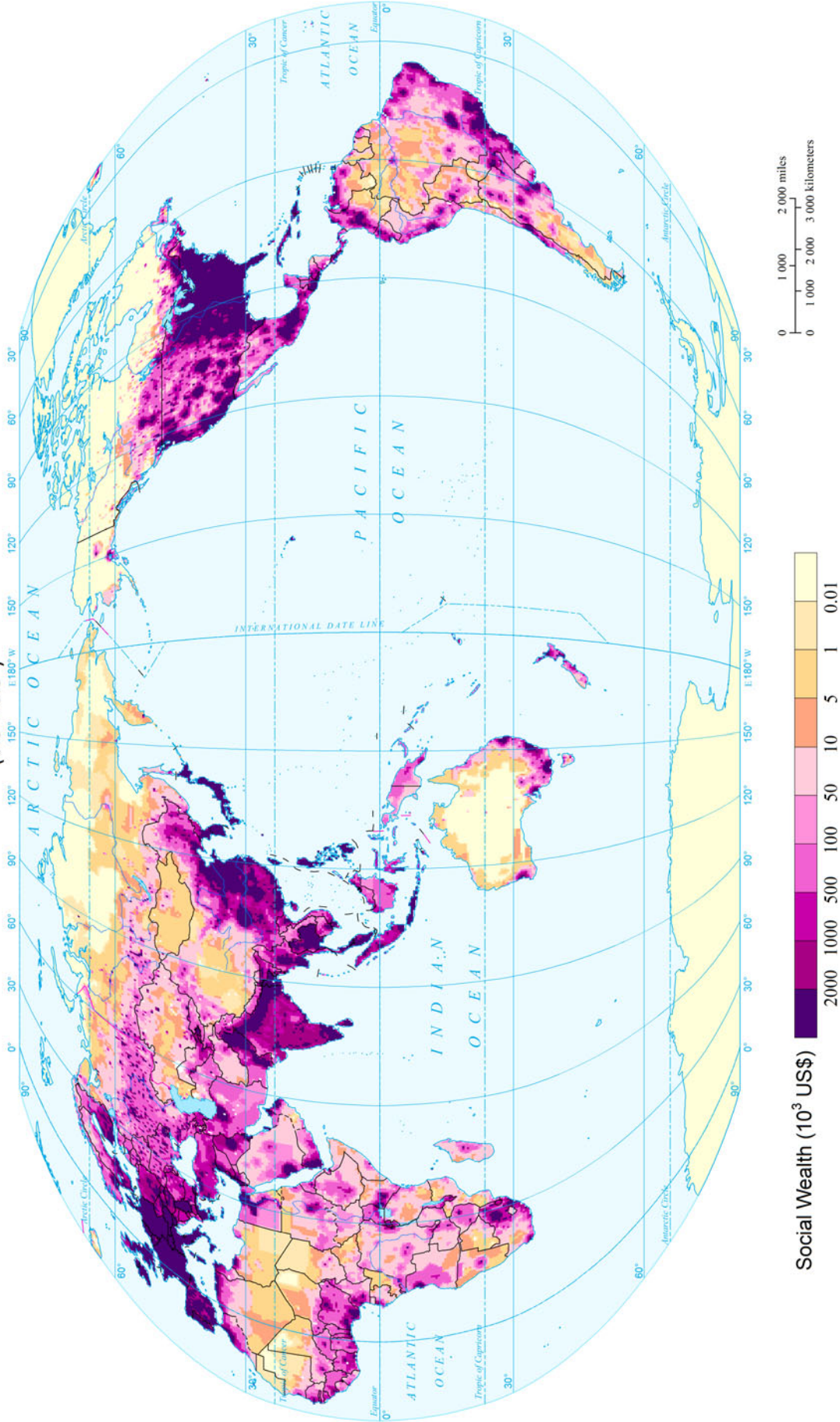


Social Wealth

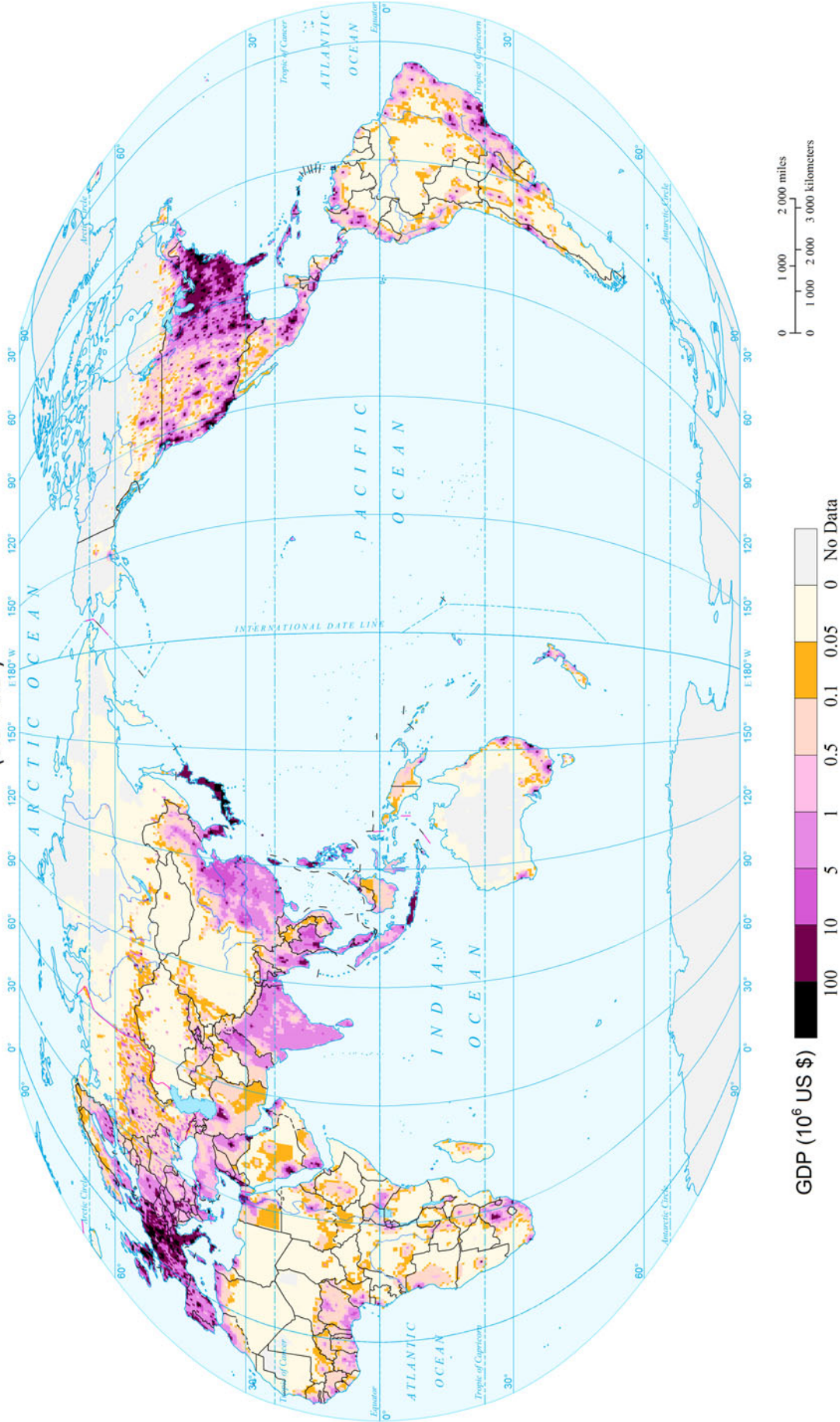
Environments and Exposures

### Economic-social Wealth of the World (2013)

(0.5°x0.5°)

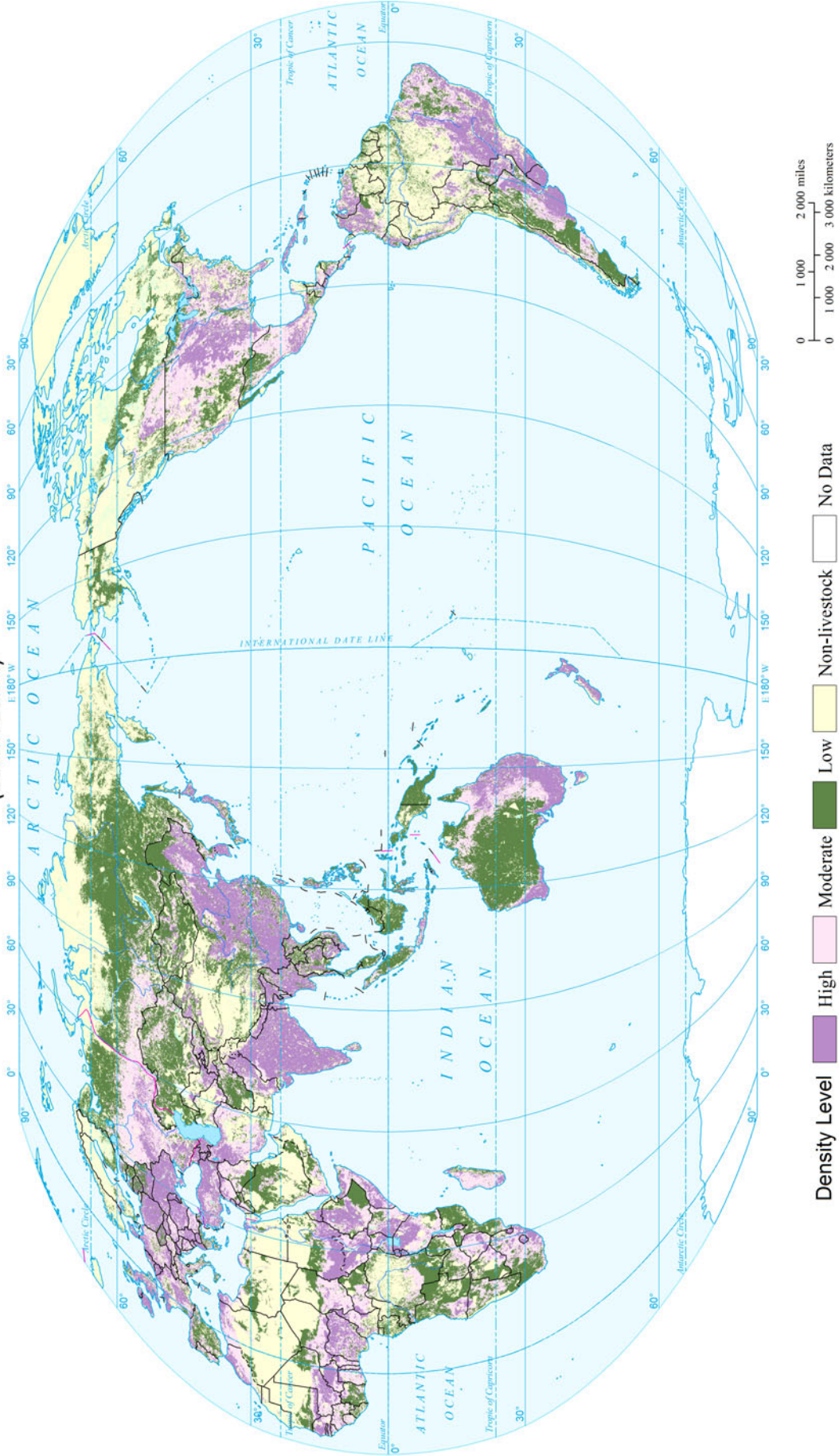


### Gross Domestic Product (GDP) of the World (2010) (0.5°x0.5°)



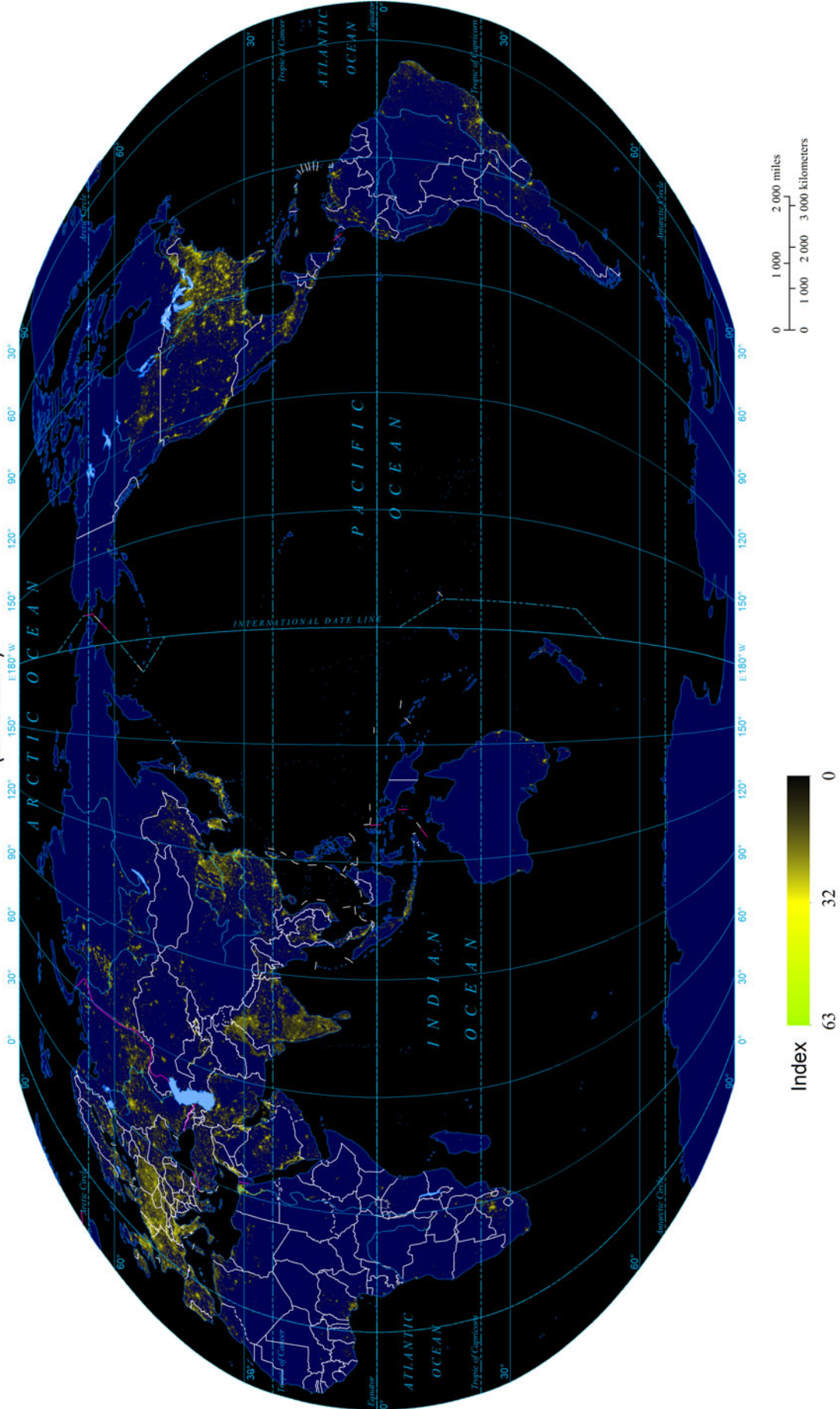
Data Source: Greenhouse Gas Initiative (GGI) Program of the International Institute for Applied Systems Analysis (IIASA)  
<http://www.iiasa.ac.at/Research/GGI/DB/>

### Livestock Density of the World (2010) (10kmx10km)



Data Source: Food and Agriculture Organization (FAO) United Nations Environment Programme (UNEP) Land Degradation Assessment in Drylands (LDAD) Project <http://www.fao.org/geonetwork/srv/en/metadata.show?id=37139&currTab=distribution>

### Night Light Index of the World (2012) (1kmx1km)



Data Source: National Aeronautics and Space Administration(NASA) <http://www.earthobservatory.nasa.gov/NaturalHazards/view.php?id=79765>

## References

- Badal, J., M. Vázquez-prada, and Á. González. 2005. Preliminary quantitative assessment of earthquake casualties and damages. *Natural Hazards* 34(3): 353–374.
- Shi, P.J. 1991. Study on the theory of disaster research and its practice. *Journal of Nanjing University (Natural Sciences)* 11(Supplement): 37–42. (in Chinese).
- Shi, P.J. 1996. Theory and practice of disaster study. *Journal of Natural Disasters* 5(4): 6–17. (in Chinese).
- Shi, P.J. 2002. Theory on disaster science and disaster dynamics. *Journal of Natural Disasters* 11(3): 1–9. (in Chinese).
- Shi, P.J. 2005. Theory and practice on disaster system research—The fourth discussion. *Journal of Natural Disasters* 14(6): 1–7. (in Chinese).
- Shi, P.J. 2009. Theory and practice on disaster system research—The fifth discussion. *Journal of Natural Disasters* 18(5): 1–9. (in Chinese).

---

**Part II**

**Earthquake, Volcano and Landslide Disasters**

---

# Mapping Earthquake Risk of the World

Man Li, Zhenhua Zou, Guodong Xu, and Peijun Shi

---

## 1 Background

In the program of Global Natural Disaster Hotspots, jointly conducted by Columbia University and the World Bank, mortality rate and economic loss rate caused by earthquake disaster are calculated as vulnerability coefficient based on mortality and economic losses in the historical earthquake records. Then the vulnerability coefficient is adjusted by earthquake density which is measured by earthquake frequency to estimate mortality risk and economic loss risk in the world (Dilley et al. 2005). In the program of Global Risk and Vulnerability Index Trends per Year (GRAVITY), hosted by the United Nations Environment Programme (UNEP)/European Global Information Resource Database, the vulnerability of earthquake is calculated based on hazard intensity, death toll, and so on in the historical earthquake records and

combined with other economic indicators to establish loss function, to estimate annual average expected losses (Peduzzi et al. 2009). These two programs are the most influential natural disaster risk assessment projects. However, in the Global Natural Disaster Hotspots, loss rate of all previous earthquakes in the same region is used to represent both hazard and vulnerability, which cannot reflect spatial differences of risk, caused by spatial distribution differences of hazard and vulnerability. Therefore the programs are only used for risk assessment at national level. The assessment results of GRAVITY are also at national level, which cannot demonstrate the risk differences within the country and region. Meanwhile, both programs take GDP as exposure for the assessment of economic losses, which describes economic flow. However, the earthquake imposes direct impact on economic stocks, which is quite different from economic flow.

Therefore, building vulnerability table at national scale and possibility of mortality caused by building collapse shall be taken into consideration to construct population vulnerability table. Combined with population density data and earthquake intensity, world earthquake mortality risk can be assessed. Meanwhile, social wealth shall be taken as social and economic exposure instead of GDP to assess world earthquake economic loss risk. Based on the above conceptions, the earthquake risk of the world is reassessed and mapped in this study at grid, comparable-geographic unit and national levels.

---

**Mapping Editors:** Jing'ai Wang (Key Laboratory of Regional Geography, Beijing Normal University, Beijing 100875, China) and Chunqin Zhang (School of Geography, Beijing Normal University, Beijing 100875, China).

**Language Editor:** Lianyou Liu (Key Laboratory of Environmental Change and Natural Disaster, Ministry of Education, Beijing Normal University, Beijing 100875, China).

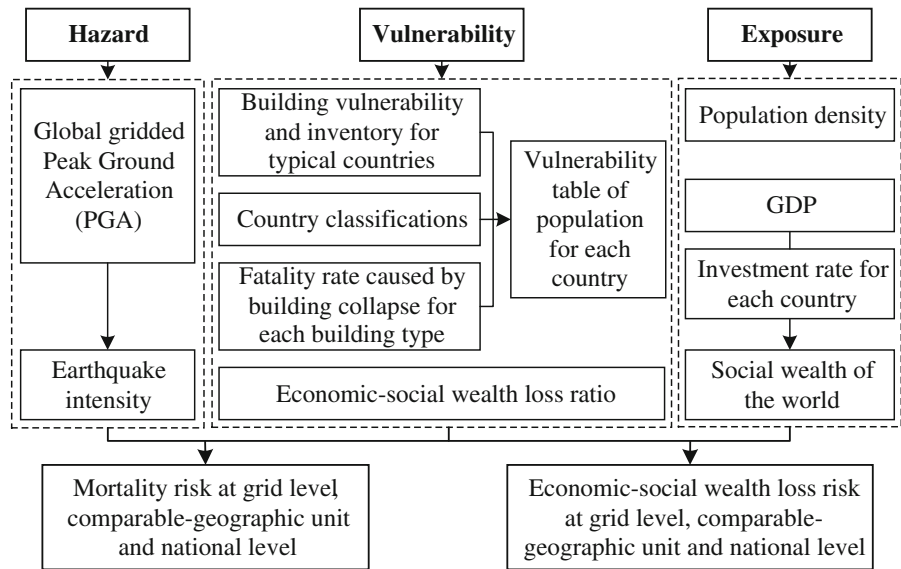
---

M. Li · Z. Zou  
Academy of Disaster Reduction and Emergency Management,  
Ministry of Civil Affairs and Ministry of Education, Beijing  
Normal University, Beijing 100875, China

G. Xu  
Disaster Prevention Institute of Science and Technology, Beijing  
101601, China

P. Shi (✉)  
State Key Laboratory of Earth Surface Processes and Resource  
Ecology, Beijing Normal University, Beijing 100875, China  
e-mail: spj@bnu.edu.cn

**Fig. 1** Technical flowchart for mapping earthquake risk of the world



## 2 Method

Figure 1 shows the technical flowchart for mapping earthquake risk of the world.

### 2.1 Mortality Risk

#### 2.1.1 Population Vulnerability Table at National Level

This study utilizes building vulnerability table (Appendix III, Exposures data 3.6) and mortality probability due to building collapse to establish population vulnerability at national

level. The building vulnerability table includes two parts: building types in each country and their collapse probabilities caused by earthquake with intensity over V level; proportion of resident population in buildings of each type, including urban and rural population. Take the United Kingdom (UK) as an example, as shown in Table 1, for unreinforced brick masonry in mud mortar, the collapse probability by earthquakes with intensity of IX, VIII, VII, and VI are 15 %, 4 %, 0.6 %, and 0 %, respectively. Proportions of population in such buildings in urban and rural areas are 35 % and 50 %, respectively.

Fatality ratio caused by collapse of 8 types of common buildings is the empirical data applied to prompt loss assessment obtained by USGS (Appendix III, Exposures

**Table 1** Building construction vulnerability and inventory of the UK

Construction material	Construction subtype	Probability of collapse (%) of building type when subjected to the specified shaking intensity				Fraction of population who lives in this building type	
		IX (0.65–1.24g)	VIII (0.34–0.65g)	VII (0.18–0.34g)	VI (0.092–0.18g)	Urban	Rural
Masonry	Unreinforced brick masonry in mud mortar	15	4	0.6	0	35	50
Masonry	Unreinforced brick masonry in cement mortar with reinforced concrete floor/roof slabs	6	1	0.1	0	63	50
Structural concrete	Concrete moment resisting frames designed for gravity loads only	11	2	0.2	0	2	0
Steel	Steel moment resisting frame with brick masonry partitions	1.5	0.2	0	0	0	0

**Table 2** Population vulnerability of the UK

	Fatality ratio (%) when subjected to the specified shaking intensity			
	IX (0.65–1.24g)	VIII (0.34–0.65g)	VII (0.18–0.34g)	VI (0.092–0.18g)
In urban areas	0.771	0.167	0.021	0
In rural areas	0.819	0.183	0.024	0

data 3.7), representing population vulnerability due to collapse of buildings of different types (Jaiswal et al. 2009).

The building vulnerability tables are jointed to mortality probabilities caused by building collapse according to building types. Population vulnerability in urban and rural areas are calculated separately according to Eq. (1) to get vulnerability function for each country.

$$FR_{ij} = \sum_{n=1}^4 V_{nj} \times R_{nj} \times CR_{nij} \quad (1)$$

where  $j$  refers to the  $j$ th nation, and  $FR_{ij}$  refers to fatality ratio due to earthquake with intensity  $i$ ,  $i = 1, 2, 3, 4$ .  $V_{nj}$  represents mortality probability caused by collapse of  $n$ -type building,  $n = 1, 2, 3, 4$ .  $R_{nj}$  represents population proportion in  $n$ -type building, and  $CR_{nij}$  refers to collapse probability of  $n$ -type building in earthquake with intensity  $i$ .

Take UK as an example (Table 2), in urban areas, population mortalities in earthquake with VI, VII, VIII, and IX magnitudes are 0, 0.021, 0.167, and 0.771 %, respectively; while for rural areas, they are 0, 0.024, 0.183, and 0.819 %, respectively.

Due to limited data, we divide the world into 28 regions (UNDP 2010) according to economic development levels and geographic positions, one country is selected to represent the whole region and its population vulnerability is taken as representation of the other countries. If such data are not available in one region, another country with data at the same development level in adjacent region shall be chosen. The following representative countries are selected: Algeria, Argentina, Chile, China, Cyprus, Greece, India, Indonesia, Japan, Macedonia, Mexico, Morocco, Nepal, Pakistan, Peru, Romania, Slovenia, Sweden, Thailand, Turkey, and UK, and the representative countries in 7 regions are replaced by suitable countries in adjacent regions. Accordingly, population vulnerability table for all countries and regions are established.

### 2.1.2 Seismic Intensity Map

Peak ground acceleration (PGA) (Appendix III, Hazards data 4.1) is widely used to earthquake disaster risk assessment and mapping. Its probability of exceedance is 10 % in 50 years, i.e., once in 475 years. The PGA is converted into intensity map according to Table 3. The grid layer with seismic intensity information is vectorized and spatially overlaid with country unit map, thus the state attributes are generated. There are two kinds of resolution for the grid layer:  $0.1^\circ \times 0.1^\circ$  for economic-social wealth (ESW) loss risk assessment and  $0.5^\circ \times 0.5^\circ$  for mortality risk assessment.

### 2.1.3 Mortality Risk

In combination with intensity vector layer with national information and population vulnerability table of each country, and based on intensity information of each vector block patch ( $0.5^\circ \times 0.5^\circ$ ), mortality risk is calculated according to Eq. (2), corresponding to earthquake mortality probability of urban and rural areas of each country under the intensity in vulnerability table.

$$FR_j = \sum FR_{jUrban} \times UR_j + \sum FR_{jRural} \times (1 - UR_j) \quad (2)$$

where  $FR_j$  refers to the mortality of vector block in country  $j$ ;  $FR_{jUrban}$  refers to the mortality probability in urban area of country  $j$ ;  $FR_{jRural}$  refers to the mortality probability in the

**Table 3** Transformation of PGA and intensity ( $g = 9.81 \text{ m/s}^2$ )

Intensity	PGA (g)	PGA ( $\text{m/s}^2$ )
<VI	<0.05	<0.491
VI	0.05–0.1	0.491–0.981
VII	0.1–0.2	0.981–1.962
VIII	0.2–0.4	1.962–3.924
≥IX	≥0.4	≥3.924

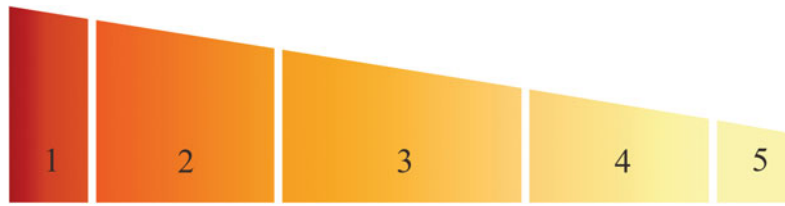


**Fig. 2** Expected annual earthquake mortality risk of the world. 1 (0, 10 %] India, Indonesia, Pakistan, Bangladesh, China, Philippines, Burma, Iran, Afghanistan, Uzbekistan, Nepal, and Ethiopia. 2 (10, 35 %] Egypt, Guatemala, Turkey, Kyrgyzstan, Tanzania, Japan, Syria, Bolivia, Tajikistan, Kenya, Mexico, Congo (Democratic Republic of the), Honduras, Uganda, Peru, Chile, Gaza Strip, Georgia, Vietnam, Ecuador, Papua New Guinea, Colombia, Malawi, Nicaragua, United States, Burundi, Algeria, and Moldova. 3 (35, 65 %] Venezuela, Rwanda, Bhutan, Haiti, Kazakhstan, Russia, Laos, El Salvador, Iraq, Azerbaijan, Romania, Costa Rica, Morocco, Turkmenistan, Mozambique, Jordan, Mongolia, Dominican Republic, Albania, Italy,

Armenia, Tunisia, Bosnia and Herzegovina, Eritrea, Lebanon, Serbia, Libya, Argentina, Canada, Ukraine, Djibouti, Greece, Cuba, Croatia, and Sudan. 4 (65, 90 %] Somalia, Jamaica, Panama, Gabon, Spain, Zambia, New Zealand, Israel, Germany, United Arab Emirates, Bulgaria, Thailand, Oman, Australia, Switzerland, Austria, Portugal, Macedonia, Palestine, France, Slovenia, Solomon Islands, Iceland, Belgium, Trinidad and Tobago, Congo, Montenegro, Czech Republic, and Slovakia. 5 (90, 100 %] Fiji, Brazil, Cameroon, Cyprus, Central African Republic, Kuwait, Saudi Arabia, Paraguay, Norway, New Caledonia, and Sweden

rural area of country  $j$ ;  $UR_j$  represents the urbanization rate of country  $j$  in 2010 from the World Bank.

By converting mortality to raster and overlaying it with world population density map (Appendix III, Exposures data 3.1), the map of mortality risk of the world by earthquake in  $0.5^\circ \times 0.5^\circ$  grid could be generated.

## 2.2 Economic-social Wealth (ESW) Loss Risk

### 2.2.1 ESW Loss Rate

This study calculates the economic-social wealth loss rate (Appendix III, Exposures data 3.8) using empirical relation between earthquake intensity and economic-social wealth loss. The empirical relation is provided by Munich Reinsurance Company, as shown in Eq. (3) (Badalet al. 2005):

$$\log f(I) = k_0 + k_1 I + k_2 I^2 + k_3 I^3 \quad (3)$$

where  $I$  represents the intensity value larger than  $V$ ,  $k_0$ ,  $k_1$ ,  $k_2$ , and  $k_3$  are empirical parameters, with two sets of numerical values. When  $k_0 = -10.28677$ ,  $k_1 = 2.83516$ ,  $k_2 = -0.24213$ , and  $k_3 = 0.00793$ , the maximum social wealth loss rate can be calculated. While  $k_0 = -11.29522$ ,  $k_1 = 2.72825$ ,  $k_2 = -0.20344$ , and  $k_3 = 0.00581$ , the minimum social wealth loss rate can be calculated. The two sets of parameters could describe the inherent uncertainty of

social wealth loss caused by different building structures and define the possible range of social wealth loss rate caused by earthquake. This study calculates the social wealth loss rate based on the average of the maximum and minimum values.

### 2.2.2 ESW Loss Risk

ESW loss value of each grid of the world is calculated by a combination of world social wealth data, the loss rate of each grid and earthquake intensity.

## 3 Results

### 3.1 Mortality Risk

The world earthquake mortality risk map in  $0.5^\circ \times 0.5^\circ$  grid is produced based on spatial analysis, using the world PGA data, building vulnerability data, mortality probability data caused by building collapse, and population density data. The spatial pattern of world earthquake mortality risk is similar to that of tectonic fault zone; however, the pattern is affected by the exposure.

The expected annual mortality risk of earthquake of the world at national level is derived and ranked (Fig. 2) by adding mortality risks of all grids confined by country boundary and then dividing the sum by the return period (475 years).

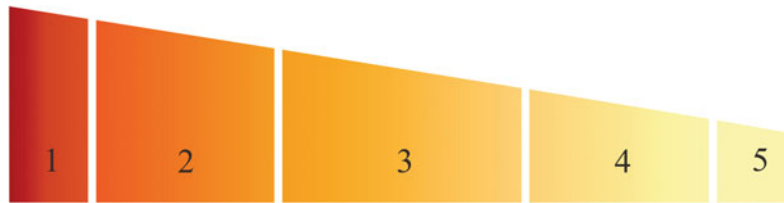


**Fig. 3** Expected annual ESW loss risk of earthquake of the world. 1 (0, 10 %) Japan, United States, China, Turkey, Italy, Mexico, Chile, Canada, Indonesia, Venezuela, Iran, Philippines, Colombia, Greece, Peru, India, Puerto Rico, Germany, and United Arab Emirates. 2 (10, 35 %) New Zealand, Russia, Spain, Pakistan, Israel, Australia, Kazakhstan, Costa Rica, United Kingdom, Romania, Guatemala, Switzerland, Uzbekistan, Ecuador, Azerbaijan, Belgium, Egypt, Croatia, Malaysia, El Salvador, Oman, Bulgaria, Gaza Strip, Thailand, Syria, Trinidad and Tobago, Hungary, Afghanistan, the Netherlands, Algeria, Brazil, Slovakia, Serbia, Saudi Arabia, Kuwait, Lebanon, Cyprus, Nepal, and Panama. 3 (35, 65 %) Bolivia, Kyrgyzstan, Slovenia, Poland, Tajikistan, Georgia, Honduras, Singapore, Iceland, Jordan, Norway, Czech Republic, Jamaica, Bosnia and Herzegovina, South Africa, Nicaragua, Tunisia, South Korea, Turkmenistan, Libya, Papua New Guinea, Albania, Armenia, Ukraine, Morocco, Kenya, Macedonia, Sweden, Montenegro, Nigeria, Vietnam, Ethiopia,

Luxembourg, Yemen, Denmark, Ireland, Uganda, Moldova, Tanzania, Liechtenstein, San Marino, Finland, Antigua and Barbuda, Haiti, Laos, Mongolia, Andorra, Ghana, Rwanda, Angola, Gabon, Congo (Democratic Republic of the), Fiji, Baker Island, Bhutan, and Malawi. 4 (65, 90 %) Cameroon, Malta, South Sudan, Zambia, Grenada, Solomon Islands, North Korea, Mozambique, Djibouti, Palestine, Qatar, Sudan, Belize, Eritrea, Dominica, Lithuania, Uruguay, Samoa, Burundi, Swaziland, Bahrain, Sri Lanka, Timor-Leste, Guinea, Paraguay, Belarus, The Republic of Côte d'Ivoire, Saint Lucia, Congo, Cambodia, Saint Vincent and the Grenadines, Latvia, Equatorial Guinea, Saint Kitts and Nevis, Chad, Togo, Estonia, Central African Republic, Zimbabwe, Benin, Barbados, Sierra Leone, Botswana, Namibia, Federated States of Micronesia, Tonga, Kiribati. 5 (90, 100 %) Guyana, Madagascar, Suriname, Senegal, Somalia, Niger, Lesotho, Liberia, Mauritania, Mali, Bahamas, Western Sahara, Guinea-Bissau, Palau, Comoros, Marshall Islands, Maldives, Gambia, and Niue

The top 1 % country with the highest expected annual earthquake mortality risk is India, and the 10 % countries are India, Indonesia, Pakistan, Bangladesh, China, Philippines, Burma, Iran, Afghanistan, Uzbekistan, Nepal, and Ethiopia.

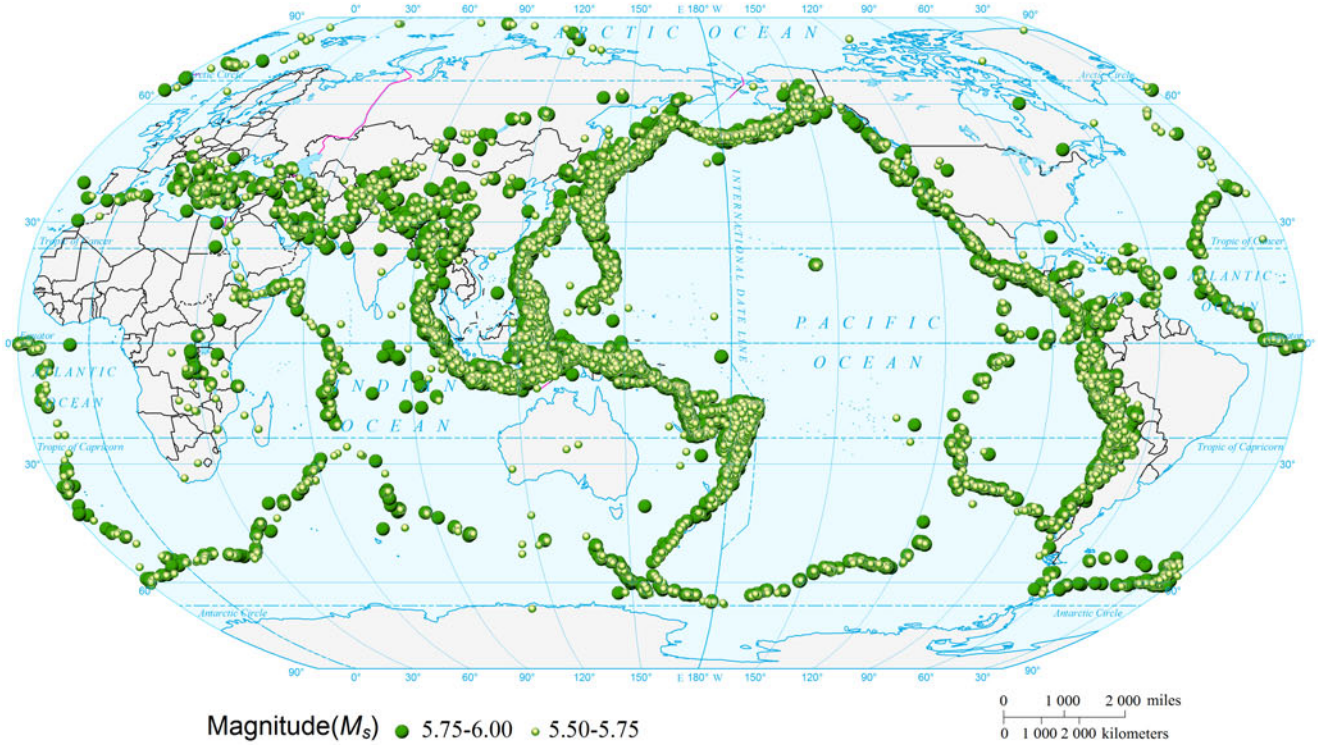
### 3.2 ESW Loss Risk

The earthquake ESW loss risk of the world in  $0.1^\circ \times 0.1^\circ$  grid is acquired based on spatial analysis. Replacing GDP with the calculated world social wealth data as the exposure of economic and combining global PGA data and the calculated social wealth loss rate, ESW loss risk is assessed. The spatial pattern of world ESW loss risk is similar to that of tectonic fault zone; however, the pattern is also affected by the exposure.

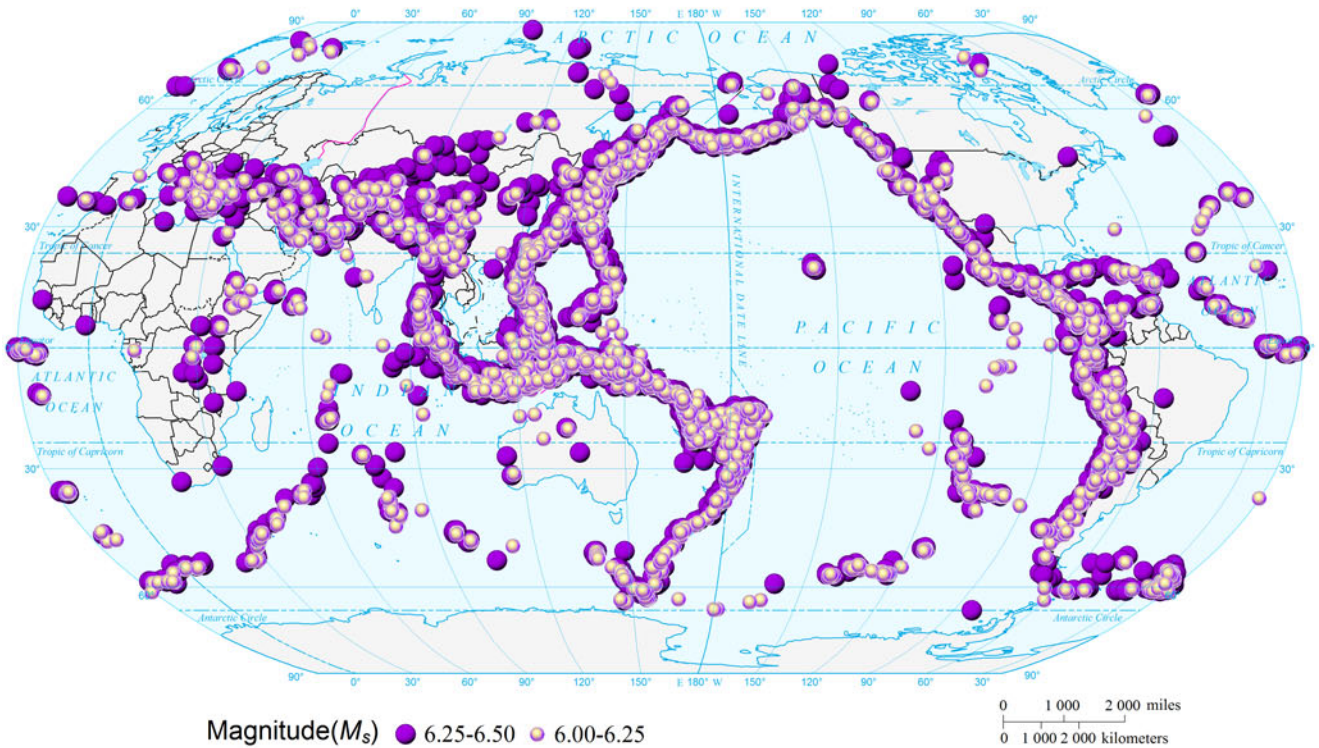
By zonal statistics of the expected risk result, the world expected annual ESW loss risk of earthquake of the world at national level is derived and ranked (Fig. 3) by adding ESW loss risks of all grids confined by country boundary and then dividing the sum by the recurrence interval (475 years). The top 1 % countries with the highest expected annual ESW risk of earthquake are Japan and United States, and the 10 % countries are Japan, United States, China, Turkey, Italy, Mexico, Chile, Canada, Indonesia, Venezuela, Iran, Philippines, Colombia, Greece, Peru, India, Puerto Rico, Germany and United Arab Emirates.

## 4 Maps

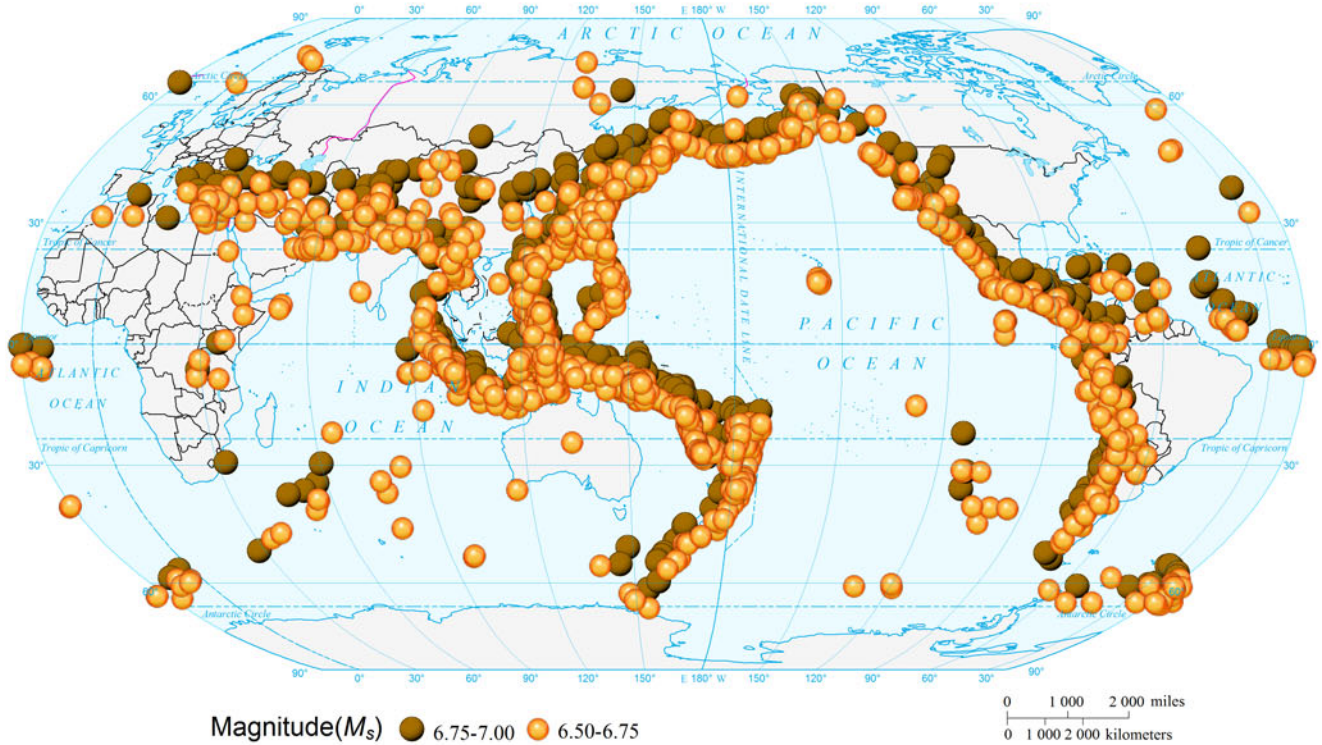
### Historical Event Locations of Global Earthquake (1900-2009, $5.50 \leq M_s < 6.00$ )



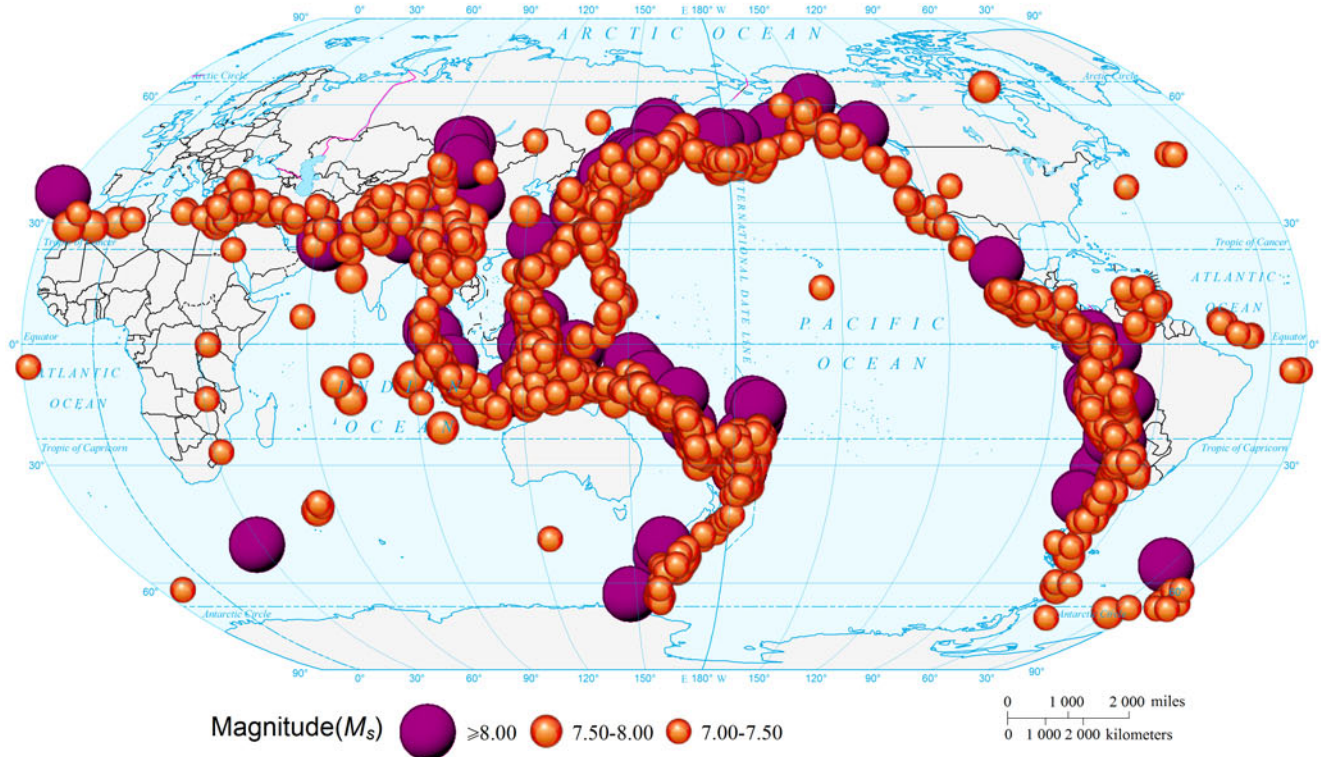
### Historical Event Locations of Global Earthquake (1900-2009, $6.00 \leq M_s < 6.50$ )



### Historical Event Locations of Global Earthquake (1900-2009, $6.50 \leq M_s < 7.00$ )

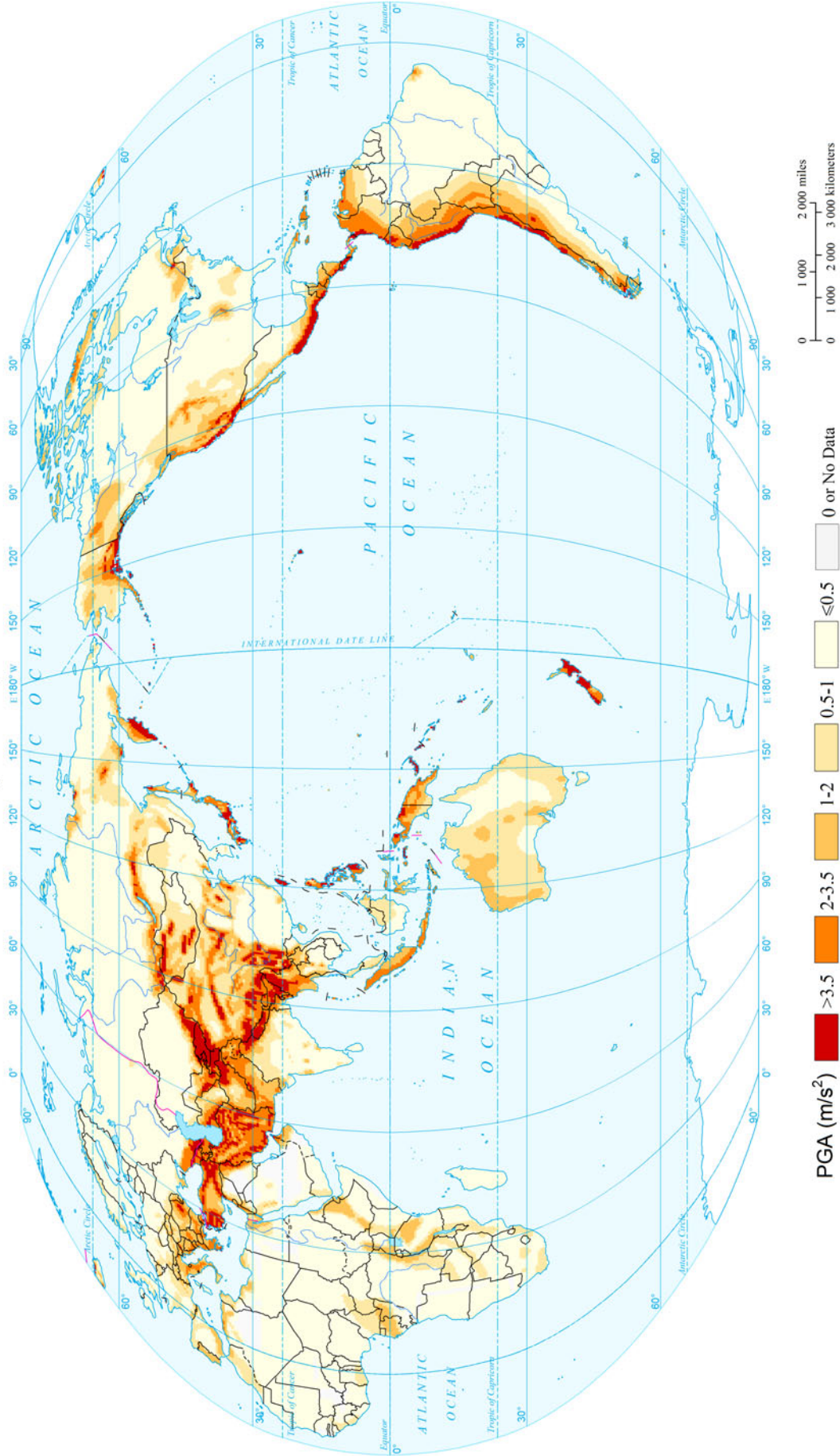


### Historical Event Locations of Global Earthquake (1900-2009, $M_s \geq 7.00$ )



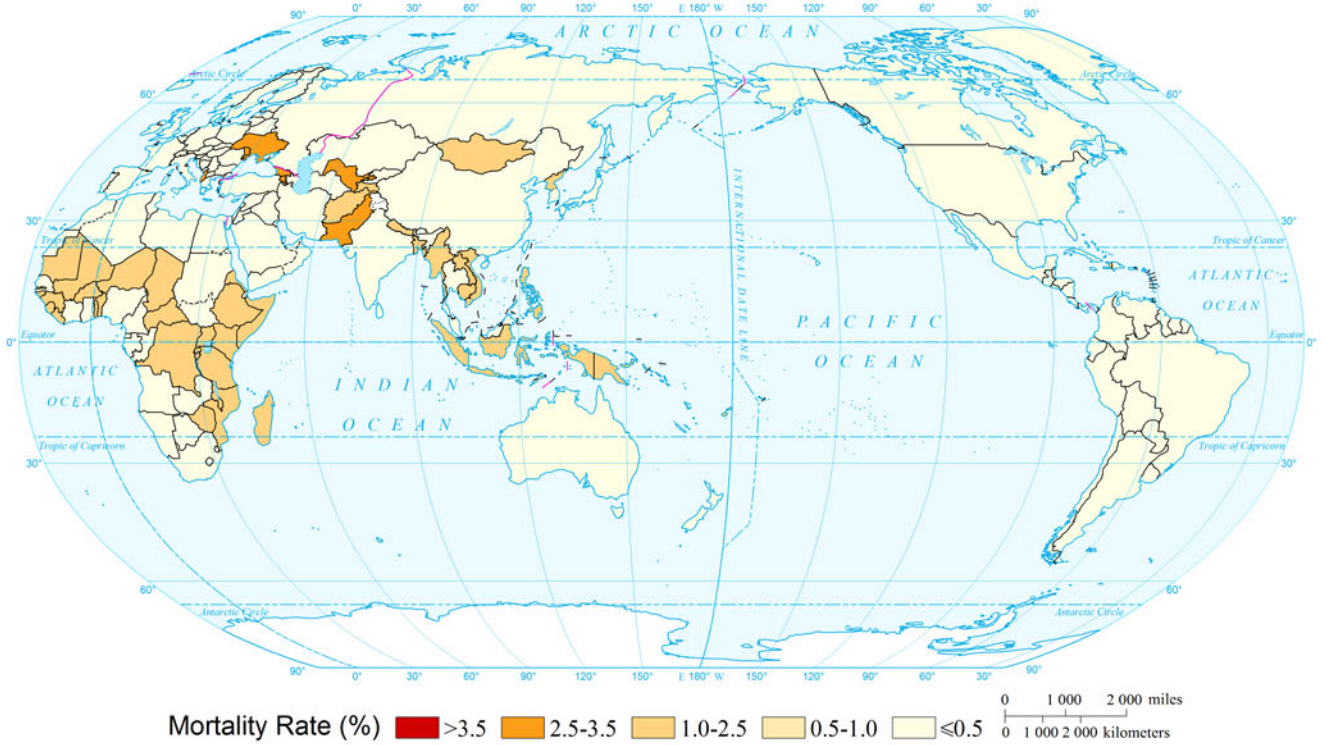


### Global Peak Ground Acceleration (PGA) ( $0.5^\circ \times 0.5^\circ$ )

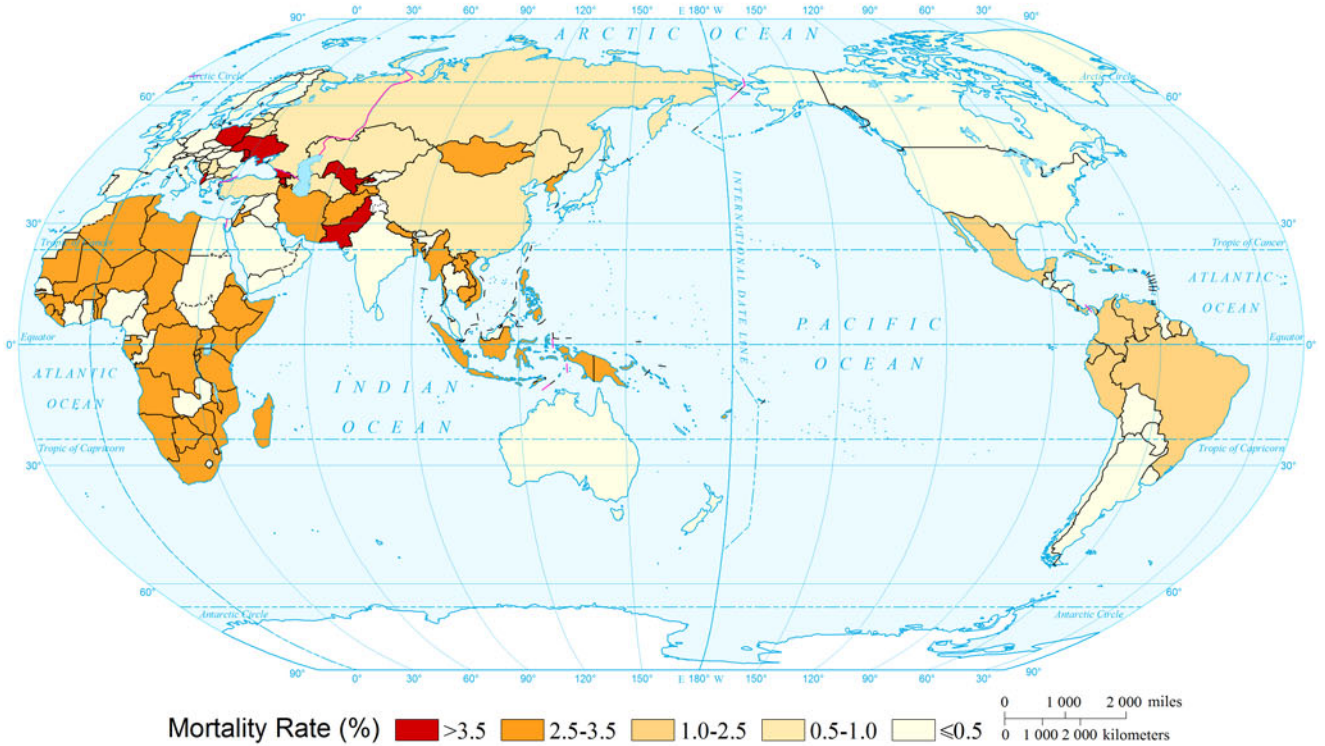


Data Source: Global Seismic Hazard Assessment Program (GSHAP) <http://www.seismo.ethz.ch/static/GSHAP/>

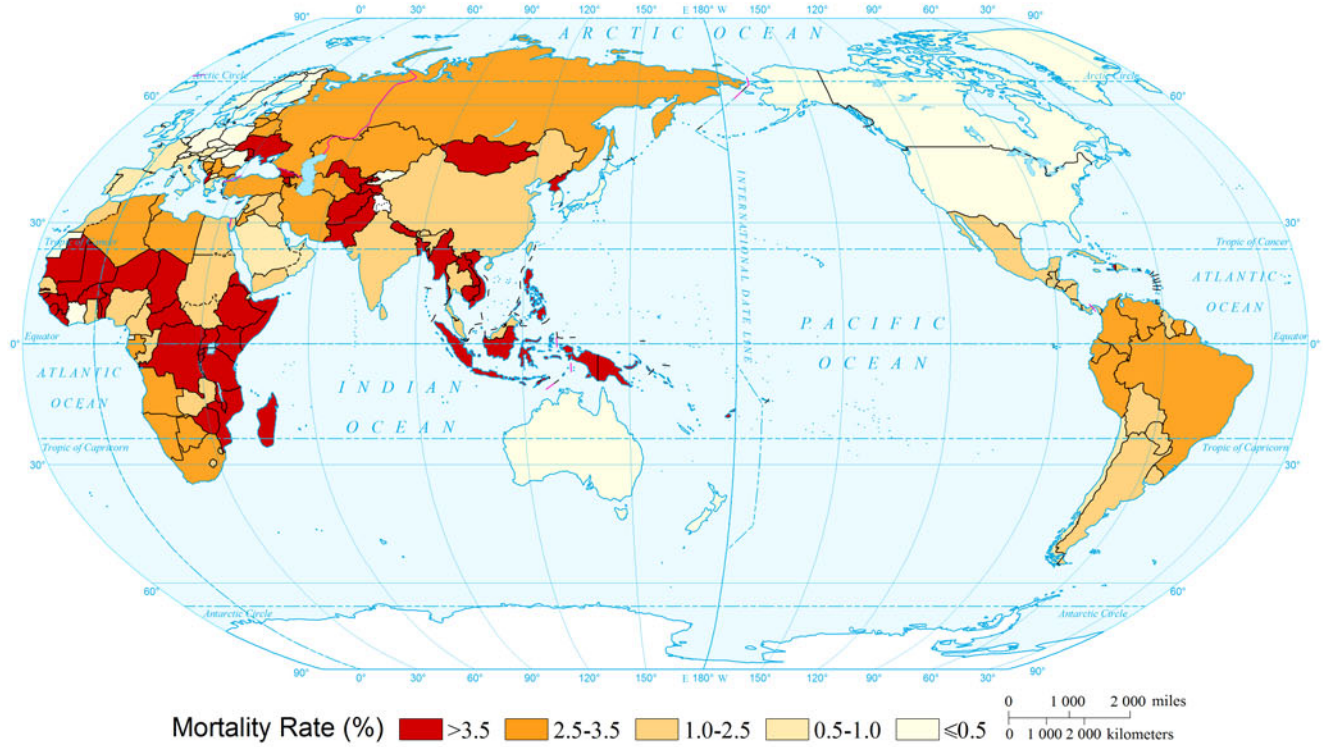
### Mortality Rate of Earthquake Disaster (Intensity =VI) of the World



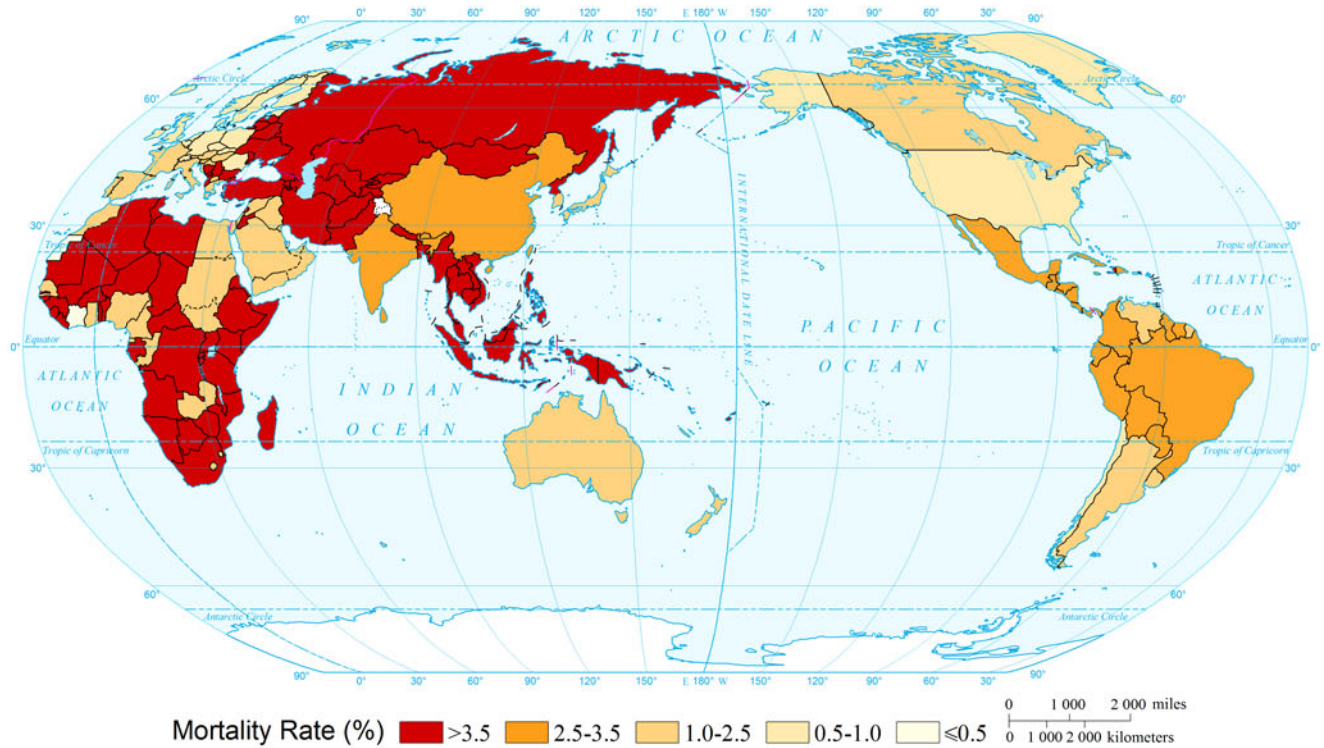
### Mortality Rate of Earthquake Disaster (Intensity =VII) of the World



### Mortality Rate of Earthquake Disaster (Intensity=VIII) of the World



### Mortality Rate of Earthquake Disaster (Intensity≥IX) of the World

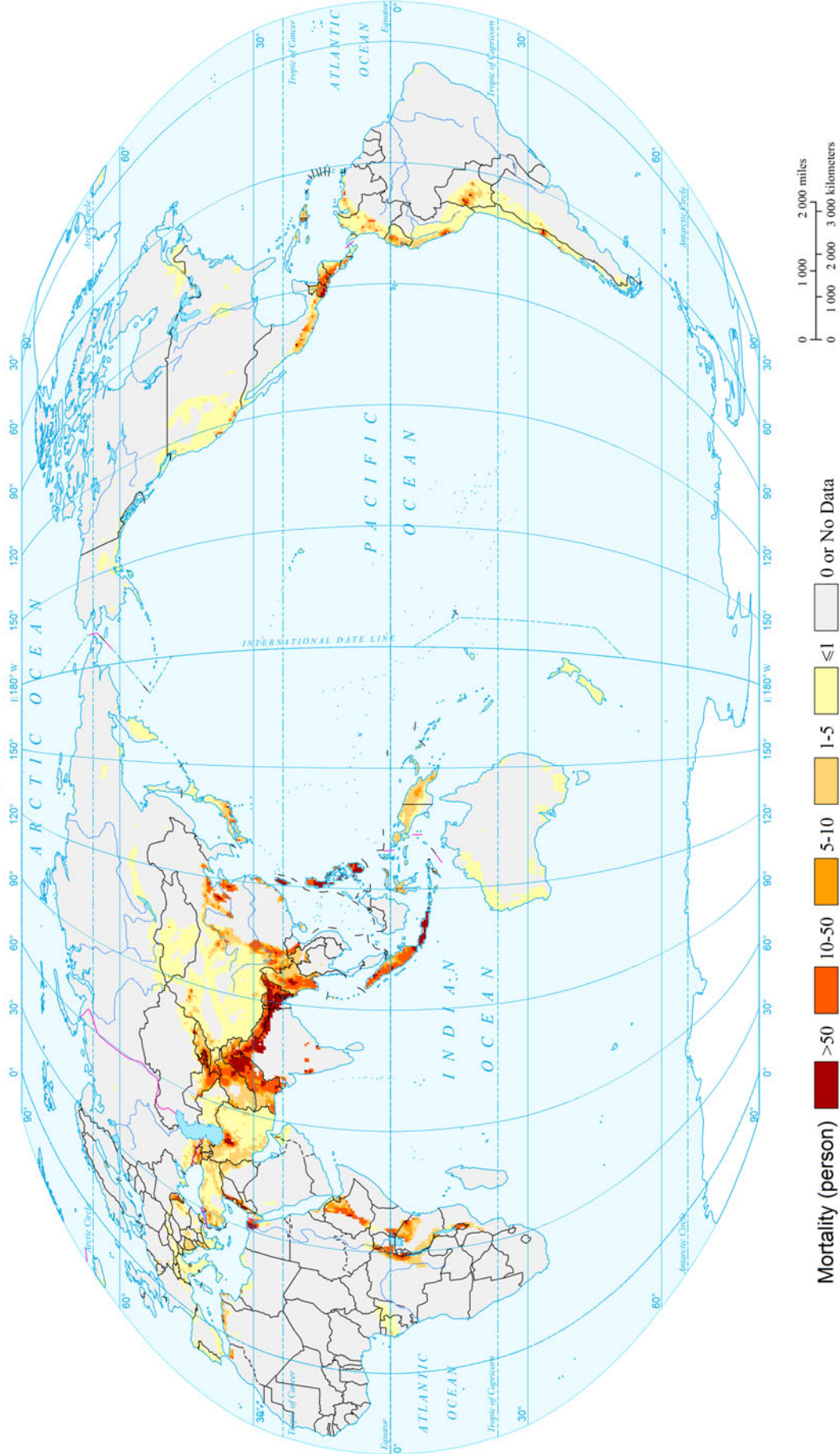




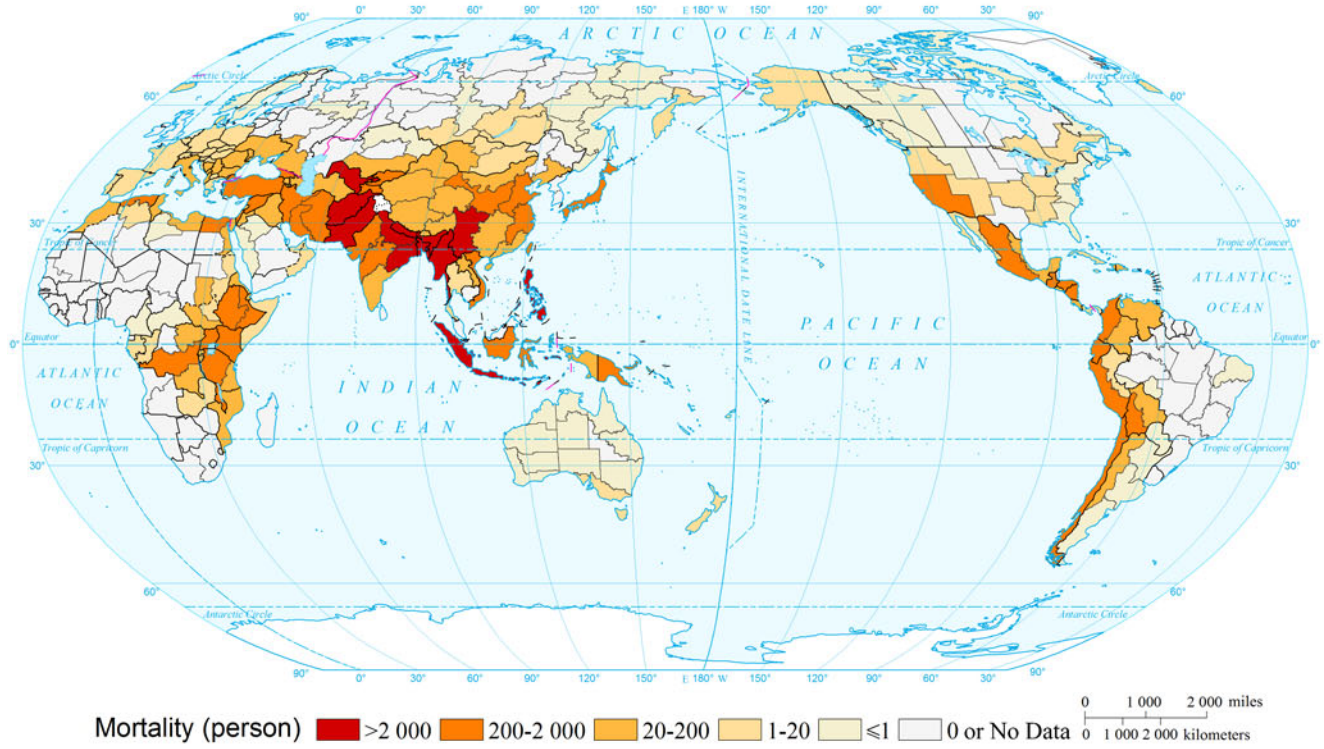
Earthquake

Earthquake, Volcano and Landslide Disasters

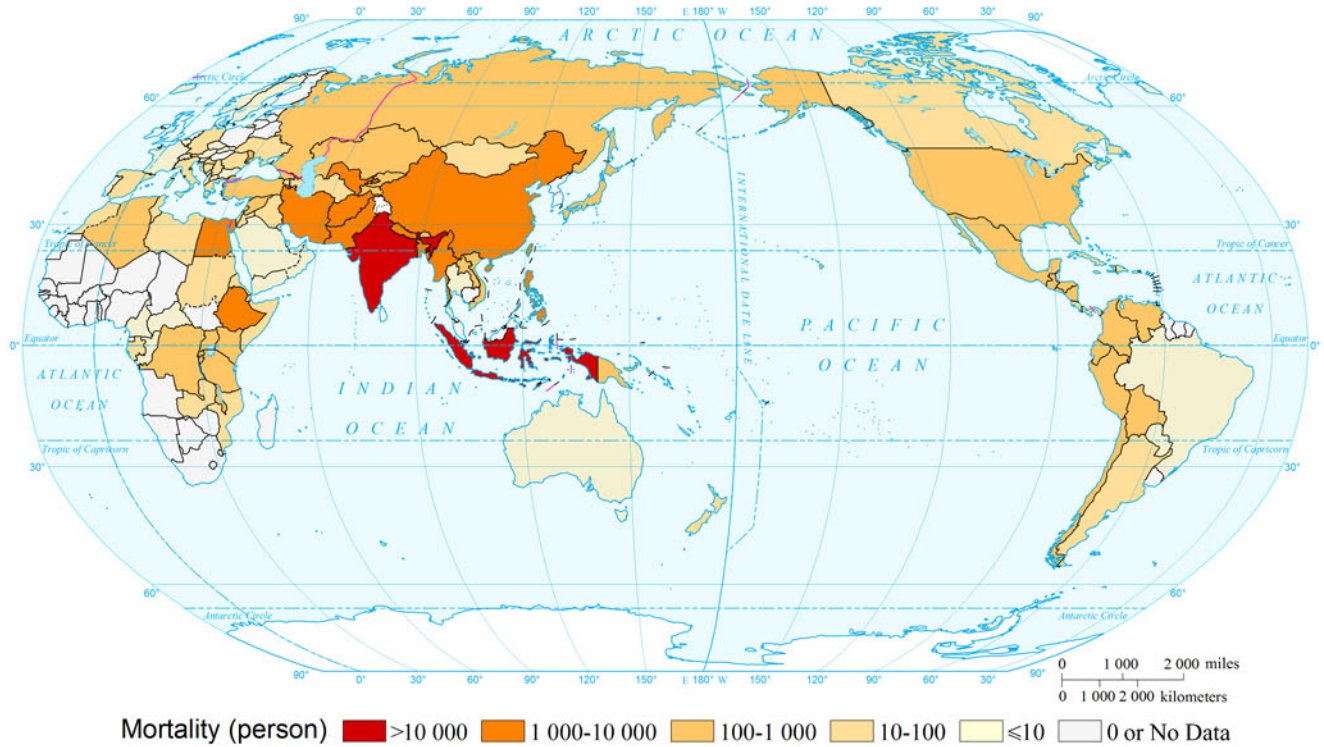
### Expected Annual Mortality Risk of Earthquake of the World (0.5° x 0.5°)



### Expected Annual Mortality Risk of Earthquake of the World (Comparable-geographic Unit)



### Expected Annual Mortality Risk of Earthquake of the World (Country and Region Unit)

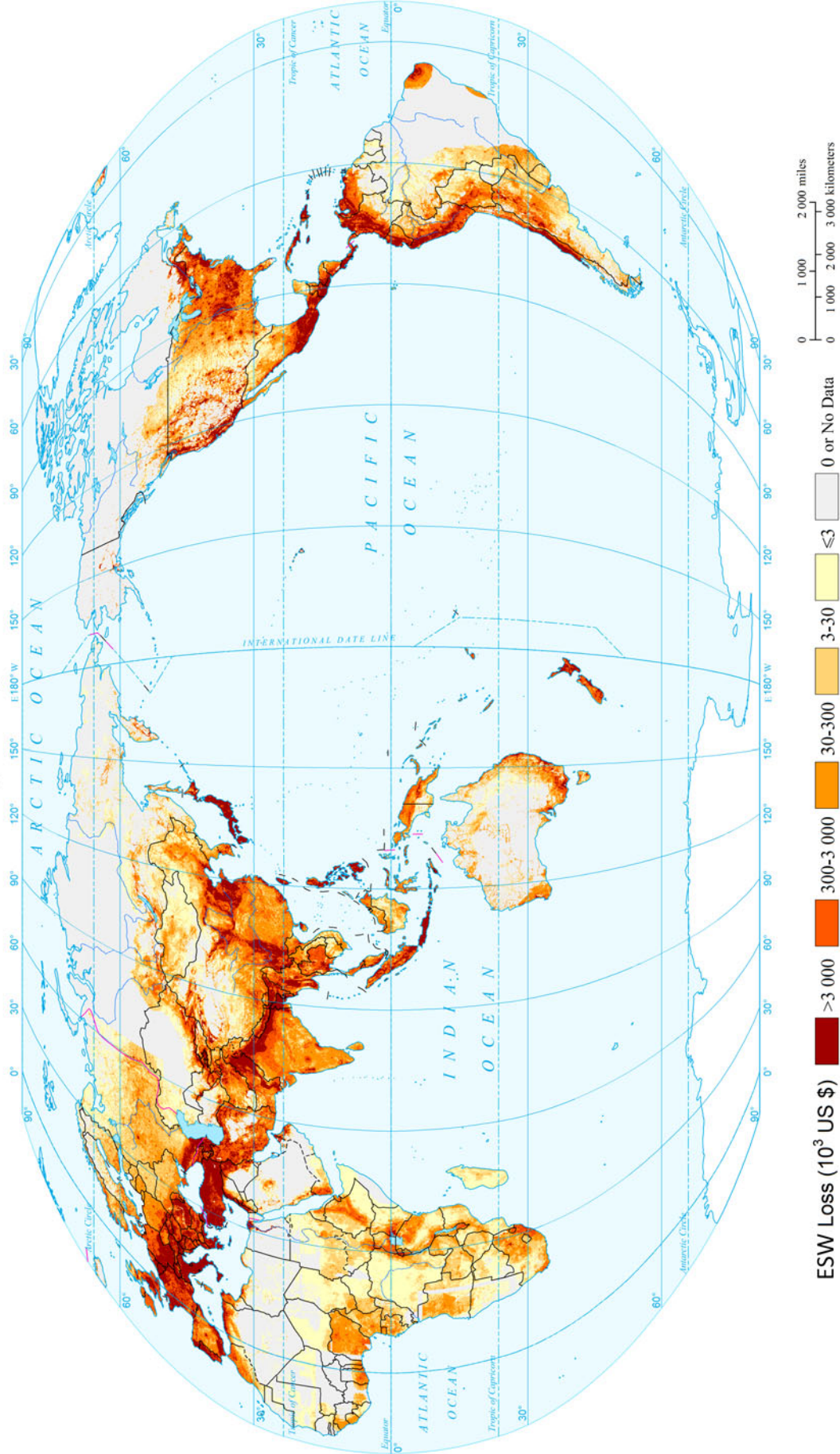




Earthquake

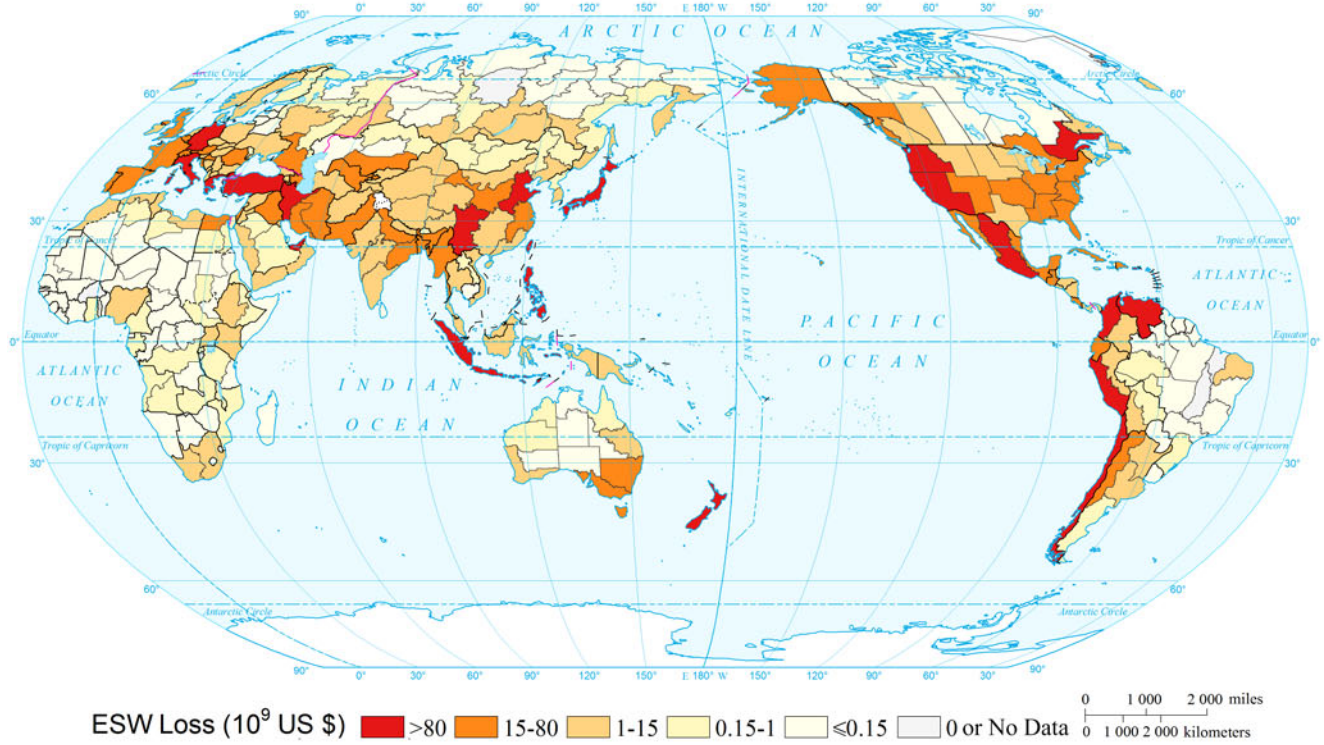
Earthquake, Volcano and Landslide Disasters

### Expected Annual Economic-social Wealth (ESW) Loss Risk of Earthquake of the World ( $0.1^\circ \times 0.1^\circ$ )

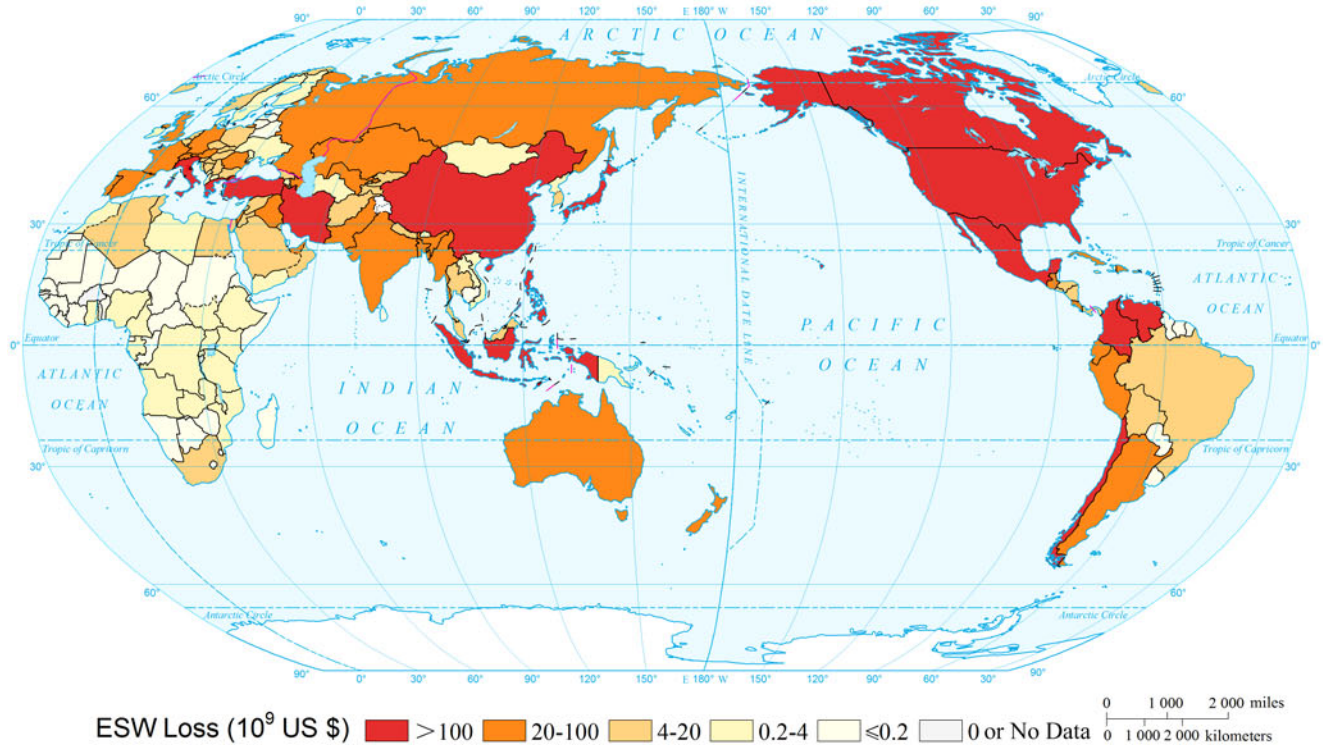


ESW Loss ( $10^3$  US \$)    >3 000    300-3 000    30-300    3-30    ≤3    0 or No Data

### Expected Annual Economic-social Wealth (ESW) Loss Risk of Earthquake of the World (Comparable-geographic Unit)



### Expected Annual Economic-social Wealth (ESW) Loss Risk of Earthquake of the World (Country and Region Unit)



## References

- Badal, J., M. Vazquez-Prada, and A. Gonzalez. 2005. Preliminary quantitative assessment of earthquake casualties and damages. *Natural Hazards* 34(3): 353–374.
- Dilley, M., U. Deichmann, and R.S. Chen. 2005. *Natural disaster hotspots: A global risk analysis*. Washington DC: World Bank Publications.
- Jaiswal, K.S., D.J. Wald, P.S. Earle, et al. 2009. Earthquake casualty models within the USGS prompt assessment of global earthquakes for response (Pager) system. In *Proceedings of the 2nd international workshop on disaster casualties*, 15–16 June, University of Cambridge, Cambridge, UK.
- Peduzzi, P., H. Dao, C. Herold, et al. 2009. Assessing global exposure and vulnerability towards natural hazards: The disaster risk index. *Natural Hazards and Earth System Sciences* 9(4): 1149–1159.
- United Nations Development Programme (UNDP). 2010. *Human development report 2010—The real wealth of nations: Pathways to human development*. New York: Palgrave Macmillan.

---

# Mapping Volcano Risk of the World

Hongmei Pan and Peijun Shi

---

## 1 Background

Previous volcanic hazard assessment has typically explored the hazard or risk from a single volcano (Pomonis et al. 1999; Thouret et al. 2000) or to a particular site (Hoblitt et al. 1995; Magill and Blong 2005). Volcanic risk analysis at the global scale is limited by the availability and quality of data. Existing data can only support semi-quantitative risk assessment and derive relative risk level. The first global volcanic mortality risk map was developed by the World Bank ‘Natural Disaster Hotspots’ program (Dilley et al. 2005). It applied an empirical method to depict global volcanic hazard and vulnerability using the historical volcano record from EM-DAT (1981–2000) and then integrated these two parts to rank the risk level. It assessed the risks of mortality and economic losses, with a spatial resolution of  $2.5' \times 2.5'$ .

Compared to the Natural Disaster Hotspots results, the present study considers both frequency and intensity of historical volcanic eruption events. It also uses longer series of volcano mortality data since 1700s, a certain time before which the completeness of the data decreases remarkably as suggested by an earlier study (Newhall and Self 1982).

---

**Mapping Editors:** Jing'ai Wang (Key Laboratory of Regional Geography, Beijing Normal University, Beijing 100875, China) and Chunqin Zhang (School of Geography, Beijing Normal University, Beijing 100875, China).

**Language Editor:** Tao Ye (State Key Laboratory of Earth Surface Processes and Resource Ecology, Beijing Normal University, Beijing 100875, China).

---

H. Pan

Academy of Disaster Reduction and Emergency Management,  
Ministry of Civil Affairs and Ministry of Education, Beijing  
Normal University, Beijing 100875, China

P. Shi (✉)

State Key Laboratory of Earth Surface Processes and Resource  
Ecology, Beijing Normal University, Beijing 100875, China  
e-mail: spj@bnu.edu.cn

When identifying the exposure for each historical event, buffer regions are generated instead of using administrative regions, an attempt actually suggested by Dilley et al. (2005). Therefore, this study intends to provide a more integrated risk assessment than previous studies, including a systematic analysis of hazard, exposure, vulnerability, and mortality risk. Risk assessment results are provided at comparable geographic unit and national level.

---

## 2 Method

Figure 1 shows the technical flow chart for mapping volcano risk of the world.

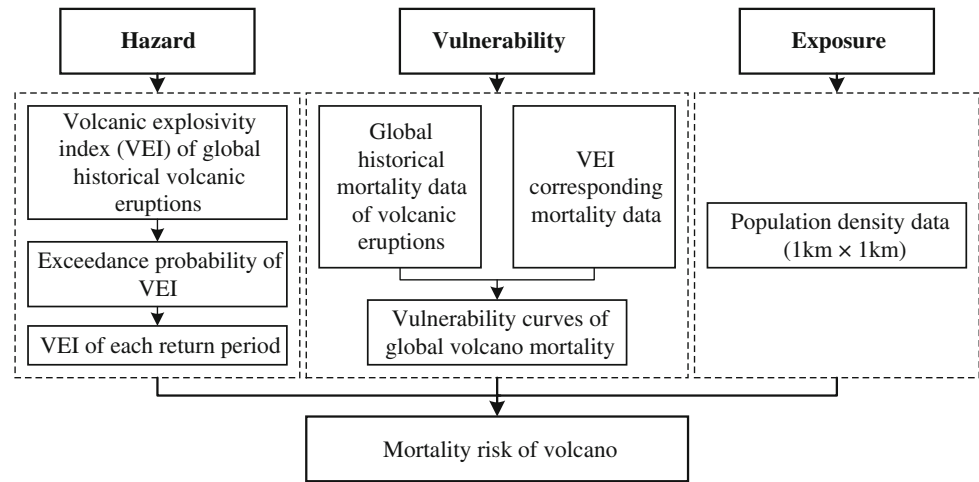
### 2.1 Intensity

The volcanic explosivity index (VEI) is a general indicator of the explosive character of an eruption (Newhall and Self 1982). It is a 0–8 index of increasing explosivity (the maximum number of categories we could realistically distinguish). Each increase in number represents an increase around a factor of ten. The VEI uses several factors to assign a number, including volume of erupted pyroclastic material (for example, ash fall, pyroclastic flows, and other ejecta), height of eruption column, duration in hours, and qualitative descriptive terms (United States Geological Survey 2014).

The historical eruptions of each volcano are derived from the Volcanoes of the World database (Appendix III, Hazards data 4.2). We assume that the eruption probability in the future is consistent with that in the past. Eruption frequency of VEI level of each volcano can be calculated by Eq. (1).

$$\lambda_{ix} = N_{ix}/T_{ix} \quad (1)$$

**Fig. 1** Technical flowchart for mapping volcano risk of the world



where  $\lambda_{ix}$  is the eruption frequency of volcano  $i$  with a VEI of  $x$ ;  $T_{ix}$  is the record time period of VEI  $x$  of  $i$  volcano, which is divided into 2 types:  $x = 0-3$  and  $x = 4-7$ . Time period is according to an earlier work on data completeness carried out by (Jenkins et al. 2012);  $N_{ix}$  is the number of eruptions within  $T_{ix}$  years.

Exceeding probability for each volcano is calculated according to the eruption frequency of each VEI level. Because the number of historical eruptions is inadequate, the method of histogram estimation is used for estimating exceeding probability (Huang 2012). Volcano intensity is represented as the corresponding VEI level of 10-year, 20-year, 50-year, and 100-year return period.

Population exposed to volcanic threats essentially decides the mortality claimed. Pyroclastic flow, lahar, and tephra are selected as volcanic threats to human lives. Influence area of pyroclastic flow of different VEI levels can be calculated according to the height of the volcanic eruption column which is directly related to jet heat flow. Volcano eruption column height is calculated with the maximum height record of large magnitude explosive volcanic eruptions (LaMEVE) database (Appendix III, Hazards data 4.3). A total of 943 maximum volcanic eruption column height records labeled as High Quality are picked from LaMEVE database, and the relationship between maximum volcanic eruption column height (MCH) and VEI is fitted as Eq. (2):

$$\text{MCH}_x = 8.5961 \text{ VEI}_x - 19.817, R^2 = 0.6456 \quad (2)$$

where  $\text{MCH}_x$  is the MCH for  $x = 3, 4, 5, 6, 7$ . It is set as 1 km when  $x < 3$  since historical records are unavailable in LaMEVE database.  $R^2$  is the measure of goodness of fit.

Influence area of pyroclastic flows is roughly calculated by the ratio of MCH and the farthest distance. The value range of the ratio is usually 0.2–0.3 (Hayashi and Self 1992; Hoblitt et al. 1995; Waythomas et al. 2003; Macías et al. 2008).

In this study, a mean value of 0.25 is used. The influence radius of lahar ( $L'$ ) is also determined by  $H/L'$ , the value range of which is 0.1–0.3 (Huggel et al. 2008), and a mean value of 0.2 is used.

The influence area of tephra is closely related to ash volume and volcanic eruption column height. A total of 1,174 tephra volume records labeled as high quality from LaMEVE database are picked out. The relationship between ash volume and VEI is fitted by Eq. (3).

$$V = \frac{10^{0.9615 \times \text{VEI}_x}}{10^{4.494}}, R^2 = 0.8899 \quad (3)$$

where  $V$  is ash volume,  $x = 3, 4, 5, 6, 7$  and set as  $0.001 \text{ km}^3$  when  $x < 3$  since historical record is unavailable in LaMEVE database.  $R^2$  is the measure of goodness of fit.

The thickness of volcano ash is computed according to Eq. (4) (Rhoades et al. 2002):

$$\log_{10} t_m = 3.13[\pm 0.14] + 0.96[\pm 0.07] \log_{10} V - 1.60[\pm 0.11] \log_{10} r \quad (4)$$

where  $t_m$  is average thickness of volcanic ash;  $V$  is ash volume;  $r$  is the radius.

A thickness of 12.5 cm of volcano ash is defined as the triggering value causing population death (Pomonis et al. 1999).

The largest radius of the influence area of pyroclastic flow, lahar, and tephra is determined as the lethal radius ( $L$ ) of each VEI.

The relationship between influence area  $L$  and VEI is fit by Eq. (5):

$$L = 3.0408e^{0.6956 \text{ VEI}}, R^2 = 0.9367 \quad (5)$$

where  $R^2$  is the measure of goodness of fit.

**Table 1** Statistics of death of each volcano VEI level

VEI	Number of data	Average mortality
0	7	15.4
1	26	45.9
2	128	194.4
3	105	429.2
4	50	1,309.8
5	6	1,001
6	4	988
7	1	10,000

## 2.2 Vulnerability

Historical volcanic disaster mortality data (Appendix III, Disasters data 5.1) are used to characterize vulnerability. Since some of the mortality data are classified by grade instead of absolute data, the median of the grade range is chosen as mortality data.

The average death of each volcano VEI level is shown in Table 1. The vulnerability curve ( $V'$ ) is fitted according to Eq. (6):

$$V' = 25.306e^{0.7942VEI}, R^2 = 0.9508 \quad (6)$$

where  $R^2$  is the measure of goodness of fit.

## 2.3 Mortality Risk

Using the world population density data as exposure (Appendix III, Exposures data 3.1), the volcanic mortality risk of each return period is calculated as Eq. (7):

$$R_{yij} = V_{yj} \times \frac{P_{ij}}{\sum_{i=1}^n P_{ij}} \quad (7)$$

where  $R_{yij}$  is the mortality risk of grid  $i$  ( $1 \text{ km} \times 1 \text{ km}$ ) of volcano  $j$  with a return period of  $y$ ;  $P_{ij}$  is the population of grid  $i$  exposed to volcano  $j$ ;  $V_{yj}$  is the vulnerability corresponding return period  $y$  of volcano  $j$ ;  $n$  is the total number of grids of volcano  $j$ .

The expected volcanic mortality is calculated as Eq. (8):

$$E(R_{yij}) = \sum_{k=0}^7 V(\text{VEI})_{kyj} \times \frac{P_{ij}}{P(\text{VEI})_{kj}} \times F(\text{VEI})_{kj} \quad (8)$$

where  $V(\text{VEI})_{kyj}$  is the vulnerability function shown in Eq. (6);  $P(\text{VEI})_{kj}$  is the total population within the influence area of volcano  $j$  with vulnerability  $k$ , and  $F(\text{VEI})_{kj}$  is the frequency of volcano  $j$  with vulnerability  $k$ .

## 3 Results

By zonal statistics of the expected risk result, the expected annual mortality risk of volcano of the world at national level is derived and ranked (Fig. 2). The top 1 % country with the highest expected annual mortality risk of volcano is Indonesia, and the top 10 % countries are Indonesia, Papua New Guinea, Japan, Philippines, Russia, and Nicaragua.

## 4 Maps

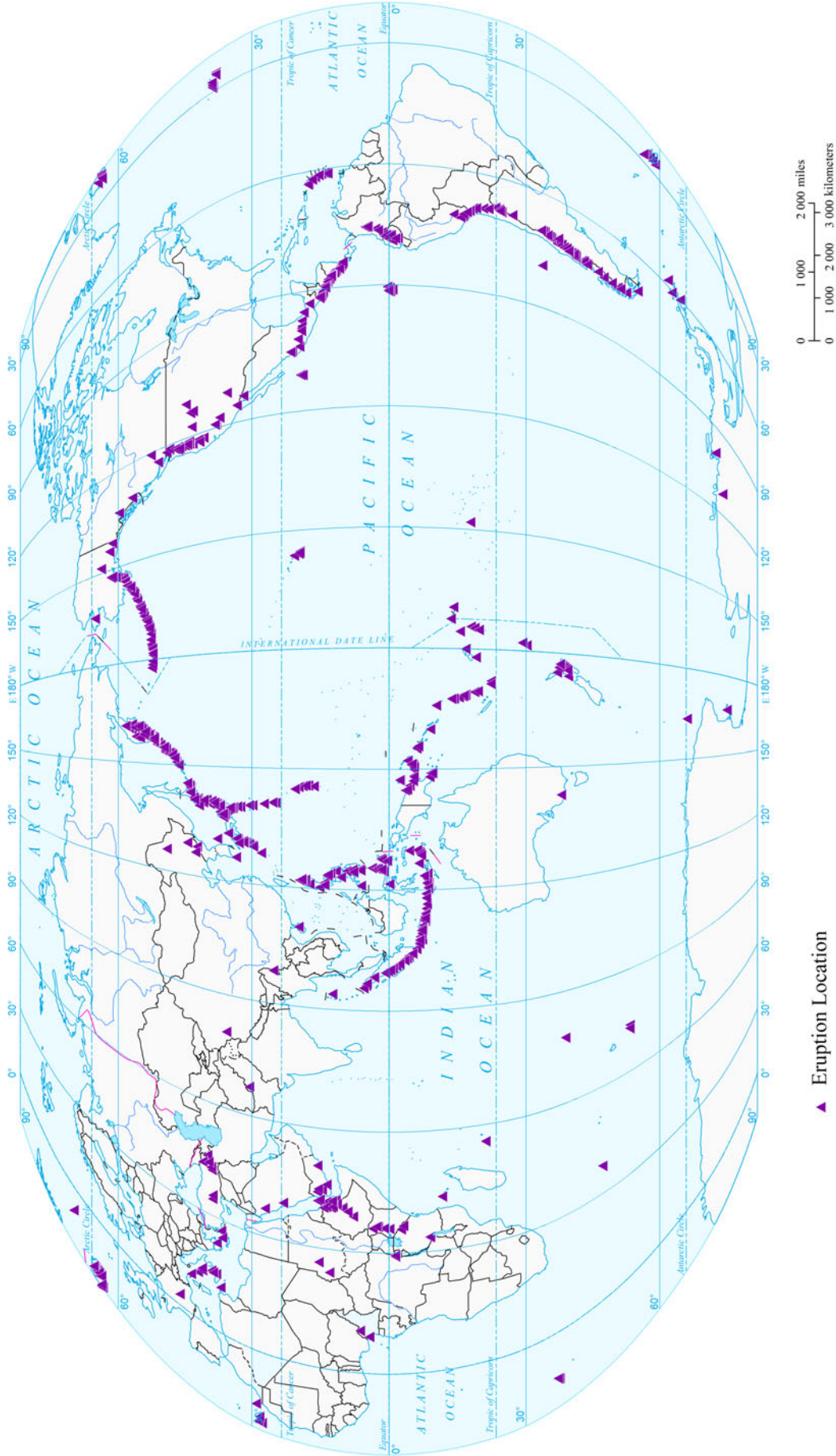


**Fig. 2** Expected annual mortality risk of volcano of the world. 1 (0, 10 %) Indonesia, Papua New Guinea, Japan, Philippines, Russia, and Nicaragua. 2 (10, 35 %) New Zealand, Chile, Ecuador, United States, Guatemala, Italy, Costa Rica, El Salvador, Palestine, Colombia, Congo (Democratic Republic of the), Mexico, Tanzania, and Iceland. 3 (35, 65 %) Peru, Ethiopia, Tonga, Cameroon, Greece, India, Portugal,

Saint Vincent and the Grenadines, Kenya, Solomon Islands, China, Spain, Turkey, Yemen, Fiji, Argentina, and Rwanda. 4 (65, 90 %) Canada, Comoros, Eritrea, Saudi Arabia, Dominica, Sudan, North Korea, South Korea, France, Djibouti, Saint Lucia, Saint Kitts and Nevis, Honduras, and Zambia. 5 (90, 100 %) Bolivia, Armenia, Australia, Pakistan, Malawi, and Iran



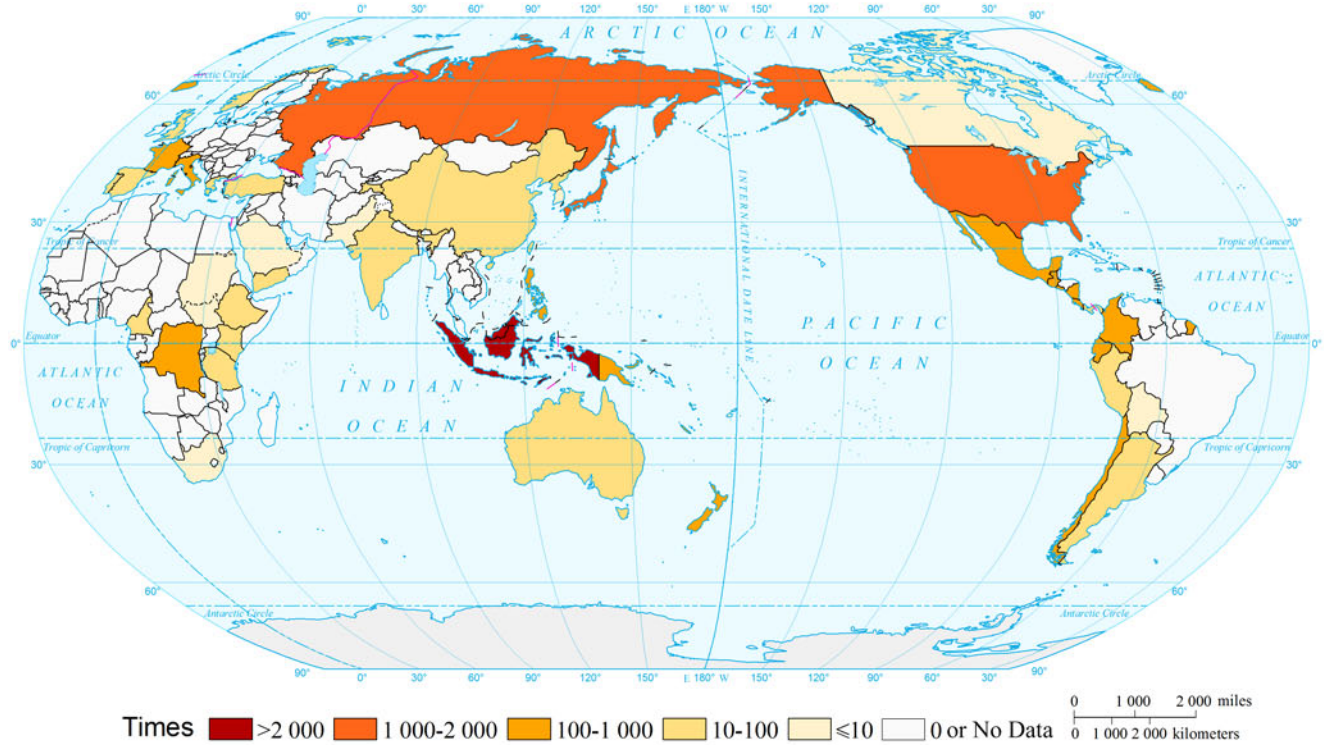
### Historical Eruption Locations of Global Volcano (4360 B.C.-2012 A.D.)



▲ Eruption Location

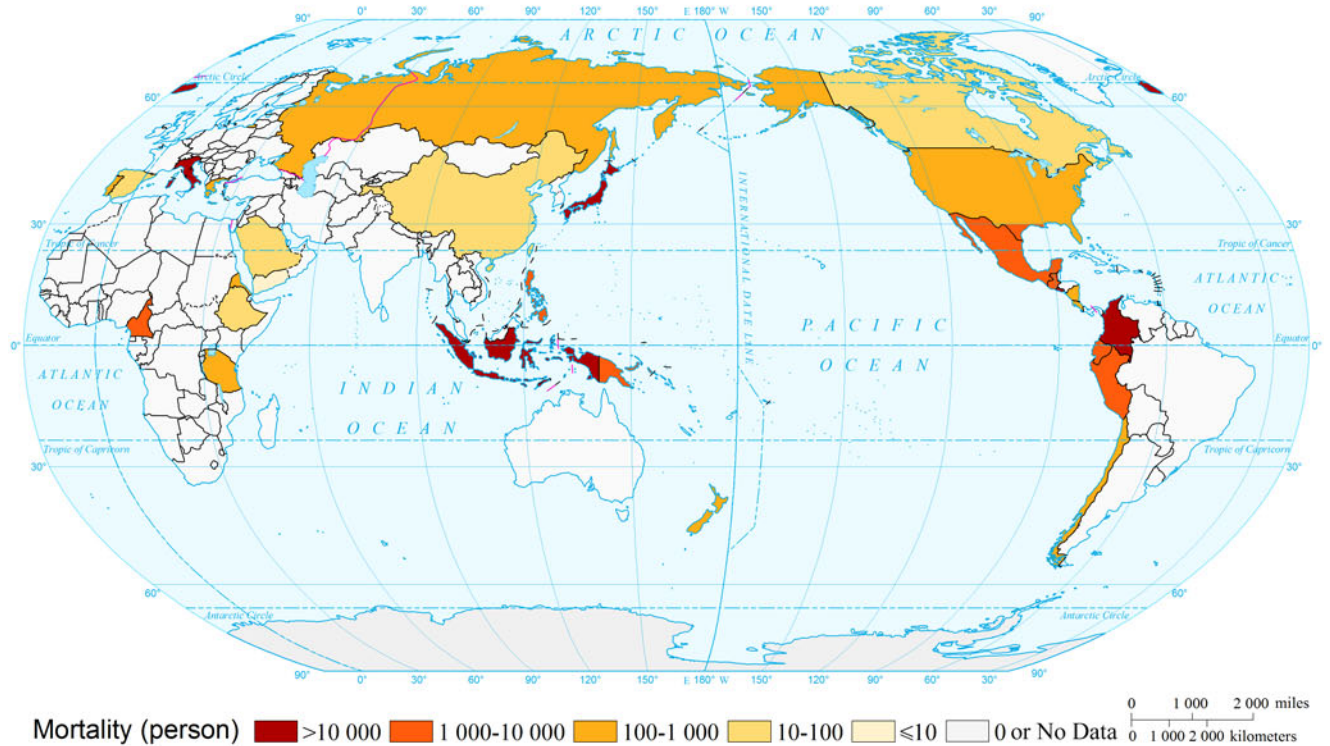
Data Source: Smithsonian Institution National Museum of Natural History (Global Volcanism Program) <http://www.volcano.si.edu>

### Historical Eruption Frequency of Global Volcano (4360 B.C.-2012 A.D.)



Data Source: NOAA <http://www.ngdc.noaa.gov/hazard/volcano.shtml>

### Historical Mortality Record of Global Volcano (1900-2009)



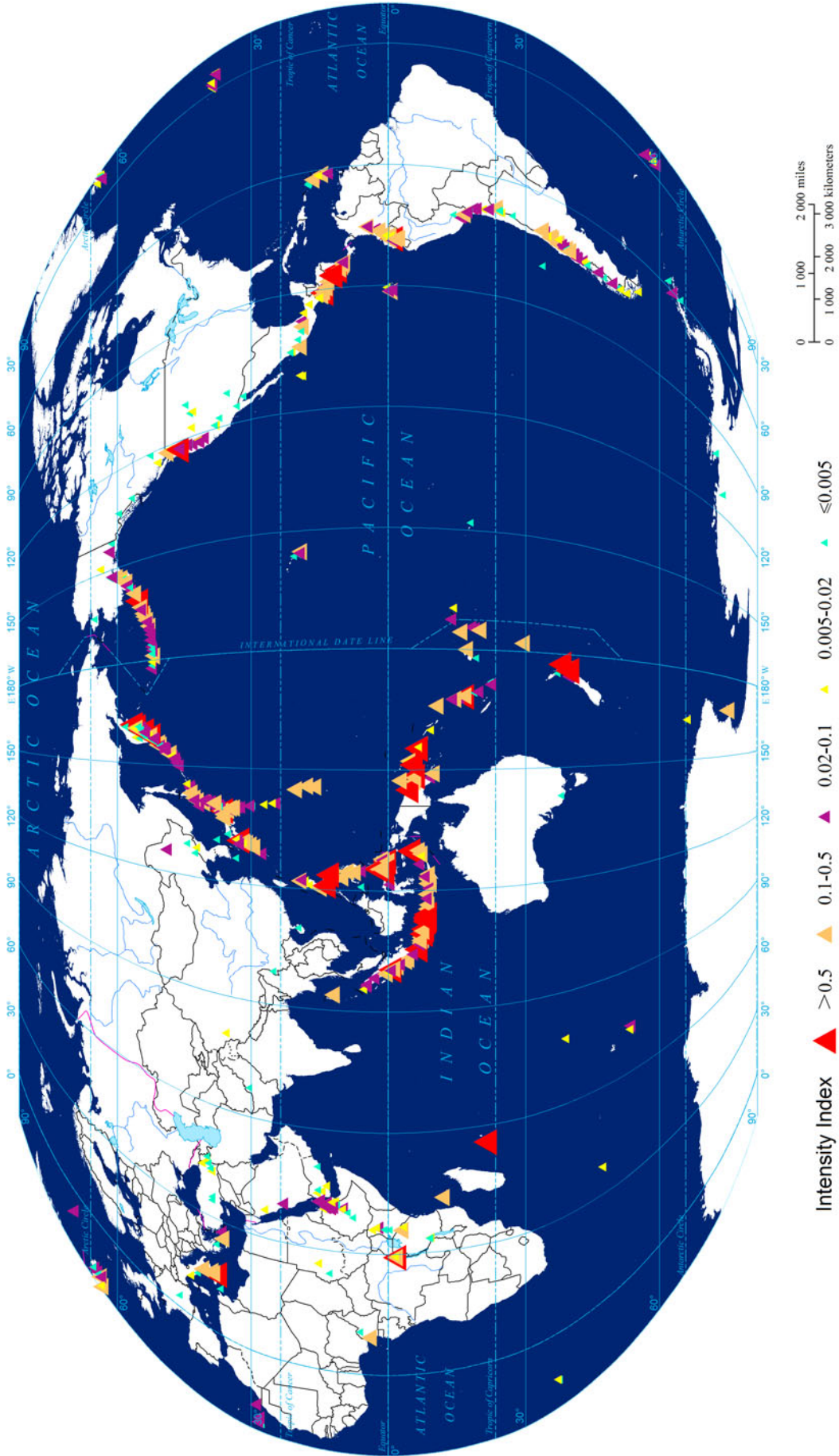
Data Source: EM-DAT <http://www.emdat.be/database>



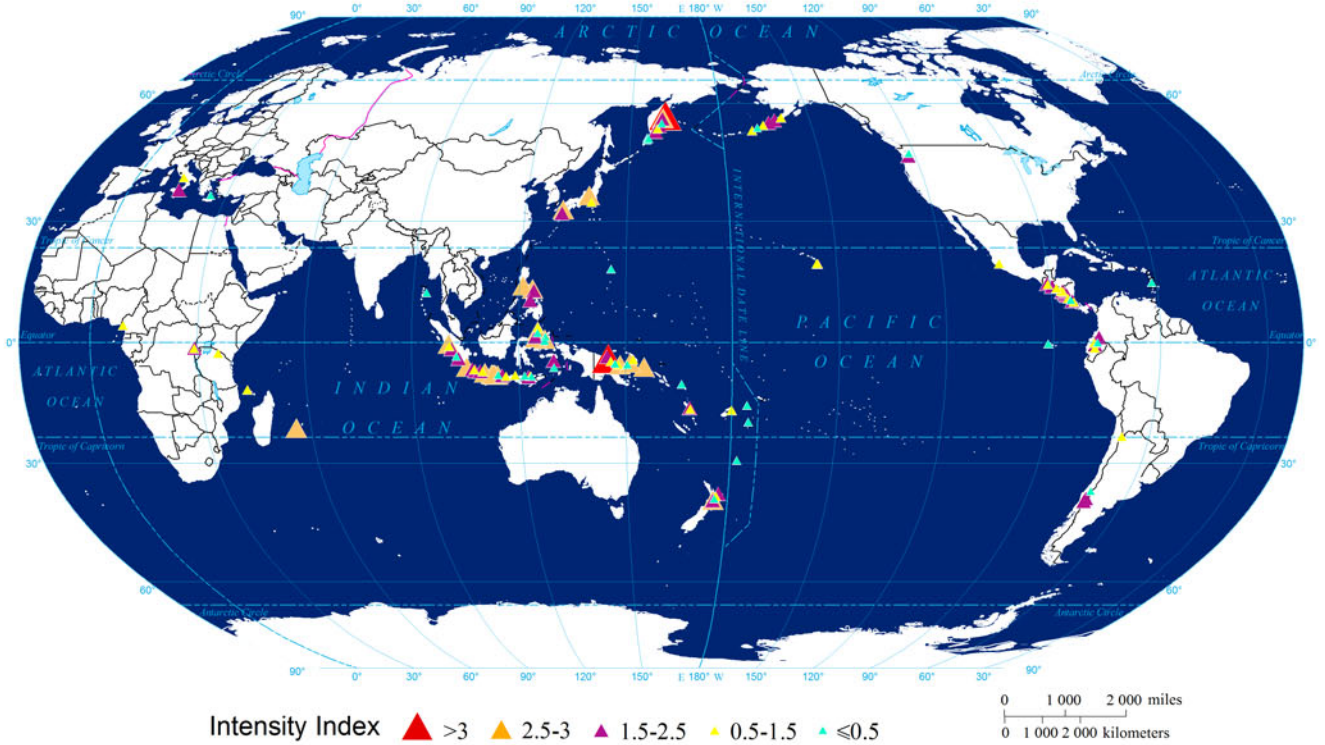
Volcano

Earthquake, Volcano and Landslide Disasters

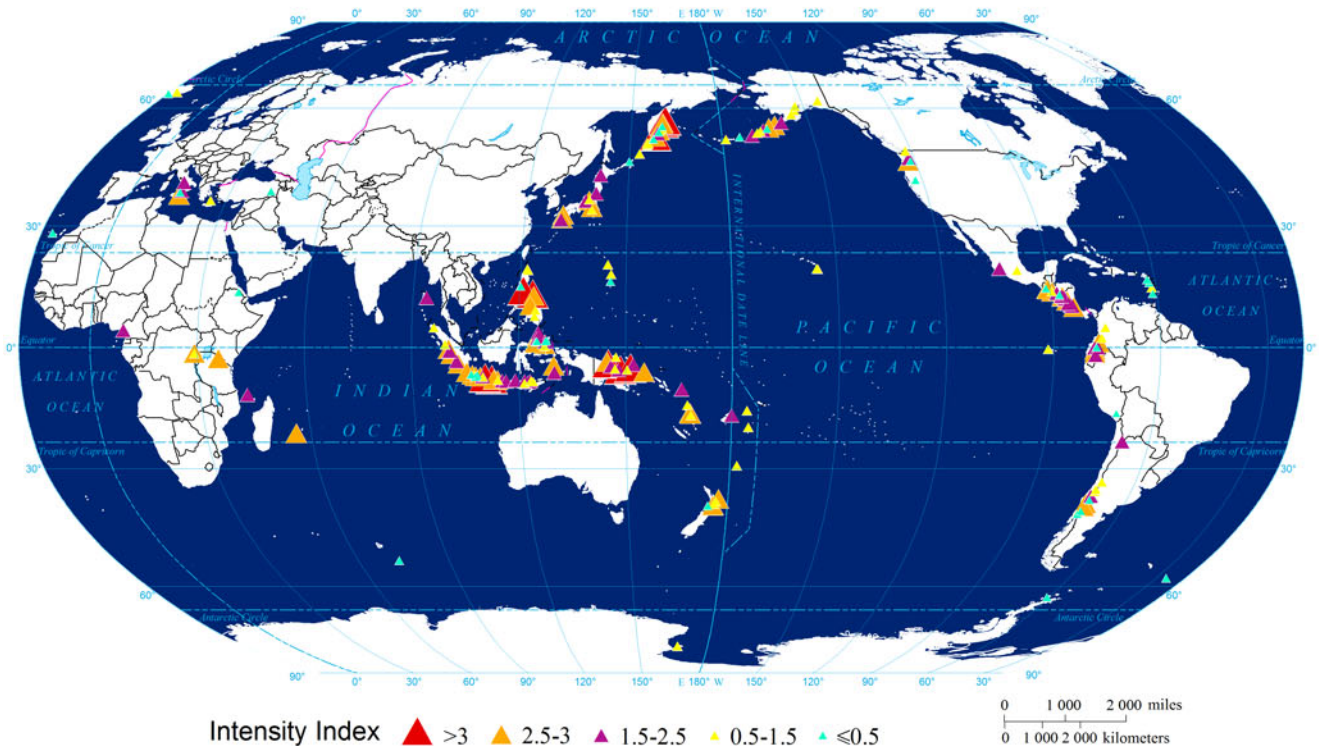
### Expected Annual Intensity of Global Volcano



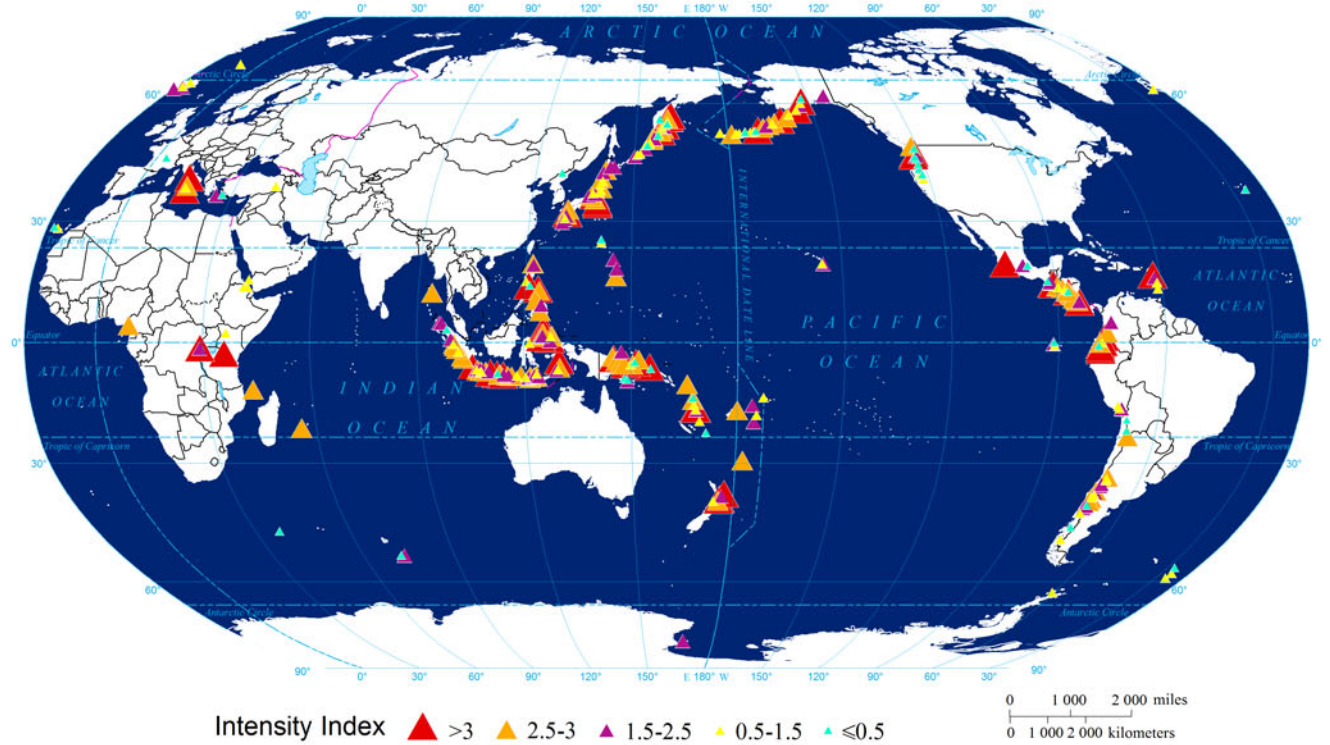
Global Volcano Intensity by Return Period (10a)



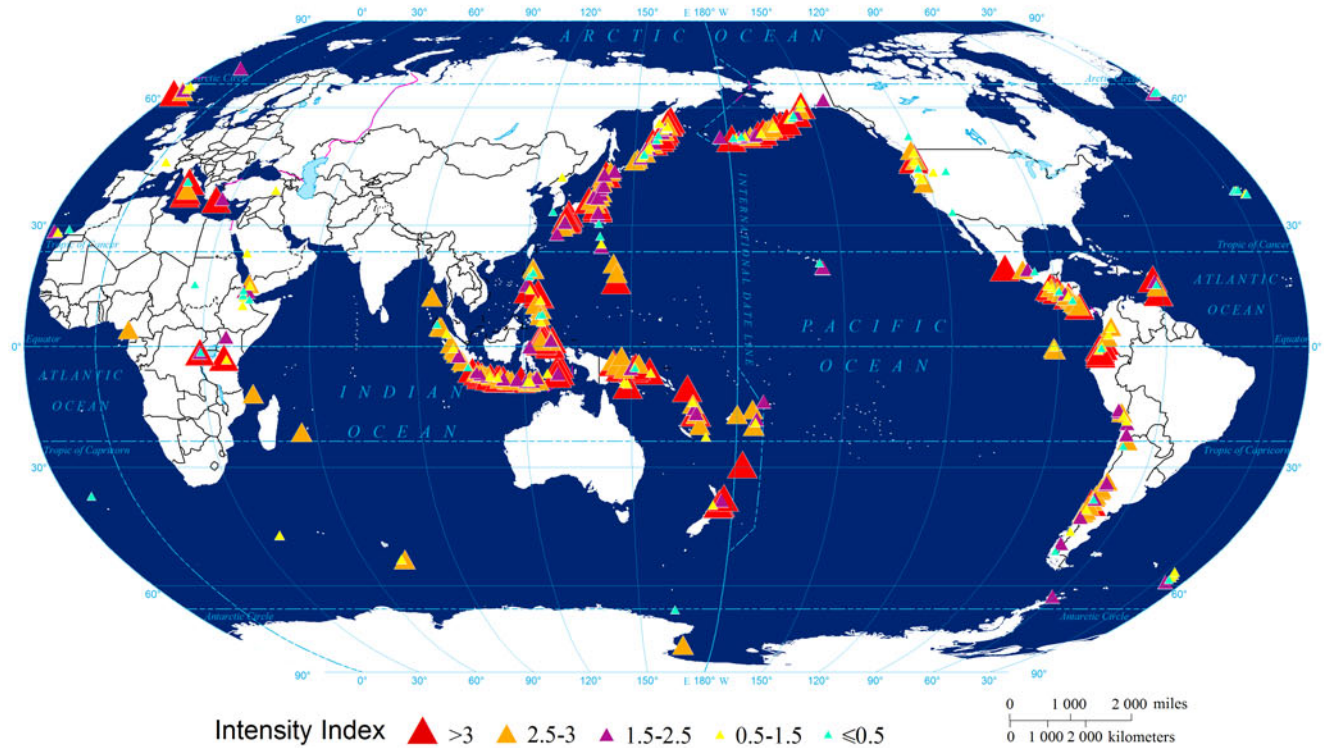
Global Volcano Intensity by Return Period (20a)



Global Volcano Intensity by Return Period (50a)



Global Volcano Intensity by Return Period (100a)

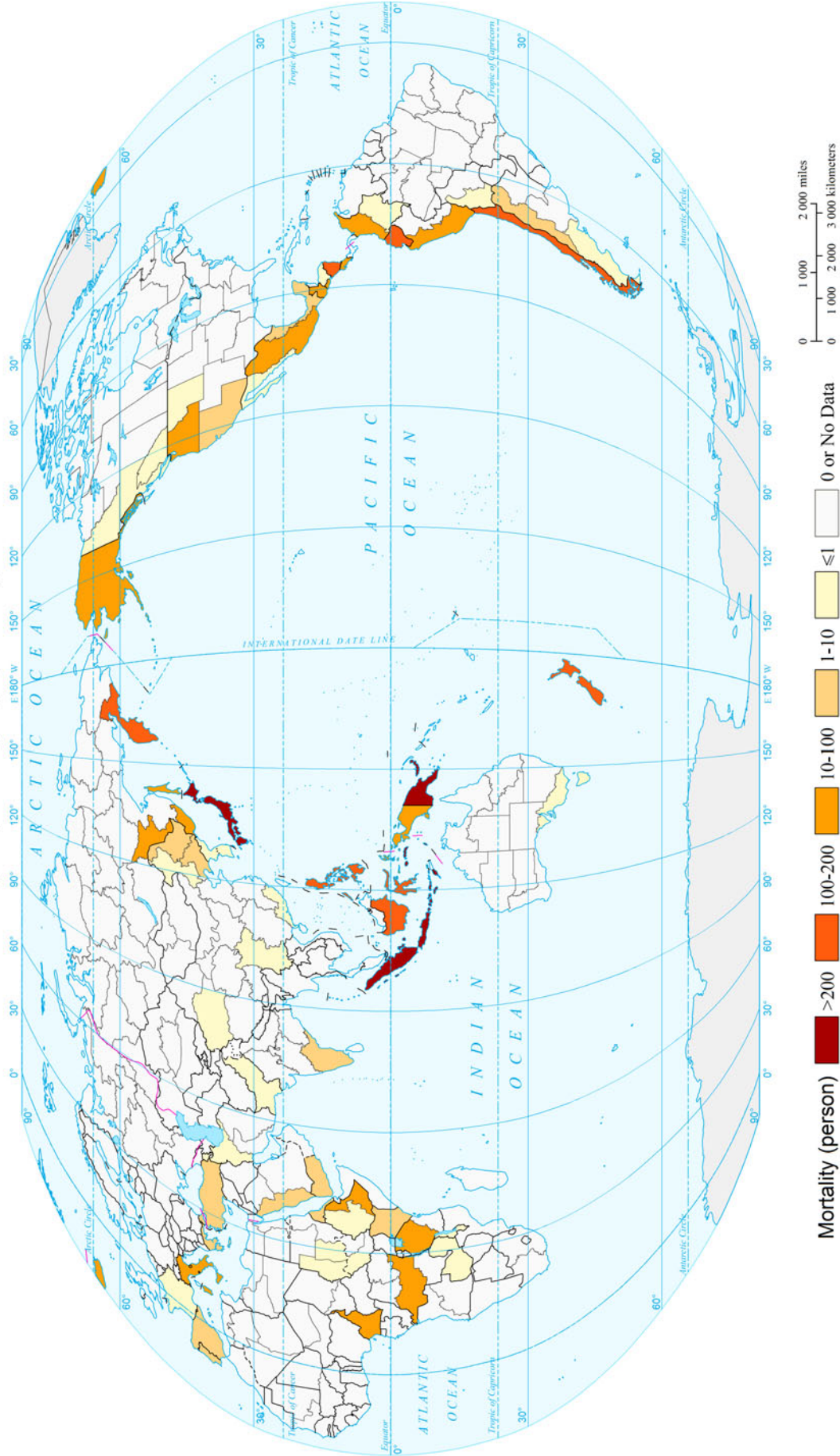




Volcano

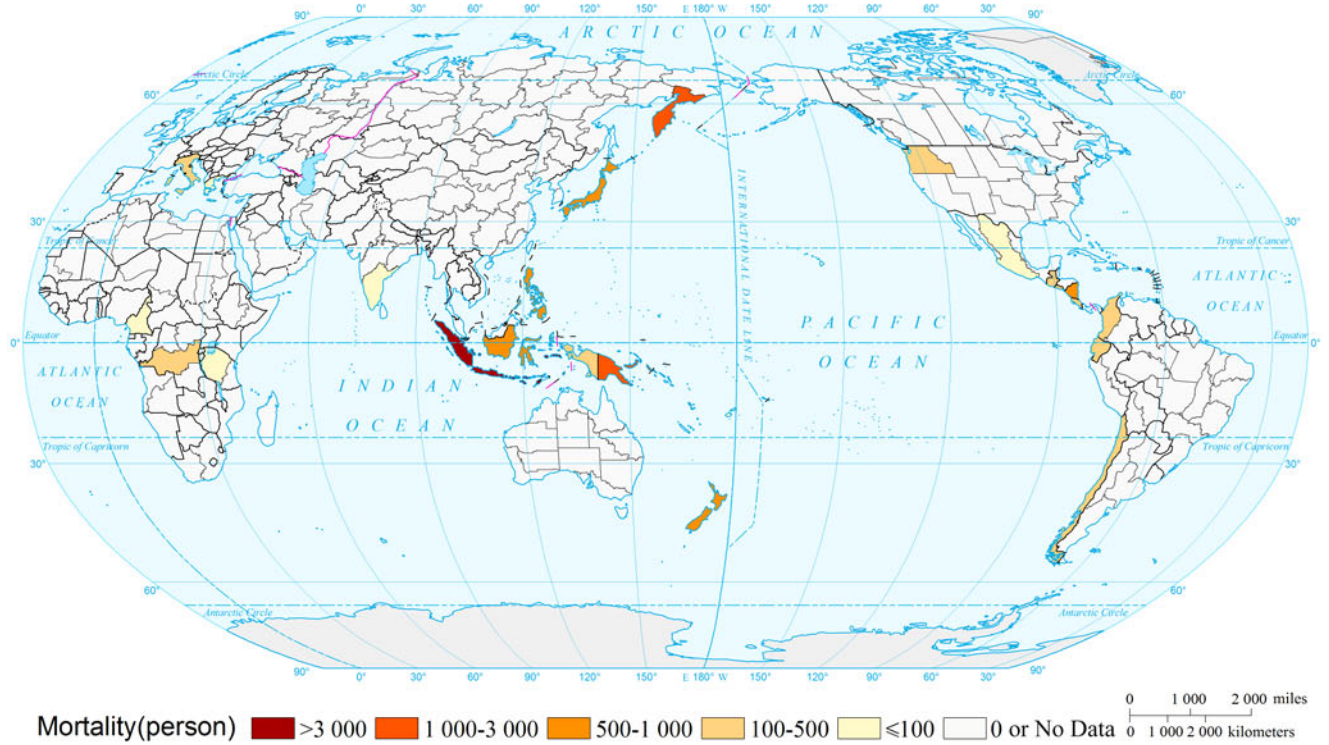
Earthquake, Volcano and Landslide Disasters

### Expected Annual Mortality Risk of Volcano of the World (Comparable-geographic Unit)

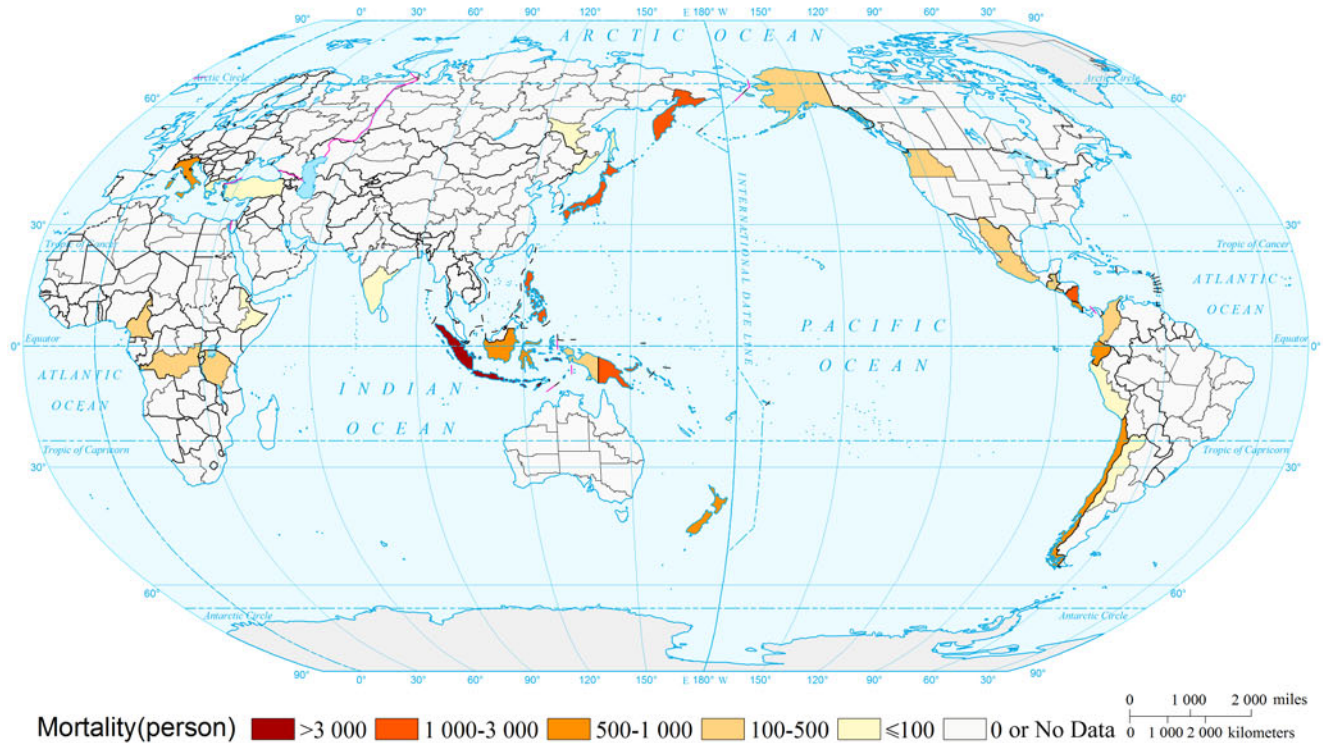


Mortality (person) [Color Scale Legend]

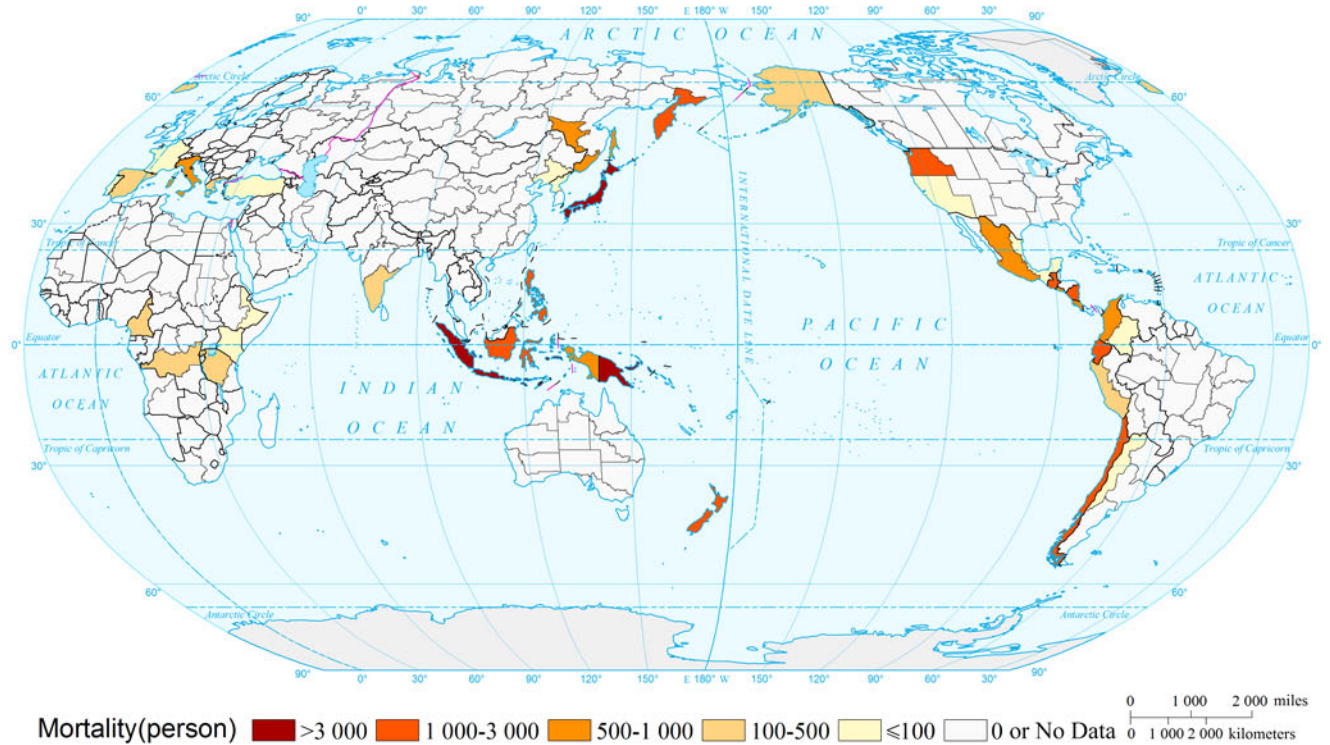
### Mortality Risk of Volcano of the World by Return Period (10a) (Comparable-geographic Unit)



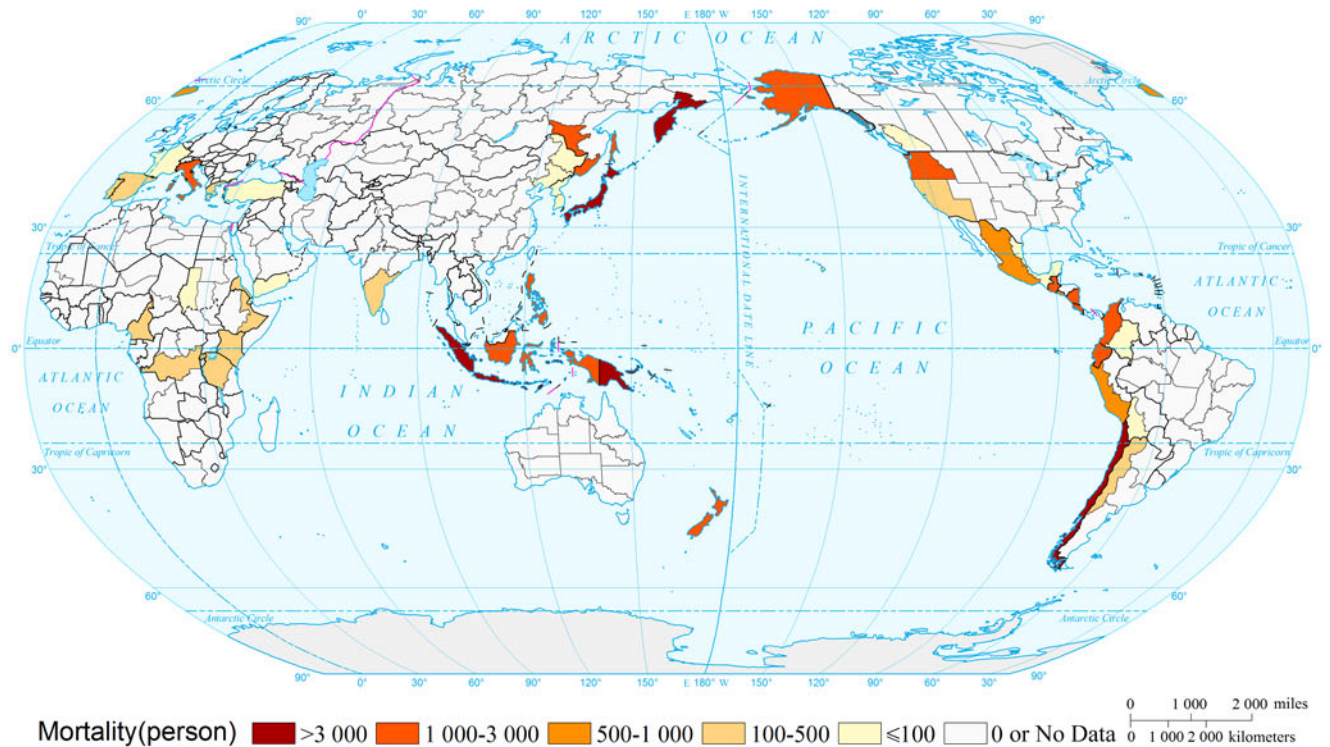
### Mortality Risk of Volcano of the World by Return Period (20a) (Comparable-geographic Unit)



### Mortality Risk of Volcano of the World by Return Period (50a) (Comparable-geographic Unit)

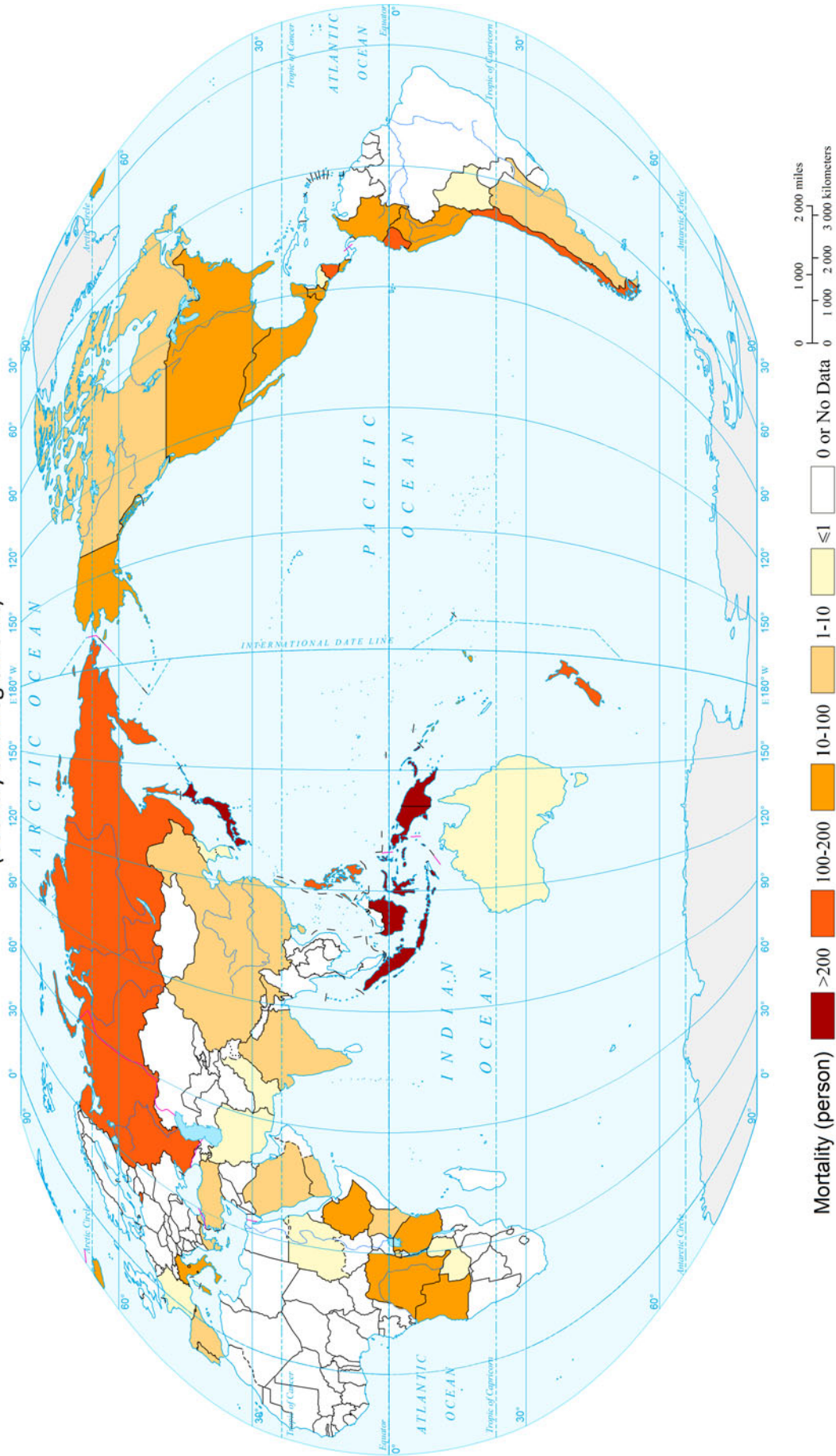


### Mortality Risk of Volcano of the World by Return Period (100a) (Comparable-geographic Unit)

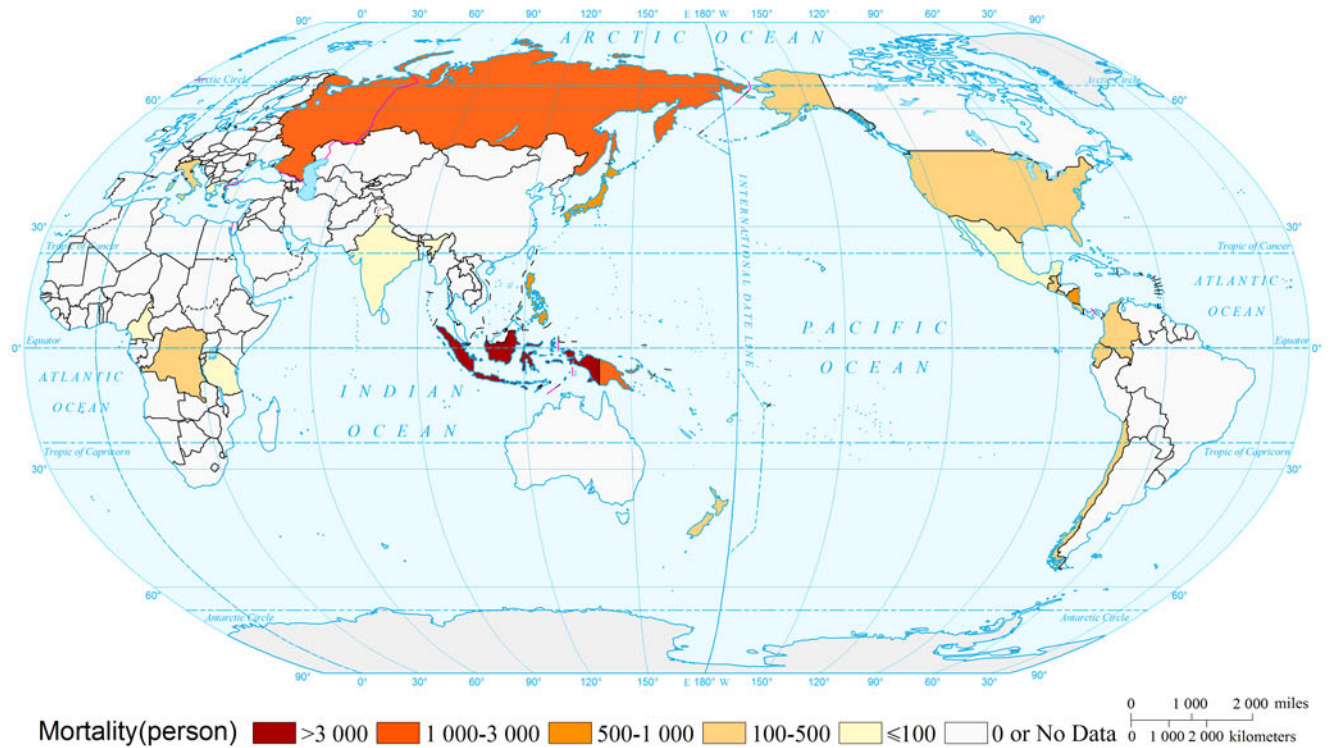




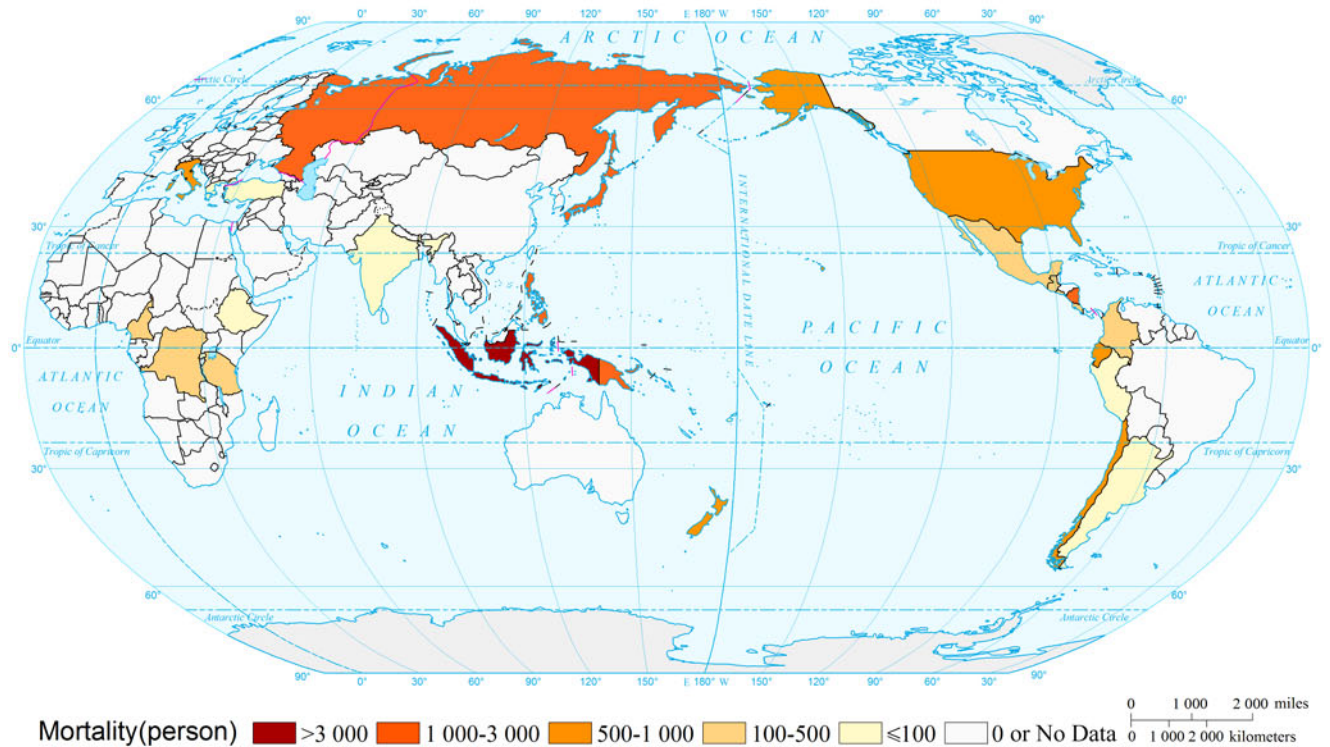
Expected Annual Mortality Risk of Volcano of the World  
(Country and Region Unit)



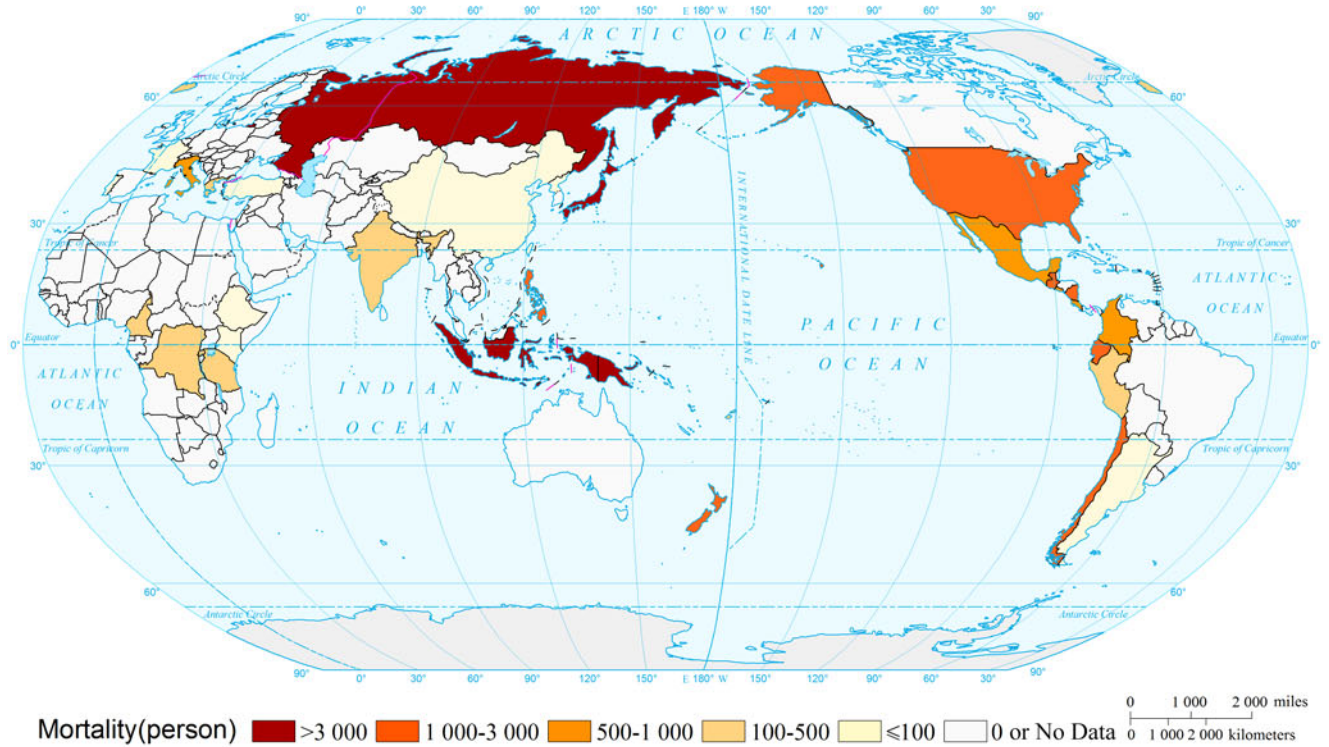
### Mortality Risk of Volcano of the World by Return Period (10a) (Country and Region Unit)



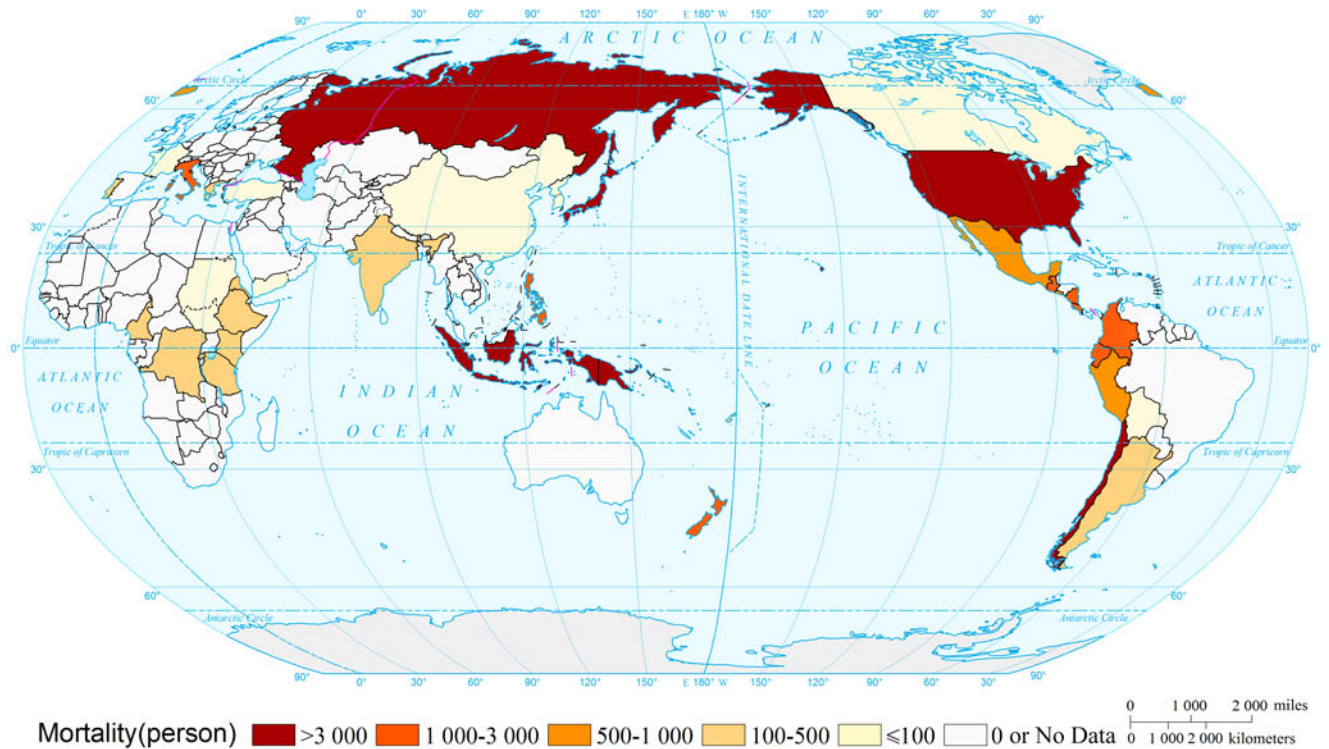
### Mortality Risk of Volcano of the World by Return Period (20a) (Country and Region Unit)



### Mortality Risk of Volcano of the World by Return Period (50a) (Country and Region Unit)



### Mortality Risk of Volcano of the World by Return Period (100a) (Country and Region Unit)



## References

- Dilley, M., U. Deichmann, and R.S. Chen. 2005. *Natural Disaster Hotspots: A global risk analysis*. Washington DC: World Bank Publications.
- Hayashi, J.N., and S. Self. 1992. A comparison of pyroclastic flow and debris avalanche mobility. *Journal of Geophysical Research: Solid Earth (1978–2012)* 97(B6): 9063–9071.
- Hoblitt, R.P., J.S. Walder, and C.L. Dreidger, et al. 1995. *Volcano hazards from Mount Rainier, Washington: USGS Open-File Report 98–4*.
- Huang, C.F. 2012. *Natural disaster risk analysis and management*. Beijing: Science Press. (in Chinese).
- Huggel, C., D. Schneider, P.J. Miranda, et al. 2008. Evaluation of ASTER and SRTM DEM data for lahar modeling: A case study on lahars from Popocatepetl Volcano, Mexico. *Journal of Volcanology and Geothermal Research* 170(1): 99–110.
- Jenkins, S., C. Magill, J. McAneney, et al. 2012. Regional ash fall hazard I: A probabilistic assessment methodology. *Bulletin of Volcanology* 74(7):1699–1712.
- Macías, J.L., L. Capra, J.L. Arce, et al. 2008. Hazard map of El Chichón Volcano, Chiapas, México: Constraints posed by eruptive history and computer simulations. *Journal of Volcanology and Geothermal Research* 175(4): 444–458.
- Magill, C., and R. Blong. 2005. Volcanic risk ranking for Auckland, New Zealand II: Hazard consequences and risk calculation. *Bulletin of volcanology* 67(4): 340–349.
- Newhall, C.G., and S. Self. 1982. The volcanic explosivity index (VEI): An estimate of explosive magnitude for historical volcanism. *Journal of Geophysical Research: Oceans (1978–2012)*, 87 (C2):1231–1238.
- Pomonis, A., R. Spenceand, and P. Baxter. 1999. Risk assessment of residential buildings for an eruption of Furnas Volcano, Sao Miguel, the Azores. *Journal of Volcanology and Geothermal Research* 92 (1): 107–131.
- Rhoades, D.A., D.J. Dowrick, and C.J.N. Wilson. 2002. Volcanic hazard in New Zealand: Scaling and attenuation relations for tephra fall deposits from Taupo Volcano. *Natural Hazards* 26(2): 147–174.
- Thouret, J.C., F. Lavigne, K. Kelfoun, et al. 2000. Toward a revised hazard assessment at Merapi Volcano, Central Java. *Journal of Volcanology and Geothermal Research* 100(1): 479–502.
- United States Geological Survey. 2014. Volcano hazards program. <http://volcanoes.usgs.gov/images/pglossary/vei.php>. Accessed in March 2014.
- Waythomas, C.F., T.P. Miller, and C.J. Nye. 2003. Preliminary volcano-hazard assessment for Great Sitkin Volcano, Alaska. *US Department of the Interior, USGS*.

---

# Mapping Landslide Risk of the World

Wentao Yang, Lingling Shen, and Peijun Shi

---

## 1 Background

Landslide inventory, susceptibility, and hazard mapping are different steps toward landslide risk mapping (Fell et al. 2008). Landslide inventory can be regarded as a simple form of landslide susceptibility map by showing the location of existing landslides. Besides, other kinds of landslide susceptibility map scan also show the location of potential landslides by incorporating environmental factors, which serve as the basis for hazard and risk mapping (Fell et al. 2008). Although susceptibility map shows the potential location of landslides, it does not give the information of temporal probability. For every location, landslide hazard map shows the spatial and temporal probability of landslides under given intensity (UNESCO 1985), whereas landslide risk map denotes the annual probability of people or economic loss expected. Risk is the interaction of hazard intensity, the vulnerability of elements at risk, and the corresponding environment (Shi 2002).

There are many methods for landslide mapping and landslide disaster, hazard, and risk map are among those popular landslide mappings. Durham Fatal Landslide Database

(Petley 2012) and Landslide Disaster Database from NASA Goddard Space Flight Center (GSFC) (Kirschbaum et al. 2010) are two landslide disaster databases at the global scale. Both databases are collected from worldwide reports of landslide disasters, while the latter has an expansion for other losses except human casualty. Global landslide hazard was mapped by Nadim et al. (2006), who considered global lithology, slope, seismic activity, etc., and assigned hazard probability based on expert judgment. Based on the Gridded Population of the World (GPW), global landslide risk was also estimated in the work carried out by Nadim et al. (2006). Using 3-h resolution TRMM rainfall data, Hong et al. (2006) developed a real-time global landslide warning system based on global landslide susceptibility map. Based on support vector machines (SVM), Farahmand and AghaKouchak (2013) developed a quasi-global landslide susceptibility model using satellite precipitation data, land use and cover change maps, and 250-m resolution topography information.

Previous researches show that slope, altitude, lithology, land use, and soil property can influence landslide susceptibility (Nadim et al. 2006; Cui et al. 2008; Minder et al. 2009; Huang 2011). Coe et al. (2004) and Fabbri et al. (2003) found that slope and altitude are two most important contributing factors of landslide occurrence.

Although Hong et al. (2006) argued that it was possible to map global-scale landslide susceptibility map based on incomplete information layers, the lack of lithology and seismicity layers in this model might impair the hazard map. Compared to the global landslide risk map developed by Nadim et al. (2006), factors including fine temporal resolution rainfall data, tectonic faults, and land use type are considered in this study. By using 15-year consecutive 3-h resolution precipitation data, this study examined every rainfall event over the rainfall threshold for the initiation of landslide. Based on information diffusion theory, information diffusion method was used to fit the 15-year samples to get the expected annual numbers of landslide events.

---

**Mapping Editors:** Jing'ai Wang (Key Laboratory of Regional Geography, Beijing Normal University, Beijing 100875, China) and Chunqin Zhang (School of Geography, Beijing Normal University, Beijing 100875, China).

**Language Editor:** Liu Lianyou (Laboratory of Environmental Change and Natural Disaster, Ministry of Education, Beijing Normal University, Beijing 100875, China).

---

W. Yang · L. Shen  
Academy of Disaster Reduction and Emergency Management,  
Ministry of Civil Affairs and Ministry of Education, Beijing  
Normal University, Beijing 100875, China

P. Shi (✉)  
State Key Laboratory of Earth Surface Processes and Resource  
Ecology, Beijing Normal University, Beijing 100875, China  
e-mail: spj@bnu.edu.cn

By combining these results, landslide hazard map with the LandScan population and global landslide disaster database (Kirschbaum et al. 2010), population vulnerability and mortality risk of landslide of the world were calculated. In this study, the environmental factors denote the background of hazard formation, while the probability of hazard is estimated from precipitation data. At global scale, vulnerability of human is estimated from the ratio of casualties to exposed population at national level.

## 2 Method

Figure 1 shows the technical flow chart for mapping landslide risk of the world.

### 2.1 Hazard

This study can be divided into three components: landslide susceptibility, hazard, and mortality risk mapping. By weighting layers such as slope, elevation, land use type, lithology, fault, and semi-quantitative seismic hazard map, landslide susceptibility map was developed. TRMM 3B42 3-h precipitation data (Appendix III, Hazards data 4.4) were used to generate hazard map by integrating previously developed landslide susceptibility map. Finally, LandScan population data (Appendix III, Exposures data 3.1) and global landslide casualty data (Appendix III, Disasters data 5.2) were used to calculate population vulnerabilities of each country and landslide risk to population. Due to limited data at the global scale, the global hazard mapping was validated by the global landslide hotspot hazard map.

#### 2.1.1 Global Landslide Susceptibility

Landslide susceptibility map was calculated by weighting different layers of preparatory or environmental layers, including slope, elevation, lithology, active fault line density, and seismicity (Eq. 1). The weight of each layer is given according to their importance to landslides referring to past research (Nadim et al. 2006; Hong et al. 2007).

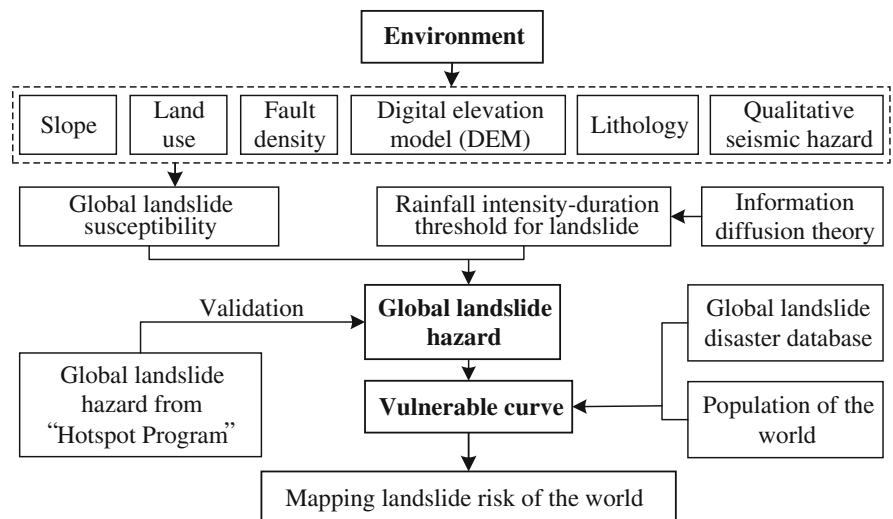
$$\text{Sus} = 0.25 \times \text{Slo} + 0.15 \times \text{DEM} + 0.15 \times \text{LUCC} + 0.15 \times \text{Lith} + 0.15 \times \text{Fault} + 0.15 \times \text{Seis} \quad (1)$$

where Sus denotes landslide susceptibility, Slo denotes reclassified global slope percentage (Appendix III, Environments data 2.2), DEM denotes normalized global elevation (Appendix III, Environments data 2.1), LUCC denotes reclassified global land use data in 2012 (Appendix III, Environments data 2.8), Lith denotes reclassified global lithology data (Appendix III, Environments data 2.4), Fault denotes reclassified global active fault line density (Appendix III, Environments data 2.4), and Seis denotes seismicity (PGA) (Appendix III, Hazards data 4.1).

#### 2.1.2 Global Landslide Hazard

By considering the temporal occurrence of landslide triggers such as precipitation, landslide hazard map can be made based on susceptibility map (van Westen et al. 2008). Fine-temporal resolution precipitation data are vital for estimating the occurrence of rainfall-induced landslides. However, rain gauge stations are unevenly distributed and cover very limited areas around the world. Thus, the homogeneous global coverage TRMM data are ideal for calculating the occurrence of landslides.

**Fig. 1** Technical flowchart for mapping landslide risk of the world



The data used were TRMM 3B42. However, there are some deviations between station-based precipitation and TRMM-based data (Qi et al. 2013). Most existing station-based precipitation threshold are not necessarily sufficient for landslide hazard analysis. Based on global landslide records and TRMM data, Hong et al. (2006) established a global rainfall threshold for the initiation of landslides. This study used Hong's threshold to examine every rainfall event in each pixel from the beginning of 1998 to the end of 2012 (Eq. 2).

$$I = 12.45D^{-0.42} \quad (2)$$

where  $I$  is the precipitation intensity (mm/h) and  $D$  is the rainfall duration (h).

After examining every rainfall event, we summed up the number of events that exceed the threshold each year for each pixel. So, there are 15 years data with the number of landslide events from 1998 to 2012.

For the hazard factors with limited samples, it is a better choice to apply information diffusion theory (Huang and Moraga 2004). The normal diffusion model was the most frequently used kind of information diffusion model. The process of information diffusion was actually to diffuse the information in single sample to the whole sample space, which obeys the principle of conservation of the amount of information.

The data scope of TRMM was among 50° latitude north and south. For areas beyond this scope, the NCEP/NCAR reanalysis data (Appendix III, Hazards data 4.5) were used. The high-latitude areas had less landslide occurrences due to relatively high vegetation cover, soil freezing, sparsely populated, and subdued topography. Applying the methods and processes mentioned above, with the same period as TRMM (January 1, 1998—December 31, 2012), the

cumulative value of global precipitation–landslide exceedance threshold was calculated.

After getting global precipitation–landslide frequency, according to the different weights of susceptibility map, the global landslide hazard map can be estimated (Eq. 3):

$$H(\text{pre}) = \text{Sus} \times \text{Pre} \quad (3)$$

where  $H(\text{pre})$  is the number of rainfall-induced landslides (times/a/km<sup>2</sup>),  $\text{Sus}$  is the landslide susceptibility, and  $\text{Pre}$  is the annual expectation numbers of exceedance precipitation–landslide threshold (times/a/km<sup>2</sup>).

## 2.2 Mortality Risk

Vulnerability typified the loss and damage of exposure by hazard. Generally, the loss was estimated from statistical history loss data. Population vulnerability of landslide is estimated by the statistical casualties and population exposure. NASA's global landslide early warning system based on TRMM data had collected the data of human death and missing due to precipitation-induced landslide in 2003 and 2007–2011 (Appendix III, Disasters data 5.2). According to corresponding year, the exposed population of each country and region was calculated in the light of LandScan 2010 and the hazard in the same site; the landslide–casualties vulnerability curve was made by combing casualties (Fig. 2).

There were 76 countries with available statistical mortality data in 2003 and 2007–2011 (Kirschbaum et al. 2010). To supplement the inadequate data, similar vulnerability value was assigned to countries with geographical proximity.

On the basis of global landslide hazard raster map (0.25° × 0.25°) and global landslide–casualties vulnerability, adding the layer of global population density raster map

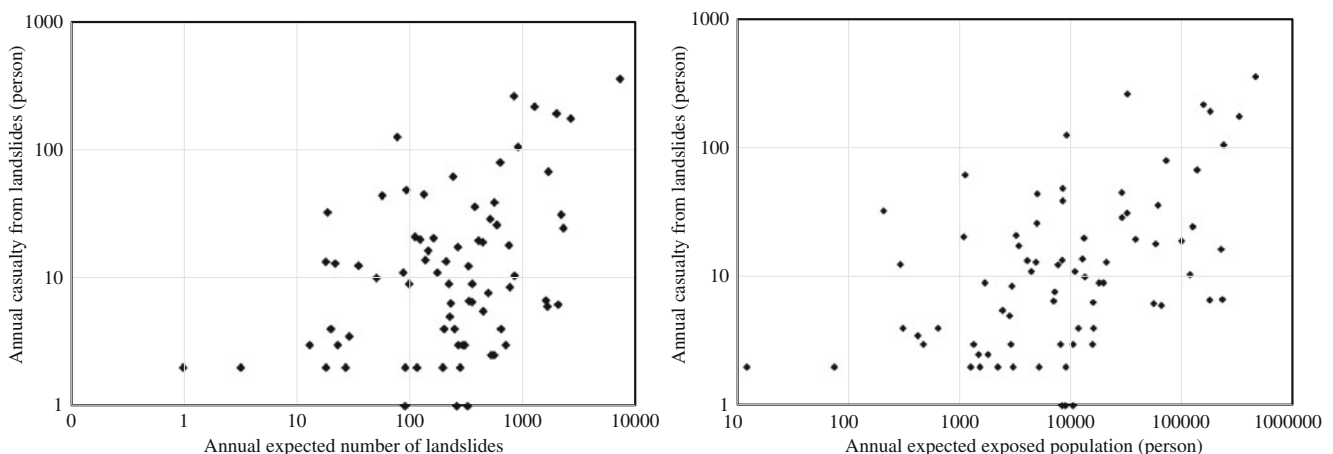


**Fig. 2** Landslide–casualties vulnerability curve

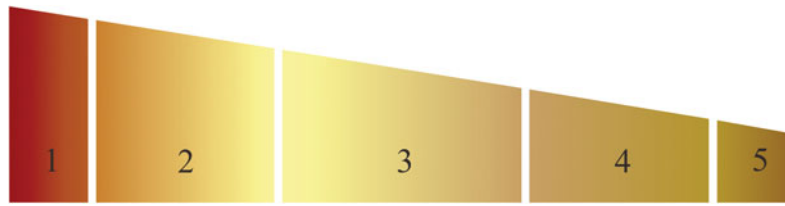


**Fig. 3** Expected annual mortality risk levels of landslide of the world 1 (0, 10 %) China, Brazil, Iran, Uganda, Philippines, Indonesia, India, Nepal, Paraguay, Bolivia, Burundi, Colombia. 2 (10, 35 %) Switzerland, Pakistan, Bangladesh, Afghanistan, Guatemala, Portugal, South Korea, Peru, Sierra Leone, Cameroon, Vietnam, Central African Republic, Guinea-Bissau, Kazakhstan, Congo (Democratic Republic of the), Mexico, Angola, Nigeria, Syria, Dominican Republic, Ethiopia, Tajikistan, Costa Rica, Sri Lanka, Jordan, Malaysia, El Salvador, North Korea, Haiti, Tanzania, Senegal, 3 (35, 65 %) Spain, Guinea, Iraq, Kyrgyzstan, Mali, Liberia, Uzbekistan, Thailand, Mozambique, Kenya, Rwanda, Romania, Madagascar, Malawi, Italy, Sudan, Ecuador,

Zambia, Papua New Guinea, Yemen, Japan, Uruguay, France, Turkey, Zimbabwe, Georgia, Venezuela, United States, Azerbaijan, Panama, South Africa, Honduras, Poland, Niger, Laos, Chile, Cuba, New Zealand. 4 (65, 90 %) Ghana, Burkina Faso, Algeria, Slovakia, Russia, Nicaragua, Argentina, Armenia, Morocco, Serbia, Jamaica, Bhutan, Palestine, Bosnia and Herzegovina, Trinidad and Tobago, Bulgaria, Moldova, Ukraine, Australia, Tunisia, Israel, Mauritania, Chad, Germany, Togo, Hungary, Lebanon, Austria, Greece, Croatia, Albania 5 (90, 100 %) Macedonia, Saudi Arabia, Somalia, Eritrea, Lesotho, Slovenia, Czech Republic, Montenegro, Cambodia, Turkmenistan, Mongolia, Libya

(1 km × 1 km) from American LandScan program, world mortality risk of landslide was obtained (Eq. 4).

$$R_{\text{pop}} = V \times H \times E_{\text{pop}} \quad (4)$$

where  $R_{\text{pop}}$  is landslide-induced mortality risk,  $V$  is the population vulnerability,  $H$  is landslide hazard, and  $E_{\text{pop}}$  is global population density.

### 3 Results

Susceptibility represents the likelihood of landslide occurrence, that is, how easily landslide could occur under a certain environment. From the aspect of disaster system theory, susceptibility is subjected to the instability of landslide hazard-background environment. Global landslide susceptibility is divided into 5 classes, from high to low, expressing a stable progressive decrease. The highest class is distributed mainly around the major structural mountains, especially in the Alpine–Himalayan mountain tectonic belt, the Pacific Rim, and the Great Rift Valley. The medium and lower classes are scattered in plateaus, such as African plateau, Chinese Loess plateau, Yunnan–Guizhou plateau, Inner Mongolian plateau, India’s Deccan plateau, and the edge of Brazil plateau.

Rainfall-induced landslide hazard indicates the estimation of landslide numbers in different susceptibility classes under different precipitation intensities. Global rainfall-induced landslides are mainly scattered in humid areas with large undulating terrain, such as windward slope of the southern Himalayas, China Longmen Mountain area Mt. Alps, and the Andes.

Global landslide mortality risk mainly distributes in mountain areas with high population density, especially in the developing countries. Countries with high landslide mortality risk include China (southwestern area), India (northern part, southern Himalayas), Nepal, Pakistan (northern area), Italy, and countries in Central and South America.

By zonal statistics of the expected risk result, the expected annual mortality risk of landslide of the world at national level is derived and ranked (Fig. 3). The top 1 % country with the highest mortality risk of landslide is China, and the top 10 % countries are China, Brazil, Iran, Uganda, Philippines, Indonesia, India, Nepal, Paraguay, Bolivia, Burundi, and Colombia.

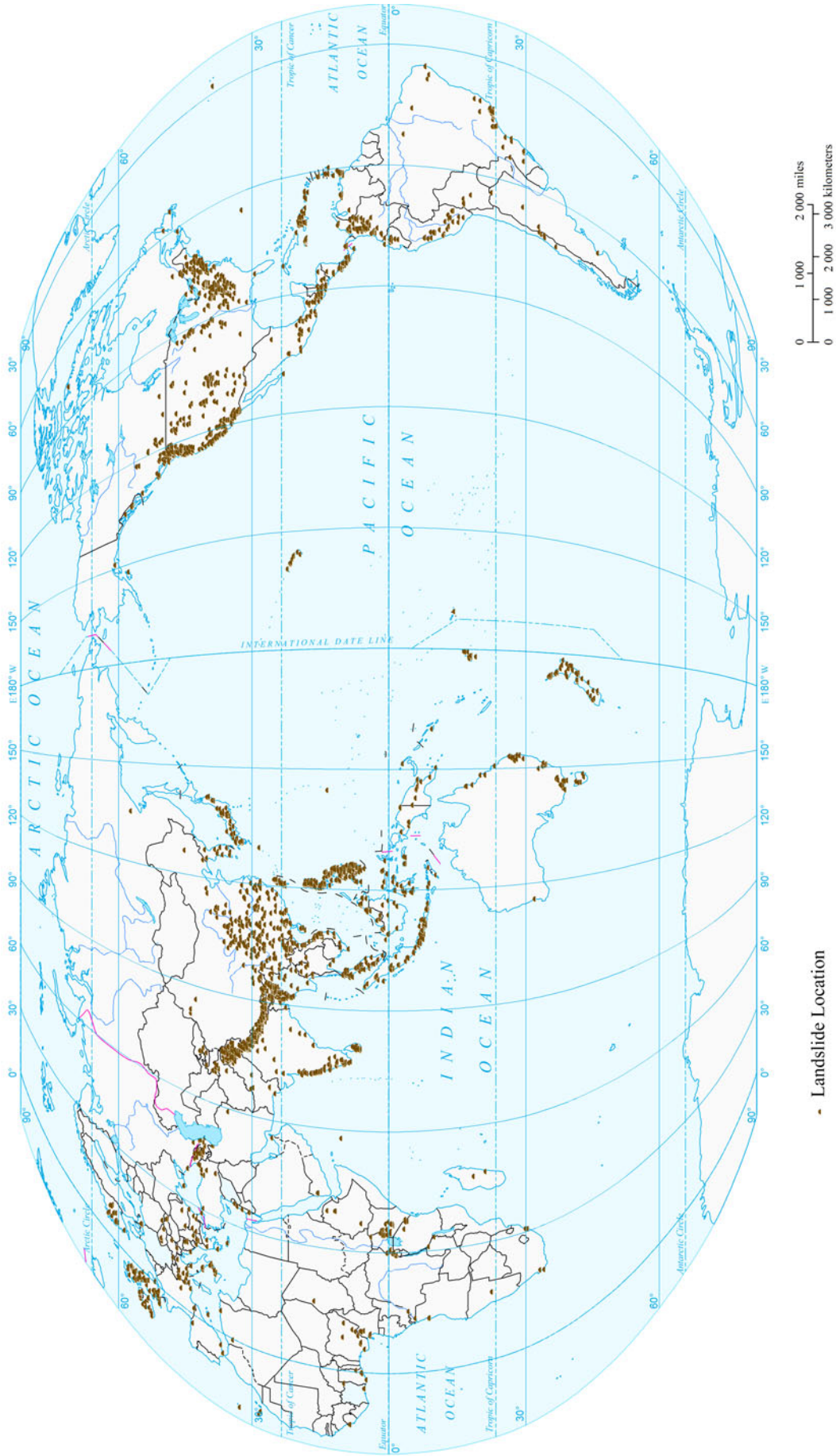
### 4 Maps



Landslide

Earthquake, Volcano and Landslide Disasters

### Historical Event Locations of Global Landslide (2003 and 2007-2011)

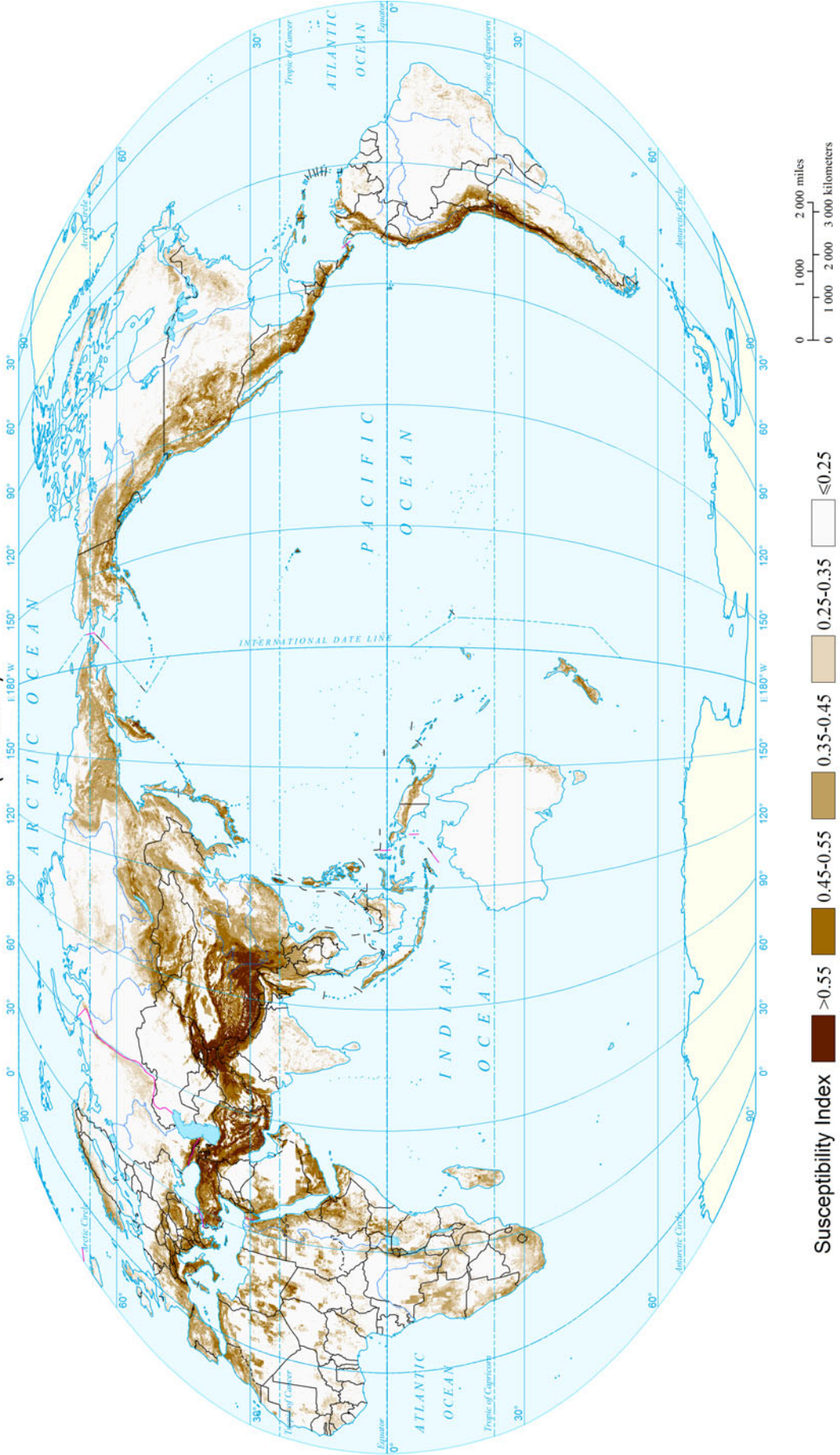


Data Source: National Aeronautics and Space Administration(NASA)  
[http://gcmd.nasa.gov/records/GCMD\\_NASA\\_GSFC\\_TRMM\\_LANDSLIDE\\_INVENTORY.html](http://gcmd.nasa.gov/records/GCMD_NASA_GSFC_TRMM_LANDSLIDE_INVENTORY.html)



### Global Landslide Susceptibility

( $0.1^\circ \times 0.1^\circ$ )

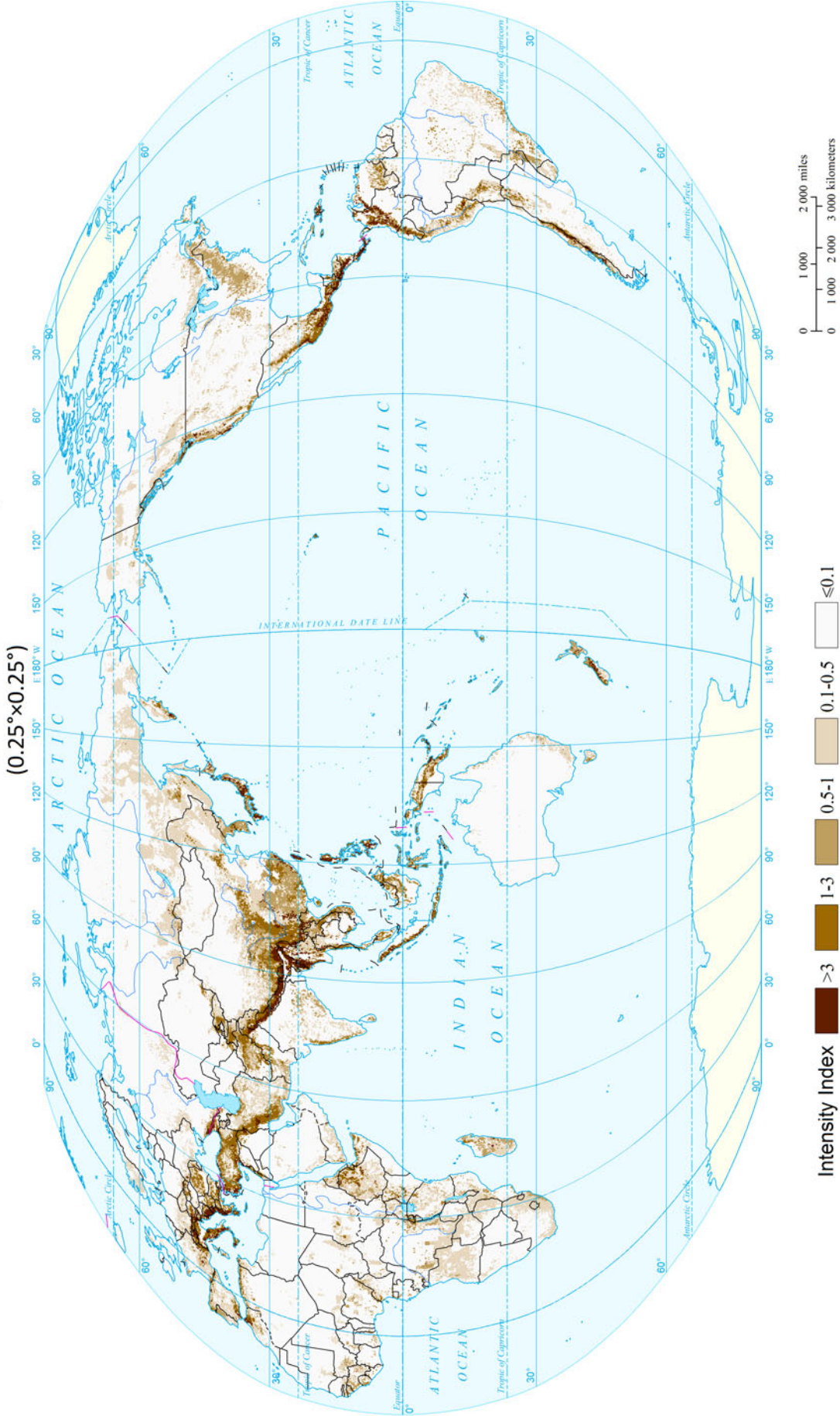




Landslide

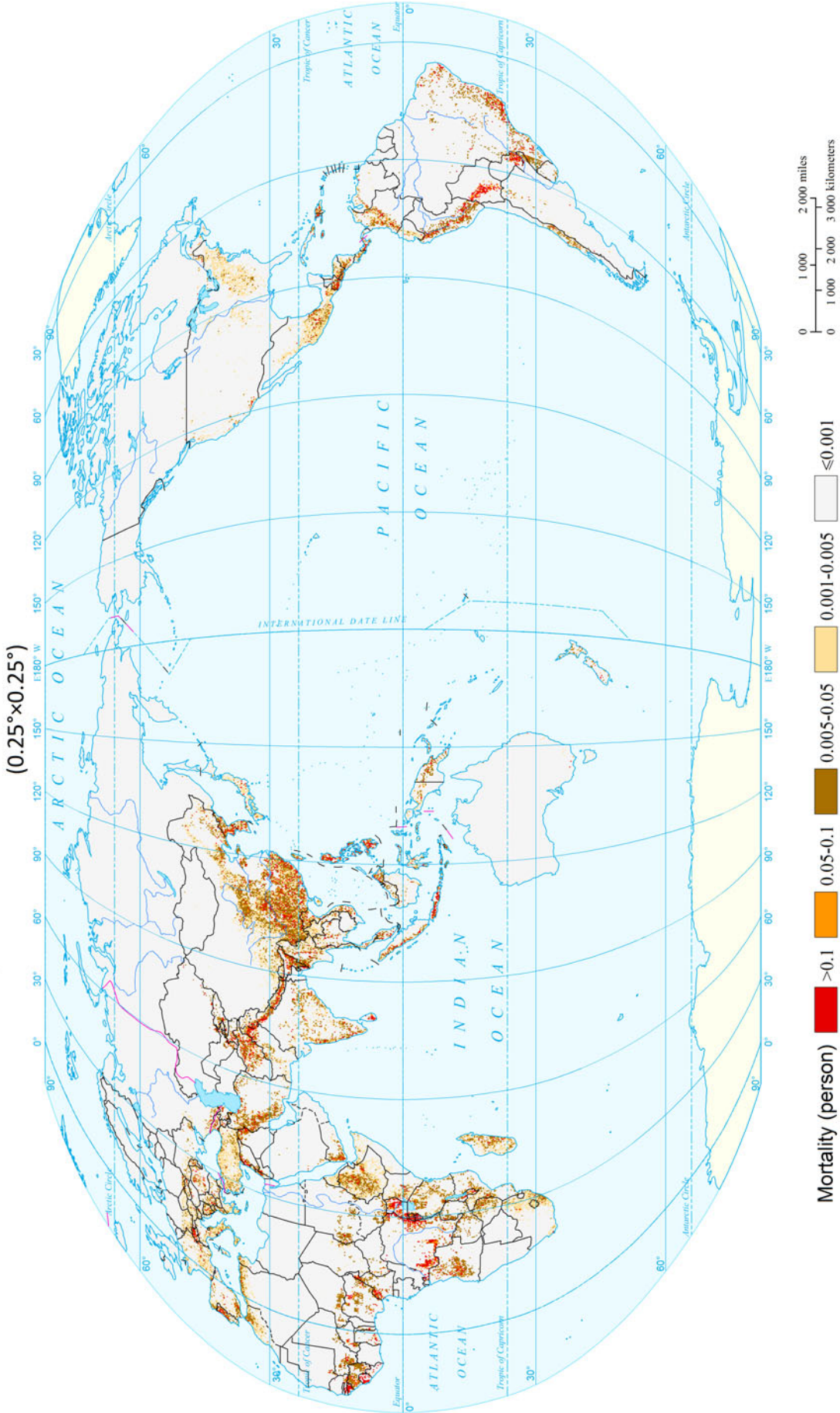
Earthquake, Volcano and Landslide Disasters

### Global Rainfall-induced Landslide Intensity (0.25°x0.25°)

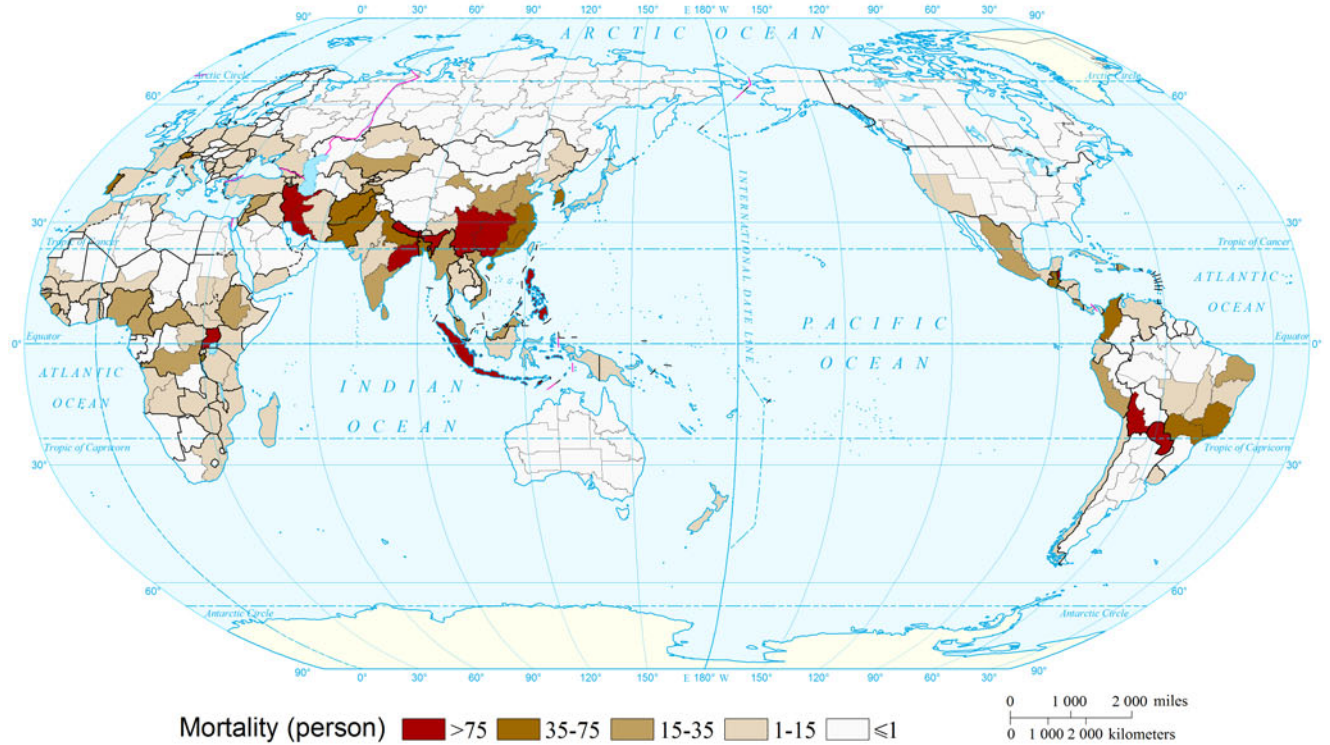




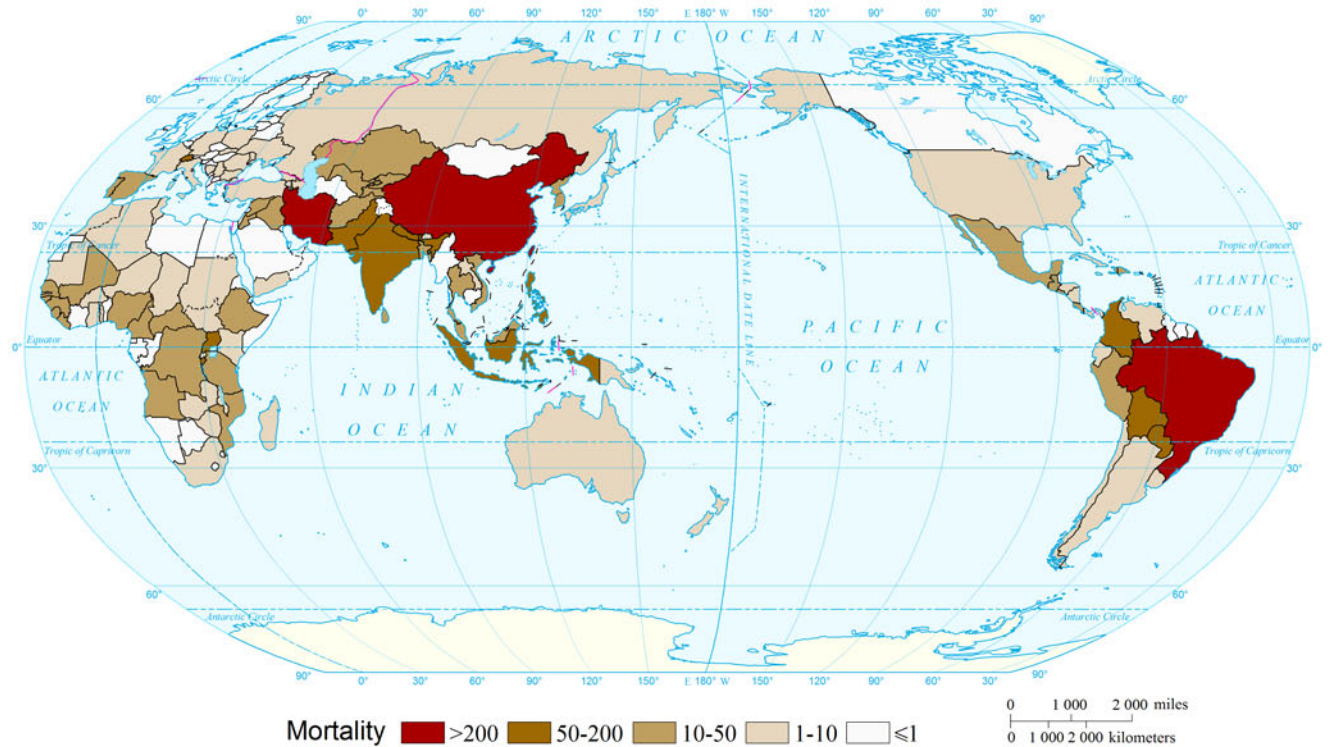
### Expected Annual Mortality Risk of Landslide of the World ( $0.25^\circ \times 0.25^\circ$ )



Expected Annual Mortality Risk of Landslide of the World  
( Comparable-geographic Unit)



Expected Annual Mortality Risk of Landslide of the World  
( Country and Region Unit)



## References

- Coe, J.A., J.W. Godt, R.L. Baum, et al. 2004. Landslide susceptibility from topography in Guatemala. In *Landslides: Evaluation and stabilization*, vol. 1, ed. W.A. Lacerda, M. Ehrlich, and S.A.B. Fontura, et al. 69–78. London: Taylor & Francis Group.
- Cui, P., F.Q. Wei, S.M. He, et al. 2008. Mountain disasters induced by the earthquake of May 12 in Wenchuan and the disasters mitigation. *Journal of Mountain Science* 26(3): 280–282. (in Chinese).
- Fabbri, A.G., C.J.F. Chung, A. Cendrero, et al. 2003. Is prediction of future landslides possible with a GIS? *Natural Hazards* 30(3): 487–503.
- Farahmand, A., and A. AghaKouchak. 2013. A satellite-based global landslide model. *Natural Hazards and Earth System Science* 13(5): 1259–1267.
- Fell, R., J. Corominas, C. Bonnard, et al. 2008. Guidelines for landslide susceptibility, hazard and risk zoning for land use planning. *Engineering Geology* 102(3–4): 99–111.
- Hong, Y., R. Adler, and G. Huffman. 2006. Evaluation of the potential of NASA multi-satellite precipitation analysis in global landslide hazard assessment. *Geophysical Research Letters* 33(22). doi:10.1029/2006GL028010.
- Hong, Y., R. Adlerand, and G. Huffman. 2007. Use of satellite remote sensing data in the mapping of global landslide susceptibility. *Natural Hazards* 43(2): 245–256.
- Huang, C.F., and C. Moraga C. 2004. A diffusion-neural-network for learning from small samples. *International Journal of Approximate Reasoning* 35: 137–161.
- Huang, R.Q. 2011. After effect of geohazards induced by the Wenchuan earthquake. *Journal of Engineering Geology* 19(2): 145–161. (in Chinese).
- Kirschbaum, D.B., R. Adler, Y. Hong, et al. 2010. A global landslide catalog for hazard applications: Method, results, and limitations. *Natural Hazards* 52(3): 561–575.
- Minder, J.R., G.H. Roeand, and D.R. Montgomery. 2009. Spatial patterns of rainfall and shallow landslide susceptibility. *Water Resources Research* 45(4). doi:10.1029/2008WR007027.
- Nadim, F., O. Kjekstad, P. Peduzzi, et al. 2006. Global landslide and avalanche hotspots. *Landslides* 3(6): 159–173.
- Petley, D. 2012. Global patterns of loss of life from landslides. *Geology* 40(10): 927–930.
- Qi, W.W., B.P. Zhang, Y. Pang, et al. 2013. TRMM-data-based spatial and seasonal patterns of precipitation in the Qinghai-Tibet Plateau. *Scientia Geographica Sinica* 33(8): 999–1005. (in Chinese).
- Shi, P.J. 2002. Theory on disaster science and disaster dynamics. *Journal of Natural Disasters* 11(3): 1–9. (in Chinese).
- United Nations Educational, Scientific and Cultural Organization (UNESCO). 1985. *Landslide hazard zonation: A review of principles and practice*. Paris: United Nations Educational Scientific and Cultural Organization.
- van Westen, C.J., E. Castellanos, and S.L. Kuriakose. 2008. Spatial data for landslide susceptibility, hazard, and vulnerability assessment: An overview. *Engineering Geology* 102(3): 112–131.

---

**Part III**

**Flood and Storm Surge Disasters**

---

# Mapping Flood Risk of the World

Jian Fang, Mengjie Li, and Peijun Shi

---

## 1 Background

The flood risk assessment on regional and small/medium watershed scales has been extensively carried out all around the world, yielding various risk maps through both model simulations and historical data analysis, to guide regional flood risk management (Apel et al. 2004; Kim et al. 2012; Li et al. 2012; Su et al. 2012; Wang et al. 2011). However, on a global scale, much less relevant research is available due to the limitation of data availability and the lack of large-scale modeling methods.

On a global scale, the *Identification of Global Natural Disaster Risk Hotspots* project, conducted by Columbia University and the World Bank, studied the distribution and frequency of global flood with historical flood event records archived by Dartmouth Flood Observatory (DFO), evaluated flood economic and population vulnerability for each country using EM-DAT historical flood loss data and, finally, assessed the risk of mortality and economic loss for global floods (Dilley et al. 2005). Additionally, Winsemius et al. (2012) proposed a framework for high-resolution

global flood risk assessment in which global meteorological datasets were coupled with a hydrological and river routing model to simulate floods and then estimate the high-resolution risk through a downscaling scheme with the simulated floods and the overlay of the world economy and population distribution. Herold and Mouton (2011) combined the statistical analysis of historical peak flow for major global hydrological stations and GIS-based modeling to simulate the inundation extent and depth for global floods with various return periods. UNISDR (2009) used the global inundation datasets of flood hazard created by Herold and Mouton (2011) to assess global flood economic and population exposure risk in the Global Assessment Report on Disaster Risk Reduction (GAR). Jongman et al. (2012) used the same global inundation datasets (Herold and Mouton 2011) to estimate global exposure to river flooding.

From an overview of the existing literature, it can be inferred that the assessment of flood risk on a global scale has been very limited; the GAR and the Hotspots project report are the most cited and influential ones. UNISDR (2009) employed an analytical method to investigate the potential loss of flood. But they focused on modeling flood hazards and lacked vulnerability analysis. The Hotspots project applied an empirical method to depict the hazard and vulnerability and integrated these two parts to rank the risk levels. However, it relied only on historical flood records yet lacked consideration of various important factors in the flood disaster system such as hazards and disaster environment; therefore, its analysis on disaster systems was not comprehensive sufficiently.

Thus, this study combines both analytical and empirical methods to provide more comprehensive risk assessment. Both the aspect of estimation of potential flood loss and mortality and the aspect of the comprehensive analysis of flood hazard, stability of disaster environment, and vulnerability of exposure were addressed here. The global flood risk was assessed at 4 levels: grid, comparable geographic

---

**Mapping Editors:** Jing'ai Wang (Key Laboratory of Regional Geography, Beijing Normal University, Beijing 100875, China) and Chunqin Zhang (School of Geography, Beijing Normal University, Beijing 100875, China).

**Language Editor:** Ming Wang (State Key Laboratory of Earth Surface Processes and Resource Ecology, Beijing Normal University, Beijing 100875, China).

---

J. Fang · M. Li

Academy of Disaster Reduction and Emergency Management,  
Ministry of Civil Affairs and Ministry of Education, Beijing  
Normal University, Beijing 100875, China

P. Shi (✉)

State Key Laboratory of Earth Surface Processes and Resource  
Ecology, Beijing Normal University, Beijing 100875, China  
e-mail: spj@bnu.edu.cn

unit, watershed unit, and country and region unit in order to provide risk information from different scales for global flood reduction.

## 2 Method

Figure 1 shows the technical flowchart for mapping flood risk of the world.

### 2.1 Mapping Flood Risk at National Level

#### 2.1.1 Economic Loss Risk

At national level, the method used by Jongman et al. (2012) was adopted to calculate urban losses initially and then the agriculture economic losses were added to obtain a more accurate total loss estimation. The main steps are as follows:

Firstly, a global flood inundation-extent dataset (Appendix

Exposures data 3.5) to calculate the average losses per square meter of both urban and crop land for each country using Eqs. (1) and (2):

$$\frac{\text{Damage}_{\text{urban}_i}}{\text{Damage}_{\text{urban}_0}} = \frac{\text{GDP}_{\text{PPP}_i}}{\text{GDP}_{\text{PPP}_0}} \quad (1)$$

$$\frac{\text{Damage}_{\text{crop}_i}}{\text{Damage}_{\text{crop}_0}} = \frac{\text{GDP}_{\text{PPP}_i}}{\text{GDP}_{\text{PPP}_0}} \quad (2)$$

where  $\text{Damage}_{\text{urban}_i}$  is the unit-area monetization loss (in US \$) of inundated urban land of country  $i$ ,  $\text{Damage}_{\text{urban}_0}$  is the unit-area monetization loss (in US\$) of inundated urban land of the Netherlands,  $\text{Damage}_{\text{crop}_i}$  is the unit-area monetization loss (in US\$) of inundated crop land of country  $i$ ,  $\text{Damage}_{\text{crop}_0}$  is unit-area monetization loss (in US\$) of inundated crop land of the Netherlands,  $\text{GDP}_{\text{PPP}_i}$  is the GDP of country  $i$  in US\$ at purchase power parity (PPP),  $\text{GDP}_{\text{PPP}_0}$  is the GDP of the Netherlands in US\$ at PPP.

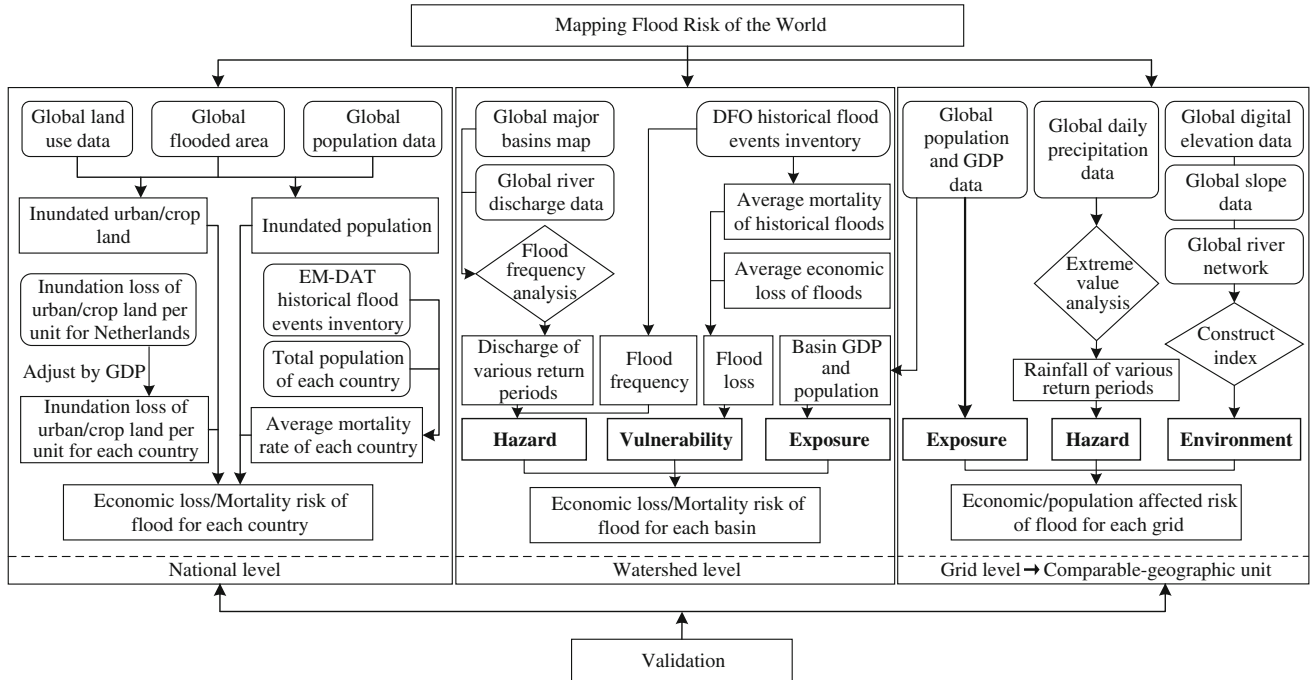


Fig. 1 Technical flowchart for mapping flood risk of the world

III, Hazards data 4.6) was overlaid with the global land-use data to extract the urban and crop land in the inundated area.

Secondly, based on the international boundary data, for each country, the areas of inundated urban and crop land were calculated.

Thirdly, for damage evaluation, the Dutch flood damage calculation specifications (Kok et al. 2005) were applied to all nations through the adjustment of GDP (Appendix III,

Fourthly, summing the total inundated area losses led to an estimation of the potential total economic loss caused by flood in each country, using Eq. (3), which indicates the economic risk of flood

$$\text{Economic\_loss} = \text{Damage}_{\text{urban}} \times \text{Area}_{\text{urban}} + \text{Damage}_{\text{crop}} \times \text{Area}_{\text{crop}} \quad (3)$$

### 2.1.2 Mortality Risk

The mortality risk at national level was assessed through a combination of flood hazard modeling and flood mortality rate estimation. It mainly consists of the following three steps:

Firstly, the global flood inundation-extent dataset was overlaid with gridded global population density data (Appendix III, Exposures data 3.1) to calculate total population in the inundated area for each country.

Secondly, flood mortality rate for each country was estimated as the average ratio of annual flood mortality to total population using the mortality data from EM-DAT (Appendix III, Disasters data 5.4) and population data from World Bank (Appendix III, Exposures data 3.2). It can be given in Eq. (4) and indicates the vulnerability in each country.

$$V = \frac{1}{N} \sum_{i=1}^N \frac{\text{Mortality}_i}{\text{Total}_{p_i}} \quad (4)$$

where  $N$  is the number of years;  $\text{Mortality}_i$  is the flood mortality in year  $i$ ;  $\text{Total}_{p_i}$  is the total population of the country in year  $i$ .

Thirdly, the number of exposed population in flood inundated areas for each country was multiplied by the mortality rate of the country, and as a result, the flood mortality risk was obtained.

## 2.2 Mapping Flood Risk at Watershed Level

The risk assessment at watershed level can provide better understanding of flooding process and benefit flood risk management. Flood risk was assessed mainly by hazard, exposure, and vulnerability, with the consideration of specific hydrological features within watersheds. The main steps are as follows:

Firstly, representative hydrological stations were selected for each of the global major basins according to the criteria locating in the low reach of the main stream, and covering over 30 years discharge observation.

Secondly, flood frequency analysis was conducted with monthly discharge data of these representative stations (Appendix III, Hazards data 4.8), and extreme value method was used to fit the extreme discharge data considering the statistical characteristic of hydrological phenomenon (Kidson and Richards 2005). According to the extreme value theory, extreme events or samples on the tails are subject to specific distributions. The extreme data sampled through the annual maximum (AM) and peak over threshold (POT) methods can be fitted to generalized extreme value

distributions (GEV) and generalized Pareto distributions (GPD), respectively (Coles et al. 2001). Here, we used the generalized Pareto distribution to calculate extreme discharge with various return periods and expected extreme discharge. The probability density function of this distribution and the calculation of return period given a specific amount of precipitation are described in Eqs. (5) and (6):

$$f(x; \mu, \sigma, \beta) = 1 - \left(1 + \beta \frac{x - \mu}{\sigma}\right)^{-1/\beta} \quad (5)$$

$$p = \frac{1}{1 - F(x < x_m)} = \frac{1}{\int_{x_m}^{\infty} f(x) dx} \quad (6)$$

where  $f(x)$  is the probability density function (PDF);  $F(x)$  is the cumulative distribution function (CDF);  $\mu$  is the location parameter;  $\sigma$  is the scale parameter;  $\beta$  is the shape parameter;  $p$  denotes the return period of precipitation  $x_m$ . The parameters are estimated through the method of maximum-likelihood, and the precipitation corresponding to return periods of 10, 20, 50, and 100 years is calculated using the inverse function of Eq. (6).

Thirdly, for each river basin, the flood hazard index  $H$  was calculated by multiplying the extreme discharge with historical flood frequency using Eq. (7).

$$H = \text{Dis}_n \times \text{Freq}_n \quad (7)$$

where  $H$  is the flood hazard index,  $\text{Dis}_n$  is normalized extreme discharge, and  $\text{Freq}_n$  is normalized flood frequency. All the normalization procedures in this study adopt the Eq. (8) in which  $A$  is the variable to be normalized.

$$A_n = \frac{A - A_{\min}}{A_{\max} - A_{\min}} \quad (8)$$

Fourthly, for each river basin, the average economic loss and mortality of historic floods were evaluated to obtain the vulnerability index using Eqs. (9) and (10).

$$V_{\text{ecom}} = \frac{\text{Loss} - \text{Loss}_{\min}}{\text{Loss}_{\max} - \text{Loss}_{\min}} \quad (9)$$

$$V_{\text{mort}} = \frac{\text{Mortality} - \text{Mortality}_{\min}}{\text{Mortality}_{\max} - \text{Mortality}_{\min}} \quad (10)$$

Fifthly, the exposure index was calculated through the normalization of population and GDP within each river basin using Eqs. (11) and (12)

$$E_{\text{pop}} = \frac{\text{pop} - \text{pop}_{\min}}{\text{pop}_{\max} - \text{pop}_{\min}} \quad (11)$$

$$E_{\text{gdp}} = \frac{\text{gdp} - \text{gdp}_{\text{min}}}{\text{gdp}_{\text{max}} - \text{gdp}_{\text{min}}} \quad (12)$$

Sixthly, flood risk was calculated by multiplying hazard index, vulnerability index, and exposure index using Eq. (13).

$$R = H \times E \times V \quad (13)$$

Finally, flood risk maps corresponding to hazard index ( $H$ ) containing extreme discharge with return periods of 10, 20, 50, and 100 years were obtained, and the results were normalized using Eq. (8) and classified into various levels for each basin.

### 2.3 Mapping Flood-Affected Risk at Grid Level and Comparable Geographic Unit

For the grid level ( $1^\circ \times 1^\circ$ ), the global-gridded data of precipitation, digital elevation, slope, river network, GDP, and population were mainly used to evaluate flood hazard and exposure of population and economy. Then, through a comprehensive analysis, the global flood-affected risk at the grid level was evaluated.

In this study, from the Global Precipitation Climatology Project (GPCP) daily dataset (Appendix III, Hazards data 4.7), the series of extreme precipitation defined as consecutive 3-day accumulative precipitation above the 95th percentile was firstly extracted and then fitted to the generalized Pareto distribution. The least square method was used to estimate the GPD parameters. Then, the precipitation with return periods of 10, 20, 50, and 100 years and the expected extreme precipitation were calculated.

In each grid, the hazard index is a function of precipitation, slope, and elevation and its distance from the river, as Eq. (14)

$$H = \frac{\text{Pre}_n}{\text{Ele}_n + \text{Slp}_n + \text{Dis}_n} \quad (14)$$

where  $\text{Pre}_n$  is the normalized 3-day accumulative precipitation index;  $\text{Ele}_n$  is the normalized elevation index;  $\text{Slp}_n$  is the normalized slope index; and  $\text{Dis}_n$  is the normalized distance index.

The economy and population-affected risk for each grid were calculated by multiplying hazard index and the exposure index of population and GDP using Eqs. (15) and (16)

$$R_{\text{pop}} = H \times E_{\text{pop}} = H \times \frac{\text{pop} - \text{pop}_{\text{min}}}{\text{pop}_{\text{max}} - \text{pop}_{\text{min}}} \quad (15)$$

$$R_{\text{gdp}} = H \times E_{\text{gdp}} = H \times \frac{\text{gdp} - \text{gdp}_{\text{min}}}{\text{gdp}_{\text{max}} - \text{gdp}_{\text{min}}} \quad (16)$$

After obtaining grid-level risks, through spatial statistical analysis, the flood-affected population and economic risk at the comparable geographic unit level were calculated by aggregating the grid risks within each unit area.

Finally, flood-affected risk maps corresponding to hazard index ( $H$ ) containing extreme discharge with return periods of 10, 20, 50, and 100 years at grid level and comparable geographic unit level were obtained and the results were normalized using Eq. (8), respectively.

## 3 Results

### 3.1 Mortality and Affected Population Risk

Countries with high-mortality risk are mainly located in tropical and subtropical areas, especially in the Indian peninsula, the southern and eastern China, the Indo-China peninsula, Western Europe, and part of eastern America. These regions are densely populated and usually have abundant rainfall and surface water.

By zonal statistics of the expected risk result, the expected annual mortality risk of flood at national level is derived and ranked. The top 1 % country with the highest mortality risk of flood is Bangladesh, and the top 10 % countries are Bangladesh, China, India, Cambodia, Pakistan, Brazil, Nepal, the Netherlands, Indonesia, United States, Vietnam, Burma, Thailand, Nigeria, and Japan (Fig. 2).

### 3.2 Economic Loss and Damage Risk

From the world economic loss risk map of a 100-year flood at national level, countries with high risk are mainly distributed in areas along rivers, lakes, or the coasts of Asia, Europe, and North America. With flat landscapes and abundant water resources, these regions are also often more economically developed; therefore, these regions suffer in higher GDP losses per square meter and have greater economic risk when flood occurs. The difference in GDP leads to different potential losses per square meter for various nations. The more developed a country is, the higher its potential loss per square meter is.

By zonal statistics of the expected risk result, the expected annual economic loss risk of flood at national level is derived and ranked (Fig. 3). The top 1 % country with the highest economic loss risk of flood is United States, and the

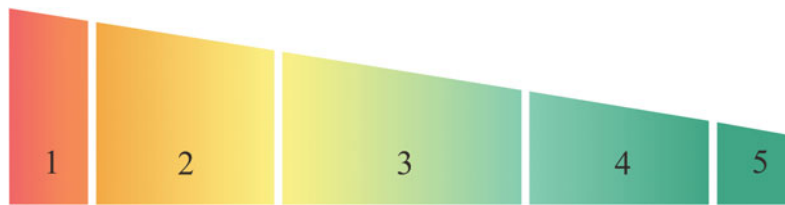


**Fig. 2** Expected annual mortality risk of flood of the world. 1 (0, 10 %) Bangladesh, China, India, Cambodia, Pakistan, Brazil, Nepal, the Netherlands, Indonesia, United States, Vietnam, Burma, Thailand, Nigeria, Japan. 2 (10, 35 %) Iraq, Argentina, Russia, Mexico, Germany, Mozambique, Egypt, South Korea, Ukraine, France, Democratic Republic of the Congo, Paraguay, Iran, Senegal, Poland, Venezuela, Ghana, Ecuador, United Kingdom, Colombia, Philippines, Canada, Laos, Italy, Guatemala, Tanzania, The Republic of Côte d'Ivoire, Hungary, Sudan, Belgium, Togo, Burkina Faso, Mali, Romania, Niger, Malaysia, Kenya, Syria. 3 (35, 65 %) Somalia, Ethiopia, Turkey, Peru, Chile, Cameroon, Sri Lanka, Azerbaijan, Madagascar, North Korea, Malawi, Serbia, Angola, South Africa, Belarus, Uganda, Chad, Uzbekistan, Spain, Kazakhstan, Uruguay, Mauritania, Australia,

Guinea, Algeria, Jordan, South Sudan, Benin, Bulgaria, Gambia, Morocco, Bosnia and Herzegovina, Slovakia, Papua New Guinea, Bolivia, Croatia, Nicaragua, Zambia, Zimbabwe, Gabon, Cuba, Afghanistan, Czech Republic, Moldova, Sierra Leone, Portugal. 4 (65, 90 %) Turkmenistan, Latvia, Liberia, Austria, Sweden, Central African Republic, Honduras, Tajikistan, Finland, Lithuania, Tunisia, Panama, Yemen, Greece, Haiti, Congo, Estonia, Saudi Arabia, Libya, Switzerland, Dominican Republic, Eritrea, Israel, Costa Rica, Norway, Burundi, Kyrgyzstan, Rwanda, Ireland, Macedonia, Armenia, Guinea-Bissau, Namibia, Denmark, Botswana, Swaziland, Georgia, Slovenia. 5 (90, 100 %) Oman, Belize, Guyana, Lesotho, Albania, Mongolia, Suriname, Equatorial Guinea, United Arab Emirates, Djibouti, Bhutan, New Zealand, Montenegro, Western Sahara, Kuwait, Iceland

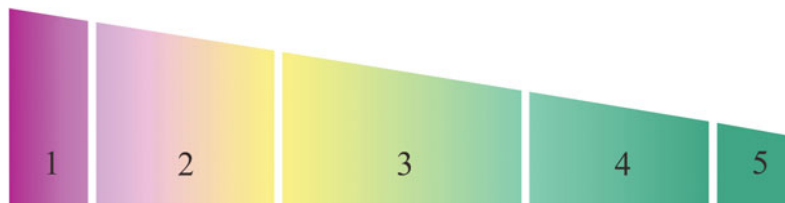


**Fig. 3** Expected annual economic loss risk of flood of the world. 1 (0, 10 %) United States, China, Japan, the Netherlands, India, Germany, France, Argentina, Bangladesh, Brazil, United Kingdom, Thailand, Myanmar, Cambodia, Canada. 2 (10, 35 %) Iraq, Belgium, Mexico, Italy, South Korea, Russia, Indonesia, Spain, Pakistan, Australia, Paraguay, Nigeria, Nepal, Poland, Finland, Hungary, Venezuela, Serbia, Colombia, Vietnam, Iran, Chile, Philippines, Malaysia, Ukraine, Romania, Egypt, Ireland, Saudi Arabia, Austria, Laos, North Korea, South Africa, Belarus, Czech Republic, Ecuador, Portugal, Ghana. 3 (35, 65 %) Switzerland, Senegal, Kazakhstan, Sweden, The Republic of Côte d'Ivoire, Norway, Turkey, Cameroon, Gabon, Cuba, Papua New Guinea, Libya, Guatemala, Slovakia, Uzbekistan, Algeria, Democratic Republic of the Congo, Azerbaijan, Togo, Sudan, Greece,

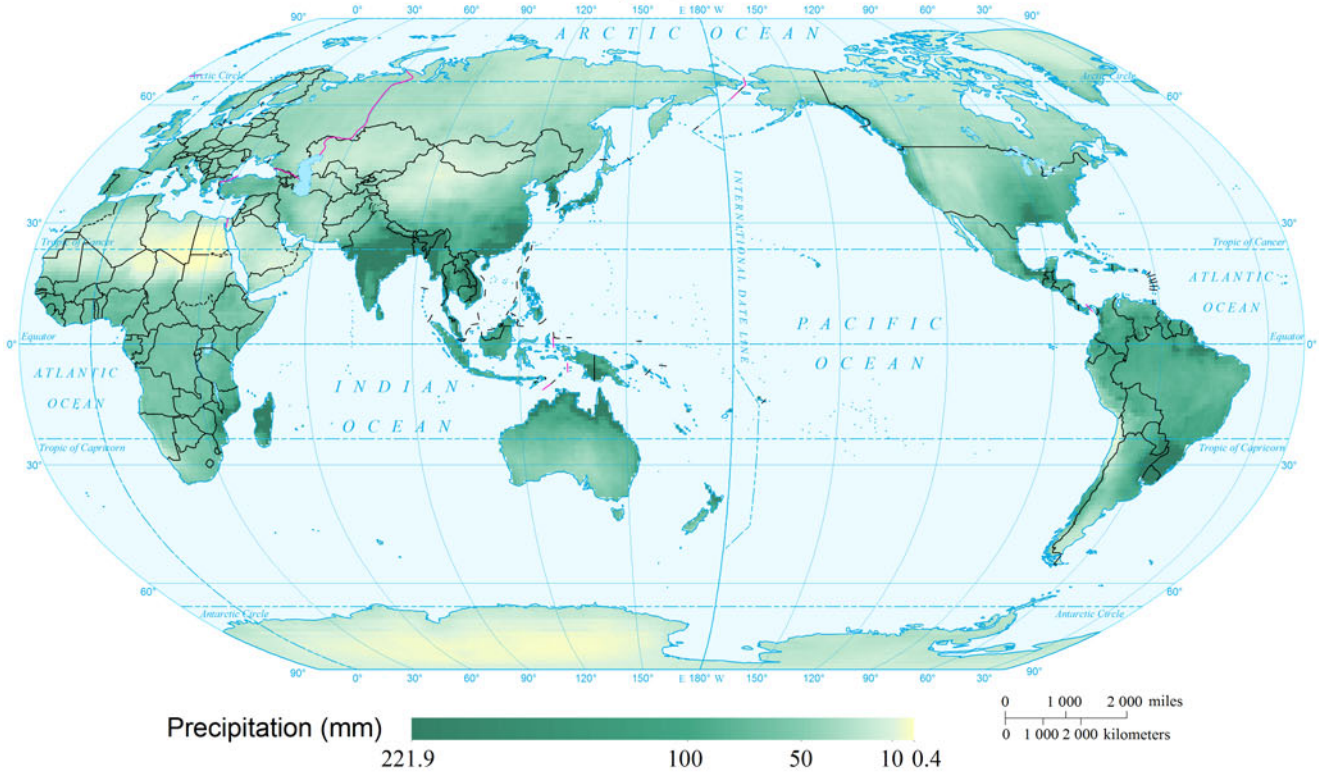
Angola, Syria, Morocco, Turkmenistan, Latvia, Niger, Peru, Tunisia, Bulgaria, Yemen, Panama, Lithuania, Burkina Faso, Somalia, Mozambique, Mauritania, Macedonia, Uruguay, Oman, Slovenia, Zimbabwe, Tanzania, Denmark, Uganda. 4 (65, 90 %) Israel, Guinea, Zambia, Benin, Kenya, Estonia, Sri Lanka, Georgia, Mali, Jordan, Malawi, Chad, Madagascar, Congo, Ethiopia, Bosnia and Herzegovina, Moldova, Bolivia, Albania, South Sudan, Nicaragua, Haiti, United Arab Emirates, Croatia, Honduras, Tajikistan, Armenia, Kyrgyzstan, Liberia, Guyana, Central African Republic, Namibia, Gambia, Afghanistan, Suriname, Botswana, Sierra Leone, Montenegro. 5 (90, 100 %) New Zealand, Costa Rica, Mongolia, Eritrea, Guinea-Bissau, Belize, Djibouti, Lesotho, Swaziland, Burundi, Rwanda, Equatorial Guinea, Bhutan, Western Sahara, Iceland

top 10 % countries are United States, China, Japan, the Netherlands, India, Germany, France, Argentina, Bangladesh, Brazil, United Kingdom, Thailand, Myanmar, Cambodia, and Canada.

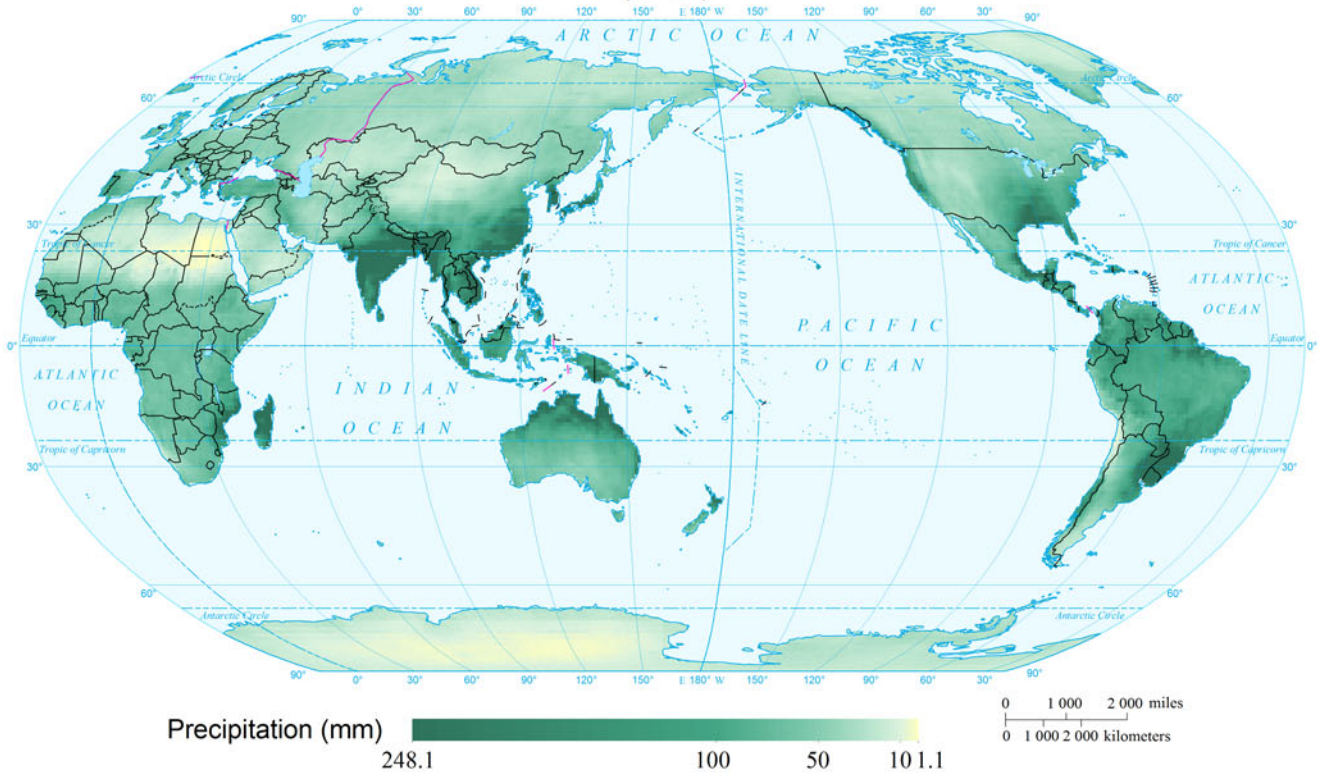
## 4 Maps



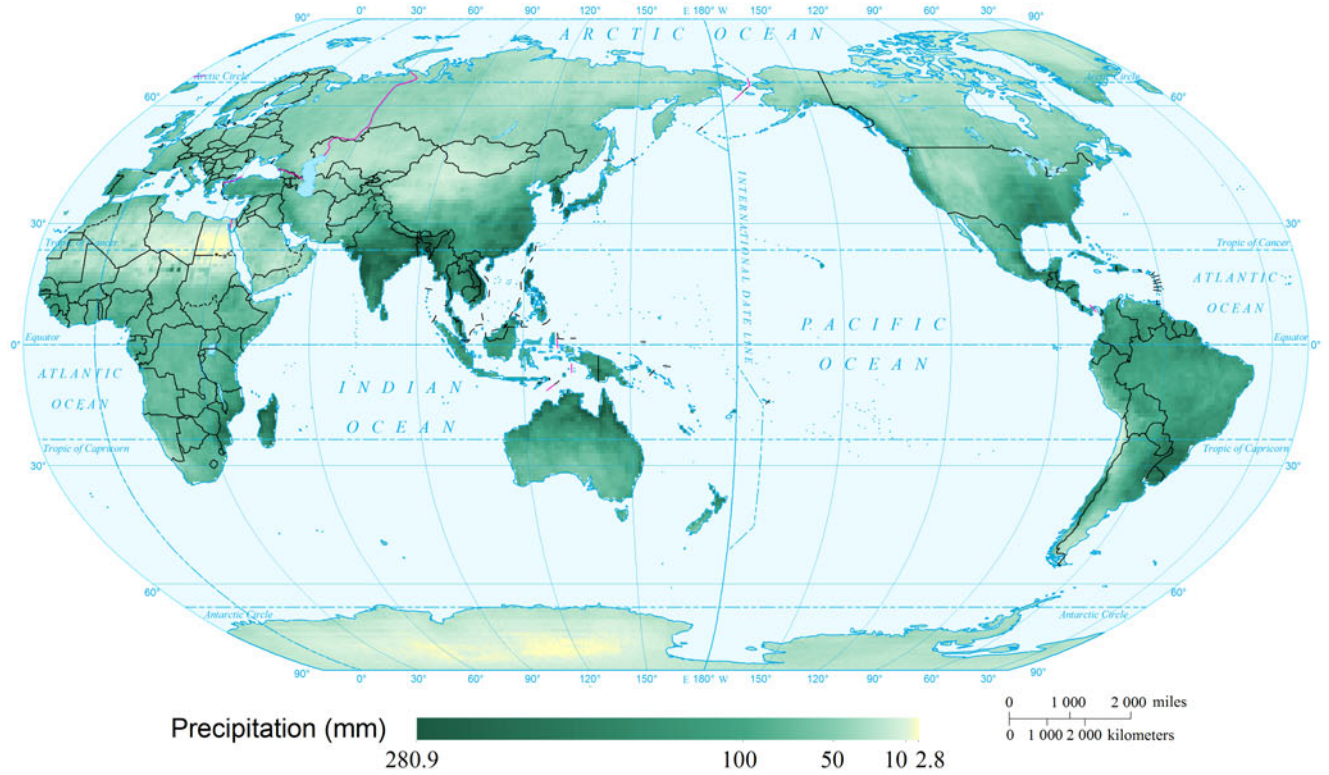
Global Accumulated 3-day Extreme Precipitation by Return Period (10a)  
(1°×1°)



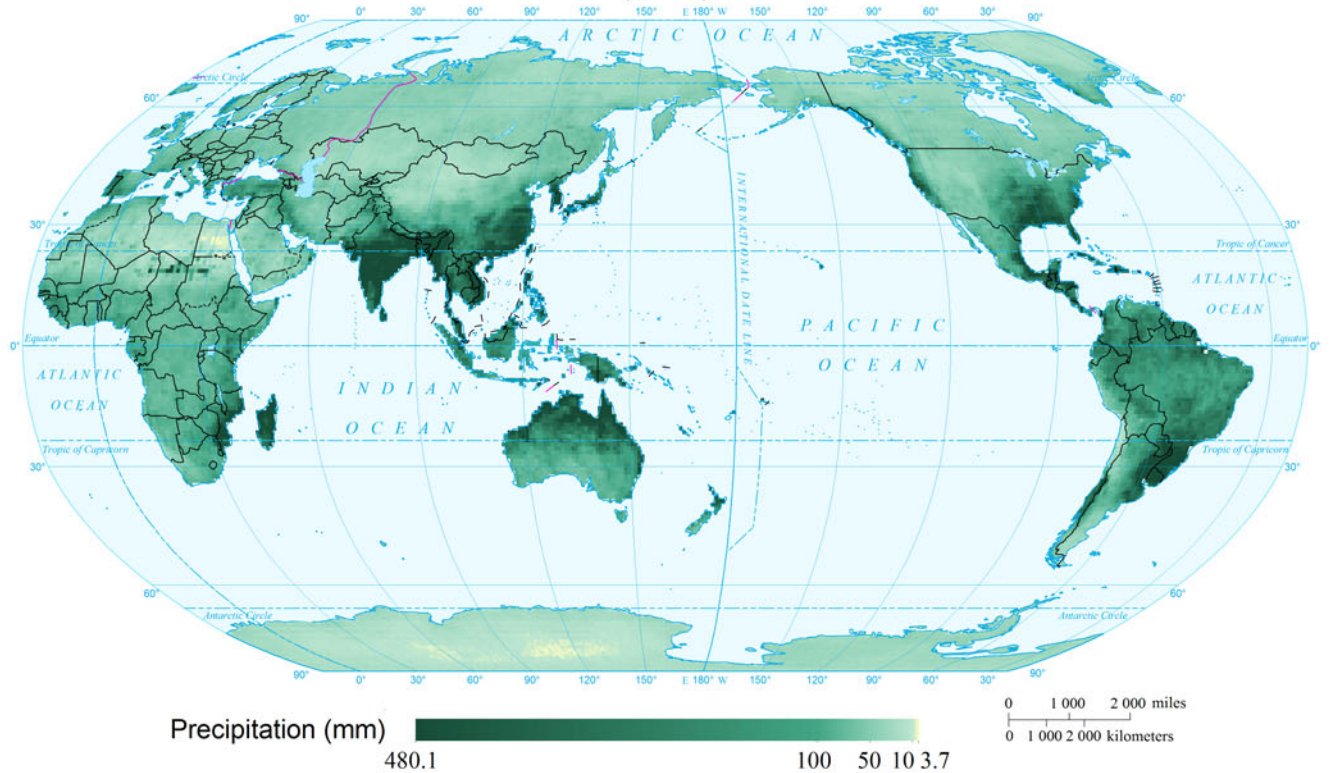
Global Accumulated 3-day Extreme Precipitation by Return Period (20a)  
(1°×1°)



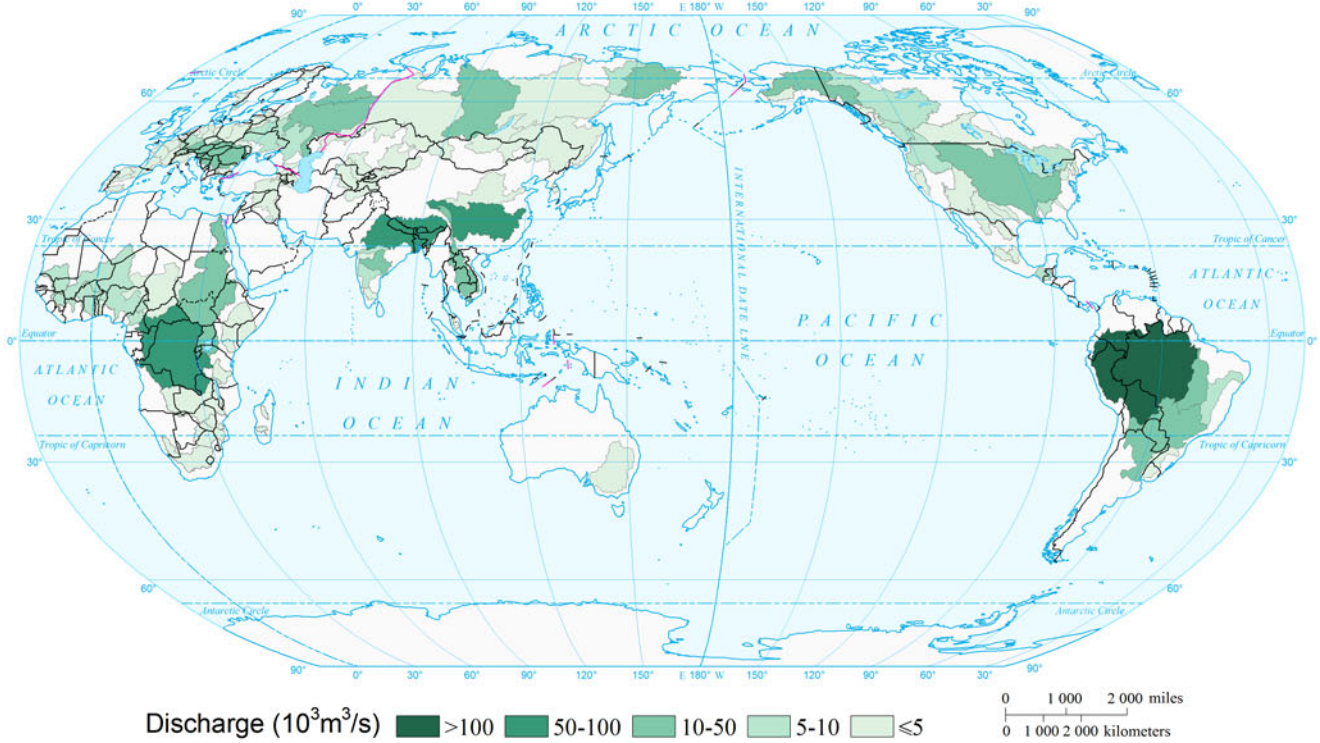
Global Accumulated 3-day Extreme Precipitation by Return Period (50a)  
(1°×1°)



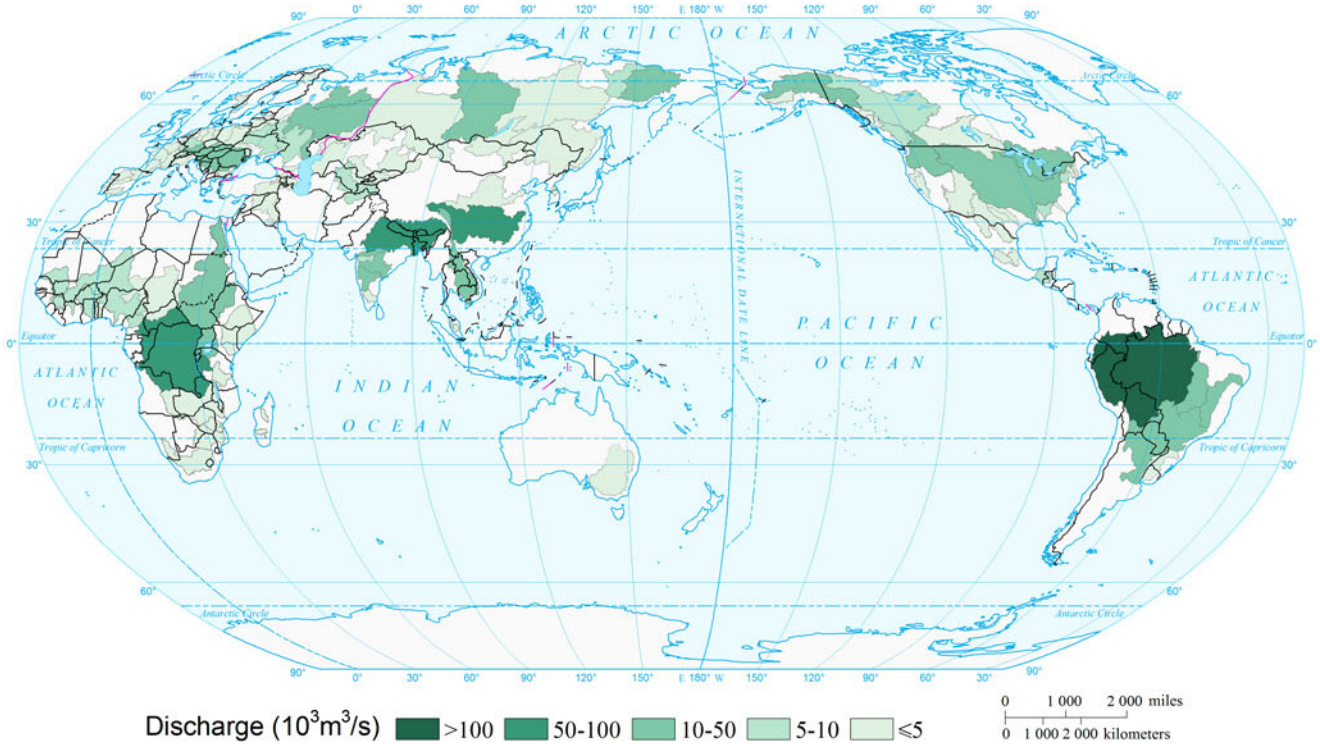
Global Accumulated 3-day Extreme Precipitation by Return Period (100a)  
(1°×1°)



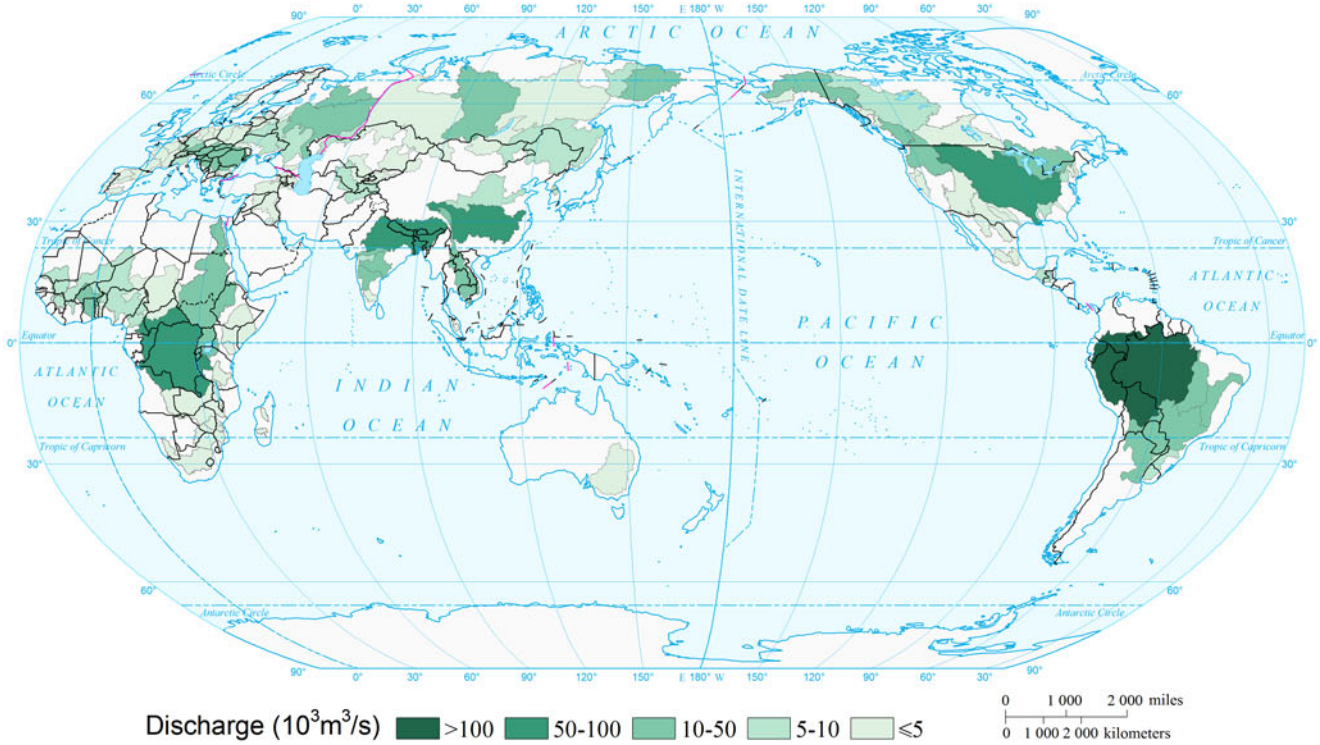
### Extreme Discharge of Global Main Watersheds by Return Period (10a)



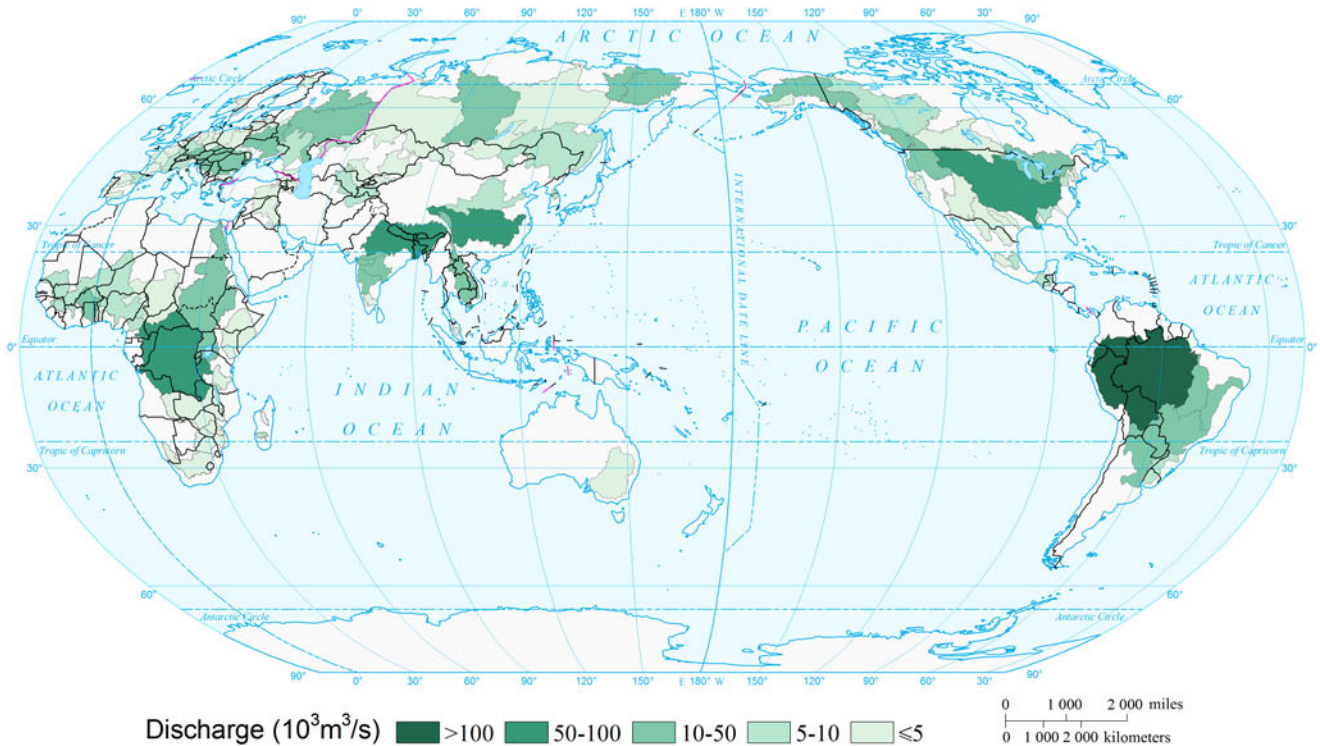
### Extreme Discharge of Global Main Watersheds by Return Period (20a)



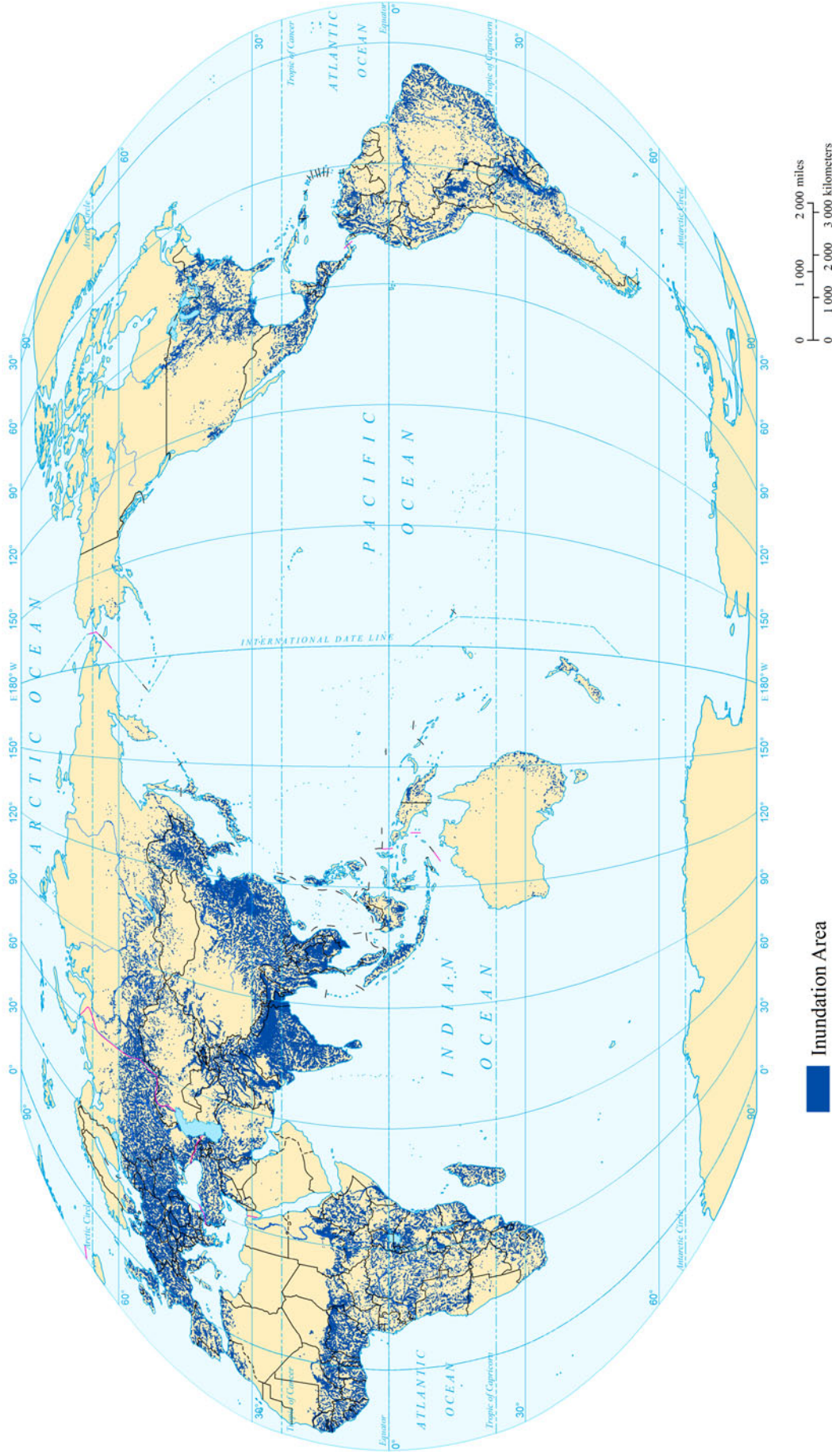
### Extreme Discharge of Global Main Watersheds by Return Period (50a)



### Extreme Discharge of Global Main Watersheds by Return Period (100a)

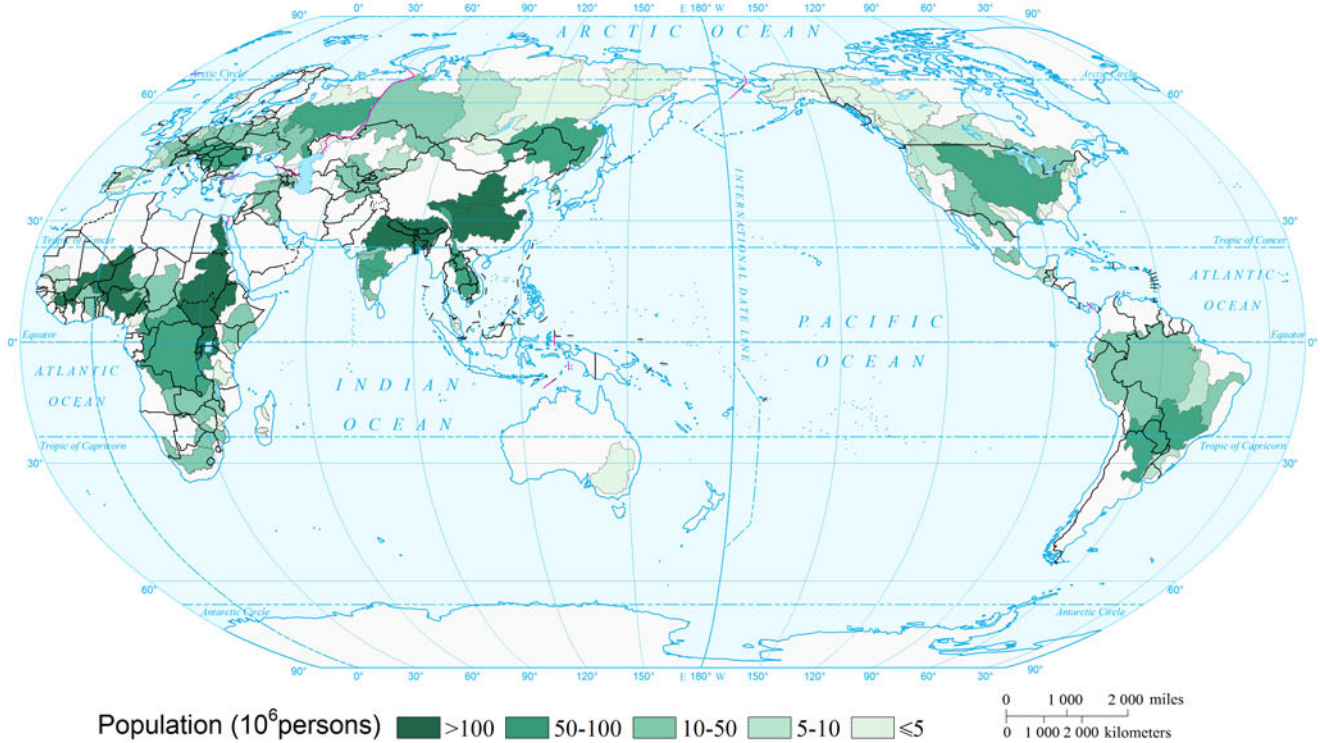


Global Flood Inundation Area by Return Period (100a)

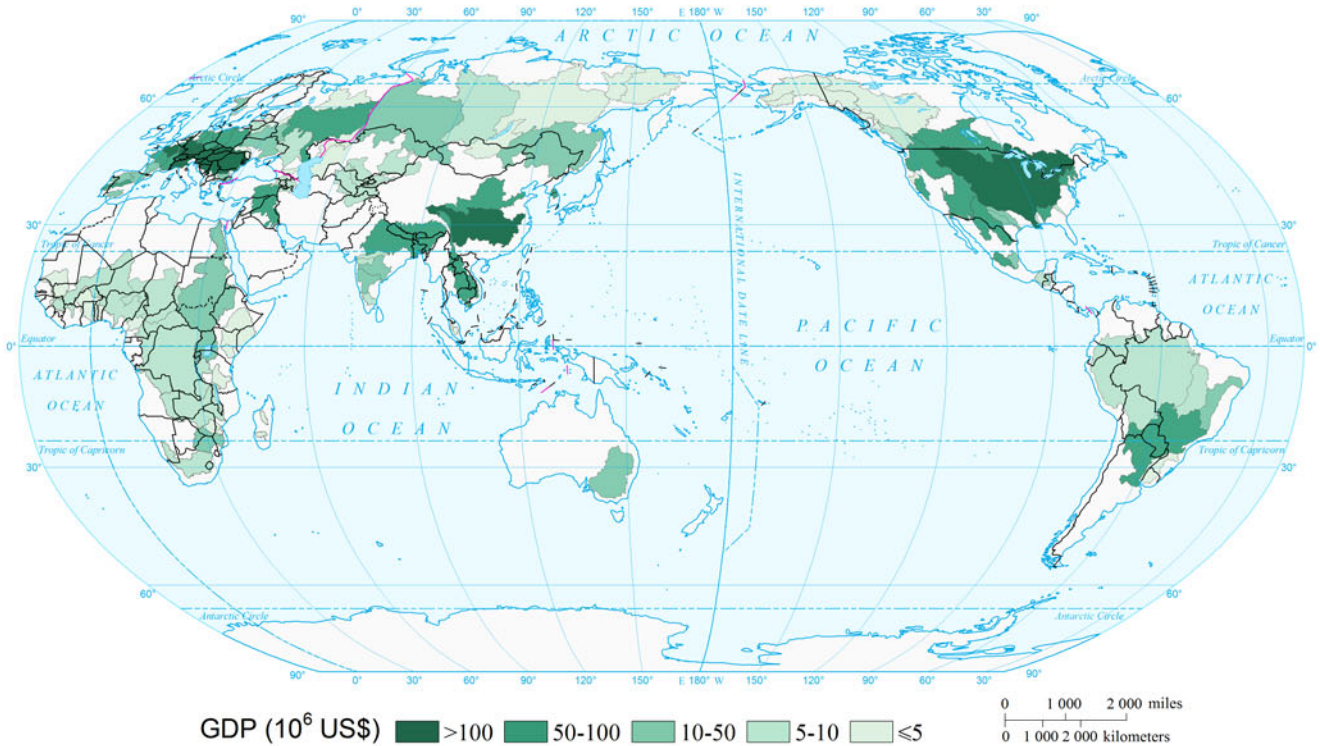


Data Source: United Nations Environment Programme (UNEP) / Global Resource Information Database (GRID)-Europe  
<http://preview.grid.unep.ch/>

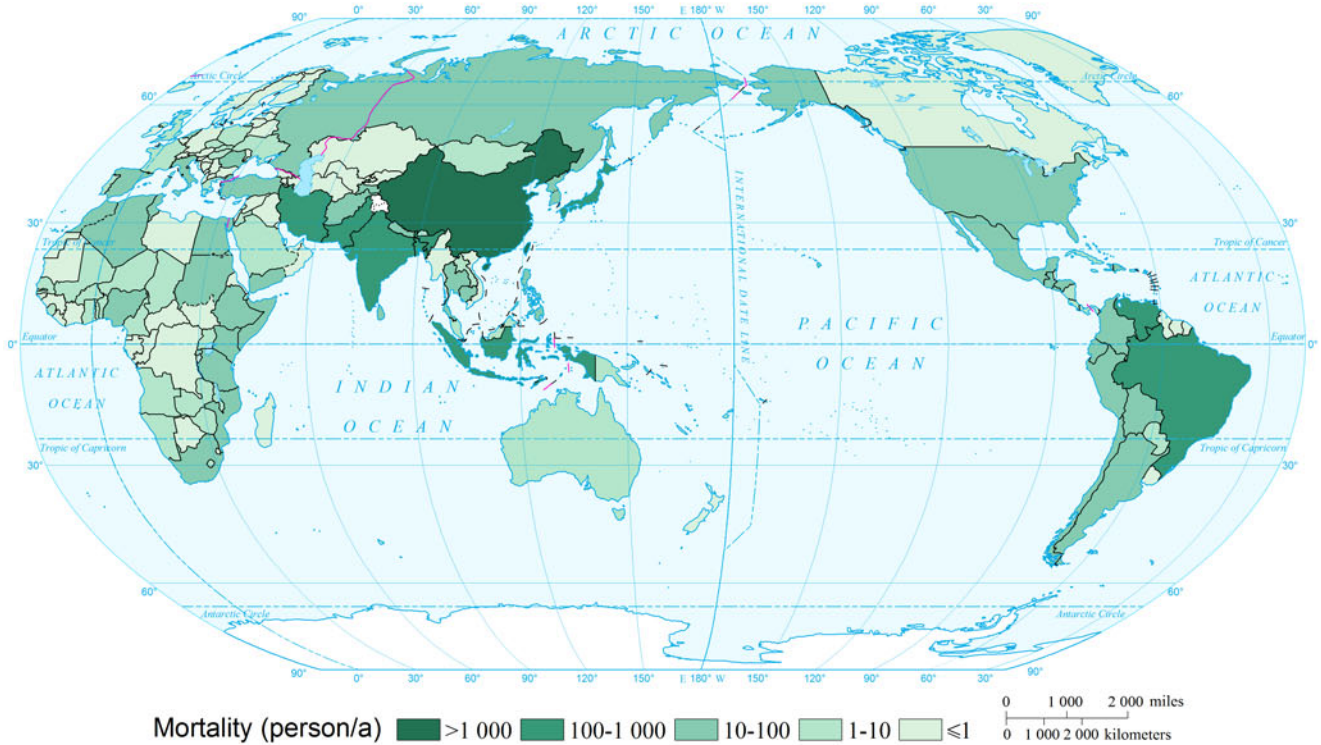
### Population of Main Watersheds of the World (2010)



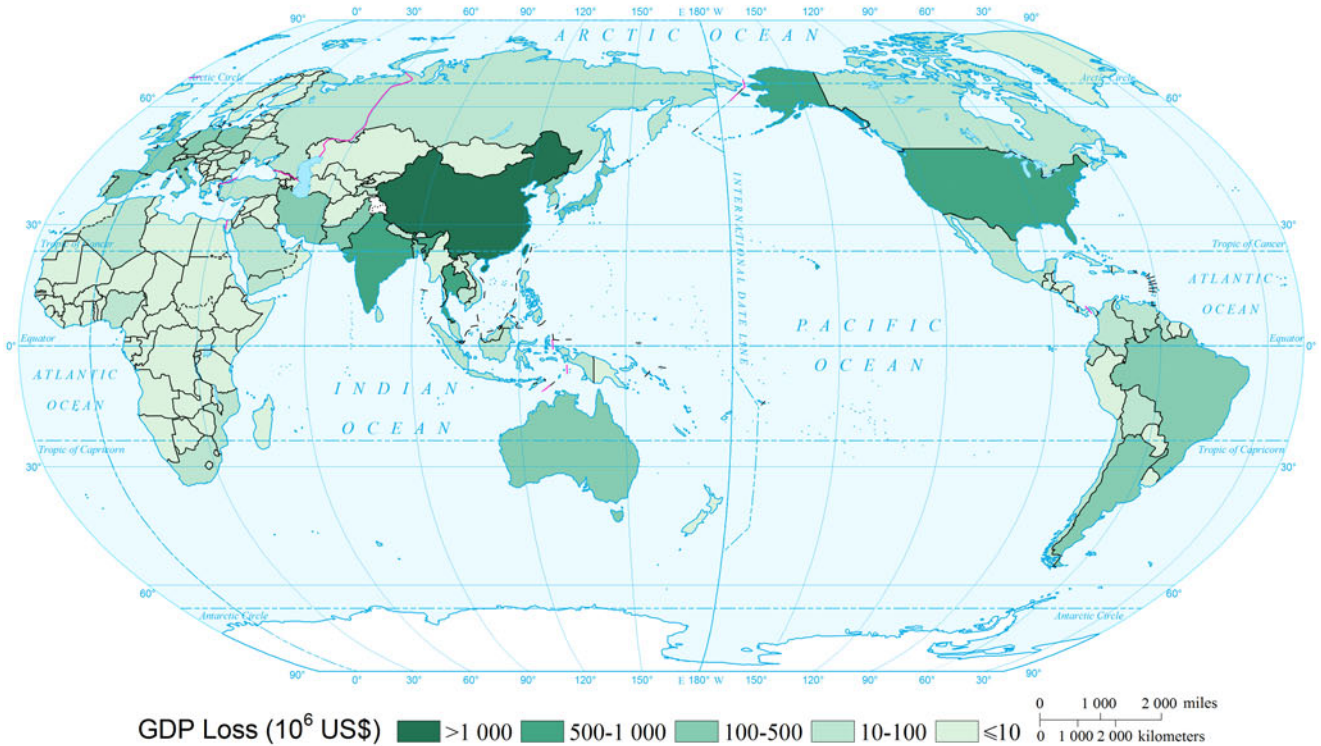
### GDP of Main Watersheds of the World (2010)



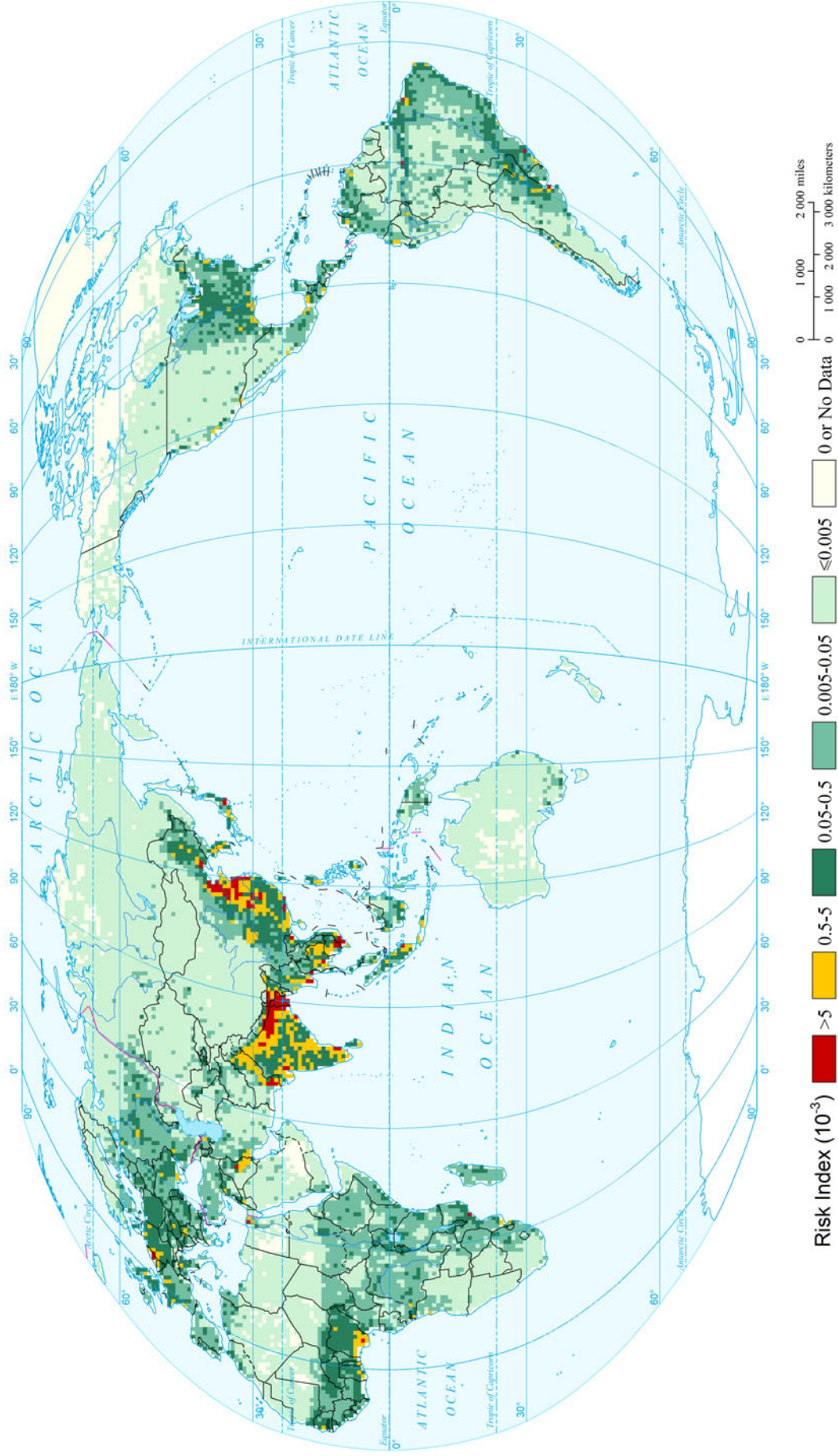
### Annual Mortality in Historical Flood Disaster of the World (1950-2012)



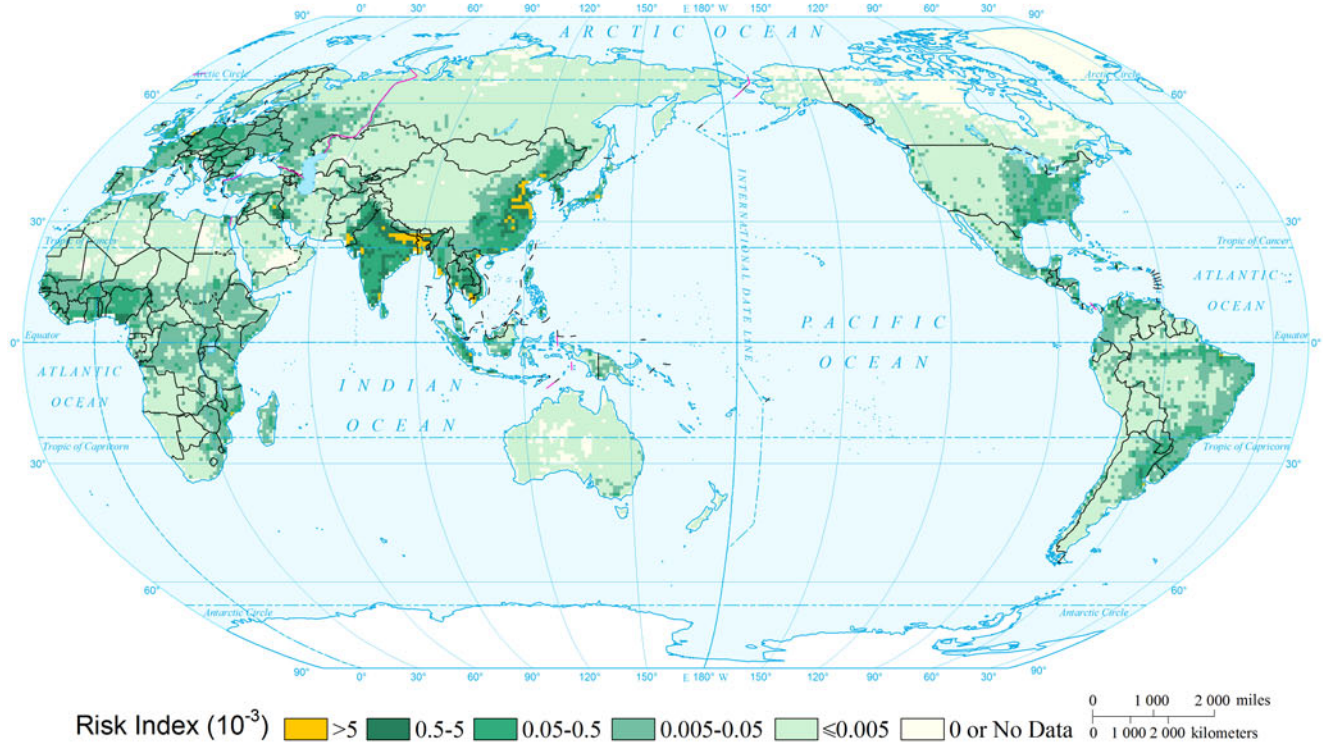
### Annual GDP Loss in Historical Flood Disaster of the World (1950-2012)



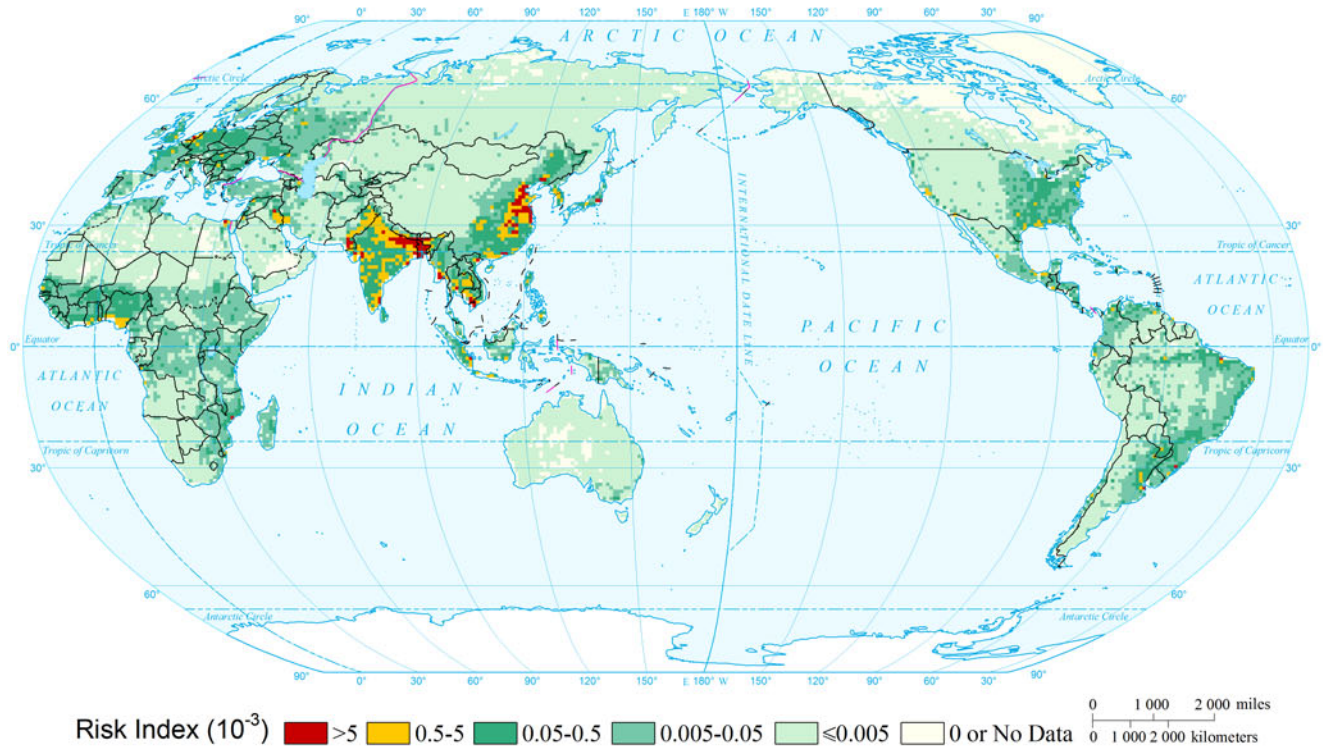
Expected Annual Affected Population Risk of Flood of the World  
( $1^{\circ} \times 1^{\circ}$ )



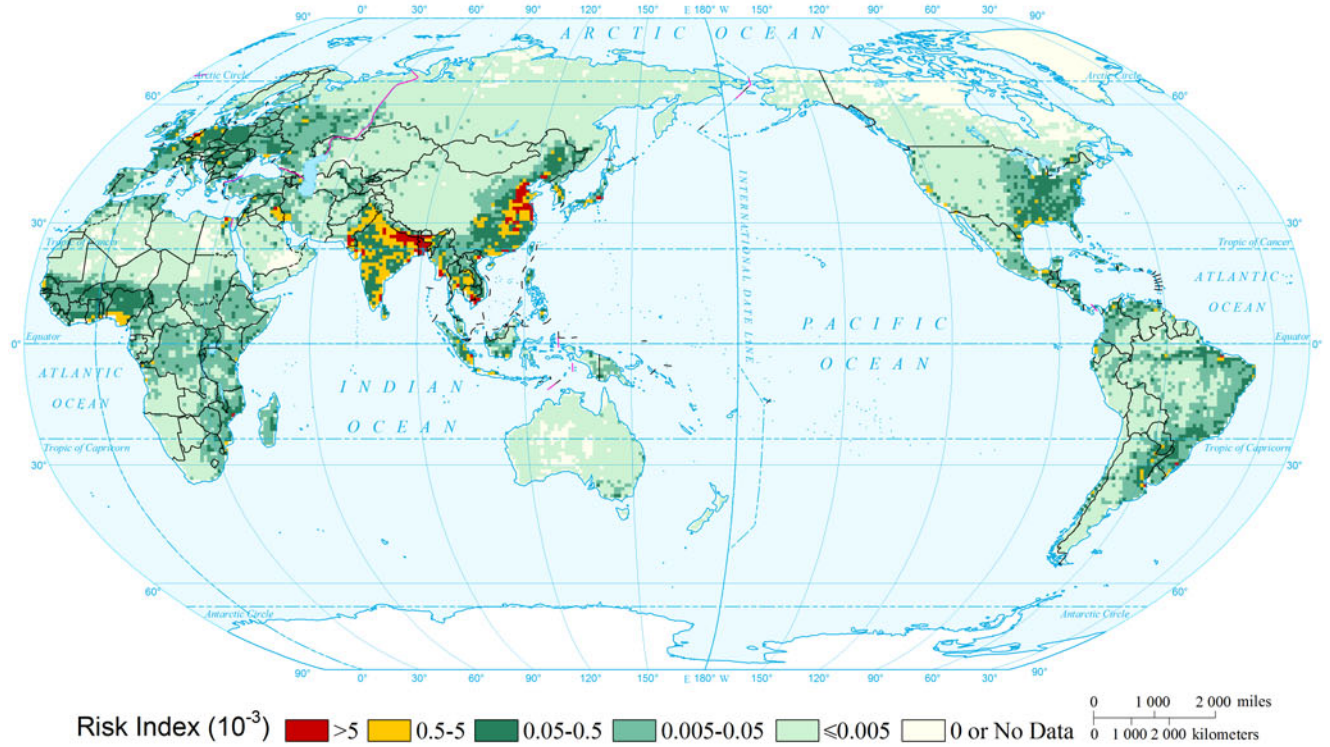
Affected Population Risk of Flood of the World by Return Period (10a)  
(1°×1°)



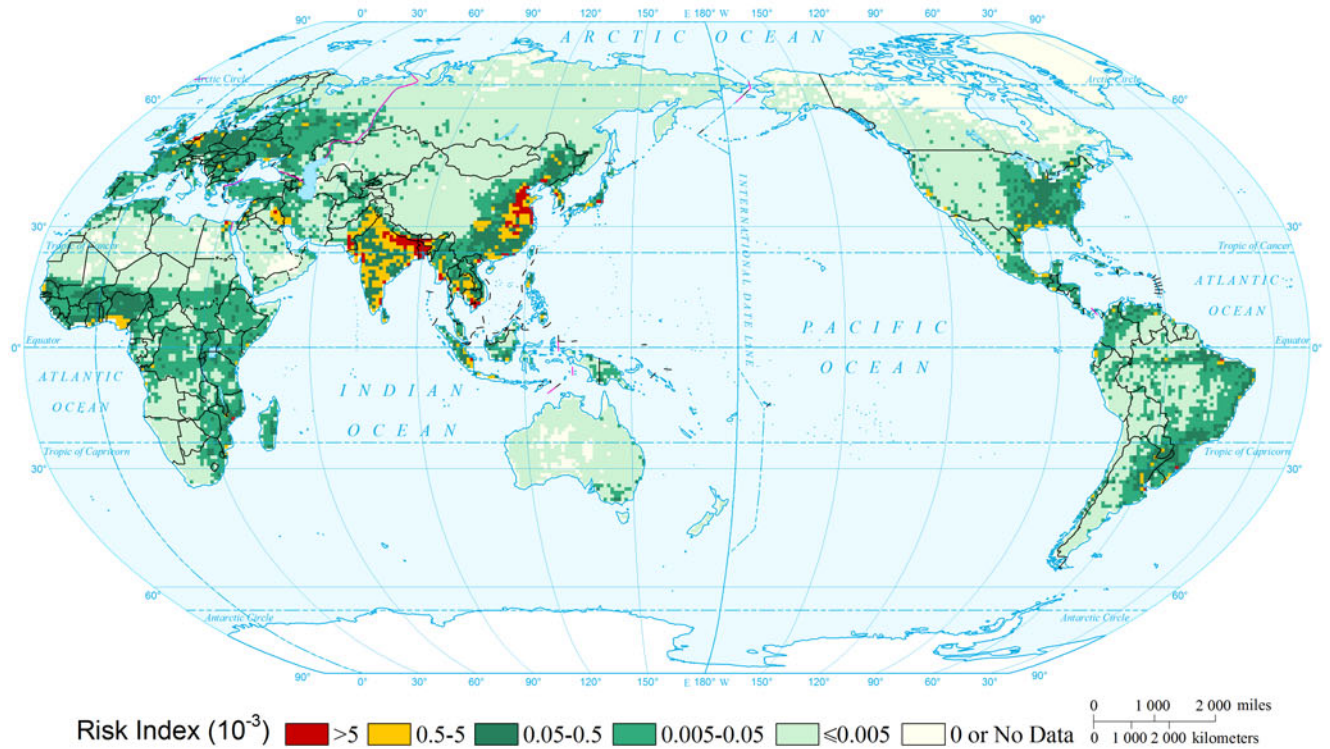
Affected Population Risk of Flood of the World by Return Period (20a)  
(1°×1°)



### Affected Population Risk of Flood of the World by Return Period (50a) (1°×1°)



### Affected Population Risk of Flood of the World by Return Period (100a) (1°×1°)

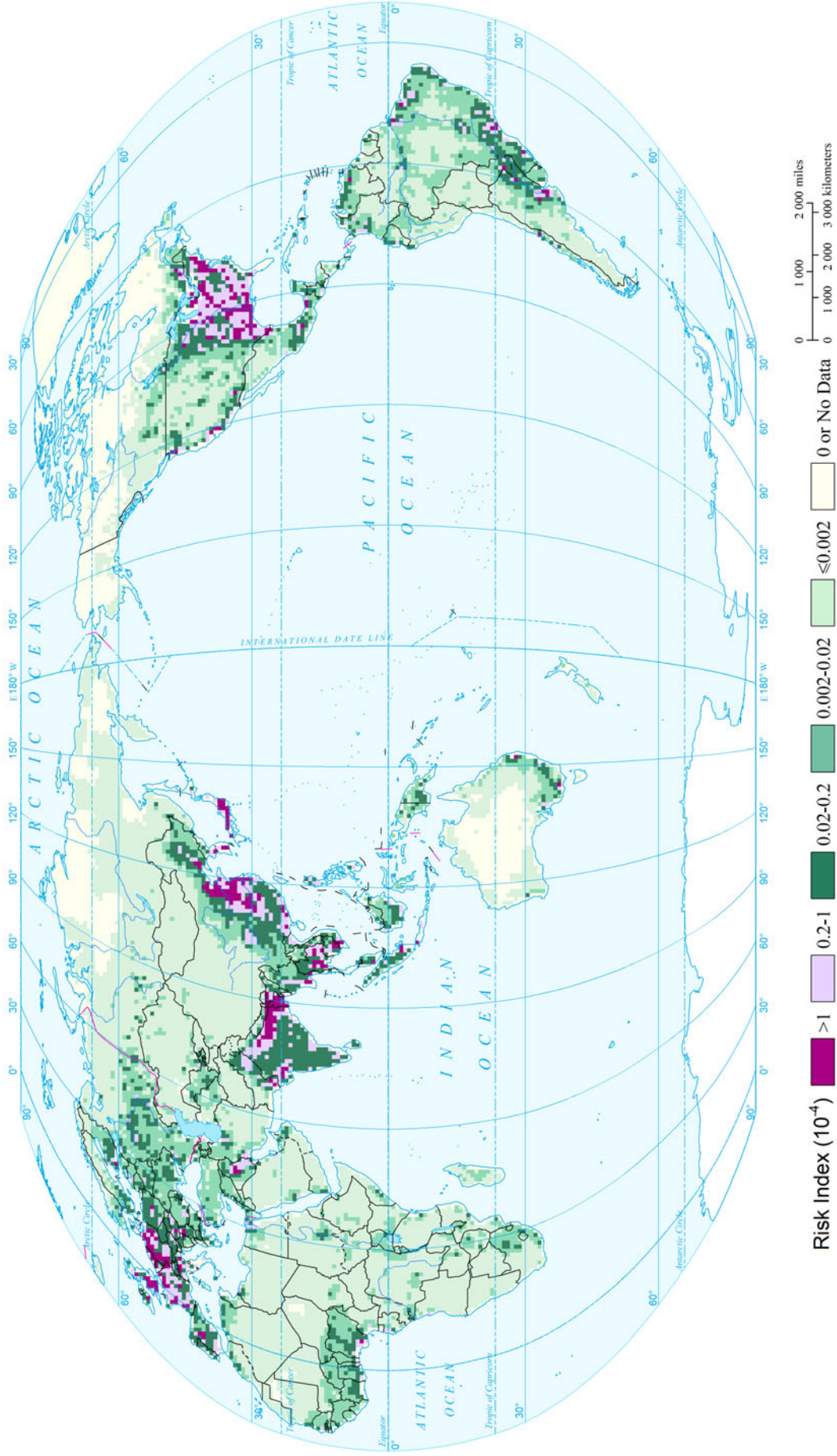




Flood

Flood and Storm Surge Disasters

### Expected Annual Affected GDP Risk of Flood of the World (1°x1°)

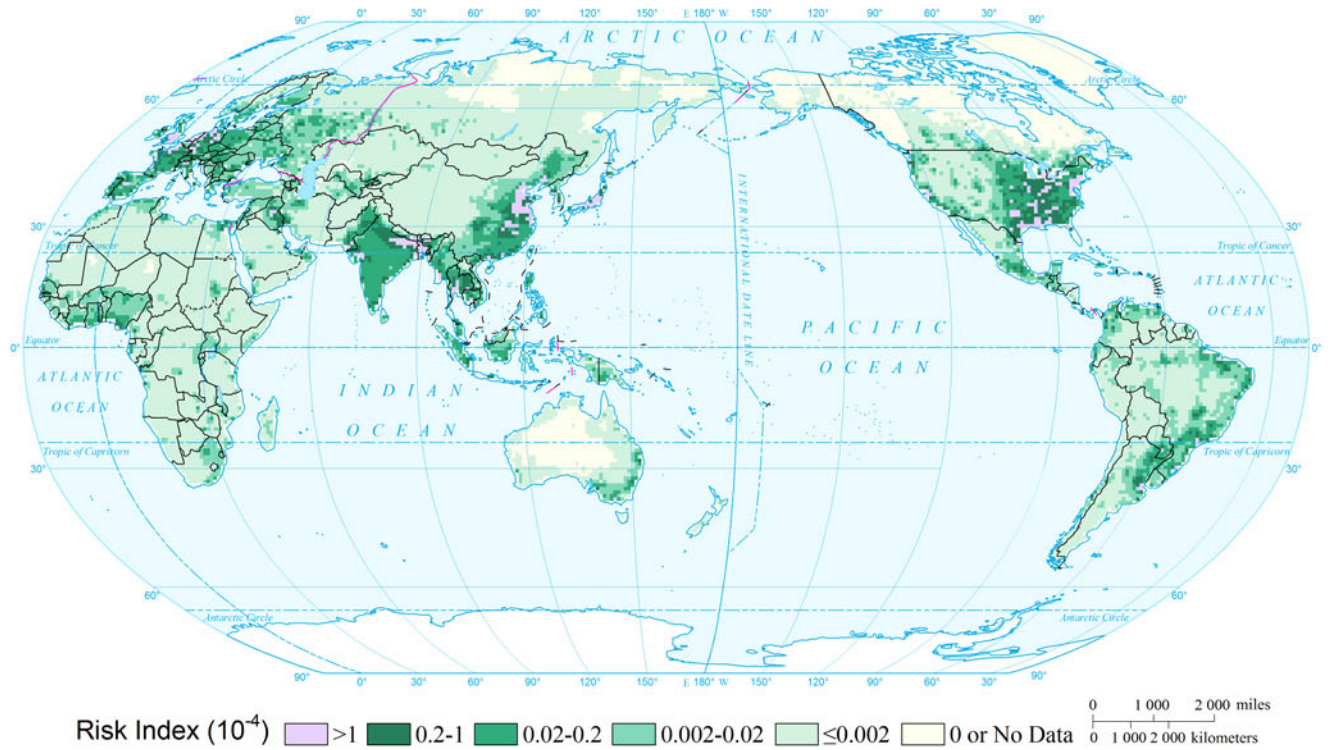


Risk Index (10<sup>-4</sup>)

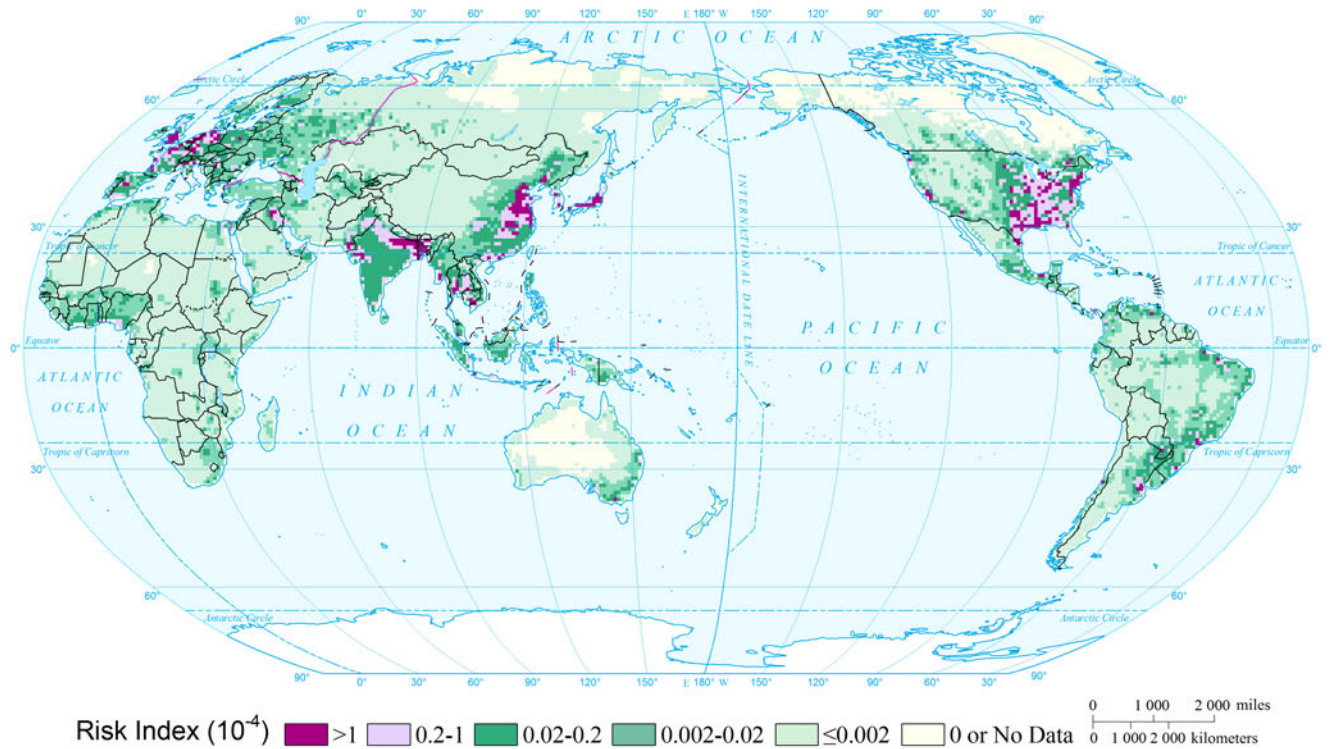
- >1
- 0.2-1
- 0.02-0.2
- 0.002-0.02
- ≤0.002
- 0 or No Data

0 1 000 2 000 miles  
0 1 000 2 000 3 000 kilometers

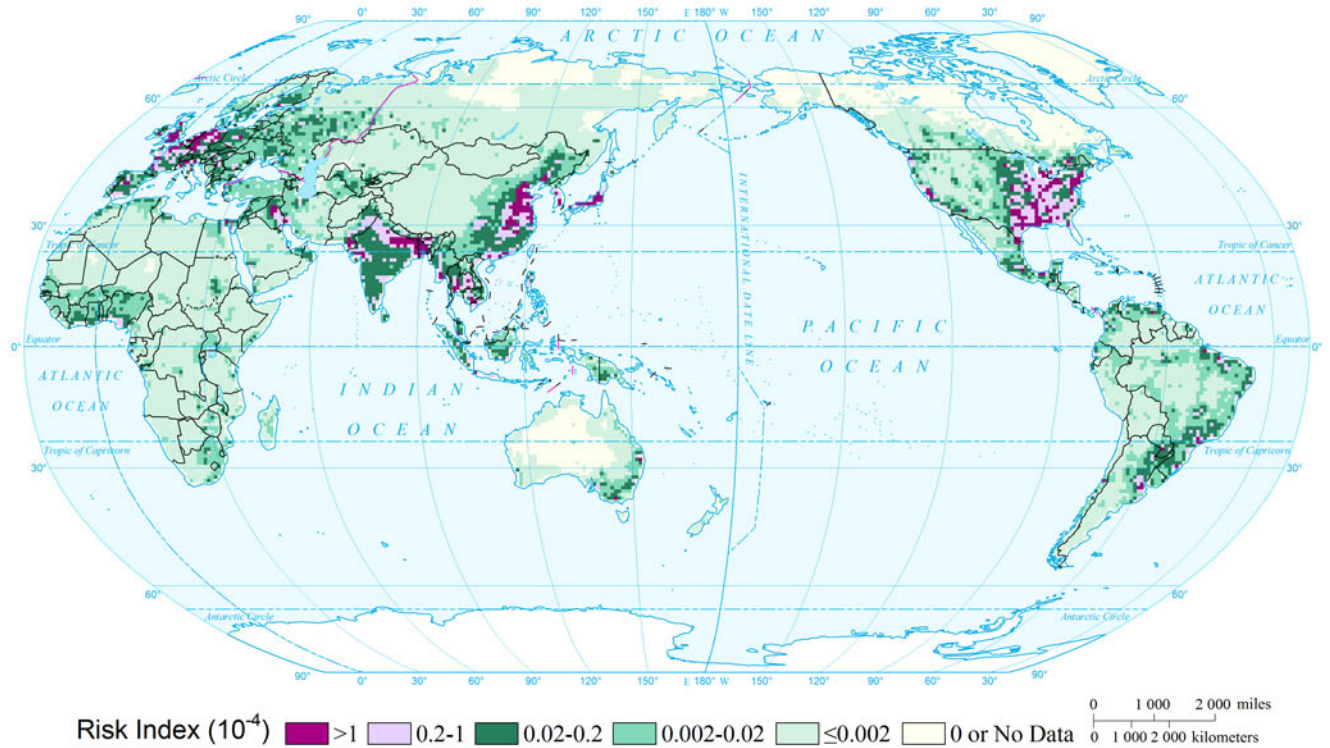
### Affected GDP Risk of Flood of the World by Return Period (10a) (1°×1°)



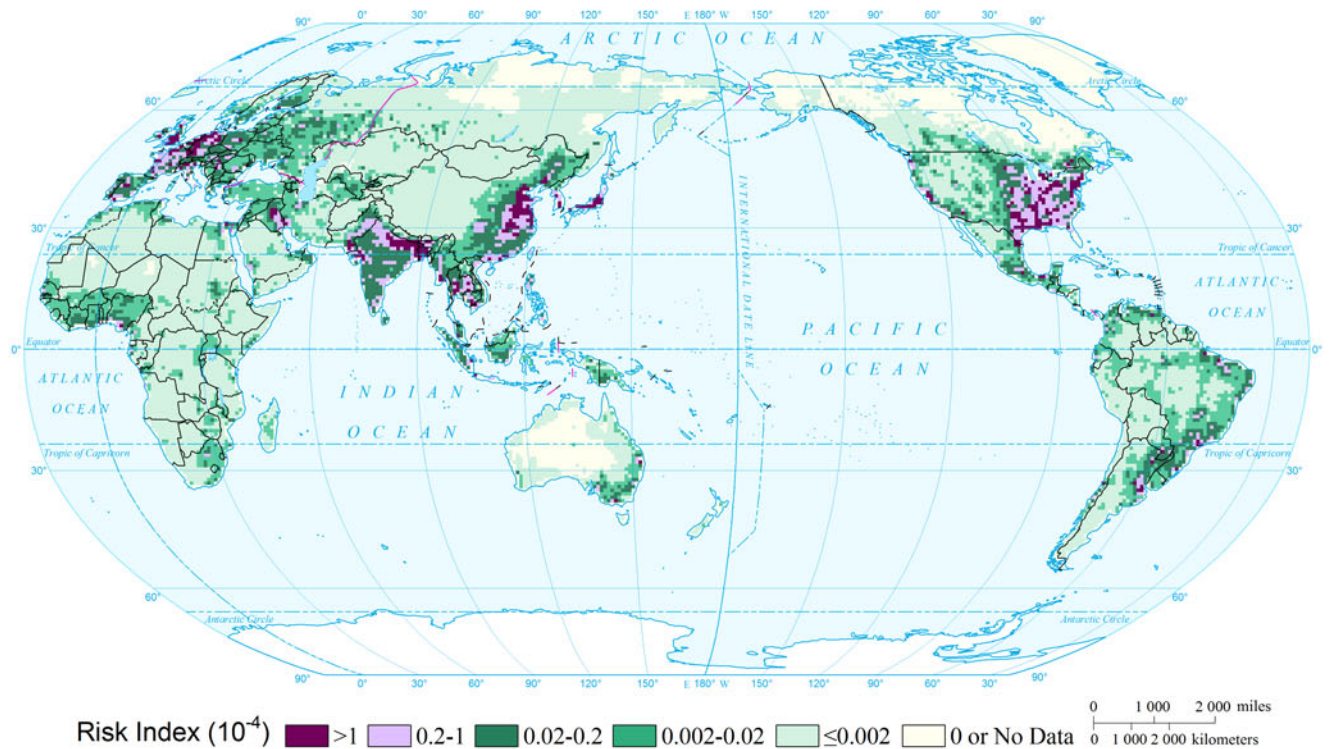
### Affected GDP Risk of Flood of the World by Return Period (20a) (1°×1°)



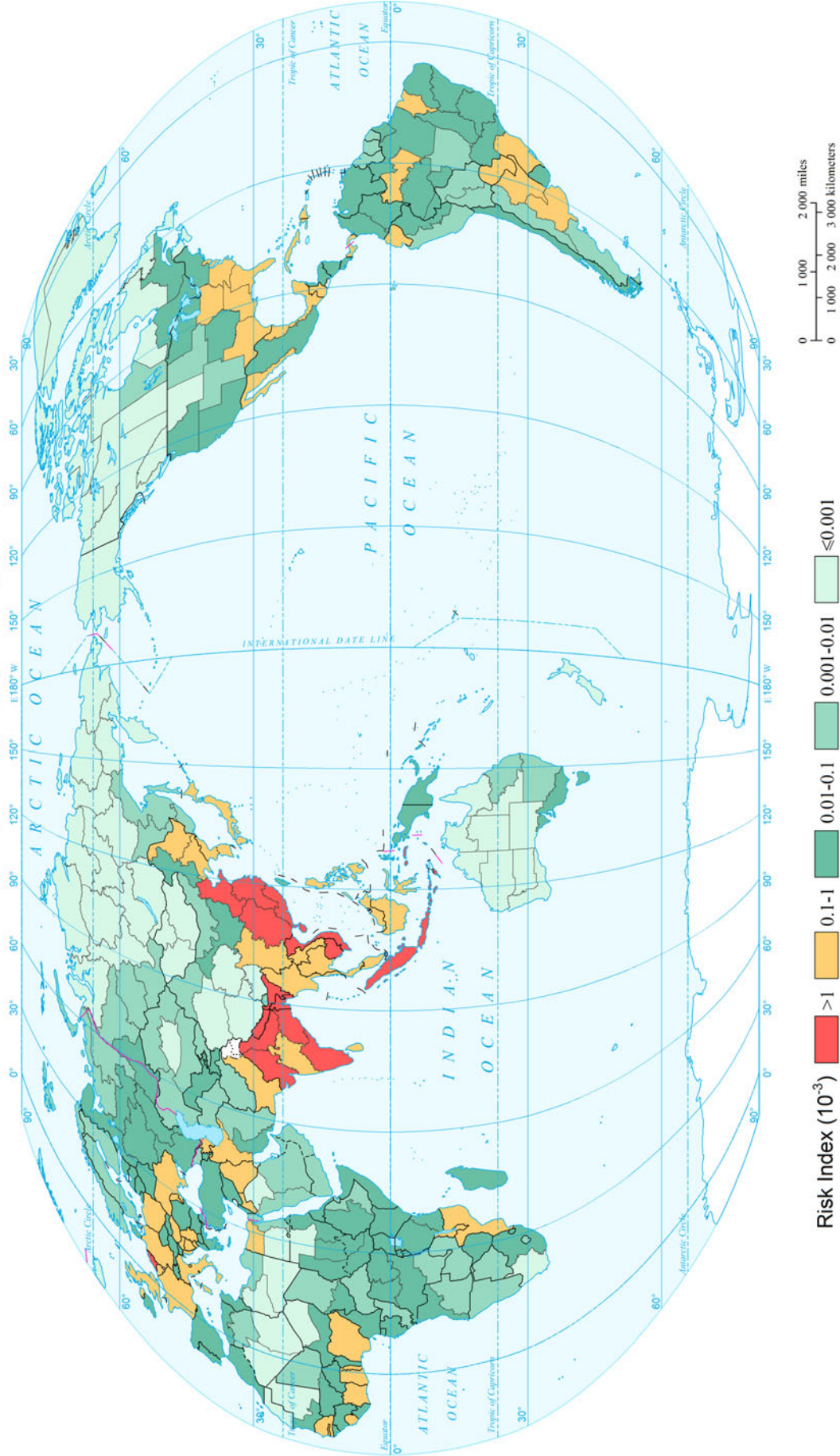
### Affected GDP Risk of Flood of the World by Return Period (50a) (1°×1°)



### Affected GDP Risk of Flood of the World by Return Period (100a) (1°×1°)



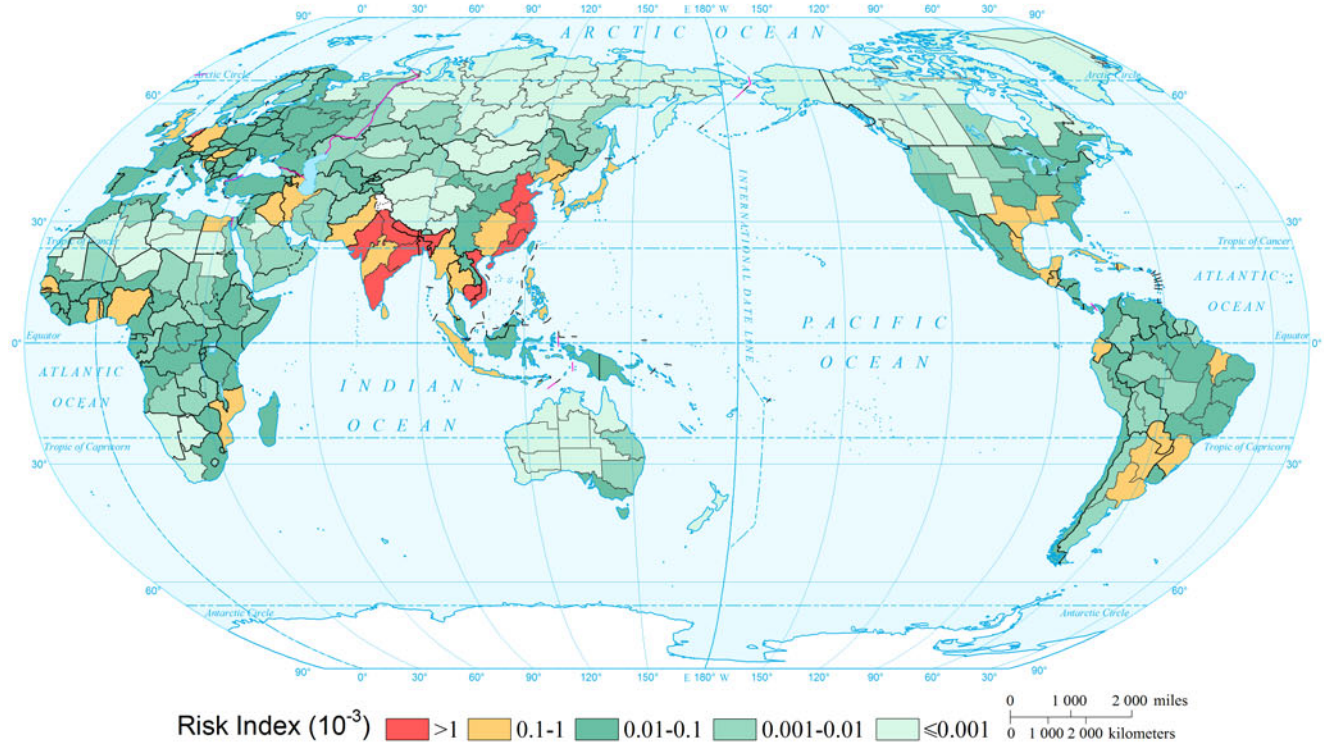
Expected Annual Affected Population Risk of Flood of the World  
(Comparable-geographic Unit)



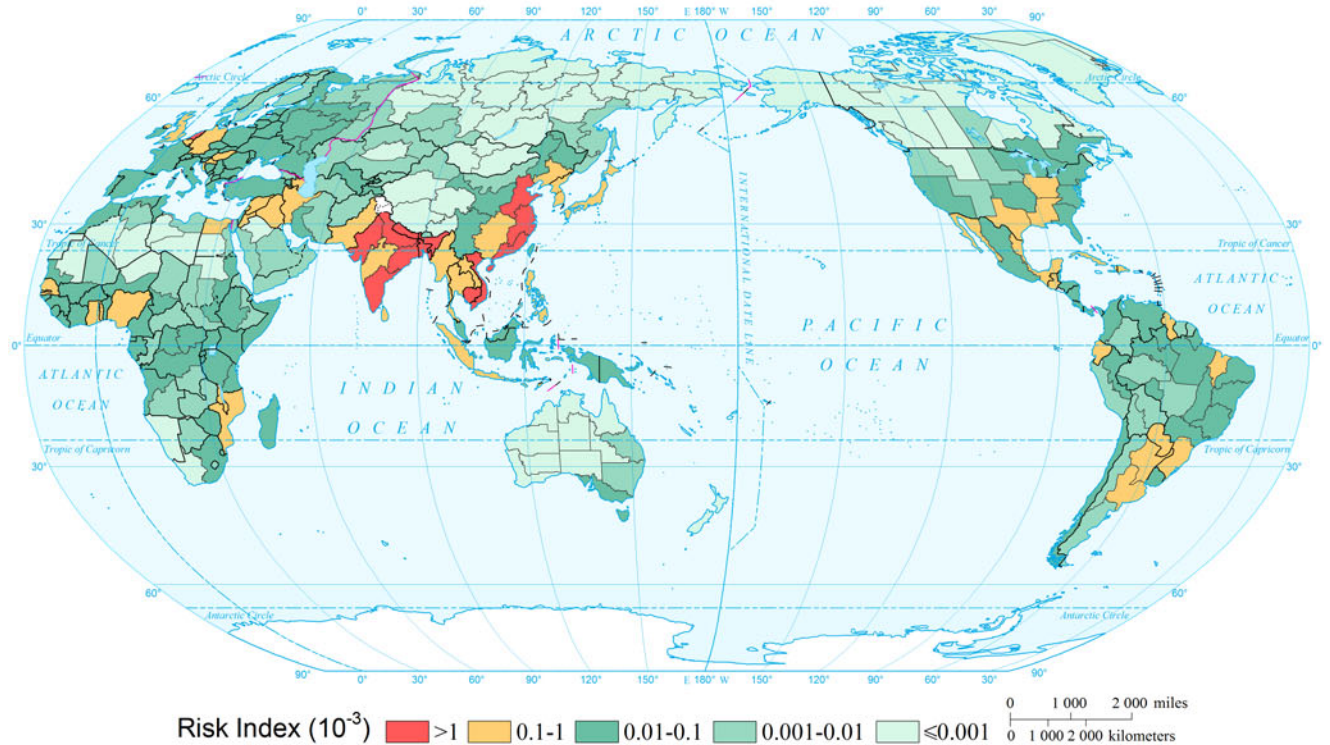
0 1 000 2 000 miles  
0 1 000 2 000 3 000 kilometers

Risk Index (10<sup>-3</sup>) >1 0.1-1 0.01-0.1 0.001-0.01 ≤0.001

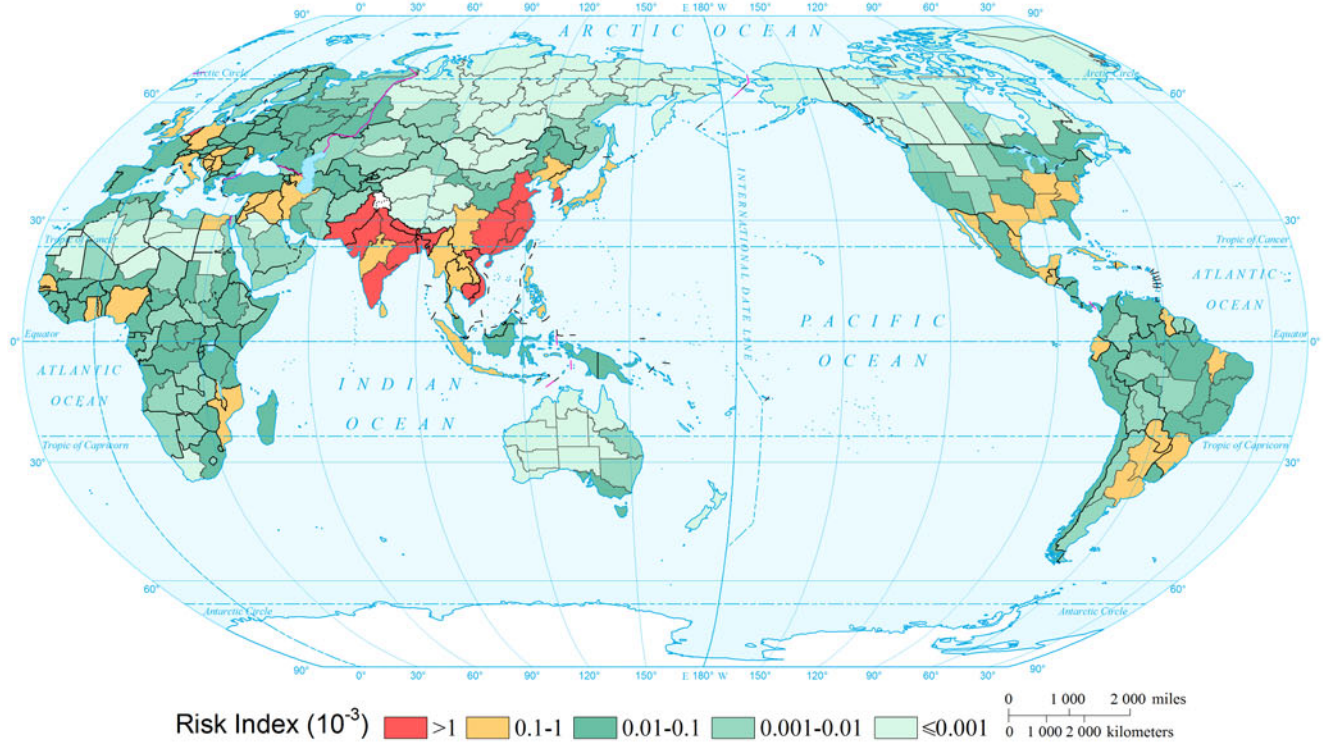
### Affected Population Risk of Flood of the World by Return Period (10a) (Comparable-geographic Unit)



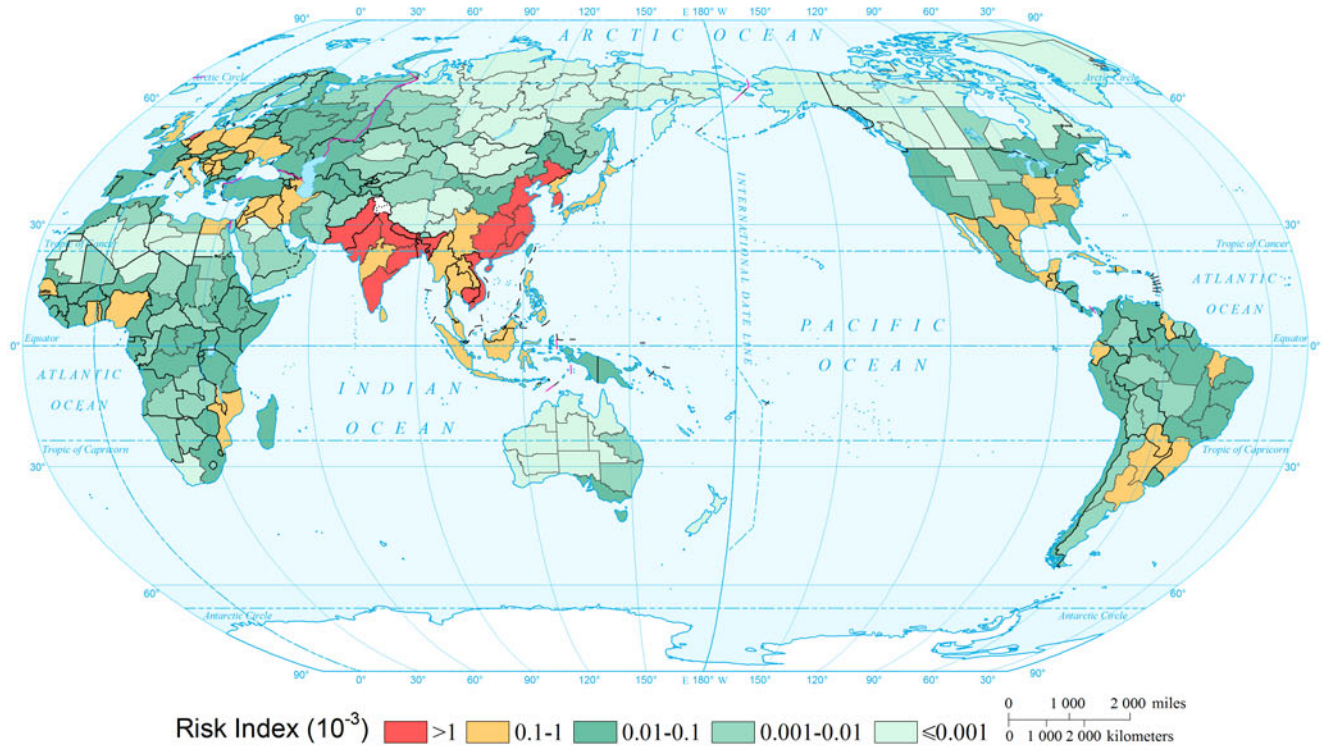
### Affected Population Risk of Flood of the World by Return Period (20a) (Comparable-geographic Unit)



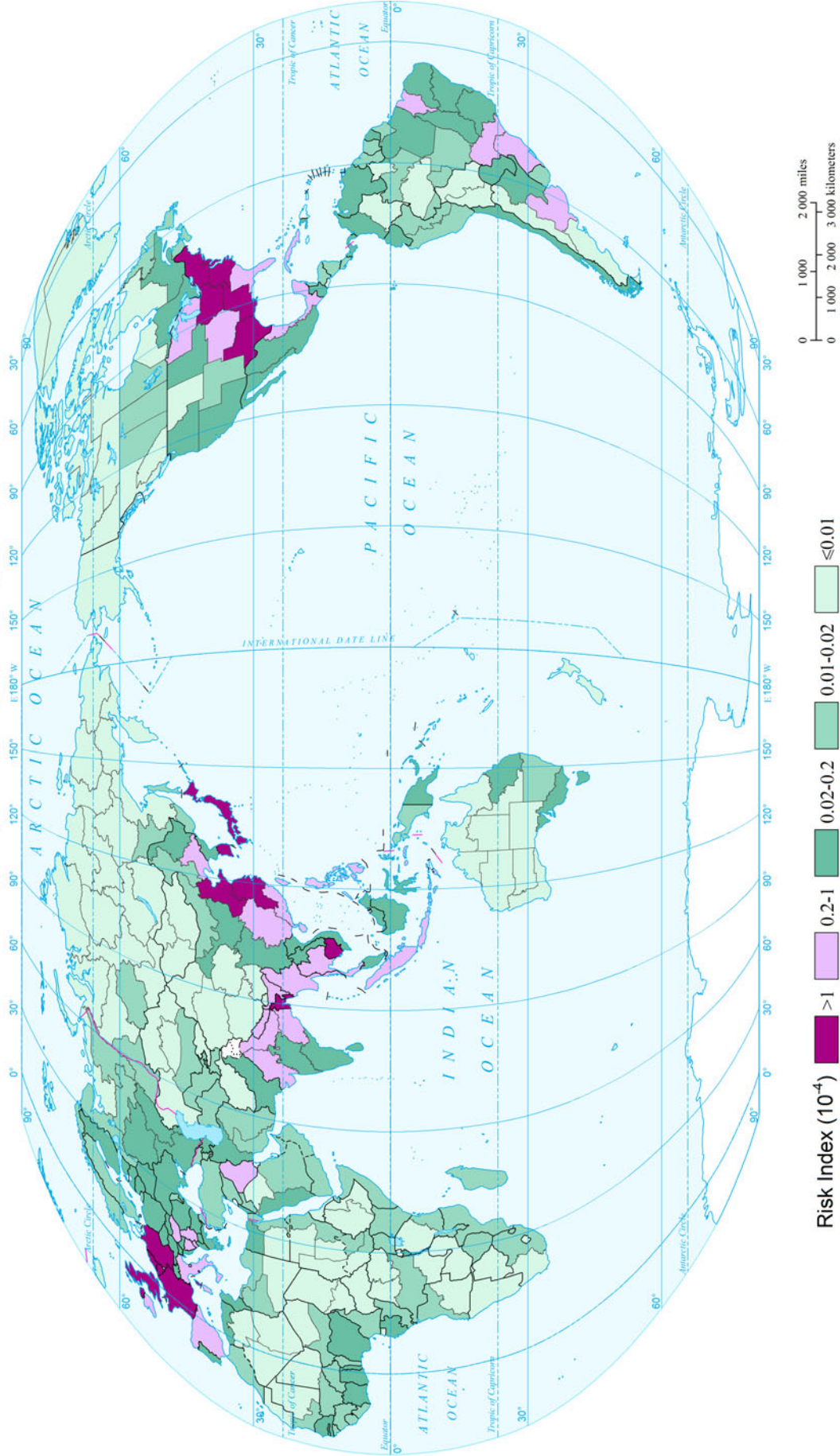
### Affected Population Risk of Flood of the World by Return Period (50a) (Comparable-geographic Unit)



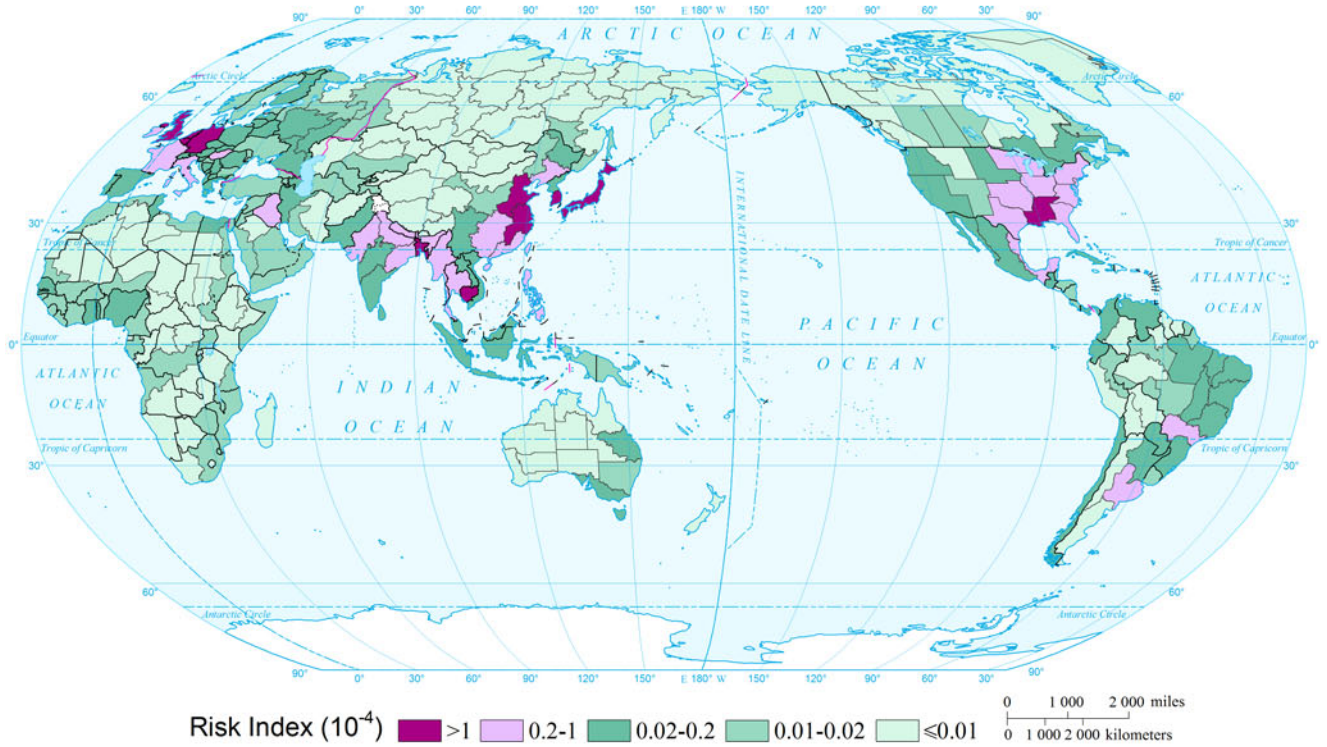
### Affected Population Risk of Flood of the World by Return Period (100a) (Comparable-geographic Unit)



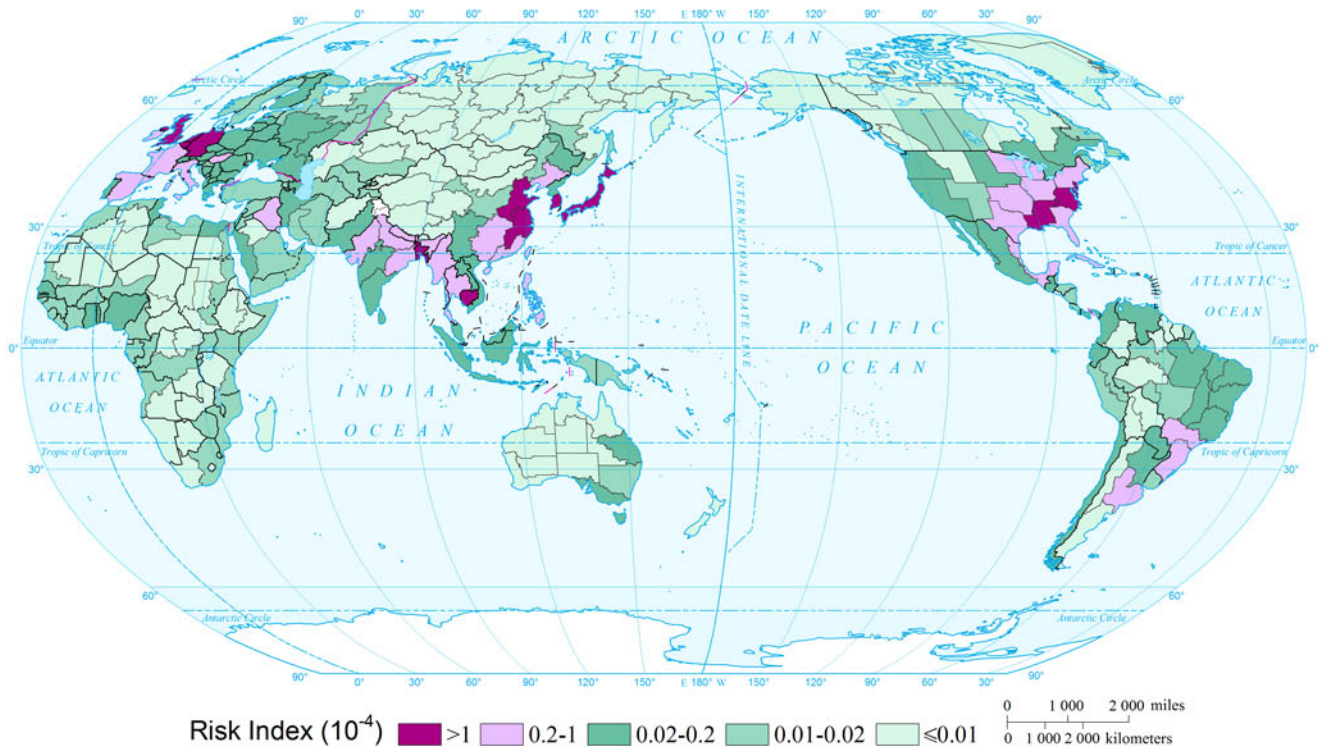
Expected Annual Affected GDP Risk of Flood of the World  
(Comparable-geographic Unit)



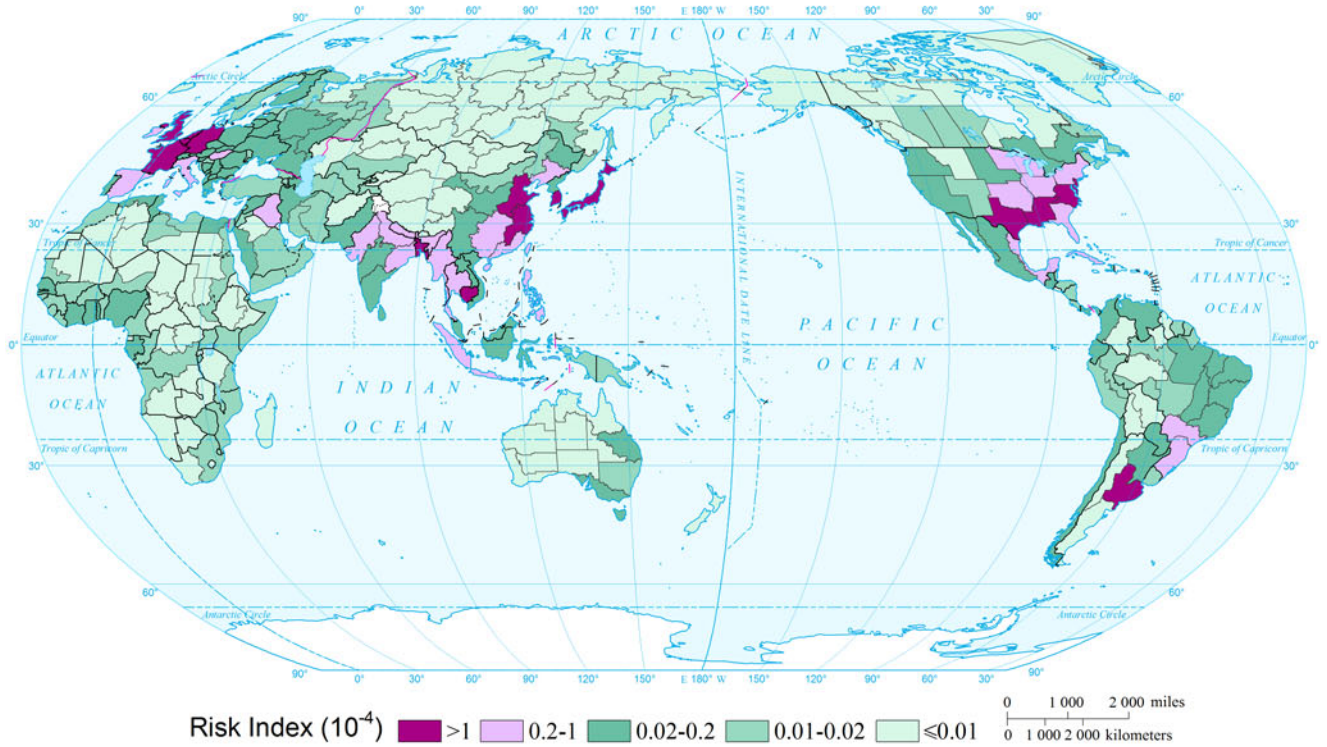
Affected GDP Risk of Flood of the World by Return Period(10a)  
(Comparable-geographic Unit)



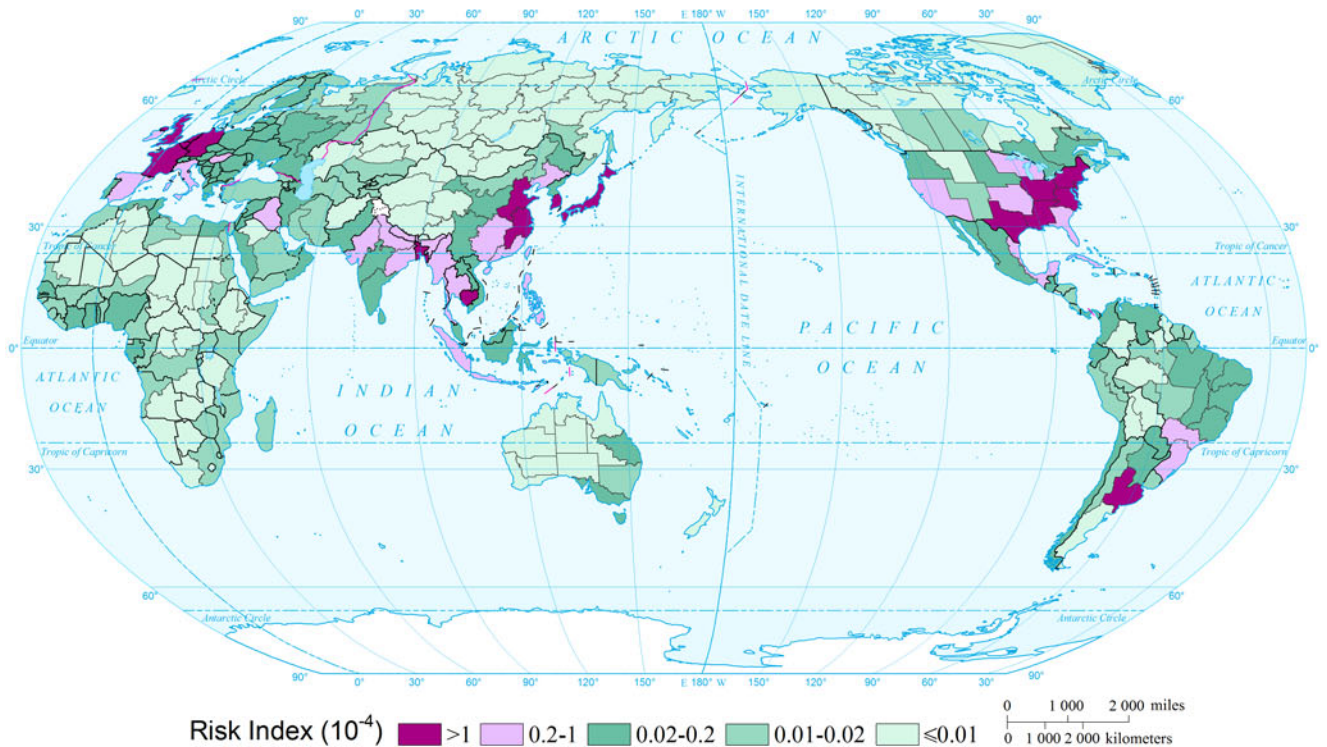
Affected GDP Risk of Flood of the World by Return Period(20a)  
(Comparable-geographic Unit)



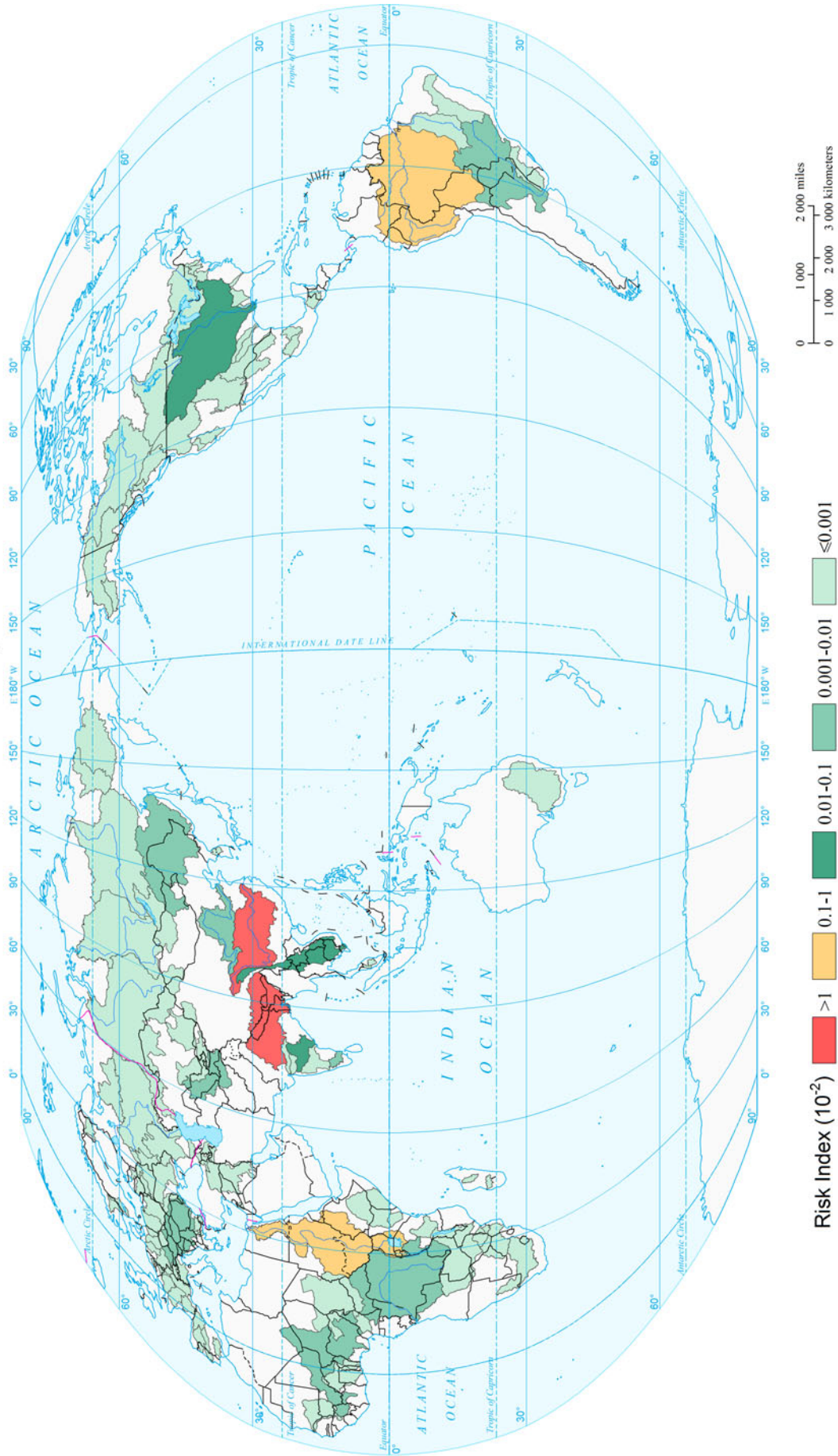
Affected GDP Risk of Flood of the World by Return Period(50a)  
(Comparable-geographic Unit)



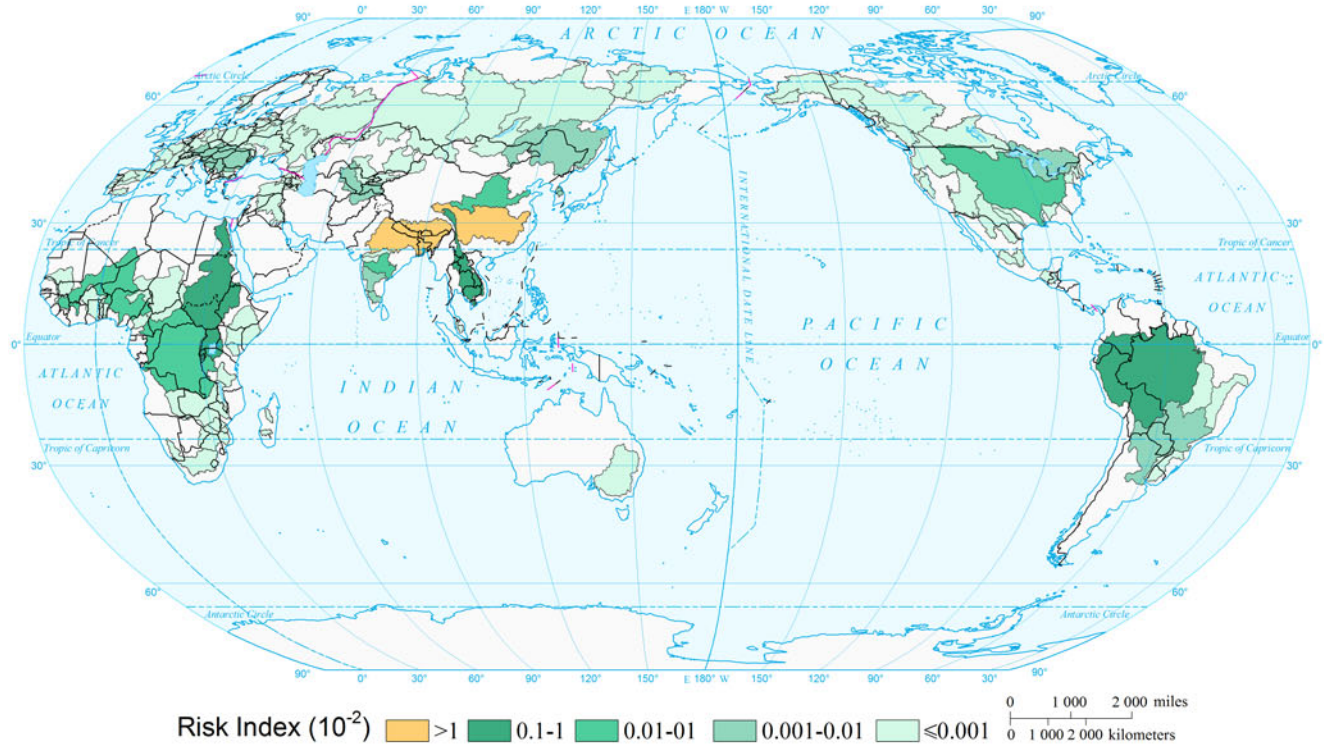
Affected GDP Risk of Flood of the World by Return Period(100a)  
(Comparable-geographic Unit)



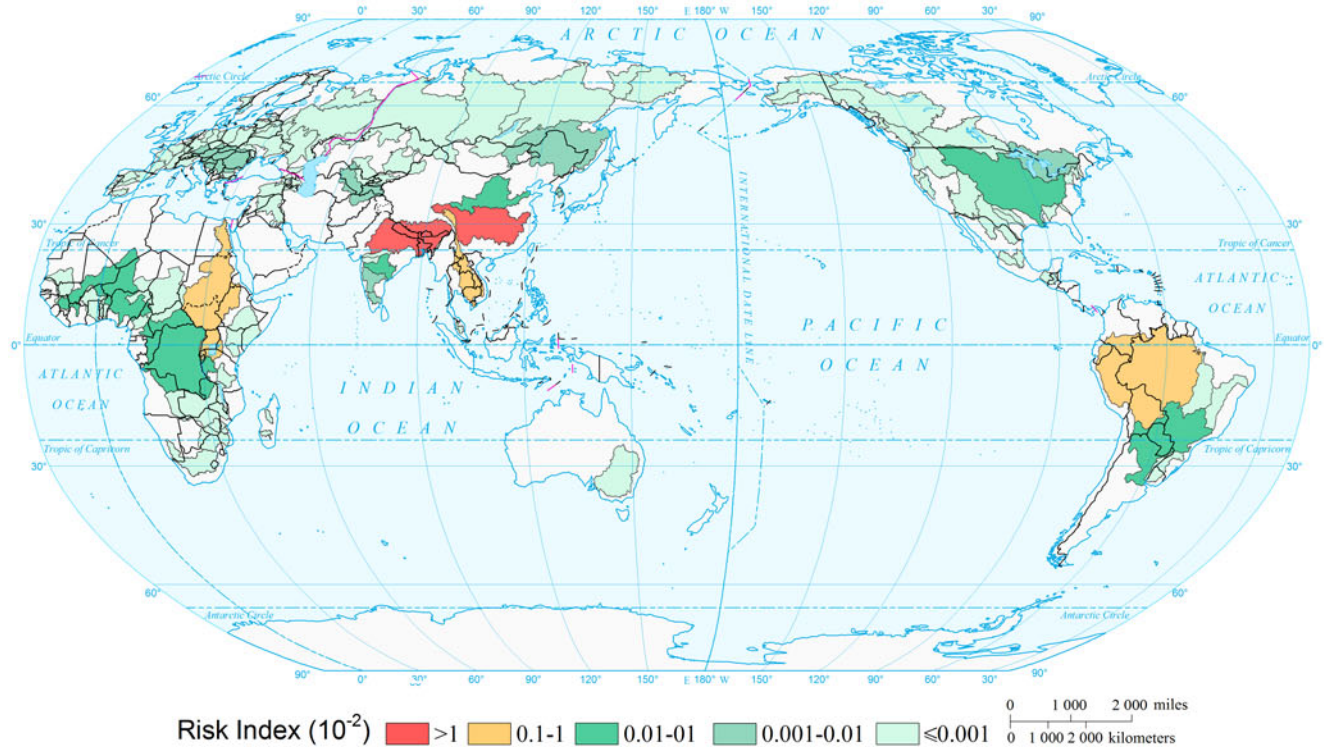
Expected Annual Affected Population Risk of Flood of the World (Watershed Unit)



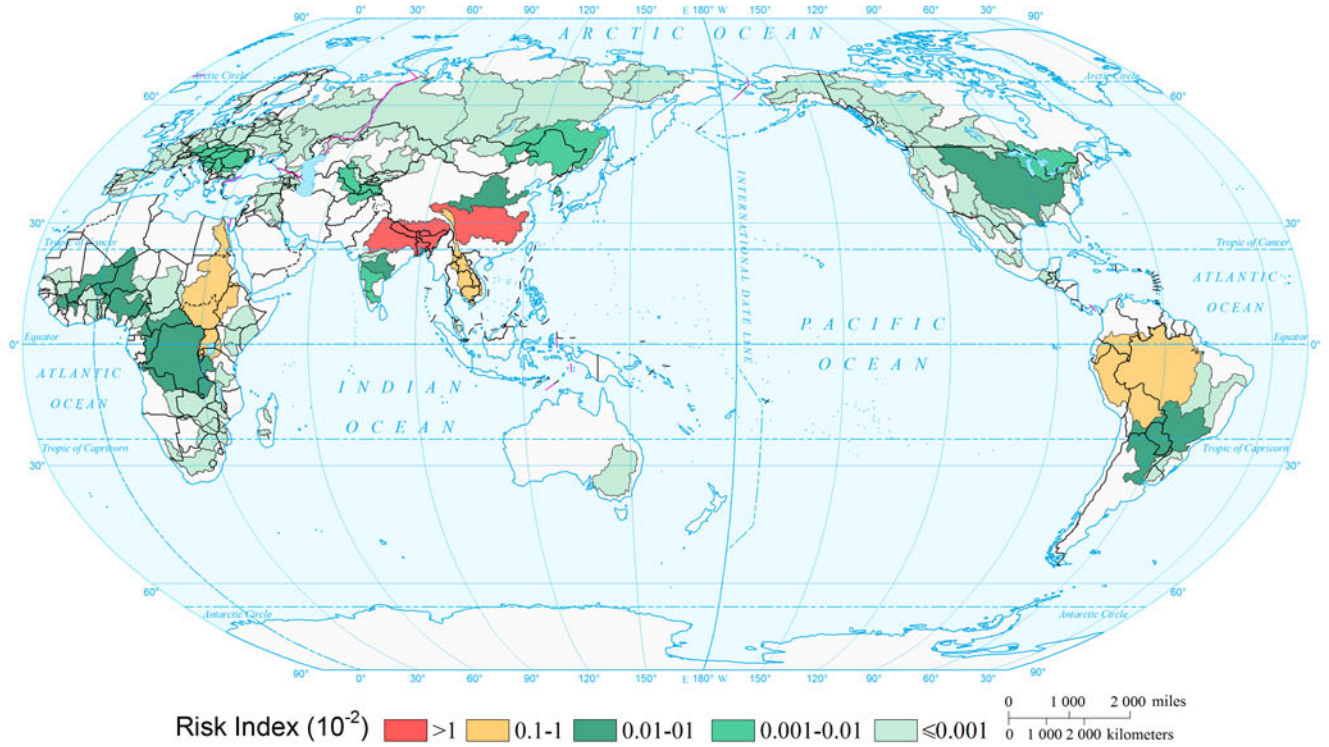
### Affected Population Risk of Flood of the World by Return Period (10a) (Watershed Unit)



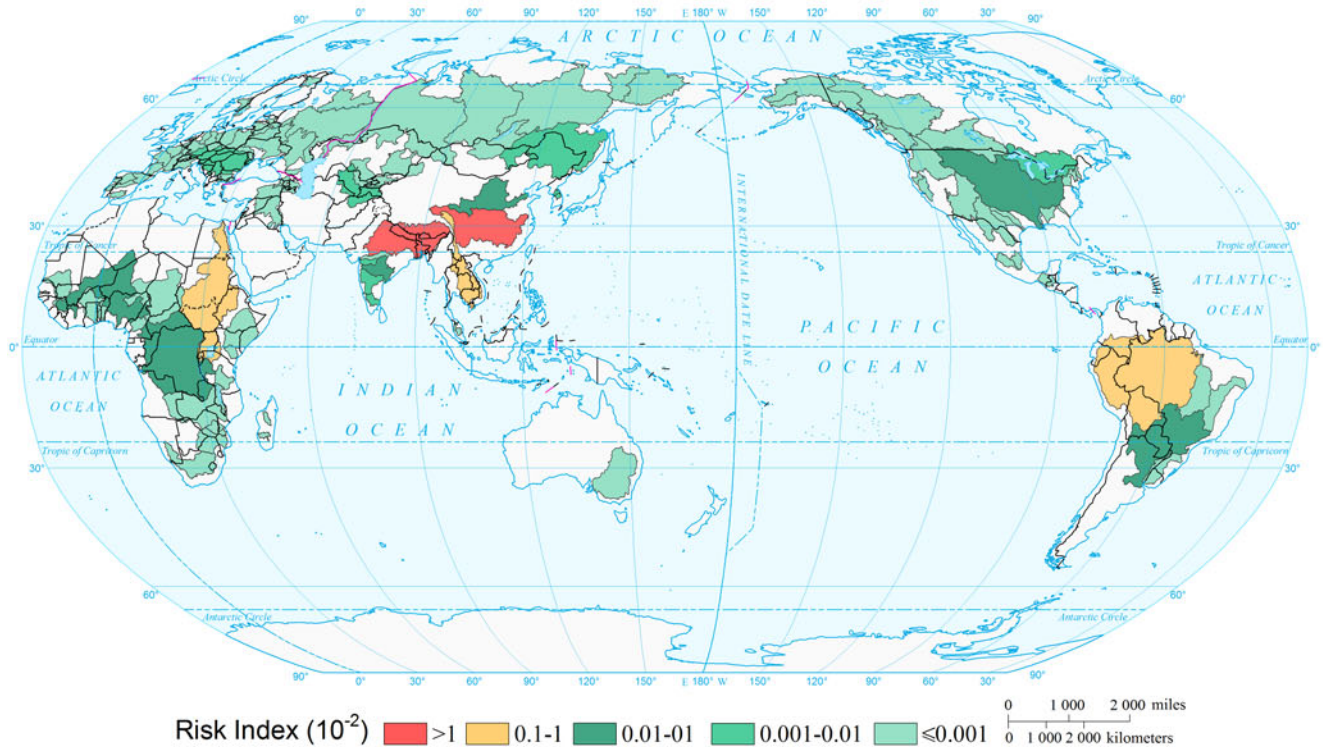
### Affected Population Risk of Flood of the World by Return Period (20a) (Watershed Unit)



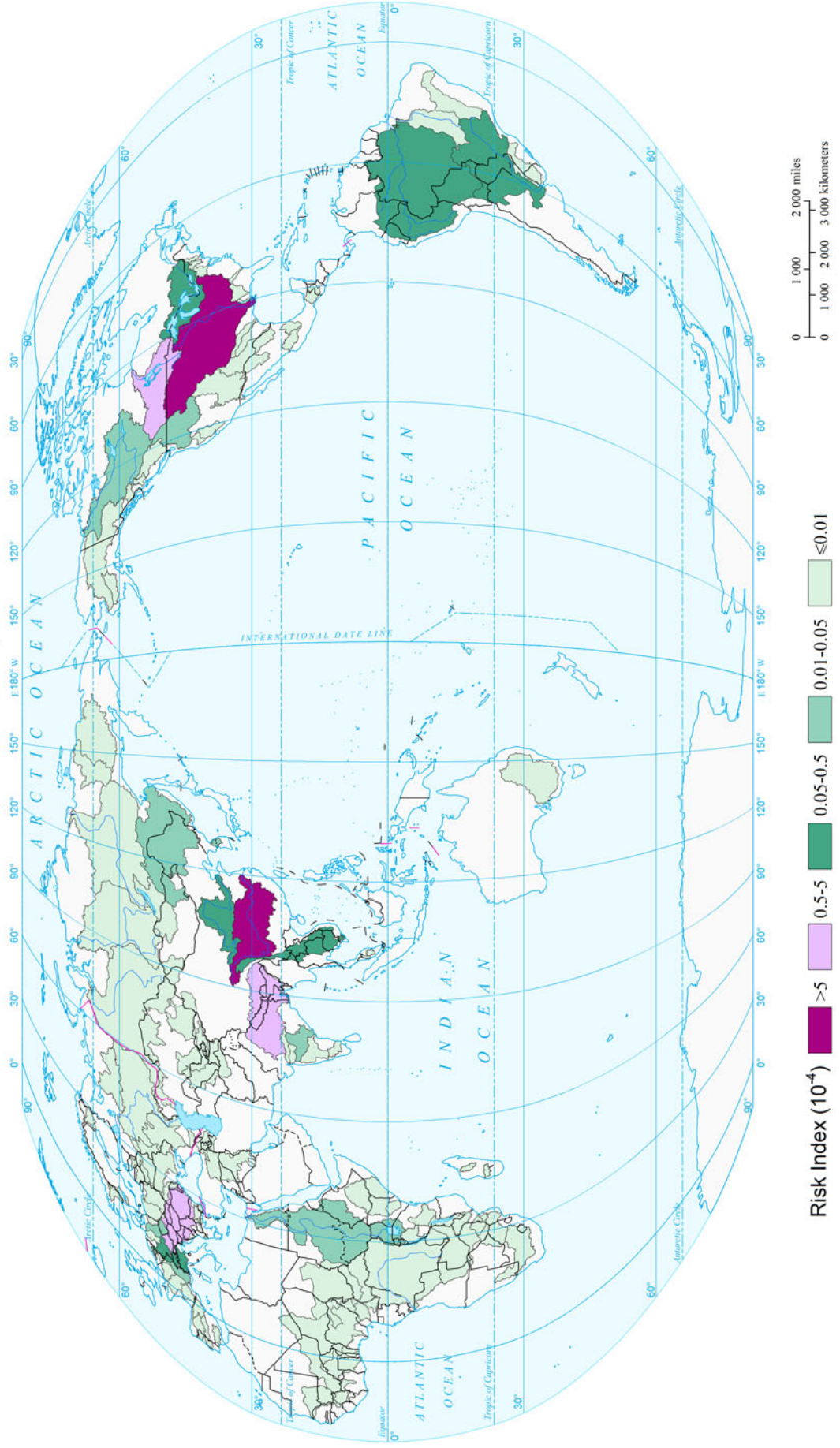
### Affected Population Risk of Flood of the World by Return Period (50a) (Watershed Unit)



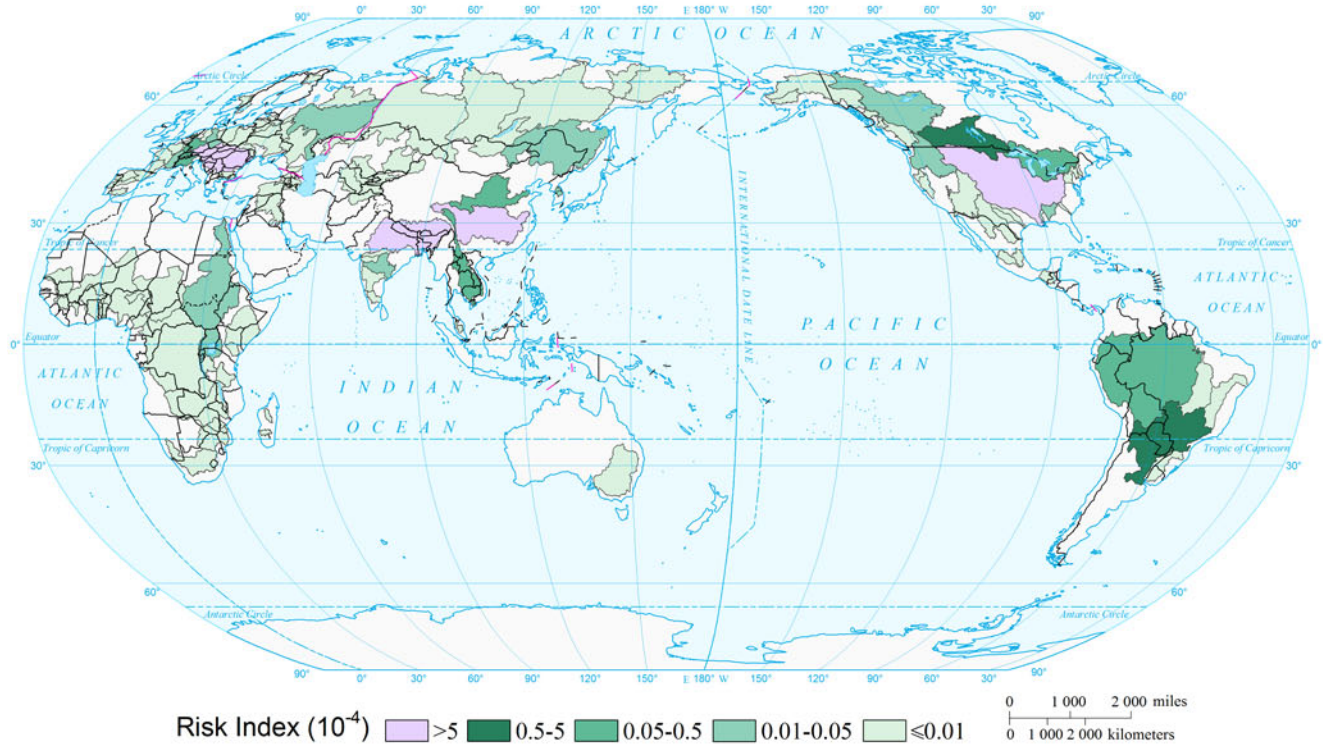
### Affected Population Risk of Flood of the World by Return Period (100a) (Watershed Unit)



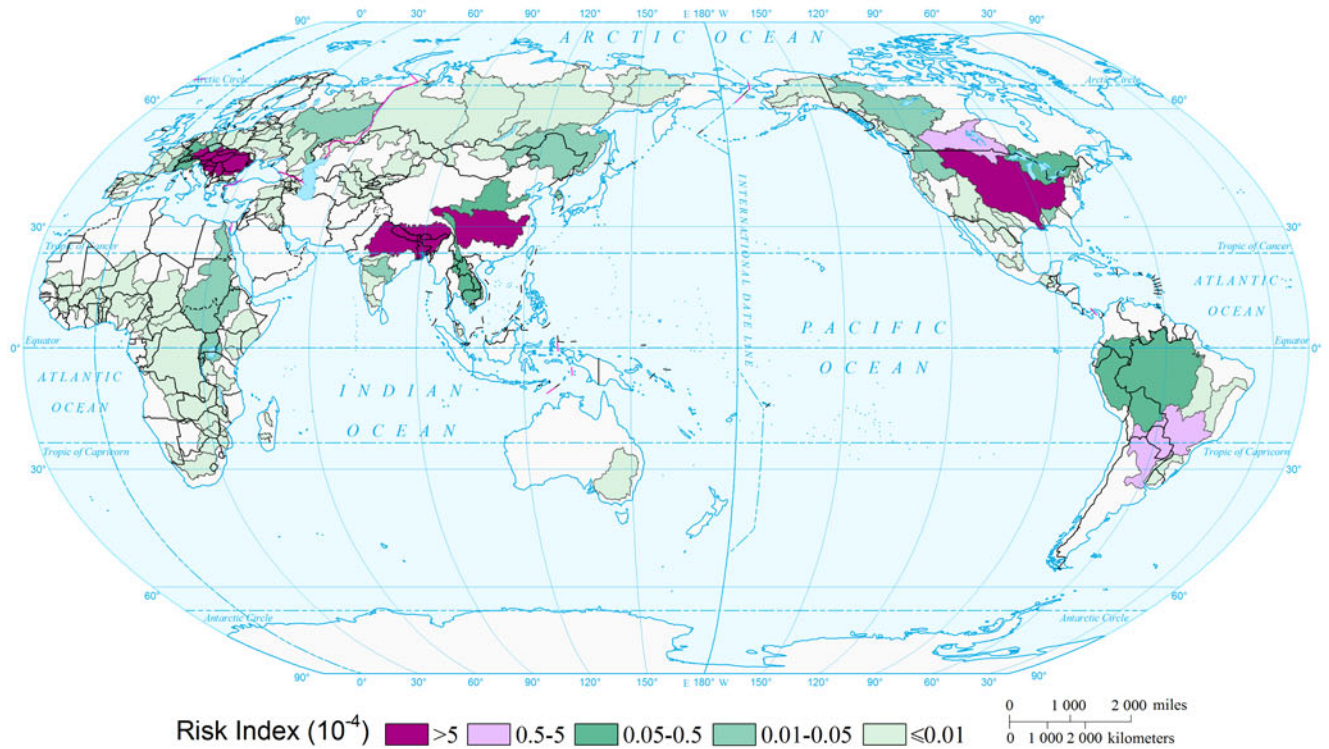
Expected Annual Affected GDP Risk of Flood of the World  
(Watershed Unit)



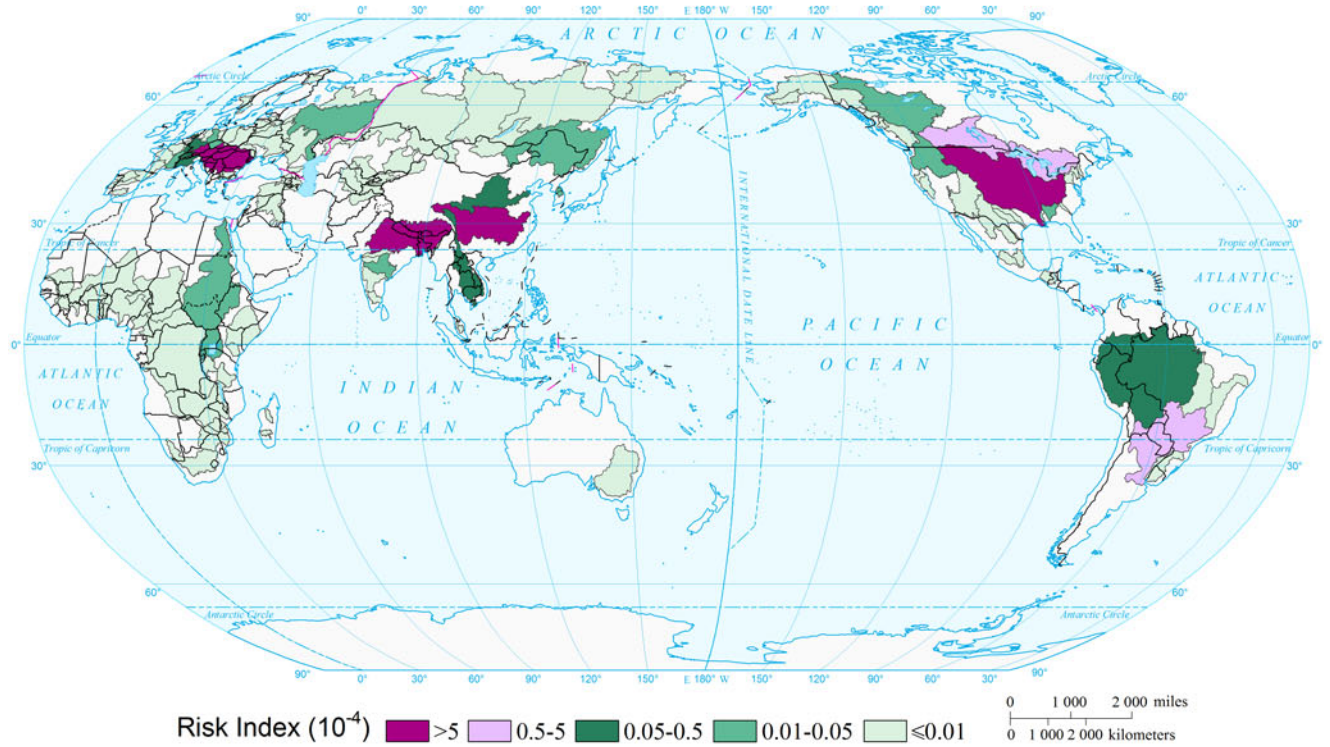
Affected GDP Risk of Flood of the World by Return Period (10a)  
(Watershed Unit)



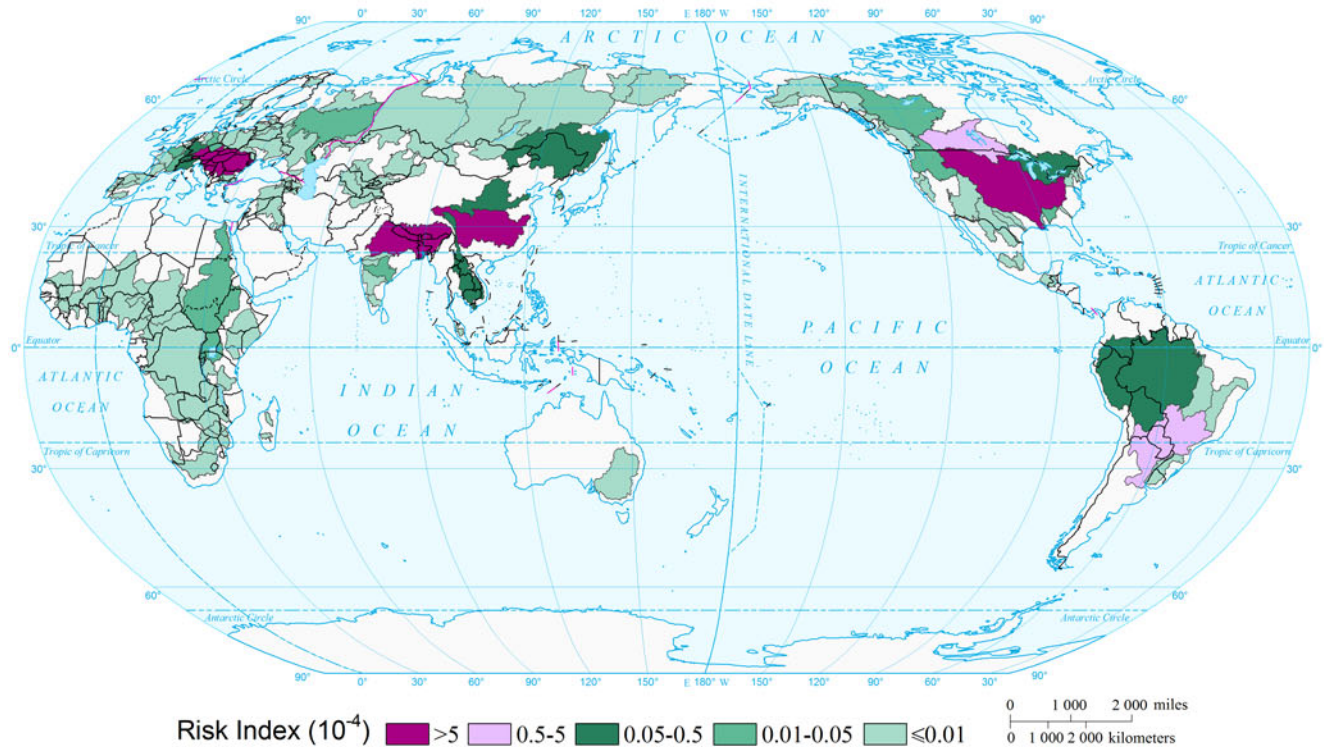
Affected GDP Risk of Flood of the World by Return Period (20a)  
(Watershed Unit)



### Affected GDP Risk of Flood of the World by Return Period (50a) (Watershed Unit)



### Affected GDP Risk of Flood of the World by Return Period (100a) (Watershed Unit)

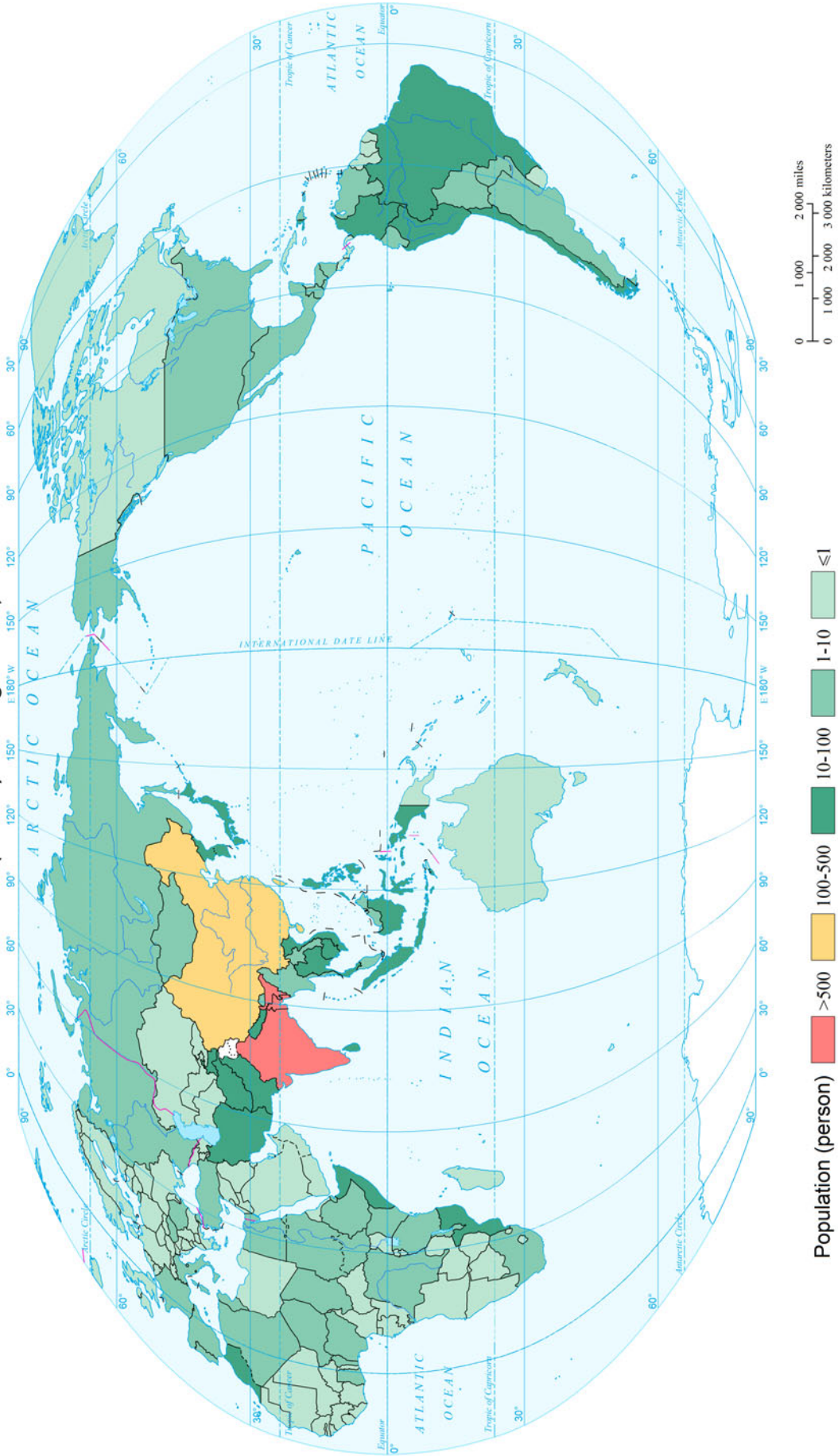




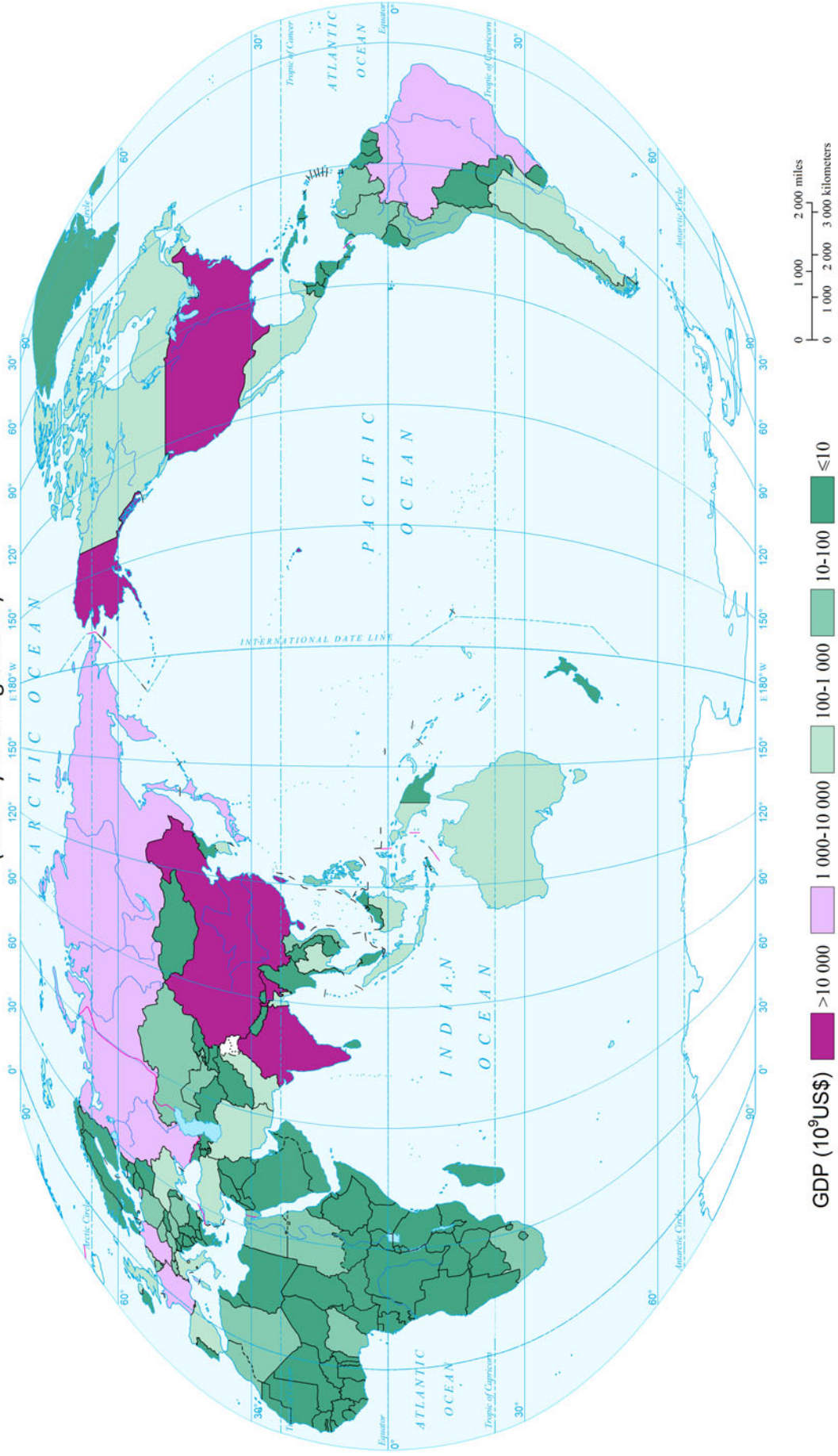
Flood

Flood and Storm Surge Disasters

Mortality Risk of Flood of the World by Return Period (100a)  
(Country and Region Unit)



GDP Loss Risk of Flood of the World by Return Period (100a)  
(Country and Region Unit)



## References

- Apel, H., A.H. Thieken, B. Merz, et al. 2004. Flood risk assessment and associated uncertainty. *Natural Hazards and Earth System Sciences* 4: 295–308.
- Coles, S. 2001. *An introduction to statistical modeling of extreme values*, Springer, Berlin.
- Dilley, M., U. Deichmann, and R.S. Chen. 2005. *Natural disaster hotspots: A global risk analysis*. Washington DC: World Bank Publications.
- Herold, C., and F. Mouton. 2011. Global flood hazard mapping using statistical peak flow estimates. *Hydrology and Earth System Sciences Discussions* 8(1): 305–63.
- Jongman, B., P.J. Ward, and J.C.J.H. Aerts. 2012. Global exposure to river and coastal flooding: Long term trends and changes. *Global Environmental Change* 22: 823–35.
- Kidson, R., and K.S. Richards. 2005. Flood frequency analysis: Assumptions and alternatives. *Progress in Physical Geography* 29 (3): 392–410.
- Kim, Y.O., S.B. Seo, and O.J. Jang. 2012. Flood risk assessment using regional regression analysis. *Natural Hazards* 63: 1203–17.
- Kok, M., H.J. Huizinga, A.C.W.M. Vrouwenvelder, et al. 2005. *Standard Method 2004: Damage and casualties caused by flooding*. Netherlands: Road and Hydraulic Engineering Institute.
- Li, K.Z., S.H. Wu, E.F. Dai, et al. 2012. Flood loss analysis and quantitative risk assessment in China. *Natural Hazards* 63: 737–60.
- Su, X.H., X.D. Zhang, S.Q. Yang, et al. 2012. County-level flood risk level assessment in China using geographic information system. *Sensor Letters* 10: 379–386.
- United Nations International Strategy for Disaster Reduction (UNISDR). 2009. *Global assessment report on disaster risk reduction*. United Nations.
- Wang, H., X. Li, H. Long, et al. 2011. Development and application of a simulation model for changes in land-use patterns under drought scenarios. *Computers and Geosciences* 37: 831–843.
- Winsemius, H.C., L.P.H. Van Beek, B. Jongman, et al. 2012. A framework for global river flood risk assessments. *Hydrology and Earth System Sciences* 9(8): 9611–59.

---

# Mapping Storm Surge Risk of the World

Shao Sun, Jiayi Fang, and Peijun Shi

---

## 1 Background

Storm surge can be ranked as the most serious disaster among the marine disasters. Most of the serious disasters that occurred along the coastal zones are associated with storm surges induced by extreme weather systems. Storm surge is primarily caused by wind pushing on the water surface, causing the water to pile up above ordinary levels (Feng 1982). Severe storm surge hazard with destructive power could occur when abnormal weather system, astronomical tide period, and suitable geographic environment conditions meet coincidentally (Le 1998). The Intergovernmental Panel on Climate Change (IPCC) has reported that global climate change will lead to sea-level rise which further increase occurrences of typhoon and storm surge (IPCC 2013).

At the regional scale, coastal countries and regions around the world have developed a wide range of storm surge risk assessment. The existing models can accurately

simulate storm surge processes in local coastal areas, for instance, SLOSH, DELFT3D, MIKE 12, ADCIRC, GCOM 2D/3D, and TAOS storm surge assessment models (Shi et al. 2013), but they are not applicable to a larger extent, or even the global scope. Hinkel et al. (2014) emphasized coastal flood damage and adaptation costs on a global scale under a range of sea-level rise scenarios in twenty-first century. Thus, it can be inferred that systematic assessment and mapping of storm surge risk at a global scale is very limited, and the related risk was usually assessed from the aspects of sea-level rise, flood, tropical cyclones, and so on. However, systematic assessment of storm surge risk should not only be associated with the intensity and the frequency of the hazard, but also with the vulnerability of exposure.

According to the basic theory framework of natural disaster system, we initially mapped the population and GDP risk affected by storm surge at the global scale. The historical water level records observed (Appendix III, Hazards data 4.9) were used to analyze the intensity of storm surge through the information diffusion theory.

---

## 2 Method

Figure 1 shows the technical flowchart for mapping affected population and GDP risk from storm surge of the world.

### 2.1 Intensity

As the available dataset was too short to analyze by the traditional method for extreme value fitting, the information diffusion theory (Huang 2012; Qi et al. 2010) was

---

**Mapping Editors:** Jing'ai Wang (Key Laboratory of Regional Geography, Beijing Normal University, Beijing 100875, China) and Chunqin Zhang (School of Geography, Beijing Normal University, Beijing 100875, China).

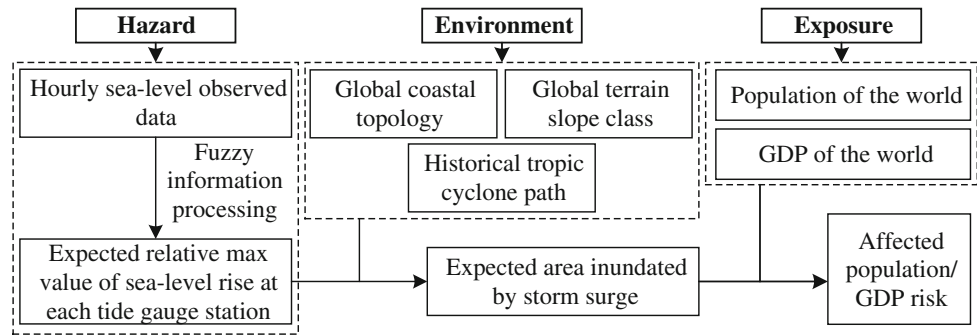
**Language Editor:** Zhao Zhang (State Key Laboratory of Earth Surface Processes and Resource Ecology, Beijing Normal University, Beijing 100875, China).

---

S. Sun · J. Fang  
Academy of Disaster Reduction and Emergency Management,  
Ministry of Civil Affairs and Ministry of Education, Beijing  
Normal University, Beijing 100875, China

P. Shi (✉)  
State Key Laboratory of Earth Surface Processes and Resource  
Ecology, Beijing Normal University, Beijing 100875, China  
e-mail: spj@bnu.edu.cn

**Fig. 1** Technical flowchart for mapping affected population and GDP risk of storm surge of the world



introduced to solve this problem. The study assumes that the storm surge system is a stochastic Markov chain process, and its state changes according to a transition rule that only depends on the known past  $N$  years' state. We used the expected relative maximum value of sea-level rise as the indicator of hazard intensity for each tide gauge station, which can be obtained by fitting the probability distribution curve based on the annual maximum dataset of the relative increasing sea level ( $H_{\text{relative}}$ ) using fuzzy mathematic method (Huang 2012).  $H_{\text{relative}}$  can be calculated according to Eq. (1).

$$H_{\text{relative}} = H_{\text{max}} - H_{\text{mean}} \quad (1)$$

where  $H_{\text{max}}$  is the annual maximum water level and  $H_{\text{mean}}$  is the annual mean of water level.

The global expected relative maximum value of sea-level rise for coastal areas was obtained by interpolating through spatial interpolation method in ArcGIS.

## 2.2 Affected Population and GDP Risk

Geo-environment has a significant influence on the damages induced by different magnitude of storm surge. The geo-environment in coastal zone can be classified into bedrock coast and plain coast (Dürr et al. 2011; Appendix III, Environments data 2.12). The storm surge reaches bedrock coast after a shorter distance than those to plain coast. However, topographical environment in loose sedimentary coast is usually flat, especially for the silty mud coast which is characterized by broadness and flat with a slope less than 0.5 %. Taking into account of the historical path records of tropical cyclones (Appendix III, Disasters data 5.5), we divided global coastline into plain-storm, plain-no-storm, bedrock-storm, and bedrock-no-storm coastal areas. Storm coastal area is referred to the area affected seriously by cyclones, while no storm area not affected. The assessment processes are as follows: Firstly, the maximum inundation distance expected ( $D_{\text{inundated}}$ ) can be calculated from the slope dataset (Appendix III, Environments data 2.2). Then,

the maximum inundation area expected at the global scale can be marked using altitude-area method and geo-statistics method. After superimposing the global GDP distribution data (Appendix III, Exposures data 3.4) and the global population density data (Appendix III, Exposures data 3.1), the global population and GDP risk affected by storm surge can be calculated, respectively.

## 3 Results

### 3.1 Intensity Map

The maximum inundation areas expected are concentrated on the areas which are frequently hit by strong tropical cyclones with plain-storm coastal environment. These areas are mainly located in the coasts of the East Asia, West Europe, northern Australia, and eastern and western North America. Due to the high intensity of tropical cyclones, storm surges can generally bring dramatic changes in the water level. Although the inundation area is not so wide, some coastal area could experience a severe damage due to an extreme increase in maximum relative water level since it is located in a bedrock environment. West coast in Canada is a great example for this.

By zonal statistics of the expected inundation area, the expected annual inundation area of storm surge of the world at national level is derived and ranked. The top 1 % country with the highest inundation area of storm surge is Australia, and the top 10 % countries are Australia, USA, Mexico, Bangladesh, Cuba, and India.

### 3.2 Affected Population Risk

A large variability for the affected population exists due to the huge differences of population density at grid level among countries. High risk areas for the population exposure to storm surge are located in the Caribbean region, the Bay of Bengal, East Asia, etc. Although some areas were shown

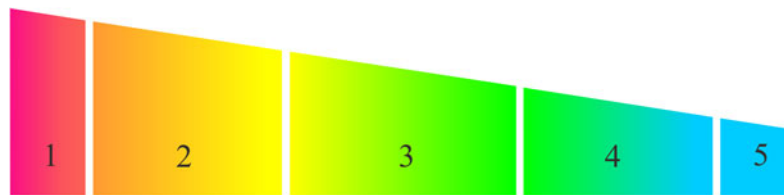


**Fig. 2** Expected annual affected population risk of storm surge of the world. 1 (0, 10 %] Bangladesh, India, China, and Vietnam. 2 (10, 35 %] USA, Sri Lanka, Japan, Australia, Mozambique, Thailand, Philippines, Burma, Mexico, and Tonga. 3 (35, 65 %] Fiji, North Korea, New Zealand, Palestine, Canada, Belize, Madagascar, Marshall Islands,

Saint Kitts and Nevis, Antigua and Barbuda, Honduras, Dominica, and Palau. 4 (65, 90 %] Federated States of Micronesia, Haiti, South Korea, Cuba, Bahamas, Pakistan, Cook Islands, Samoa, Saint Vincent and the Grenadines, and Grenada. 5 (90, 100 %] Seychelles, Venezuela, Nicaragua, and Mauritius



**Fig. 3** Expected annual affected GDP risk of storm surge of the world. 1 (0, 10 %] USA, China, and Japan. 2 (10, 35 %] Australia, Ireland, Bangladesh, India, Thailand, Vietnam, Sri Lanka, and Mexico. 3 (35, 65 %] New Zealand, Mozambique, Canada, Philippines, Fiji, Antigua

and Barbuda, South Korea, Tonga, Cuba, and Saint Kitts and Nevis. 4 (65, 90 %] Palestine, Dominican Republic, Honduras, Burma, Belize, Bahamas, Dominica, and Federated States of Micronesia. 5 (90, 100 %] Madagascar, Palau, Marshall Islands, and Mauritius

with a high value of inundation area, the risk is still low due to its sparse population along the coastline. In this case, Australia is a good example.

By zonal statistics of the expected risk result, the expected annual affected population risk of storm surge of the world at national level is derived and ranked (Fig. 2). The top 1 % country with the highest affected population risk of storm surge is Bangladesh, and the top 10 % countries are Bangladesh, India, China, and Vietnam.

### 3.3 Affected GDP Risk

A large variability for the affected GDP exists due to the huge differences of GDP at grid level among countries. It is found that higher economic loss risk will be encountered following with the rapid economic development of a

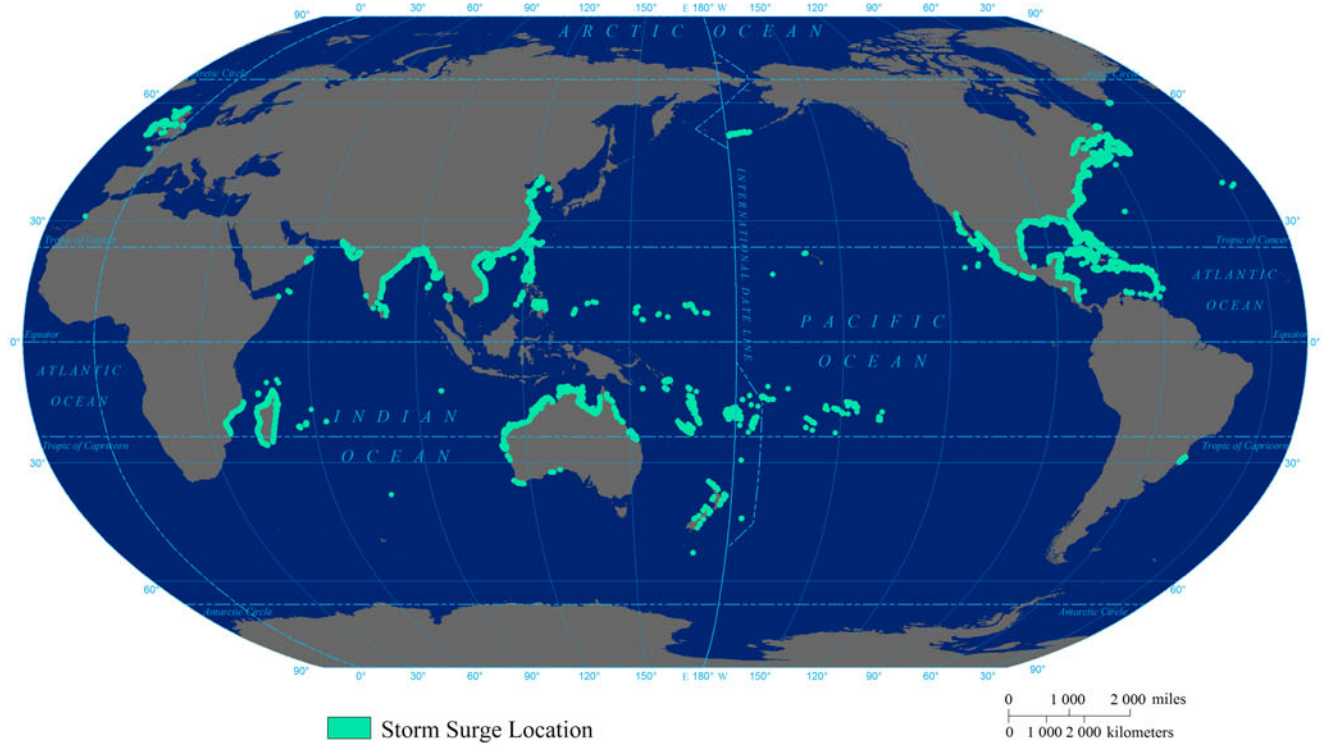
country. Areas with high economic loss risk are mainly distributed in some coastal parts of England, other developed countries in Europe, the Yangtze River Delta in China, the eastern coast of America, the Gulf of Mexico, etc. As for the Bay of Bengal, even though it is characterized by a high risk of population exposure, the economic risk is not such remarkable because of its underdeveloped economic.

By zonal statistics of the expected risk result, the expected annual affected GDP risk of storm surge of the world at national level is derived and ranked (Fig. 3). The top 1 % country with the highest expected annual affected GDP risk of storm surge is USA, and the top 10 % countries are USA, China, and Japan.

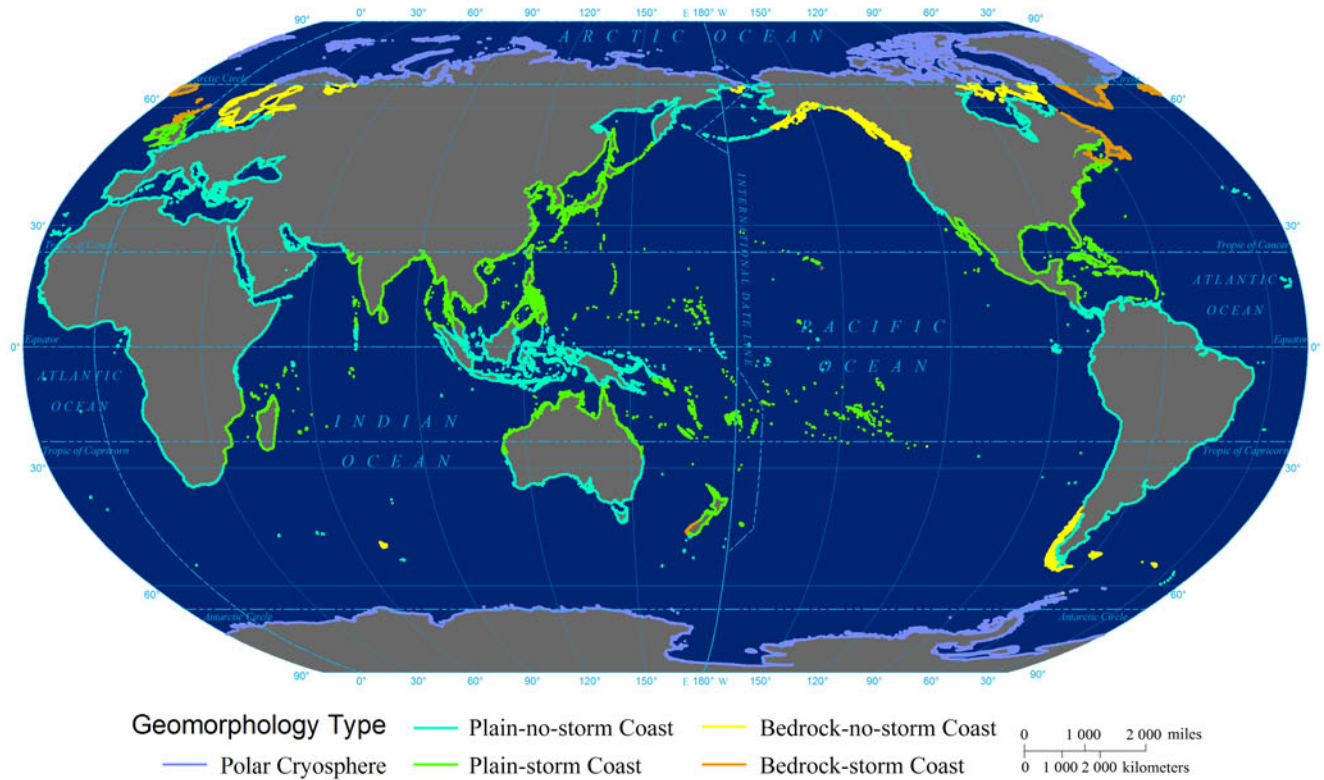
---

## 4 Maps

### Historical Event Locations of Global Storm Surge (1975-2007)



### Global Coastal Geomorphology

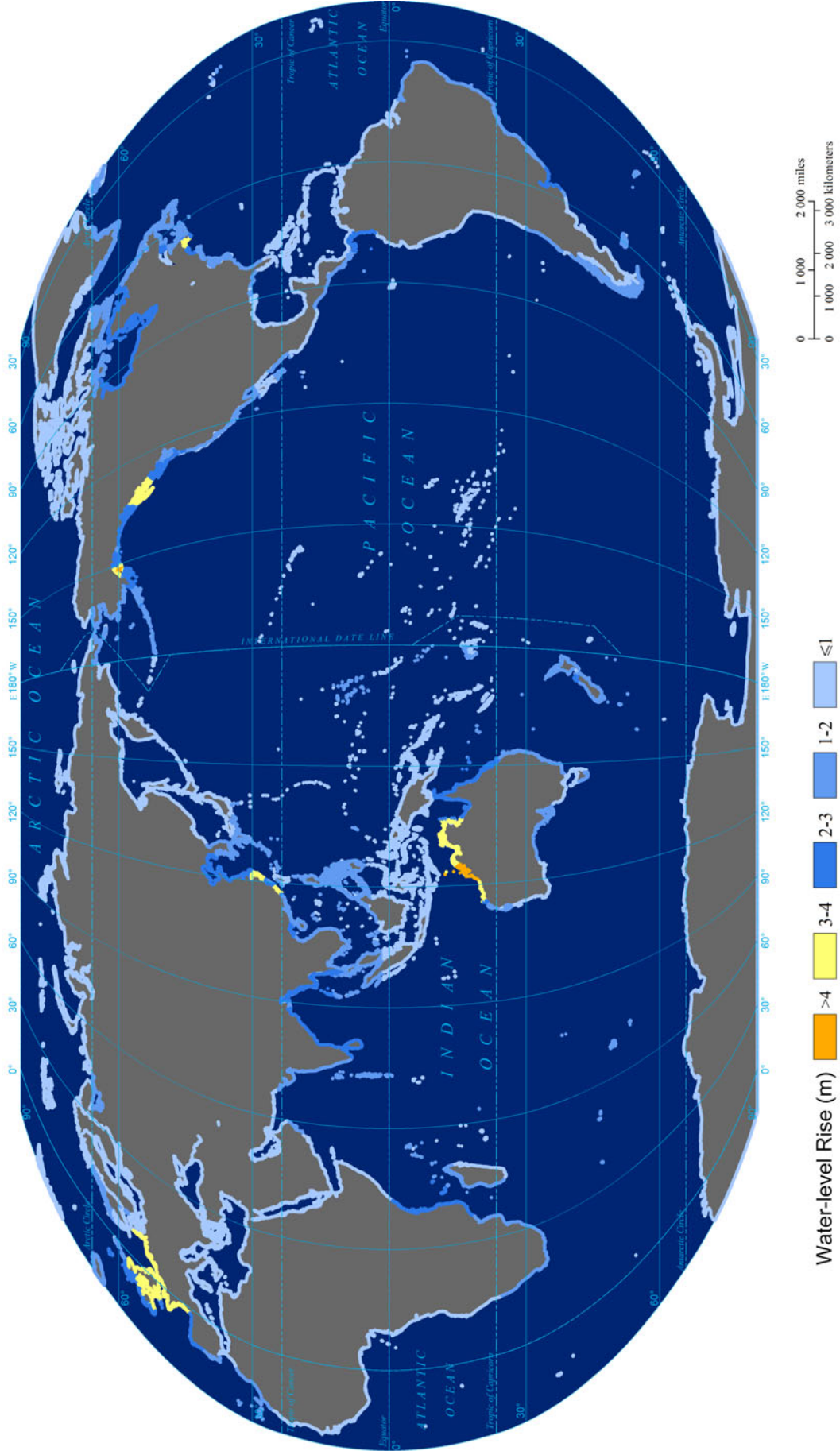




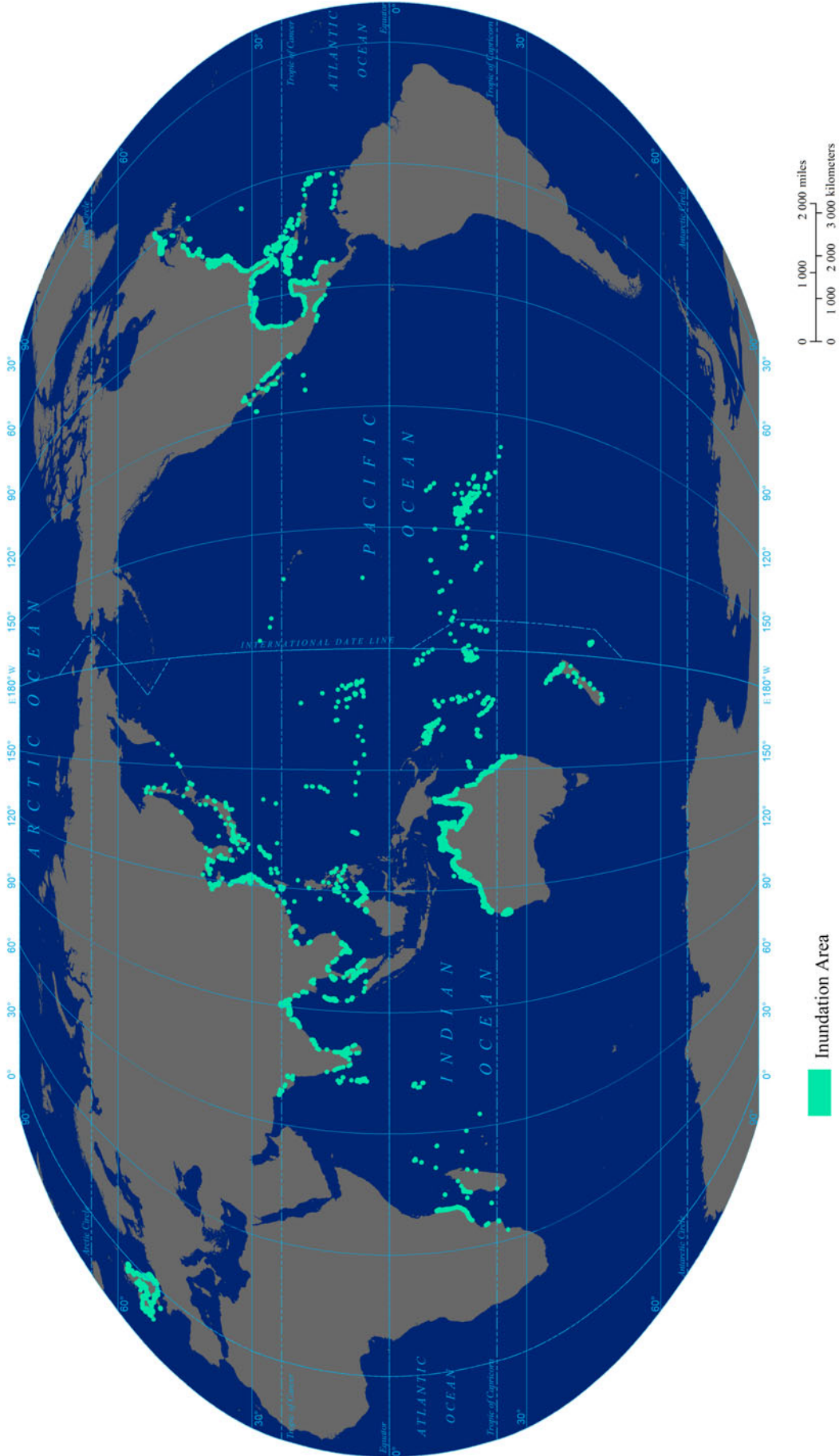
Storm Surge

Flood and Storm Surge Disasters

### Expected Annual Relative Maximum Value of Water-level Rise of Global Coastal Zones



### Expected Annual Inundation Area of Global Coastal Zones

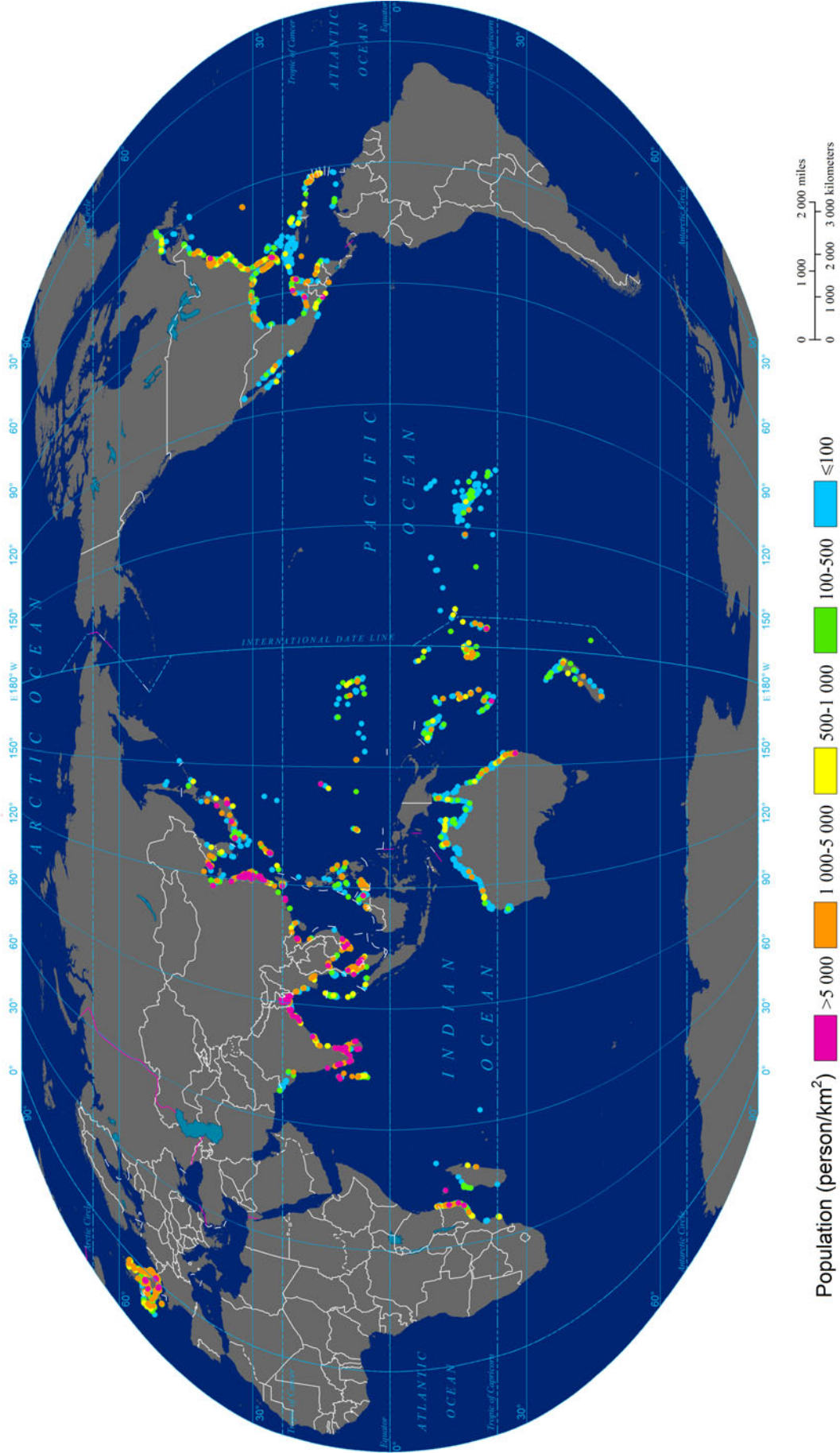




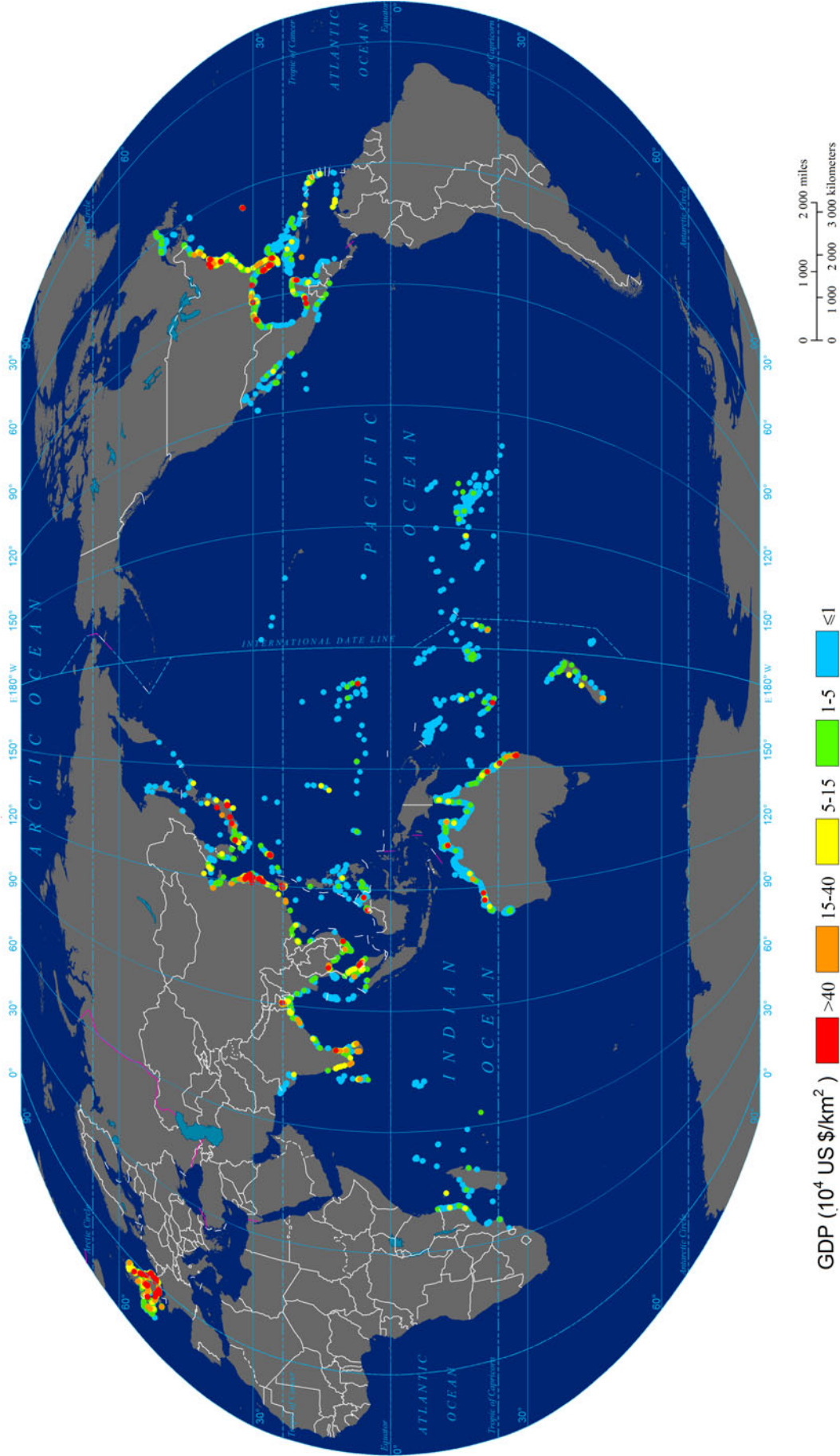
Storm Surge

Flood and Storm Surge Disasters

### Expected Annual Affected Population Risk of Storm Surge of the World



Expected Annual Affected GDP Risk of Storm Surge of the World



## References

- Dürr, H.H., G.G. Laruelle, C.M. van Kempen, et al. 2011. Worldwide typology of nearshore coastal systems: Defining the estuarine filter of river inputs to the oceans. *Estuaries and Coasts* 34(3): 441–58.
- Feng, S.Z. 1982. *Introduction to storm surge*. Beijing: Science Press. (in Chinese).
- Hinkel, J., D. Lincke, A.T. Vafeidis, et al. 2014. Coastal flood damage and adaptation costs under 21st century sea-level rise. *Proceedings of the National Academy of Science* 111(9): 3292–297.
- Huang, C.F. 2012. *Natural disaster risk analysis and management*. Beijing: Science Press. (in Chinese).
- Intergovernmental Panel on Climate Change (IPCC). 2013. *Summary for policymakers*. In *Climate change 2013: The physical science basis*. Contribution of Working Group I to the fifth assessment report of the intergovernmental panel on climate change. Cambridge and New York: Cambridge University Press.
- Le, K.T. 1998. The basic problem of the storm surge disaster risk assessment method in China. *Marine Forecasts* 15: 38–44. (in Chinese).
- Qi, P., M.J. Li, and Y.J. Hou. 2010. Risk assessment of storm surge disaster in the coastal areas of Bohai Sea and Yellow Sea based on information diffusion principle. *Oceanologia Et Limnologia Sinica* 4: 628–32. (in Chinese).
- Shi, X.W., J. Tan, Z.Y. Guo, et al. 2013. A review of risk assessment of storm surge disaster. *Advances in Earth Science* 28(8): 866–74. (in Chinese).

---

**Part IV**

**Sand-dust Storm and Tropical Cyclone Disasters**

---

# Mapping Sand-dust Storm Risk of the World

Huimin Yang, Xingming Zhang, Fangyuan Zhao, Jing'ai Wang,  
Peijun Shi, and Lianyou Liu

---

## 1 Background

Sand-dust storm (SDS) refers to extreme events in which great quantities of ground sand and dust particles are blown around by strong winds, air becomes extremely turbid, and the horizontal visibility is less than 1 km (CMA 2006). SDS can be classified into SDS, strong SDS, and extremely strong SDS. SDS disaster causes massive losses and damages to the socioeconomic and ecological systems.

Global SDS-prone areas are located in North Africa, the Middle East, Central Asia, North America, Australia, and other places (Kalderon-Asael et al. 2009; Formenti et al. 2011). The global spatial distribution reported by Engelstaedter et al. (2003) shows that regions with high SDS frequency are distributed in North Africa, the Middle East, and the Iberian Peninsula, and regions with moderate and low frequencies are distributed in Australia, northern China,

and southern and southwestern America. Scholars from different countries have studied on the temporal and spatial pattern of SDS from a regional perspective, such as Central Asia (Indoitu et al. 2012), Turkmenistan (Orlovsky et al. 2005), and China (Qiu et al. 2001; Wang et al. 2001; Kang and Wang 2005; Liu et al. 2012).

Many studies have focused on the spatial-temporal distribution, causes, source regions, and disaster characteristics of SDS. SDS disaster risk assessment is important for SDS disaster reduction, especially from regional perspective to a global scale. In this study, the global SDS risk is evaluated in terms of disaster system theory (Shi 1996). Using kinetic energy as the SDS indicator, regional aridity as the environment indicator, and GDP, population, and livestock as exposure indicators, this study is intended to provide an initiative approach for mapping SDS disaster risk potential of the world.

---

## 2 Method

Figure 1 shows the technical flowchart for mapping SDS risk of the world.

### 2.1 Environments

Desertification mainly occurs in the land degradation areas of extremely arid, arid, semiarid, and dry subhumid regions (UNCCD 1994; Wang et al. 2011), and SDS rarely occurs in continuous permafrost regions (Appendix III, Environments data 2.9). In this study, areas prone to SDS were taken as mapping area. Aridity (Appendix III, Environments data 2.13) is used as a factor of the environments. In order to make the data comparable, the aridity index data were normalized by Eq. (1):

$$I_x = \frac{\max - x}{\max - \min} \quad (1)$$

---

**Mapping Editors:** Jing'ai Wang (Key Laboratory of Regional Geography, Beijing Normal University, Beijing 100875, China) and Fang Lian (School of Geography, Beijing Normal University, Beijing 100875, China).

**Language Editor:** Lianyou Liu (Key Laboratory of Environmental Change and Natural Disaster, Ministry of Education; Beijing Normal University, Beijing 100875, China).

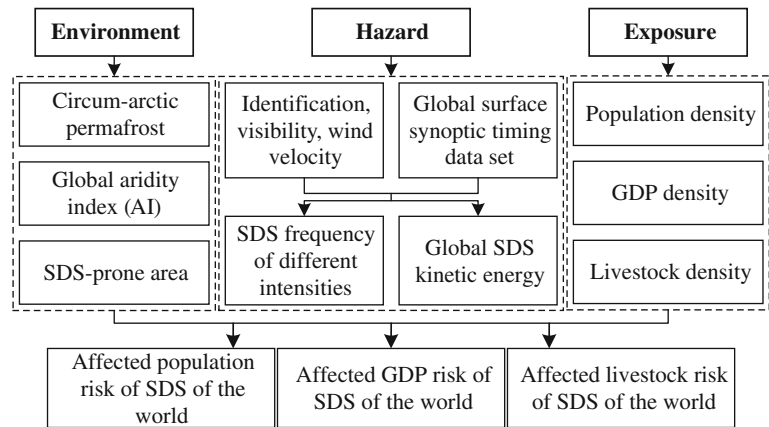
H. Yang · X. Zhang · F. Zhao  
School of Geography, Beijing Normal University, Beijing 100875,  
China

J. Wang  
Key Laboratory of Regional Geography, Beijing Normal  
University, Beijing 100875, China

P. Shi  
State Key Laboratory of Earth Surface Processes and Resource  
Ecology, Beijing Normal University, Beijing 100875, China

L. Liu (✉)  
Key Laboratory of Environmental Change and Natural Disaster,  
Ministry of Education, Beijing Normal University,  
Beijing 100875, China  
e-mail: lyliu@bnu.edu.cn

**Fig. 1** Technical flowchart for mapping SDS risk of the world



where  $I_x$  is the normalized aridity value,  $x$  is the original data, and min and max are the minimum and maximum of the original value, respectively.

## 2.2 Intensity

Wind speed and visibility of SDS events were obtained from the global surface synoptic timing data set with 9,435 stations (Appendix III, Hazards data 4.13). During typical SDS events,  $PM_{10}$  accounts for the majority of the particulate matter in atmosphere (Zhuang et al. 2001; Jayaratne et al. 2011). In sand desert areas,  $PM_{10}$  has negative power functions with visibility (Yang et al. 2006; Wang et al. 2008). Using data monitored by Tazhong weather Station, which is located in the hinterland of the Taklimakan desert in Xinjiang, relationship between  $PM_{10}$  and visibility is revealed in Eq. (2) (Yang et al. 2006).

$$PM_{10} = 5 \times 10^8 \times V_{vis}^{-1.5977} \quad (2)$$

where  $V_{vis}$  is visibility and  $PM_{10}$  is in  $\mu g/m^3$ .

With the classical kinetic energy formula, the kinetic energy per cubic meter of dust-laden airflow in SDS ( $E_p$ ) can be expressed by Eq. (3).

$$E_p = \frac{1}{4} \times V_{vis}^{-1.5977} \times v^2 \quad (3)$$

where  $v$  is the maximum wind velocity (m/s) at 10 m high.

Using method of information diffusion (Huang 2012), expected value and different return periods (10a, 20a, 50a, and 100a) of kinetic energy were calculated.

Using the inverse distance-weighted method, maps of SDS expected value and different return periods (10a, 20a,

50a, and 100a) were generated. For comparability, the SDS kinetic energy is normalized with Eq. (4).

$$I_x = \frac{x - \min}{\max - \min} \quad (4)$$

where  $I_x$  is normalized dimensionless data,  $x$  is the original data, and min and max are the minimum and maximum of the original data, respectively.

## 2.3 Exposures

World population (Appendix III, Exposures data 3.1), world GDP (Appendix III, Exposures data 3.3), and world livestock (Appendix III, Exposures data 3.10) data of exposures were normalized with Eq. (4).

## 2.4 Affected Population Risk

Based on the formula  $R = H \times E \times V$  (Shi 1996, 2002, 2005; UNDP 2004; Blaikie et al. 2003), we assessed and mapped affected population, GDP, and livestock risks of SDS. Finally, the affected exposure risk of SDS was normalized with Eq. (4).

At grid level ( $0.5^\circ \times 0.5^\circ$ ), extremely high and high values of population risk are mainly distributed in the southeastern, southwestern, and northwestern regions of the Sahara desert, northern and southeastern regions of Rub Al Khali Desert, the areas surrounding the Thar desert in western India, Iran and Turkey's desert areas, the Taklimakan deserts, the farming-pastoral regions in China and the Mongolian Gobi desert, the scattered areas of southeastern Australia, wide areas in the southwestern American deserts, the central Great Plains and the northern regions of Mexico, west coast of South America, and northeastern Brazil.

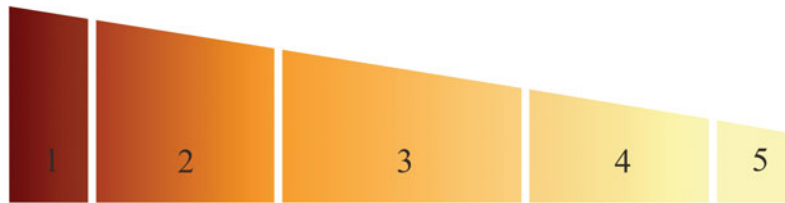


**Fig. 2** Expected annual affected population risk of SDS of the world. 1 (0, 10 %] Pakistan, USA, India, Saudi Arabia, Sudan, Mali, Burkina Faso, Ethiopia, Yemen, China. 2 (10, 35 %] Niger, Mexico, Russia, Uzbekistan, Iraq, Tunisia, Iran, Kenya, South Sudan, Syria, Algeria, Nigeria, Tanzania, Afghanistan, Mauritania, Senegal, Eritrea, Kazakhstan, Ghana, Azerbaijan, Turkey, Morocco, Brazil, Mongolia, Spain, Somalia, Benin. 3 (35, 65 %] Uganda, Myanmar, Chad, Romania, Georgia, Argentina, Ecuador, Columbia, Libya, South Africa, Tajikistan, Angola, The Democratic Republic of Congo, Peru, Israel, Chile,

Togo, Zimbabwe, Greece, Mozambique, Jordan, Italy, Turkmenistan, Venezuela, Australia, Malawi, Cameroon, Palestine, Côte d'Ivoire, Namibia, Kyrgyzstan, Rwanda. 4 (65, 90 %] Canada, Zambia, Madagascar, Hungary, Macedonia, Western Sahara, Portugal, the United Arab Emirates, Gambia, Dominica, Serbia, Djibouti, Thailand, Guinea, Bolivia, Czech, Ukraine, Botswana, Central Africa, Oman, Slovakia, Armenia, Guatemala, Kuwait, Bulgaria, Lesotho, Moldova. 5 (90, 100 %] Bhutan, Swaziland, Honduras, Cyprus, Paraguay, Germany, Lebanon, New Zealand, Nicaragua, East Timor

By zonal statistics of the expected risk result, the expected annual affected population risk of SDS of the world at national level is derived and ranked (Fig. 2). The top 1 % country with the highest expected annual affected population risk of SDS is Pakistan, and the top 10 % countries are Pakistan, USA, India, Sudan, Saudi Arabia, Mali, Burkina Faso, Ethiopia, Egypt, Yemen, and China.

## 2.5 Affected GDP Risk

By zonal statistics of the expected risk result, the expected annual affected GDP risk of SDS of the world at national level is derived and ranked (Fig. 3). The top 1 % country with the highest expected annual affected GDP risk of SDS

is USA, and the top 10 % countries are USA, Saudi Arabia, Pakistan, India, Spain, Sudan, Iran, Iraq, Algeria, China, and Egypt.

## 2.6 Affected Livestock Risk

At grid level ( $0.5^\circ \times 0.5^\circ$ ), extremely high and high values of the risk are mainly distributed in southwestern, southeastern, and northern regions of the Sahara desert, south Arabian desert, north and surroundings of the Thar desert in northwestern India, the Iranian desert, Turkestan desert, the Taklimakan desert in China, surroundings of the Gobi desert in Mongolia, central and south section of Australia, surroundings of North



**Fig. 3** Expected annual affected GDP risk of SDS of the world. 1 (0, 10 %] USA, Saudi Arabia, Pakistan, India, Spain, Iran, Sudan, Iraq, Algeria, China, Egypt. 2 (10, 35 %] Mexico, Russia, Syria, Turkey, Kuwait, Libya, Yemen, Argentina, Tunisia, Israel, Uzbekistan, Afghanistan, Chile, Kazakhstan, Greece, Brazil, Australia, Georgia, the United Arab Emirates, Jordan, Kenya, Canada, Romania, Columbia, Burkina Faso, Italy, Mongolia. 3 (35, 65 %] Azerbaijan, Mali, Cameroon, Venezuela, Ethiopia, South Africa, Morocco, Nigeria, Peru, Oman, Portugal, Hungary, Namibia, Tanzania, Palestine, South Sudan,

Niger, Macedonia, Slovakia, Turkmenistan, Senegal, Qatar, Ecuador, Ghana, Botswana, Mauritania, Serbia, Tajikistan, Bulgaria, Kyrgyzstan, Dominica, Ukraine. 4 (65, 90 %] Myanmar, Benin, Somalia, Côte d'Ivoire, Eritrea, Uganda, Chad, Angola, Czech, Thailand, Guatemala, Zambia, Togo, The Democratic Republic of Congo, Germany, Mozambique, Cyprus, Armenia, Zimbabwe, Malawi, Rwanda, Bolivia, Lebanon, Gambia, Lesotho, Madagascar, Guinea. 5 (90, 100 %] Djibouti, Moldova, Bhutan, Central Africa, Swaziland, Honduras, Paraguay, New Zealand, Nicaragua, East Timor

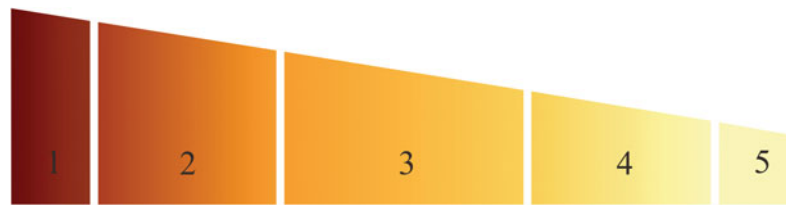


**Fig. 4** Expected annual affected livestock risk of SDS of the world. 1 (0, 10 %) China, Pakistan, Sudan, Mali, India, Mongolia, Algeria, USA, Mauritania, Iran, Burkina Faso. 2 (10, 35 %) Libya, Afghanistan, Niger, Ethiopia, Syria, South Sudan, Kazakhstan, Uzbekistan, Iraq, Egypt, Morocco, Kenya, Yemen, Mexico, Australia, Chad, Spain, Saudi Arabia, Somalia, Argentina, Tanzania, Nigeria, Tunisia, Jordan, Eritrea, Senegal, Azerbaijan, Turkmenistan. 3 (35, 65 %) Russia, Turkey, Brazil, Namibia, Ghana, Benin, South Africa, Greece, Uganda, Oman, Chile, Western Sahara, Peru, Angola, Tajikistan, Hungary, Kyrgyzstan,

Georgia, Portugal, Kuwait, Togo, Djibouti, Botswana, Canada, Myanmar, the United Arab Emirates, Zimbabwe, Rwanda, The Democratic Republic of Congo, Côte d'Ivoire, Gambia, Venezuela, Italy. 4 (65, 90 %) Romania, Israel, Ecuador, Macedonia, Bolivia, Mozambique, Madagascar, Central Africa, Zambia, Cameroon, Dominica, Paraguay, Ukraine, Serbia, Bulgaria, Malawi, Guinea, Armenia, Qatar, Columbia, France, Palestine, Slovakia, Nepal, Guatemala, Cyprus, Bhutan, Thailand. 5 (90, 100 %) Lebanon, Lesotho, Nicaragua, Moldova, Swaziland, East Timor, Honduras, Czech, New Zealand, Germany

American deserts, central Great Plain, northern Mexico, and west coast and northeastern parts of South America.

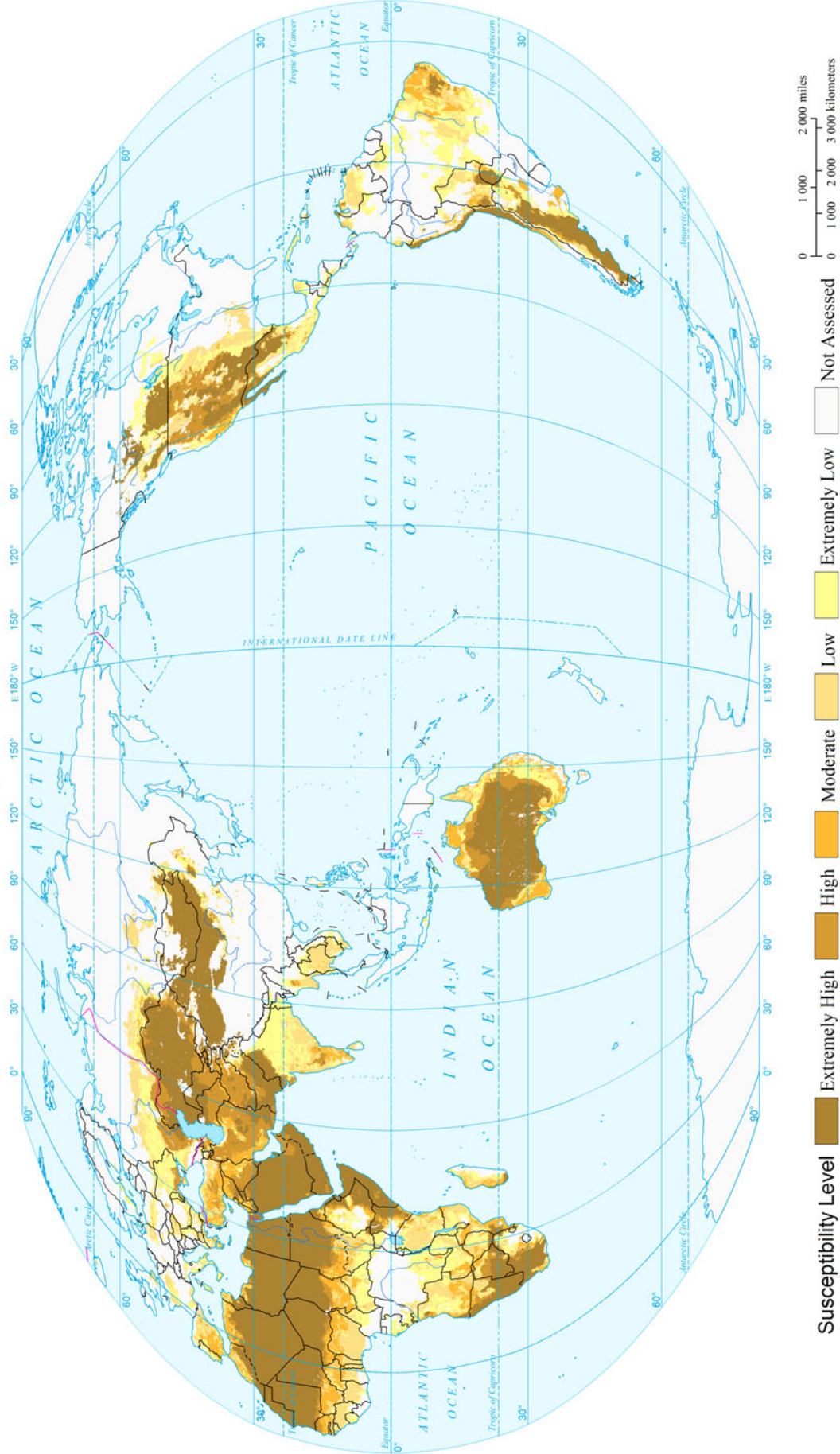
By zonal statistics of the expected risk result, the expected annual affected livestock risk of SDS of the world at national level is derived and ranked (Fig. 4). The top 1 % country with the highest expected annual affected livestock

risk of SDS is China, and the top 10 % countries are China, Sudan, Pakistan, Mali, India, Mongolia, Algeria, USA, Mauritania, Iran, and Burkina Faso.

---

### 3 Maps

Susceptibility of Global Sand-dust Storm  
(0.5°x0.5°)

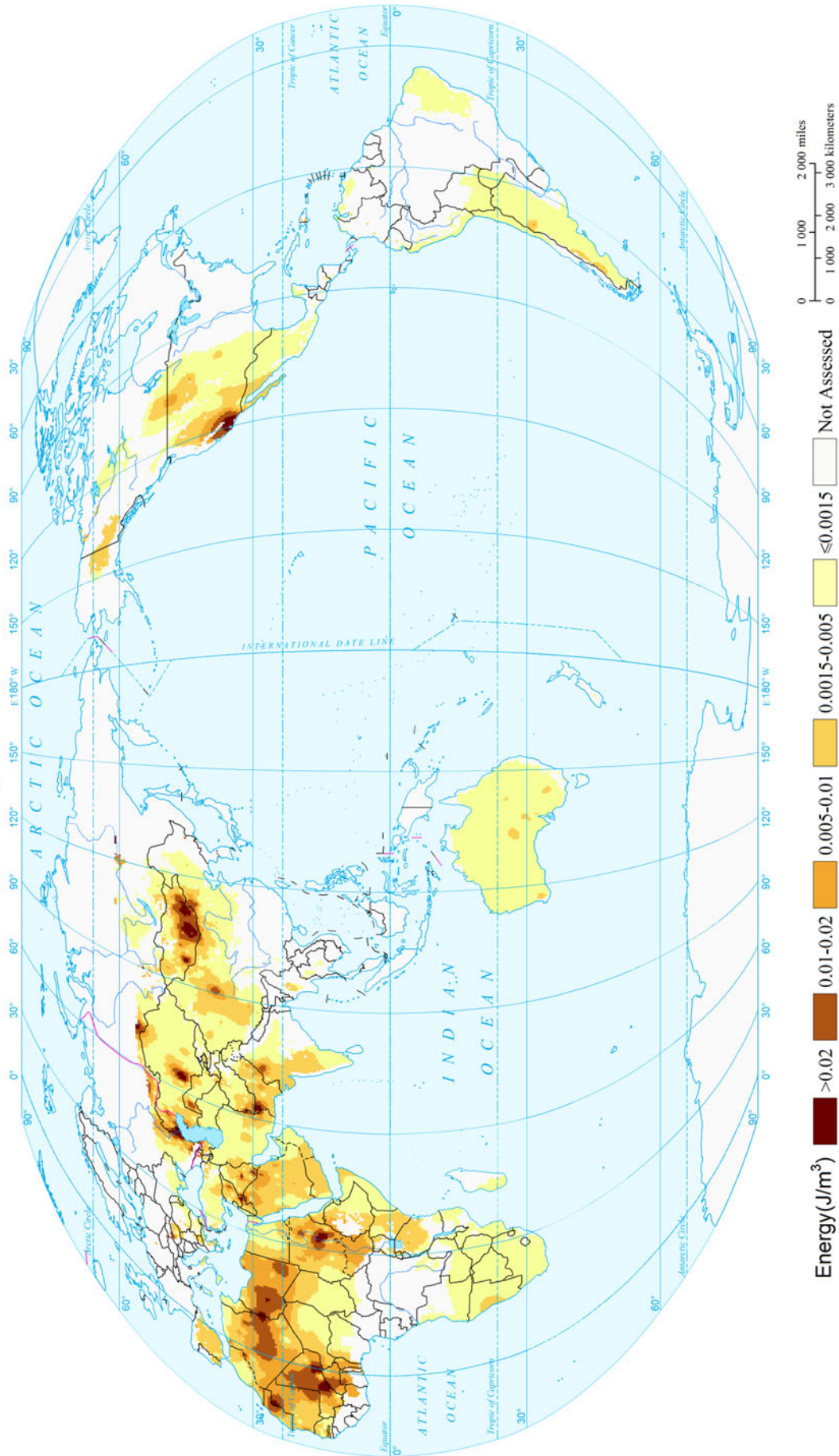


**Susceptibility Level** ■ Extremely High ■ High ■ Moderate ■ Low ■ Extremely Low ■ Not Assessed

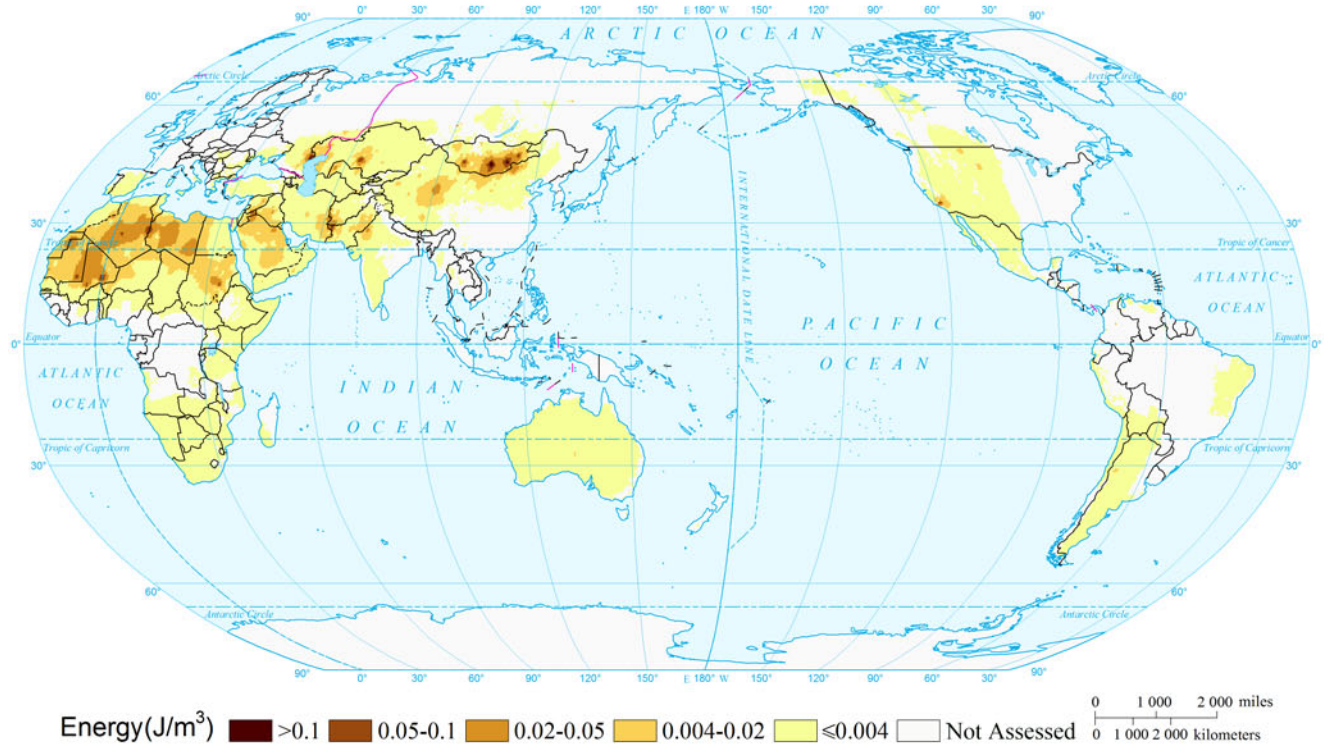
0 1 000 2 000 miles  
0 1 000 2 000 3 000 kilometers



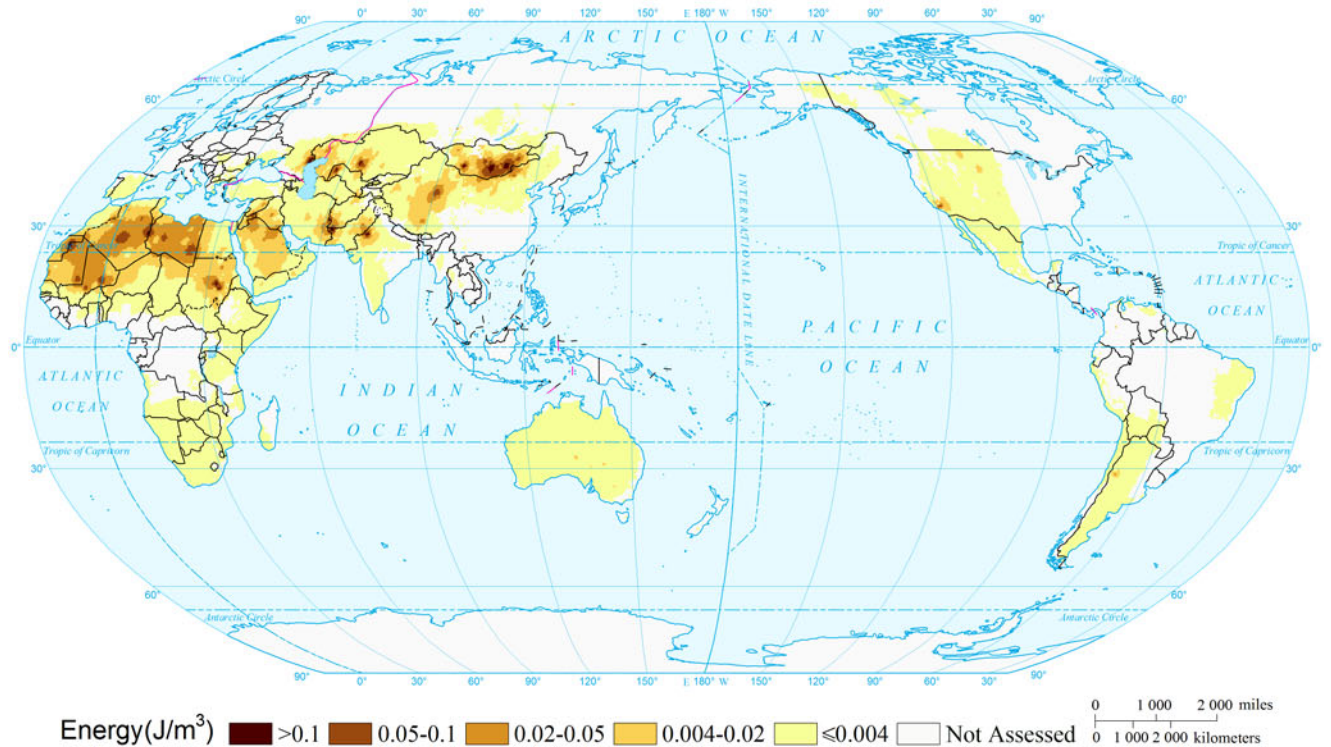
Expected Annual Kinetic Energy of Global Sand-dust Storm (PM<sub>10</sub>)  
(0.5°×0.5°)



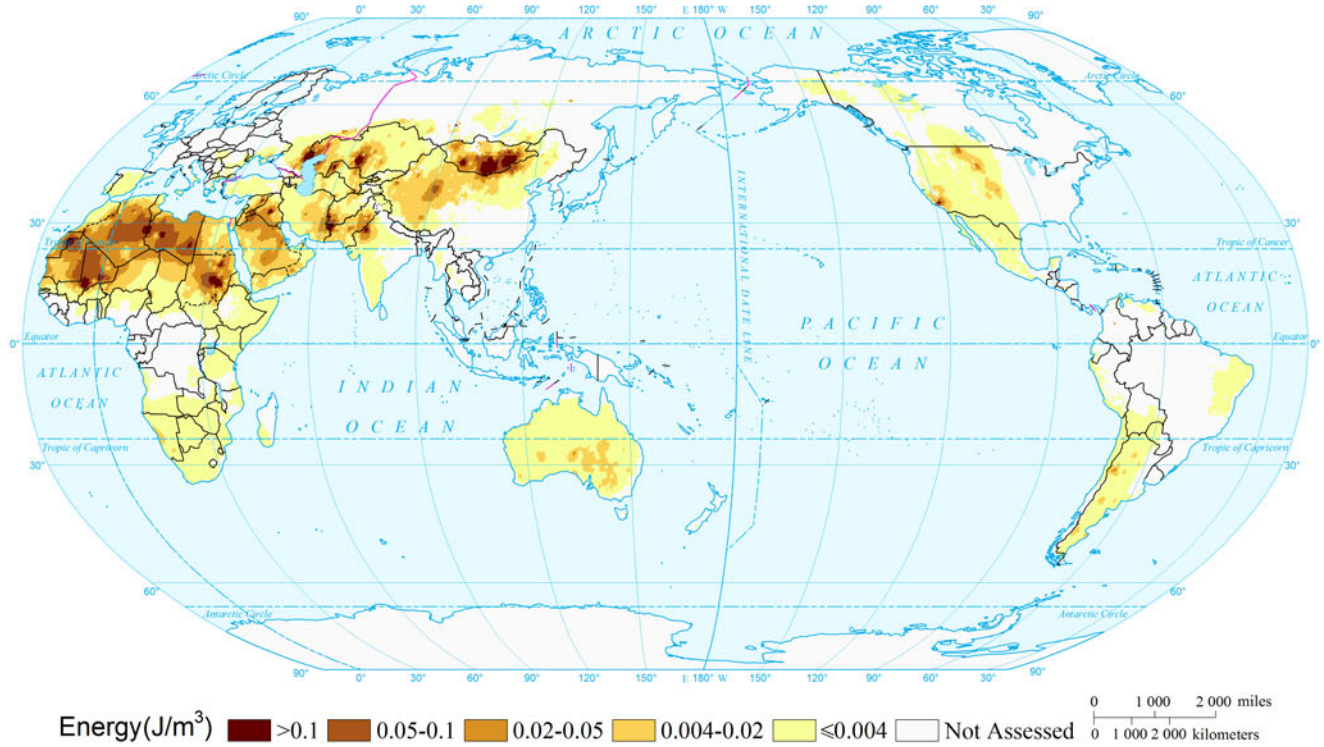
Kinetic Energy of Global Sand-dust Storm (PM<sub>10</sub>) by Return Period (10a)  
(0.5°×0.5°)



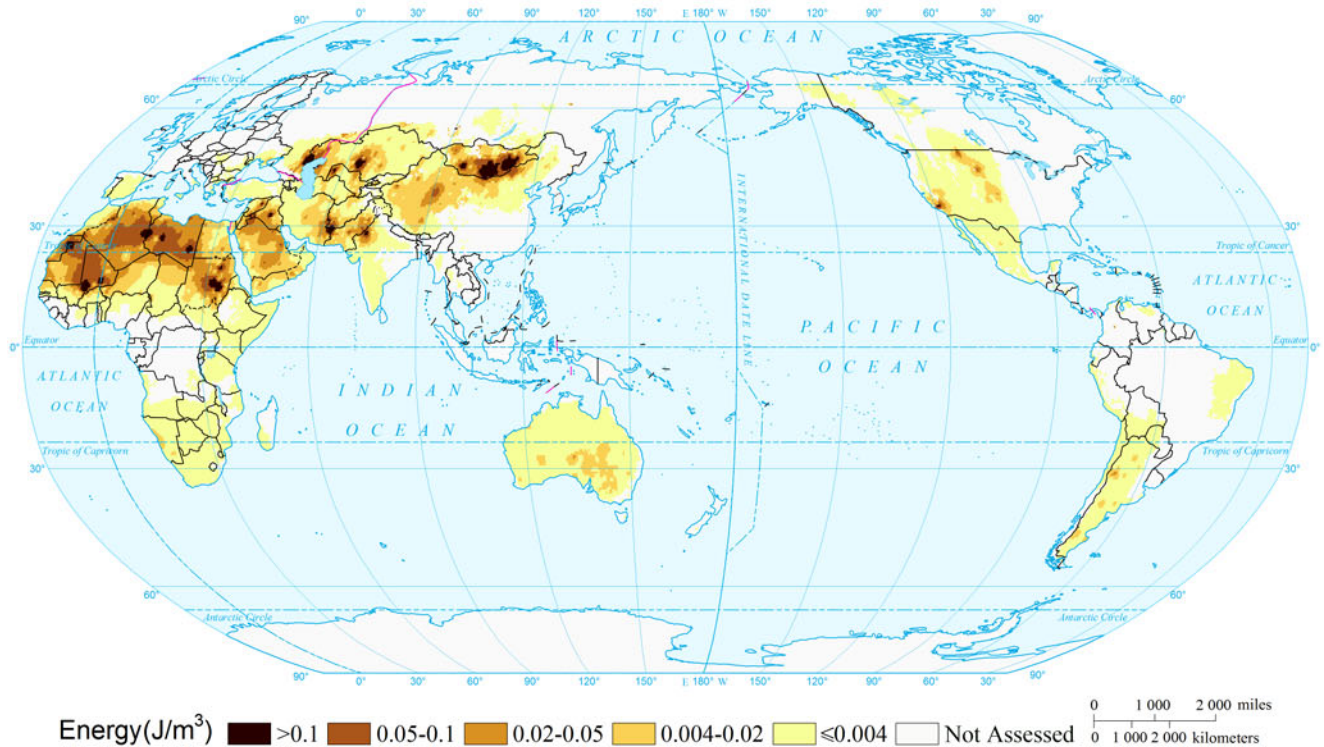
Kinetic Energy of Global Sand-dust Storm (PM<sub>10</sub>) by Return Period (20a)  
(0.5°×0.5°)



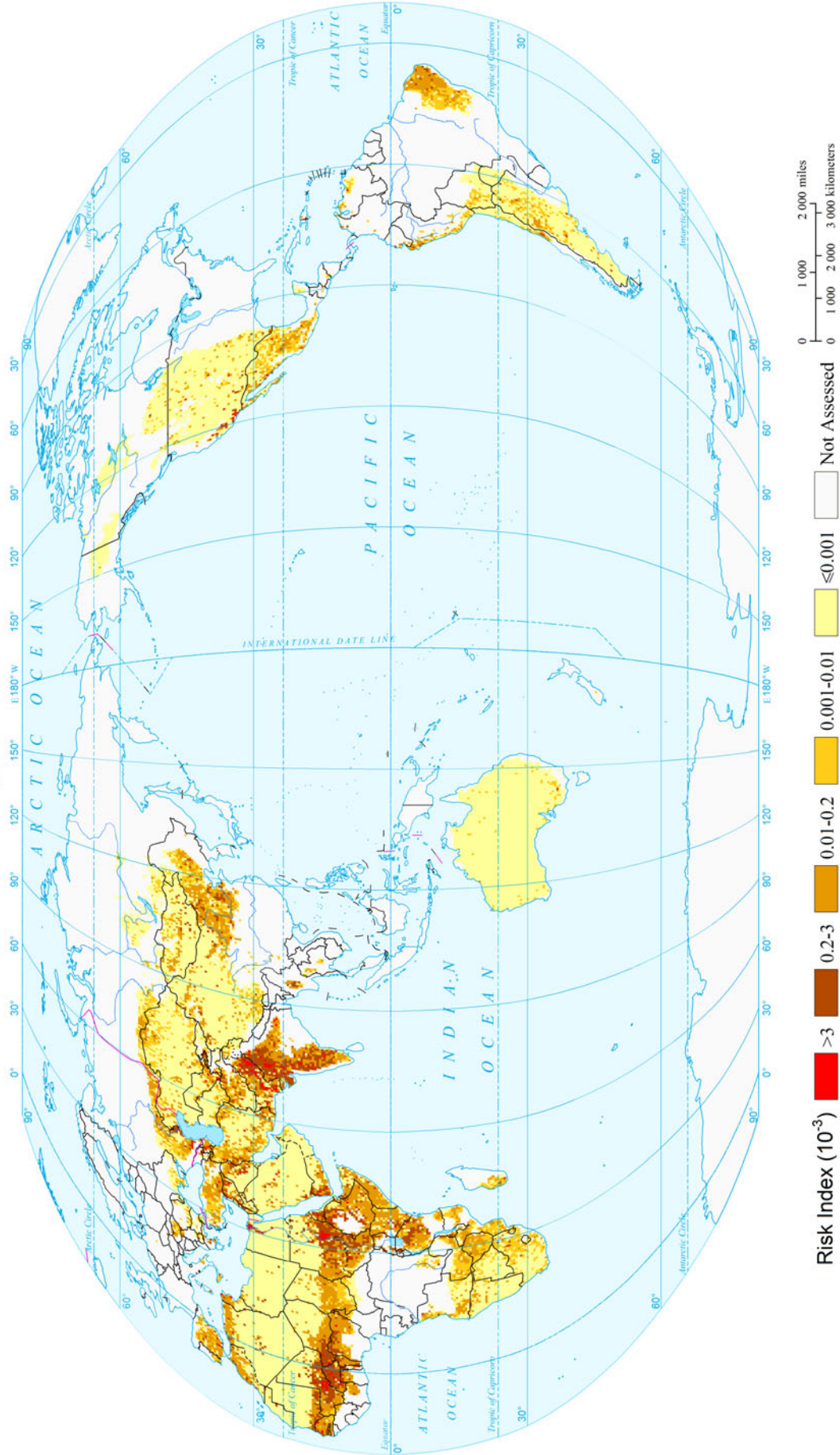
Kinetic Energy of Global Sand-dust Storm (PM<sub>10</sub>) by Return Period (50a)  
(0.5°×0.5°)



Kinetic Energy of Global Sand-dust Storm (PM<sub>10</sub>) by Return Period (100a)  
(0.5°×0.5°)



Expected Annual Affected Population Risk of Sand-dust Storm of the World  
( $0.5^\circ \times 0.5^\circ$ )

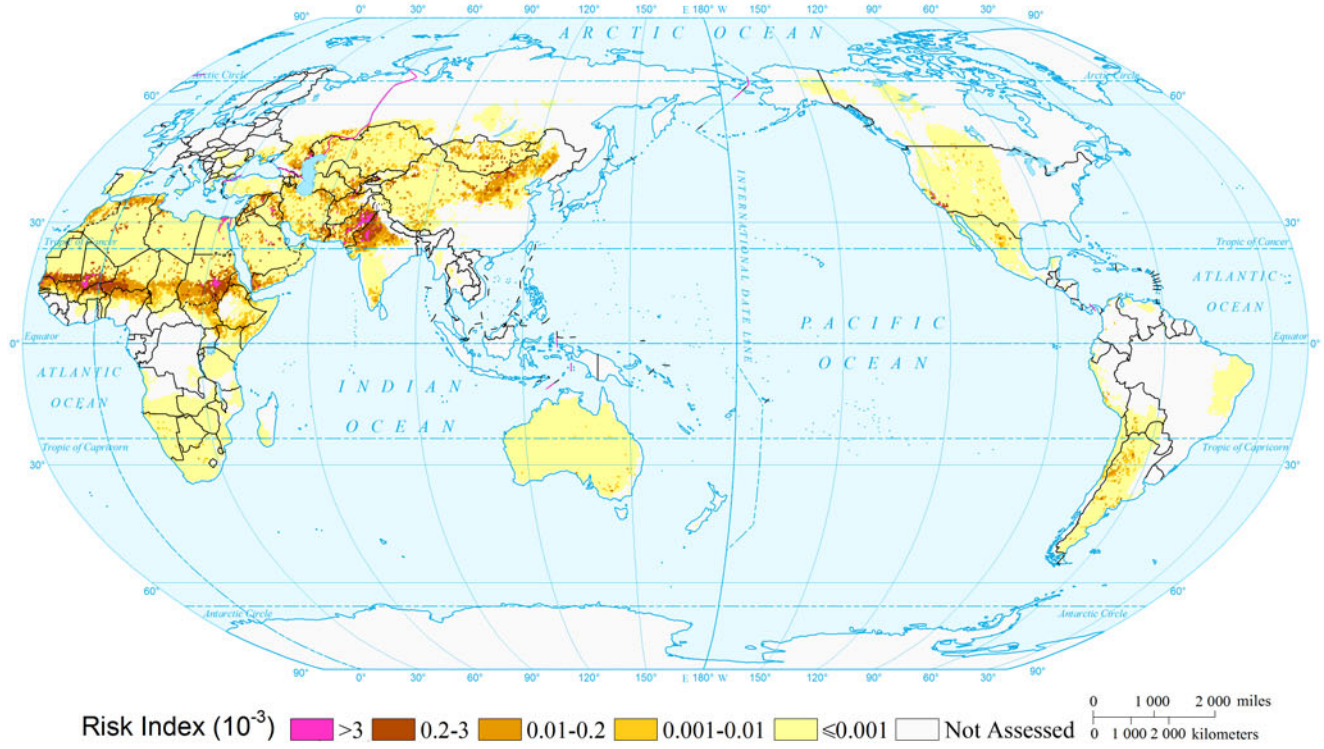


Risk Index ( $10^{-3}$ )

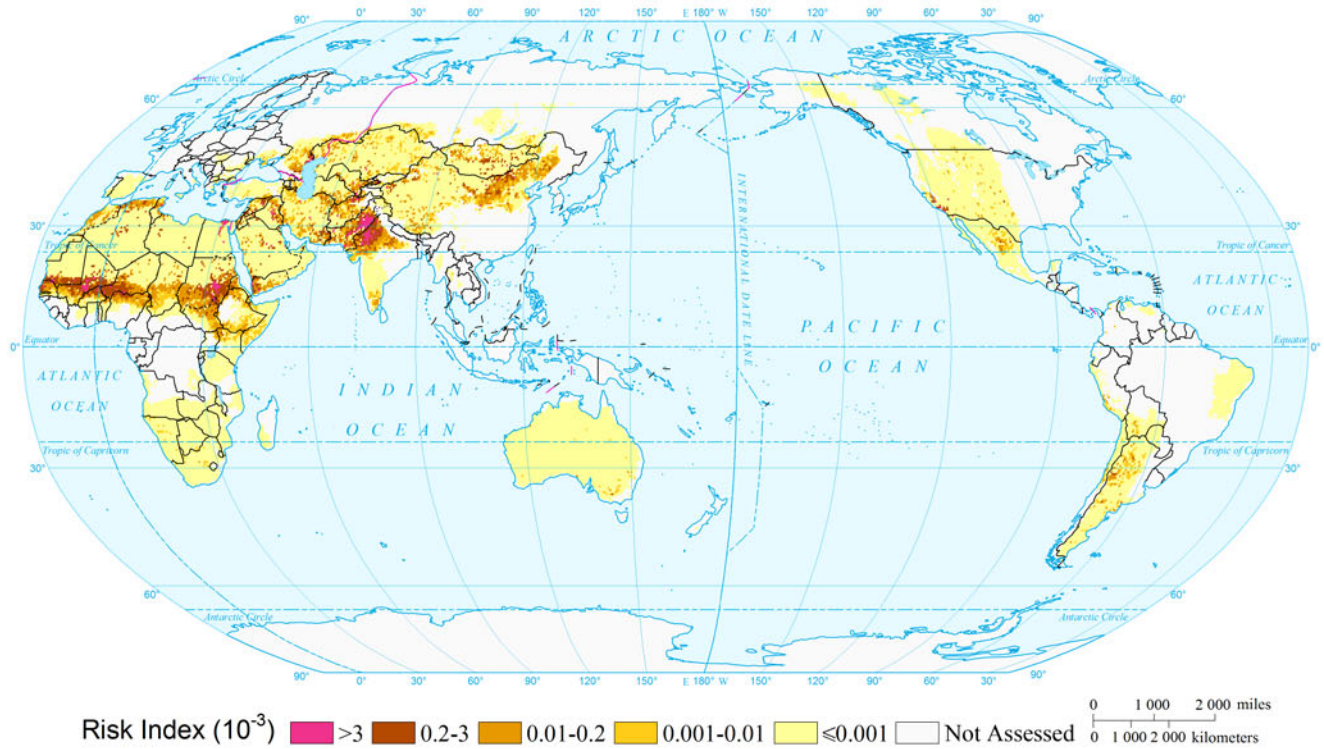
- >3
- 0.2-3
- 0.01-0.2
- 0.001-0.01
- ≤0.001
- Not Assessed

0 1 000 2 000 miles  
0 1 000 2 000 3 000 kilometers

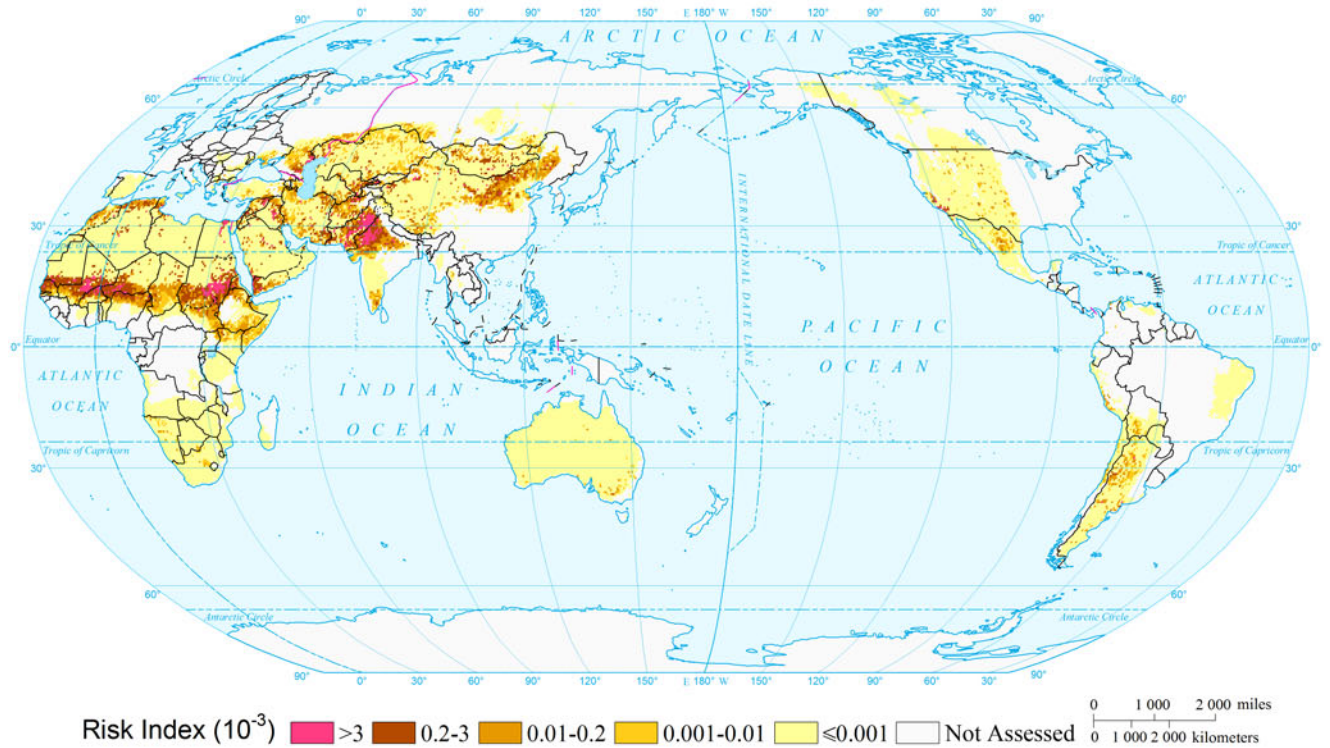
Affected Population Risk of Sand-dust Storm of the World by Return Period (10a)  
(0.5°×0.5°)



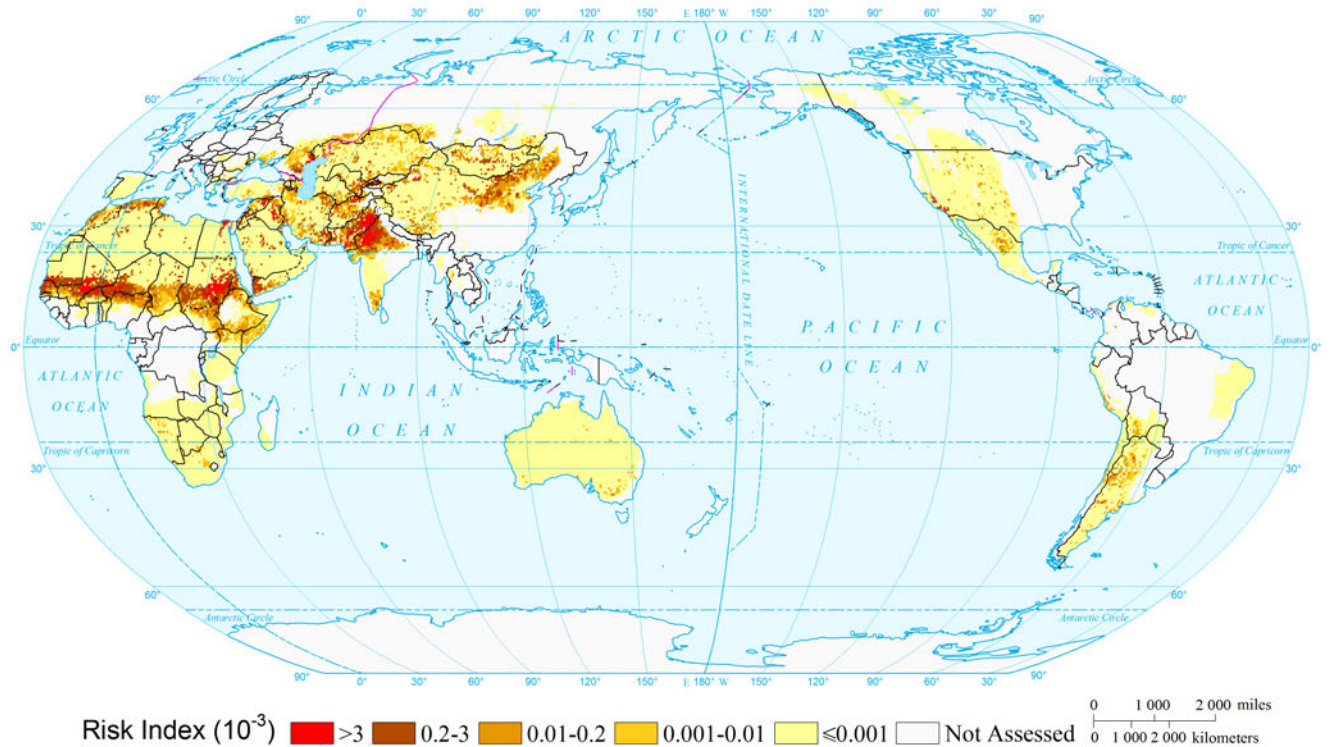
Affected Population Risk of Sand-dust Storm of the World by Return Period (20a)  
(0.5°×0.5°)



Affected Population Risk of Sand-dust Storm of the World by Return Period (50a)  
(0.5°×0.5°)

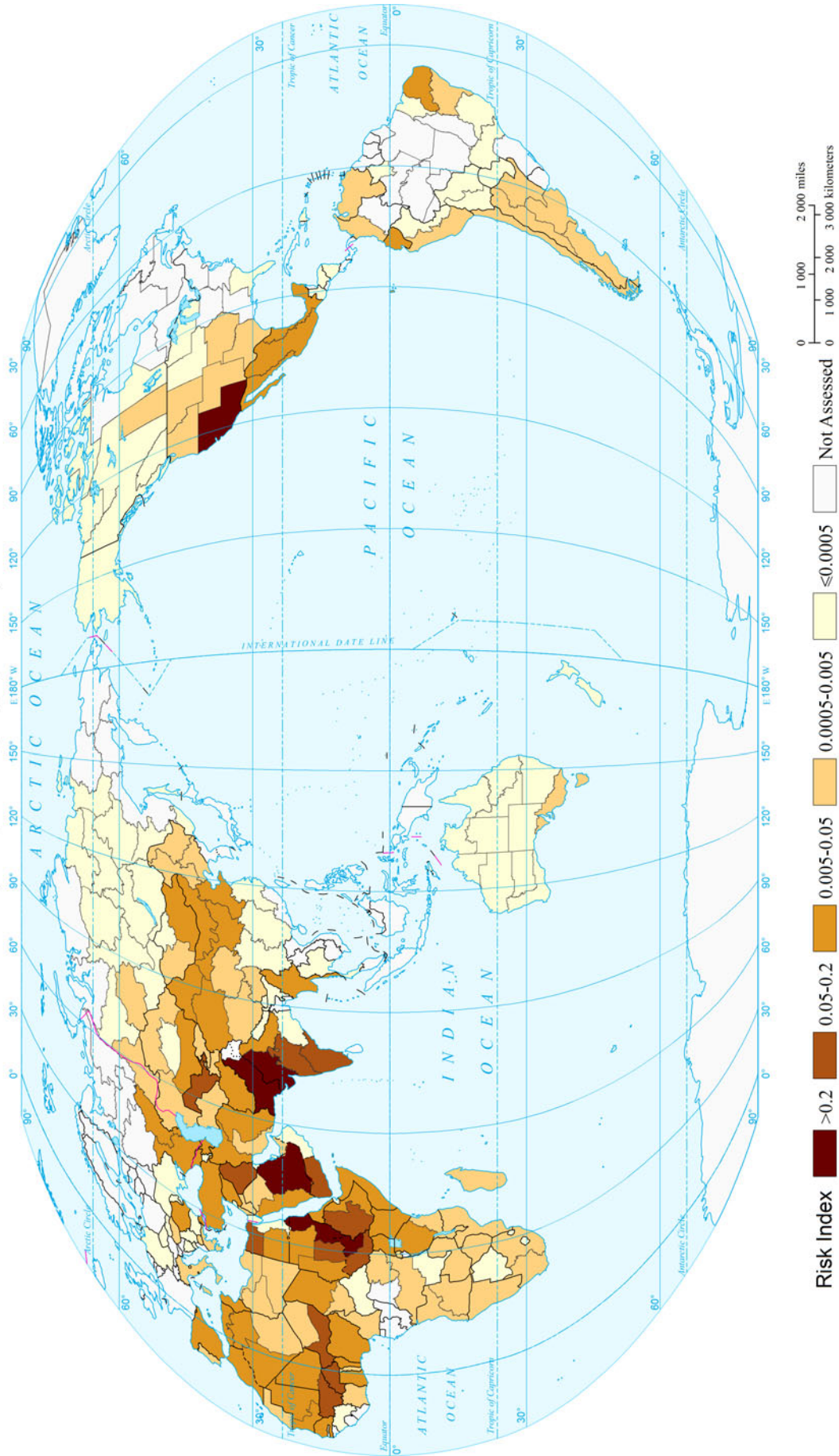


Affected Population Risk of Sand-dust Storm of the World by Return Period (100a)  
(0.5°×0.5°)

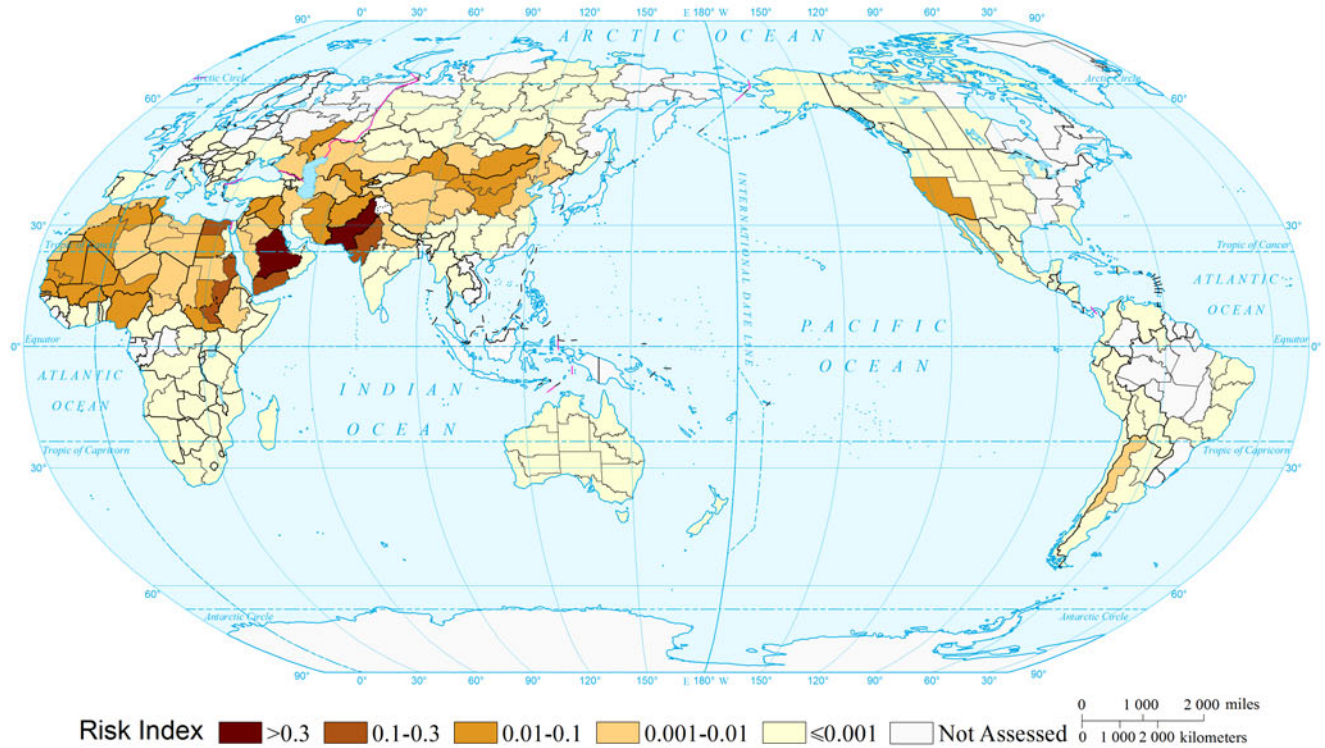




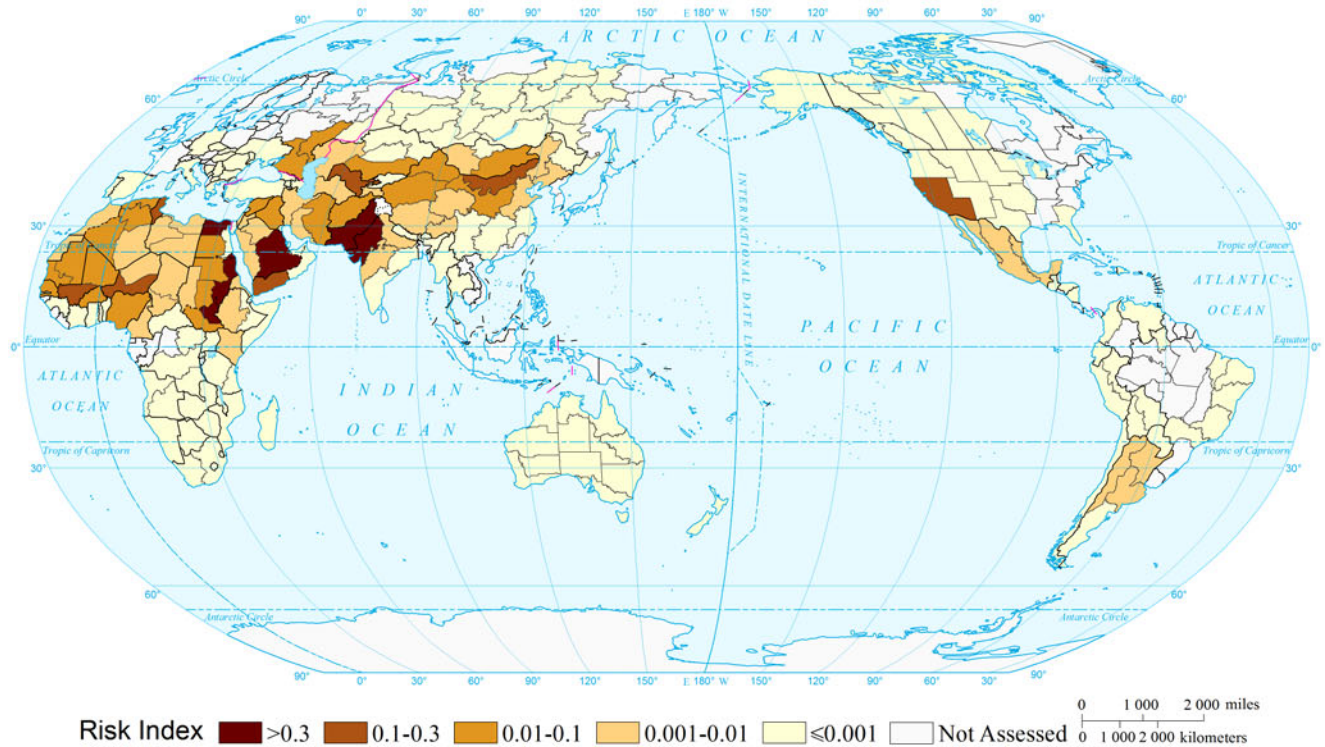
Expected Annual Affected Population Risk of Sand-dust Storm of the World  
(Comparable-geographic Unit)



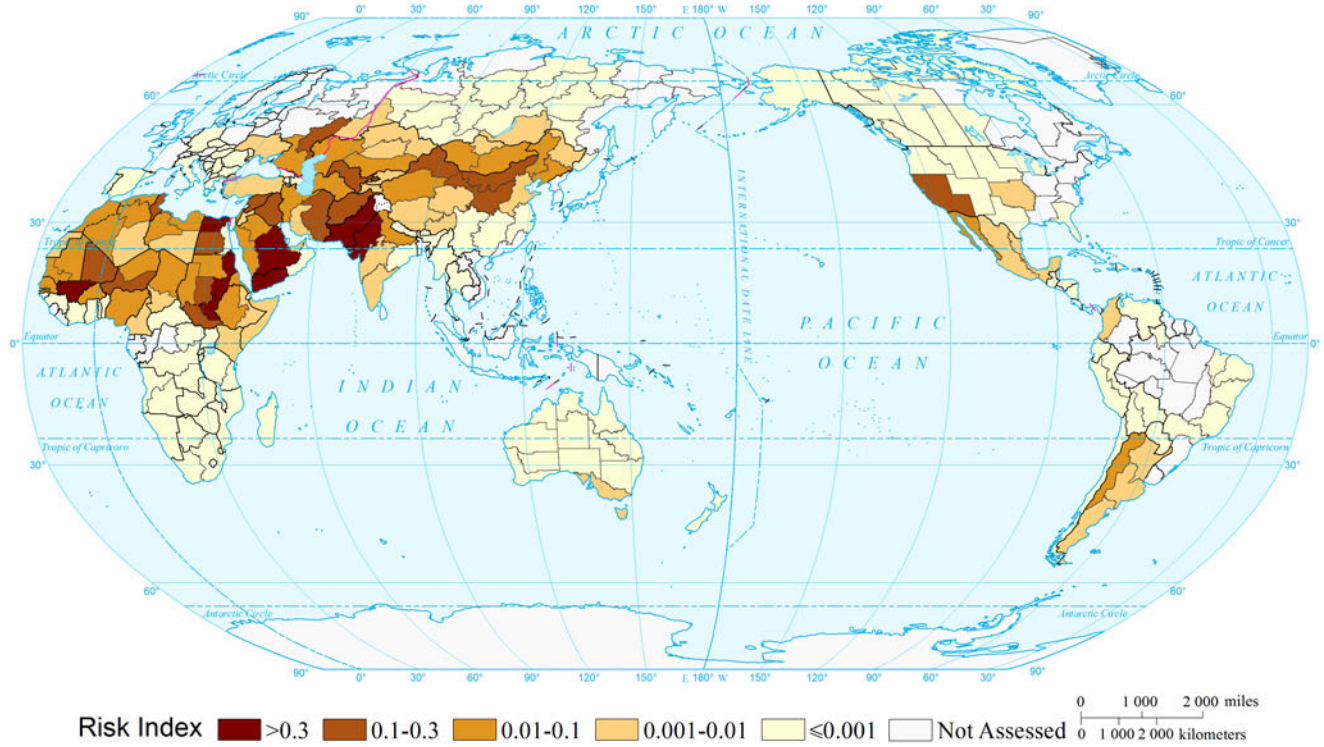
Affected Population Risk of Sand-dust Storm of the World by Return Period (10a)  
(Comparable-geographic Unit)



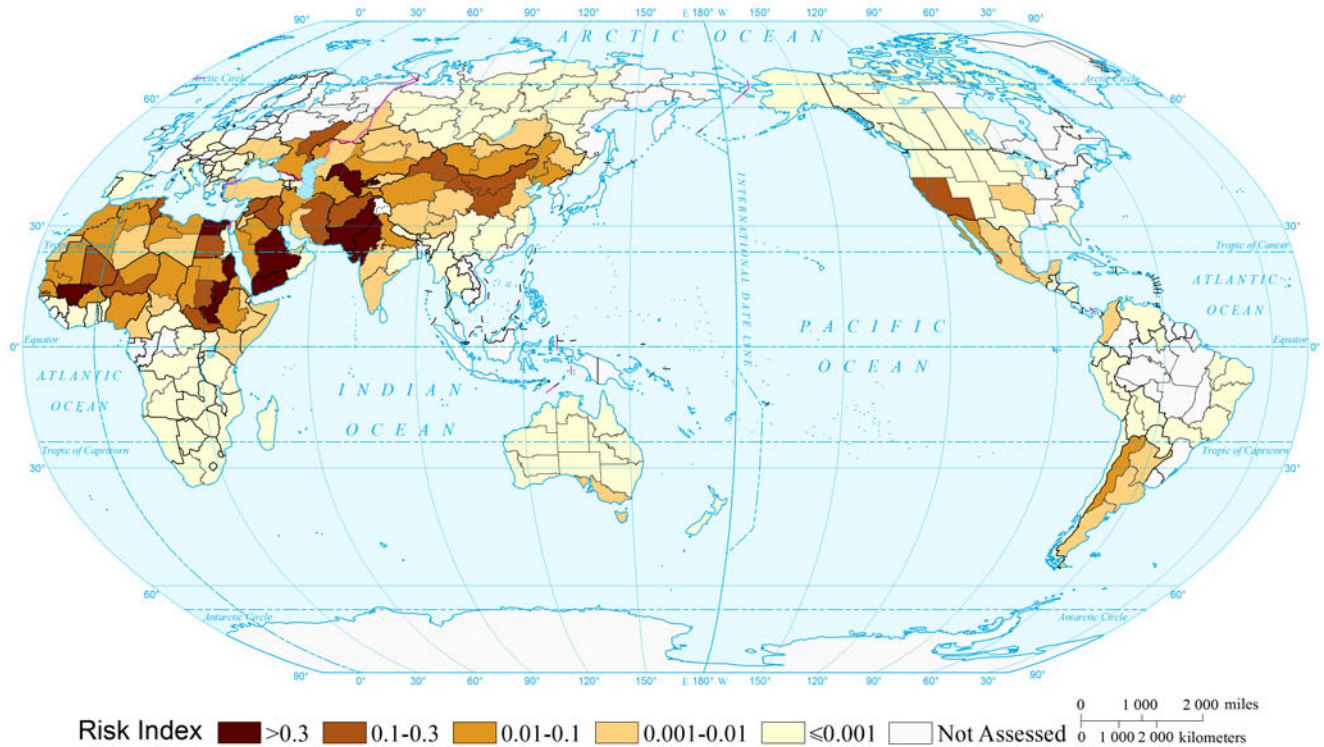
Affected Population Risk of Sand-dust Storm of the World by Return Period (20a)  
(Comparable-geographic Unit)



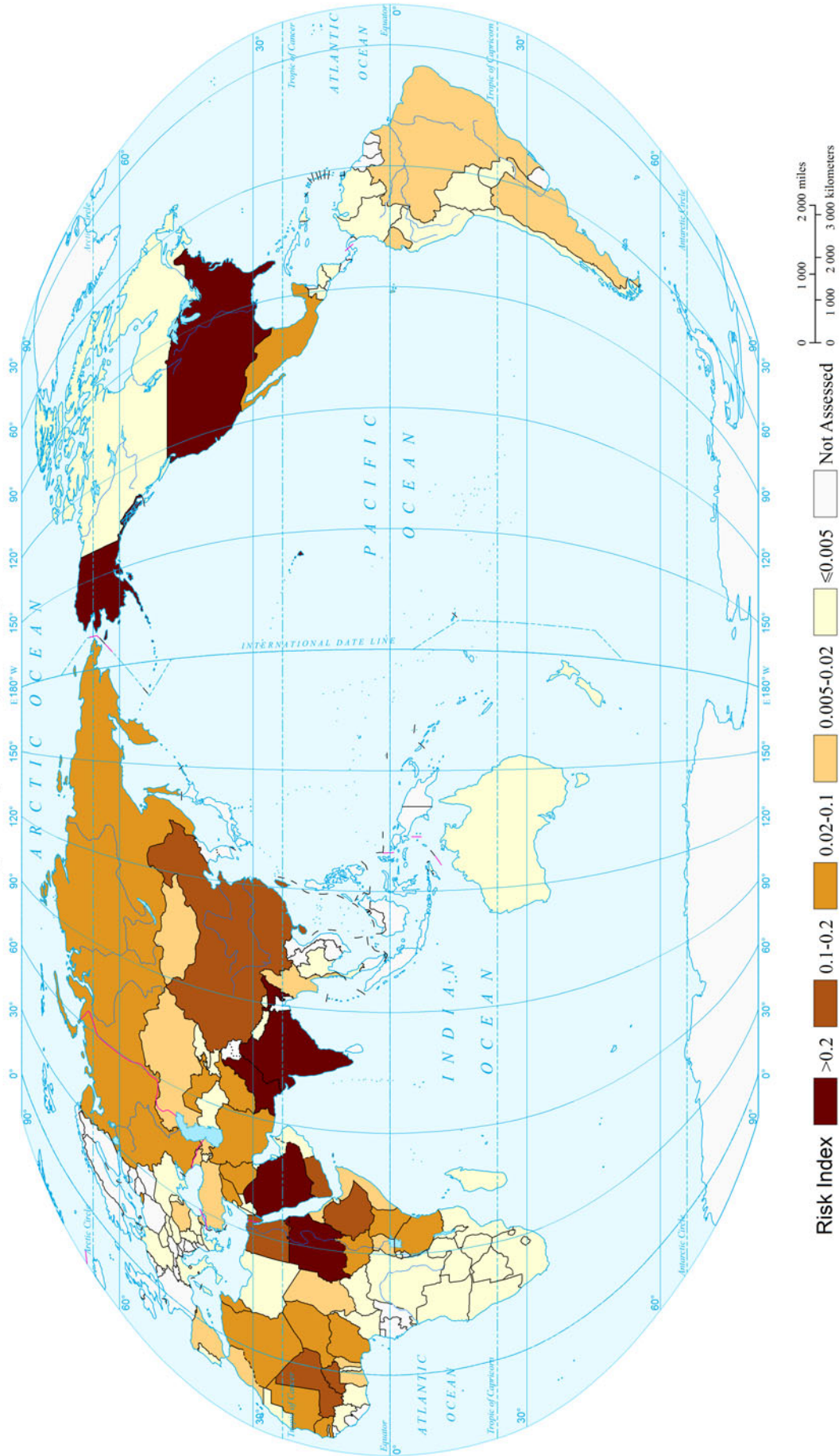
### Affected Population Risk of Sand-dust Storm of the World by Return Period (50a) (Comparable-geographic Unit)



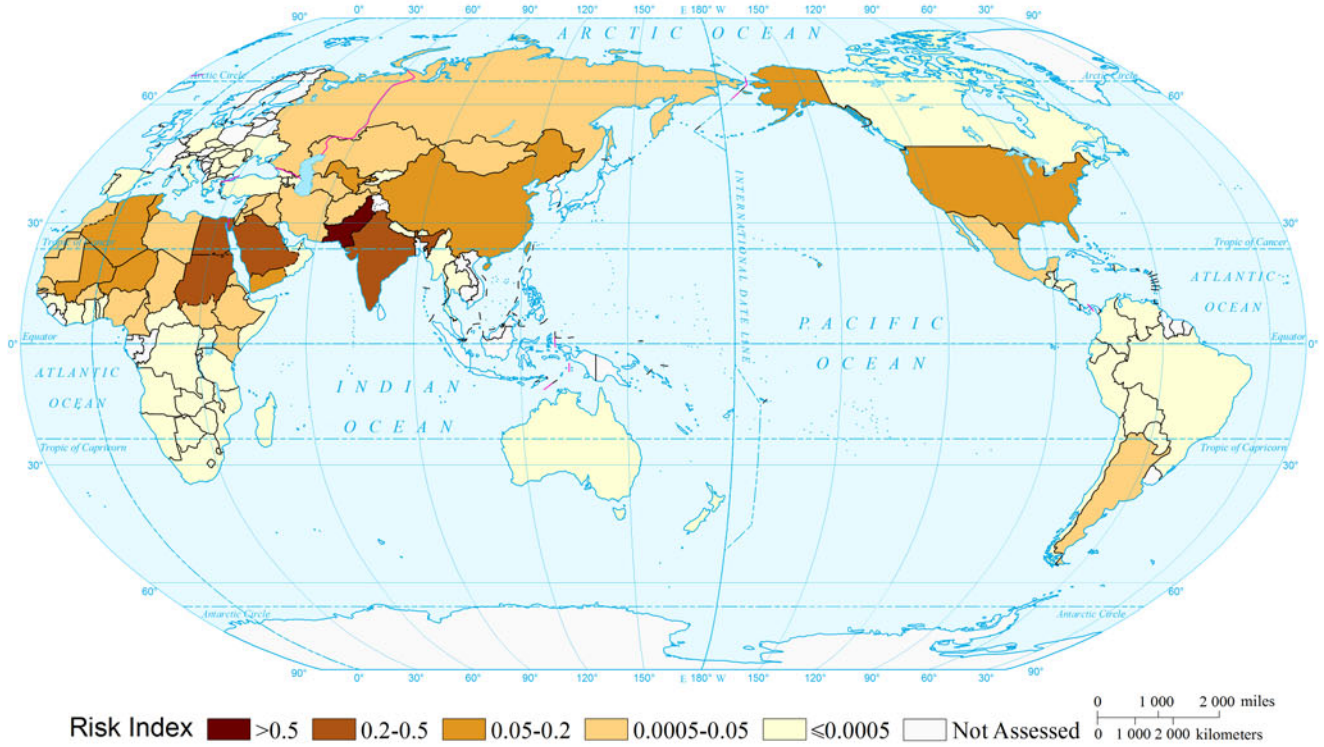
### Affected Population Risk of Sand-dust Storm of the World by Return Period (100a) (Comparable-geographic Unit)



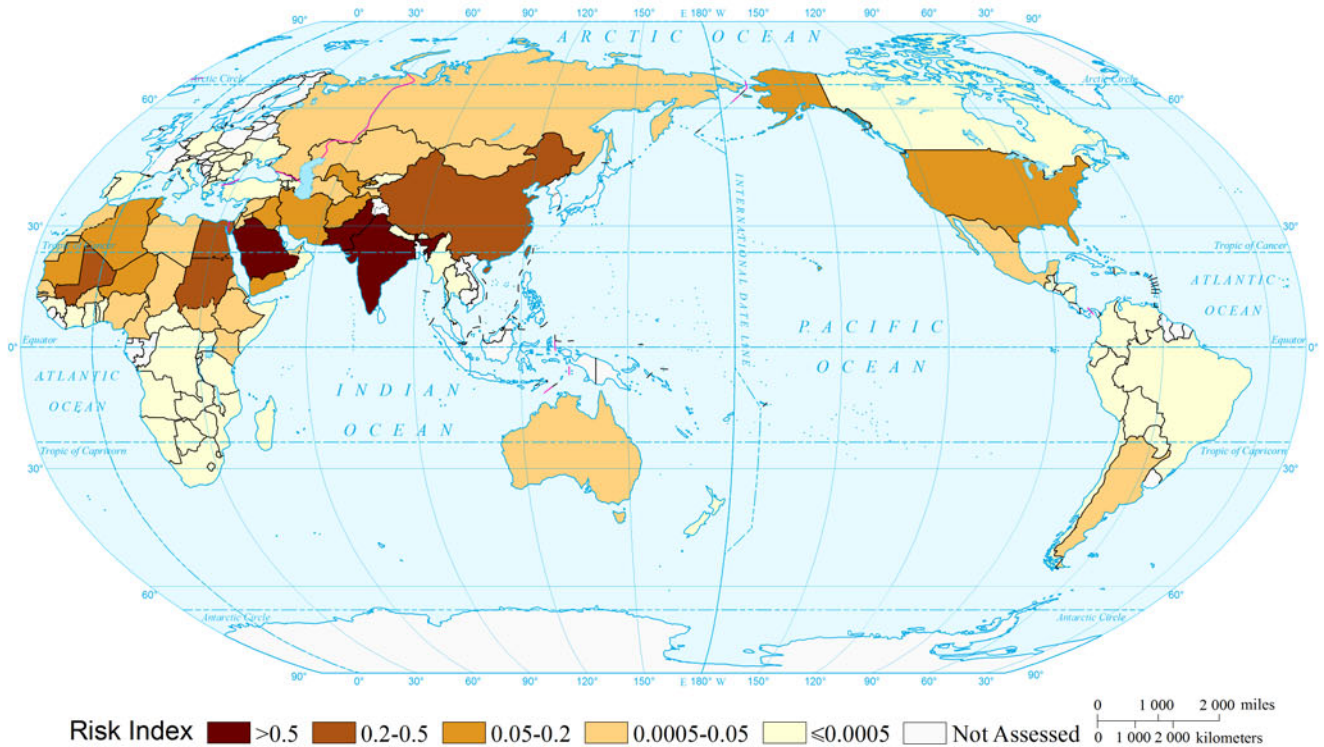
Expected Annual Affected Population Risk of Sand-dust Storm of the World  
(Country and Region Unit)



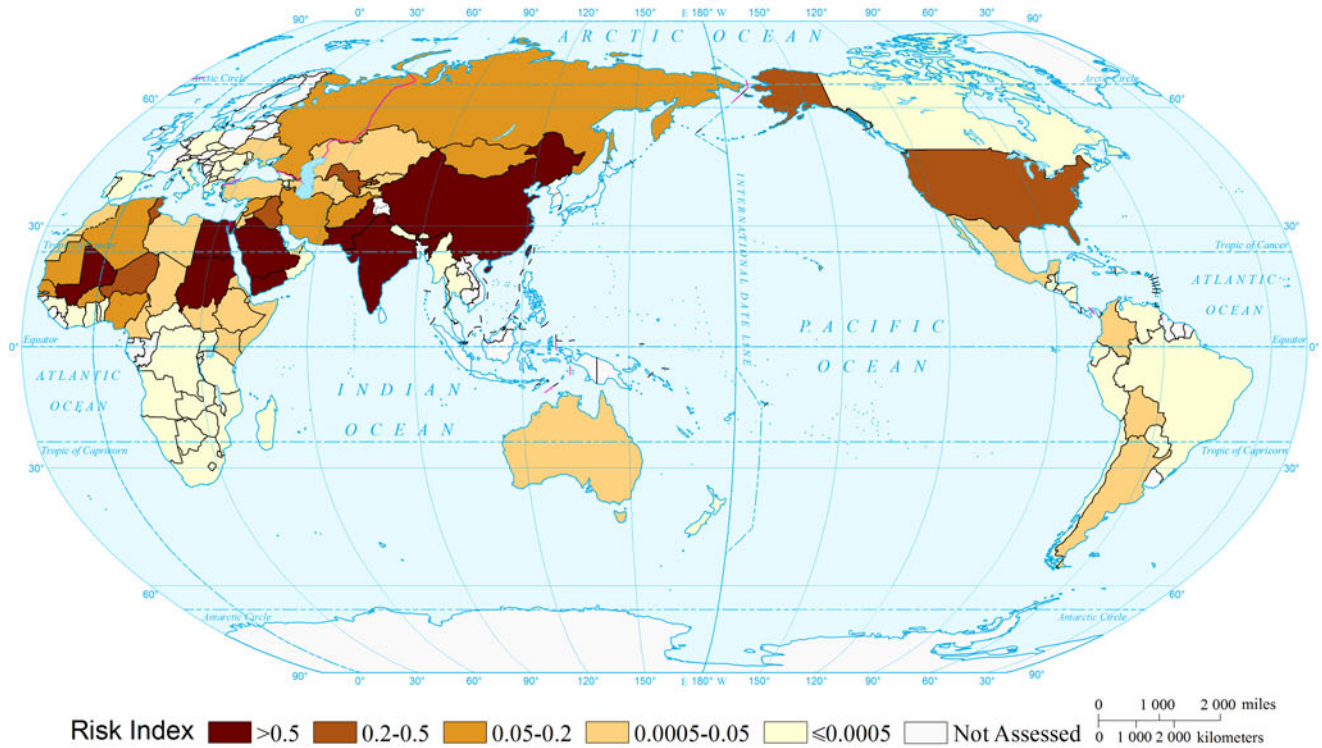
Affected Population Risk of Sand-dust Storm of the World by Return Period (10a)  
(Country and Region Unit)



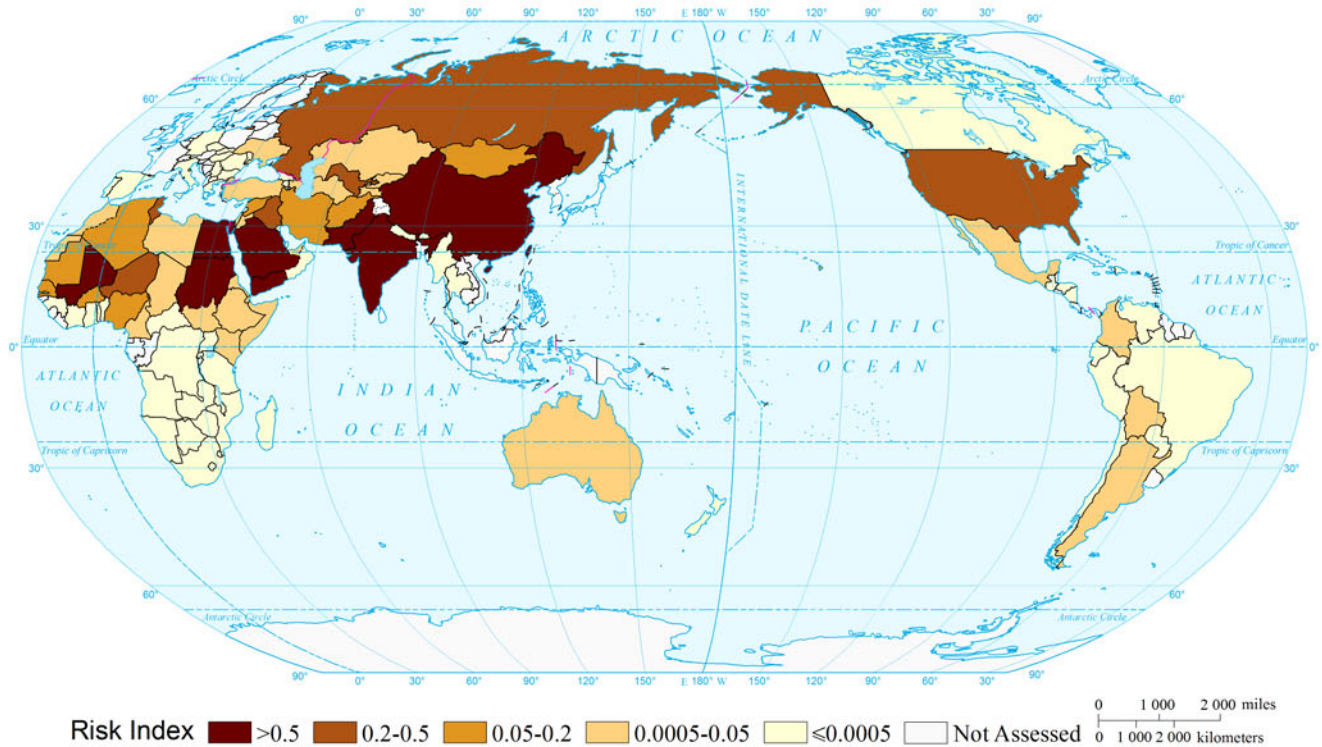
Affected Population Risk of Sand-dust Storm of the World by Return Period (20a)  
(Country and Region Unit)



### Affected Population Risk of Sand-dust Storm of the World by Return Period (50a) (Country and Region Unit)

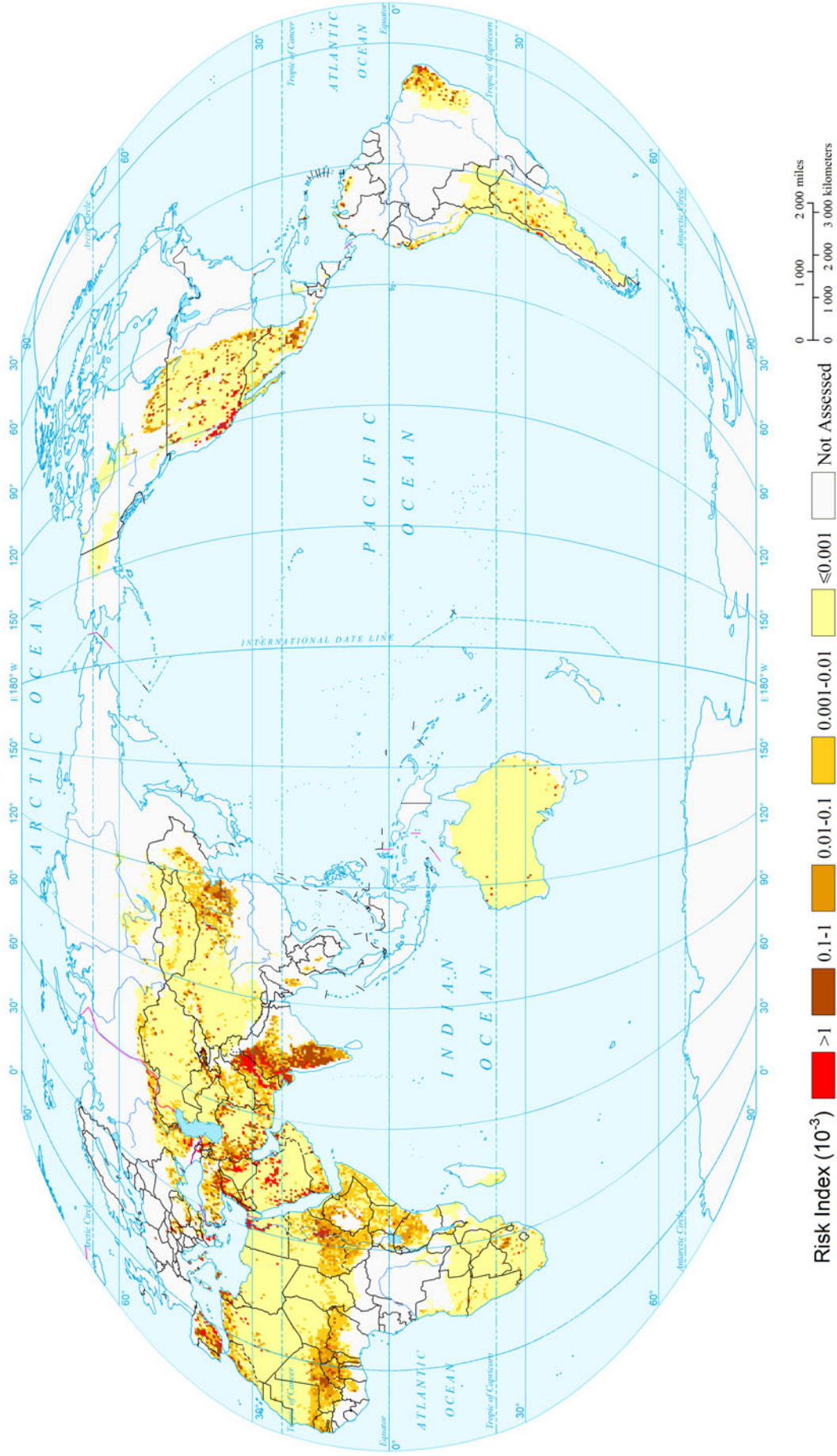


### Affected Population Risk of Sand-dust Storm of the World by Return Period (100a) (Country and Region Unit)

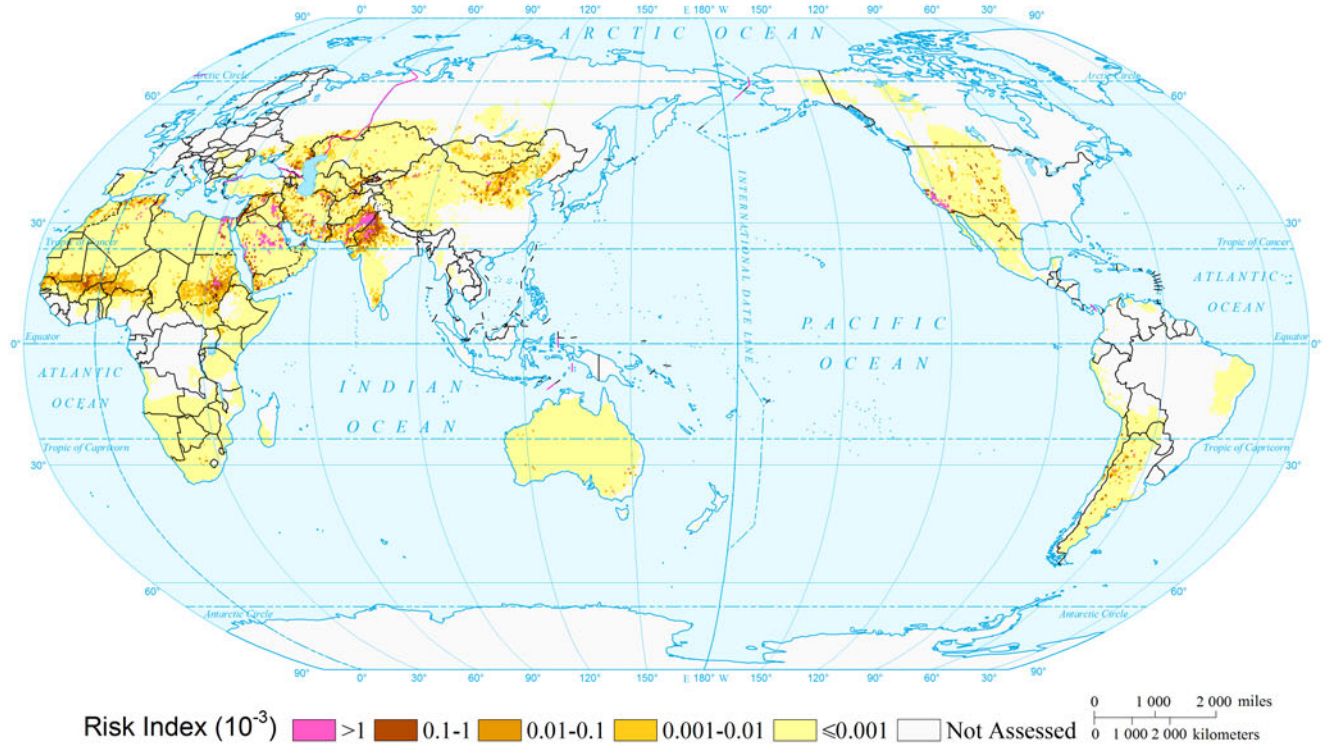




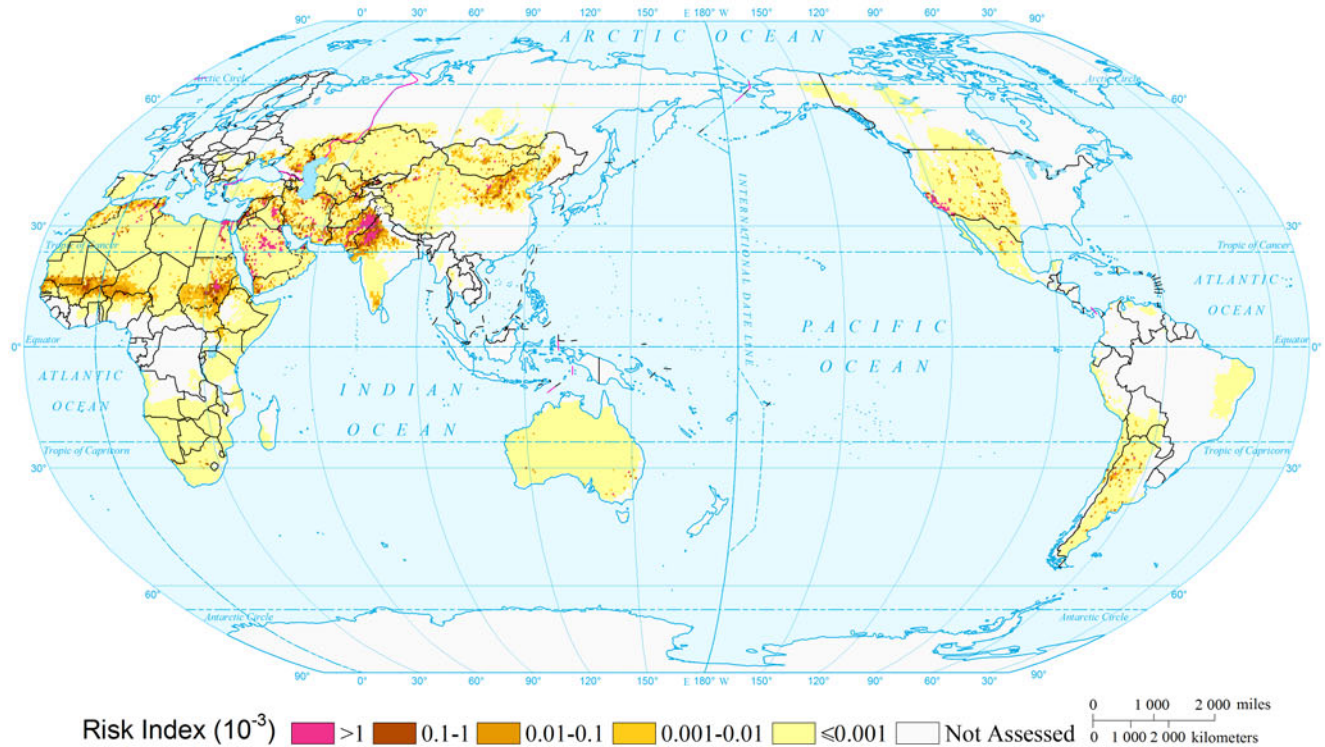
Expected Annual Affected GDP Risk of Sand-dust Storm of the World (0.5°x0.5°)



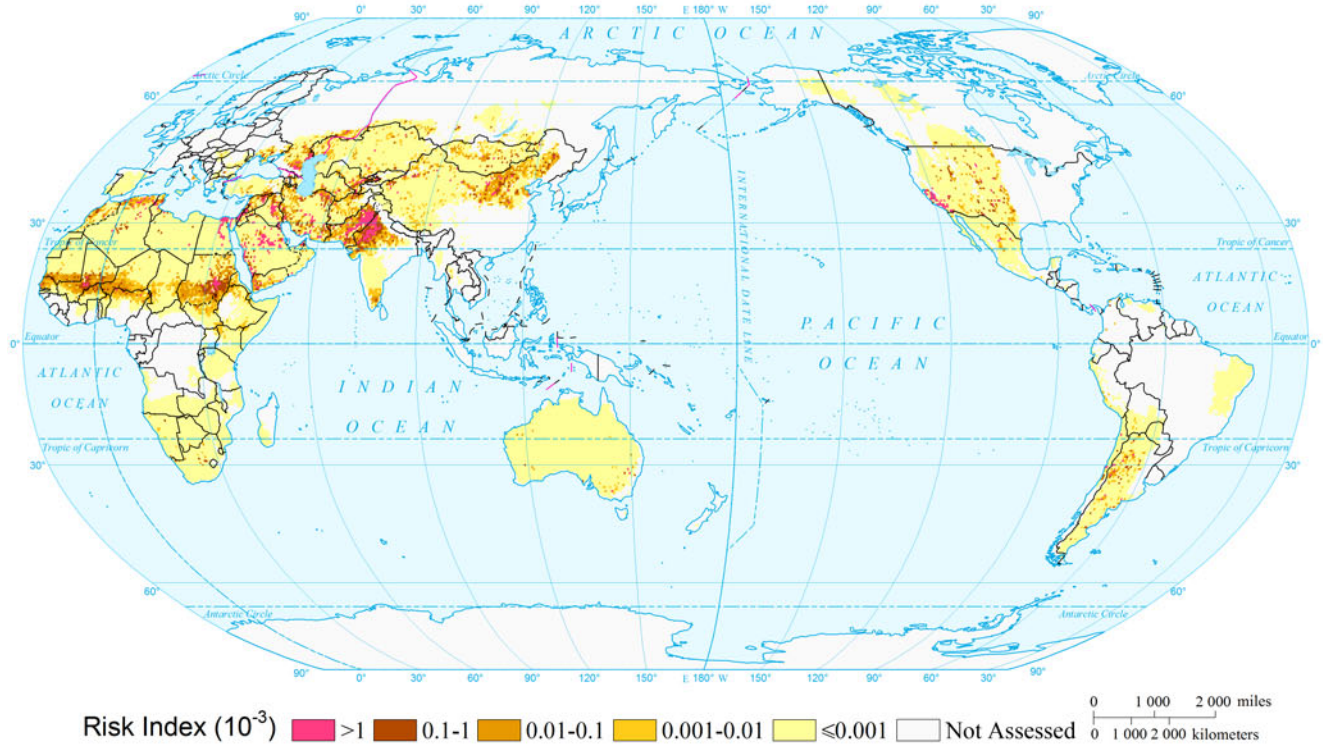
Affected GDP Risk of Sand-dust Storm of the World by Return Period (10a)  
(0.5°×0.5°)



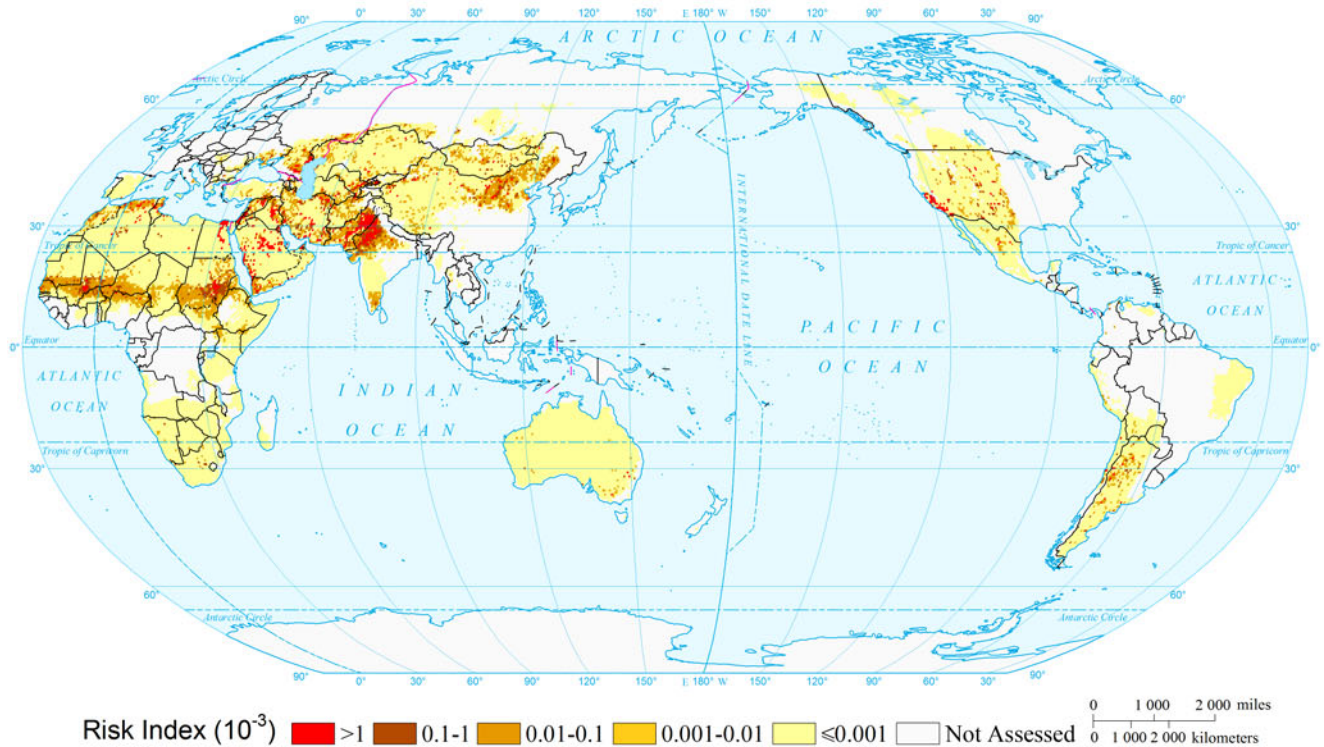
Affected GDP Risk of Sand-dust Storm of the World by Return Period (20a)  
(0.5°×0.5°)



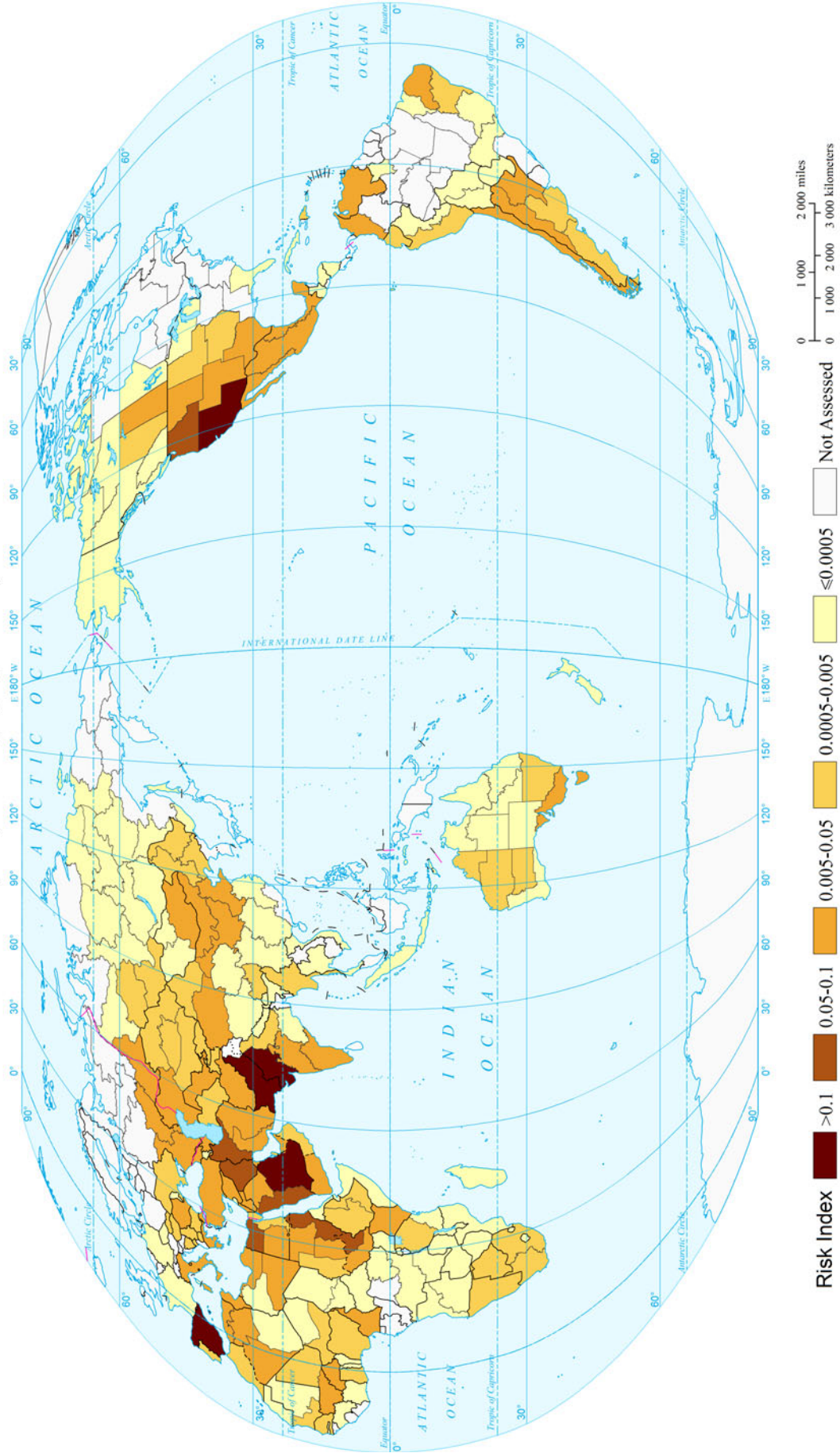
Affected GDP Risk of Sand-dust Storm of the World by Return Period (50a)  
(0.5°×0.5°)



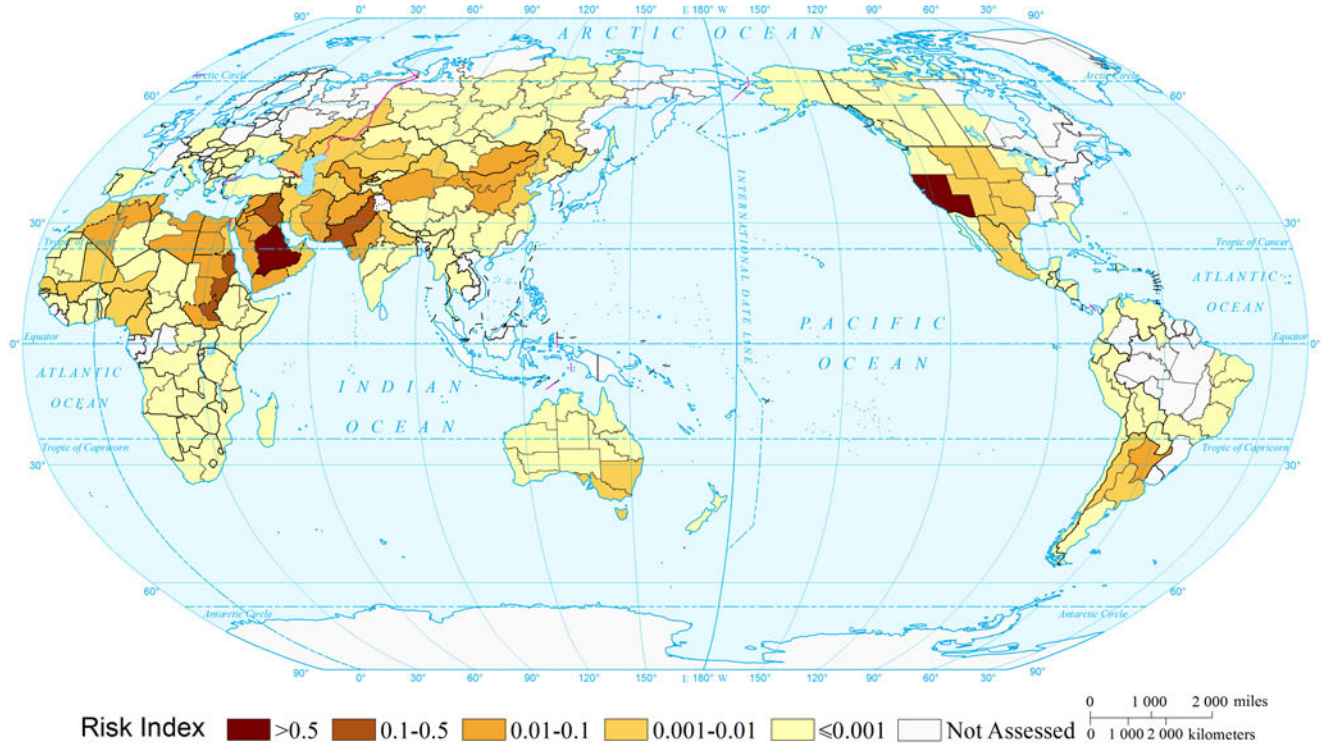
Affected GDP Risk of Sand-dust Storm of the World by Return Period (100a)  
(0.5°×0.5°)



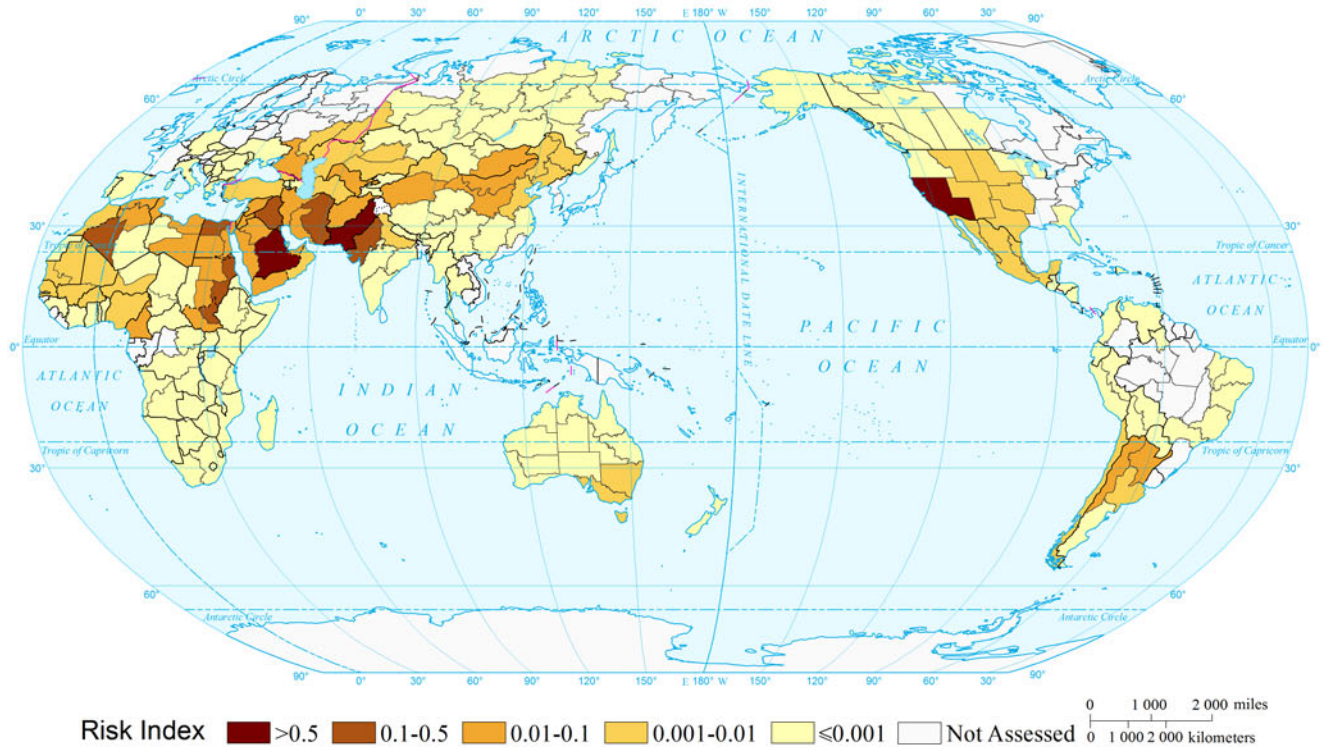
Expected Annual Affected GDP Risk of Sand-dust Storm of the World  
(Comparable-geographic Unit)



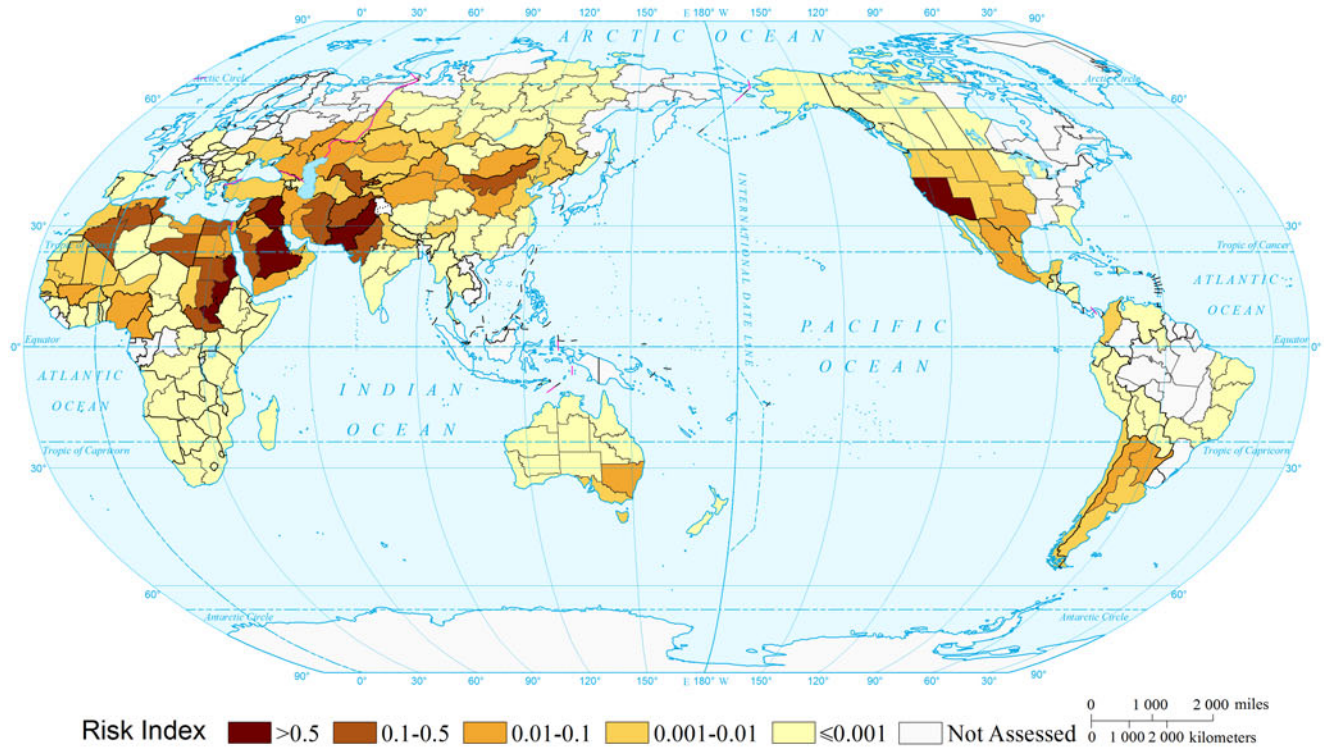
Affected GDP Risk of Sand-dust Storm of the World by Return Period (10a)  
(Comparable-geographic Unit)



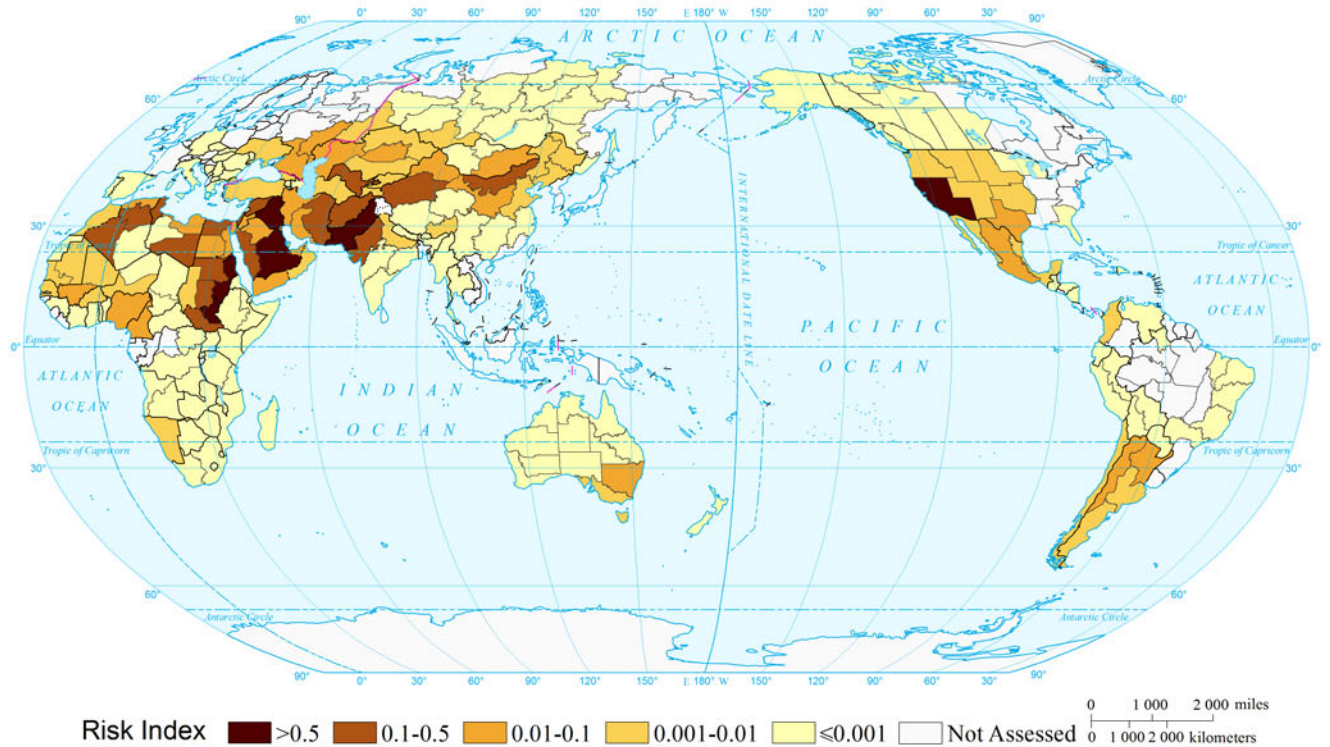
Affected GDP Risk of Sand-dust Storm of the World by Return Period (20a)  
(Comparable-geographic Unit)



Affected GDP Risk of Sand-dust Storm of the World by Return Period (50a)  
(Comparable-geographic Unit)

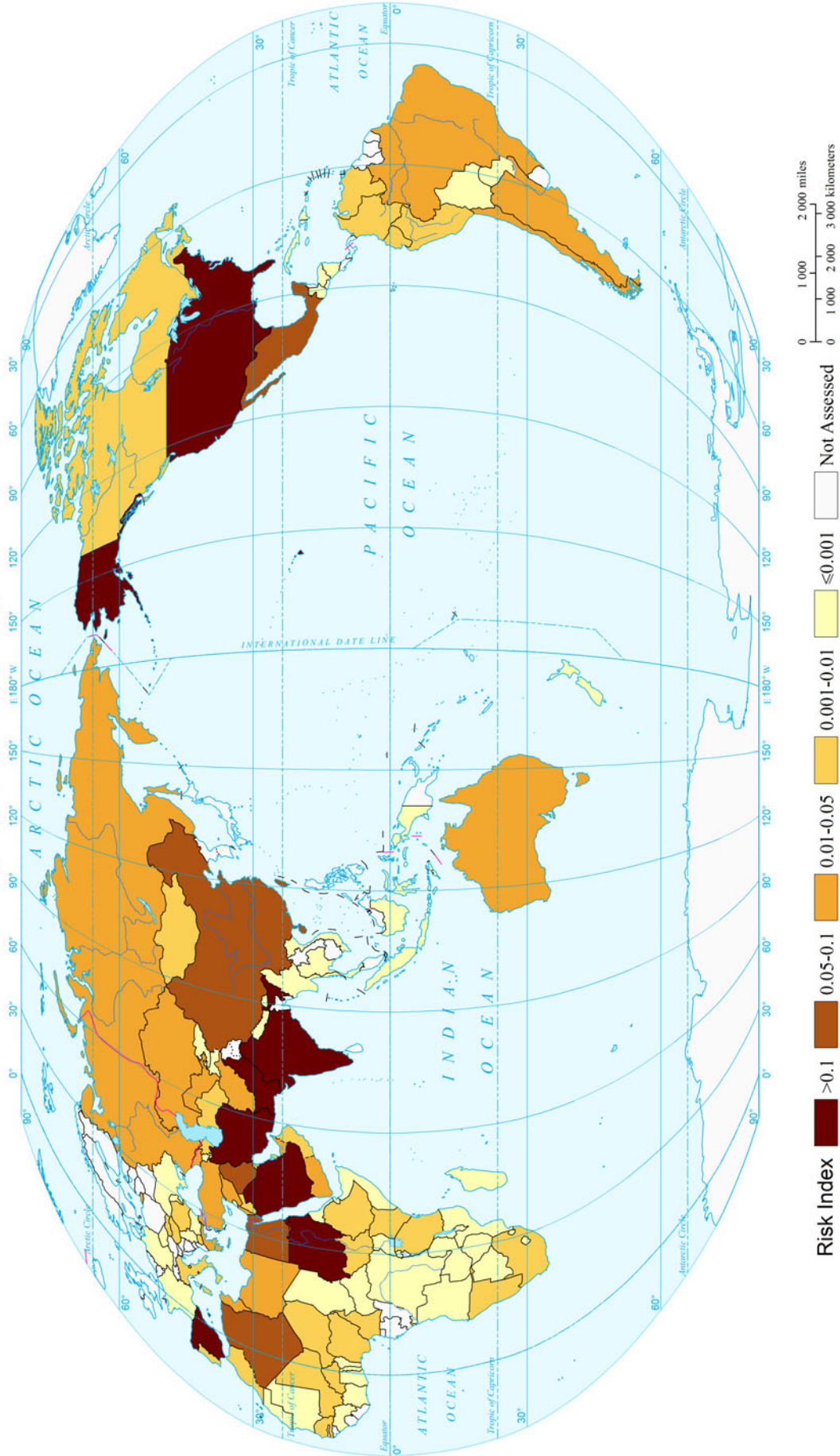


Affected GDP Risk of Sand-dust Storm of the World by Return Period (100a)  
(Comparable-geographic Unit)

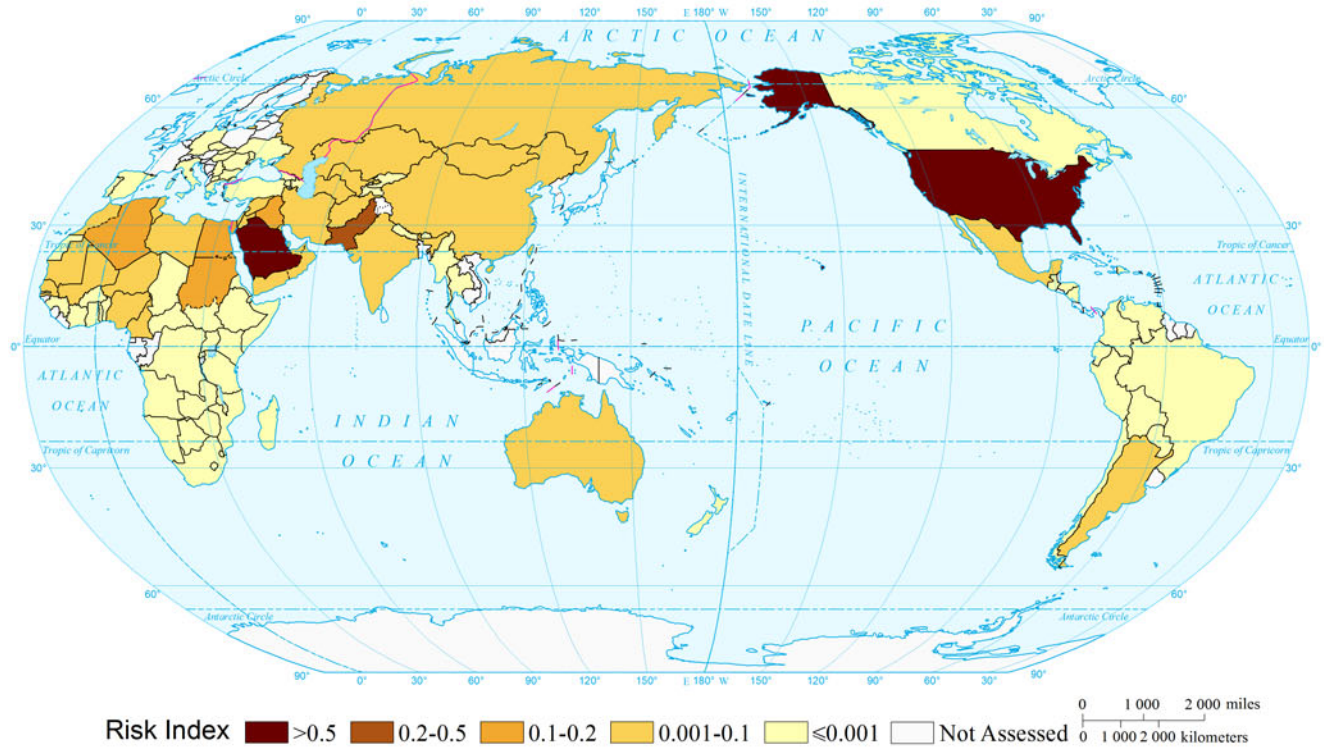




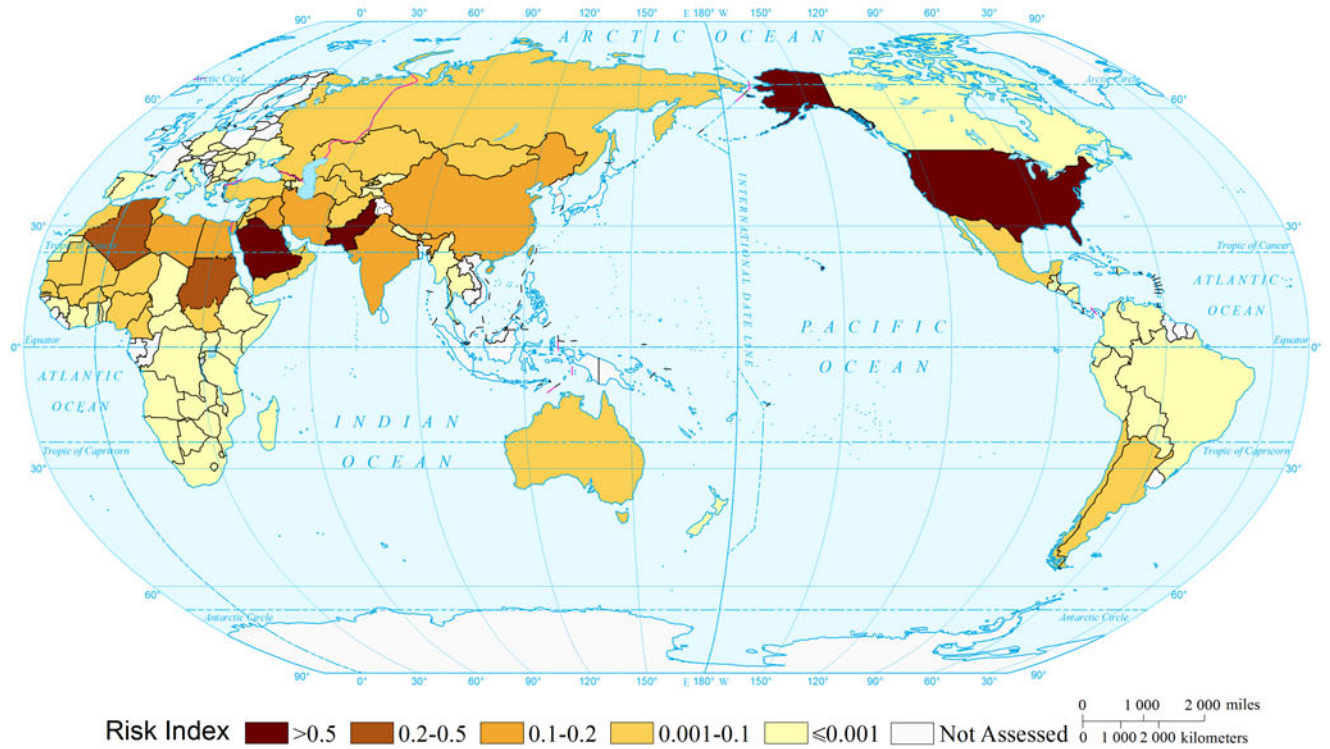
Expected Annual Affected GDP Risk of Sand-dust Storm of the World  
(Country and Region Unit)



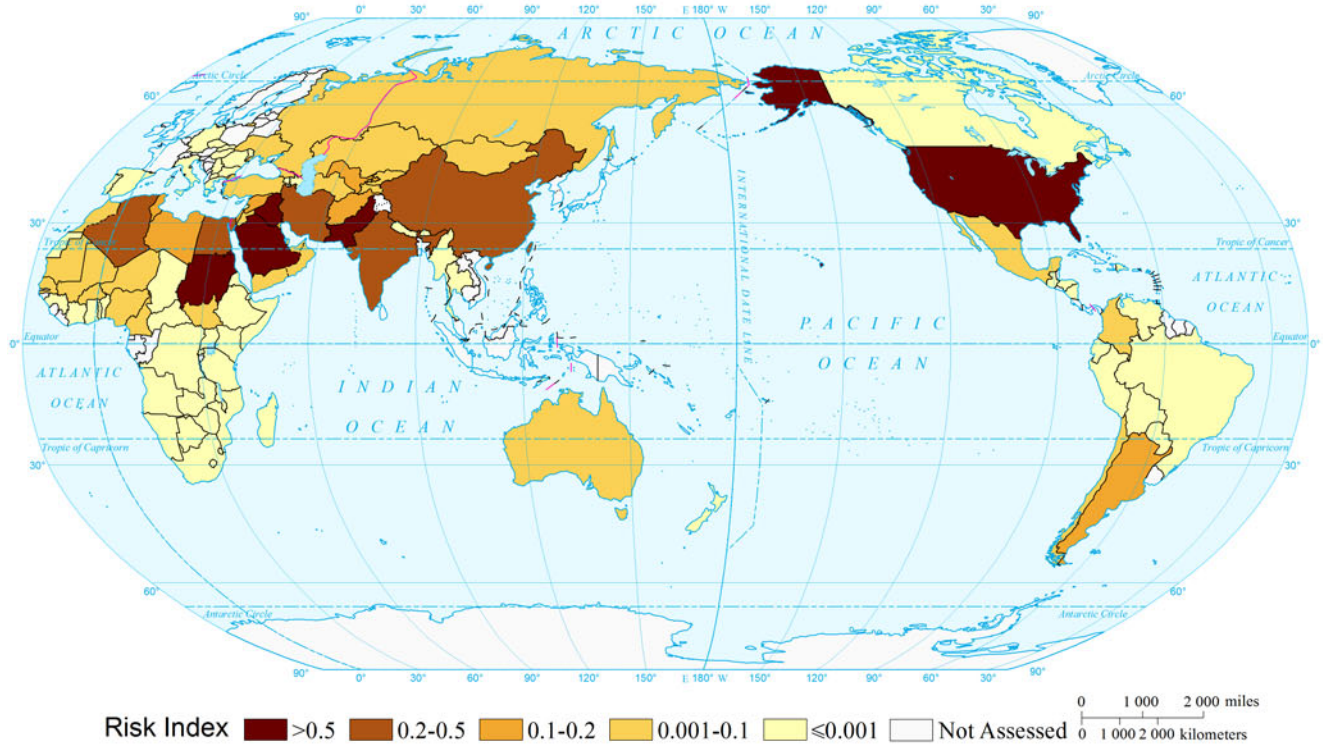
Affected GDP Risk of Sand-dust Storm of the World by Return Period (10a)  
(Country and Region Unit)



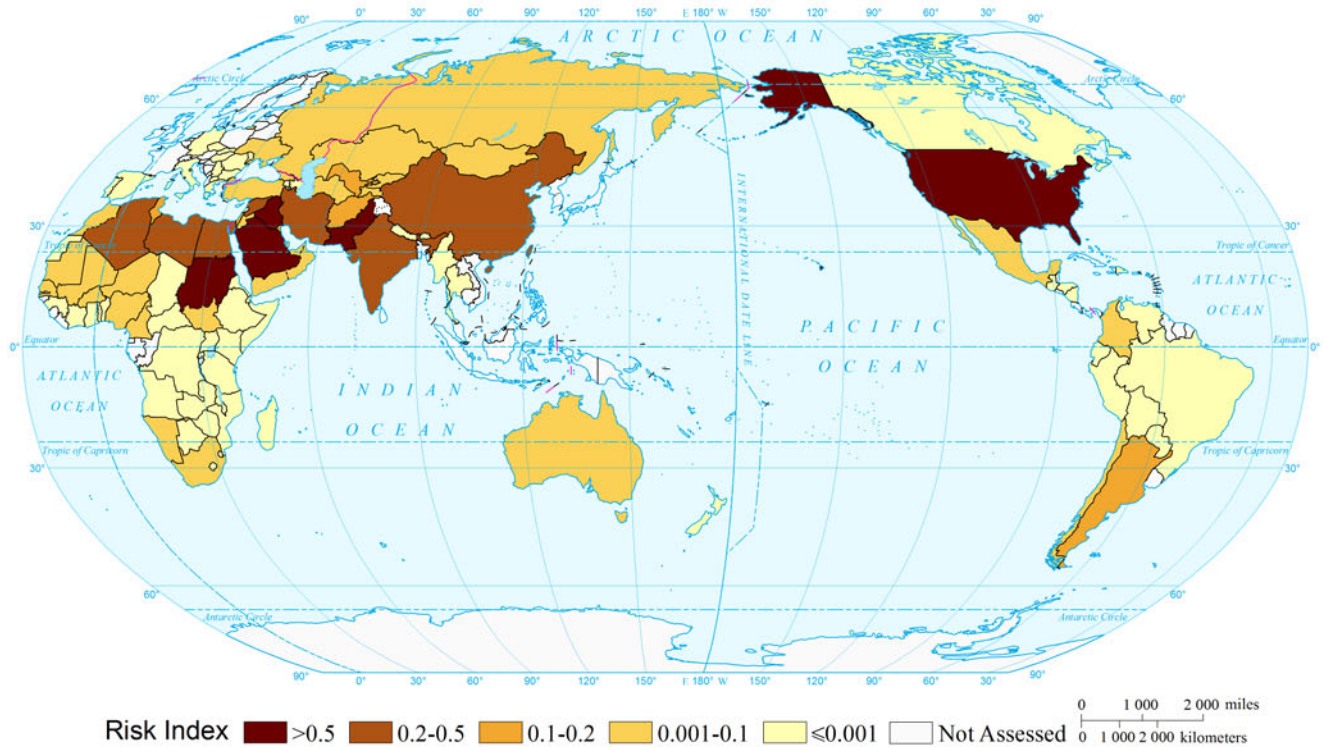
Affected GDP Risk of Sand-dust Storm of the World by Return Period (20a)  
(Country and Region Unit)



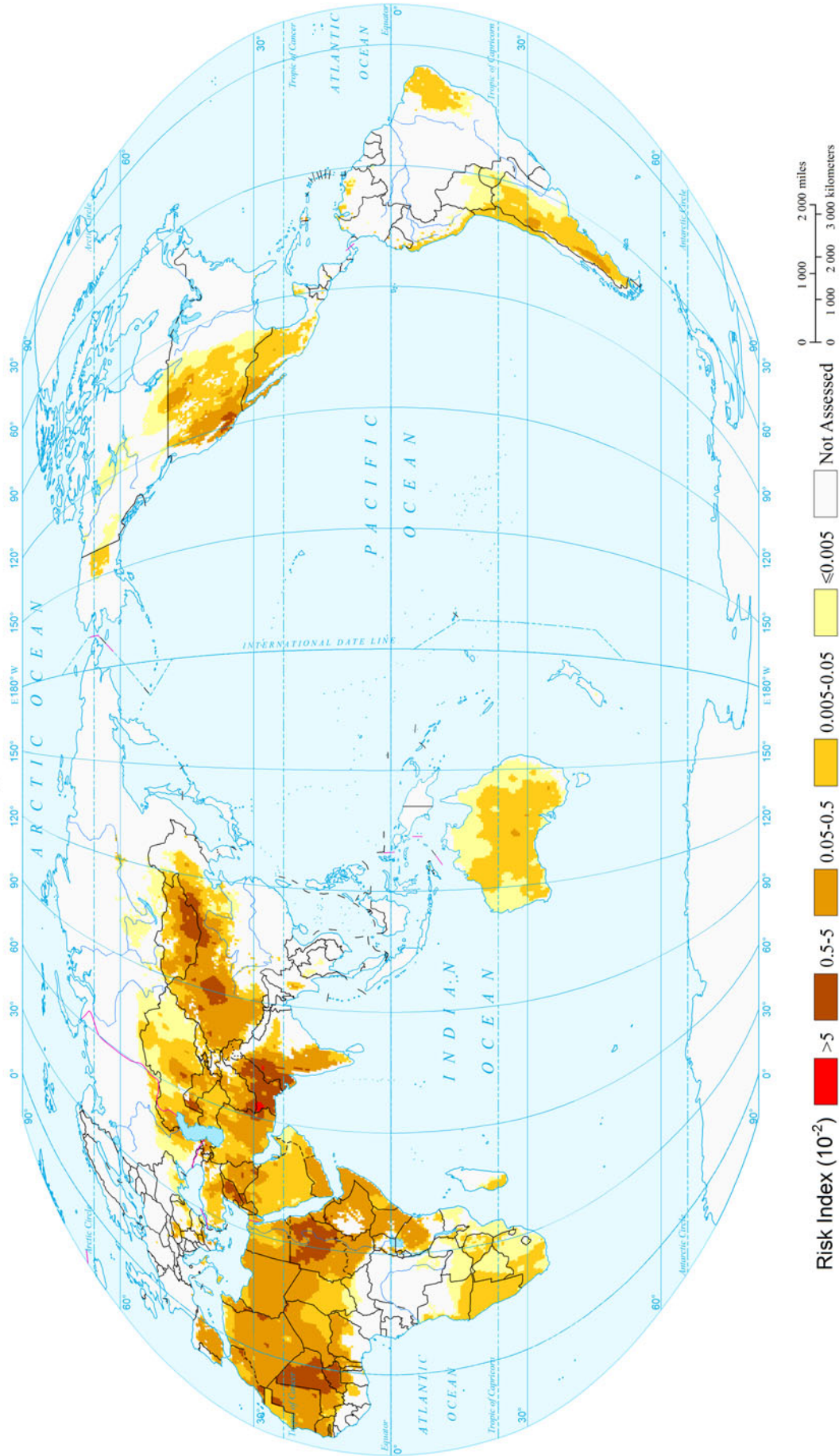
Affected GDP Risk of Sand-dust Storm of the World by Return Period (50a)  
(Country and Region Unit)



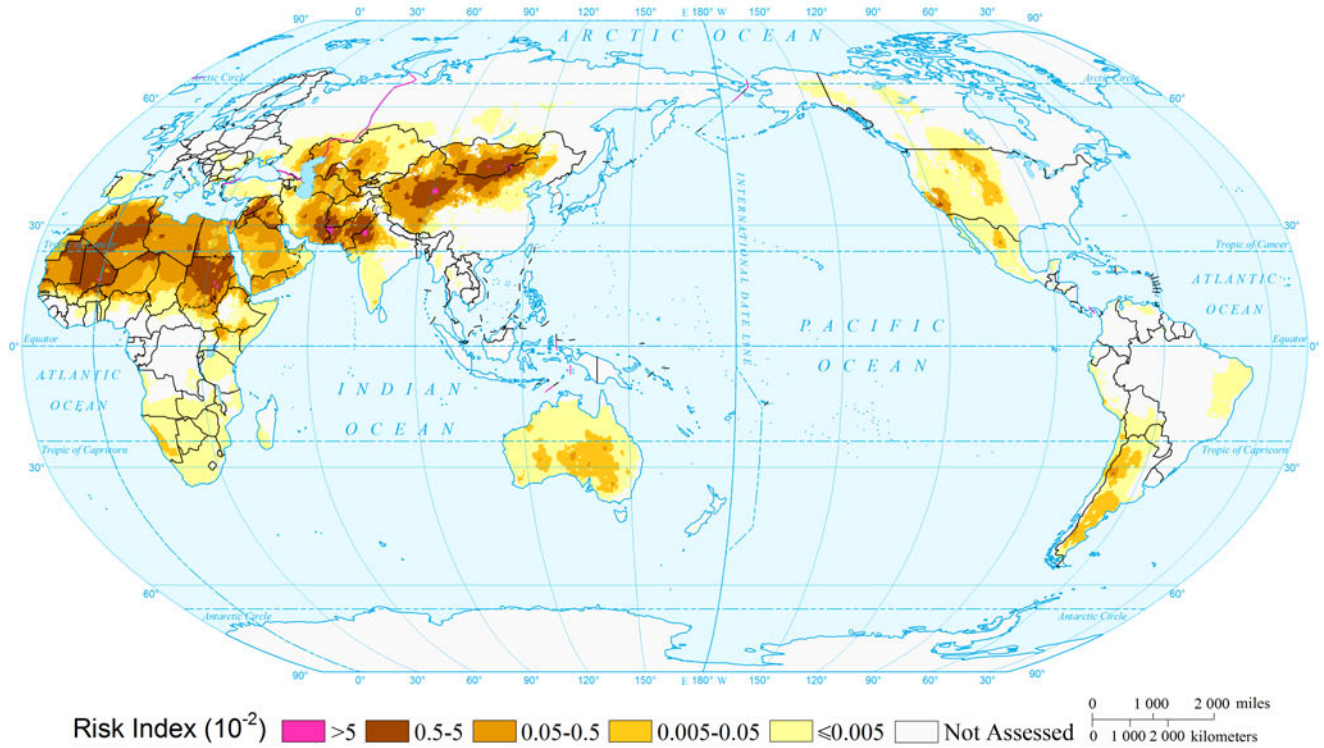
Affected GDP Risk of Sand-dust Storm of the World by Return Period (100a)  
(Country and Region Unit)



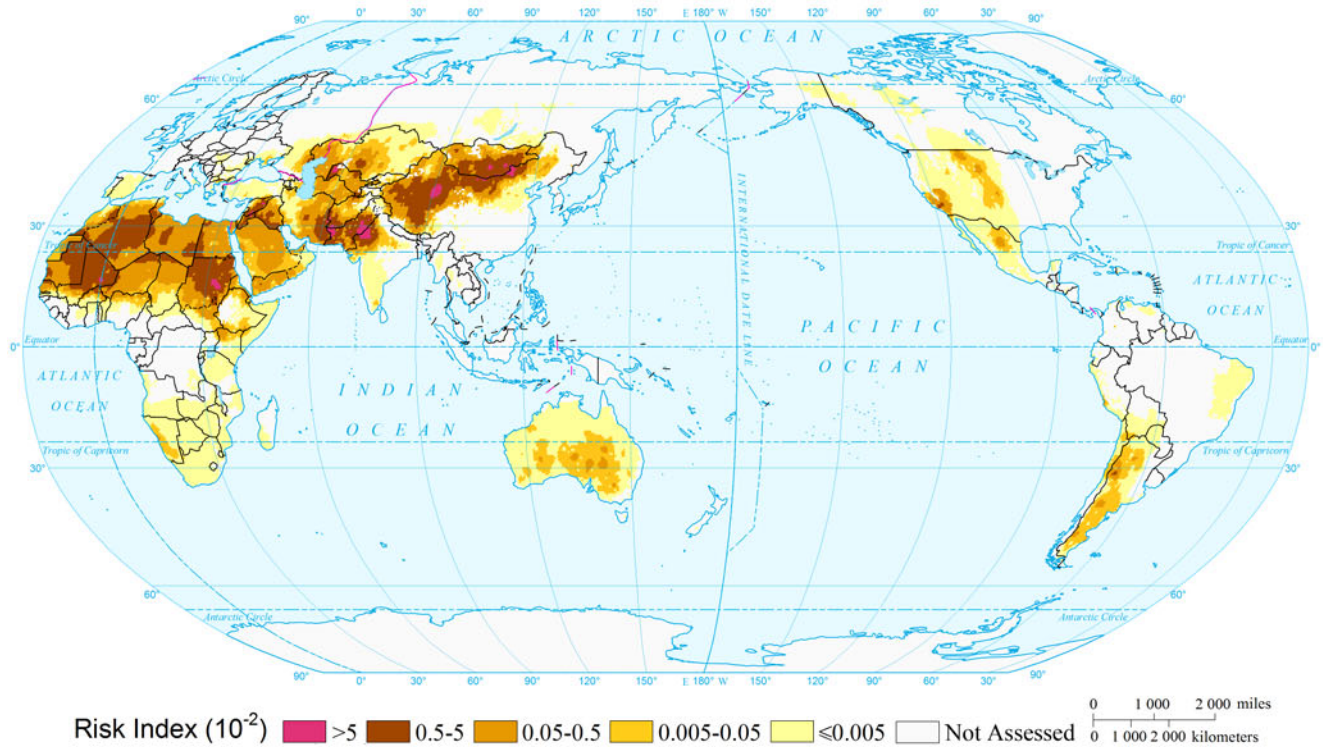
### Expected Annual Affected Livestock Risk of Sand-dust Storm of the World ( $0.5^\circ \times 0.5^\circ$ )



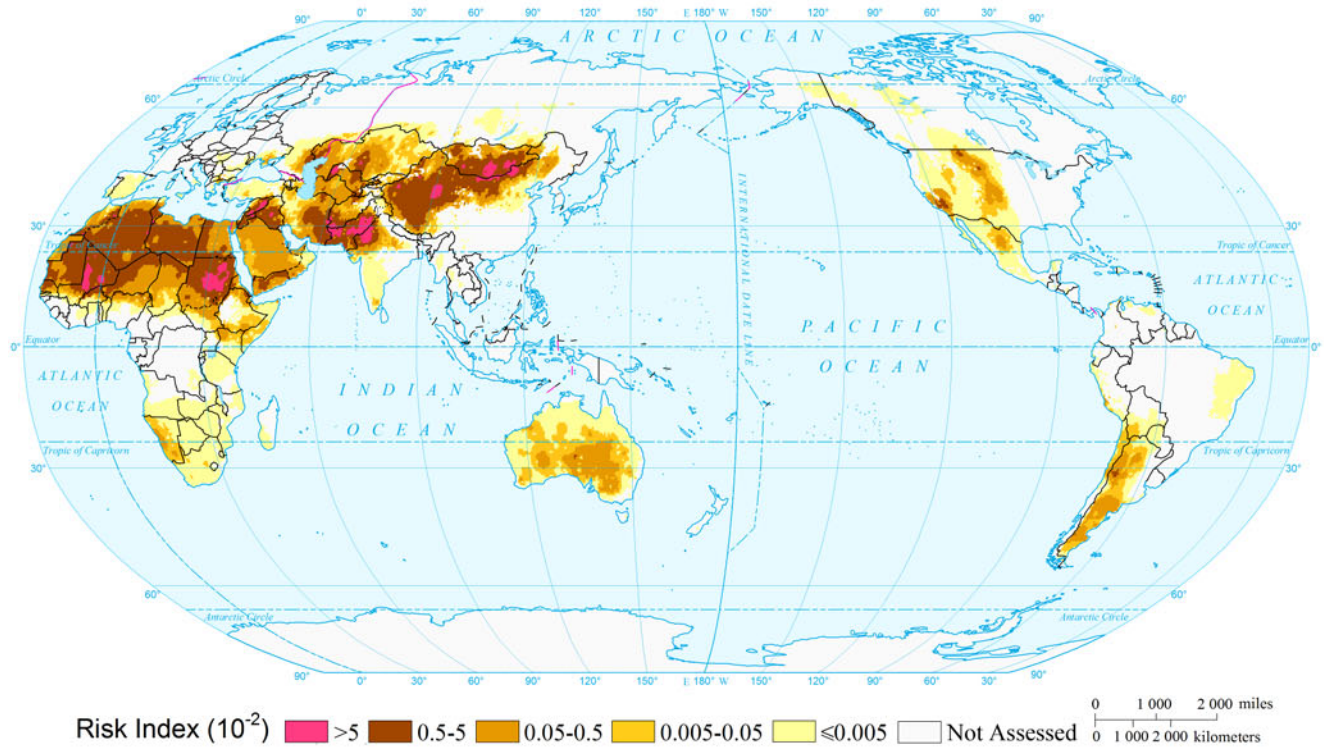
Affected Livestock Risk of Sand-dust Storm of the World by Return Period (10a)  
(0.5°×0.5°)



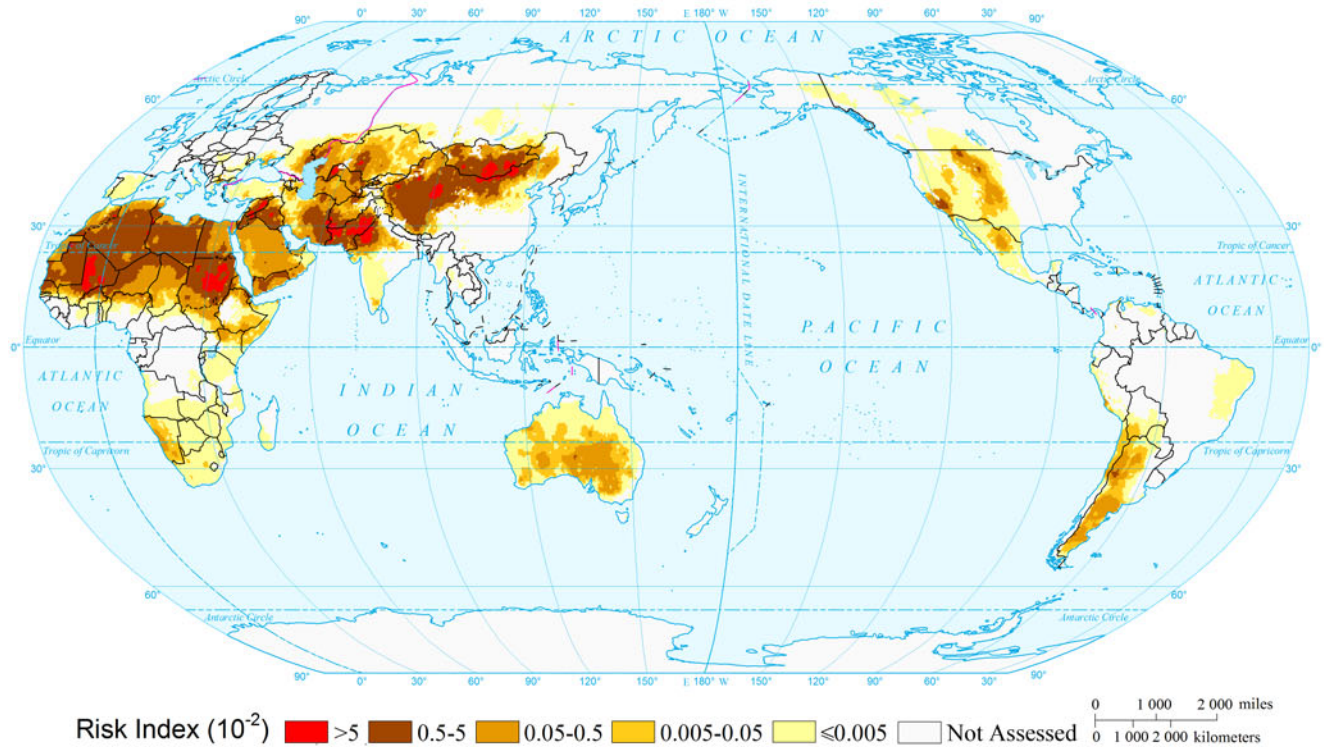
Affected Livestock Risk of Sand-dust Storm of the World by Return Period (20a)  
(0.5°×0.5°)



Affected Livestock Risk of Sand-dust Storm of the World by Return Period (50a)  
(0.5°×0.5°)

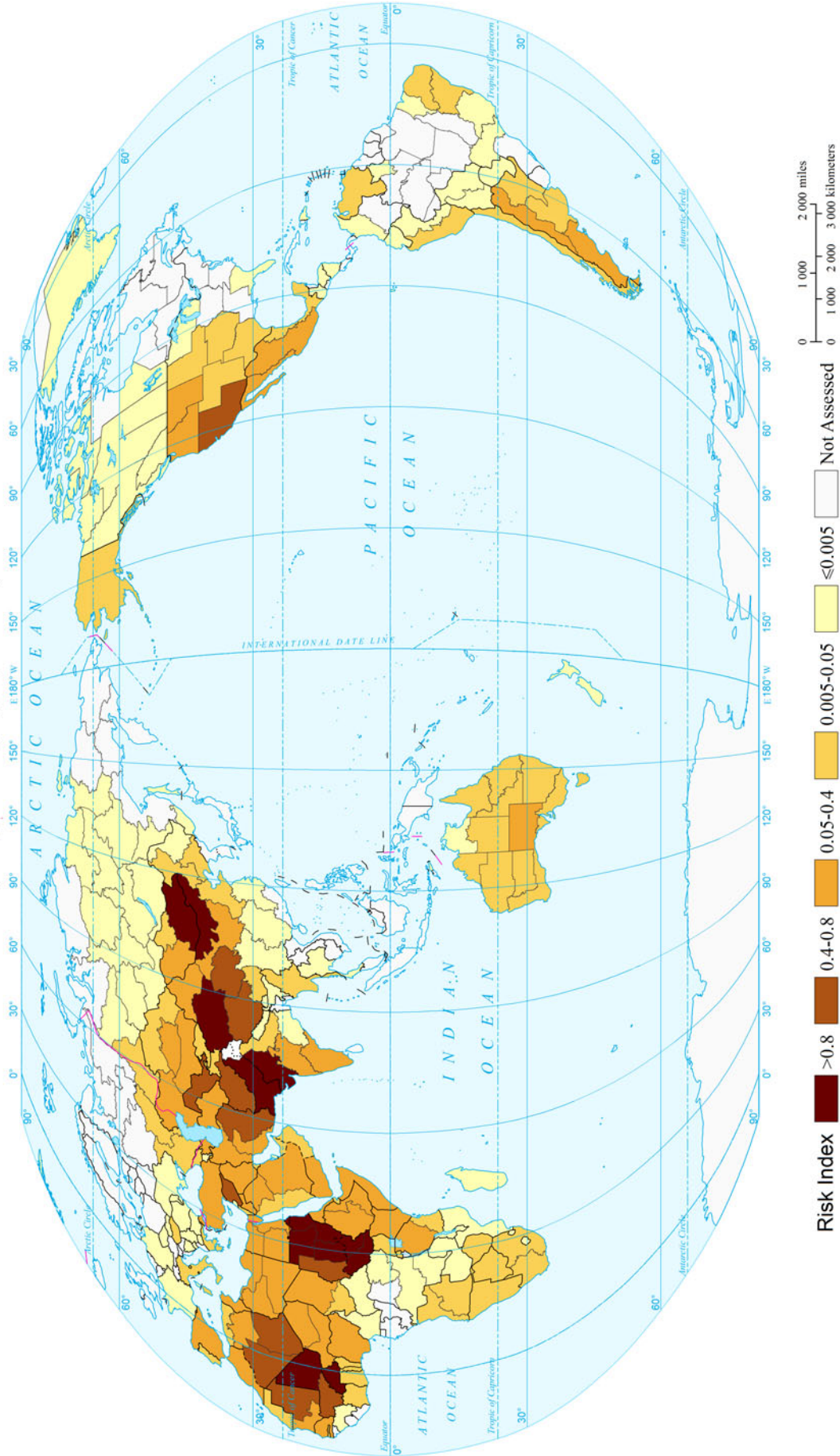


Affected Livestock Risk of Sand-dust Storm of the World by Return Period (100a)  
(0.5°×0.5°)

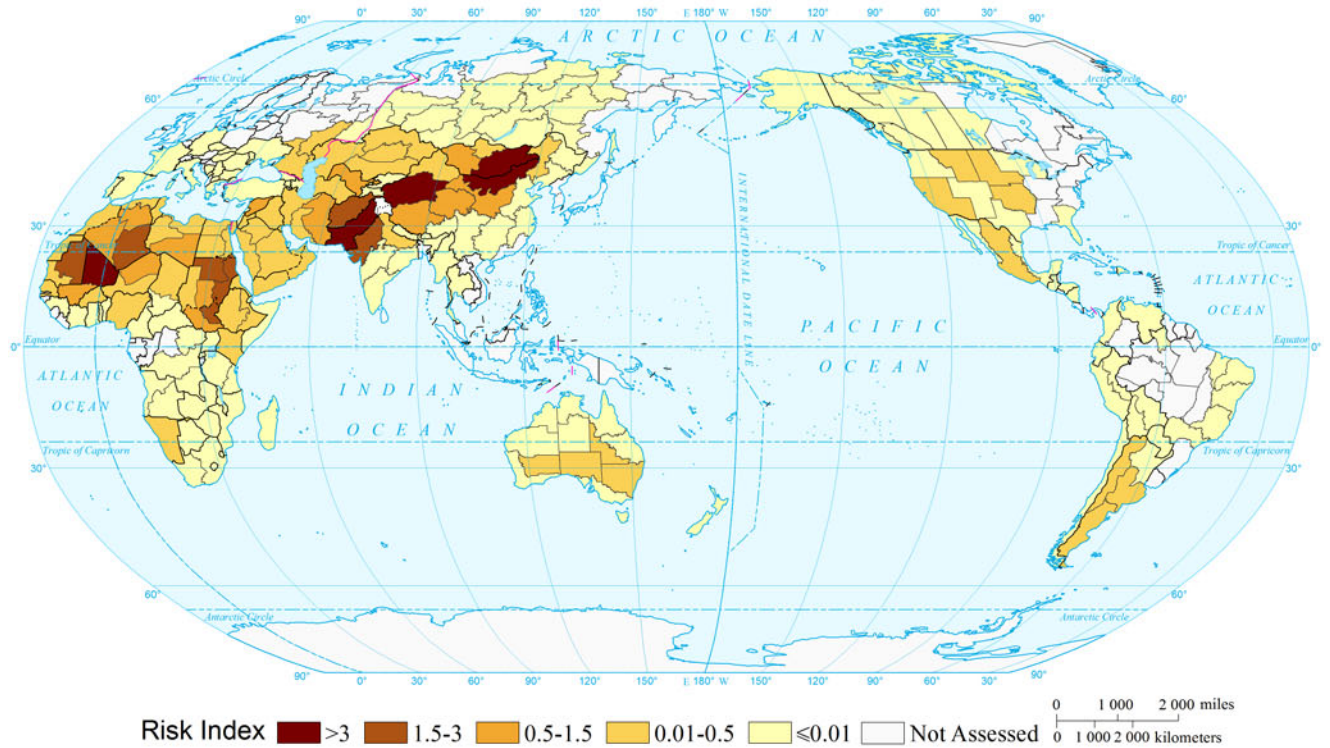




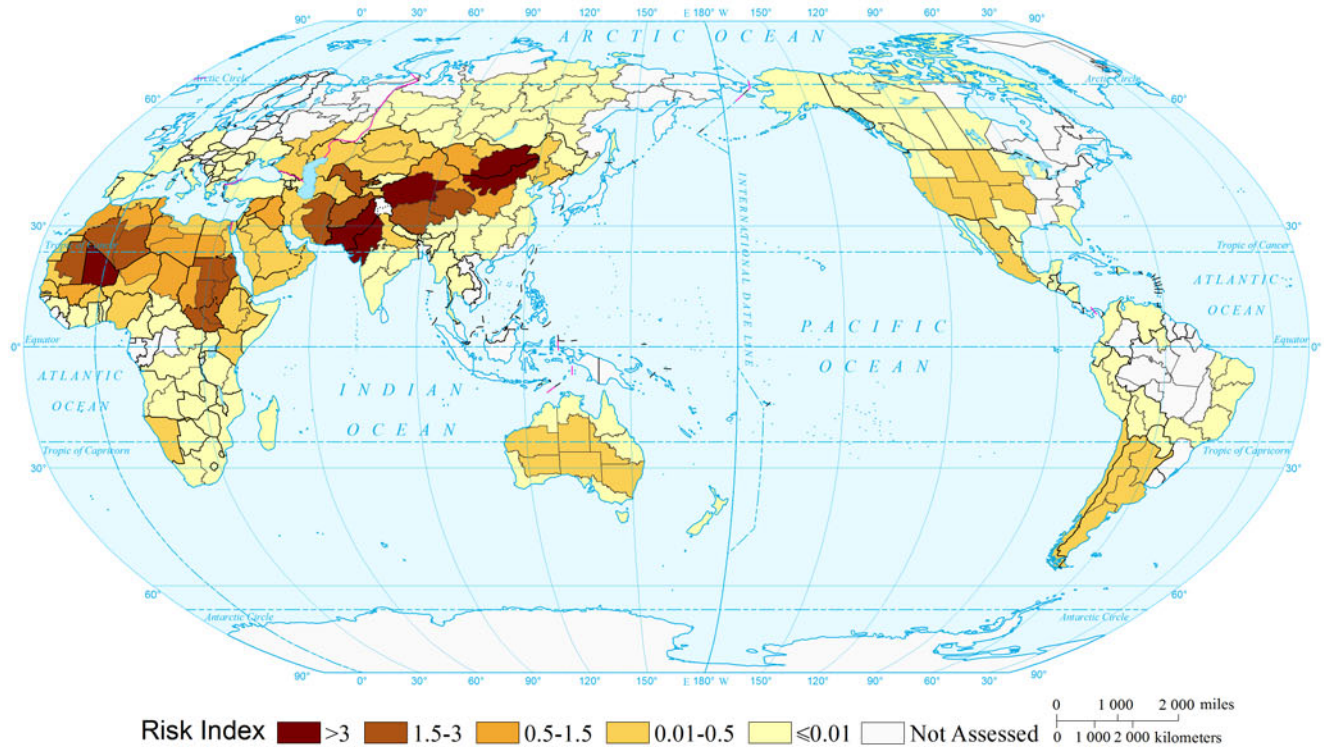
Expected Annual Affected Livestock Risk of Sand-dust Storm of the World  
(Comparable-geographic Unit)



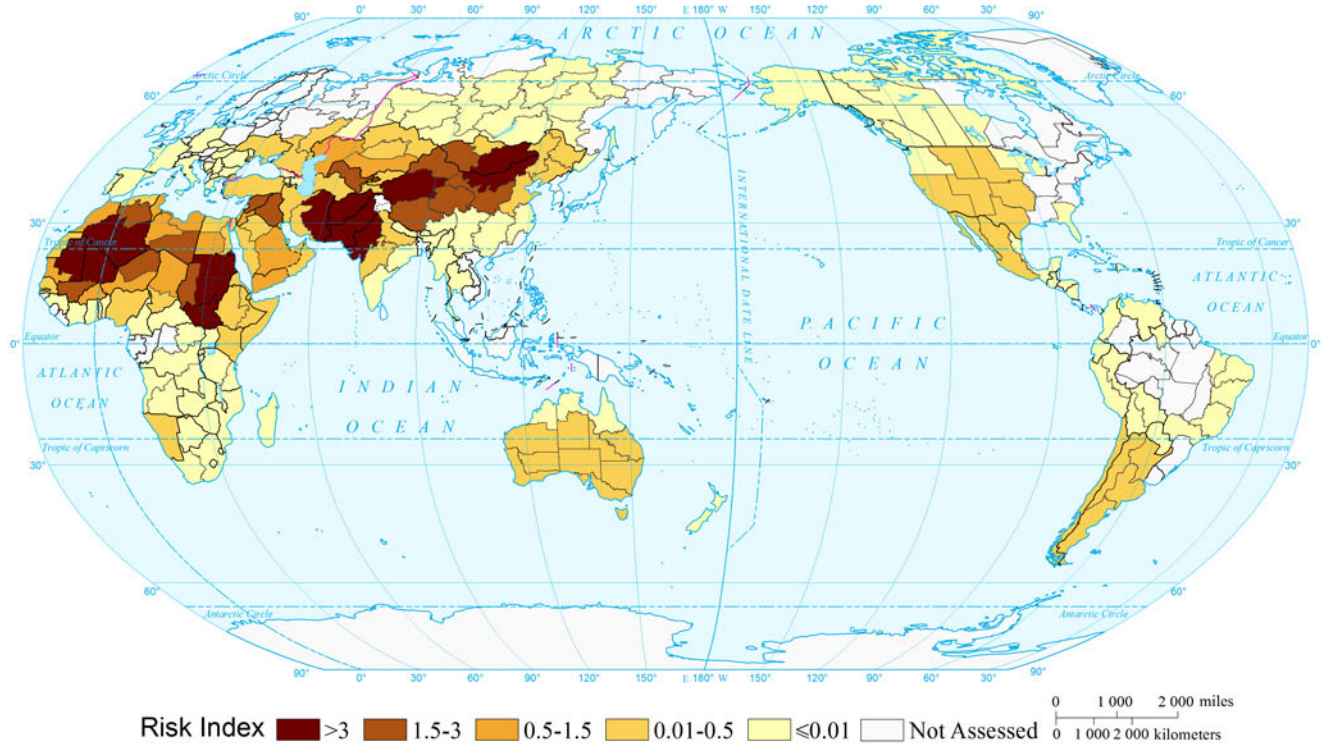
### Affected Livestock Risk of Sand-dust Storm of the World by Return Period (10a) (Comparable-geographic Unit)



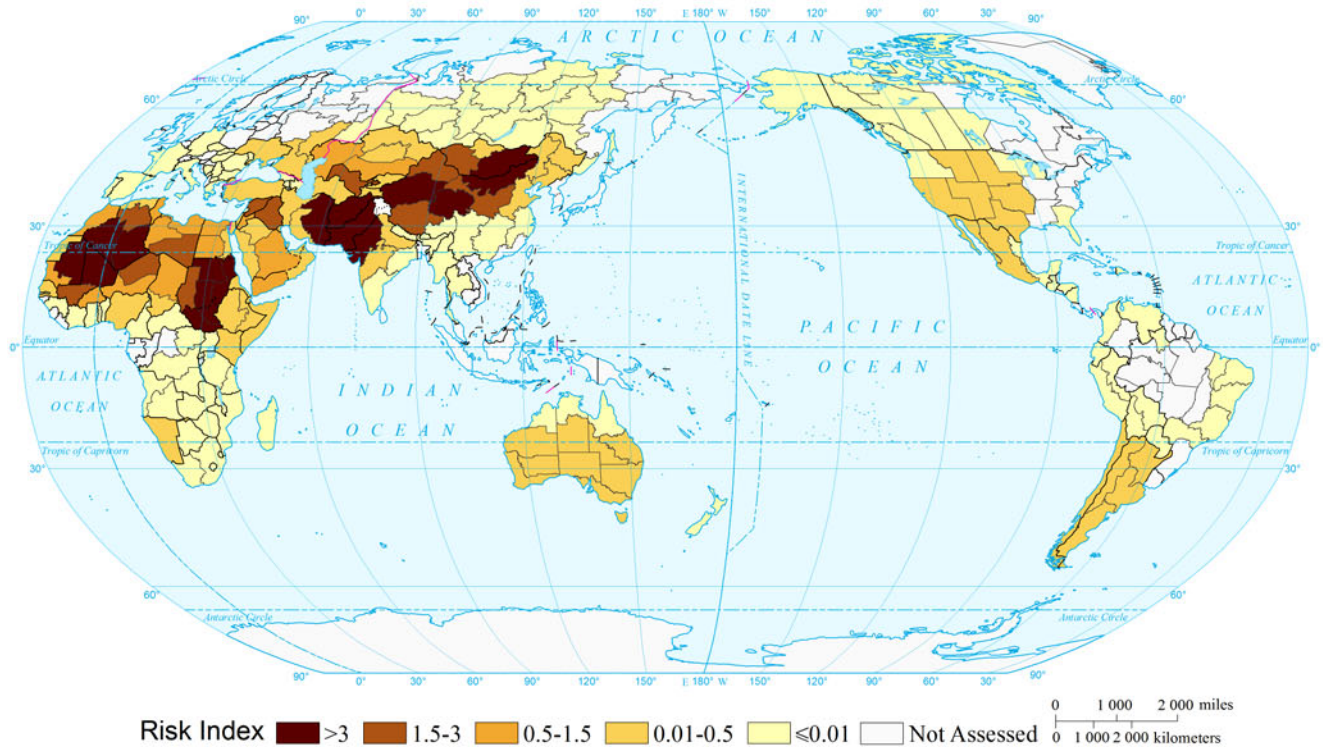
### Affected Livestock Risk of Sand-dust Storm of the World by Return Period (20a) (Comparable-geographic Unit)



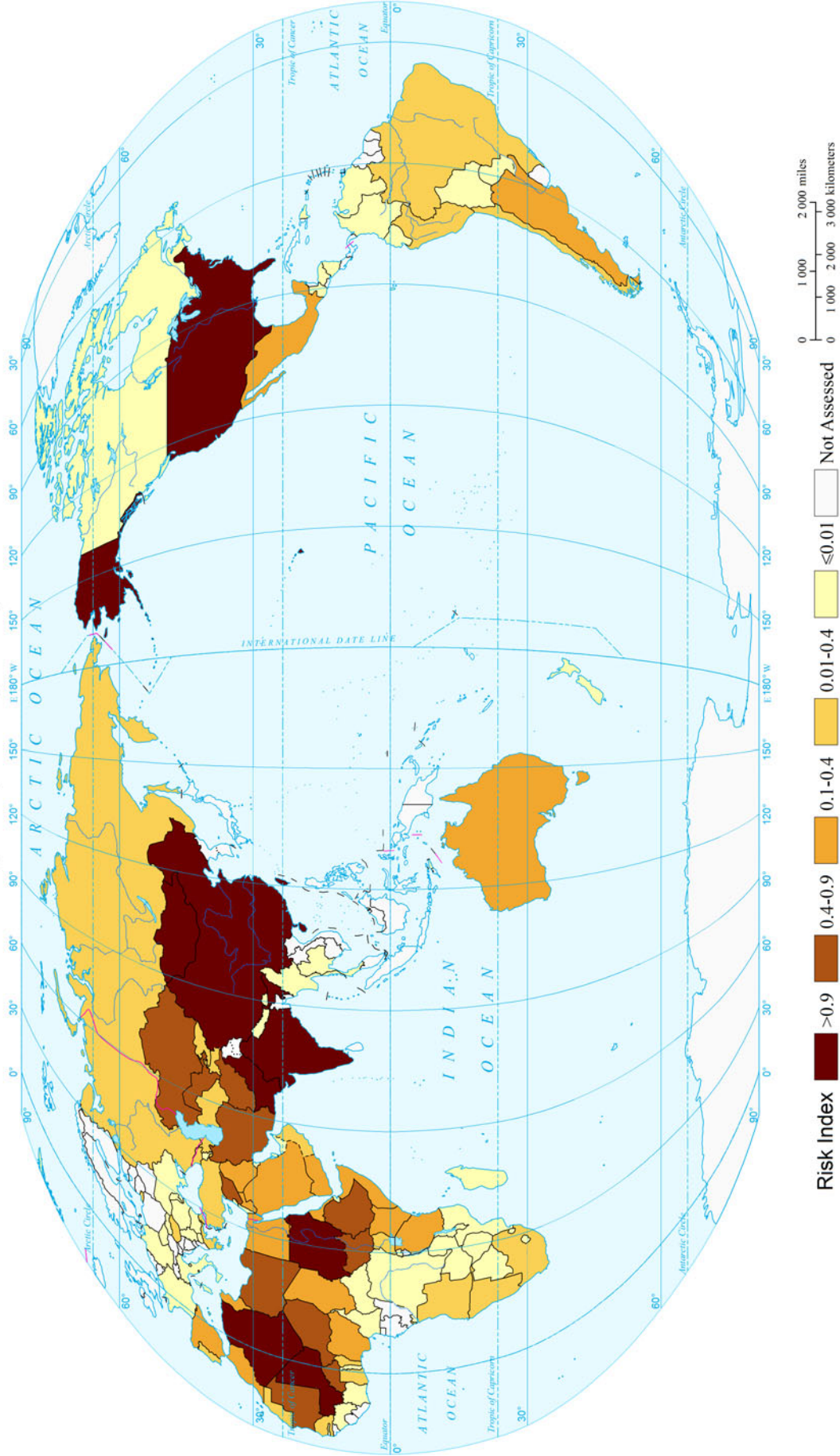
### Affected Livestock Risk of Sand-dust Storm of the World by Return Period (50a) (Comparable-geographic Unit)



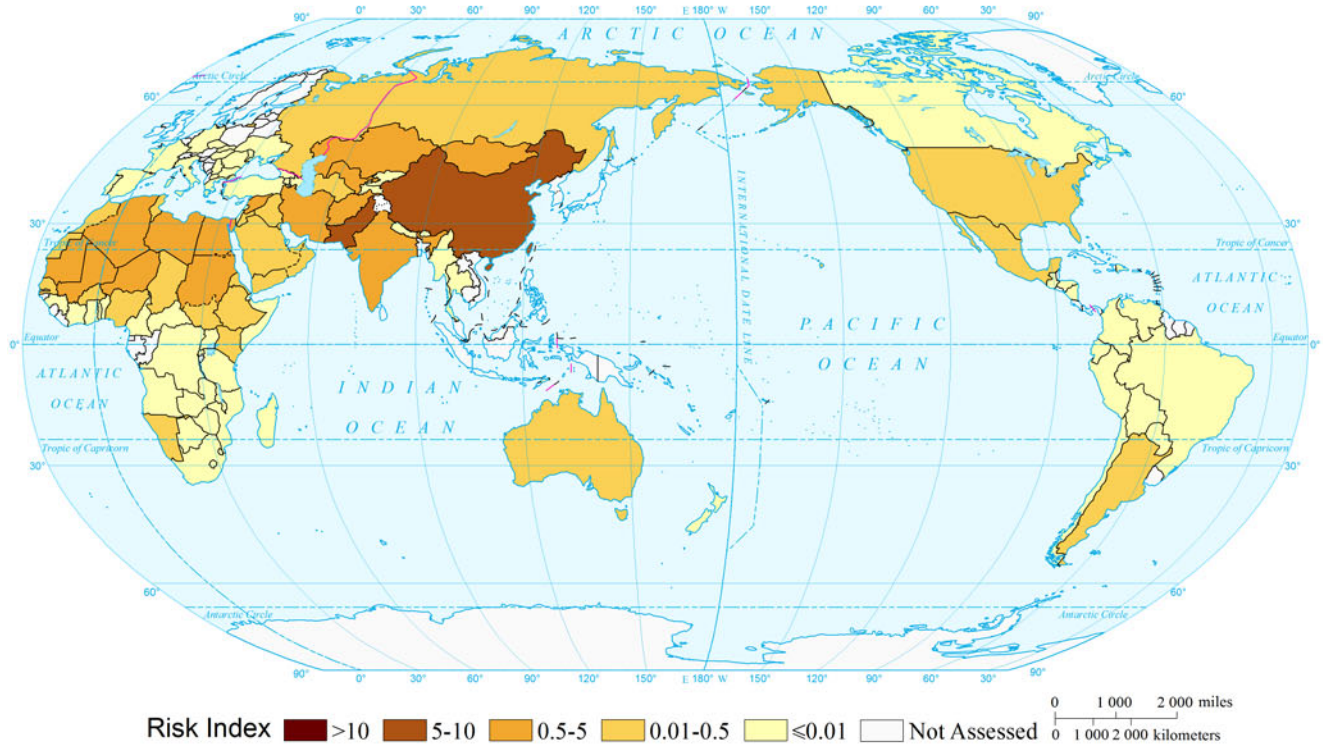
### Affected Livestock Risk of Sand-dust Storm of the World by Return Period (100a) (Comparable-geographic Unit)



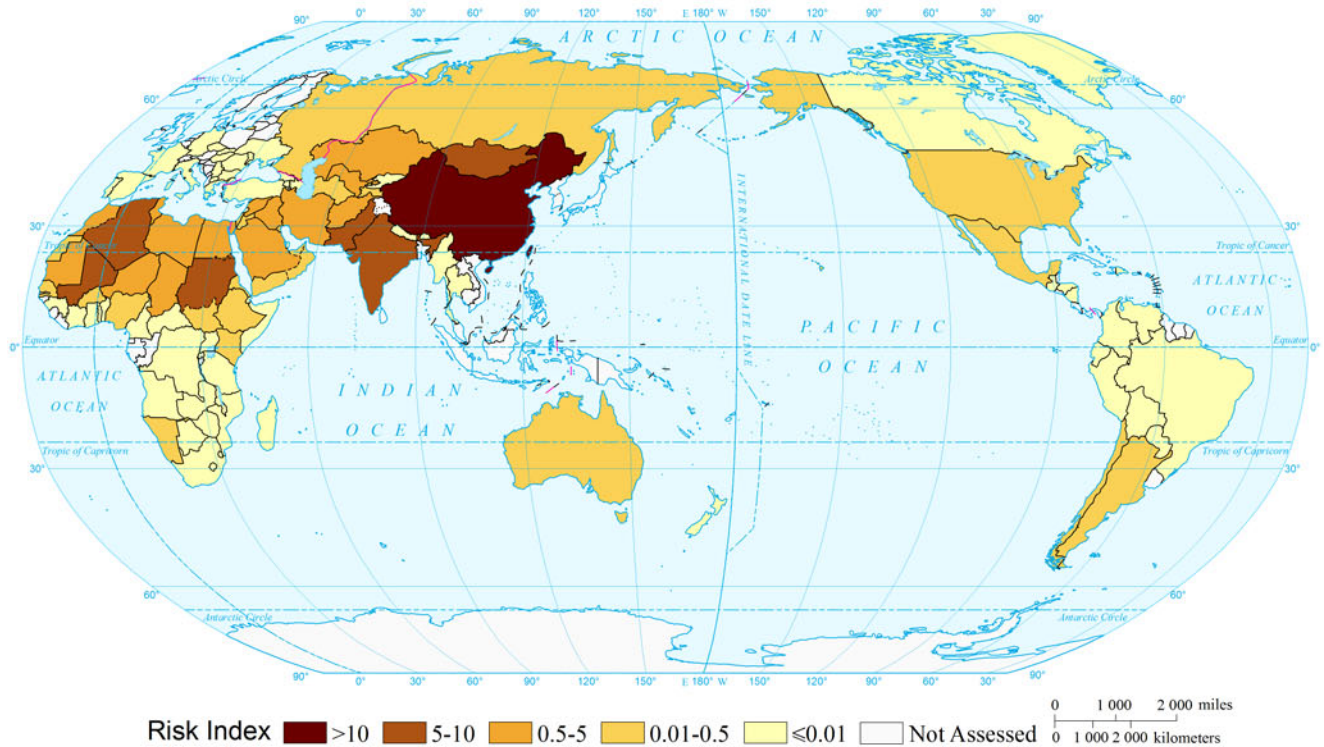
### Expected Annual Affected Livestock Risk of Sand-dust Storm of the World (Country and Region Unit)



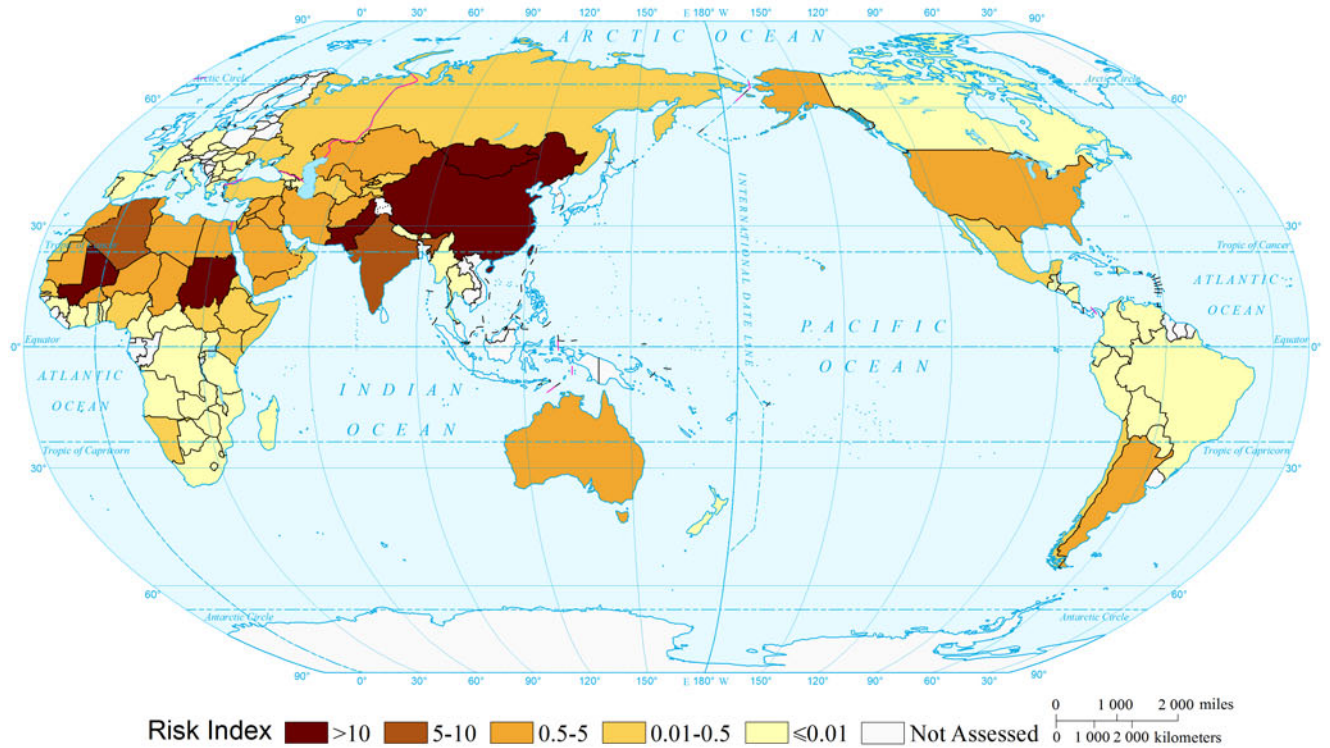
Affected Livestock Risk of Sand-dust Storm of the World by Return Period (10a)  
(Country and Region Unit)



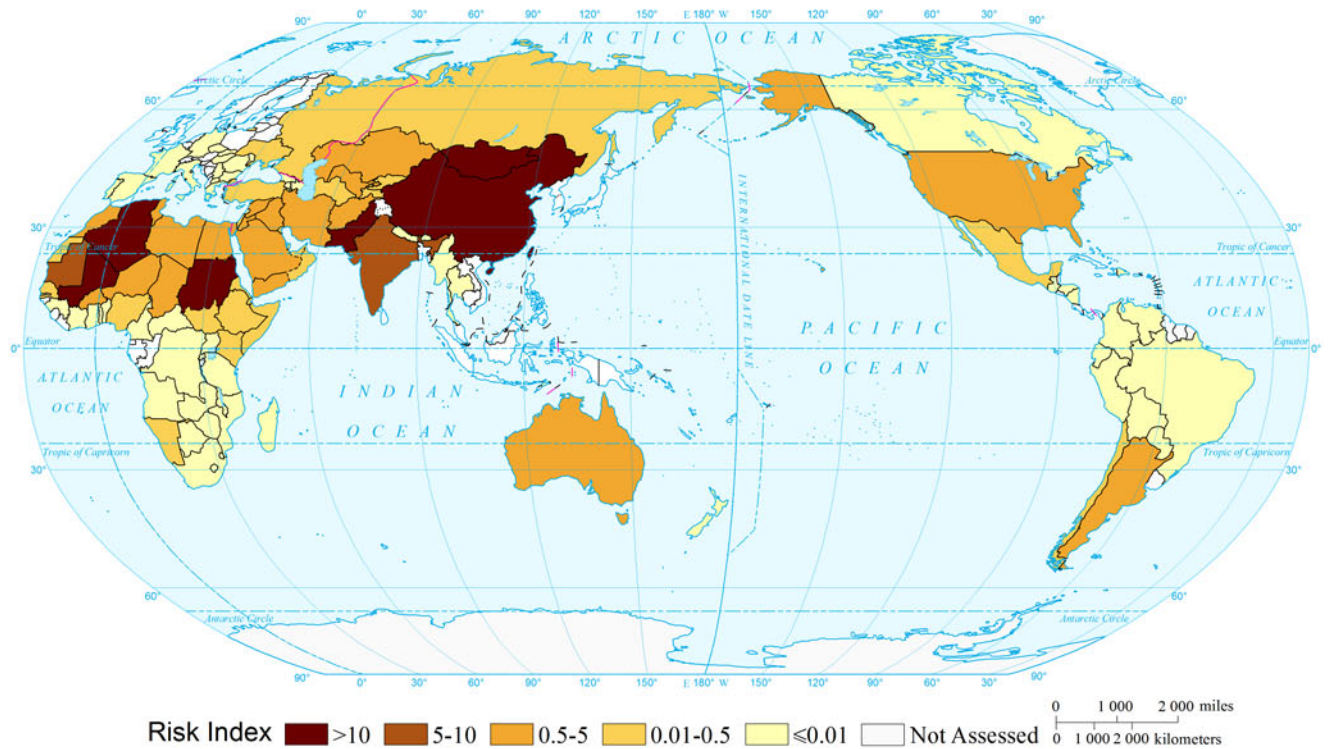
Affected Livestock Risk of Sand-dust Storm of the World by Return Period (20a)  
(Country and Region Unit)



### Affected Livestock Risk of Sand-dust Storm of the World by Return Period (50a) (Country and Region Unit)



### Affected Livestock Risk of Sand-dust Storm of the World by Return Period (100a) (Country and Region Unit)



## References

- Blaikie, P.M., C. Terry, I. Davis, et al. 2003. *At risk*, 2nd ed. New York: Routledge.
- China Meteorological Administration (CMA). 2006. *Technical regulations of sand and dust storm monitoring*. Beijing: China Standard Press. (in Chinese).
- Engelstaedter, S., K.E. Kohfeld, I. Tegen, et al. 2003. Controls of dust emissions by vegetation and topographic depressions: An evaluation using dust storm frequency data. *Geophysical Research Letters* 30(6). doi:10.1029/2002GL016471.
- Formenti, P., L. Schütz, Y. Balkanski, et al. 2011. Recent progress in understanding physical and chemical properties of African and Asian mineral dust. *Atmospheric Chemistry and Physics* 11(16): 8231–256.
- Huang, C.F. 2012. *Natural disaster risk analysis and management*. Beijing: Science Press. (in Chinese).
- Indoitu, R., L. Orlovsky, and N. Orlovsky. 2012. Dust storms in Central Asia: Spatial and temporal variations. *Journal of Arid Environments* 85: 62–70.
- Jayaratne, E., G.R. Johnson, P. McGarry, et al. 2011. Characteristics of airborne ultrafine and coarse particles during the Australian dust storm of 23 September 2009. *Atmospheric Environment* 45: 3996–4001.
- Kalderon-Asael, B., Y. Erel, A. Sandler, et al. 2009. Mineralogical and chemical characterization of suspended atmospheric particles over the east Mediterranean based on synoptic-scale circulation patterns. *Atmospheric Environment* 43: 3963–970.
- Kang, D.J. and H.J. Wang. 2005. Analysis on the decadal scale variation of the dust storm in North China. *Science in China Series D—Earth Sciences* 48:2260–266.
- Liu, X.Q., N. Li, W. Xie, et al. 2012. The return periods and risk assessment of severe dust storms in Inner Mongolia with consideration of the main contributing factors. *Environmental Monitoring and Assessment* 184: 5471–485.
- Orlovsky, L., N. Orlovsky, and A. Durdyev. 2005. Dust storms in Turkmenistan. *Journal of Arid Environments* 60: 83–97.
- Qiu, X.F., Y. Zeng, and Q.L. Miao. 2001. Sand-dust storms in China: Temporal-spatial distribution and tracks of source lands. *Journal of Geographical Sciences* 11: 253–60. (in Chinese).
- Shi, P.J. 1996. Theory and practice of disaster study. *Journal of Natural Disasters* 5(4): 6–17. (in Chinese).
- Shi, P.J. 2002. Theory on disaster science and disaster dynamics. *Journal of Natural Disasters* 11(3): 1–9. (in Chinese).
- Shi, P.J. 2005. Theory and practice on disaster system research—the fourth discussion. *Journal of Natural Disasters* 14(6): 1–7. (in Chinese).
- United Nations Convention to Combat Desertification (UNCCD). 1994. Elaboration of an international convention to combat desertification in countries experiencing serious drought and/or desertification, particularly in Africa. A. AC 241: 27.
- United Nations Development Programme (UNDP), Bureau for Crisis Prevention and Recovery. 2004. *Reducing disaster risk: A challenge for development*. New York: UNDP, Bureau for Crisis Prevention and Recovery.
- Wang, J.A., W. Xu, P.J. Shi, et al. 2001. Spatial-temporal pattern and risk assessment of wind sand disaster in China in 2000. *Journal of Natural Disasters* 10: 1–7. (in Chinese).
- Wang, Y.Q., A.F. Stein, R.R. Draxler, et al. 2011. Global sand and dust storms in 2008: Observation and HYSPLIT model verification. *Atmospheric Environment* 45: 6368–381.
- Wang, Y.Q., X.Y. Zhang, S.L. Gong, et al. 2008. Surface observation of sand and dust storm in East Asia and its application in CUACE/Dust. *Atmospheric Chemistry and Physics* 8: 545–53.
- Yang, Q., L.M. Yang, G.M. Zhang, et al. 2006. Research on classification of sandstorm intensity based on probability distribution of PM<sub>10</sub> concentration. *Journal of Desert Research* 26: 278–82. (in Chinese).
- Zhuang, G.S., J.H. Guo, H. Yuan, et al. 2001. The compositions, sources, and size distribution of the dust storm from China in spring of 2000 and its impact on the global environment. *Chinese Science Bulletin* 46: 895–900. (in Chinese).

---

# Mapping Tropical Cyclone Wind Risk of the World

Weihua Fang, Chenyan Tan, Wei Lin, Xiaoning Wu, Yanting Ye, Shijia Cao, Wanmei Mo, Ying Li, Yi Li, Yuping Wu, Guobin Lin, and Yang Yang

---

## 1 Background

A tropical cyclone (TC) is a strong low-pressure system formed on the tropical and subtropical sea surface, with top-ranking destructiveness among all kinds of meteorological hazards (Neumann 1993). TC is also referred to typhoon in Northwest Pacific (NWP) and South China Sea, hurricane in Northeast Pacific (NEP) and North Atlantic (NA), storm in North Indian (NI) Ocean and the Bay of Bengal, and TC in Central Pacific (CP), South Pacific (SP) and South Indian (SI) Ocean.

Among all basins, NWP is the most active according to historical records in terms of TC genesis. Annually, more than 90 TCs are generated, and one-third of them occur in NWP. During 1900–2012, annually TCs killed 13,000 people and caused 8.5 billion dollars economic loss (Appendix III, Disasters data 5.4).

---

**Mapping Editors:** Jing'ai Wang (Key Laboratory of Regional Geography, Beijing Normal University, Beijing 100875, China), Fang Lian (School of Geography, Beijing Normal University, Beijing 100875, China) and Chunqin Zhang (School of Geography, Beijing Normal University, Beijing 100875, China).

**Language Editor:** Weihua Fang (Key Laboratory of Environmental Change and Natural Disaster, Ministry of Education, Beijing Normal University, Beijing 100875, China).

---

W. Fang (✉)

Key Laboratory of Environmental Change and Natural Disaster,  
Ministry of Education, Beijing Normal University, Beijing  
100875, China  
e-mail: weihua.fang@bnu.edu.cn

C. Tan · W. Lin · X. Wu · Y. Ye · S. Cao · W. Mo · Y. Li · Y. Li ·  
Y. Wu · G. Lin · Y. Yang

Academy of Disaster Reduction and Emergency Management,  
Ministry of Civil Affairs and Ministry of Education, Beijing  
Normal University, Beijing 100875, China

The major hazards and secondary disasters of TC include wind, precipitation, storm surge, wave, flood, landslide, and mudslide. The risks of precipitation, storm surge, wave, flood, and landslide are separately assessed and mapped in this atlas; therefore, this study only initiates to map the wind-affected population and GDP risk of TCs of the world.

---

## 2 Method

Figure 1 shows the technical flowchart for mapping TC wind-affected population and GDP risk of the world.

### 2.1 Intensity

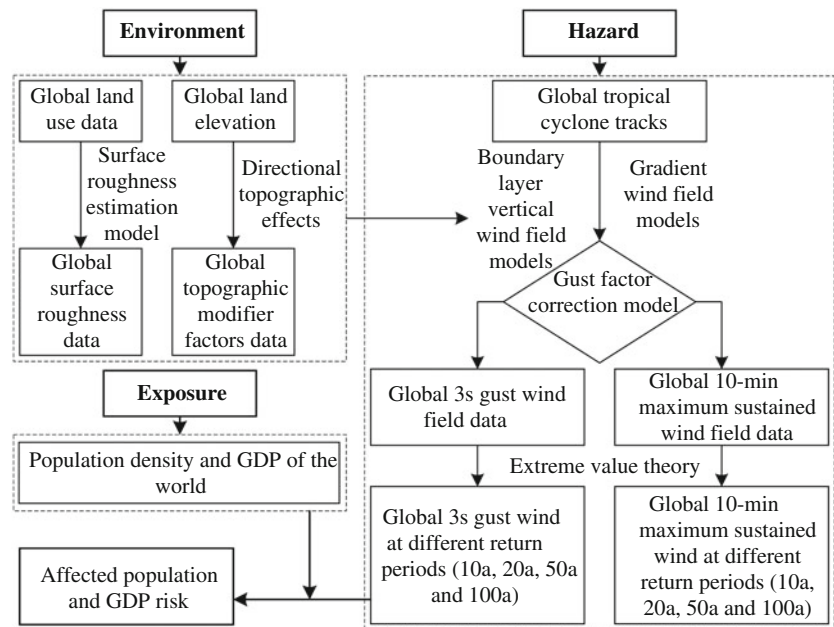
#### 2.1.1 Database

A global 6h TC track database by the year of 2012 is developed, which includes CMA-track (Appendix III, Hazards data 4.10), HURDAT (Appendix III, Hazards data 4.11), and IBTrACs (Appendix III, Hazards data 4.12). For NWP, CP, NEP and NA, data from CMA-track and HURDAT are adopted respectively, and for the other 3 basins, tracks from IBTrACs are used.

For some TCs, critical parameters, e.g., maximum wind speed (MWS) or radius of maximum wind (RMW), needed for wind field model are missing. In order to estimate these missing parameters, empirical regression functions between  $P_0$  and MWS,  $P_0$  and RMW are developed. In order to compute wind snapshot by every 10 minutes, the parameters (longitude, latitude, time,  $P_0$ , MWS, and RMW) in the best tracks with 6h time interval are interpolated linearly by every 10-min.

Global Land Cover Characteristics (GLCC) database (Appendix III, Environments data 2.6) is a global remote-sensed data collected to derive surface roughness length, a critical input of wind field model. GTOPO30 is a digital elevation model for the world (Appendix III, Environments

**Fig. 1** Technical flowchart for mapping tropical cyclone wind and affected population and GDP risk of the world



data 2.1). A global land–sea mask is rasterized into 30 arc second from a global land vector boundary.

### 2.1.2 Wind Field Modeling

A parametric wind field model usually consists of a gradient wind model and a planetary boundary layer (PBL) model. In general, for risk assessment purpose, PBL model shall consider both topographic and roughness effects. In addition, gust factor model is also included for the conversion between gust wind and sustained wind.

In different ocean basins, a variety of wind field models have been developed in the past studies. These models are reviewed in past studies (Fang and Shi 2012; Fang and Lin 2013). And in this study, for each of the seven ocean basins, one representative model is selected as shown in Table 1. The modeling parameters, such as TC center location,  $P_0$ , MWS, RMW, forward speed ( $f_s$ ), and forward direction ( $fd$ ) can be obtained from the best track dataset. A wind profile parameter, Holland B factor, is computed according to a past study (Holland 1980). The periphery pressures for each basin are also listed in Table 1.

The reliability and accuracy of the models therefore rely on both the validation of the past studies and the parameters used in this study. However, in NWP, modeled winds are validated with observed wind of ground station in China.

In order to account for topographic effect into PBL model, topographic effect factors at 8 directions are derived based on GTOPO30, following wind standard (European Committee for Standardization 2005). And roughness effect is modeled by using GLCC data, with their empirical roughness parameters derived in the past study (Wieringa 1993; Wieringa et al. 2001).

Based on the global TC track dataset and the above parametric wind field models, the 3s and 10-min wind footprints of all TCs by the year 2012 in the seven ocean basins are simulated at spatial resolution of 30 arc second, with wind field snapshots of every 10 minutes. The reconstructed historical TC events provide the data basis for wind intensity and frequency analysis.

### 2.1.3 Intensity and Frequency

In this study, the wind hazard maps with return periods of 10a, 20a, 50a, and 100a are to be produced. With the limited historical TC samples, it might become difficult or even unreliable to produce wind map with return period of 100a.

Based on extreme value theory (EVT), the intensity-frequency of 3s gust wind and 10-min sustained wind is analyzed by using Gumbel distribution, for those pixels with more than 20 historical TC events. Wind hazard maps,

**Table 1** Selected wind field models in the seven ocean basins

Basin	Track duration	Number of tracks	Gradient wind model	PBL model	Gust factor model	Holland B parameter	Periphery pressure
NWP	1949–2012	2,094	Georgiou et al. (1983)	Meng et al. (1997)	ESDU (1983)	Vickery and Wadhera (2008)	1,010
CP	1957–2012	15	Willoughby et al. (2006)	Meng et al. (1997)	ESDU (1983)	Vickery and Wadhera (2008)	1,013
NEP	1949–2012	596	Willoughby et al. (2006)	Meng et al. (1997)	ESDU (1983)	Vickery and Wadhera (2008)	1,013
NA	1851–2012	1,450	Willoughby et al. (2006)	Meng et al. (1997)	ESDU (1983)	Vickery and Wadhera (2008)	1,013
NI	1972–2012	263	Georgiou et al. (1983)	Meng et al. (1997)	ESDU (1983)	Jakobsen and Madsen (2004)	1,013
SP	1970–2012	401	McConochie et al. (2004)	Harper et al. (2001)	ESDU (1983)	Harper and Holland (1999)	1,010
SI	1973–2012	408	Georgiou et al. (1983)	Meng et al. (1997)	ESDU (1983)	Harper and Holland (1999)	1,010

with wind speeds at the return period of annual expectation, 10a, 20a, 50a, and 100a are produced, based on EVT modeling output.

## 2.2 Affected Population and GDP Risks

Affected Population and affected GDP in this study are defined as the population and GDP within the area of 2-min sustained winds equal or larger than Beaufort Scale 10. The 2-min sustained winds are computed from 3s gust winds by considering gust factors.

For each typical return period (10a, 20a, 50a and 100a) and annual expected, the affected population and GDP can be estimated by intersecting 2-min wind speeds and global population (Appendix III, Exposures data 3.1) and GDP dataset (Appendix III, Exposures data 3.3). The affected

population and GDP are aggregated to obtain affected population and GDP at national level.

## 3 Results

### 3.1 Wind Hazard

Eleven wind hazard maps are developed, including one map of track and intensity, and ten maps of 3s gust winds and 10-min winds at return periods of 10a, 20a, 50a, 100a, and annual expected.

According to these hazard maps, it can be found that the NWP tops the world in frequency of TC genesis, landing, and intensity. The most severely affected regions of TC wind include southeastern Asia, southeastern North America, Northern Australia, and southwestern Africa. At national

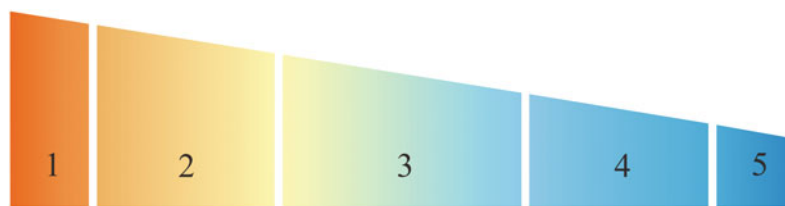


**Fig. 2** Expected annual affected population risk of tropical cyclone wind of the world. 1 (0, 10 %] China, Philippines, Japan, USA, Vietnam, South Korea. 2 (10, 35 %] India, Cuba, Mexico, Madagascar, Dominican Republic, Bangladesh, Haiti, Jamaica, North Korea, New Zealand, Australia, Canada, Burma, Mauritius, Honduras, Nicaragua. 3 (35, 65 %] Guadeloupe, Bahamas, Mozambique, Guatemala, Thailand, Laos, Fiji, Russia, Palestine, Indonesia, Belize, Trinidad and Tobago,

Pakistan, Barbados, Papua New Guinea, Saint Lucia, Solomon Islands, Grenada. 4 (65, 90 %] El Salvador, Antigua and Barbuda, Timor-Leste, Samoa, Dominica, Cambodia, Saint Vincent and the Grenadines, Sri Lanka, Tonga, Saint Kitts and Nevis, Oman, Comoros, Costa Rica, Niue, Cook Islands, Yemen. 5 (90, 100 %] Panama, Malaysia, Bhutan, Nepal, Baker Island, Tuvalu

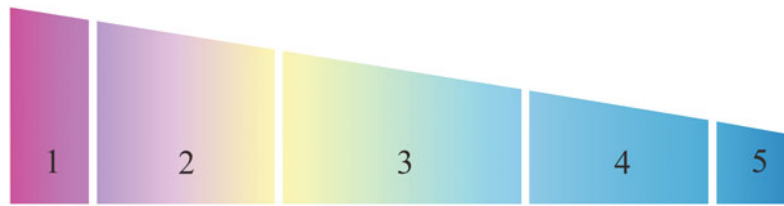


**Fig. 3** Expected annual affected GDP risk of tropical cyclone wind of the world. 1 (0, 10 %] China, Philippines, Japan, USA, Vietnam, South Korea. 2 (10, 35 %] India, Cuba, Mexico, Madagascar, Dominican Republic, Bangladesh, Haiti, Jamaica, North Korea, New Zealand, Australia, Canada, Burma, Mauritius, Honduras, Nicaragua. 3 (35, 65 %] Guadeloupe, Bahamas, Mozambique, Guatemala, Thailand, Laos, Fiji, Russia, Palestine, Indonesia, Belize, Trinidad and Tobago,

Pakistan, Barbados, Papua New Guinea, Saint Lucia, Solomon Islands, Grenada. 4 (65, 90 %] El Salvador, Antigua and Barbuda, Timor-Leste, Samoa, Dominica, Cambodia, Saint Vincent and the Grenadines, Sri Lanka, Tonga, Saint Kitts and Nevis, Oman, Comoros, Costa Rica, Niue, Cook Islands, Yemen. 5 (90, 100 %] Panama, Malaysia, Bhutan, Nepal, Baker Island, Tuvalu

level, China, Japan, the Philippines, Vietnam, USA, Mexico, Cuba, Australia, and Madagascar are the countries with the highest TC wind hazard.

### 3.2 Affected Population Risk

Five national level affected population maps are developed, including four maps of affected population at return periods of 10a, 20a, 50a, 100a, and one map on annual expectation of affected population.

By zonal statistics of the annual expectation of affected population, the expected affected population risk of typical cyclone wind of the world at national level is derived and ranked (Fig. 2). The top 1 % country with the highest annual expected affected population risk of TC wind is China, and

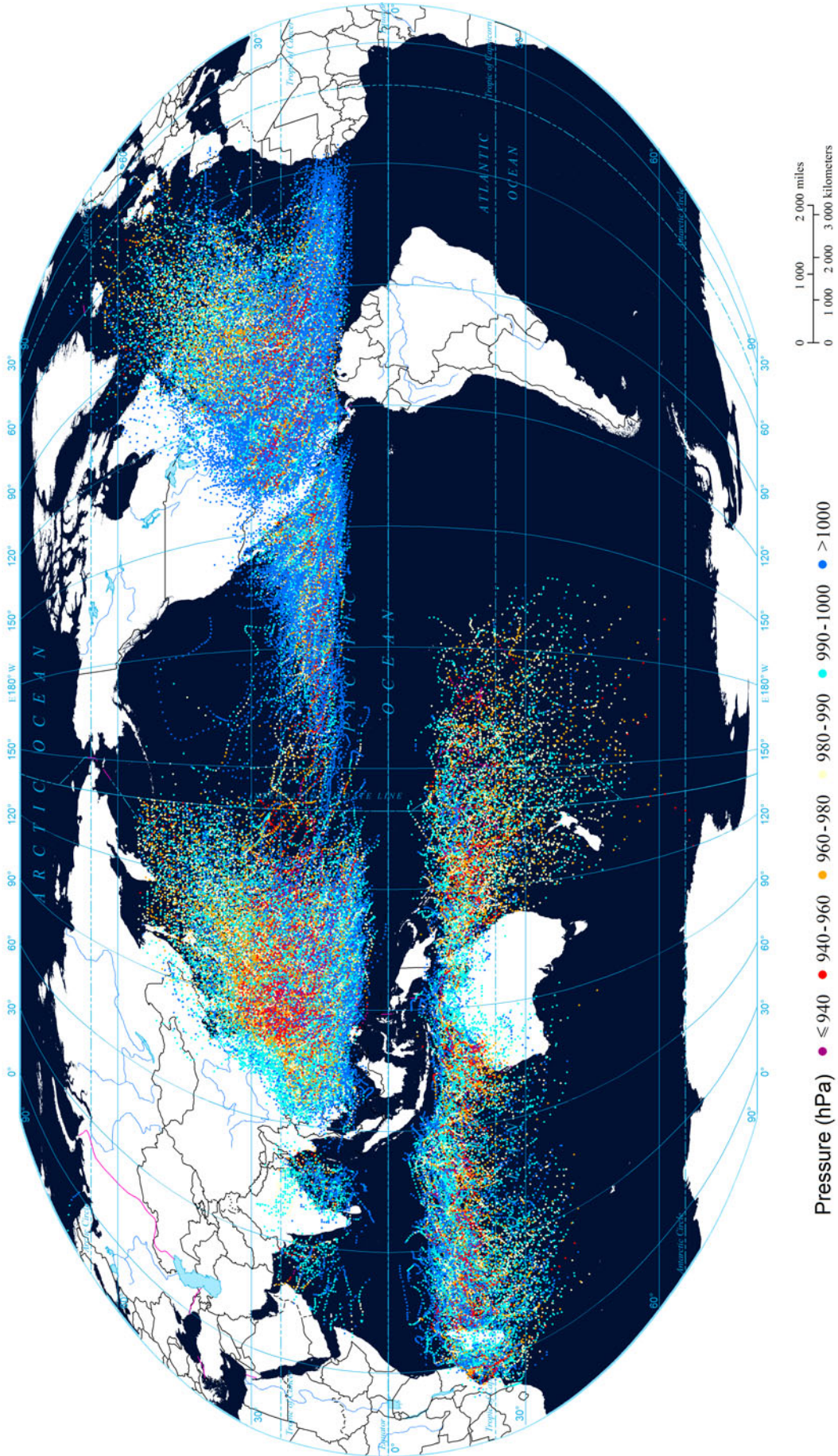
the top 10 % countries are China, Philippines, Japan, USA, Vietnam, and South Korea.

### 3.3 Affected GDP Risk

By zonal statistics of the annual expectation of affected GDP, the expected annual affected GDP risk of TC wind of the world at national level is derived and ranked (Fig. 3). The top 1 % country with the highest expected annual affected GDP risk of TC wind is China, and the top 10 % countries are China, India, USA, Japan, Philippines, and Bangladesh.

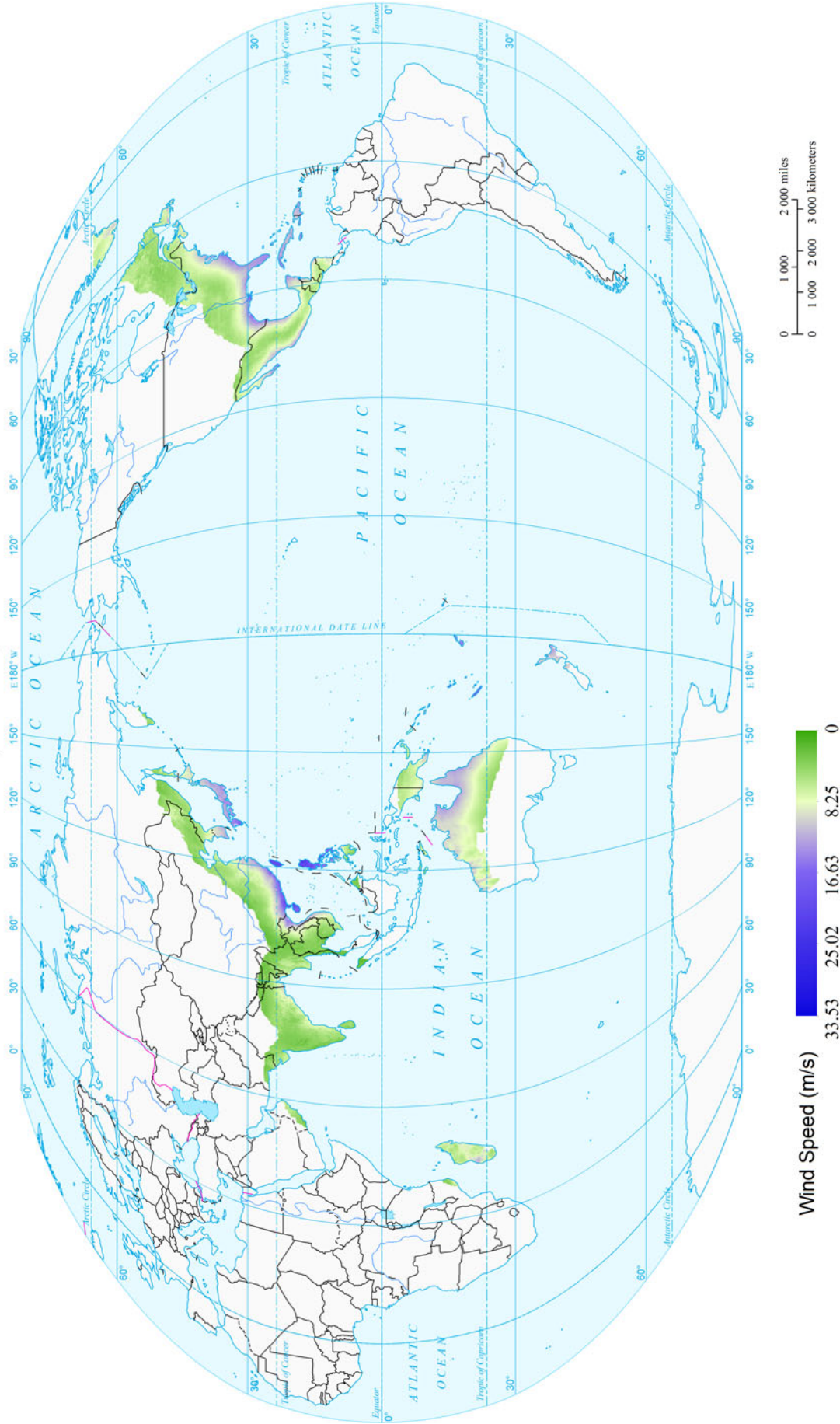
## 4 Maps

### Global Tropical Cyclone Tracks

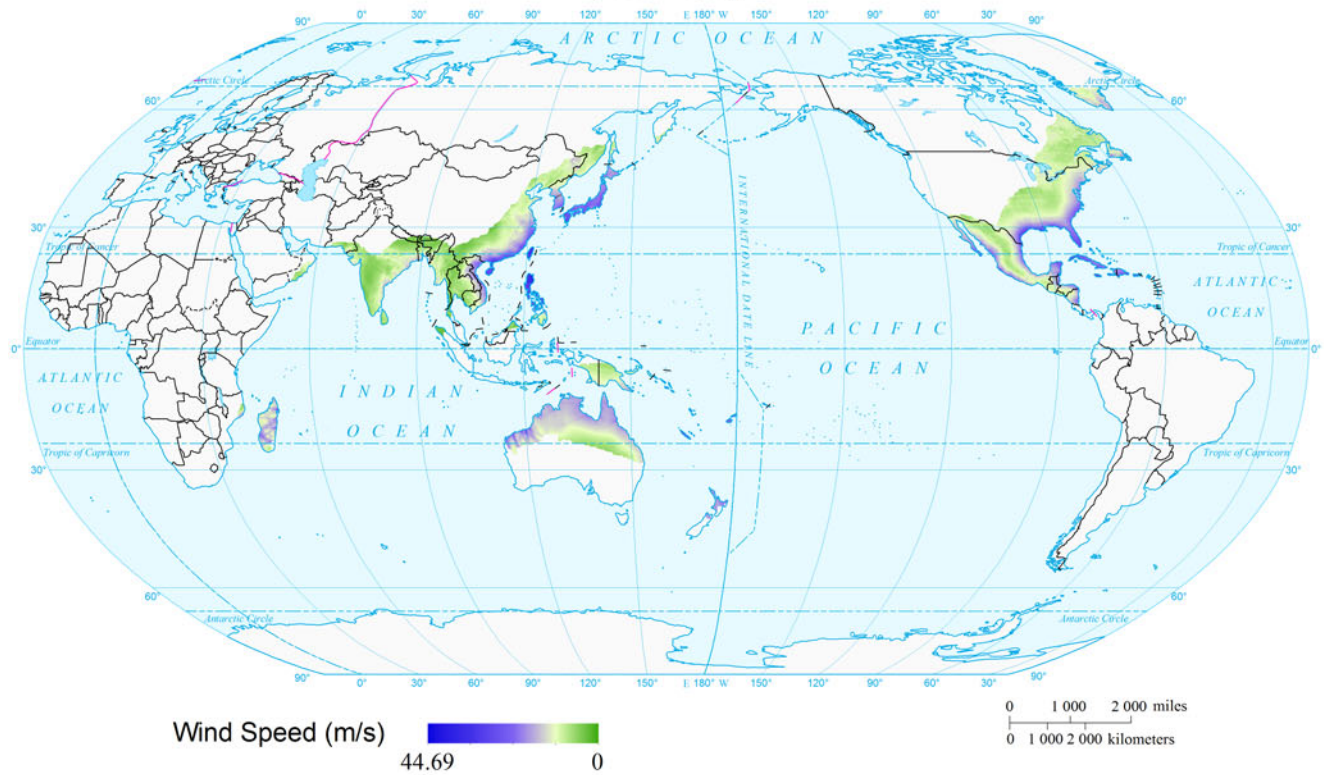




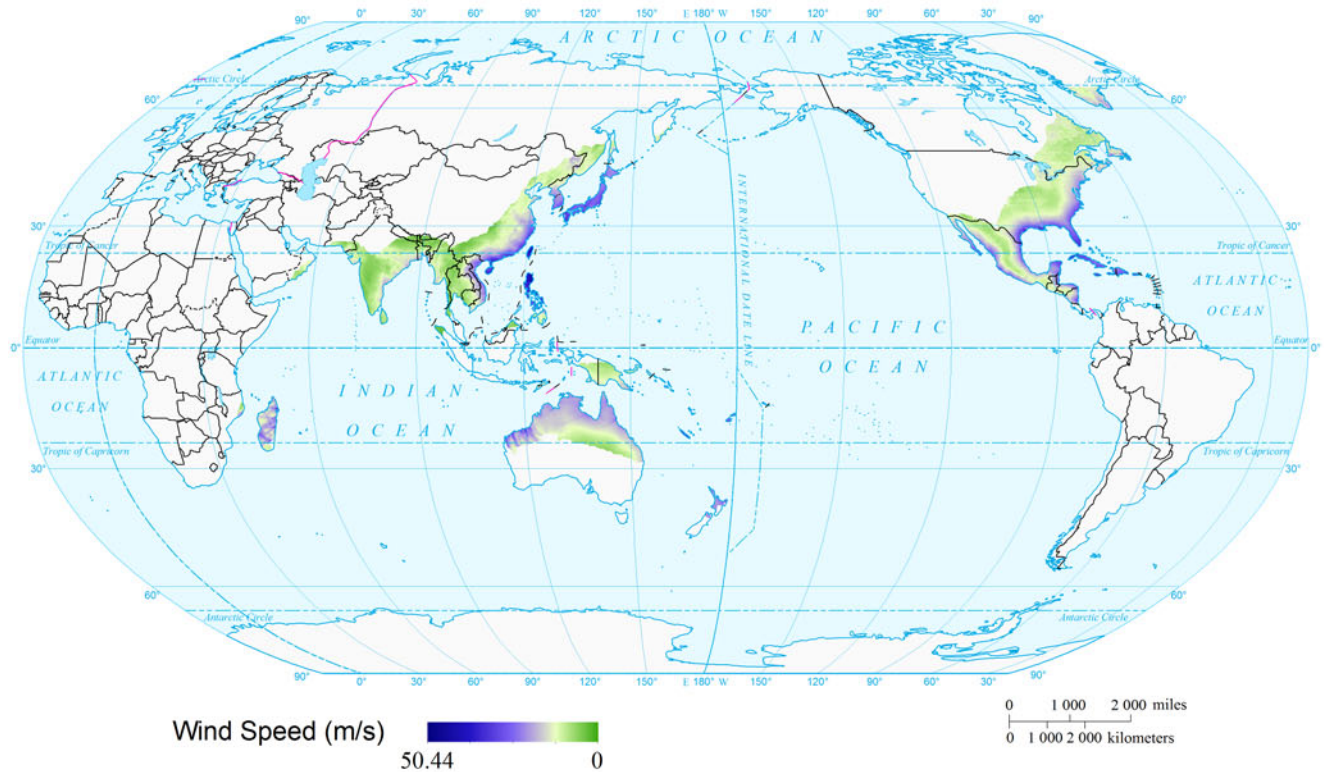
### Global Expected Annual 10-minute Maximum Sustained Wind of Tropical Cyclone (1kmx1km)



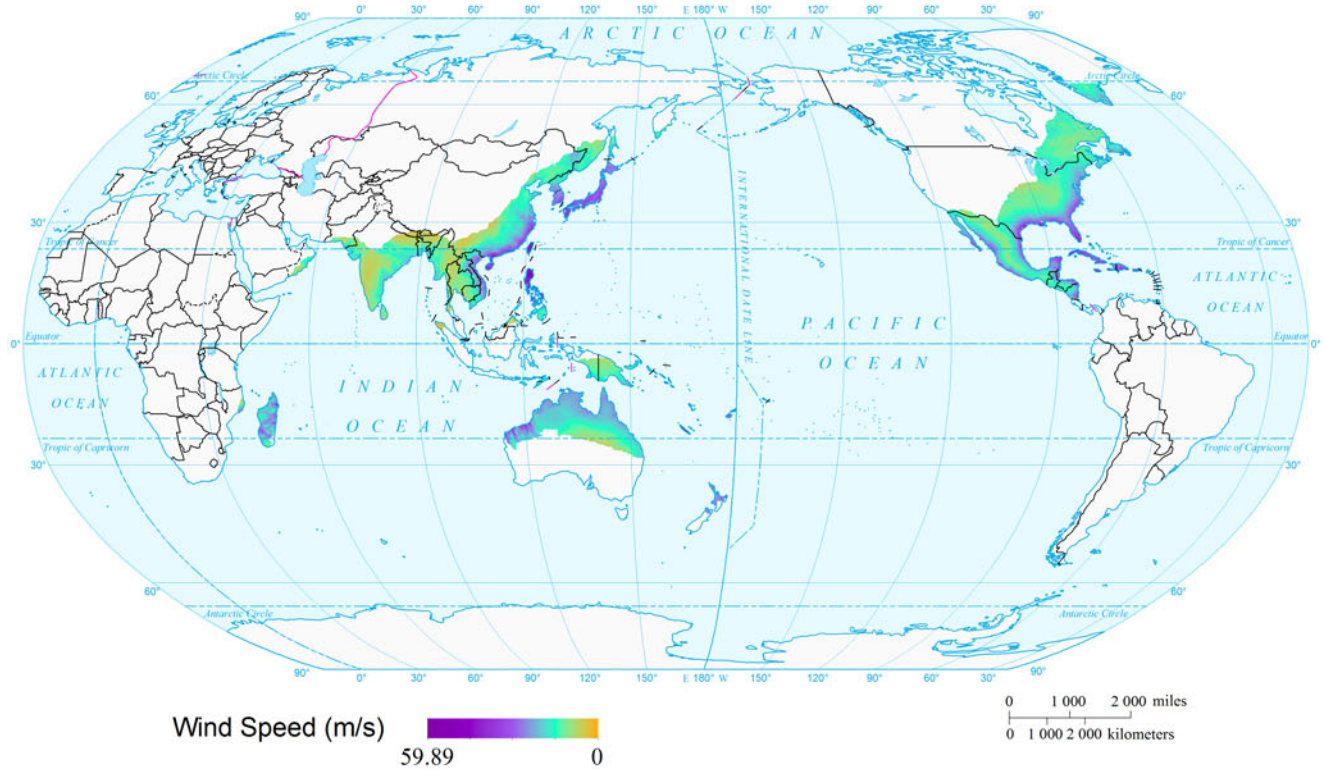
Global 10-minute Maximum Sustained Wind of Tropical Cyclone by Return Period (10a)  
(1km×1km)



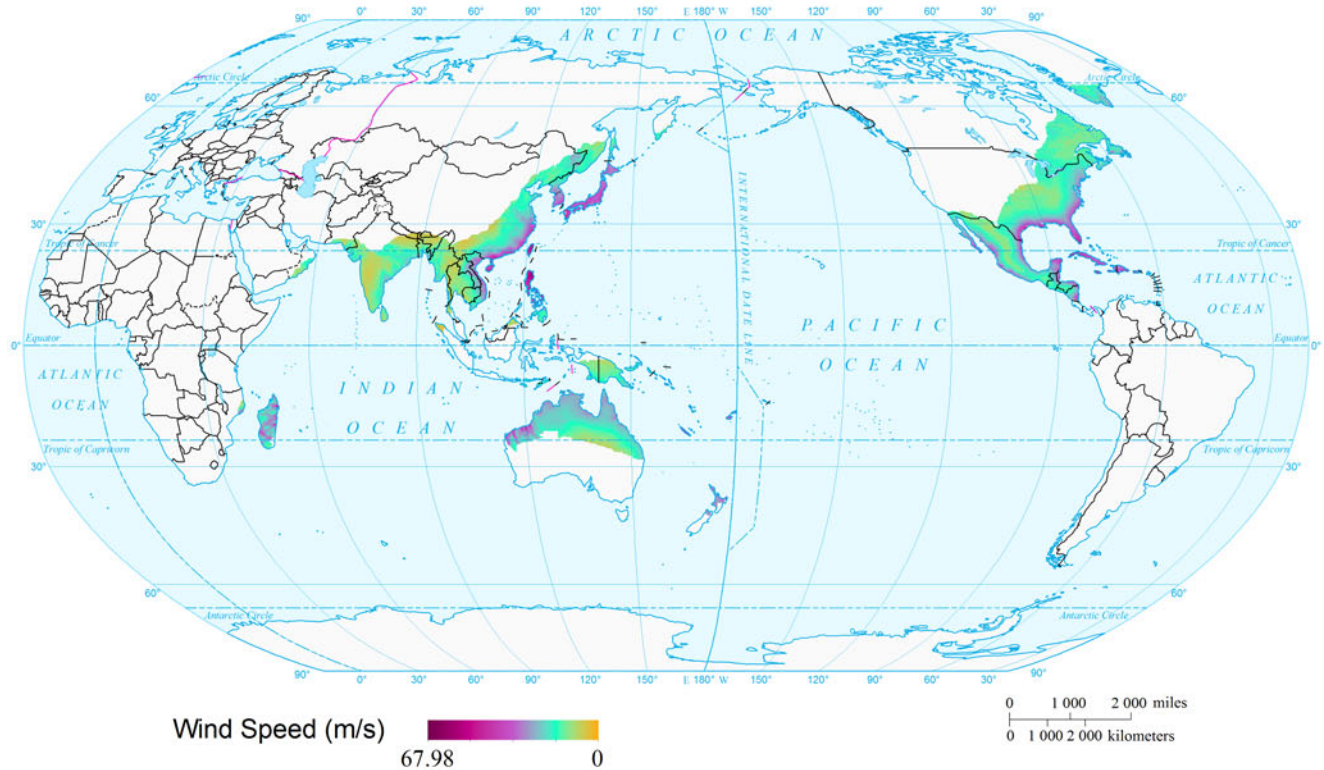
Global 10-minute Maximum Sustained Wind of Tropical Cyclone by Return Period (20a)  
(1km×1km)



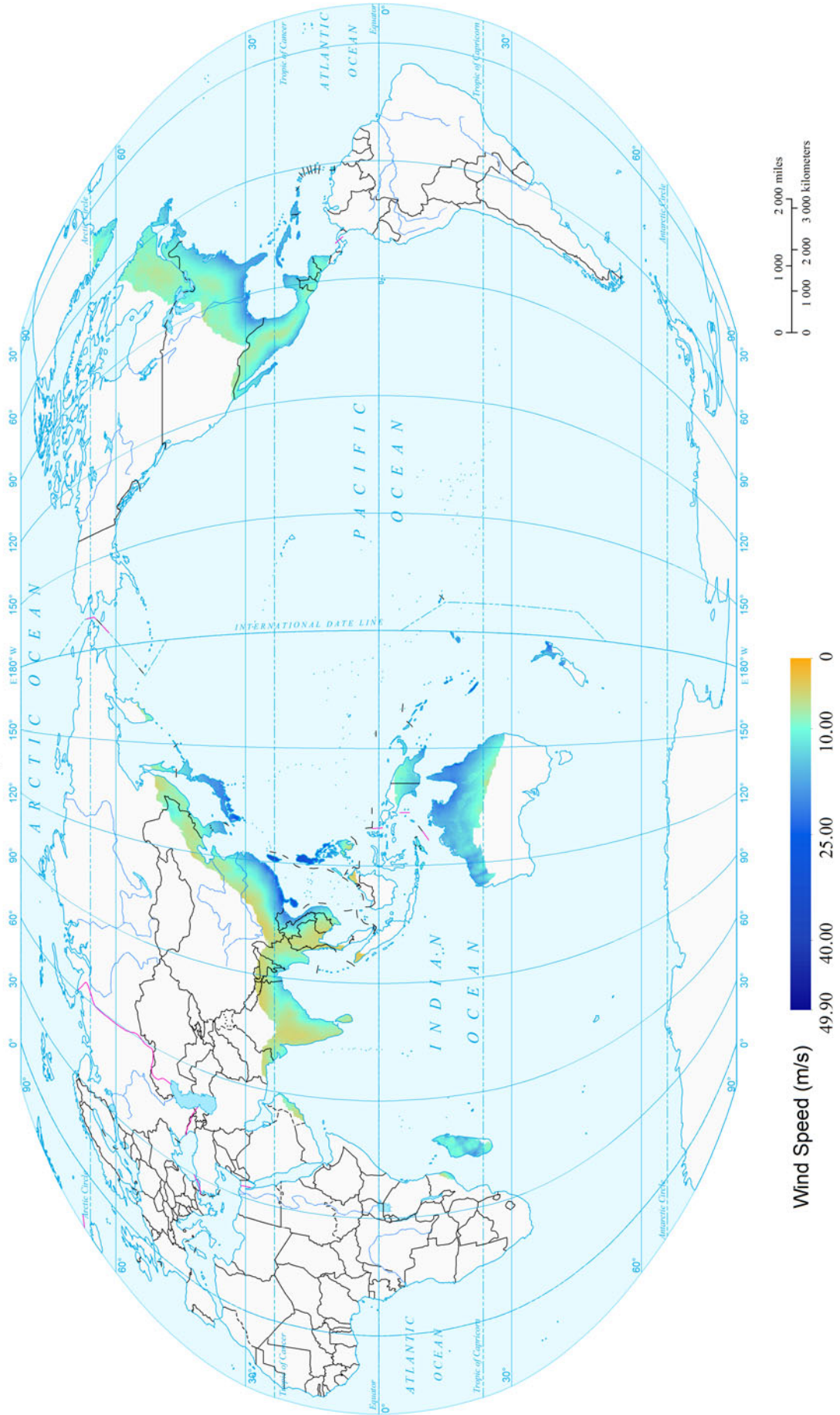
Global 10-minute Maximum Sustained Wind of Tropical Cyclone by Return Period (50a)  
(1km×1km)



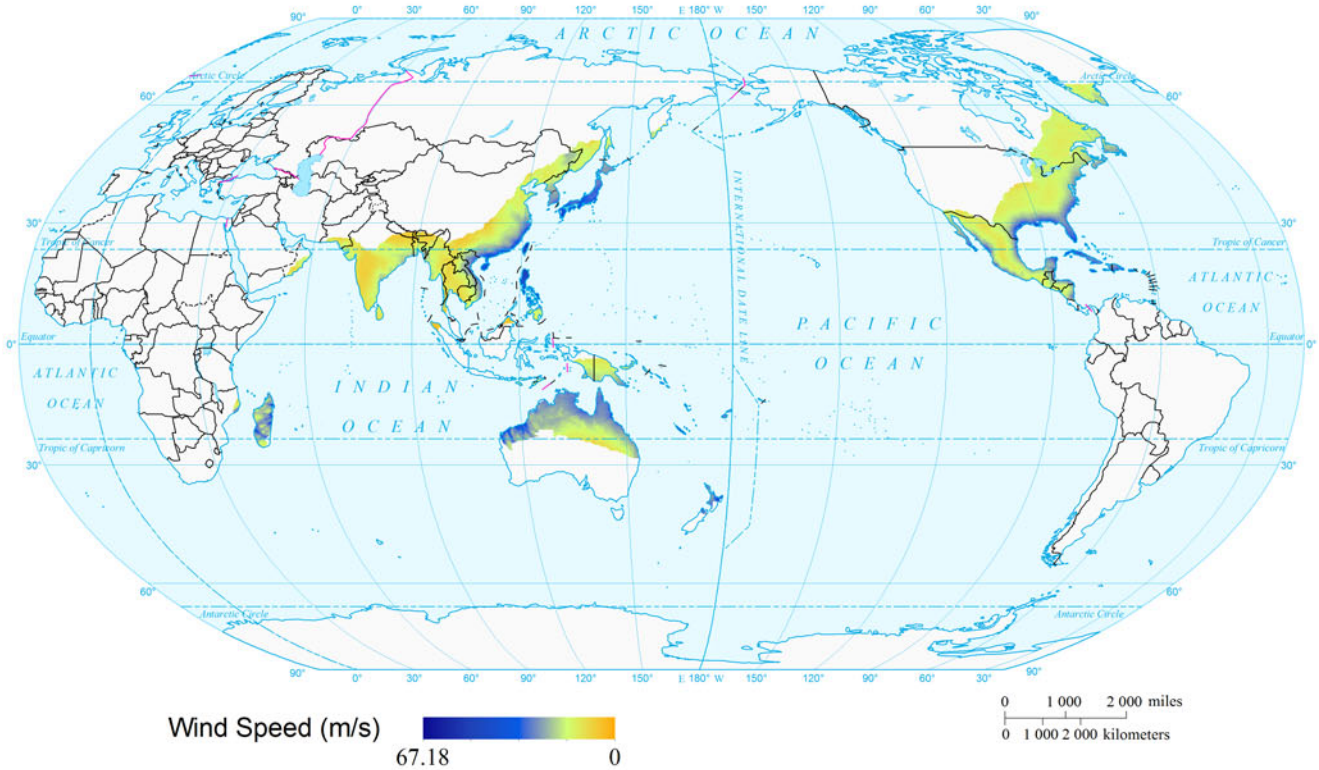
Global 10-minute Maximum Sustained Wind of Tropical Cyclone by Return Period (100a)  
(1km×1km)



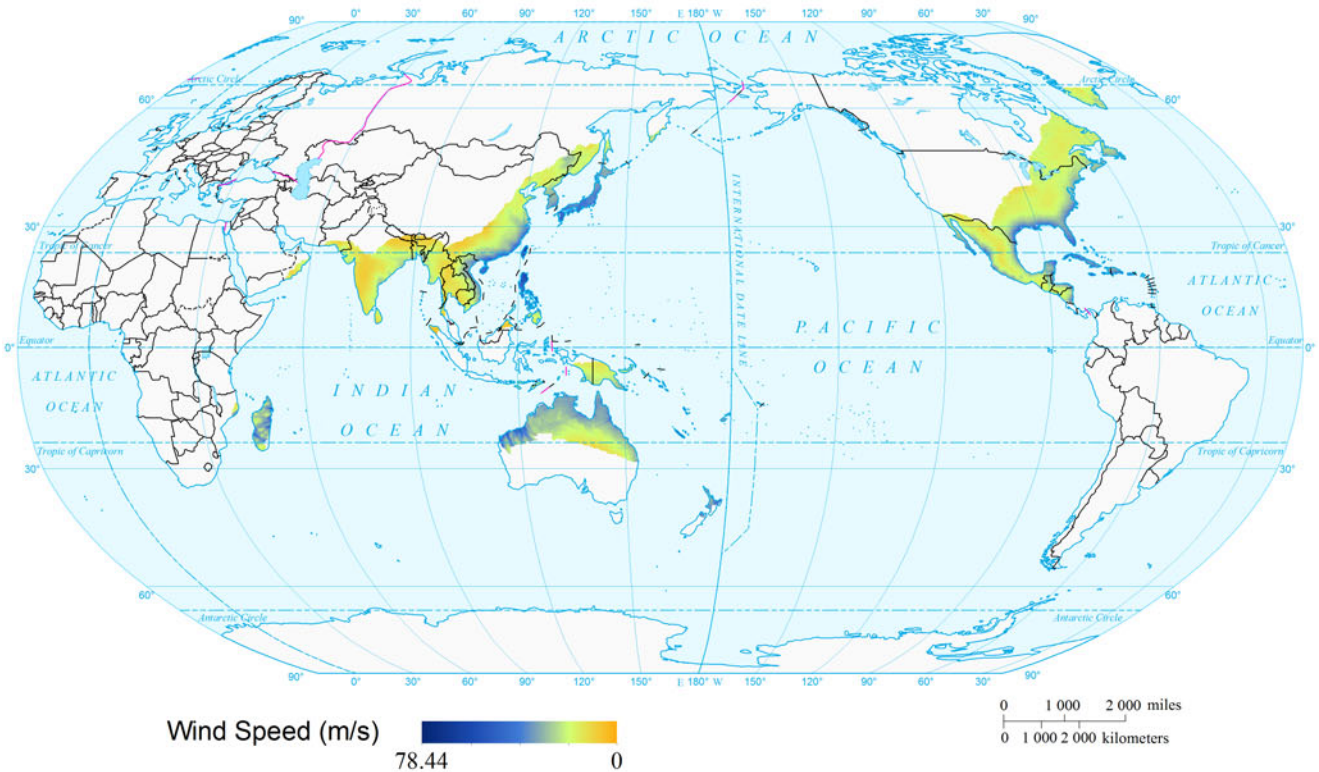
Global Expected Annual 3-second Gust Wind of Tropical Cyclone (1kmx1km)



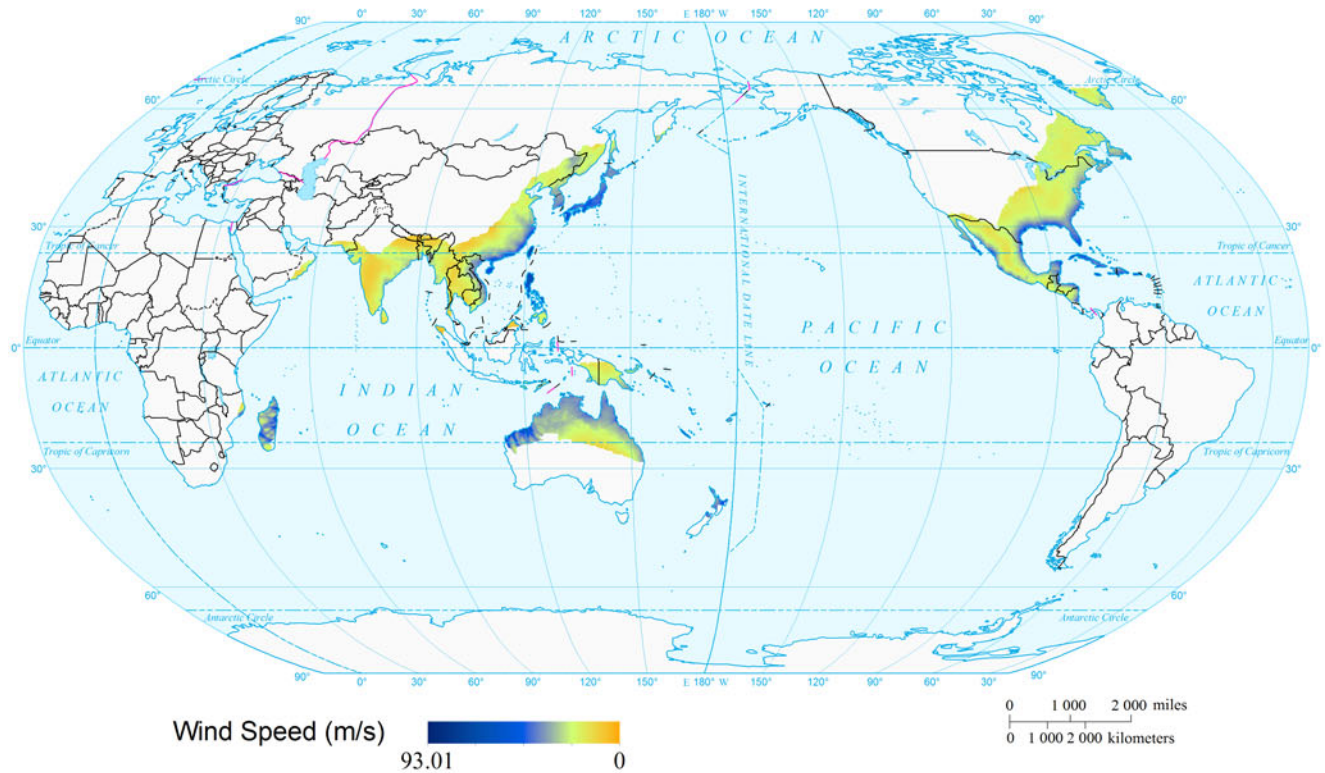
Global 3-second Gust Wind of Tropical Cyclone by Return Period (10a)  
(1km×1km)



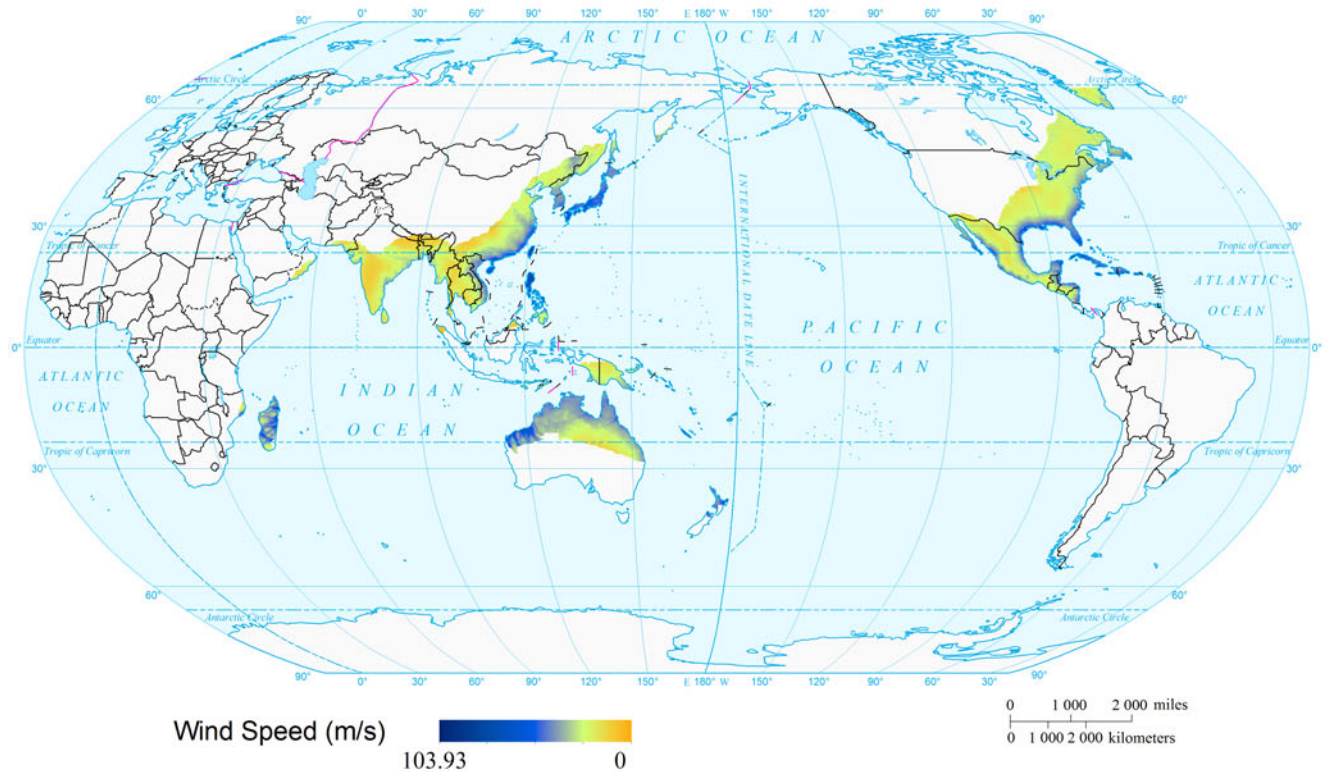
Global 3-second Gust Wind of Tropical Cyclone by Return Period (20a)  
(1km×1km)



Global 3-second Gust Wind of Tropical Cyclone by Return Period (50a)  
(1km×1km)

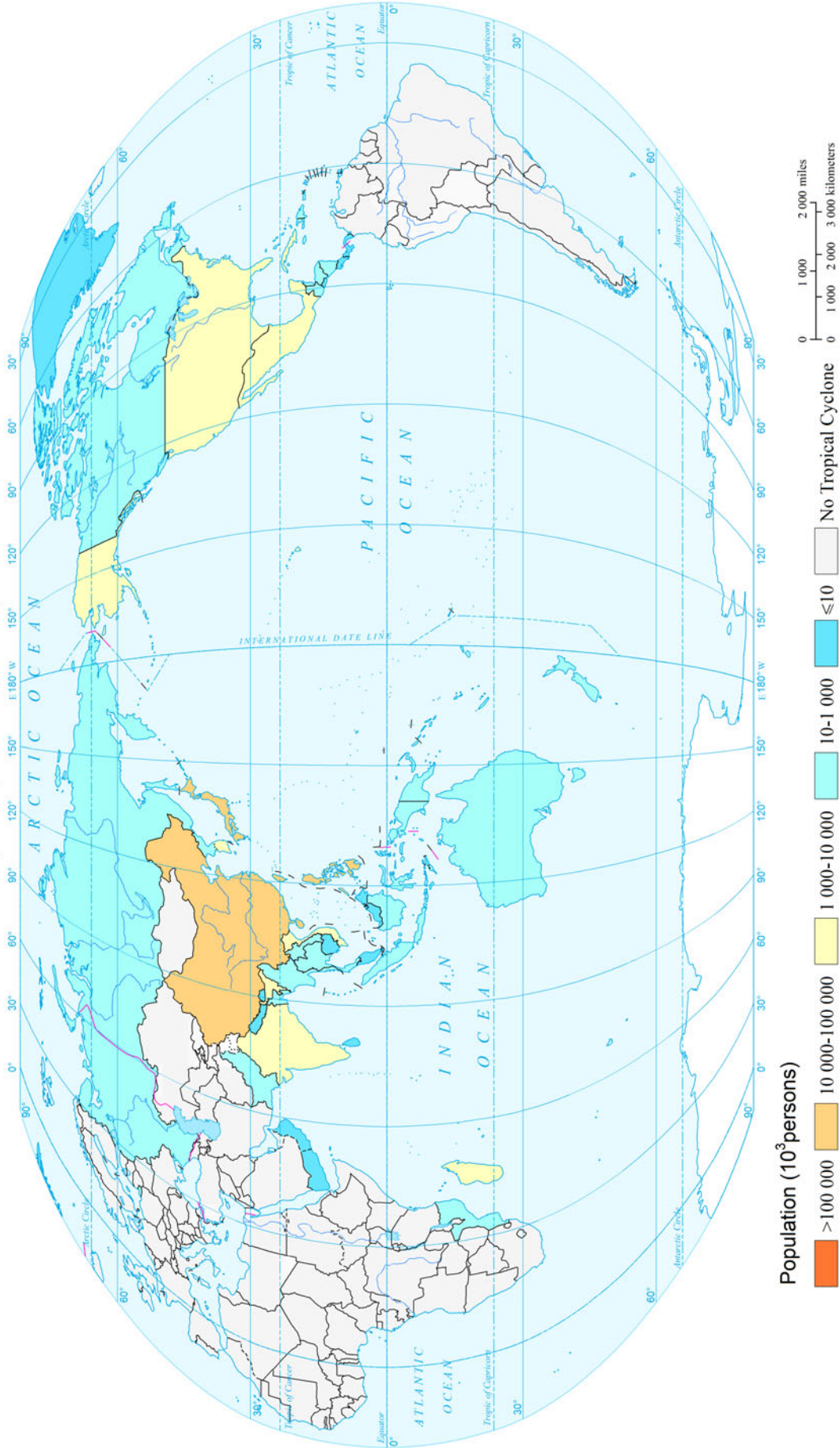


Global 3-second Gust Wind of Tropical Cyclone by Return Period (100a)  
(1km×1km)

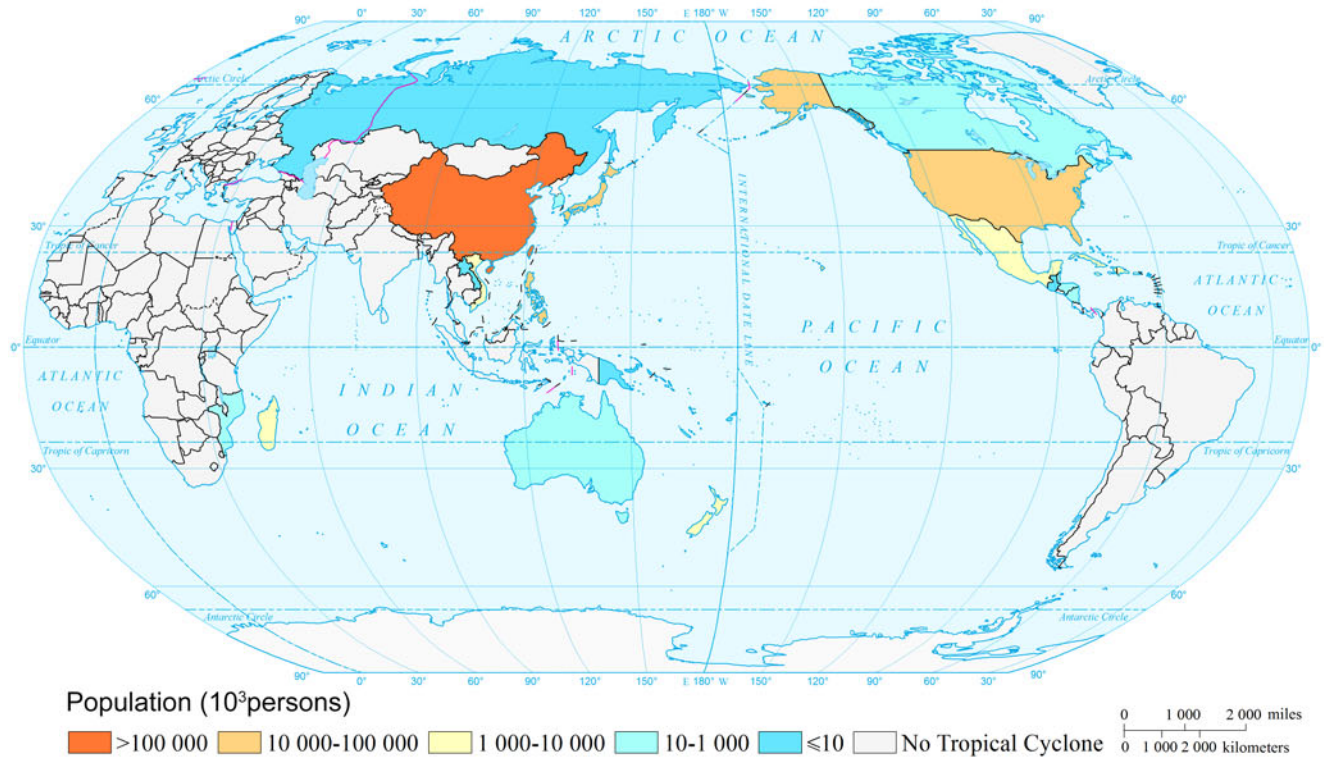




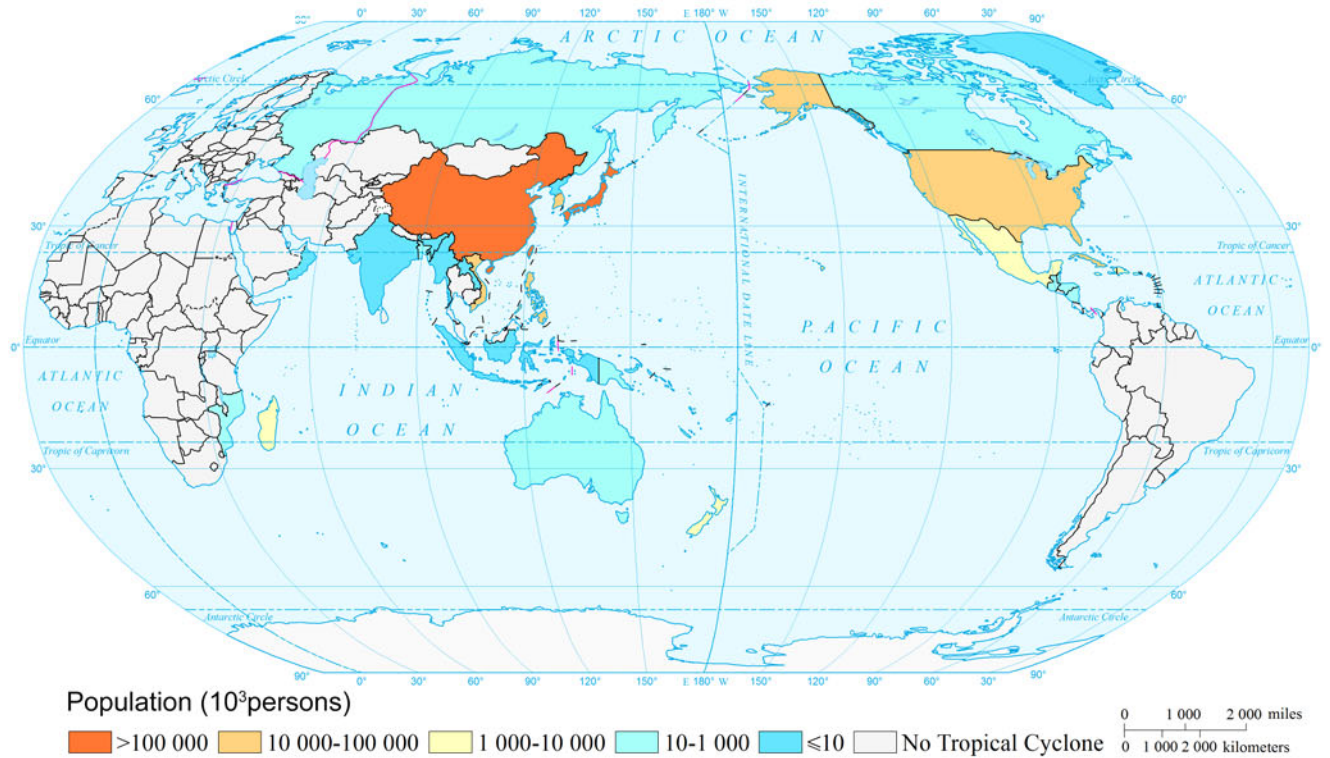
### Expected Annual Affected Population Risk of Tropical Cyclone of the World (Country and Region Unit)



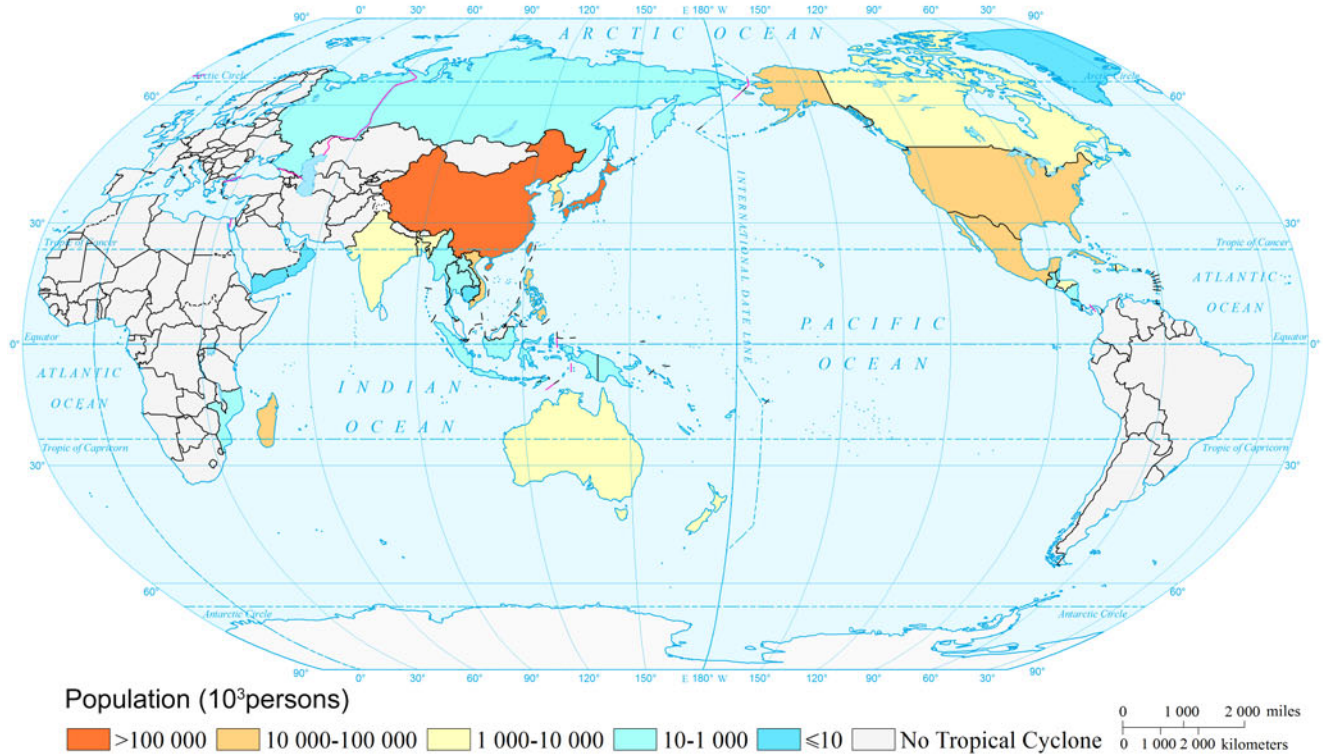
Affected Population Risk of Tropical Cyclone of the World by Return Period (10a)  
(Country and Region Unit)



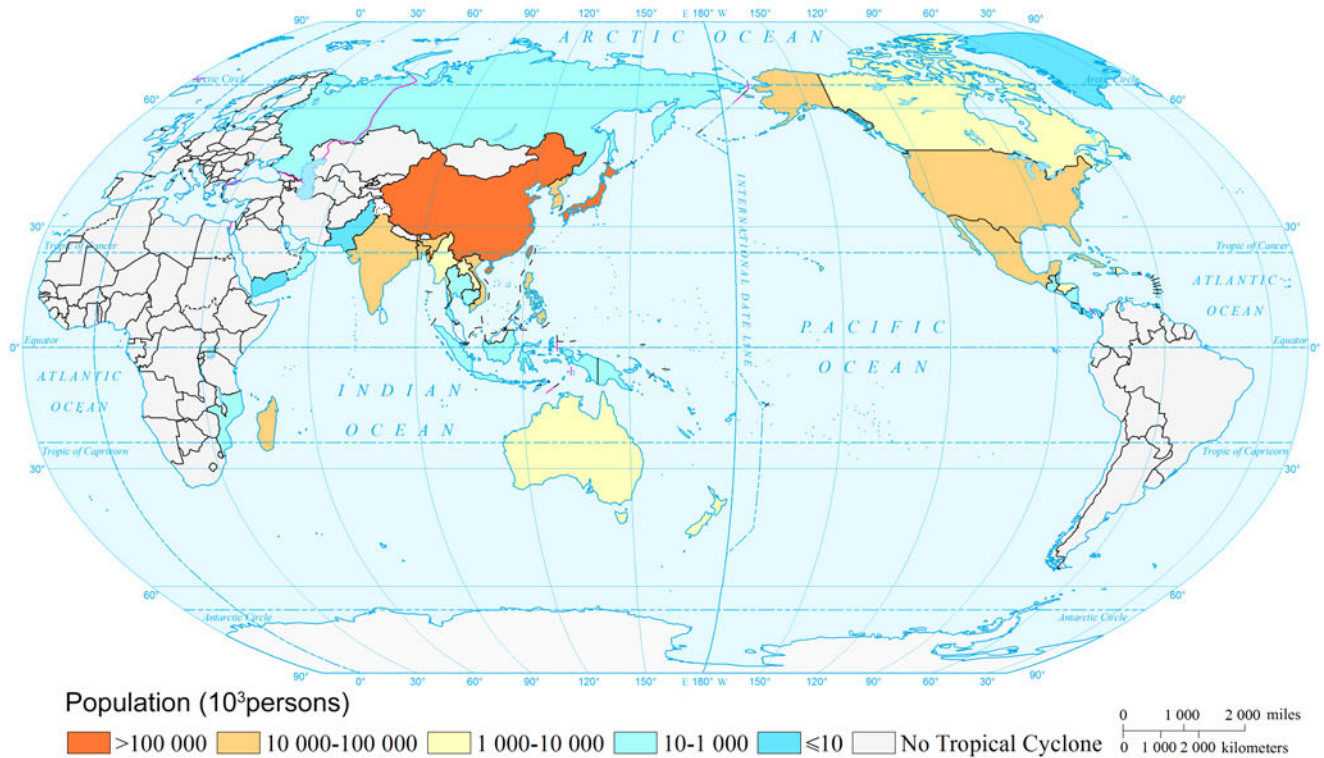
Affected Population Risk of Tropical Cyclone of the World by Return Period (20a)  
(Country and Region Unit)



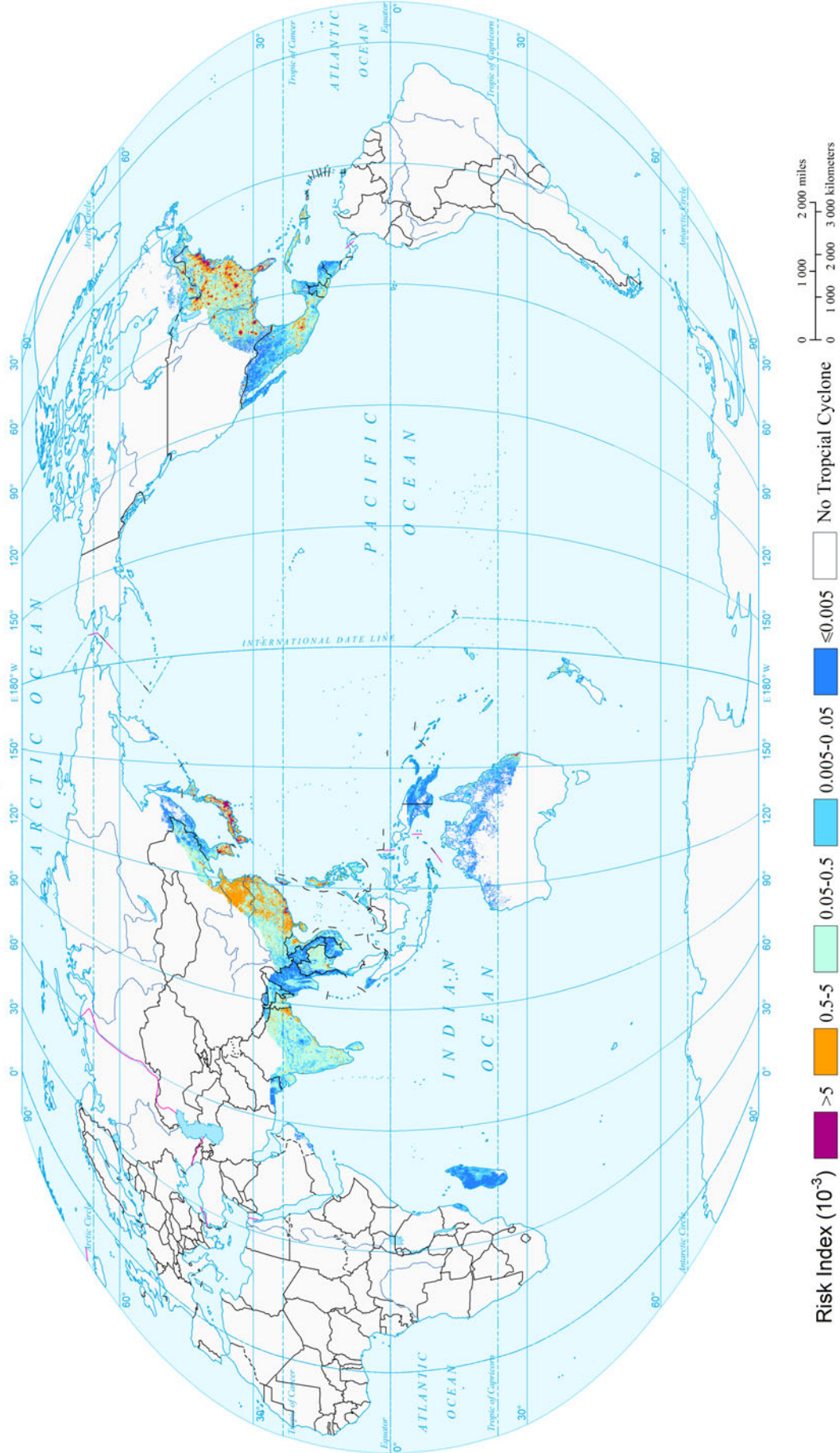
### Affected Population Risk of Tropical Cyclone of the World by Return Period (50a) (Country and Region Unit)



### Affected Population Risk of Tropical Cyclone of the World by Return Period (100a) (Country and Region Unit)



Expected Annual Affected GDP Risk of Tropical Cyclone of the World  
( $0.1^\circ \times 0.1^\circ$ )



## References

- European Committee for Standardization. 2005. Eurocode 1: Actions on structures—part 1–4: General actions—wind actions. BS EN1991-1-4.2005.
- Engineering Sciences Data Unit (ESDU). 1983. *Strong winds in the atmospheric boundary layer-part 2: Discrete gust speeds*. London: Engineering Science Data Unit.
- Fang, W.H., and X.W. Shi. 2012. A review of stochastic modeling of tropical cyclone track and intensity for disaster risk assessment. *Advances in Earth Science* 27(8): 866–75 (in Chinese).
- Fang, W.H., and W. Lin. 2013. A review on typhoon wind field modeling for disaster risk assessment. *Progress in Geography* 32(6): 852–67 (in Chinese).
- Georgiou, P.N., A.G. Davenport, and B.J. Vickery. 1983. Design wind speeds in regions dominated by tropical cyclones. *Journal of Wind Engineering and Industrial Aerodynamics* 13(1): 139–52.
- Harper, B.A., and G.J. Holland. 1999. An updated parametric model of the tropical cyclone. *Proceedings of the 23rd Conference Hurricanes and Tropical Meteorology*, 893–96, in Dallas, Texas.
- Harper, B.A., T.A. Harby, L.B. Mason et al. 2001. *Queensland climate change and community vulnerability to tropical cyclones: Ocean hazards assessment*. Stage 1 report. Queensland, Brisbane, Australia: Department of Natural Resources and Mines.
- Holland, G.J. 1980. An analytic model of the wind and pressure profiles in hurricanes. *Monthly Weather Review* 108(8): 1212–218.
- Jakobsen, F., and H. Madsen. 2004. Comparison and further development of parametric tropical cyclone models for storm surge modelling. *Journal of Wind Engineering and Industrial Aerodynamics* 92(5): 375–91.
- McConochie, J.D., T.A. Hardy, and L.B. Mason. 2004. Modelling tropical cyclone over-water wind and pressure field. *Ocean Engineering* 31(14–15): 1757–782.
- Meng, Y., M. Matsui, and K. Hibi. 1997. A numerical study of the wind field in a typhoon boundary layer. *Journal of Wind Engineering and Industrial Aerodynamics* 67–68: 437–48.
- Neumann, C.J. 1993. *Global overview: Global guide to tropical cyclone forecasting*. WMO/TC–No. 560, Report No. TCP–31. Geneva: World Meteorological Organization: 1–1–1–43.
- Vickery, P.J., and D. Wadhera. 2008. Statistical models of Holland pressure profile parameter and radius to maximum winds of hurricanes from flight-level pressure and H\*Wind data. *Journal of Applied Meteorology and climatology* 47(10): 2497–517.
- Wieringa, J. 1993. Representative roughness parameters for homogeneous terrain. *Boundary-Layer Meteorology* 63(4): 323–63.
- Wieringa, J., A.G. Davenport, C.S.B. Grimmond, et al. 2001. *New revision of Davenport roughness classification*. Eindhoven, The Netherlands: The Third European & African Conference on Wind Engineering.
- Willoughby, H., R. Darling, and M. Rahn. 2006. Parametric representation of the primary hurricane vortex—part II: A new family of sectionally continuous profiles. *Monthly Weather Review* 134(4): 1102–120.

---

**Part V**

**Heat Wave and Cold Wave Disasters**

---

# Mapping Heat Wave Risk of the World

Mengyang Li, Zhao Liu, Weihua Dong, and Peijun Shi

---

## 1 Background

Heat wave is a period of abnormally and uncomfortably hot weather (IPCC 2013). Since the 1990s, heat waves have taken place frequently, having serious impacts on human health and even leading to mortality. The European heat wave of 2003 induced more than 70,000 additional deaths in France, Germany, Italy, Spain, and other countries (Robine et al. 2008). For Russia as a whole, the death toll of 2010 summer heat wave totaled 55,000 people (Swiss Re 2011). With global warming, the frequency and intensity of heat waves have been expected to increase (Meehl and Tebaldi 2004). Heat wave has become one of the most serious climate events in the world.

---

**Mapping Editors:** Jing'ai Wang (Key Laboratory of Regional Geography, Beijing Normal University, Beijing 100875, China) and Fang Lian (School of Geography, Beijing Normal University, Beijing 100875, China).

**Language Editor:** Tao Ye (State Key Laboratory of Earth Surface Processes and Resource Ecology, Beijing Normal University, Beijing 100875, China).

---

M. Li · Z. Liu  
Academy of Disaster Reduction and Emergency Management,  
Ministry of Civil Affairs and Ministry of Education, Beijing  
Normal University, Beijing 100875, China

W. Dong  
School of Geography, Beijing Normal University, Beijing 100875,  
China

P. Shi (✉)  
State Key Laboratory of Earth Surface Processes and Resource  
Ecology, Beijing Normal University, Beijing 100875, China  
e-mail: spj@bnu.edu.cn

Special Report of the Intergovernmental Panel on Climate Change (IPCC-SREX) mapped the global warm days, warm nights, and number of days with maximal temperature larger than 30 °C (IPCC 2012). IPCC's Fifth Assessment Report pointed out that it was very likely that the number of warm days and nights had increased on the global scale between 1951 and 2010; globally, there was medium confidence that the length and frequency of warm spells, including heat waves, have increased. Nevertheless, it is likely that heat wave frequency has increased over this period in large parts of Europe, Asia, and Australia (IPCC 2013). Recently, researchers found that heat waves in northern mid-latitudes linked to a vanishing cryosphere and the changes of corresponding general atmospheric circulation (Tang et al. 2014).

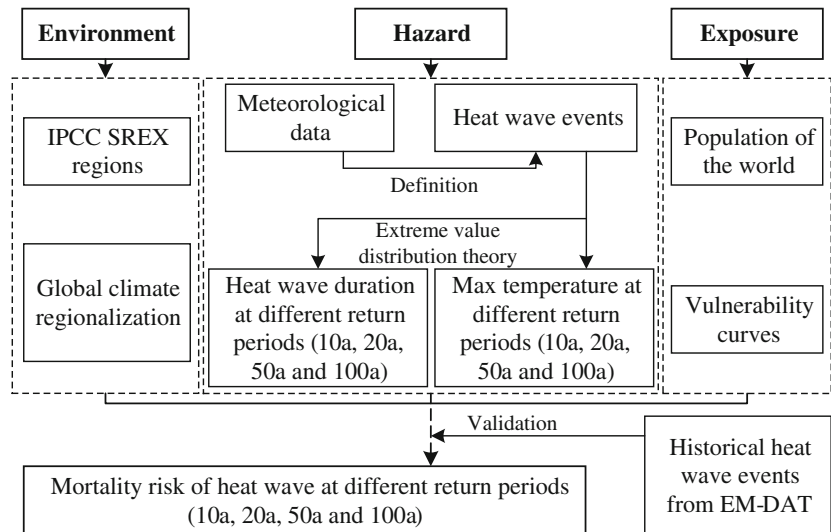
This study initiatively assesses heat wave mortality risk of the world at grid ( $0.75^\circ \times 0.75^\circ$ ), comparable geographic unit and national level based on the disaster system theory (Shi 1991, 1996, 2002).

---

## 2 Method

Figure 1 shows the technical flowchart for mapping heat wave mortality risk of the world.

**Fig. 1** Technical flowchart for mapping heat wave mortality risk of the world



## 2.1 Intensity

In this study, heat wave at grid level ( $0.75^\circ \times 0.75^\circ$ ) is defined as the climate process that daily temperature is larger than a threshold in at least three consecutive days, within which the highest temperature is at least  $3^\circ\text{C}$  higher than the threshold. The threshold for each grid is defined as the 95 percentile of daily maximum temperature during 1979–2013 (Appendix III, Hazards data 4.14). If the 95 percentile temperature is below  $25^\circ\text{C}$ , define the threshold as  $25^\circ\text{C}$ .

Heat wave intensity is measured by two steps: (1) the probability ( $p_1$ ) that daily temperature reaches the threshold and (2) number of days (duration) of the heat wave and the highest temperature in the period. The probability  $p_1$  for each grid was fitted with a binominal distribution. For duration and the highest temperature, Weibull distribution was employed [Eq. (1)].

$$f(x) = \frac{\beta}{\alpha} \left(\frac{x}{\alpha}\right)^{\beta-1} \exp\left[-\left(\frac{x}{\alpha}\right)^\beta\right], \quad x \geq 0 \quad (1)$$

where  $f(x)$  is the Weibull density function and  $\alpha$  and  $\beta$  are distribution parameters.

The return period of heat wave of specific duration highest temperature is defined in Eq. (2).

$$p = \frac{1}{1 - \frac{F(x_m)}{p_1}} \quad (2)$$

where  $F(x)$  is the cumulative Weibull density function.

Durations and highest temperatures of different return periods (10a, 20a, 50a, and 100a) can be derived using the inverse of Eq. (2).

## 2.2 Vulnerability

In this study, mortality vulnerability curves for Boston, Budapest, Dallas, Lisbon, London, and Sydney were used (Gosling et al. 2007). 26 regions suggested by IPCC-SREX were regrouped into six groups in terms of climate type and latitude zones (IPCC 2012). Each vulnerability curve is applied to each group of the IPCC-SREX regions to map heat wave mortality risk of the world. Boston: eastern North American (Region 5); Lisbon: Mediterranean region (Region 13); London: Western Europe, high latitudes of Northern Hemisphere (Regions 1, 2, 11, and 18); Sydney: mid- and high latitudes of Southern Hemisphere (Regions 9, 10, 17, 25, and 26); Dallas: mid- and low latitudes of Northern and Southern Hemispheres (Regions 4, 6, 7, 8, 14, 15, 16, 19, 20, 21, 22, 23, and 24); Budapest: south and southwest Europe (Regions 3 and 12) (IPCC 2012).

## 2.3 Risk

Heat wave mortality risk of the world is assessed with Eq. (3):

$$R = F(T_{\max}) \times P \times D \quad (3)$$

where  $R$  is the heat wave mortality risk;  $F$  represents the vulnerability function;  $T_{\max}$  refers to the maximum temperature during the heat wave;  $P$  refers to the total population of each grid; and  $D$  is the heat wave duration (days).

### 3 Results

#### 3.1 Intensity

Heat wave intensity is decreasing from the equator to the poles. The highest temperature area distributes near the latitudes 20°N/S, including North Africa, West Asia, Central Asia, South Asia, and Oceania. The longest heat wave days are in Eastern Europe, West Asia, South Asia, North America, and parts of South America. There is no heat wave in area near the equator because of the small variation of daily highest temperature.

#### 3.2 Mortality Risk

High mortality risk areas for heat wave are relatively scattered, distributed mainly in South Asia, Europe, and eastern North America at the grid level. High latitudes in the Northern Hemisphere are mainly of lower risk than other regions.

By zonal statistics of the expected risk result, the expected annual mortality risk of heat wave of the world at national level is derived and ranked (Fig. 2). The top 1 % country with the highest expected annual mortality risk of heat wave is India, and the top 10 % countries are India, Pakistan, USA, Iraq, Russia, Ukraine, Spain, China, Germany, Turkey, France, Iran, and Poland.

### 4 Maps



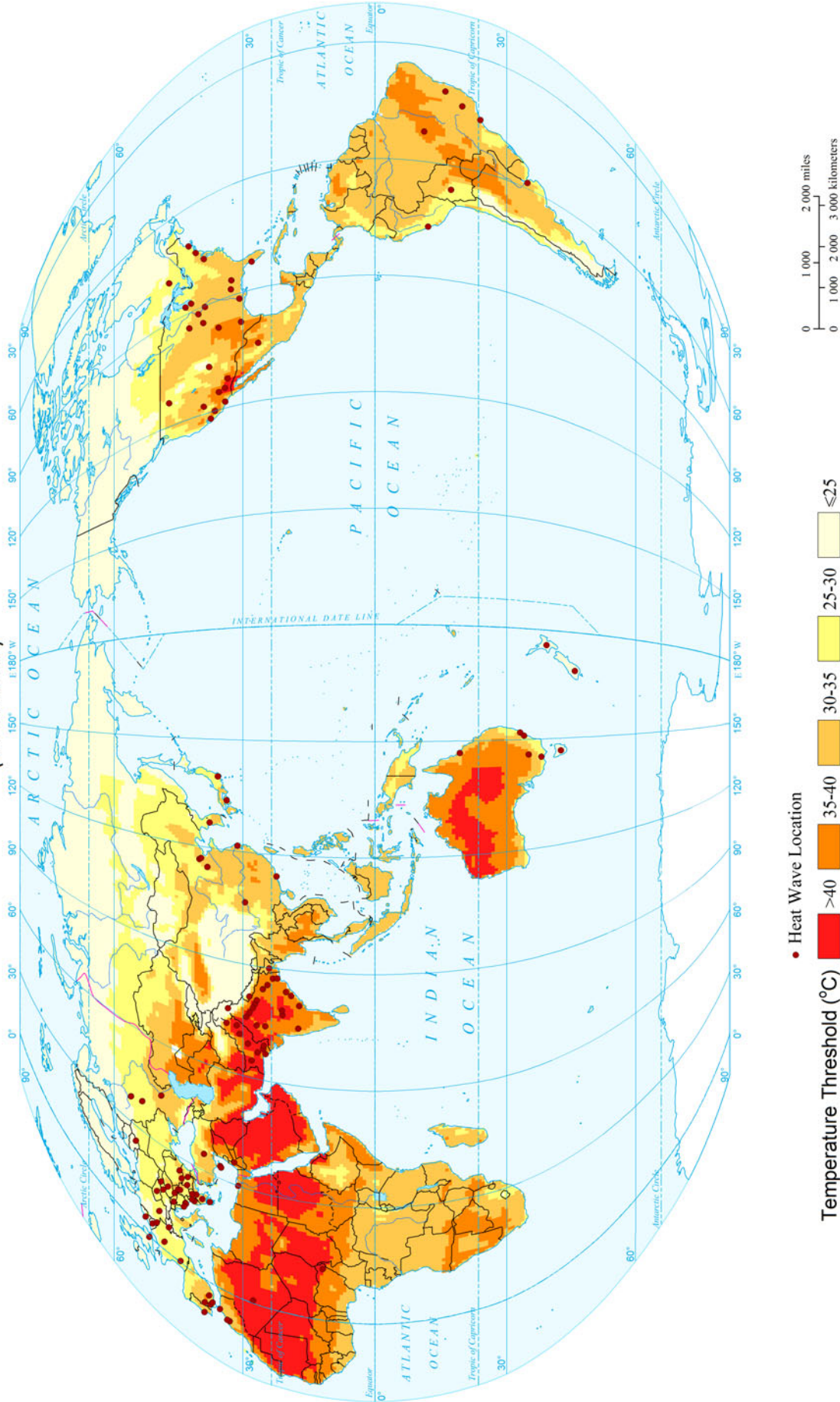
**Fig. 2** Expected annual mortality risk of heat wave of the world. 1 (0, 10 %) India, Pakistan, United States, Iraq, Russia, Ukraine, Spain, China, Germany, Turkey, France, Iran, and Poland. 2 (10 %, 35 %) Egypt, Kazakhstan, Greece, Argentina, Brazil, Romania, Kuwait, Hungary, Italy, Mexico, Afghanistan, Australia, Mozambique, South Africa, Serbia, Burma, Algeria, Syria, Uzbekistan, Slovakia, Saudi Arabia, Portugal, Sudan, Thailand, Turkmenistan, Moldova, Czech Republic, Zambia, Croatia, Canada, Bulgaria, the Netherlands, and Malawi. 3 (35 %, 65 %) Tunisia, Zimbabwe, Austria, Belarus, Morocco, Paraguay, Macedonia, Nigeria, Bosnia and Herzegovina, Bangladesh, Belgium, Albania, Slovenia, Senegal, Chile, Libya, Oman, Chad, Tajikistan, South Sudan, Botswana, Niger, Uruguay, Qatar,

Vietnam, Madagascar, United Arab Emirates, Nepal, Mauritania, Japan, Cambodia, Lithuania, Congo (Democratic Republic of the), Yemen, Angola, Cameroon, Jordan, Sweden, and Eritrea. 4 (65 %, 90 %) Central African Republic, South Korea, Laos, Namibia, Western Sahara, Montenegro, Uganda, Azerbaijan, Ethiopia, Gaza Strip, Luxembourg, The Republic of Côte d'Ivoire, Bolivia, North Korea, Latvia, Switzerland, Guinea, Venezuela, Swaziland, Mali, Finland, Lesotho, Kyrgyzstan, Ghana, Estonia, Tanzania, Sierra Leone, Indonesia, Israel, Djibouti, Burkina Faso, and Guatemala. 5 (90 %, 100 %) Lebanon, Colombia, Mongolia, Peru, Guinea-Bissau, Georgia, Congo, Armenia, Liberia, Papua New Guinea, Malaysia, Kenya, and Ecuador



### Temperature Threshold and Historical Event Locations of Global Heat Wave (1950-2013)

( $0.75^{\circ} \times 0.75^{\circ}$ )



• Heat Wave Location

Temperature Threshold (°C)

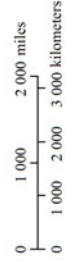
≤25

25-30

30-35

35-40

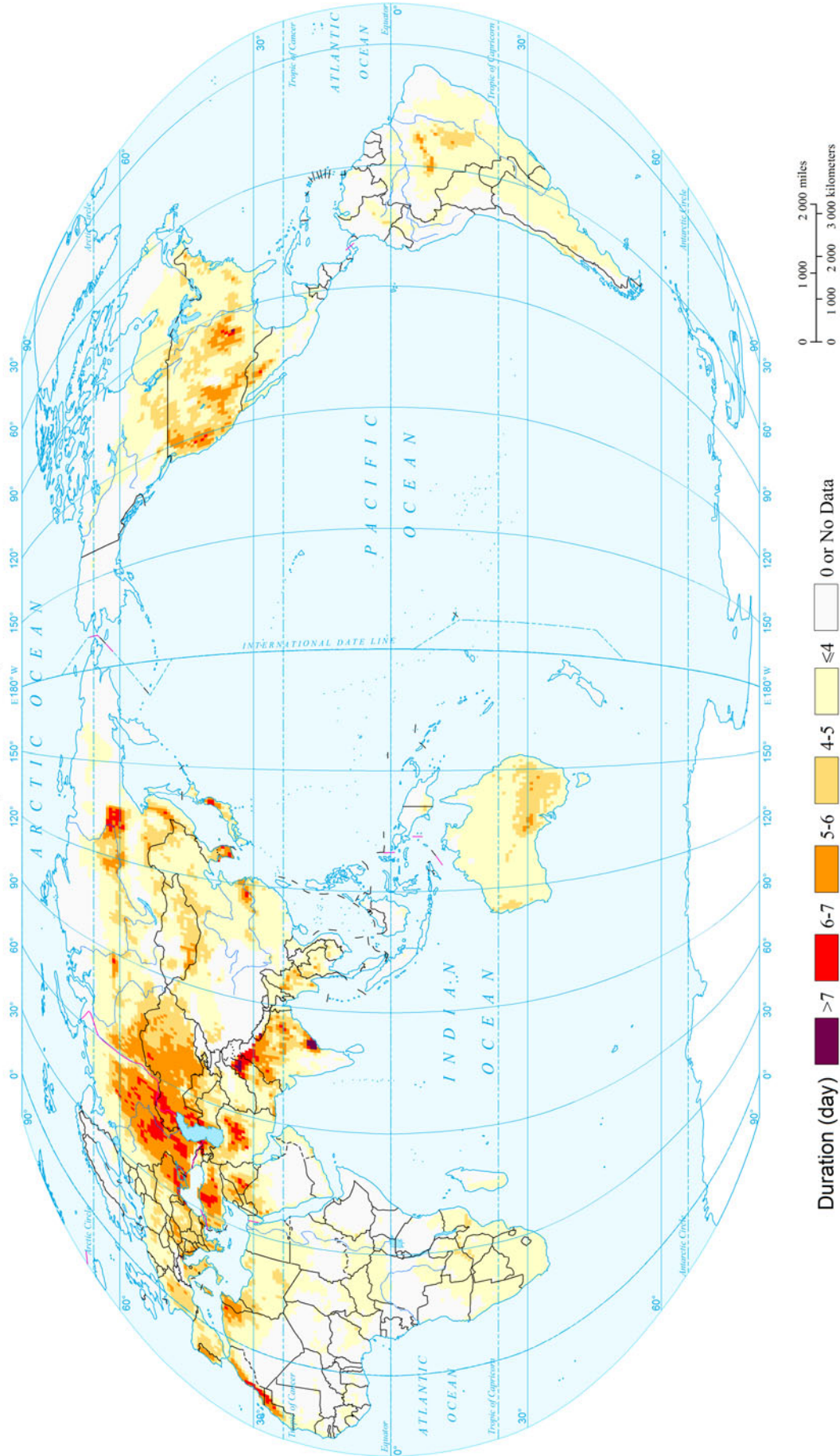
>40



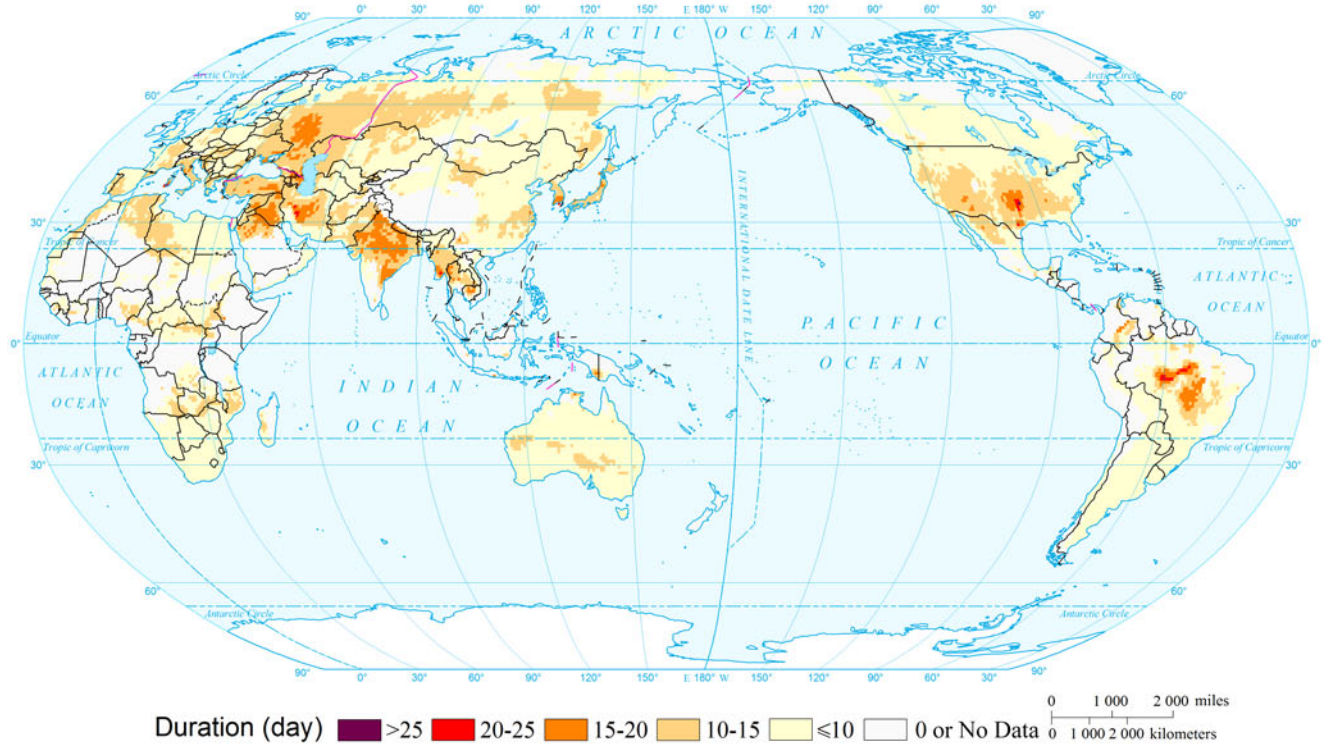
Heat Wave

Heat Wave and Cold Wave Disasters

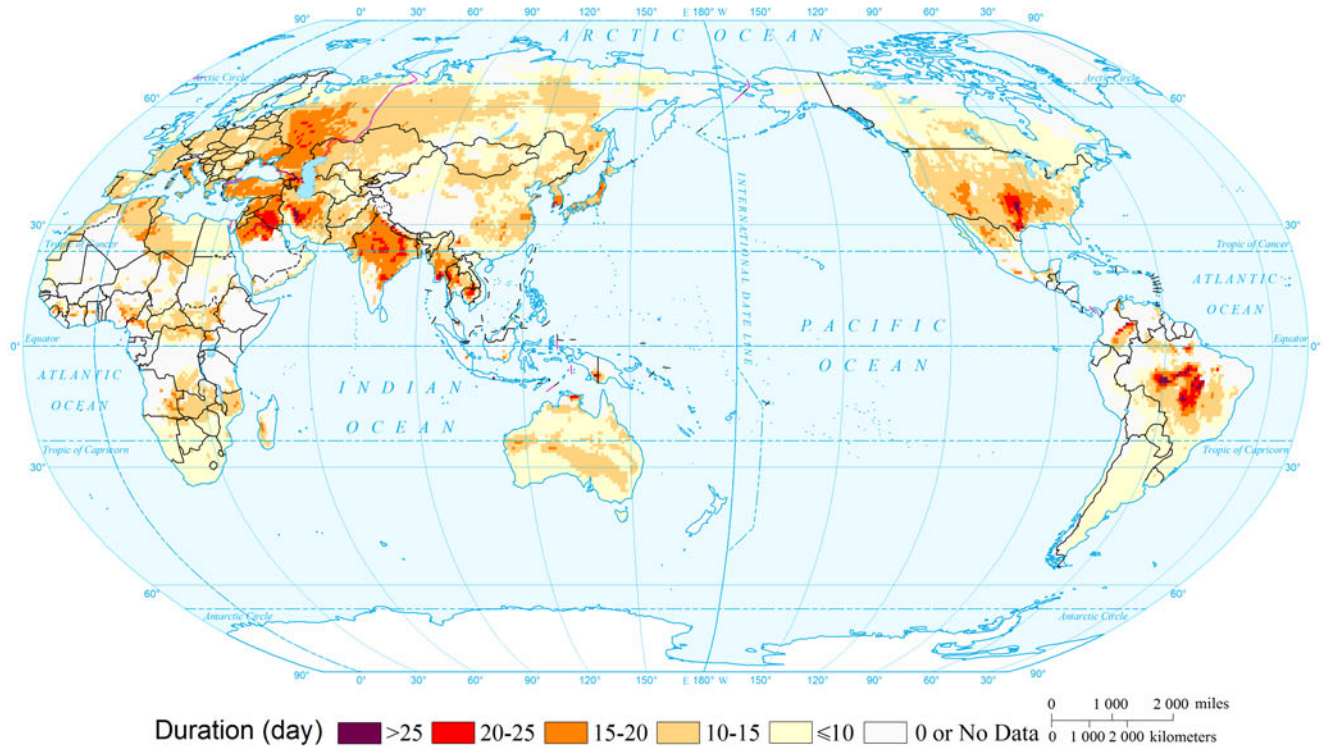
Expected Annual Duration of Global Heat Wave  
( $0.75^\circ \times 0.75^\circ$ )



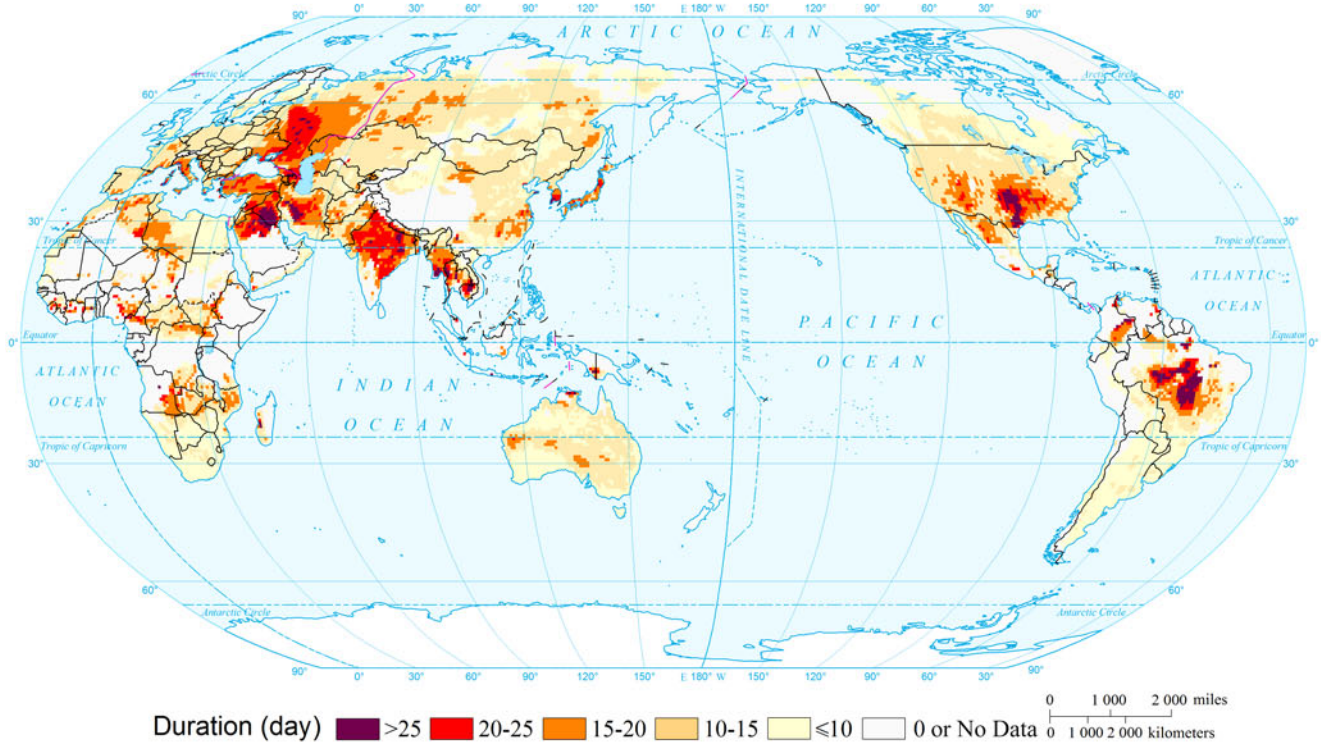
Duration of Global Heat Wave by Return Period (10a)  
(0.75°×0.75°)



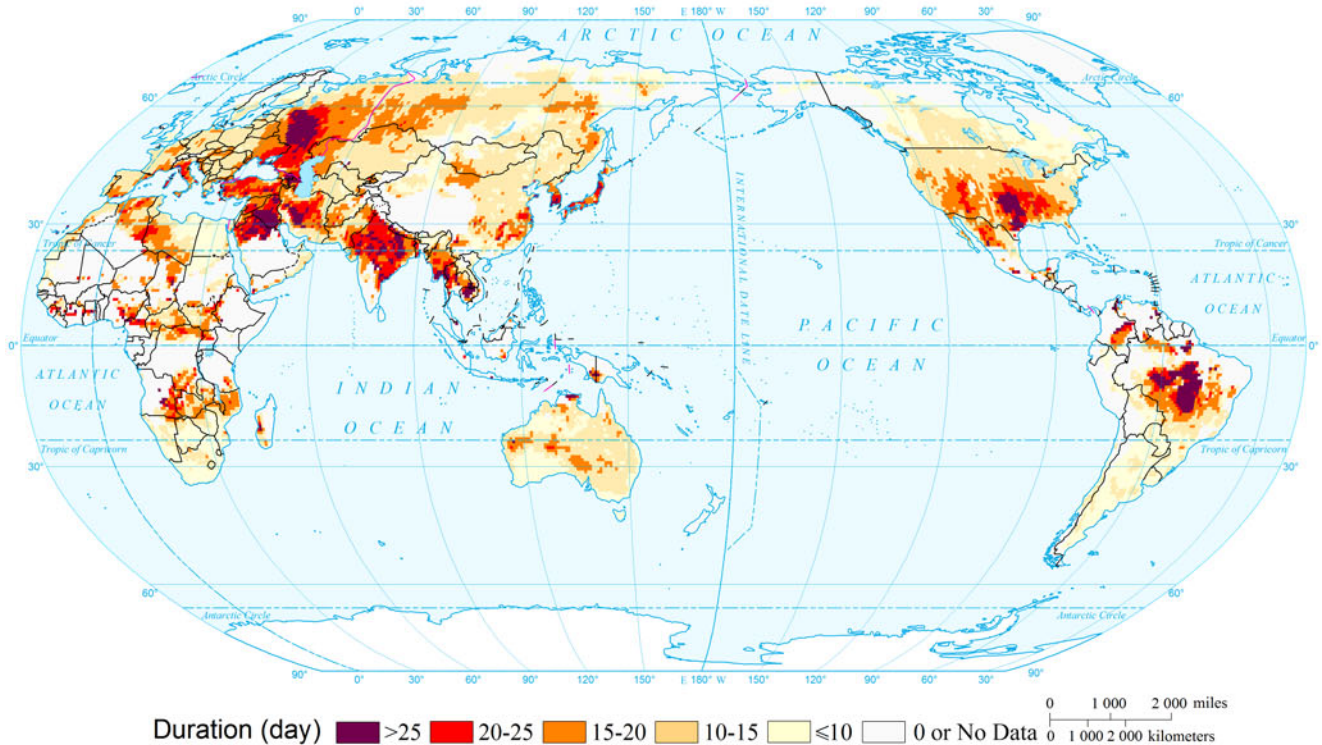
Duration of Global Heat Wave by Return Period (20a)  
(0.75°×0.75°)



Duration of Global Heat Wave by Return Period (50a)  
(0.75°×0.75°)

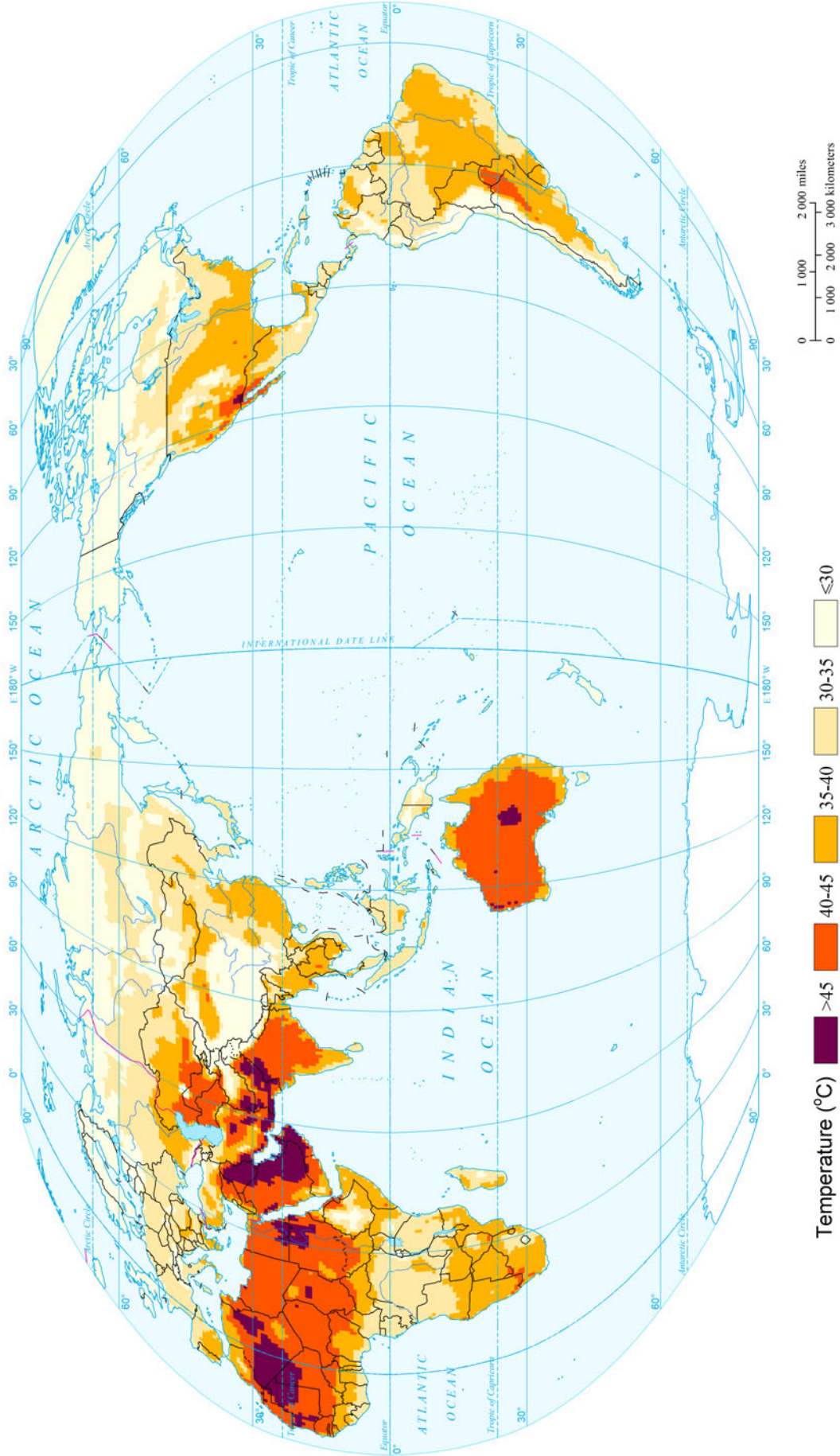


Duration of Global Heat Wave by Return Period (100a)  
(0.75°×0.75°)

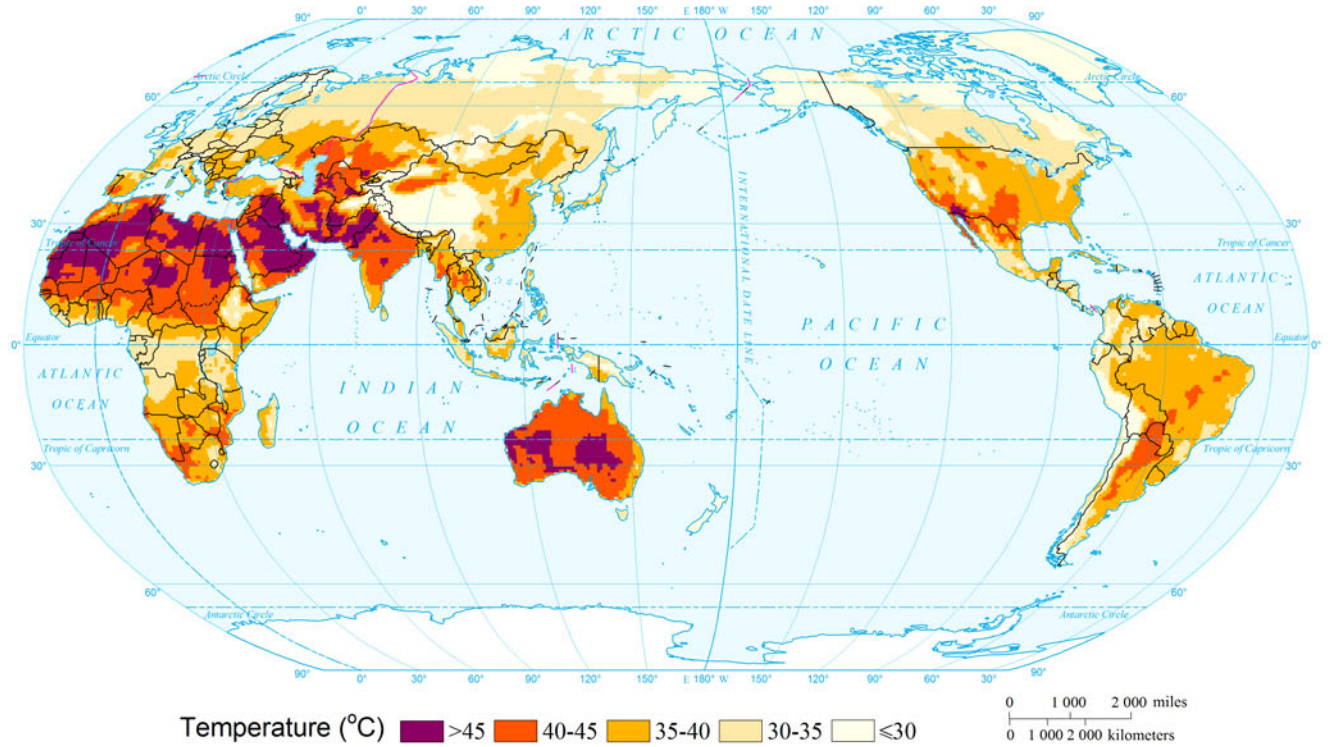




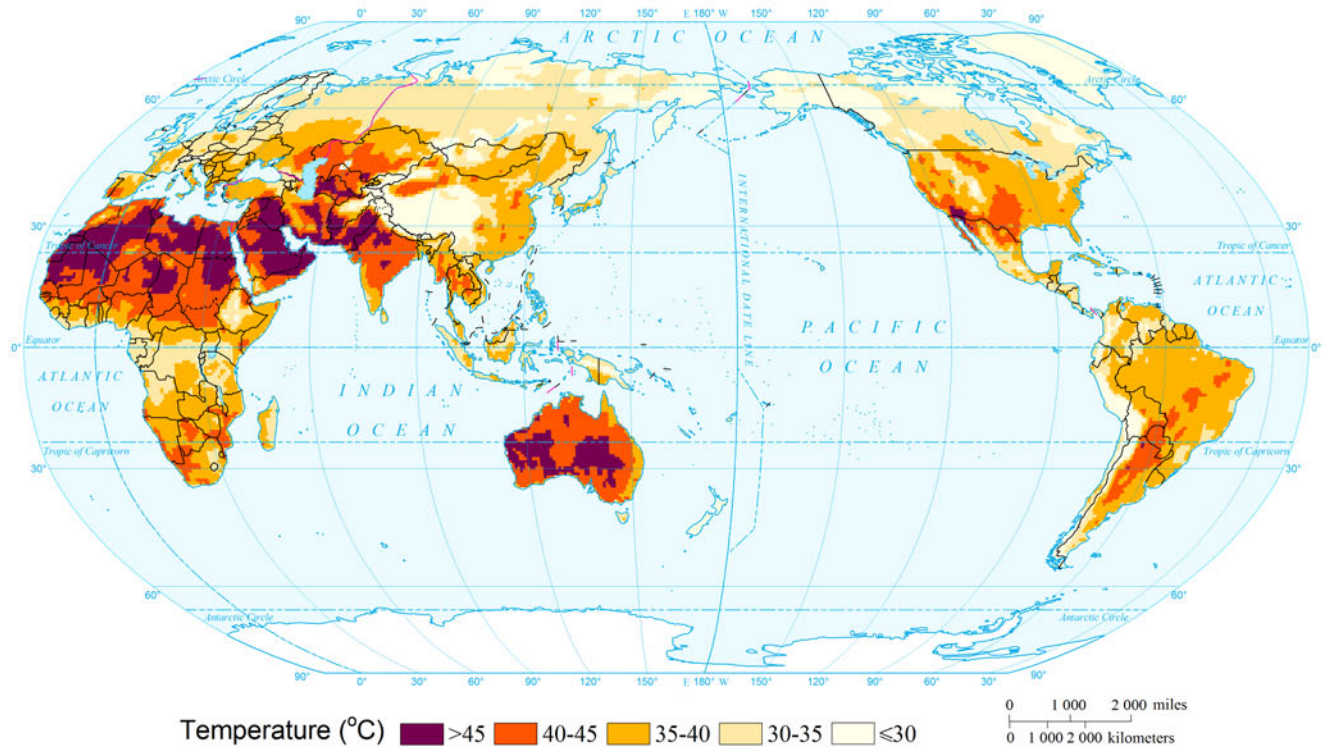
Expected Annual Maximum Temperature of Global Heat Wave  
( $0.75^{\circ} \times 0.75^{\circ}$ )



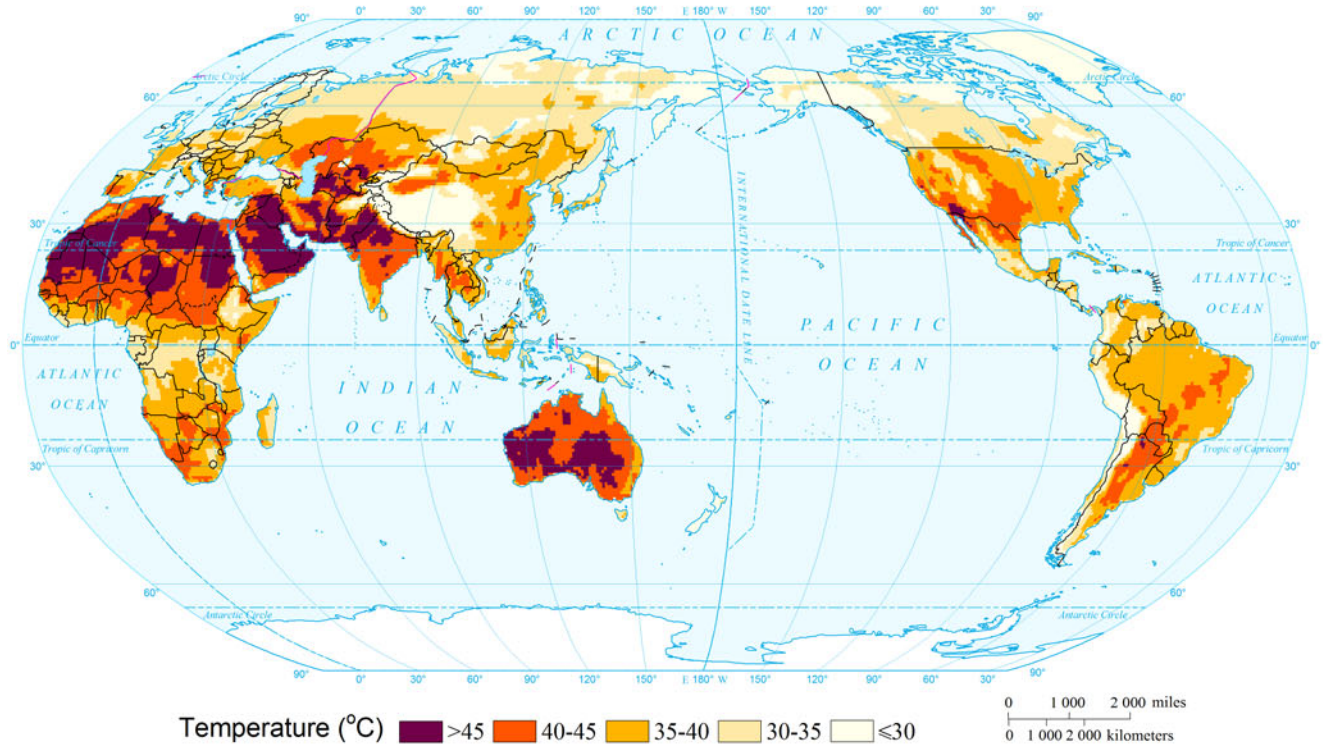
Maximum Temperature of Global Heat Wave by Return Period (10a)  
(0.75°×0.75°)



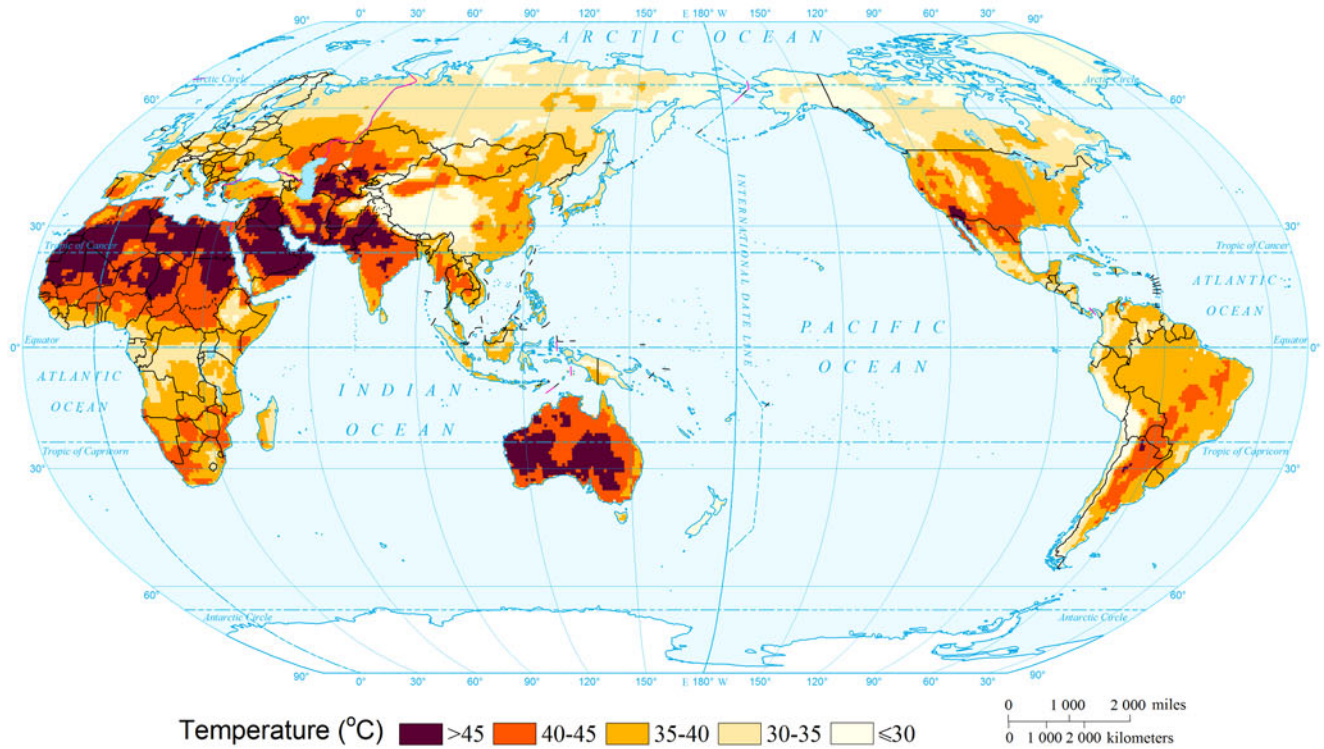
Maximum Temperature of Global Heat Wave by Return Period (20a)  
(0.75°×0.75°)



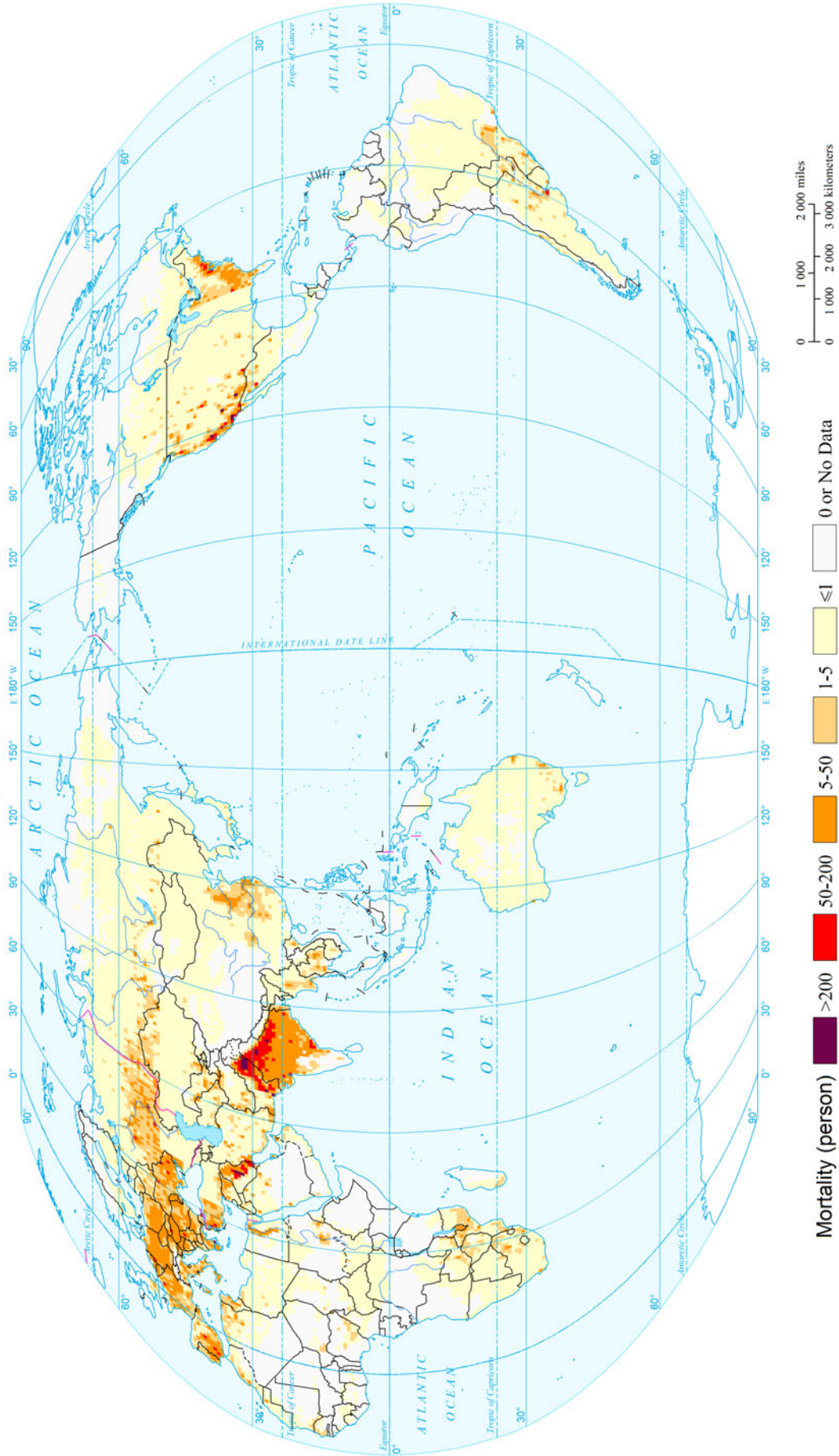
Maximum Temperature of Global Heat Wave by Return Period (50a)  
(0.75°×0.75°)



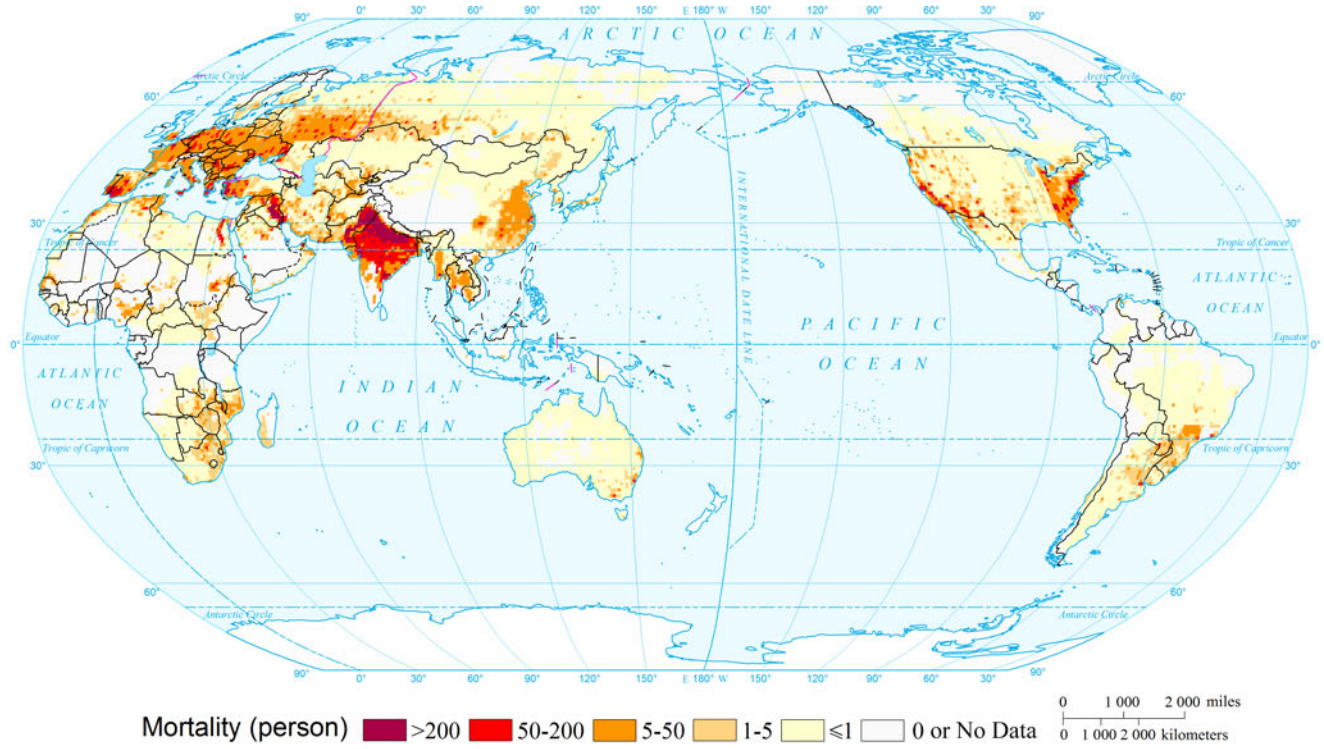
Maximum Temperature of Global Heat Wave by Return Period (100a)  
(0.75°×0.75°)



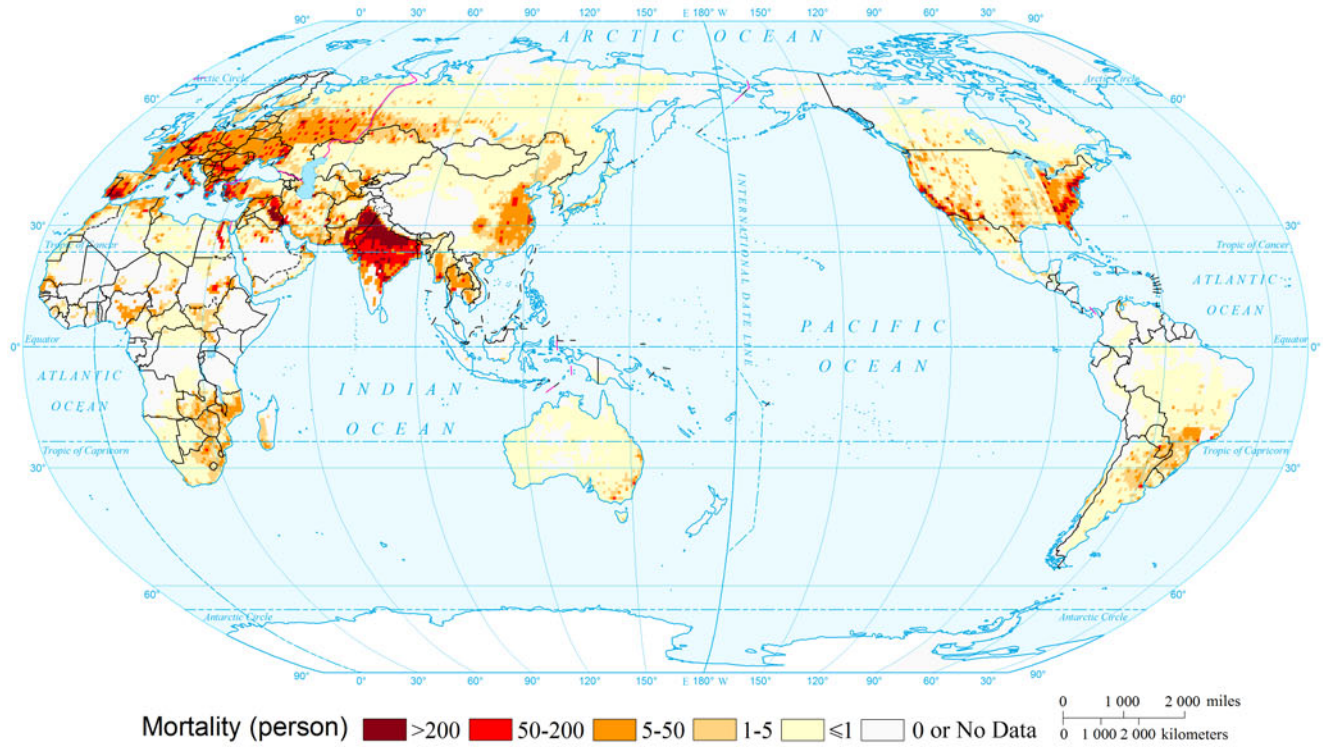
### Expected Annual Mortality Risk of Heat Wave of the World ( $0.75^{\circ} \times 0.75^{\circ}$ )



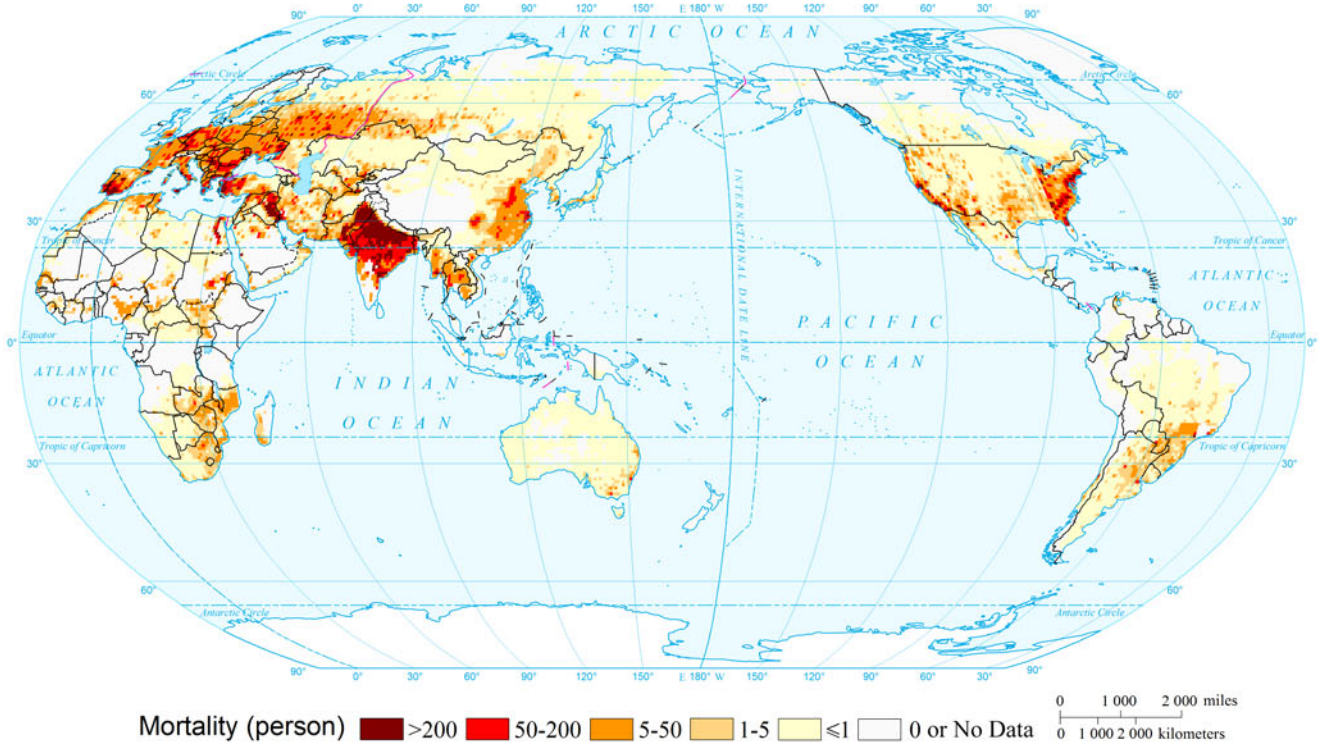
Mortality Risk of Heat Wave of the World by Return Period (10a)  
(0.75°×0.75°)



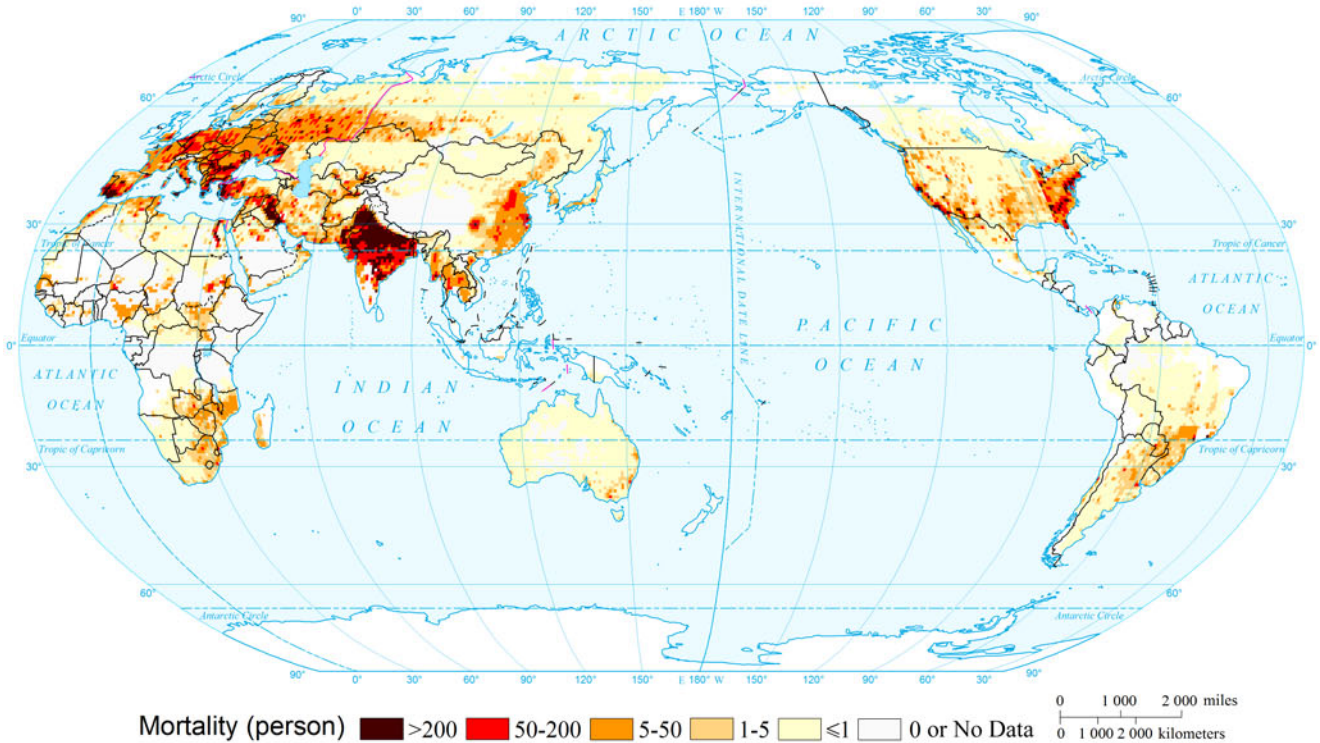
Mortality Risk of Heat Wave of the World by Return Period (20a)  
(0.75°×0.75°)



Mortality Risk of Heat Wave of the World by Return Period (50a)  
(0.75°×0.75°)

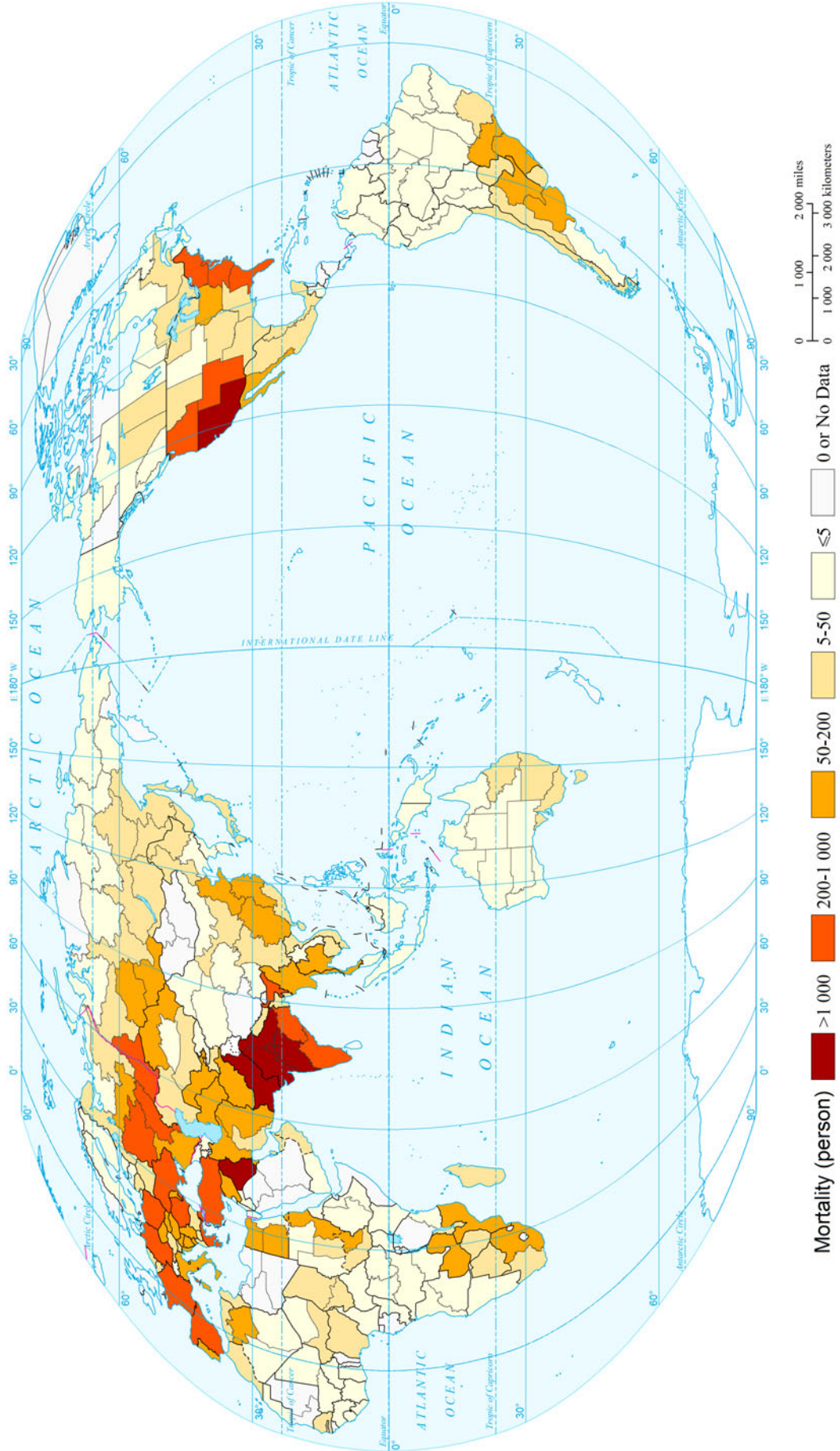


Mortality Risk of Heat Wave of the World by Return Period (100a)  
(0.75°×0.75°)

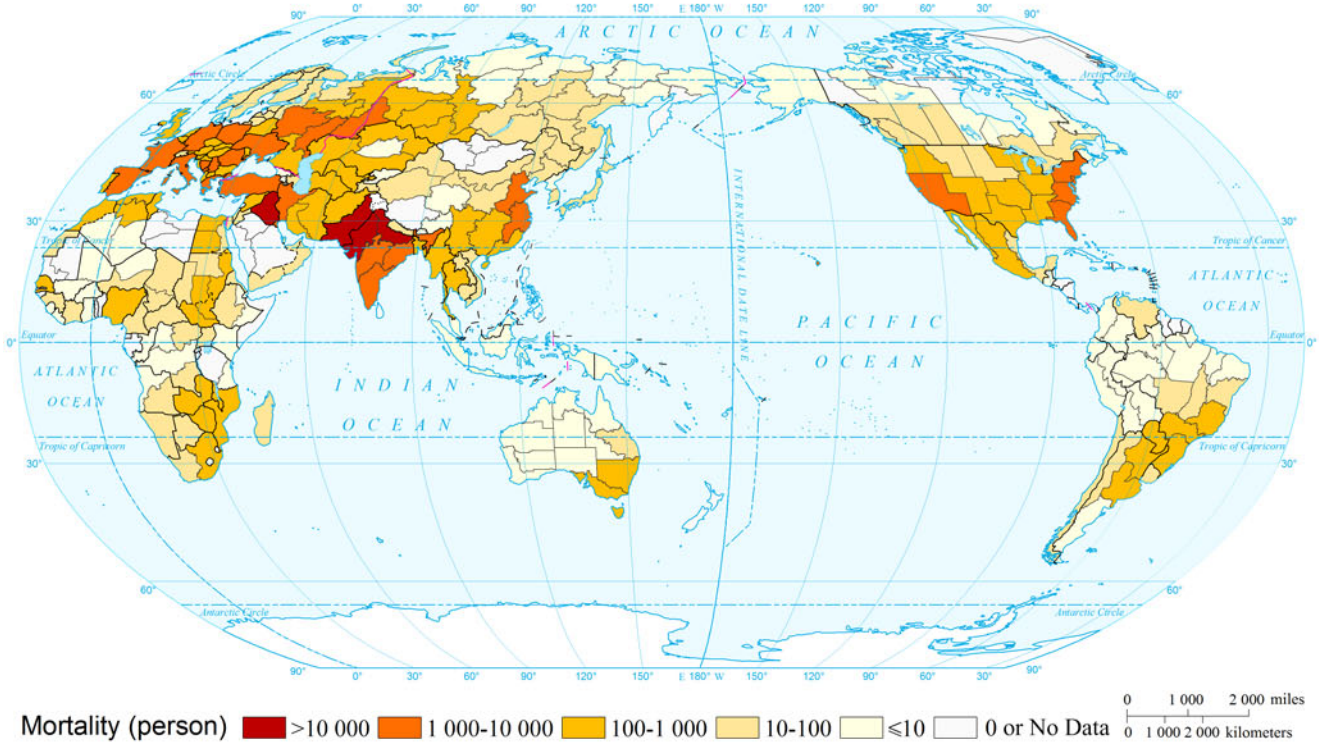




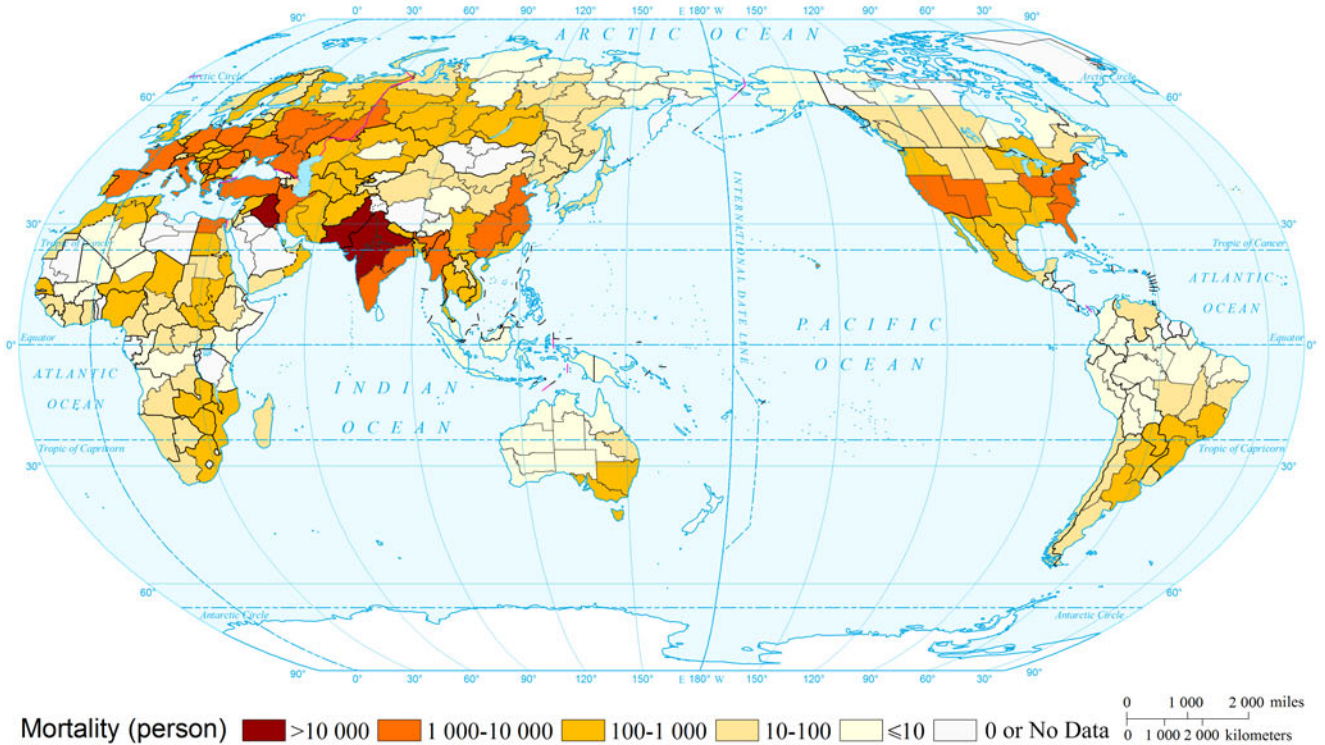
Expected Annual Mortality Risk of Heat Wave of the World  
(Comparable-geographic Unit)



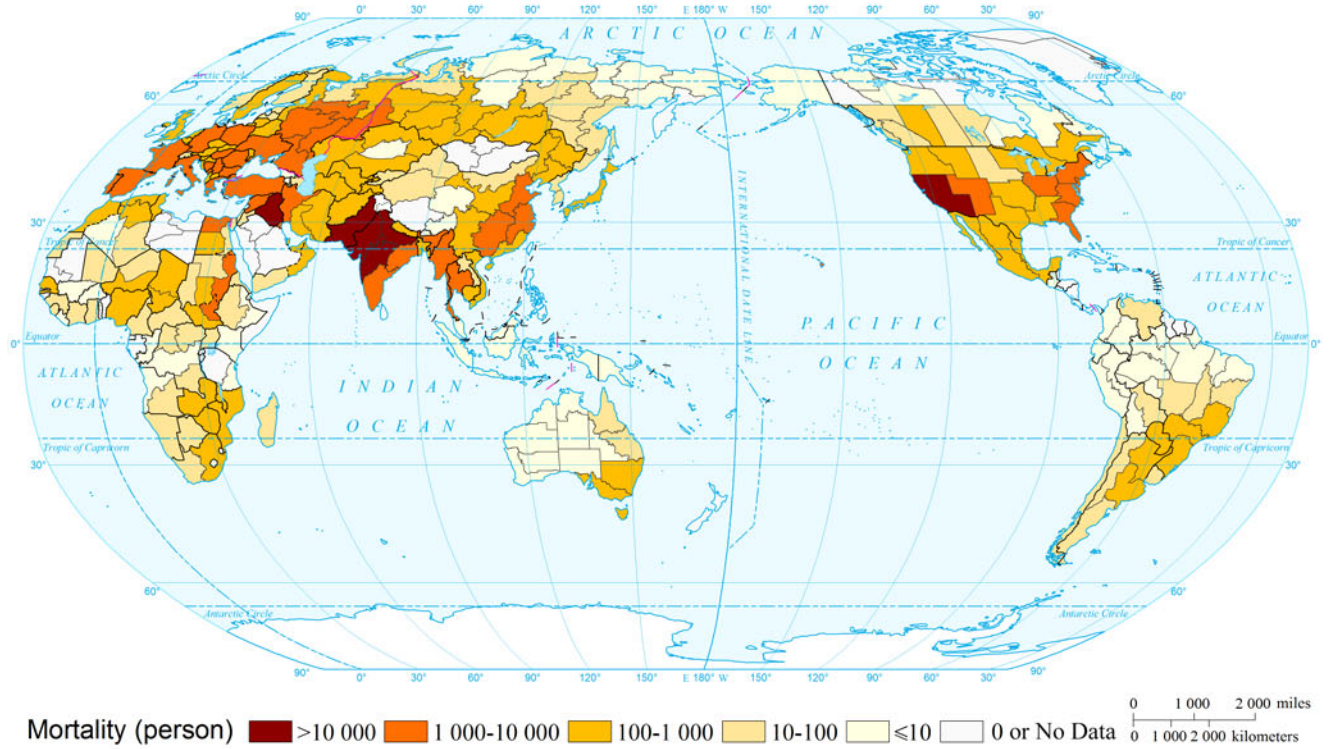
Mortality Risk of Heat Wave of the World by Return Period (10a)  
(Comparable-geographic Unit)



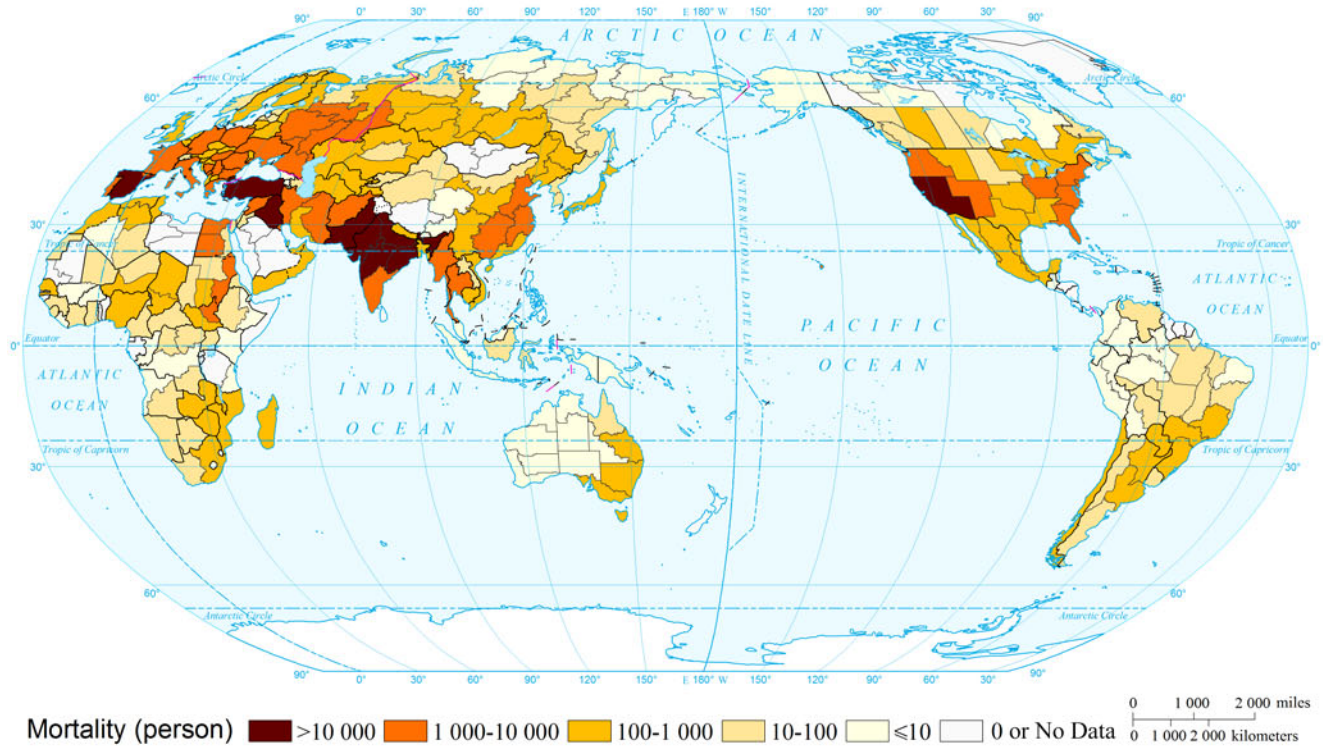
Mortality Risk of Heat Wave of the World by Return Period (20a)  
(Comparable-geographic Unit)



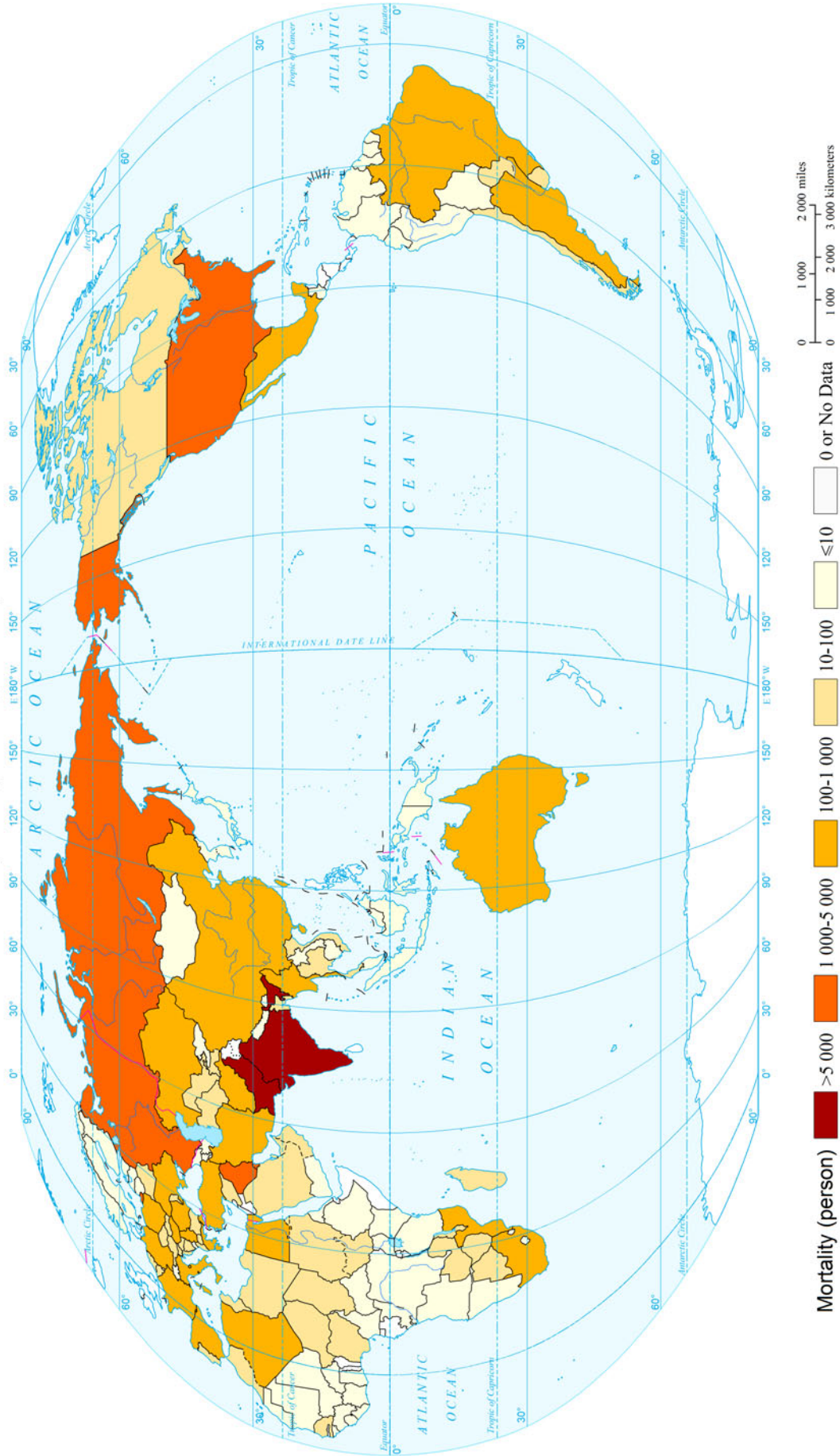
Mortality Risk of Heat Wave of the World by Return Period (50a)  
(Comparable-geographic Unit)



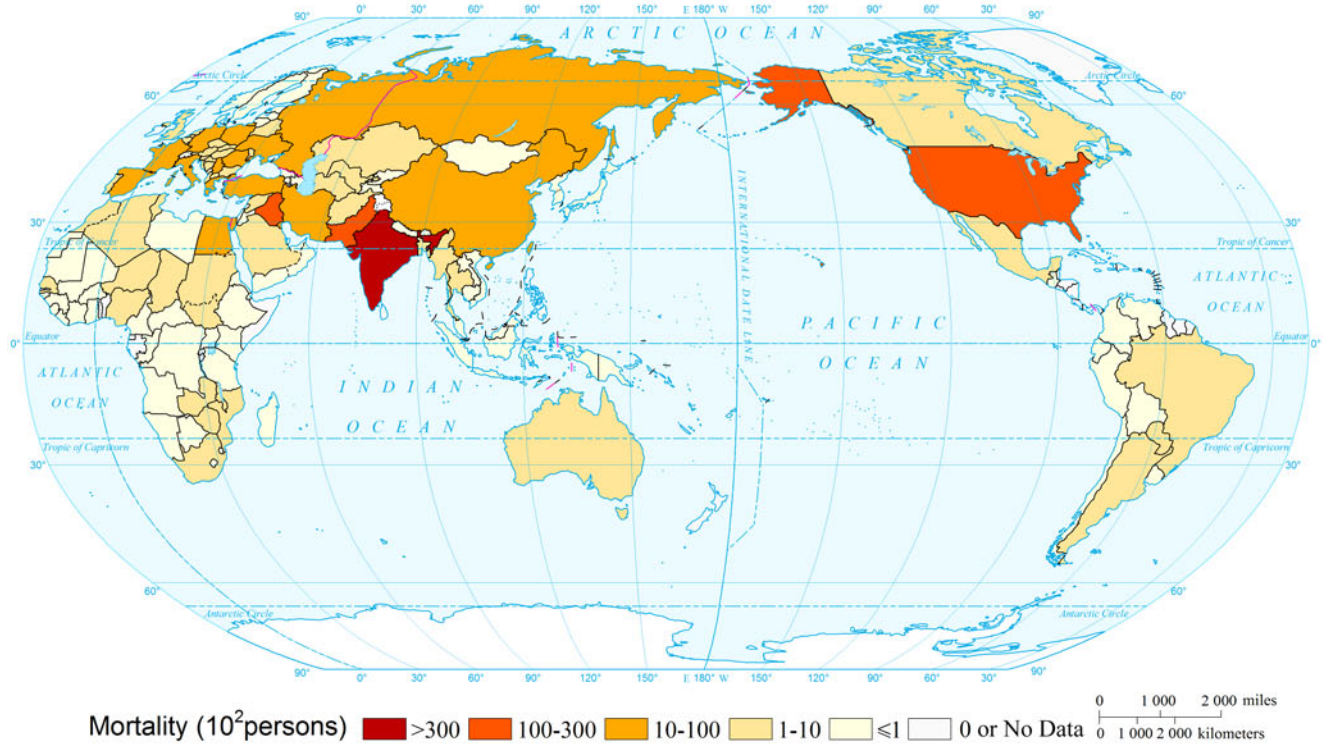
Mortality Risk of Heat Wave of the World by Return Period (100a)  
(Comparable-geographic Unit)



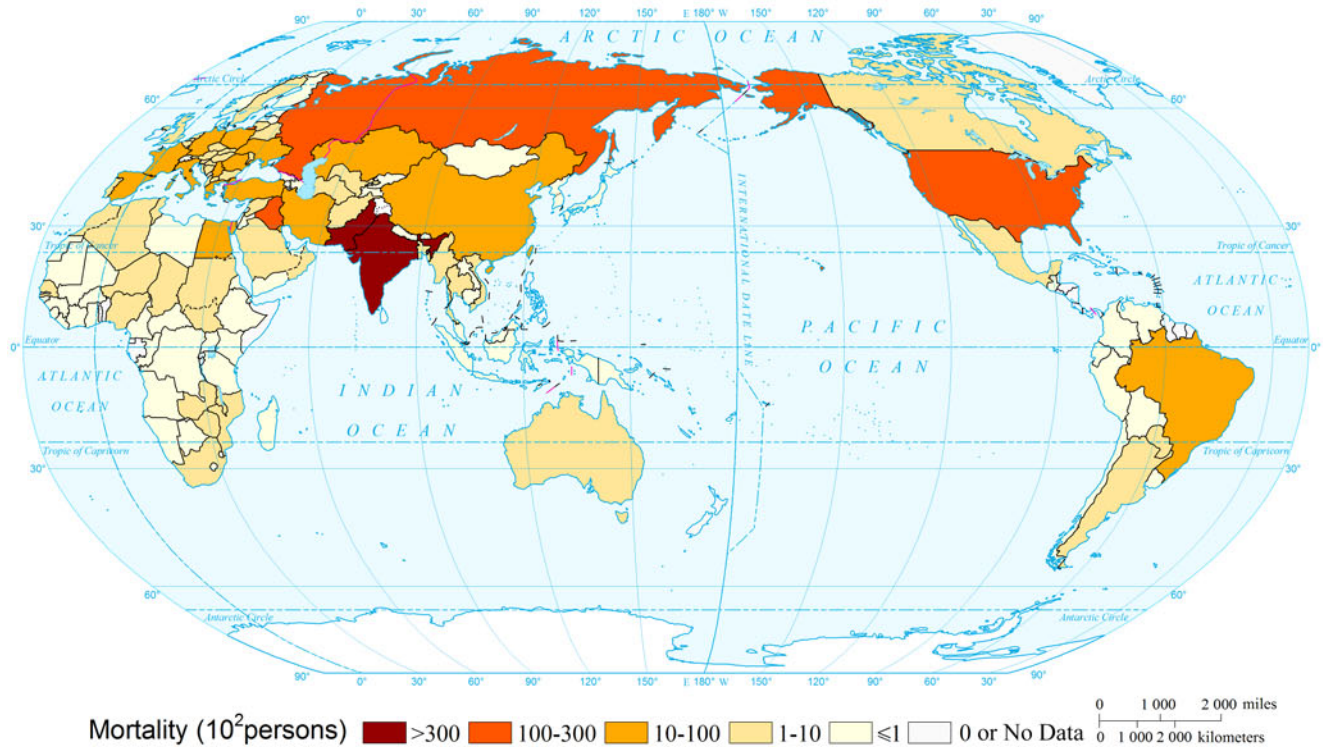
Expected Annual Mortality Risk of Heat Wave of the World  
(Country and Region Unit)



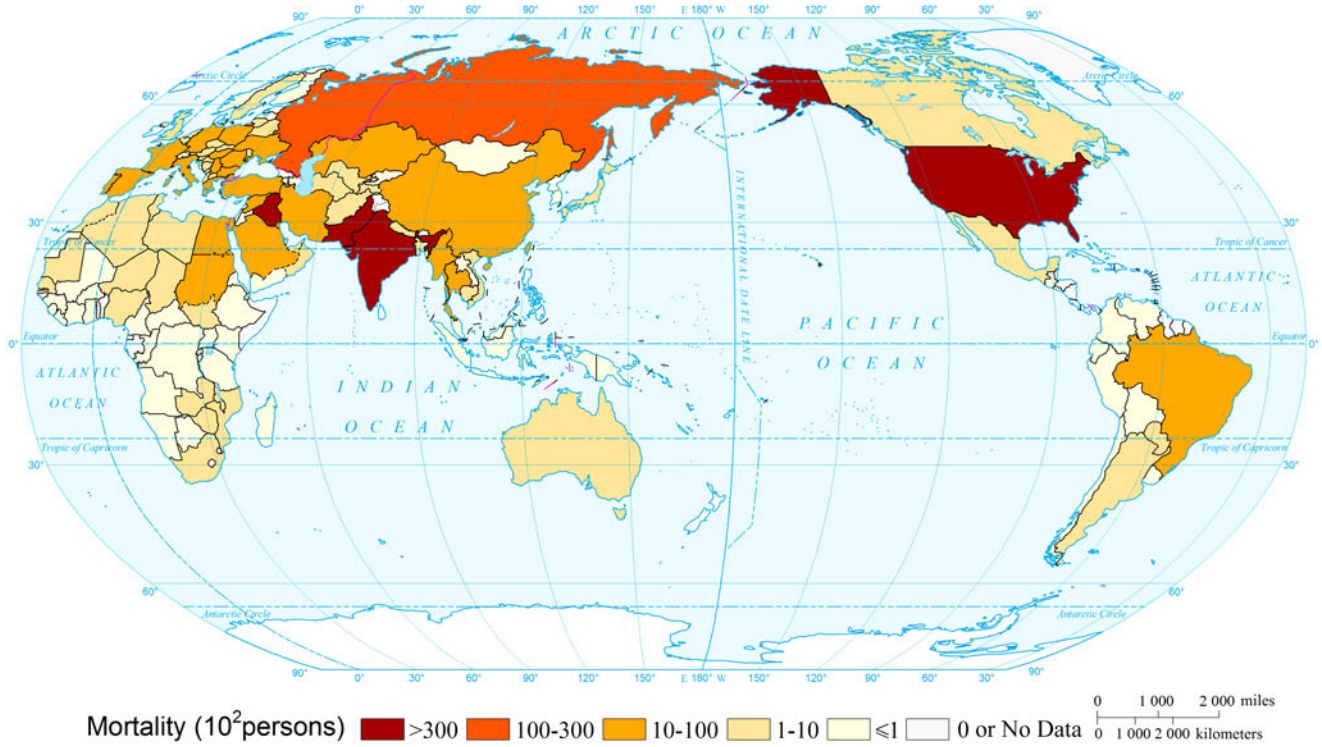
Mortality Risk of Heat Wave of the World by Return Period (10a)  
(Country and Region Unit)



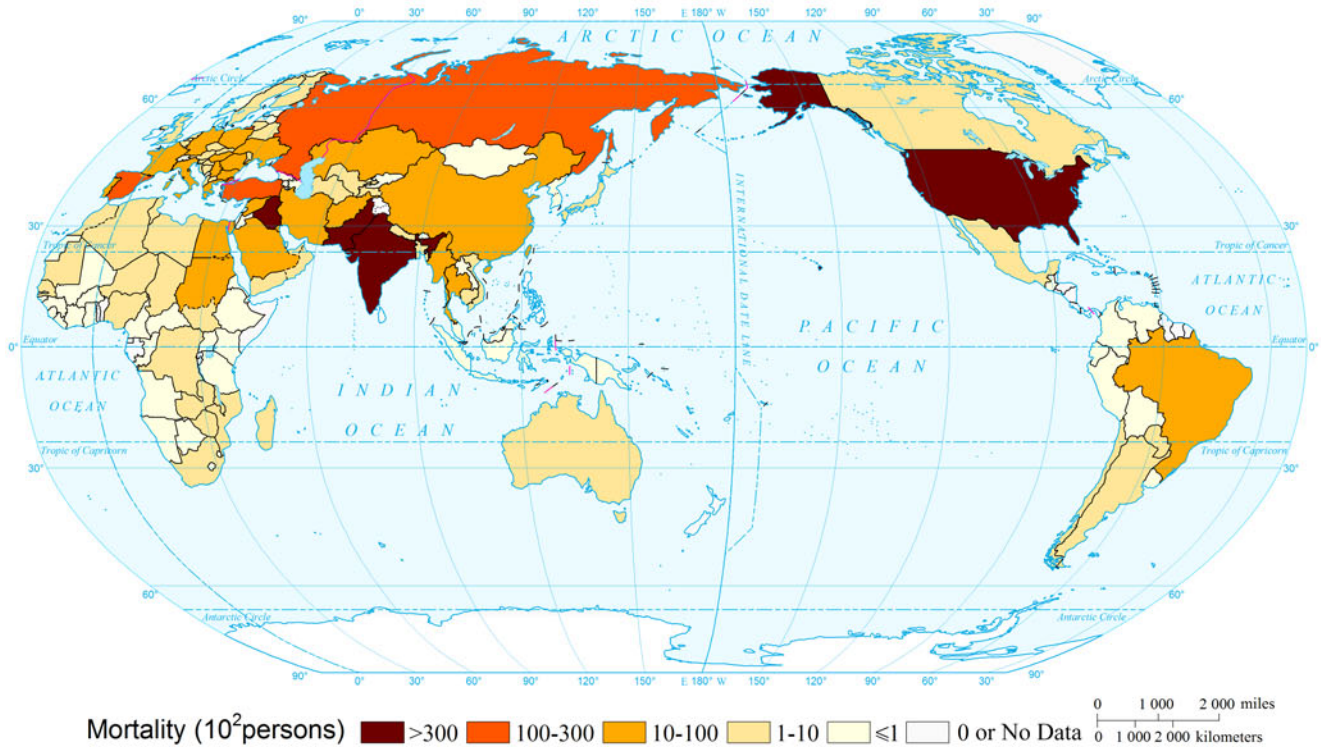
Mortality Risk of Heat Wave of the World by Return Period (20a)  
(Country and Region Unit)



Mortality Risk of Heat Wave of the World by Return Period (50a)  
(Country and Region Unit)



Mortality Risk of Heat Wave of the World by Return Period (100a)  
(Country and Region Unit)



## References

- Gosling, S.N., G.R. McGregor, and A. Páldy. 2007. Climate change and heat-related mortality in six cities—Part 1: Model construction and validation. *International Journal of Biometeorology* 51: 525–540.
- Intergovernmental Panel on Climate Change (IPCC). 2012. *Managing the risks of extreme events and disasters to advance climate change adaptation*. A special report of working groups I and II of the intergovernmental panel on climate change. Cambridge and New York: Cambridge University Press.
- Intergovernmental Panel on Climate Change (IPCC). 2013. *Summary for policymakers*. In: Climate change 2013: The physical science basis. Contribution of working group I to the fifth assessment report of the intergovernmental panel on climate change. Cambridge and New York: Cambridge University Press.
- Meehl, G.A., and C. Tebaldi. 2004. More intense, more frequent, and longer lasting heat waves in the 21st century. *Science* 305: 994–997.
- Robine, J.M., S.L.K. Cheung, S.L. Roy, et al. 2008. Death toll exceeded 70,000 in Europe during the summer of 2003. *Comptes Rendus Biologies* 331(2): 171–178.
- Shi, P.J. 1991. Study on the theory of disaster research and its practice. *Journal of Nanjing University (Natural Sciences)* 11(Supplement): 37–42. (in Chinese).
- Shi, P.J. 1996. Theory and practice of disaster study. *Journal of Natural Disasters* 5(4): 6–17. (in Chinese).
- Shi, P.J. 2002. Theory on disaster science and disaster dynamics. *Journal of Natural Disasters* 11(3): 1–9. (in Chinese).
- Swiss Re. 2011. Natural catastrophes and man-made disasters in 2010: A year of devastating and costly event. *Sigma* 1: 1–36.
- Tang, Q.H., X.J. Zhang and J.A. Francis. 2014. Extreme summer weather in northern mid-latitudes linked to a vanishing cryosphere. *Nature Climate Change* 4: 45–50. doi:[10.1038/nclimate2065](https://doi.org/10.1038/nclimate2065).

---

# Mapping Cold Wave Risk of the World

Lili Lu, Zhu Wang, and Peijun Shi

---

## 1 Background

At present, the studies on cold wave disaster focus on two aspects: the spatial–temporal distribution characteristics of cold wave and the cold wave demographic disaster risk. In the study of spatial–temporal distribution, the fourth IPCC report indicated that the occurrence of cold day, cold night, and frost is most certainly decreasing within most parts of continents. The cold wave events and the resulting mortalities both show downward trends (IPCC 2007, 2012). However, the opposite view exists that the occurrence of the cold waves has an obvious rising trend (0.064 per year,  $p < 0.01$ ) and so does the casualties (25.59 per year,  $p < 0.01$ ) through analyzing the global historical data, and they believe the instability of climate systems under the global warming background makes the cold wave disaster more severe and more damaging (Song et al. 2013).

In the aspect of cold wave population, during the period of late 1980s to early 1990s, few studies concerned about the health risk caused by extreme temperature (WHO 2003). With growing understanding of the global climate warming

and more frequently awareness of extreme temperature disasters in recent years, people began to pay more attention to the adverse effects on human health and safety caused by extreme temperature disasters (Rocklöv et al. 2011).

The European Union (EU) launched the INTERREG III INTERACT project, which gave the extreme temperature hazard risk distribution maps and indicated regions with fortification capacity within EU, based on the factors as temperature and duration of heat wave and cold wave. However, the cold wave risk was not evaluated in this project (ESPON 2006). As so far, among all the large-scale disaster risk database and disaster risk atlas, such as the PreventionWeb, the Disaster Risk Index (DRI) report by UNDP, and the hotspots atlas and Web site developed by Columbia University, there have not been any published quantitative or qualitative cold wave risk map at the global scale (UNDP 2004; Center For Hazards & Risk Research 2014; PreventionWeb 2014).

In summary, current researches on cold waves are limited in the spatial–temporal distribution characteristics of cold wave, the relationship between mortality and extreme cold at the regional scale, and the mapping of the regional extreme temperature hazard risk distribution, yet lack in-depth study of the spatial distribution of the population caused by cold waves. Based on classical disaster system theory (Shi 1991, 1996, 2002), mapping affected population risk of cold wave is initially performed at global scale.

---

**Mapping Editors:** Jing'ai Wang (Key Laboratory of Regional Geography, Beijing Normal University, Beijing 100875, China) and Chunqin Zhang (School of Geography, Beijing Normal University, Beijing 100875, China).

**Language Editor:** Ming Wang (State Key Laboratory of Earth Surface Processes and Resource Ecology, Beijing Normal University, Beijing 100875, China).

---

L. Lu · Z. Wang

Academy of Disaster Reduction and Emergency Management, Ministry of Civil Affairs and Ministry of Education, Beijing Normal University, Beijing 100875, China

P. Shi (✉)

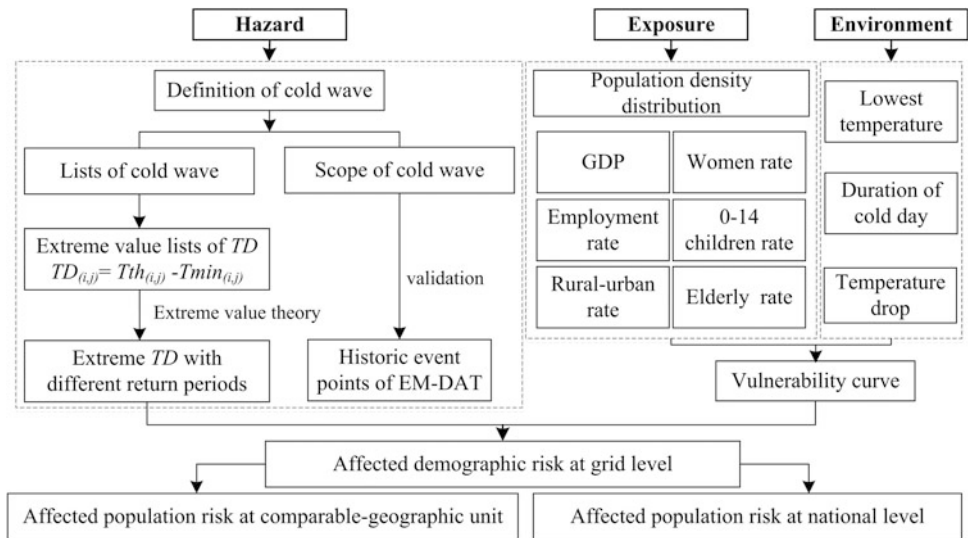
State Key Laboratory of Earth Surface Processes and Resource Ecology, Beijing Normal University, Beijing 100875, China  
e-mail: spj@bnu.edu.cn

---

## 2 Method

Figure 1 shows the technical flowchart for mapping affected population risk of cold wave of the world.

**Fig. 1** Technical flowchart for mapping affected population risk of cold wave of the world



## 2.1 Intensity

In this study, excluding summer temperatures, analyzing spring, fall, and winter temperatures in the 1979–2013 record (Appendix III, Hazards data 4.14), for each grid, the 10th percentile temperature ( $T_{th}$ ) was defined as the threshold temperature to determine whether a cold wave occurs in each grid. If the grid temperature  $T$  is below  $T_{th}$  for 3 or more consecutive days, it is considered that a cold wave occurs. It is assumed that cold wave does not occur in the areas with  $T_{th} > 15^\circ\text{C}$ . A hazard database with the information on lowest temperature, temperature drop (TD), and duration of each cold wave process was established for each grid. The concepts of concentration degree and concentration period used in precipitation study (Wang et al. 2013) were adopted to further investigate the global distribution pattern of cold wave. In this way, the two distributing characteristic parameters, cold wave occurrence concentration degree (CCD) and cold wave occurrence concentration period (CCP), were introduced to characterize the likelihood of cold wave occurrence in a month in each grid, shown from Eqs. (1) and (2):

$$\text{CCD}_i = r_i / R \quad (1)$$

$$\text{CCP}_i = i \quad (2)$$

where  $R$  is the total number of cold wave occurrences in one grid from 1979 to 2013;  $r_i$  is the total occurrence of the  $i$ th month in the past 35 years; and  $i$  is the number of each month, starting with January as 1 and ending with December as 12 ( $i = 1, 2, \dots, 12$ ).

Due to the significant differences in thermal conditions of different climate zones, extremely low temperature varies largely in different regions. Minimum extreme temperature is relatively high in a low-latitude region. With the increasing of latitude, the related extreme minimum temperature decreases gradually. The extreme minimum temperature can reach  $-70^\circ\text{C}$  in continental high latitudes and polar regions. Therefore, in this study, instead of minimum temperature, temperature drop (TD) was used in the intensity assessment, shown in Eq. (3).

$$\text{TD}(i, j) = T_{th}(i, j) - T_{\min}(i, j) \quad (3)$$

where TD is a positive number representing the largest temperature drop of the  $j$ th cold wave which happens in the  $i$ th year;  $T_{\min}(i, j)$  is the lowest minimum temperature of the  $j$ th cold wave which happens in the  $i$ th year;  $T_{th}(i, j)$  is the TD of the  $j$ th cold wave which happens in the  $i$ th year.

The intensity assessment of cold wave adopted the extreme value distribution theory to calculate the return period. This study selected the maximum annual TD of the world recorded from 1979 to 2013 as the extreme value samples, fitted the extreme value samples using Weibull distribution, and calculated the corresponding return period under certain extreme TD using Eqs. (4) and (5):

$$f(x) = \frac{\beta}{\alpha} \left(\frac{x}{\alpha}\right)^{\beta-1} \exp\left[-\left(\frac{x}{\alpha}\right)^\beta\right] \quad (4)$$

$$rp = \frac{1}{1 - F(x < x_m)} = \frac{1}{\int_{x_m}^{\infty} f(x) dx} \quad (5)$$

where  $f(x)$  is the probability density function,  $F(x)$  is the cumulative probability function,  $rp$  is the return period with certain extreme value  $x_m$ . The distribution parameters were estimated by using the method of maximum-likelihood and the corresponding temperature drop with return periods of 10, 20, 50, and 100 years and the expected temperature drop were calculated using the inverse function of Eq. (5).

## 2.2 Exposure

The United Nations Development Programme (UNDP) established multivariate linear vulnerability curves by considering various social vulnerability factors such as GDP, social development index, and urbanization rate and so on. Based on these curves, the disaster risk index (DRI) of various disasters at the global scale were evaluated (UNDP 2004). Based on the 1979–2012 EM-DAT cold wave disaster event database (Appendix III, Disasters data 5.4), 10 indices, including GDP, urban–rural demographic ratio, the employment rates, demographic rates of children under 14, elderly, and women (World Bank 2014), Population density (Pop), TD, duration and minimum temperature of cold wave, were selected for the multivariate linear regression analysis, to obtain demographic vulnerability curve affected by cold wave at global scale, as shown in Eq. (8).

$$\ln(y) = -11.401 + 22.977\overline{\ln(\text{Pop})} + 0.174\text{TD} \quad (8)$$

**Table 1** Multiple logarithmic regression model for cold wave

Parameters	B	<i>p</i> -value
Intercept	-11.401	0.000
$\overline{\ln(\text{Pop})}$	22.977	0.000
TD	0.174	0.002

$R = 0.799$ ,  $R^2 = 0.638$ , adjusted  $R^2 = 0.620$

where  $y$  is the affected population;  $\overline{\ln(\text{Pop})}$  is the normalized value of  $\ln(\text{Pop})$  by min–max normalization method; TD is the temperature drop. As shown in Table 1, all indicators in the formula passed the significant test and the  $R^2$  value of the whole model reached 0.638.

## 3 Results

### 3.1 Intensity

The highest temperature drop intensity mainly concentrated in two areas. One is Western Siberia near Kara Sea and Central Siberia, and the other is Alaska region near Bering Sea, Yukon territory, British Columbia, Alberta area, Montana region in United States, etc. The annual temperature drop in these two areas could be more than 9 °C which significantly severer than other regions of the world (include Antarctica).

### 3.2 Affected Population Risk

Globally, the regions with highlevel expected annual affected population risk at the grid scale are mainly concentrated in theses areas: North China plain, South-East China plain, North-East mountain of Indian, Bangladesh, North-west plain of Indian, Pakistan, Central and Southern mountain of China, Central Plateau of Indian, Western mountain of United States, and Germany.

By zonal statistics of the expected risk result, the expected annual affected population risk by cold wave of the world at national level is derived and ranked (Fig. 2). The top 1 % countries with the highest expected annual affected population risk by cold wave are China and India, and the top 10 % countries are China, India, United States, Russia, Pakistan, Bangladesh, Brazil, Mexico, Germany, Egypt, Japan, South Korea, Iran, United Kingdom, Turkey, and Ukraine.

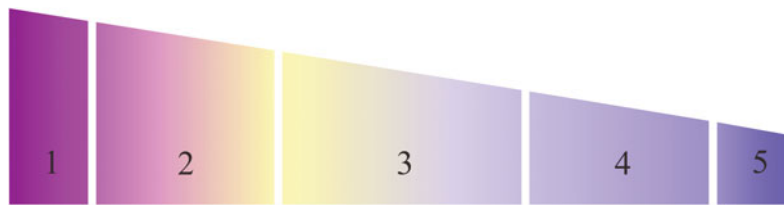
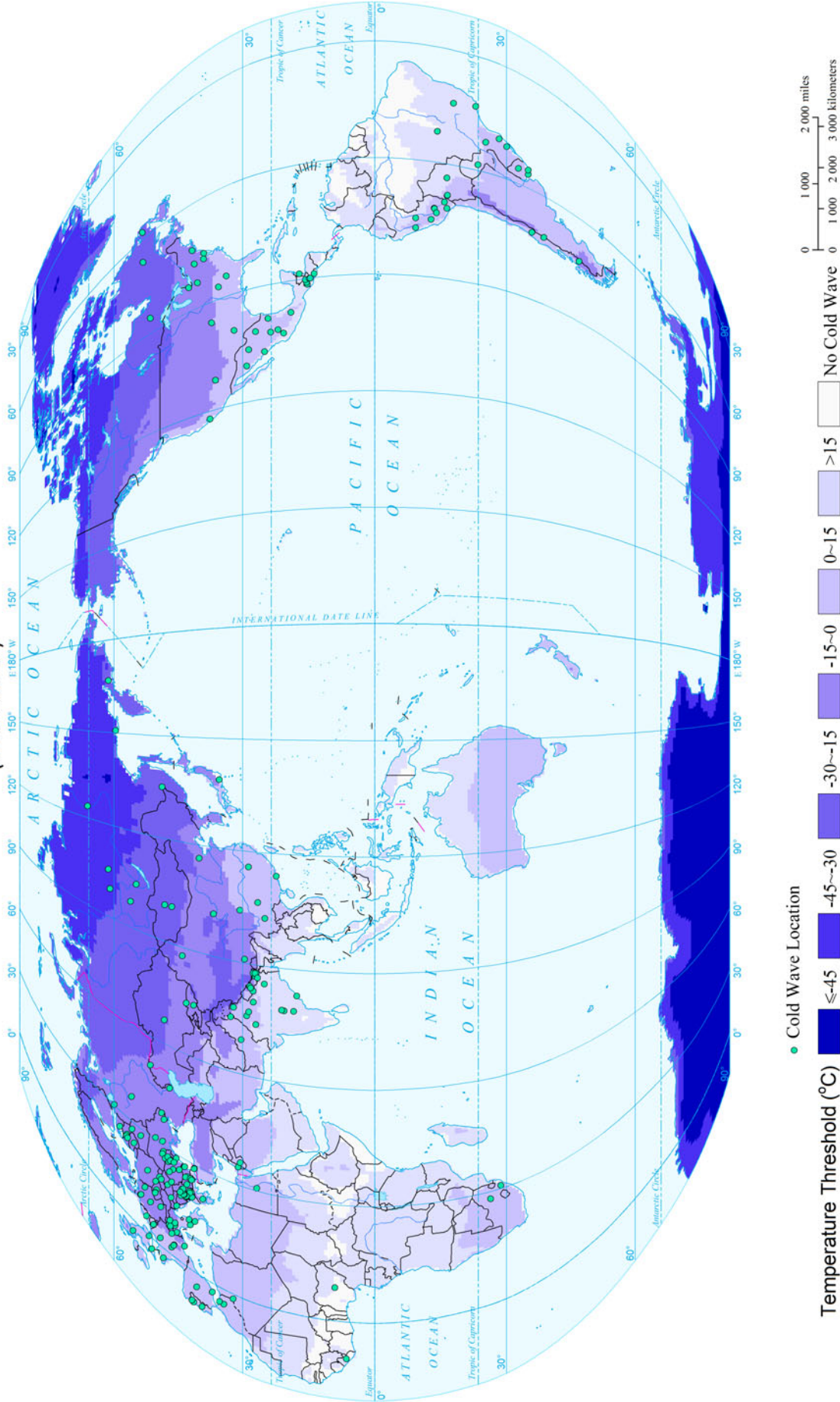


**Fig. 2** Expected annual affected population risk of cold wave of the world. 1 (0, 10 %] China, India, United States, Russia, Pakistan, Bangladesh, Brazil, Mexico, Germany, Egypt, Japan, South Korea, Iran, United Kingdom, Turkey, Ukraine. 2 (10, 35 %] France, Ethiopia, Canada, Nigeria, Vietnam, Poland, Argentina, Italy, Nepal, South Africa, Burma, Spain, Afghanistan, Iraq, Kenya, Uzbekistan, Democratic Republic of the Congo, Thailand, Indonesia, Colombia, Romania, Kazakhstan, Saudi Arabia, Algeria, North Korea, Syria, Uganda, Sudan, Morocco, Tanzania, the Netherlands, Chile, Czech Republic, Belgium, Belarus, Yemen, Hungary, Australia, Congo. 3 (35, 65 %] Venezuela, Guatemala, Cameroon, Serbia, Mozambique, Philippines, Rwanda, Niger, Madagascar, Malawi, Austria, Peru, Israel, Ecuador, Sweden, Jordan, Tajikistan, Dominican Republic, Cuba, Burundi, Tunisia, Zimbabwe, Paraguay, Bolivia, Switzerland, Kyrgyzstan,

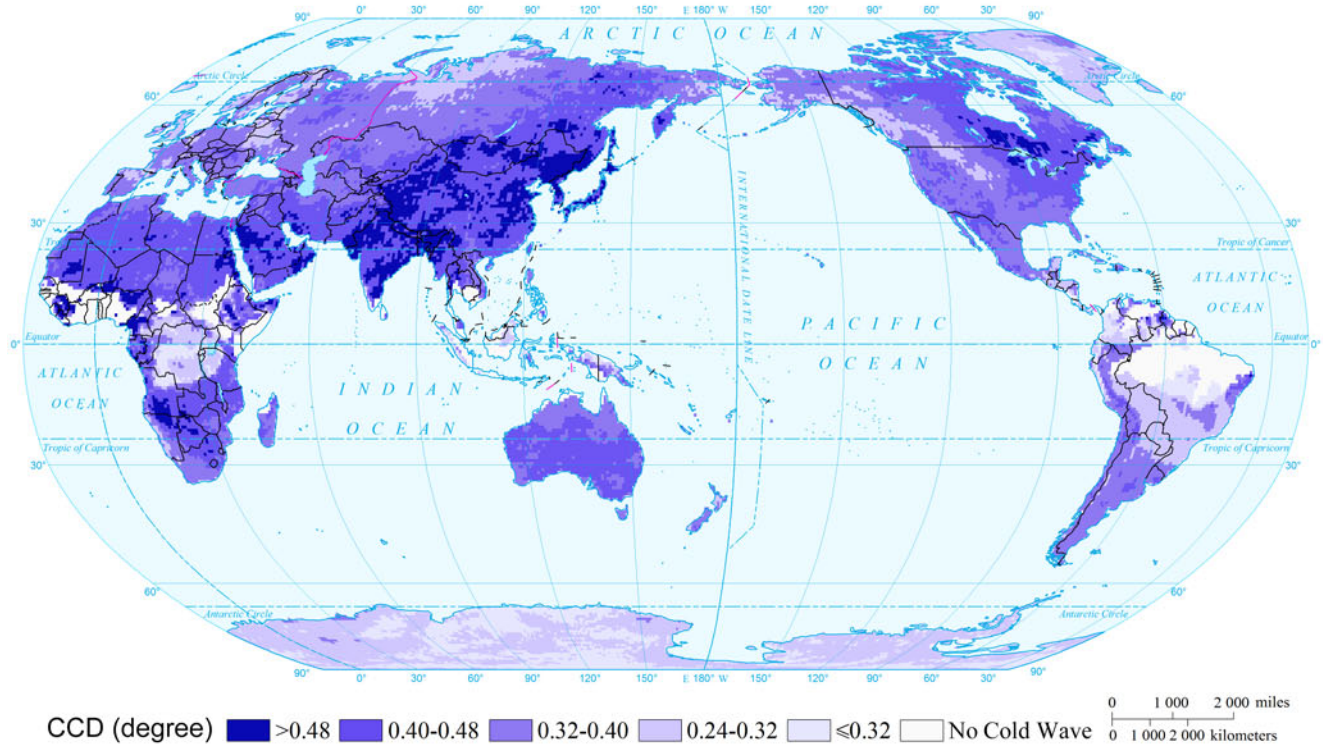
Zambia, Slovakia, Finland, Moldova, Bulgaria, El Salvador, Portugal, Haiti, Honduras, Bosnia and Herzegovina, Croatia, Denmark, Lithuania, Turkmenistan, Azerbaijan, Georgia, Greece, Norway, Chad, Angola. 4 (65, 90 %] Eritrea, Laos, Armenia, Senegal, Ireland, Costa Rica, Libya, Latvia, Albania, Guinea, Burkina Faso, Mali, Mongolia, Nicaragua, Central African Republic, Lebanon, Oman, New Zealand, Slovenia, Papua New Guinea, Kuwait, Lesotho, The Republic of Côte d'Ivoire, South Sudan, Macedonia, Malaysia, Sierra Leone, Somalia, Namibia, Uruguay, Botswana, Sri Lanka, Liberia, Cyprus, Swaziland, Qatar, Mauritania, Cambodia, Estonia. 5 (90, 100 %] Montenegro, Panama, Bhutan, Gabon, Western Sahara, Equatorial Guinea, Fiji, United Arab Emirates, Belize, Iceland, Bahamas, Palestine, Djibouti, Guyana, Cape Verde, Suriname

#### 4 Maps

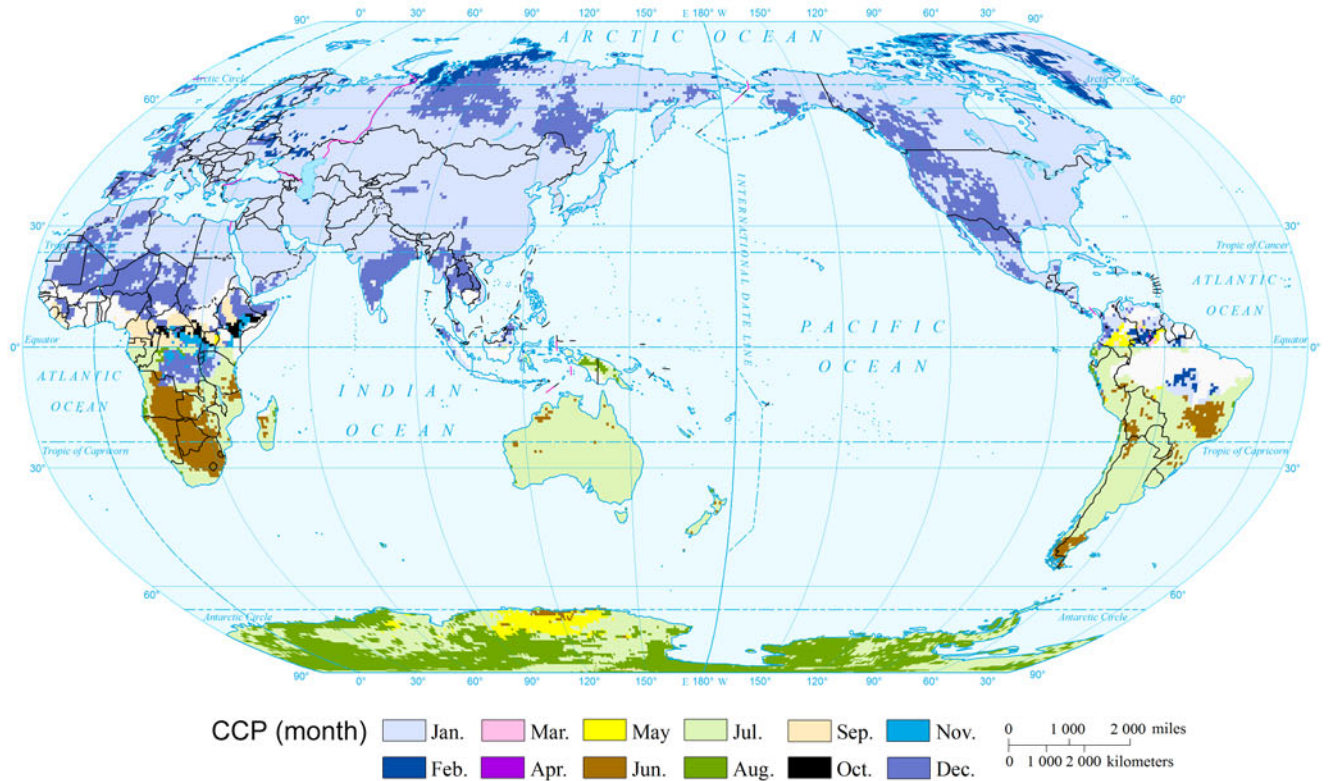
### Temperature Threshold and Historical Event Locations of Global Cold Wave (1950-2013) ( $0.75^\circ \times 0.75^\circ$ )



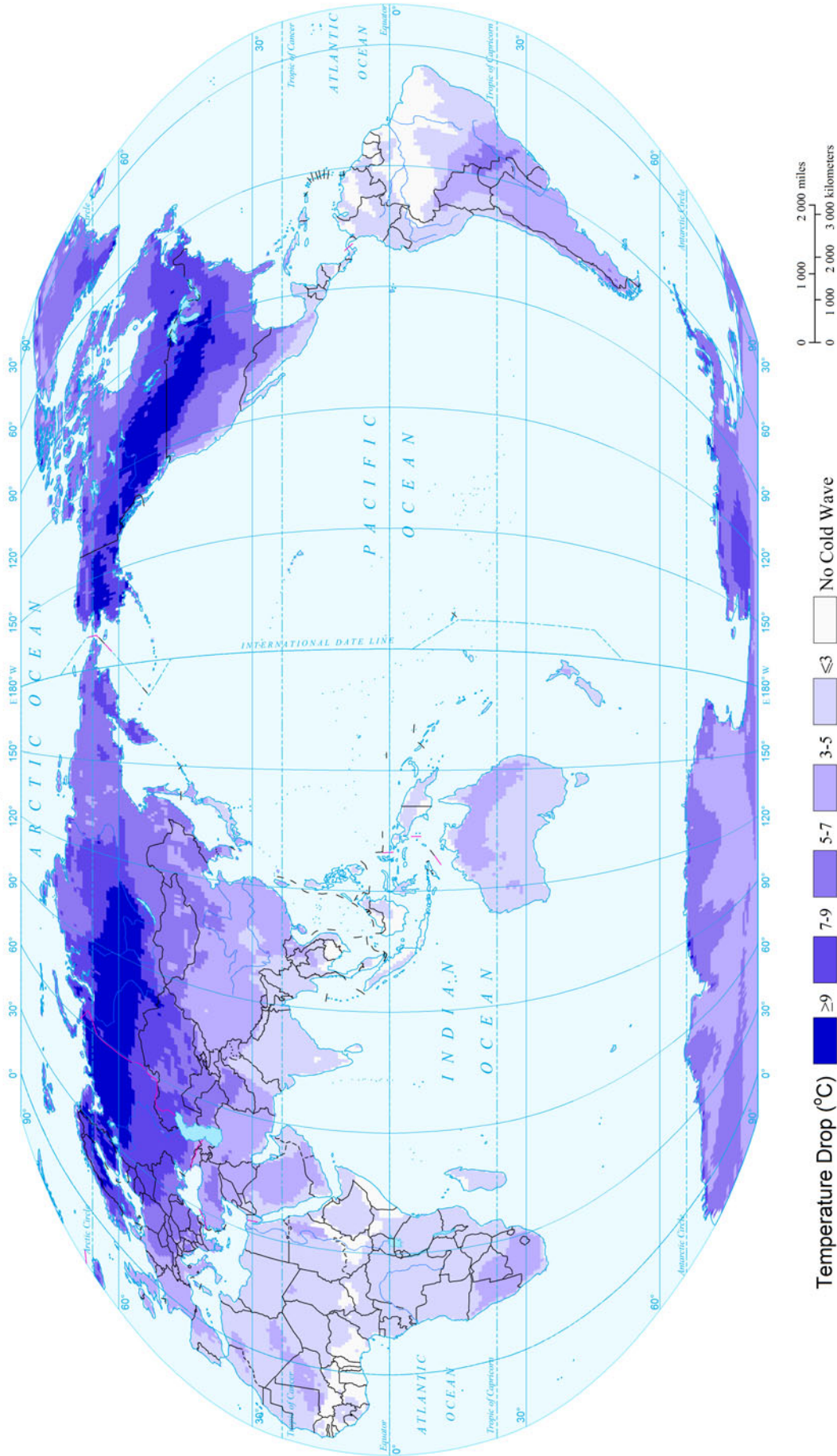
Occurrence Concentration Degree (CCD) of Global Cold Wave  
(0.75°×0.75°)



Occurrence Concentrated Period (CCP) of Global Cold Wave  
(0.75°×0.75°)

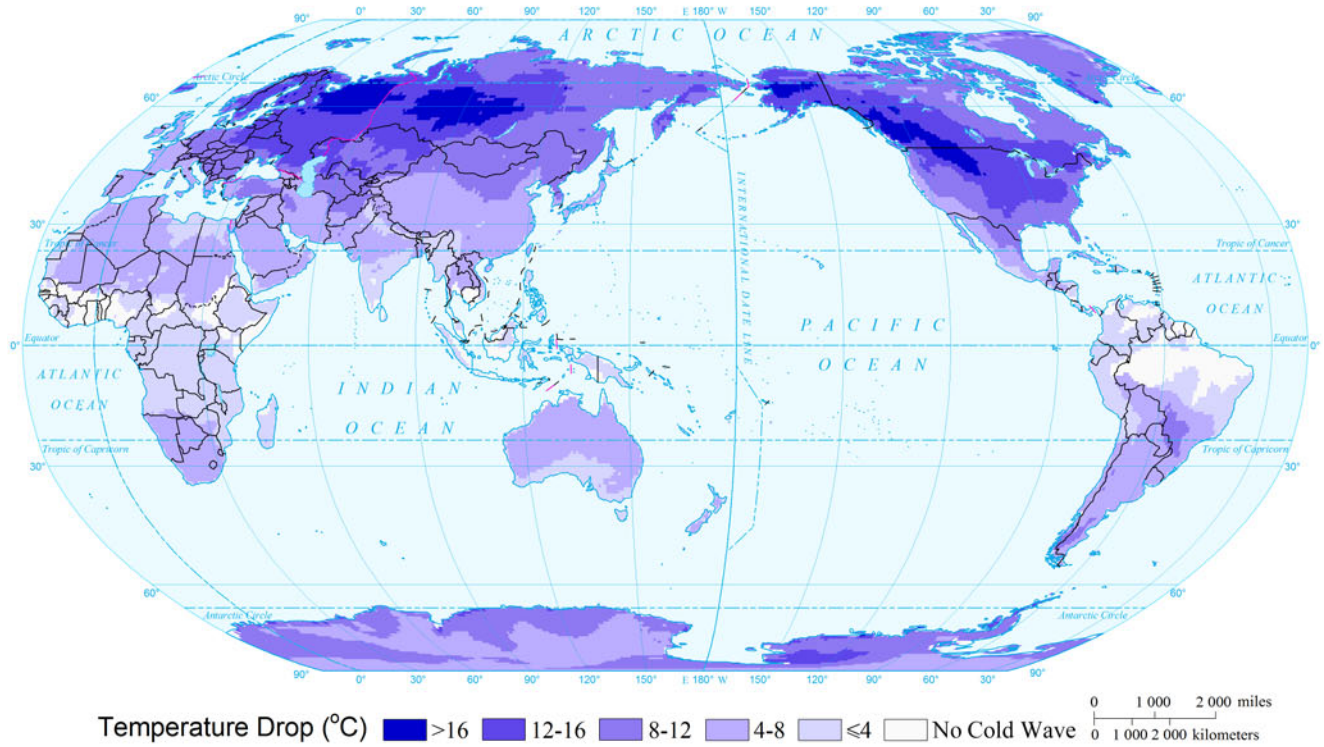


Expected Annual Global Temperature Drop  
( $0.75^\circ \times 0.75^\circ$ )

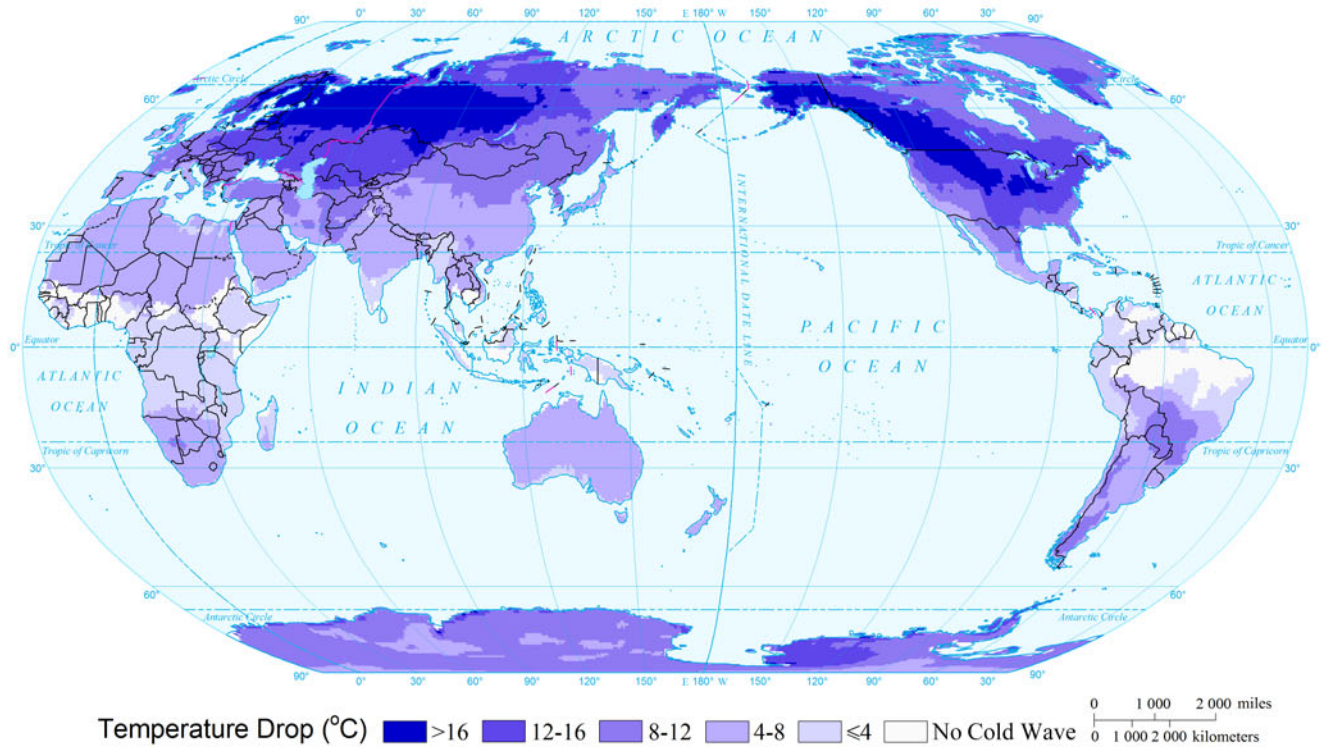


Temperature Drop (°C)  $\geq 9$  7-9 5-7 3-5  $\leq 3$  No Cold Wave

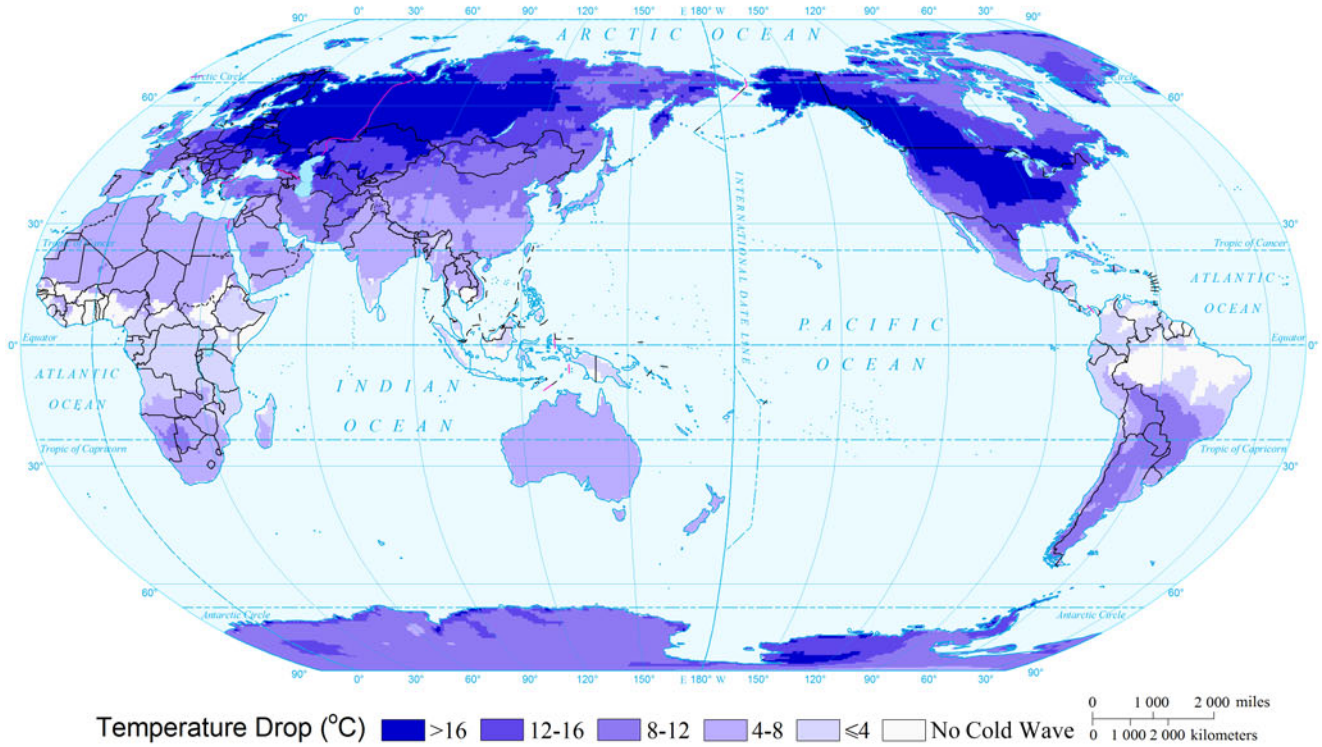
Global Temperature Drop by Return Period (10a)  
(0.75°×0.75°)



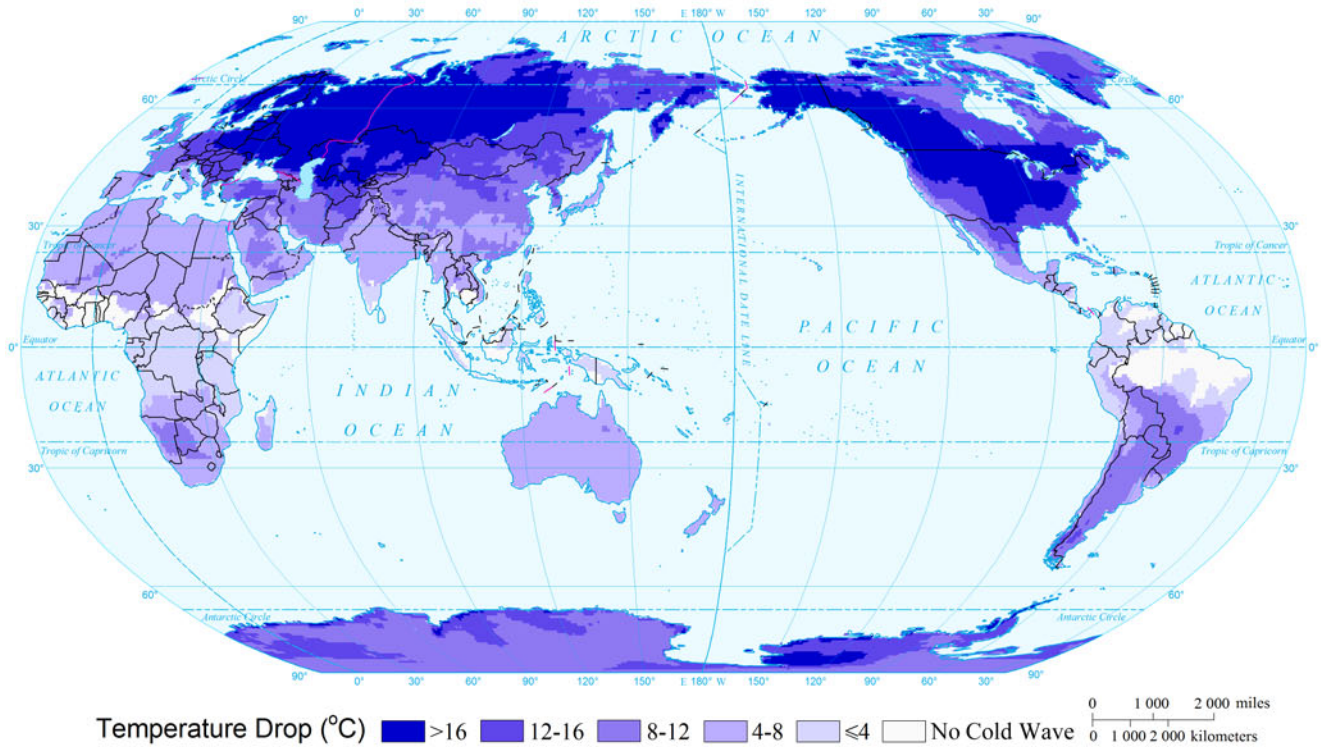
Global Temperature Drop by Return Period (20a)  
(0.75°×0.75°)



Global Temperature Drop by Return Period (50a)  
(0.75°×0.75°)

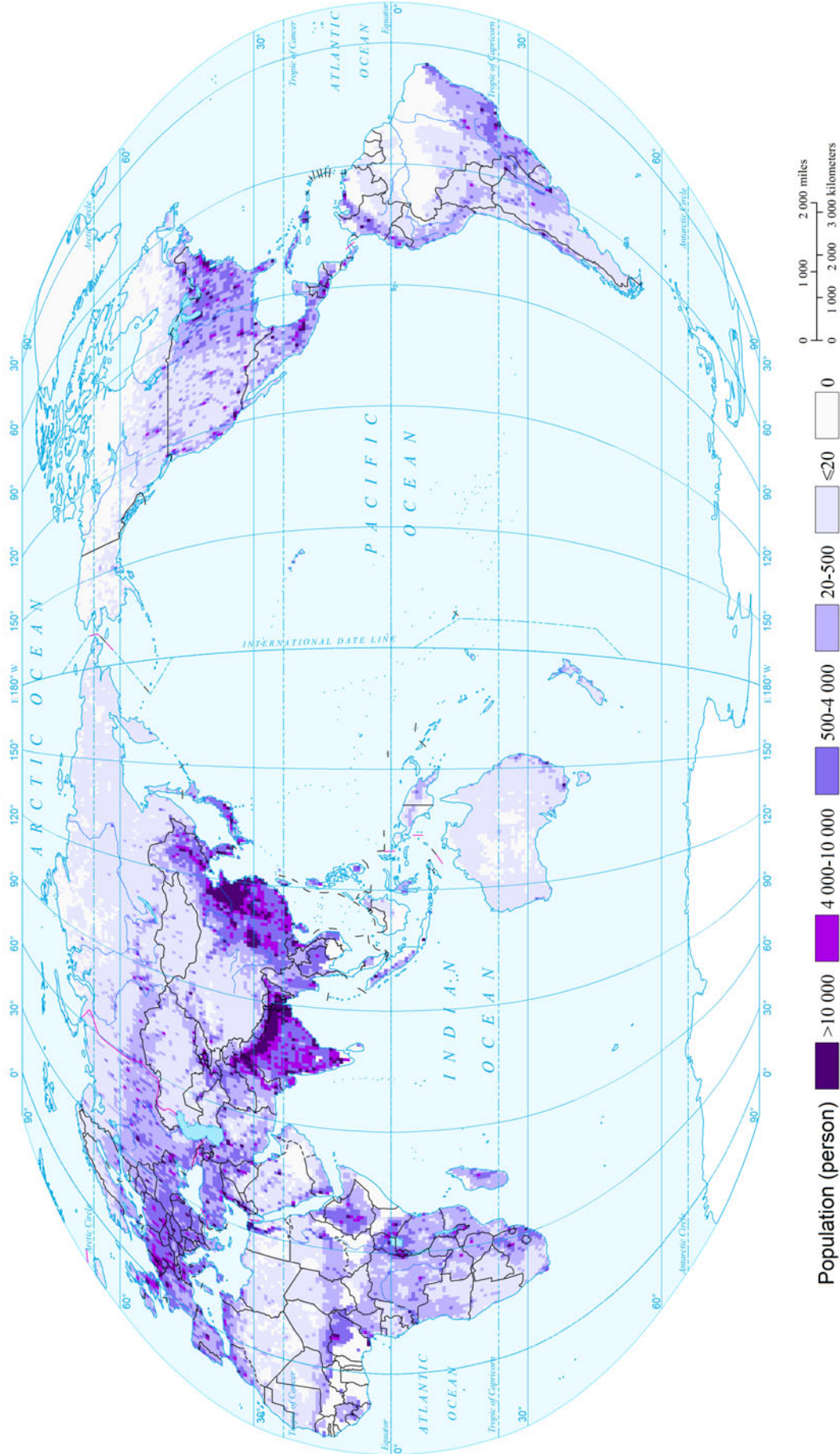


Global Temperature Drop by Return Period (100a)  
(0.75°×0.75°)

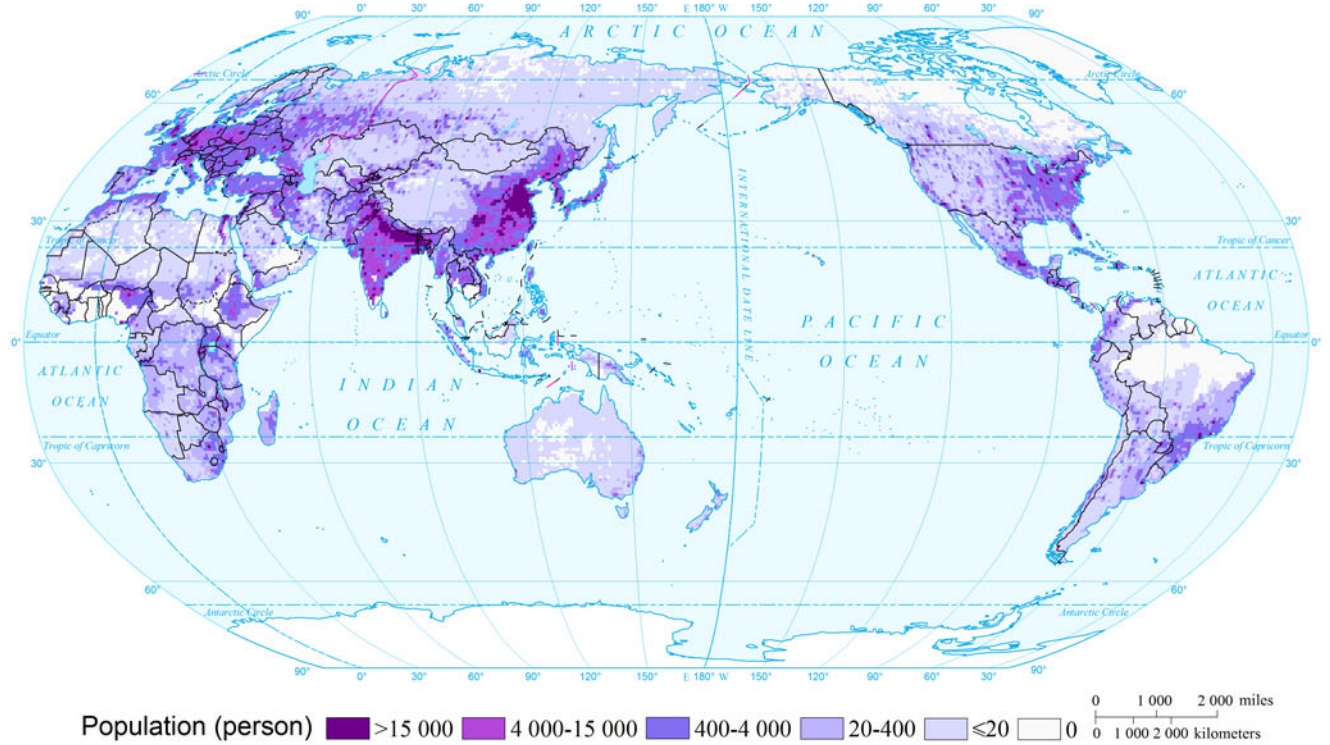




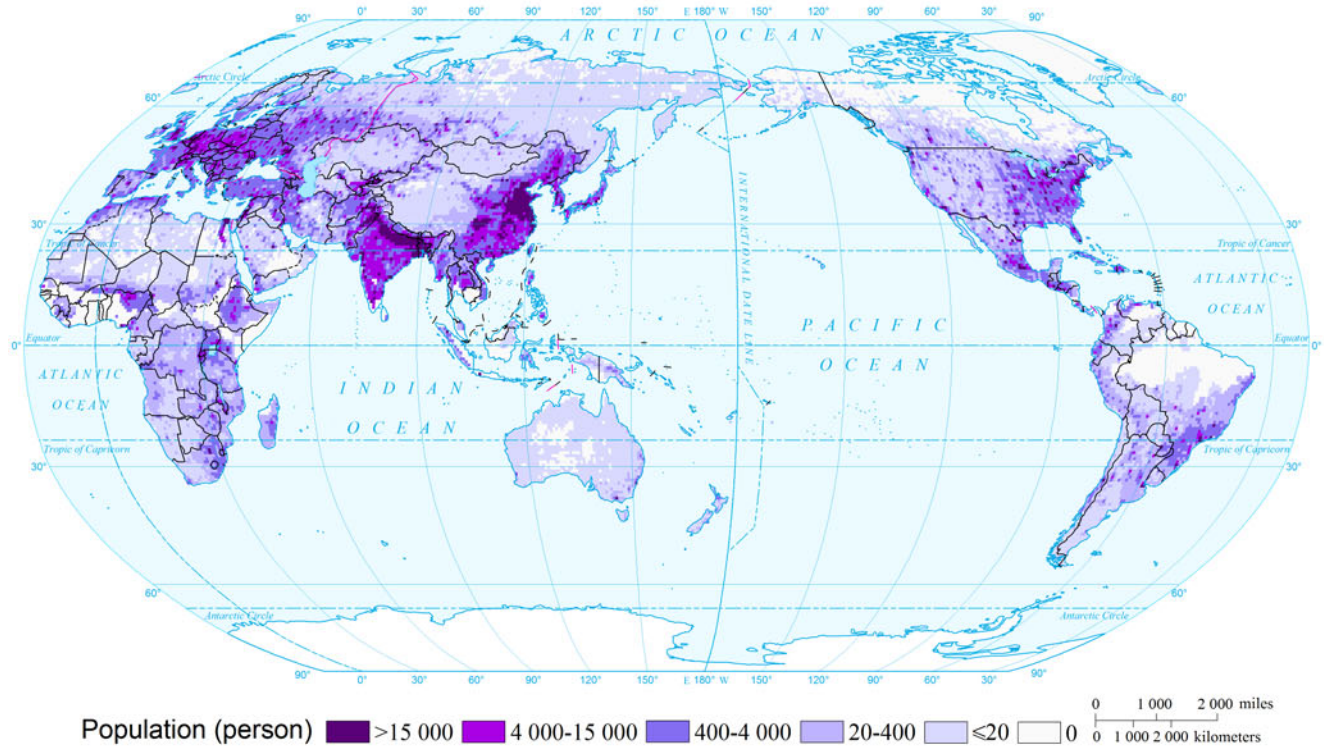
Expected Annual Affected Population Risk of Cold Wave of the World  
( $0.75^{\circ} \times 0.75^{\circ}$ )



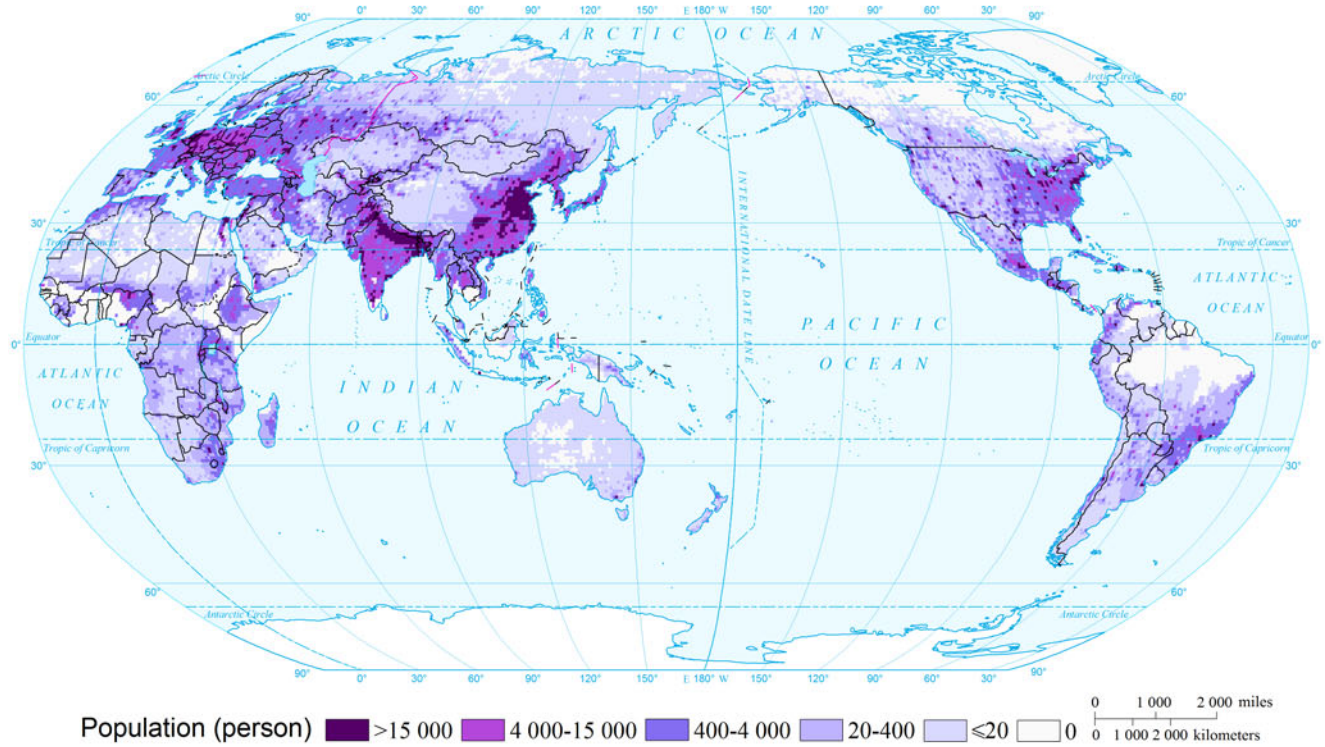
Affected Population Risk of Cold Wave of the World by Return Period (10a)  
(0.75°×0.75°)



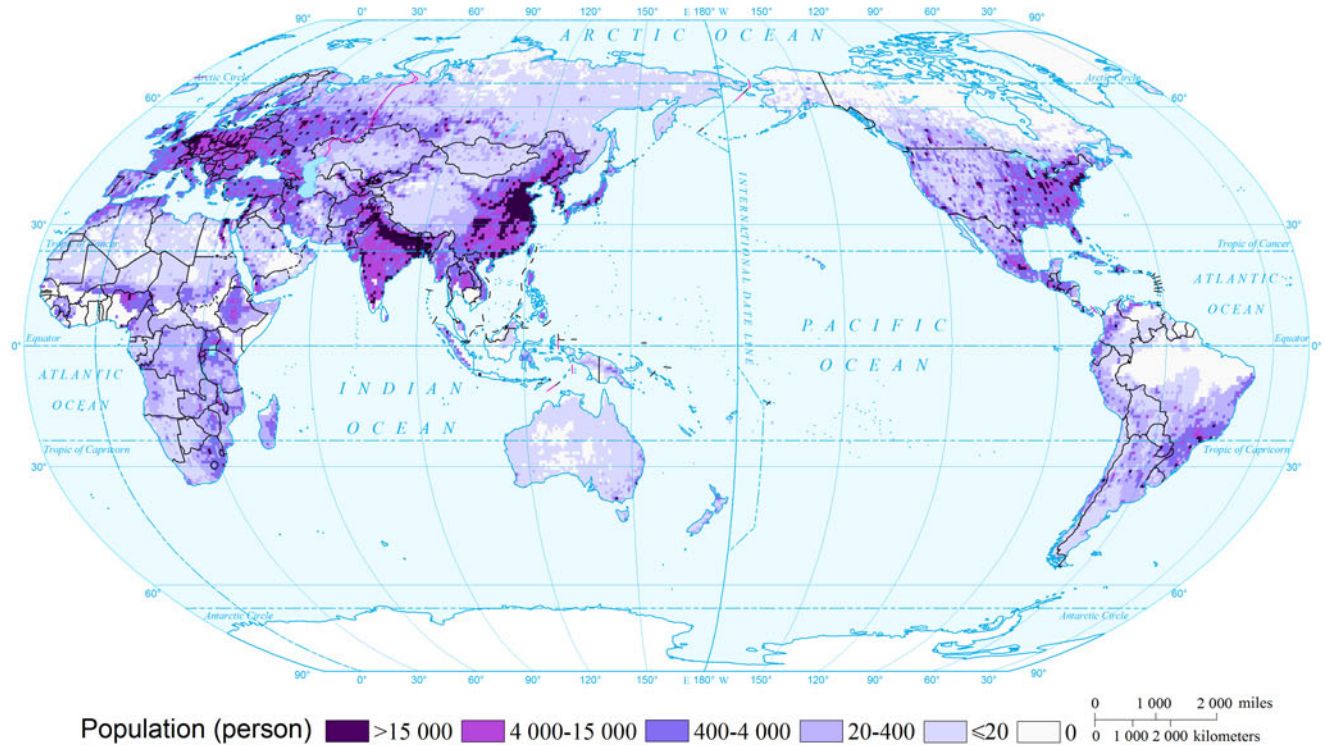
Affected Population Risk of Cold Wave of the World by Return Period (20a)  
(0.75°×0.75°)



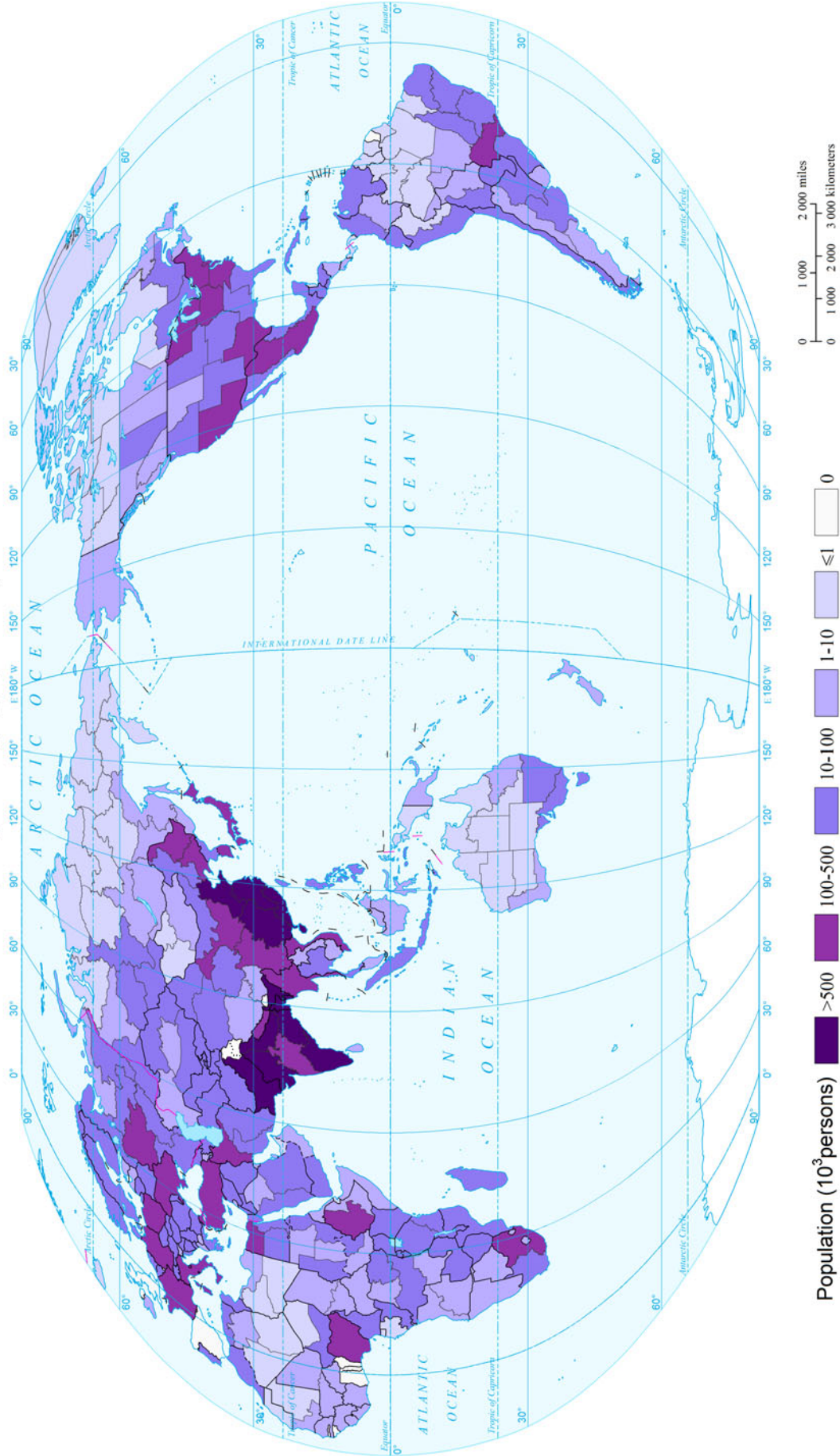
### Affected Population Risk of Cold Wave of the World by Return Period (50a) (0.75°×0.75°)



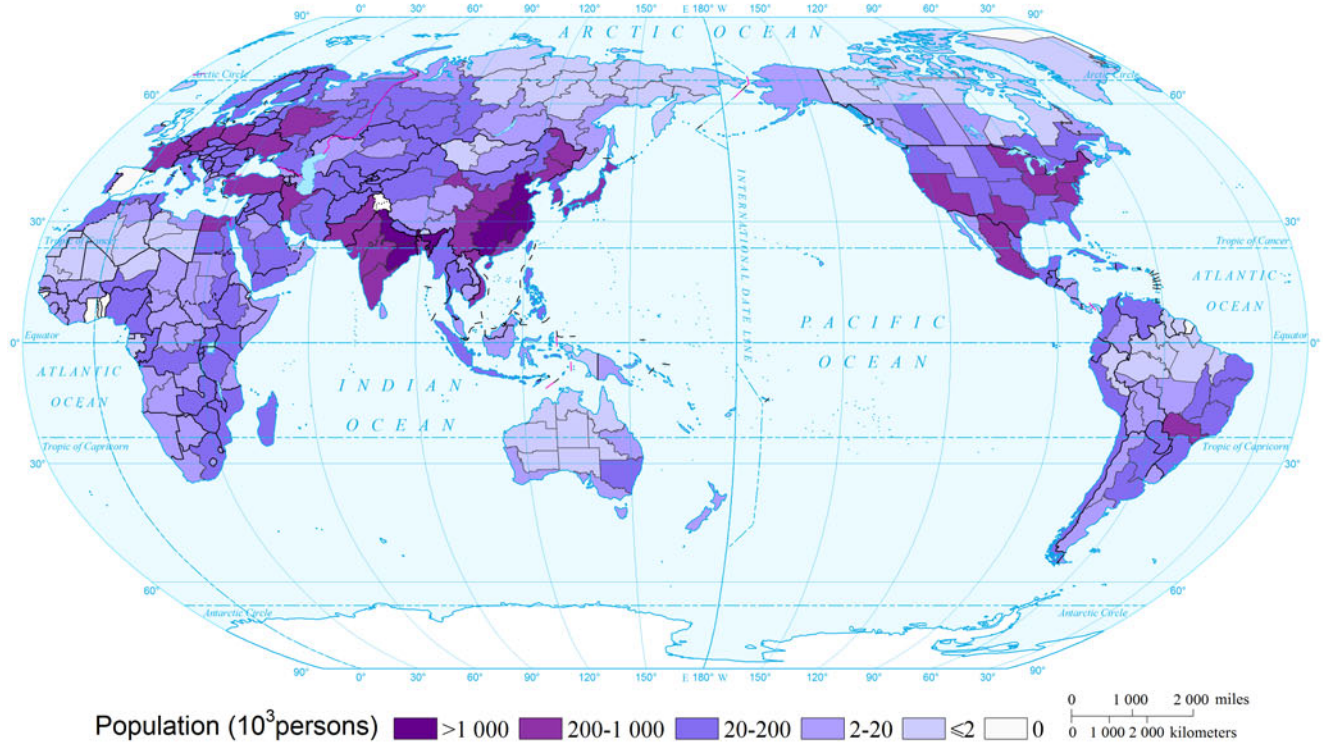
### Affected Population Risk of Cold Wave of the World by Return Period (100a) (0.75°×0.75°)



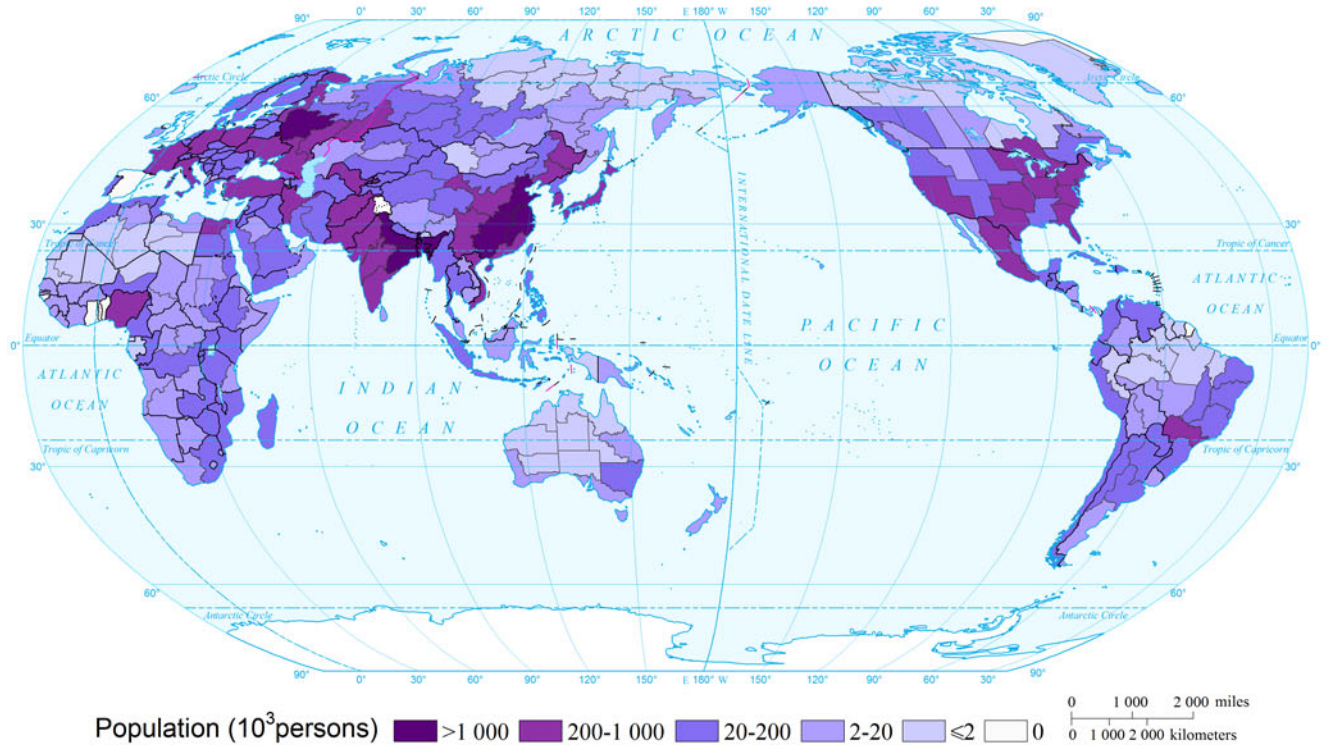
Expected Annual Affected Population Risk of Cold Wave of the World (Comparable-geographic Unit)



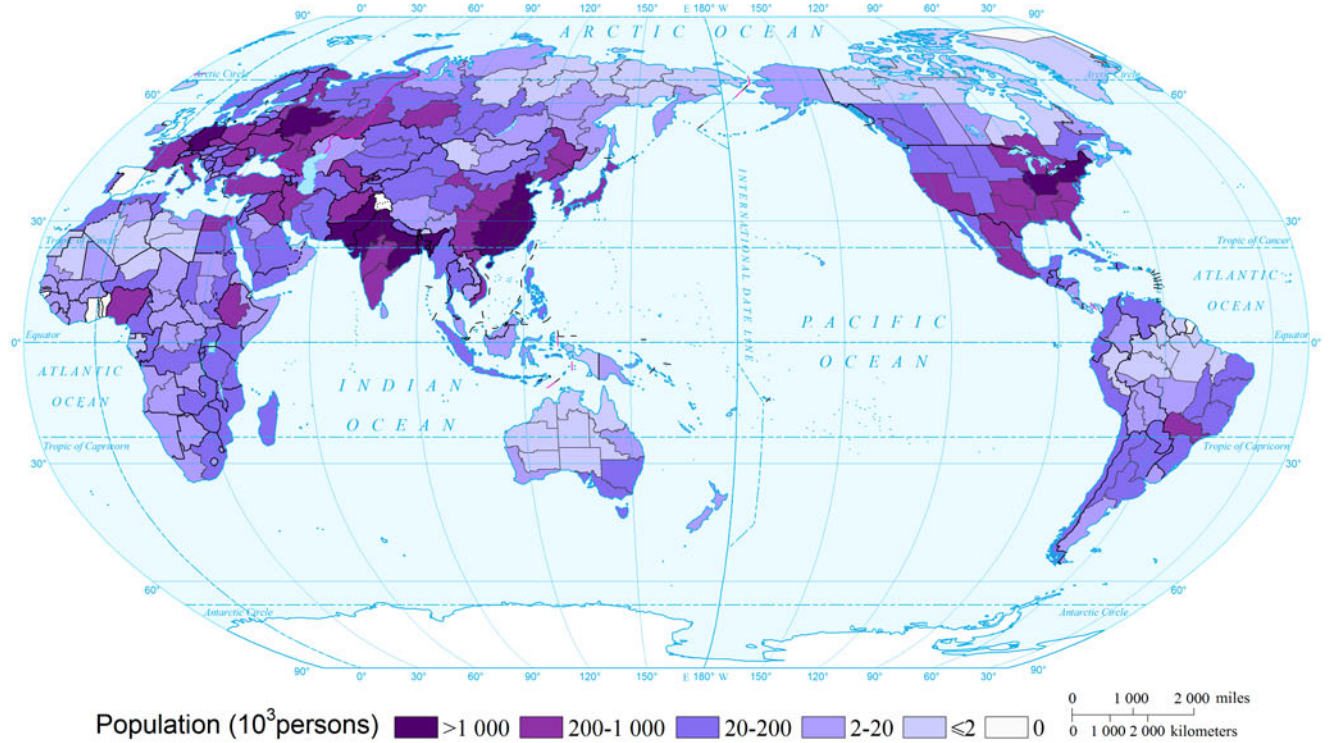
### Affected Population Risk of Cold Wave of the World by Return Period (10a) (Comparable-geographic Unit)



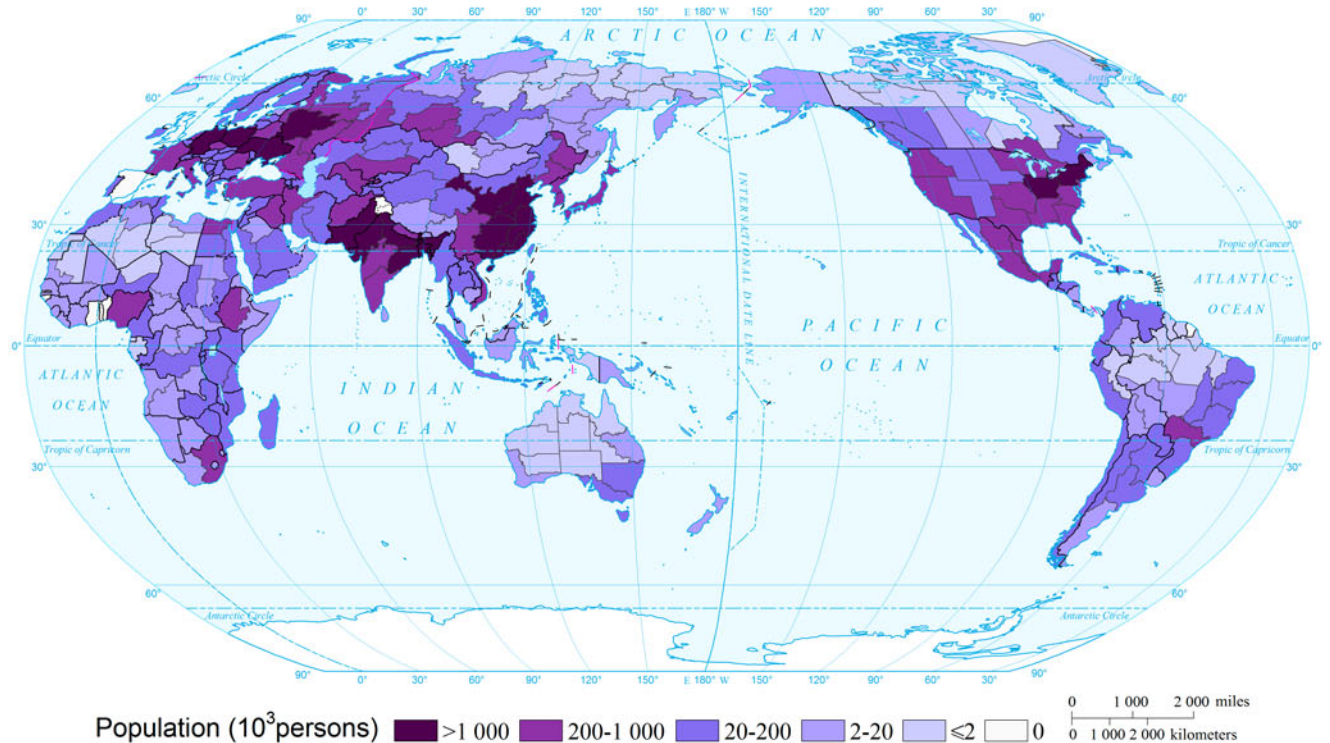
### Affected Population Risk of Cold Wave of the World by Return Period (20a) (Comparable-geographic Unit)



Affected Population Risk of Cold Wave of the World by Return Period (50a)  
(Comparable-geographic Unit)

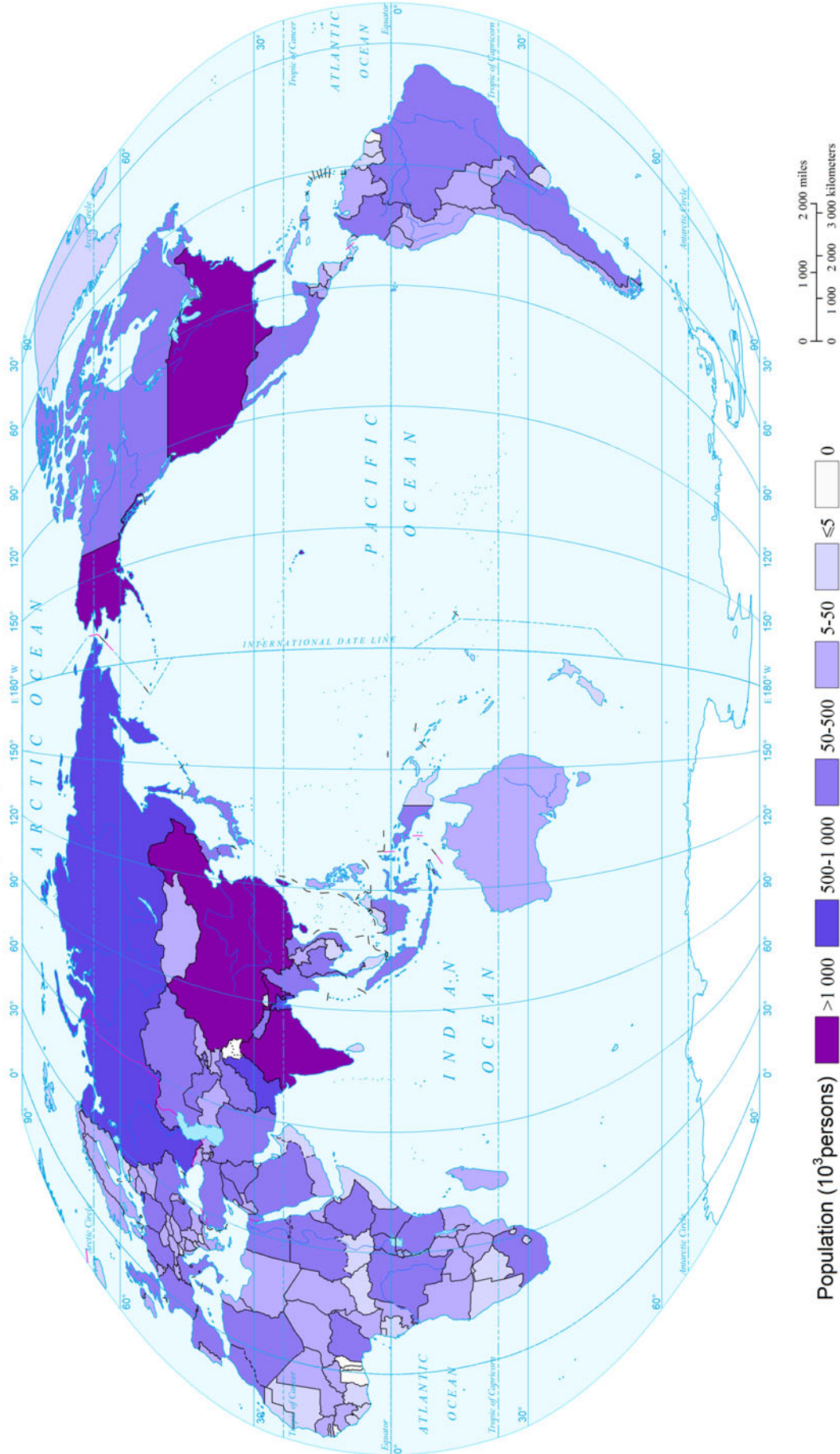


Affected Population Risk of Cold Wave of the World by Return Period (100a)  
(Comparable-geographic Unit)

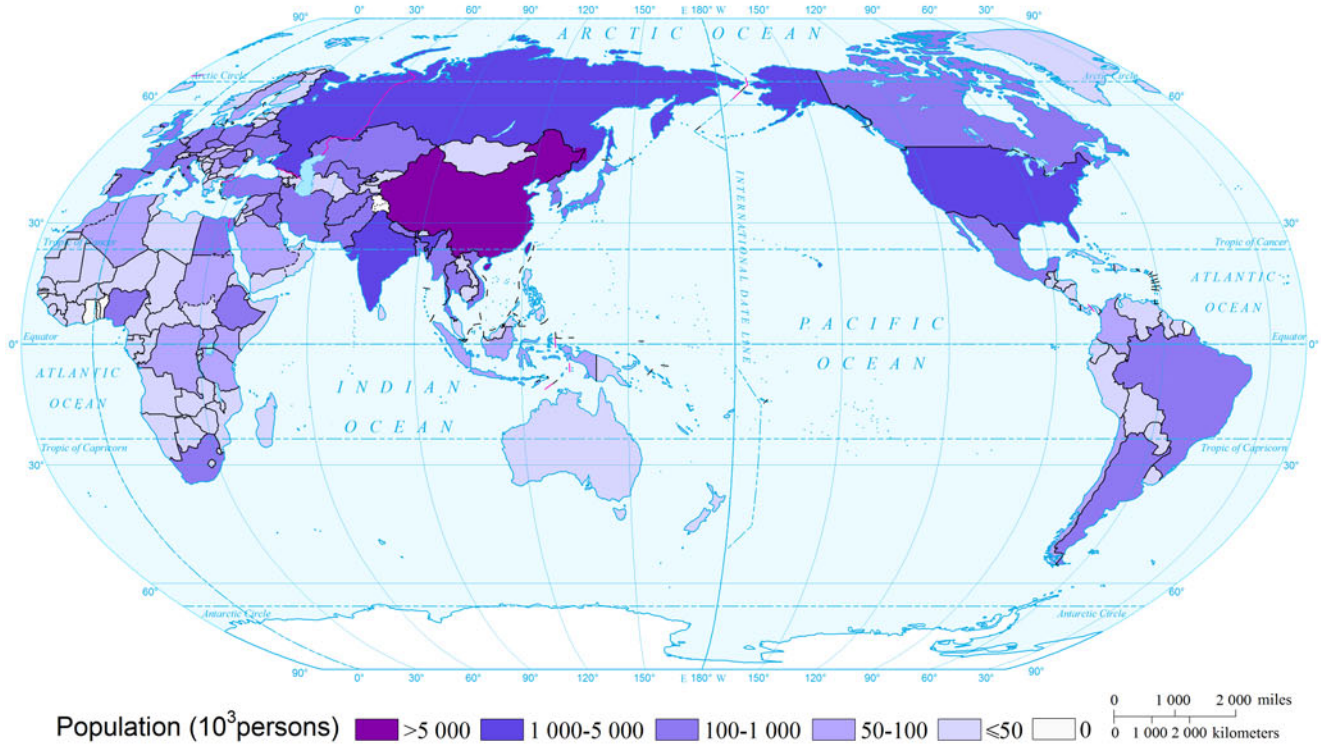




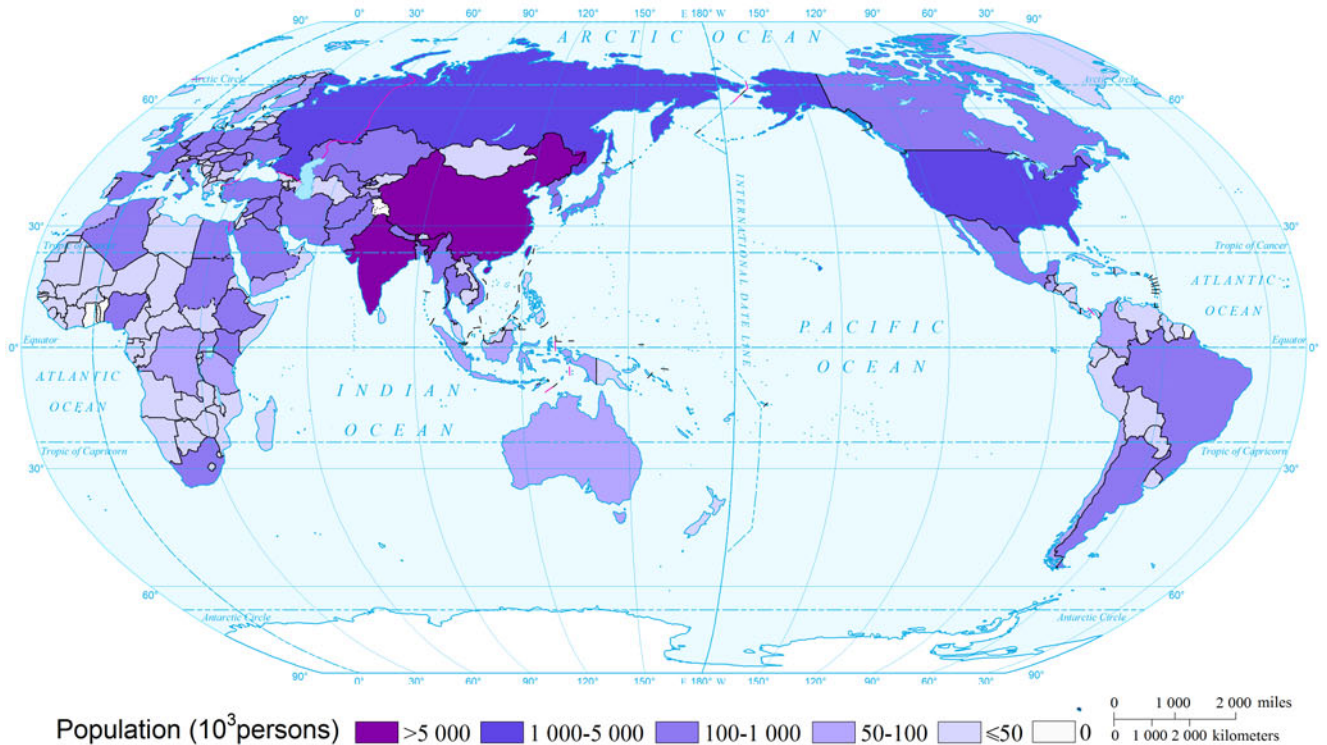
Expected Annual Affected Population Risk of Cold Wave of the World  
(Country and Region Unit)



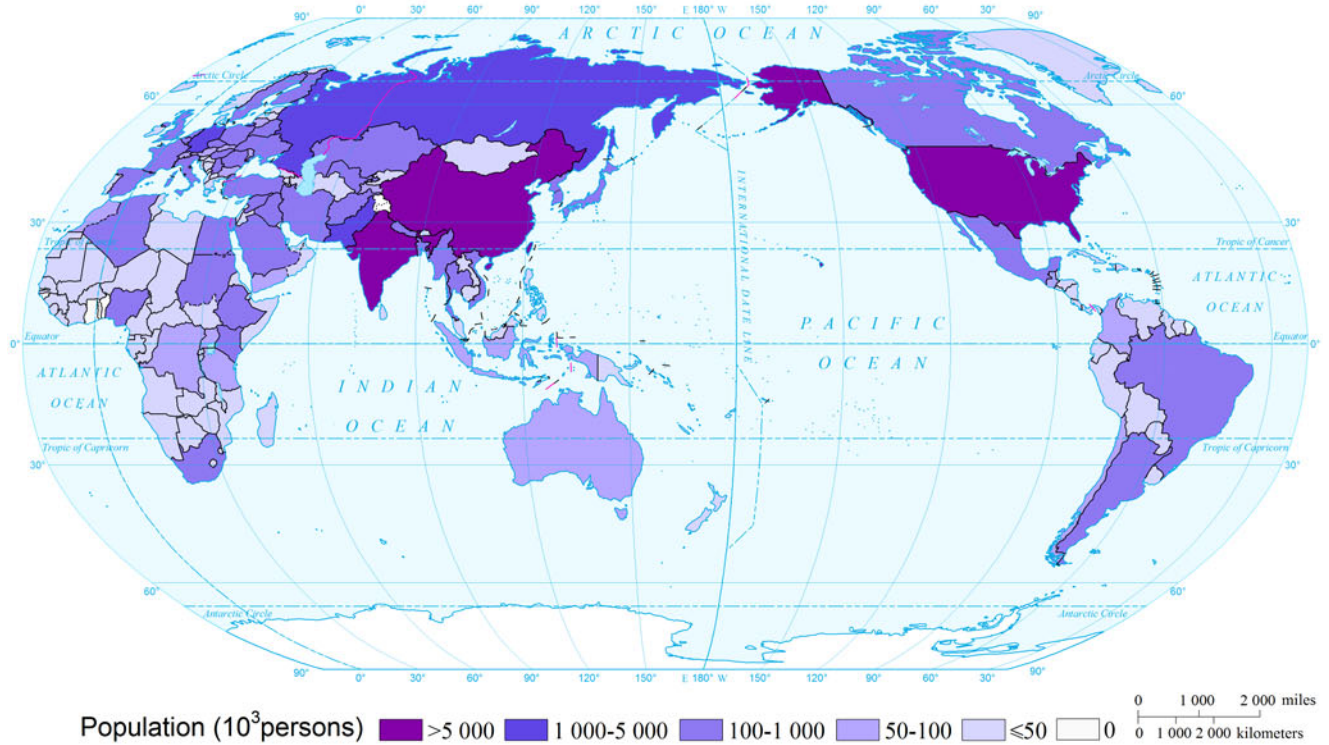
Affected Population Risk of Cold Wave of the World by Return Period (10a)  
(Comparable-geographic Unit)



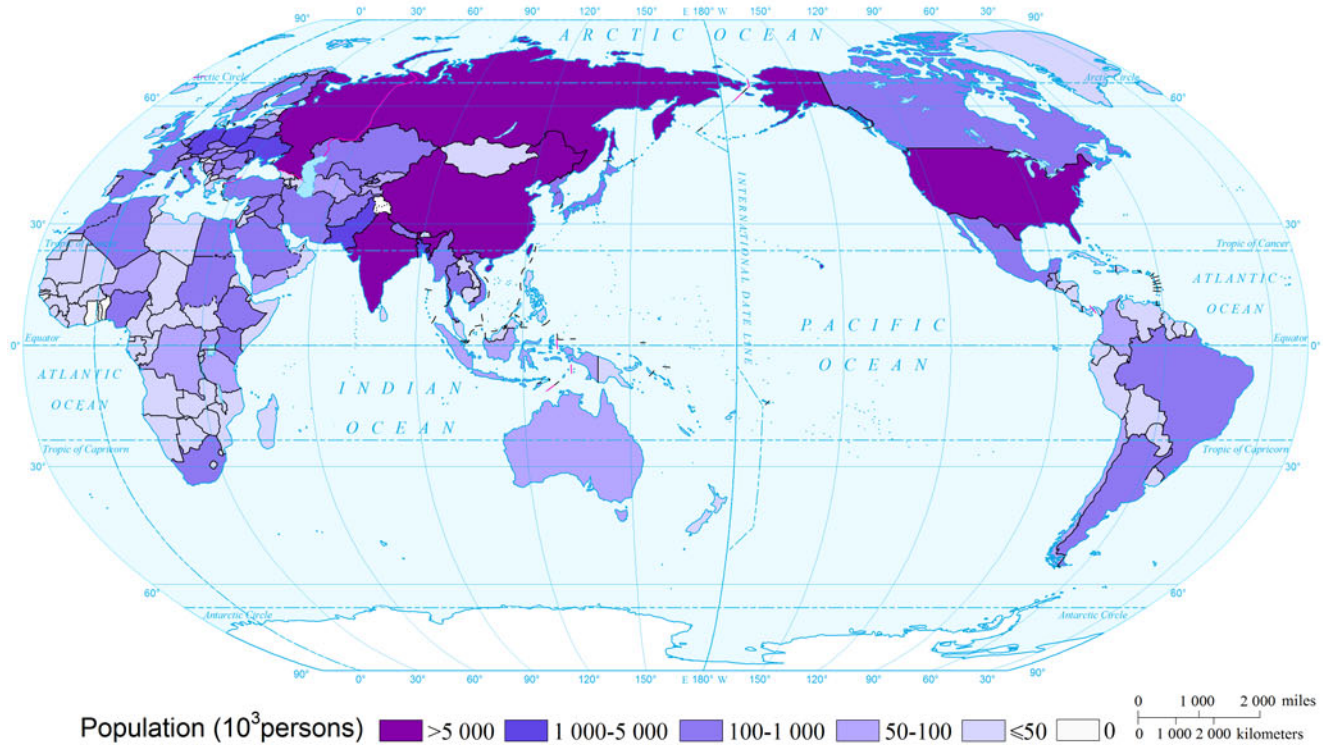
Affected Population Risk of Cold Wave of the World by Return Period (20a)  
(Comparable-geographic Unit)



Affected Population Risk of Cold Wave of the World by Return Period (50a)  
(Comparable-geographic Unit)



Affected Population Risk of Cold Wave of the World by Return Period (100a)  
(Comparable-geographic Unit)



## References

- Center for Hazards & Risk Research, Columbia University. 2014. Hotspots. <https://www.ldeo.columbia.edu/chrr/research/hotspots/>. Accessed in July 2014.
- European Spatial Planning Observation Network (ESPON). 2006. Environmental hazards and risk management—Thematic study of INTERREG and ESPON activities. Denmark.
- Intergovernmental Panel on Climate Change (IPCC). 2007. *Climate change 2007: Synthesis report*. IPCC Fourth Assessment Report (AR4). Geneva, Switzerland.
- Intergovernmental Panel on Climate Change (IPCC). 2012. *Managing the risks of extreme events and disasters to advance climate change adaptation*. A special report of working groups I and II of the intergovernmental panel on climate change. Cambridge and New York: Cambridge University Press.
- PreventionWeb. 2014. Cold wave disaster database. 2014. <http://www.preventionweb.net/english/>. Accessed in July 2014.
- Rocklöv, J., K. Ebi, and B. Forsberg. 2011. Mortality related to temperature and persistent extreme temperatures: A study of cause-specific and age-stratified mortality. *Occupational and Environmental Medicine* 68: 531–536.
- Shi, P.J. 1991. Study on the theory of disaster research and its practice. *Journal of Nanjing University (Natural Sciences)* 11(Supplement): 37–42. (in Chinese).
- Shi, P.J. 1996. Theory and practice of disaster study. *Journal of Natural Disasters* 5(4): 6–17. (in Chinese).
- Shi, P.J. 2002. Theory on disaster science and disaster dynamics. *Journal of Natural Disasters* 11(3): 1–9. (in Chinese).
- Song, X., Z. Zhang, Y. Chen, et al. 2013. Spatiotemporal changes of global extreme temperature events (ETEs) since 1981 and the meteorological causes. *Natural Hazards* 70(2): 975–994.
- United Nations Development Programme (UNDP), Bureau for Crisis Prevention and Recovery. 2004. *A global report: Reducing disaster risk: A challenge for development*, 1–161. New York: UNDP, Bureau for Crisis Prevention and Recovery.
- World Bank. 2014. Indicators. <http://data.worldbank.org/indicator>. Accessed in July 2014.
- Wang, W.G., W.Q. Xing, T. Yang, et al. 2013. Characterizing the changing behaviours of precipitation concentration in the Yangtze River Basin, China. *Hydrological Progresses* 27(6): 3375–3393.
- World Meteorological Organization (WHO). 2003. Climate change and human health—risks and responses—summary. Geneva.

---

**Part VI**

**Drought Disasters**

---

# Mapping Drought Risk (Maize) of the World

Yuanyuan Yin, Xingming Zhang, Han Yu, Degen Lin, Yaoyao Wu,  
and Jing'ai Wang

---

## 1 Background

Drought is one of the disasters that most widely affect and damage agricultural production in the world. Nearly half of the countries in the world bear severe drought (UNDP 2004; Moss et al. 2008). There is very serious drought in North America, Mexico, central and southern part of Africa, part of South America, and in northern part of China (IPCC 2012). Research shows that under the background of climate warming many regions in the world have an increasing risk of future drought because of the reduced precipitation and aggravating evaporation (IPCC 2012, 2013).

Agricultural drought risk, which is defined as the possible yield loss of crops exposed to drought, can be considered as the probability of the occurrence of agricultural drought and the negative impact on agricultural production (Yin et al. 2014). The drought risk of food production was assessed

based on drought frequency and intensity, production levels, and adaptability at global scale (Li et al. 2009). Assessing and mapping maize yield loss risk of drought of the world were made based on GEPIC-Vulnerability-Risk (GEPIC-V-R) model (Yin et al. 2014).

In this study, the maize yield loss risk of drought at global scale is assessed and mapped based on the GEPIC-V-R model developed by Yin et al. (2014). The vulnerability of maize to drought is simulated at grid level ( $0.5^\circ \times 0.5^\circ$ ), which improved the spatial resolution compared with the work of Yin et al. (2014).

---

## 2 Method

Figure 1 shows the technical flowchart for mapping maize yield loss risk of drought of the world.

### 2.1 Model

In the GEPIC-V-R model (Yin et al. 2014), drought risk is treated as the function of hazard, vulnerability of exposure, and environment (Eq. 1):

$$R = f(E, H, V) = H\{P, h_E\} \times V\{l_E, h_E\} \quad (1)$$

where  $E$  is the sensitivity of environment;  $H$  is the drought;  $V$  is the vulnerability;  $P$  is the occurrence probability of drought;  $h_E$  is the drought intensity index; and  $l_E$  is the loss rate.  $H\{P, h_E\}$  is the drought intensity under a certain probability.  $V\{l_E, h_E\}$  determines the relationship between  $h_E$  and  $l_E$ .

GEPIC-V-R model is a crop risk assessment model for large scale (i.e., regional, national, continental, and global) with functions to fit vulnerability curves and calculate risk. In this model, there are four modules: model calibration

---

**Mapping Editors:** Jing'ai Wang (Key Laboratory of Regional Geography, Beijing Normal University, Beijing 100875, China), Chunqin Zhang (School of Geography, Beijing Normal University, Beijing 100875, China), Yin Zhou (Key Laboratory of Regional Geography, Beijing Normal University, Beijing 100875, China) and Fang Chen (School of Geography, Beijing Normal University, Beijing 100875, China).

**Language Editor:** Wei Xu (Key Laboratory of Environmental Change and Natural Disaster, Ministry of Education, Beijing Normal University, Beijing 100875, China).

---

Y. Yin · J. Wang (✉)

Key Laboratory of Regional Geography,  
Beijing Normal University, Beijing 100875, China  
e-mail: jwang@bnu.edu.cn

X. Zhang · H. Yu · D. Lin · Y. Wu  
School of Geography, Beijing Normal University, Beijing 100875,  
China

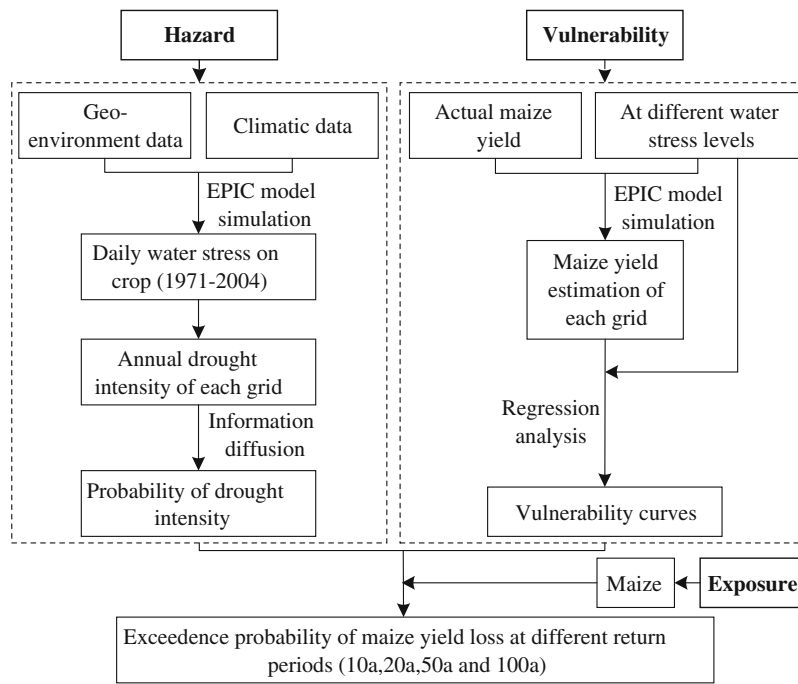


**Fig. 1** The technical flowchart for mapping maize yield loss risk of drought of the world

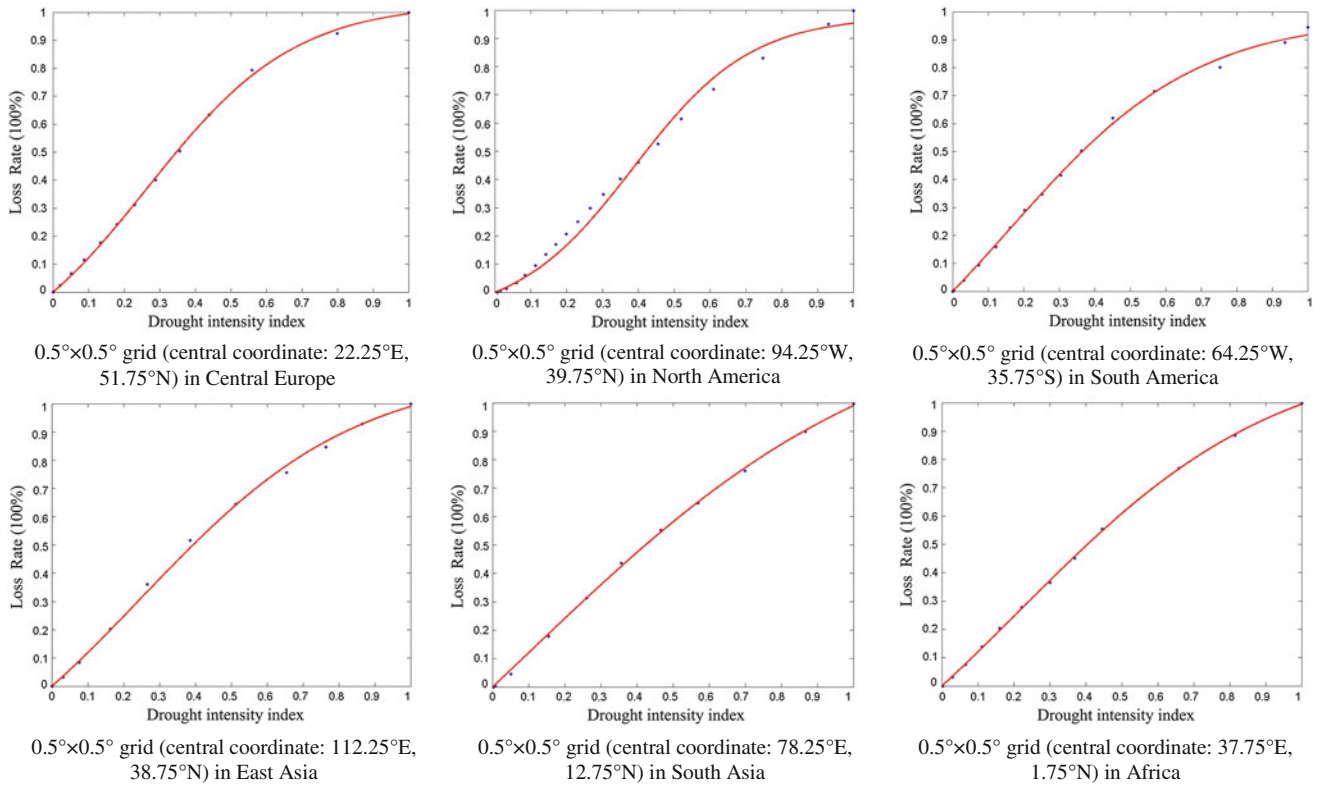


**Fig. 2** Examples of vulnerability curve of maize to drought

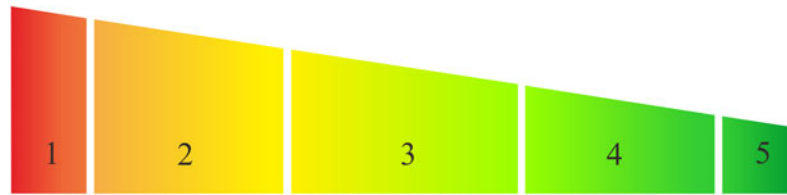


**Fig. 3** Expected annual maize yield loss risk of drought of the world. *1* (0, 10 %). USA, China, Russia, Brazil, Spain, Afghanistan, Kenya, Argentina, Mexico, Turkey, Ukraine, Kazakhstan, Iraq, South Africa, and Australia. *2* (10, 35 %). Tanzania, Peru, India, Namibia, Sudan, Ethiopia, Chile, Bolivia, Iran, Indonesia, France, Portugal, Somalia, Italy, Turkmenistan, Poland, Uzbekistan, Pakistan, Angola, Syria, Senegal, Germany, Mauritania, Kyrgyzstan, Yemen, Zimbabwe, Greece, Chad, Egypt, Ecuador, Tajikistan, Burma, Canada, Botswana, Nigeria, and Morocco. *3* (35, 65 %). Eritrea, Mali, Saudi Arabia, Burkina Faso, Mozambique, Serbia, Uruguay, Vietnam, Hungary, Azerbaijan, Bosnia and Herzegovina, Belarus, Laos, Bulgaria, Nepal, Albania, Israel, Croatia, Venezuela, Uganda, Lesotho, South Sudan, Thailand, Lebanon, Romania, Congo (Democratic Republic of the),

Gaza Strip, Benin, Macedonia, Czech Republic, Dominican Republic, Paraguay, Montenegro, the Netherlands, Slovakia, Gambia, Zambia, Georgia, Honduras, Cameroon, Nicaragua, New Zealand, and Cuba. *4* (65, 90 %). Madagascar, Moldova, the Republic of Côte d'Ivoire, Central African Republic, Jordan, Colombia, Algeria, Philippines, Swaziland, Malawi, Libya, Armenia, South Korea, Guinea-Bissau, Malaysia, Sri Lanka, Austria, Haiti, Belgium, Guyana, Guinea, North Korea, Togo, Guatemala, El Salvador, Switzerland, Niger, Slovenia, Luxembourg, Ghana, Mongolia, Belize, Kuwait, Jamaica, Timor-Leste, and Costa Rica. *5* (90, 100 %). Congo, Rwanda, Burundi, Bangladesh, Gabon, Finland, Trinidad and Tobago, San Marino, Lithuania, Latvia, Cambodia, Sierra Leone, Panama, and Bhutan

module, hazard module, vulnerability module, and risk calculation module (Yin et al. 2014).

Data for assessing the maize yield loss risk by drought of the world consist of crop growth environment data (Appendix III, Environments data 2.1, 2.2 and 2.7, Appendix III, Hazards data 4.15), crop management data (Appendix III, Environments data 3.13–3.16), crop species attribute data (Appendix III, Environments data 3.18), and actual yield data (Appendix III, Environments data 3.17).

## 2.2 Spatial Resolution

Compared with the work of Yin et al. (2014), the vulnerability of maize to drought is simulated at grid level ( $0.5^\circ \times 0.5^\circ$ ) instead of the regional level, which greatly improves the spatial resolution. Furthermore, the maize exposure is calculated and mapped at  $5' \times 5'$  grid level in this study instead of  $0.5^\circ \times 0.5^\circ$  grid level done by Yin et al. (2014).

## 3 Results

### 3.1 Intensity

Areas with high value of drought intensity on maize mainly distribute in a band along Mongolian Plateau, the Hindu Kush Mountains, Asia Minor peninsula, Balkan Peninsula,

Apennine peninsula and Iberian Peninsula in Asia and Europe, the Great Rift Valley and east margin of the Namib Desert in Africa, the Rocky Mountains, central part of Mexico Plateau, northeast of Brazil Plateau and the Andes Mountains in America, and Murray River Basin in Oceania.

### 3.2 Vulnerability

Based on the GEPIC-V-R model, vulnerability curves of maize to drought for each grid ( $0.5^\circ \times 0.5^\circ$ ) are fitted. Figure 2 shows the vulnerability curves of some selected grids.

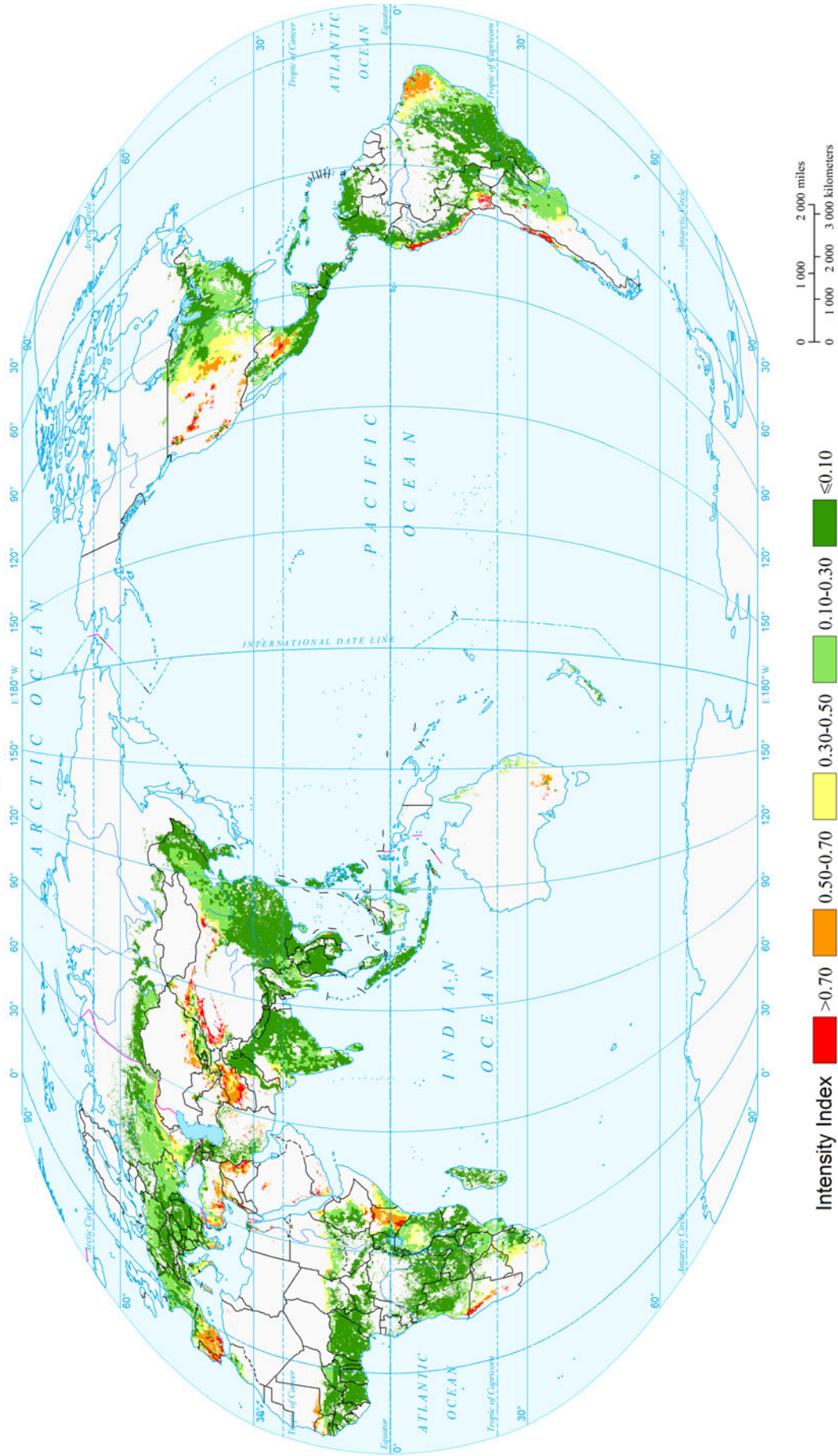
### 3.3 Risk

By zonal statistics of the expected risk result, the expected annual maize yield loss risk of drought of the world at national level is derived and ranked (Fig. 3). The top 1 % country with the highest expected annual maize yield loss risk of drought is USA, and the top 10 % countries are USA, China, Russia, Brazil, Spain, Afghanistan, Kenya, Argentina, Mexico, Turkey, Ukraine, Kazakhstan, Iraq, South Africa, and Australia.

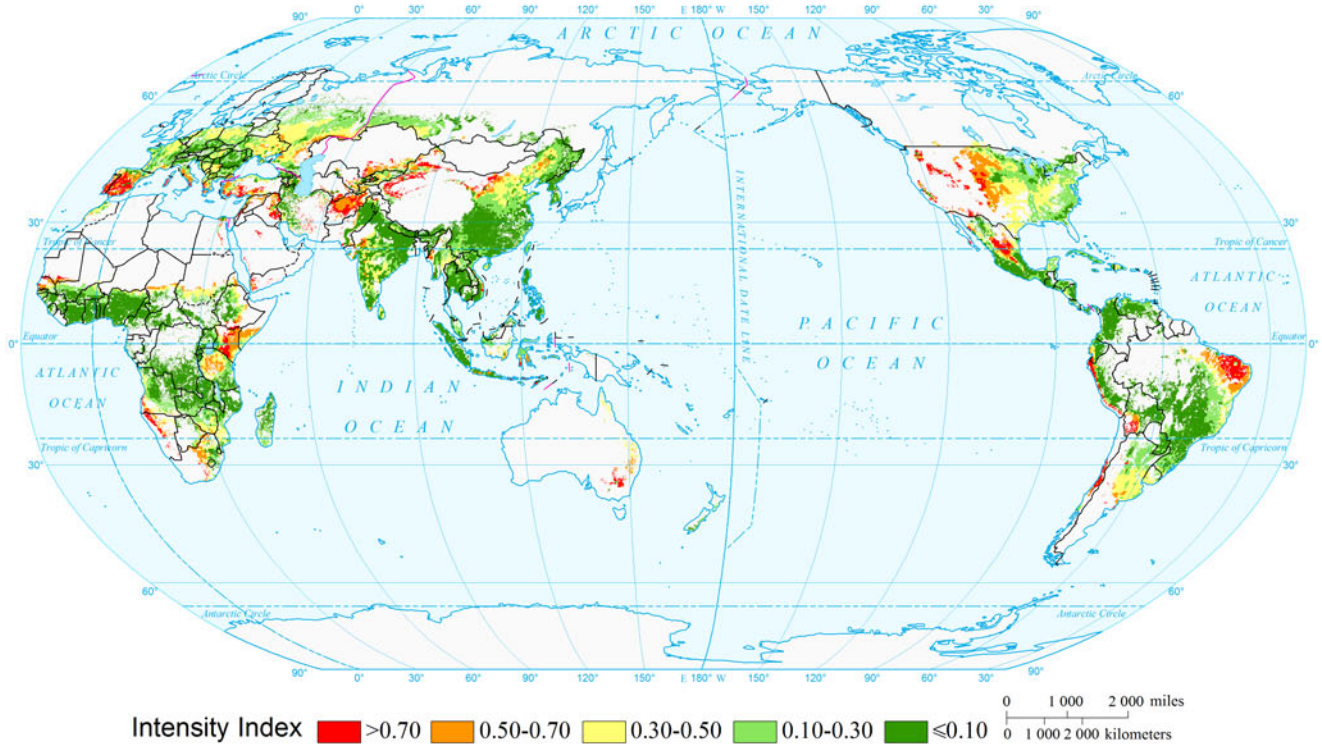
## 4 Maps



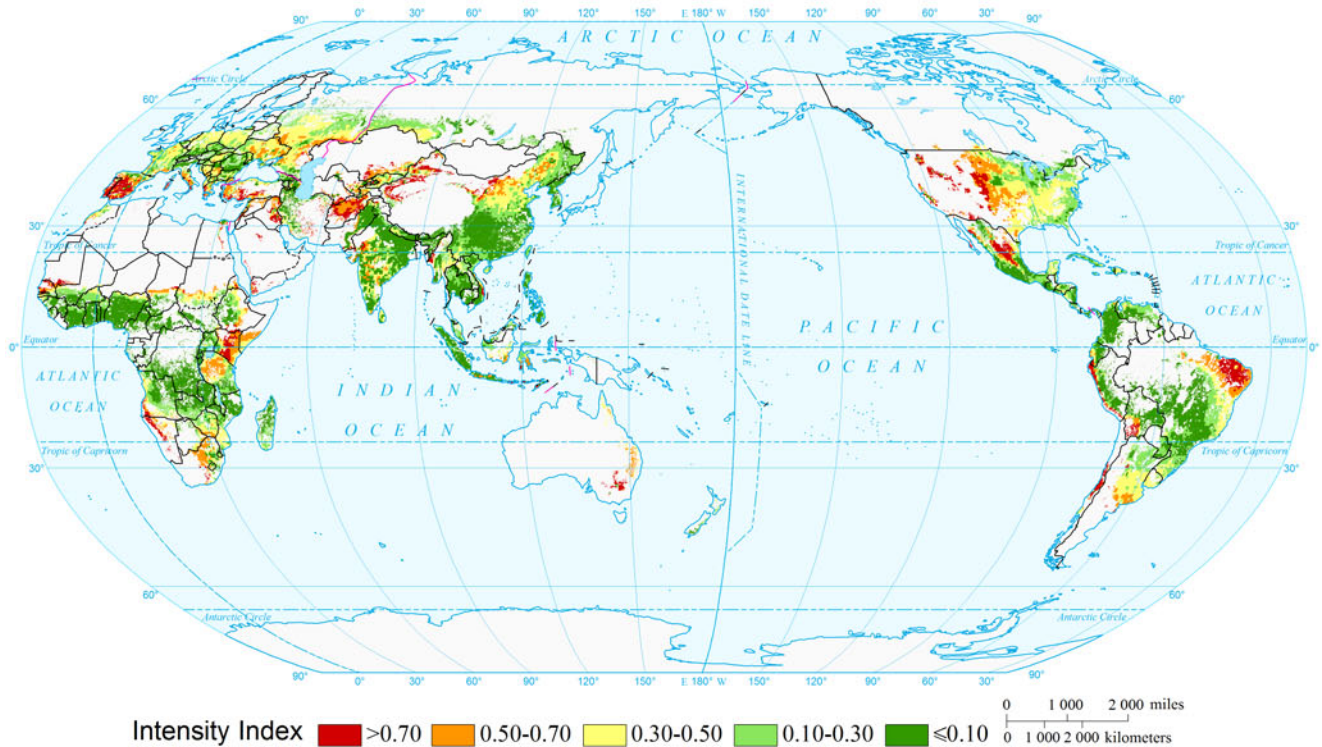
Global Expected Annual Drought Intensity for Maize  
( $0.5^\circ \times 0.5^\circ$ )



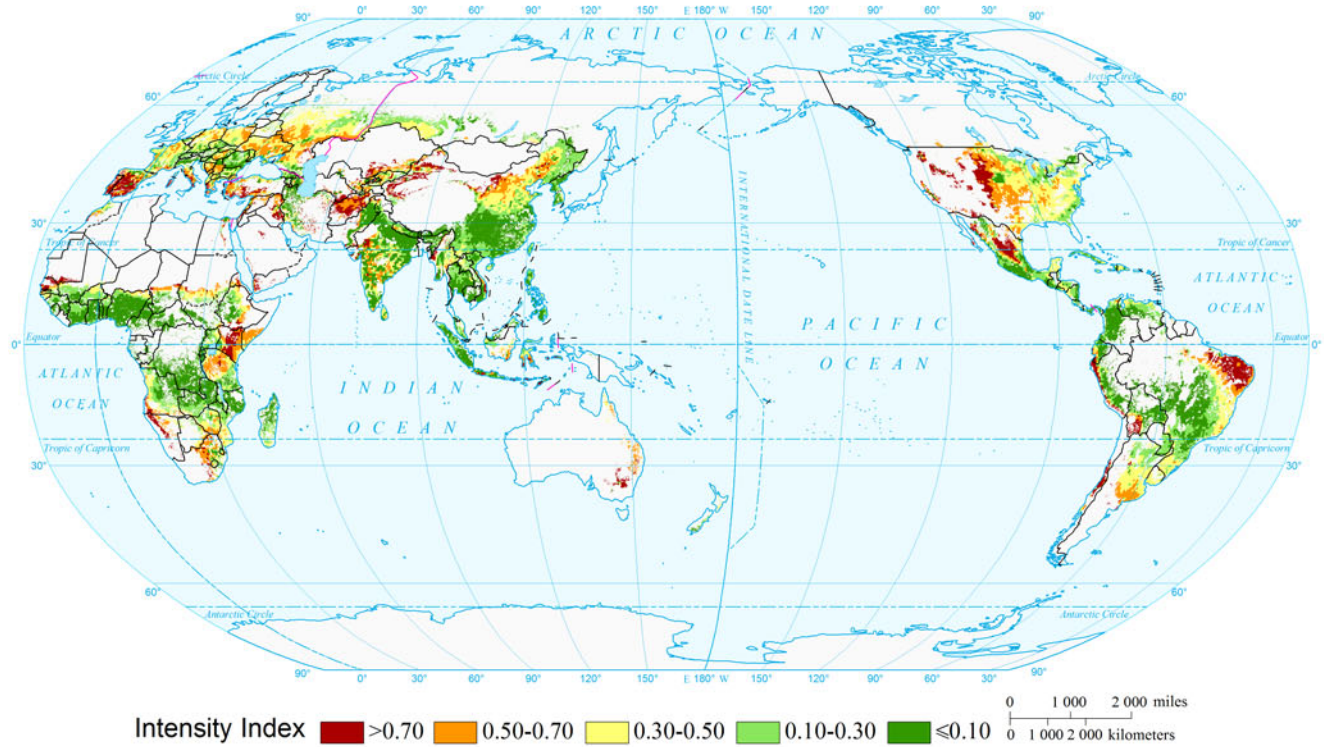
Global Drought Intensity for Maize by Return Period (10a)  
(0.5°×0.5°)



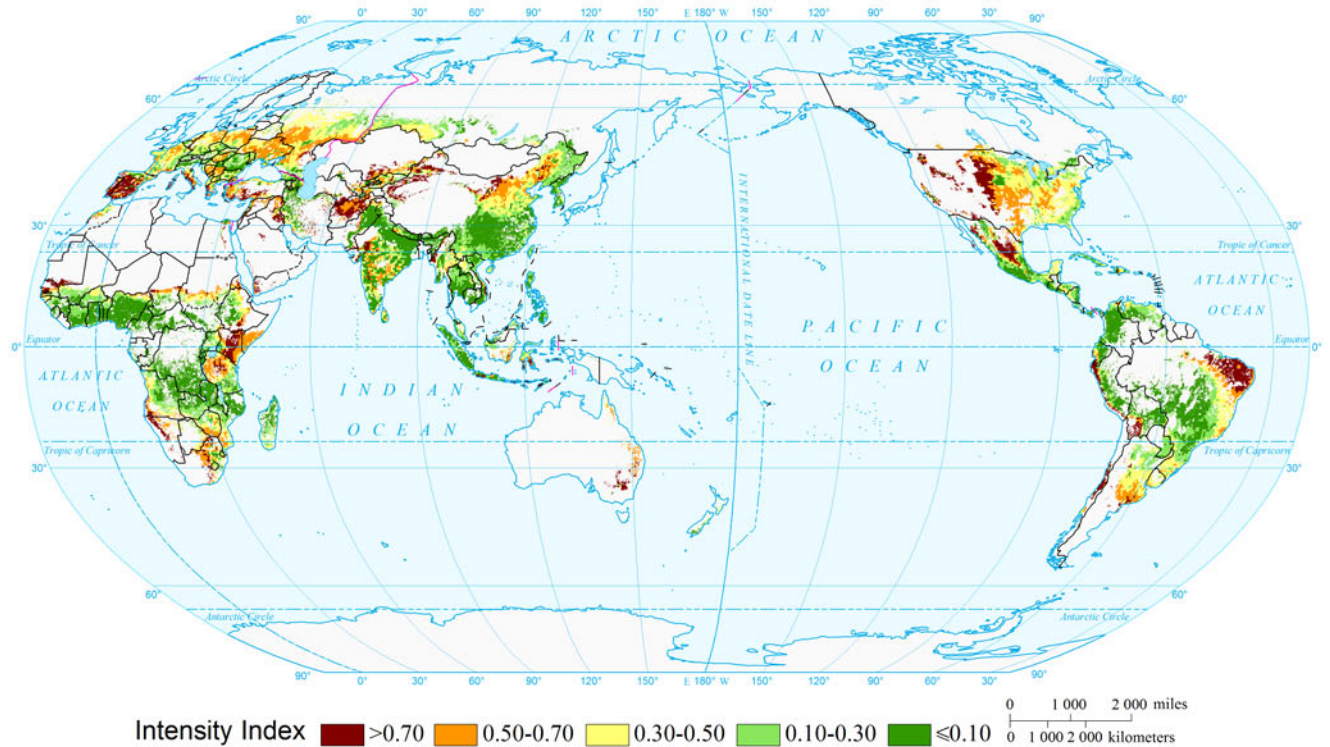
Global Drought Intensity for Maize by Return Period (20a)  
(0.5°×0.5°)



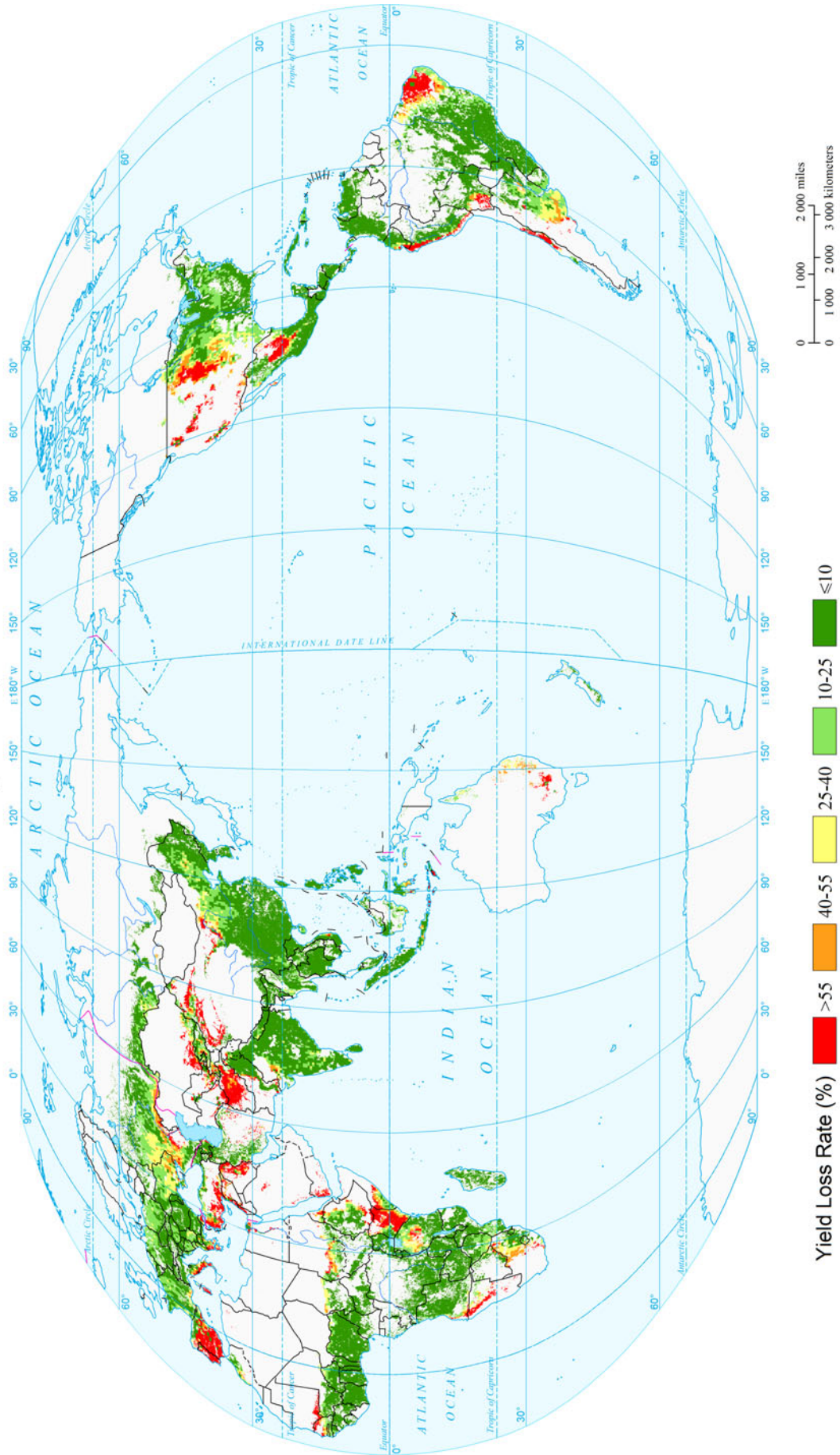
Global Drought Intensity for Maize by Return Period (50a)  
(0.5°×0.5°)



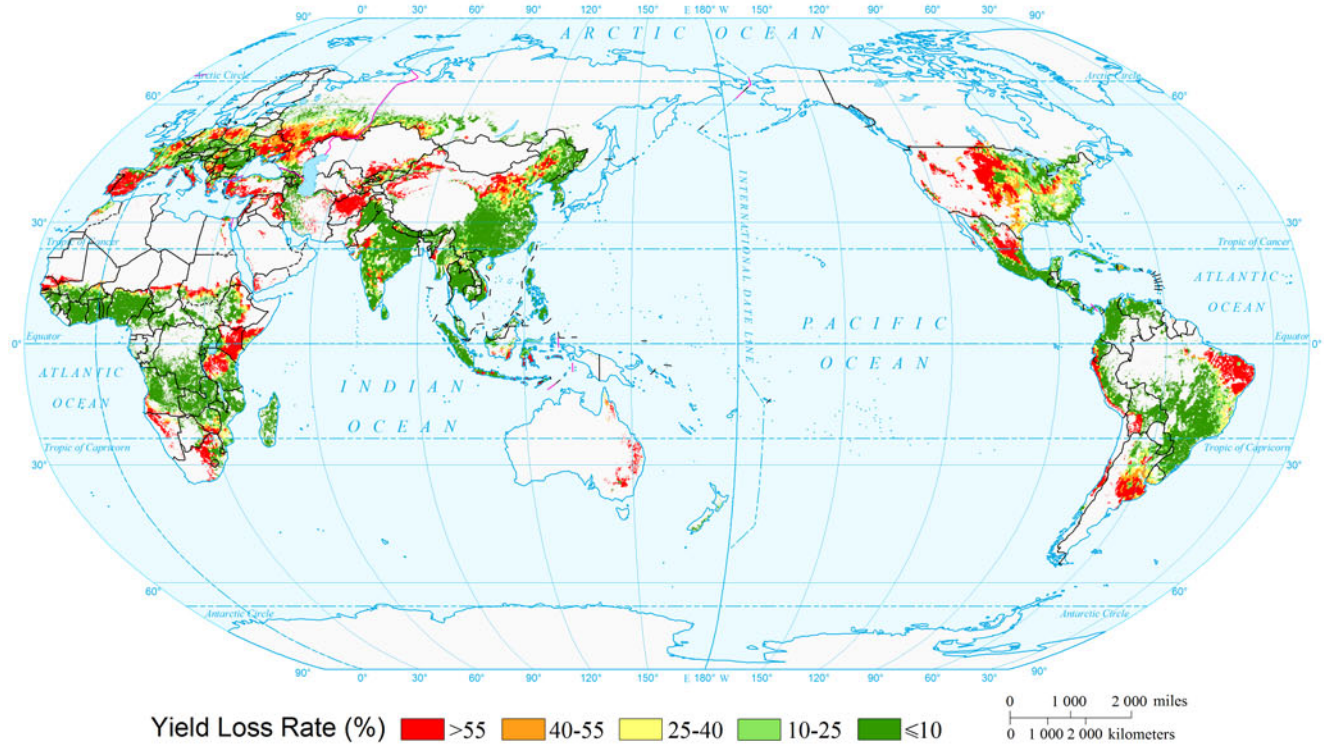
Global Drought Intensity for Maize by Return Period (100a)  
(0.5°×0.5°)



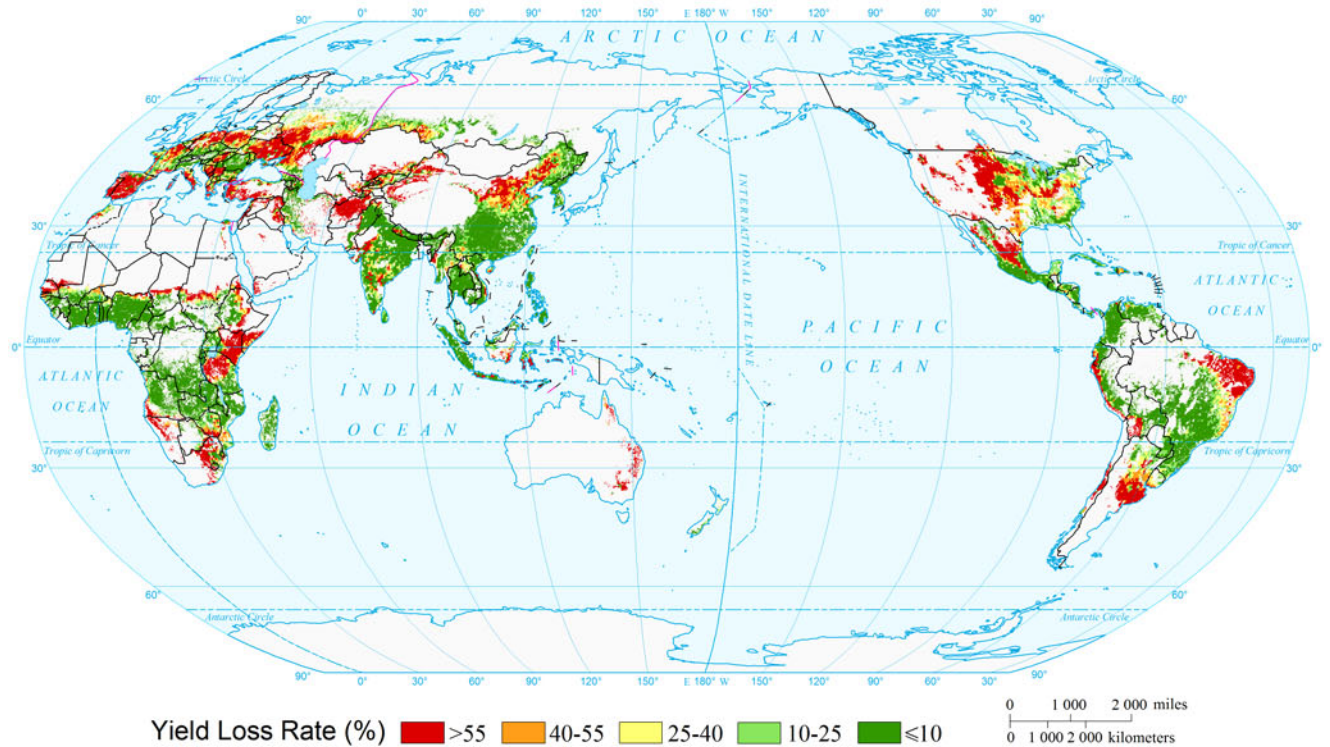
### Expected Annual Maize Yield Loss Risk of Drought of the World (0.5°x0.5°)



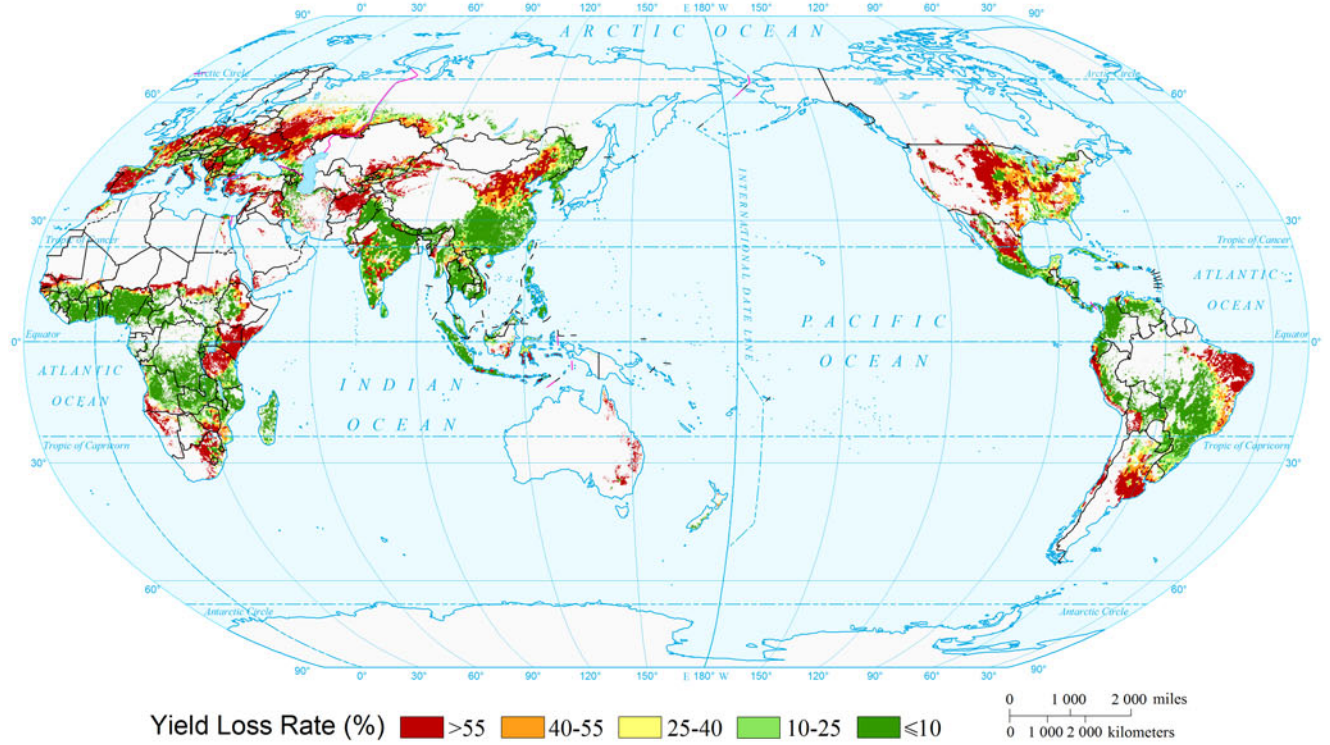
Maize Yield Loss Risk of Drought of the World by Return Period (10a)  
(0.5°×0.5°)



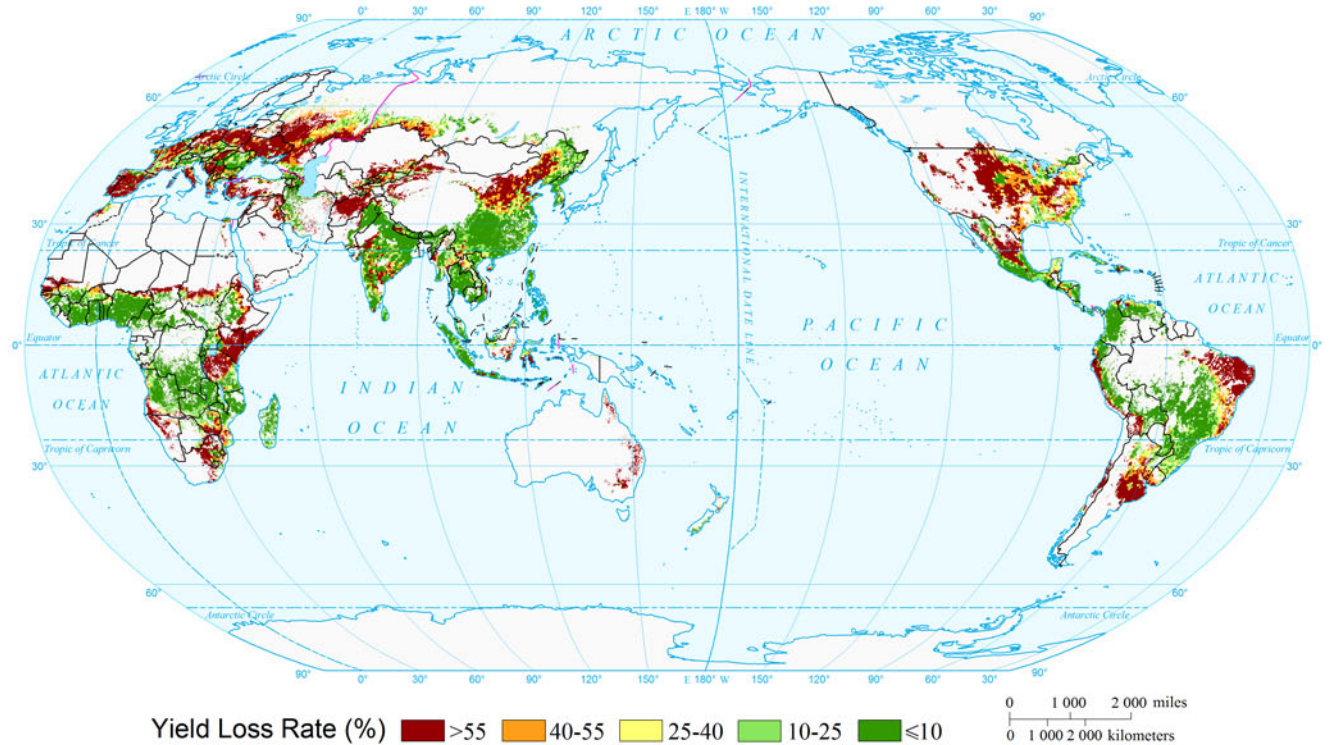
Maize Yield Loss Risk of Drought of the World by Return Period (20a)  
(0.5°×0.5°)



Maize Yield Loss Risk of Drought of the World by Return Period (50a)  
(0.5°×0.5°)



Maize Yield Loss Risk of Drought of the World by Return Period (100a)  
(0.5°×0.5°)

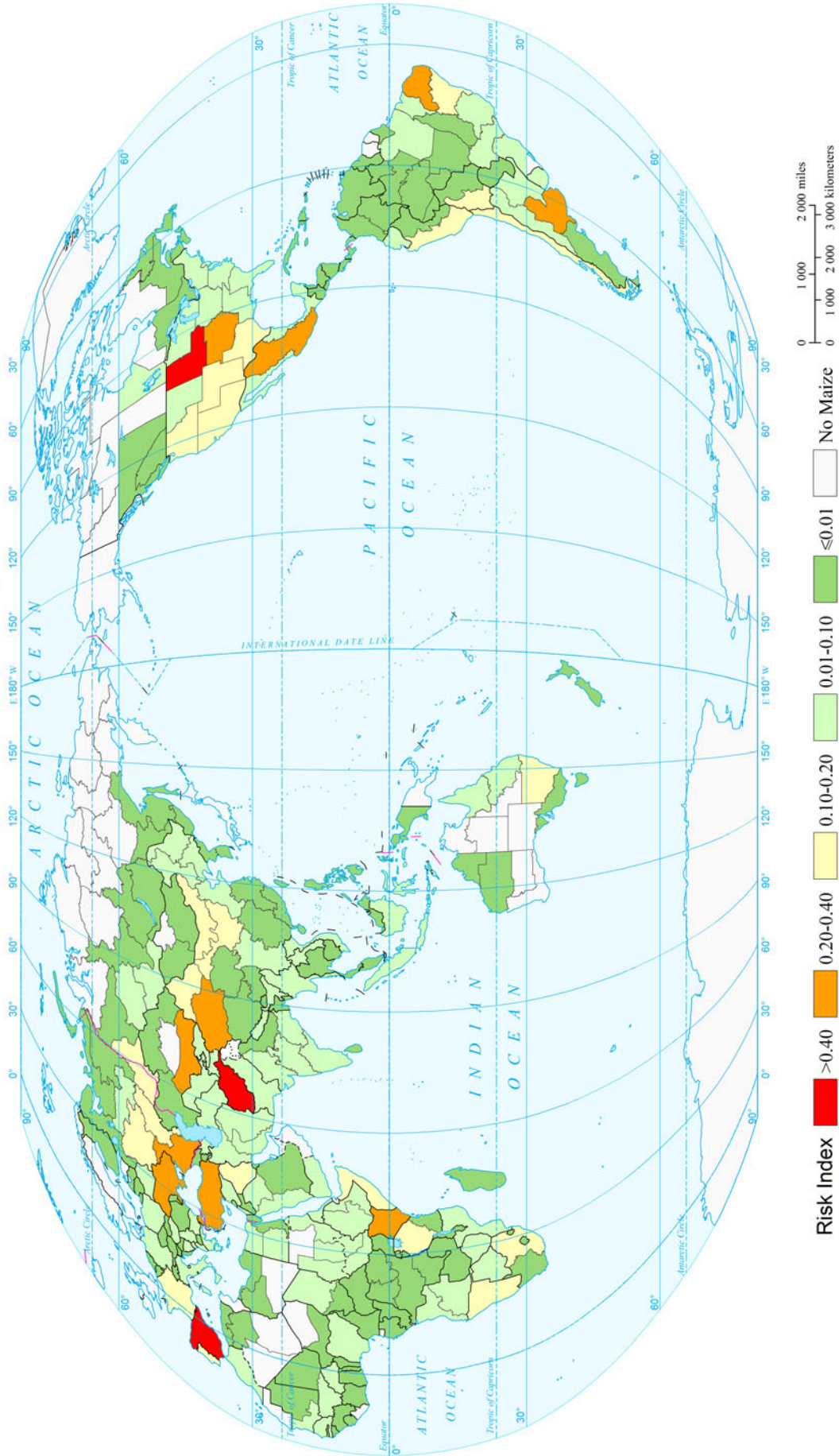




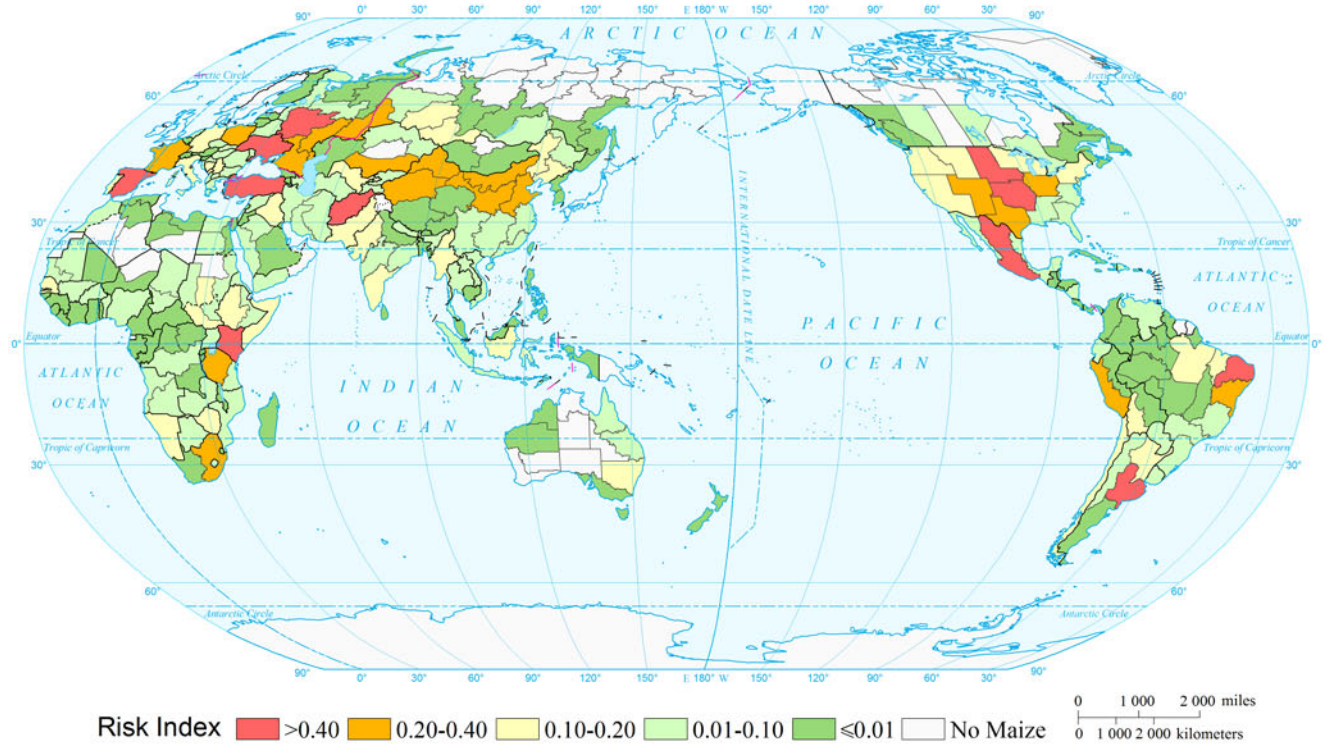
Maize

Drought Disasters

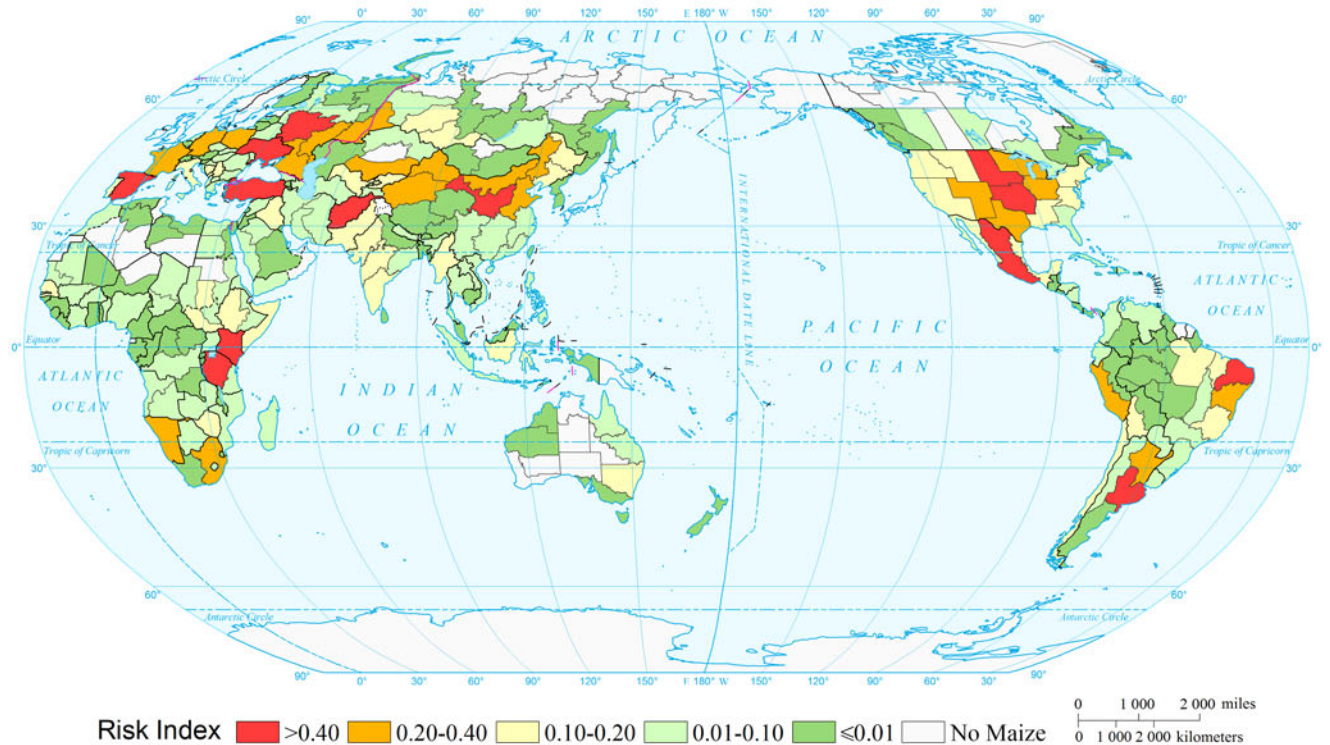
Expected Annual Maize Yield Loss Risk of Drought of the World  
(Comparable-geographic Unit)



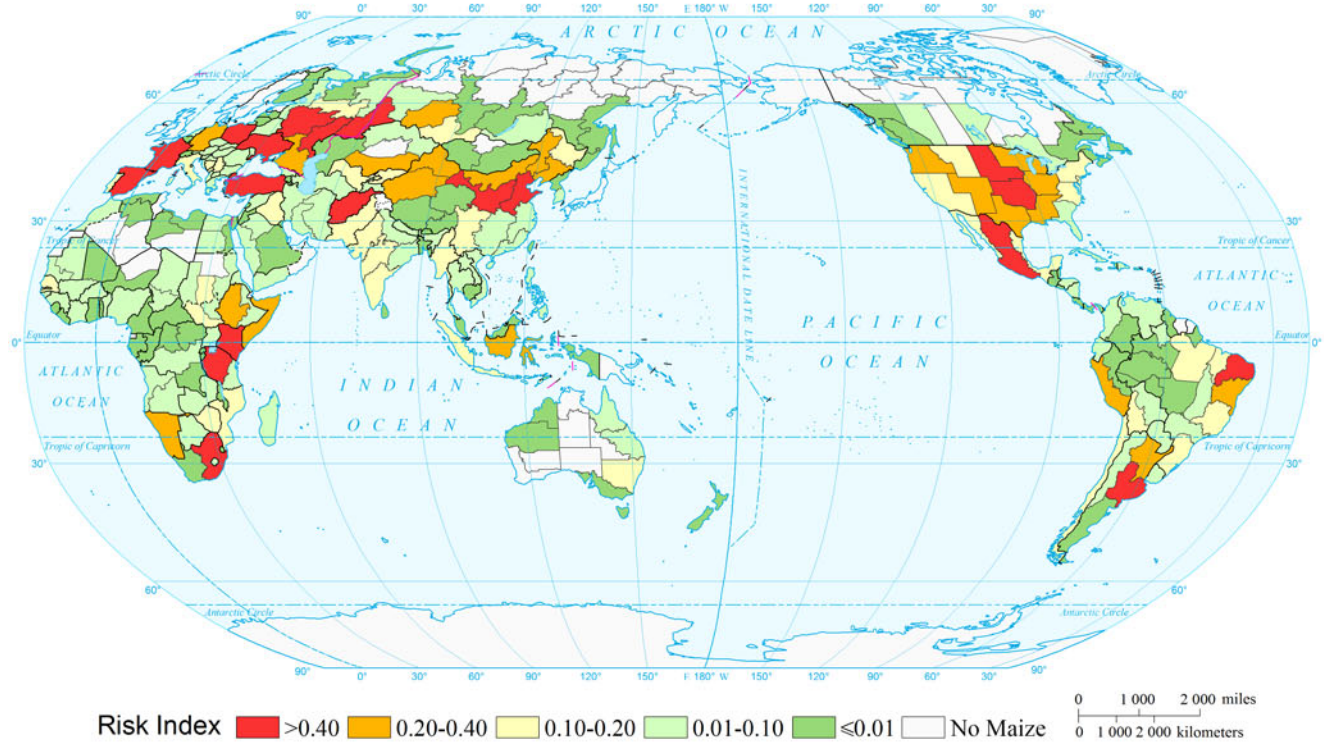
Maize Yield Loss Risk of Drought of the World by Return Period (10a)  
(Comparable-geographic Unit)



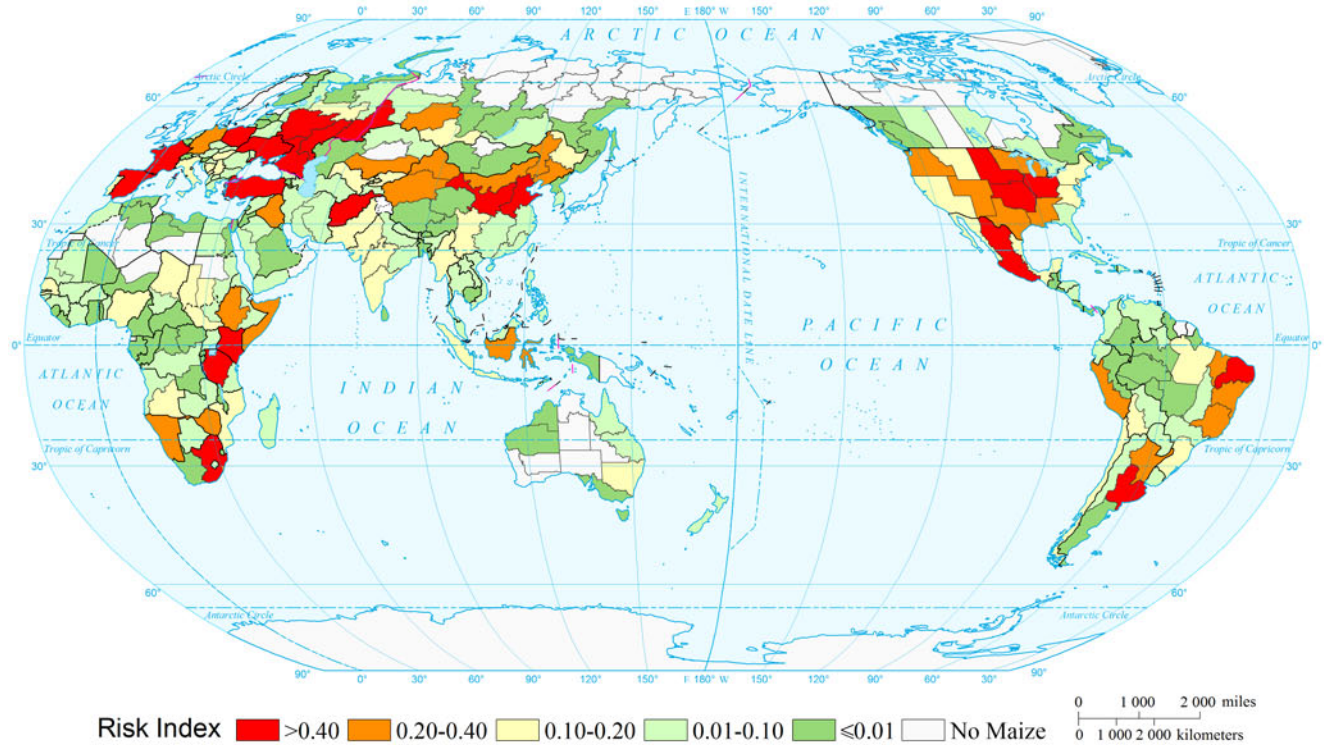
Maize Yield Loss Risk of Drought of the World by Return Period (20a)  
(Comparable-geographic Unit)



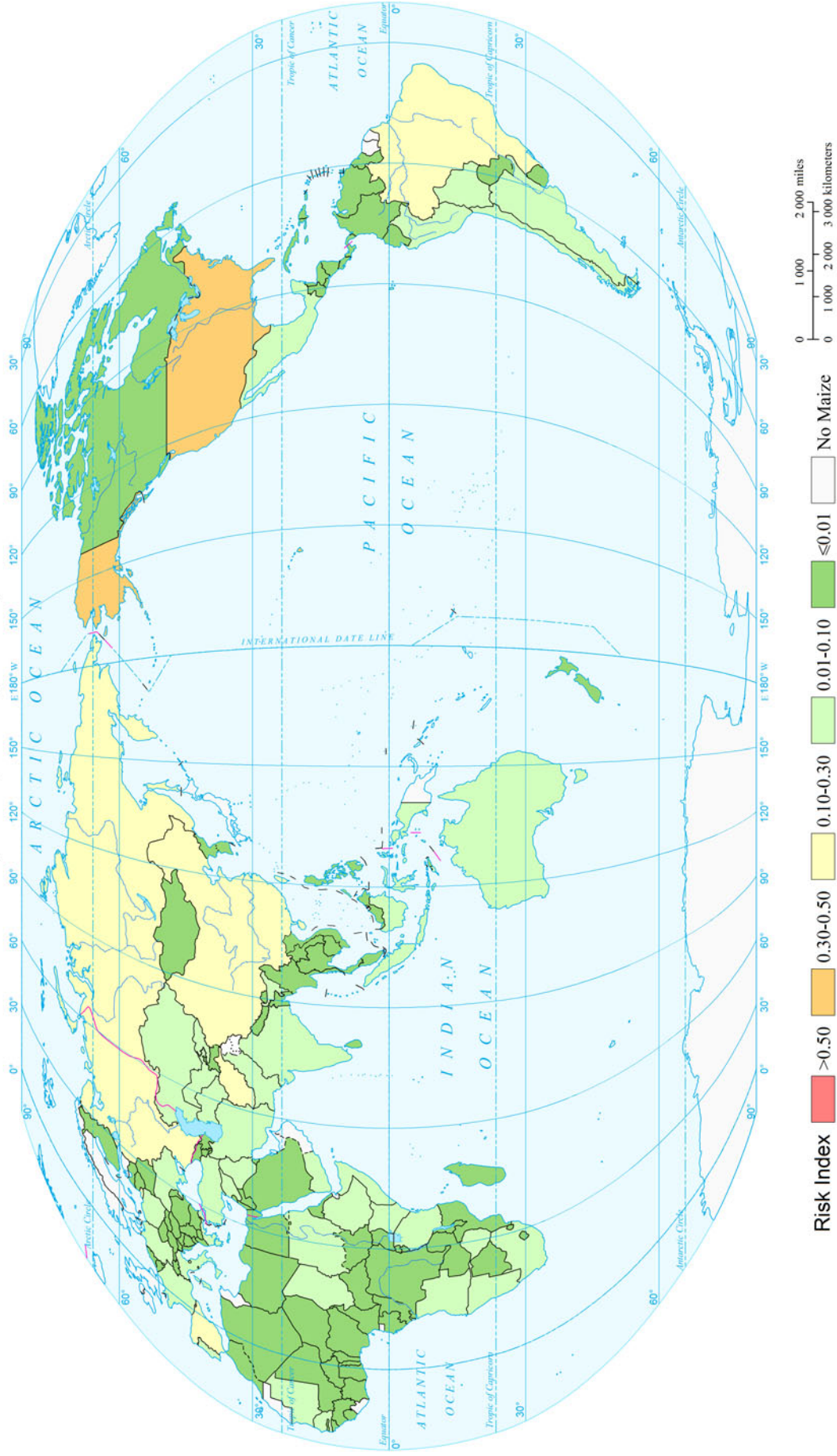
Maize Yield Loss Risk of Drought of the World by Return Period (50a)  
(Comparable-geographic Unit)



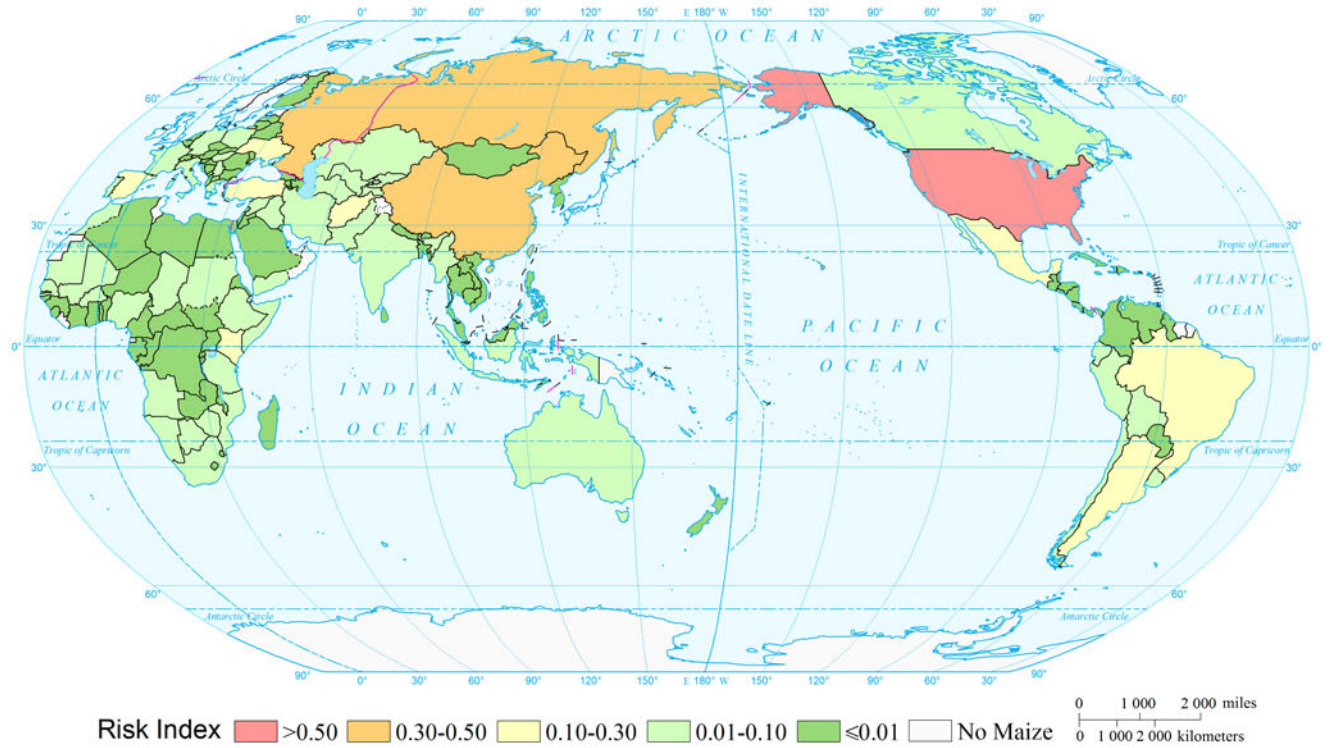
Maize Yield Loss Risk of Drought of the World by Return Period (100a)  
(Comparable-geographic Unit)



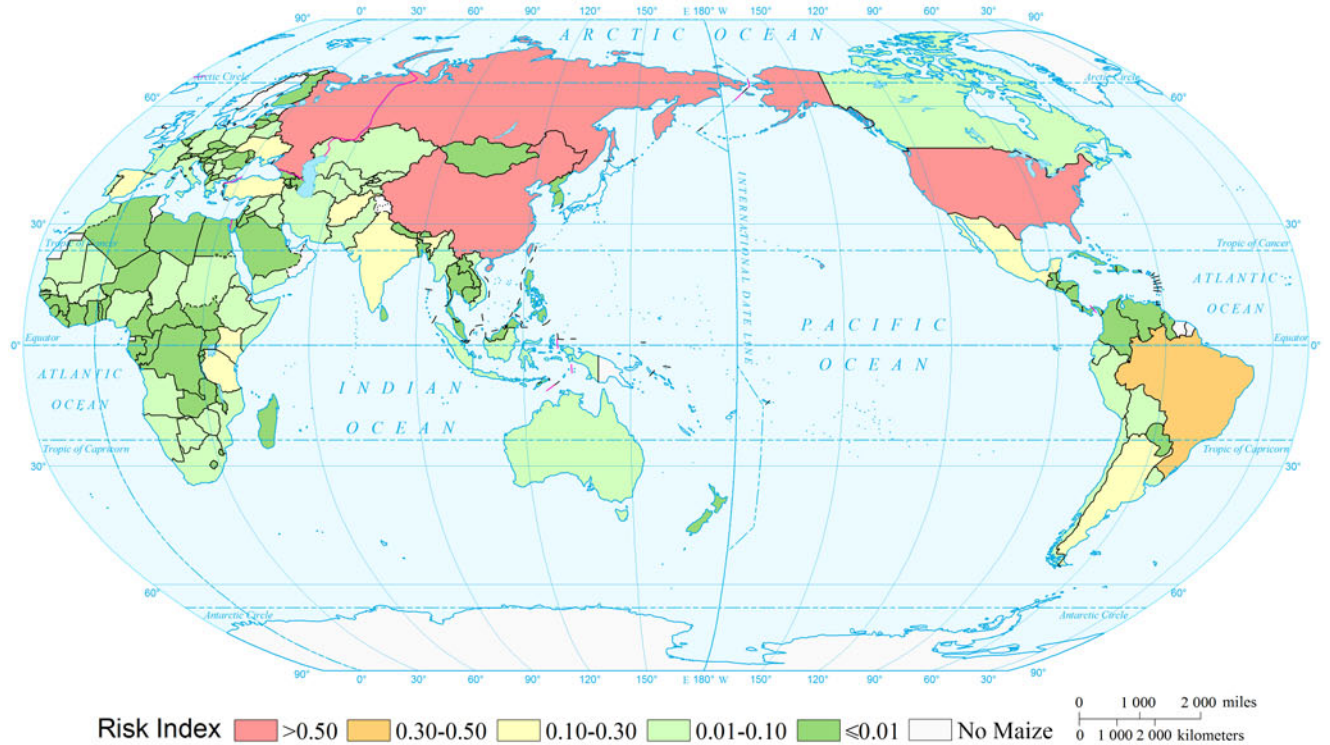
Expected Annual Maize Yield Loss Risk of Drought of the World  
(Country and Region Unit)



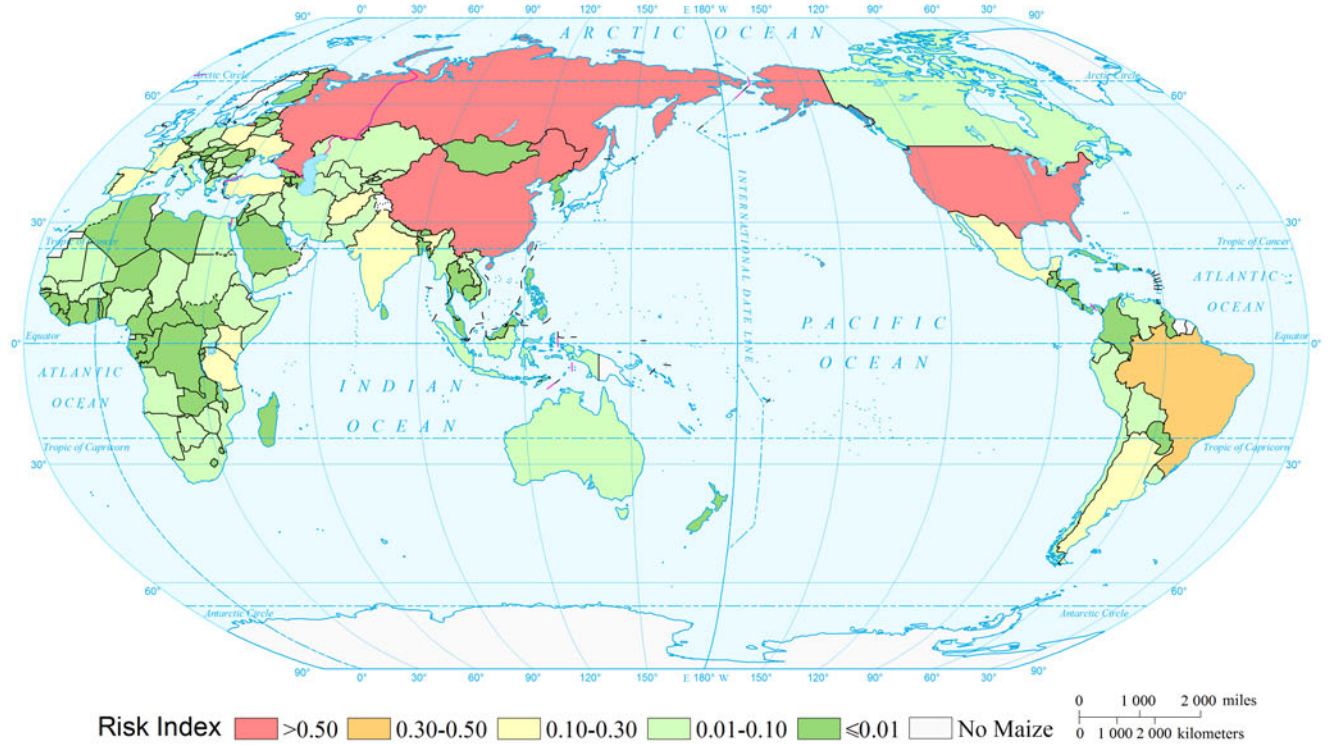
Maize Yield Loss Risk of Drought of the World by Return Period (10a)  
(Country and Region Unit)



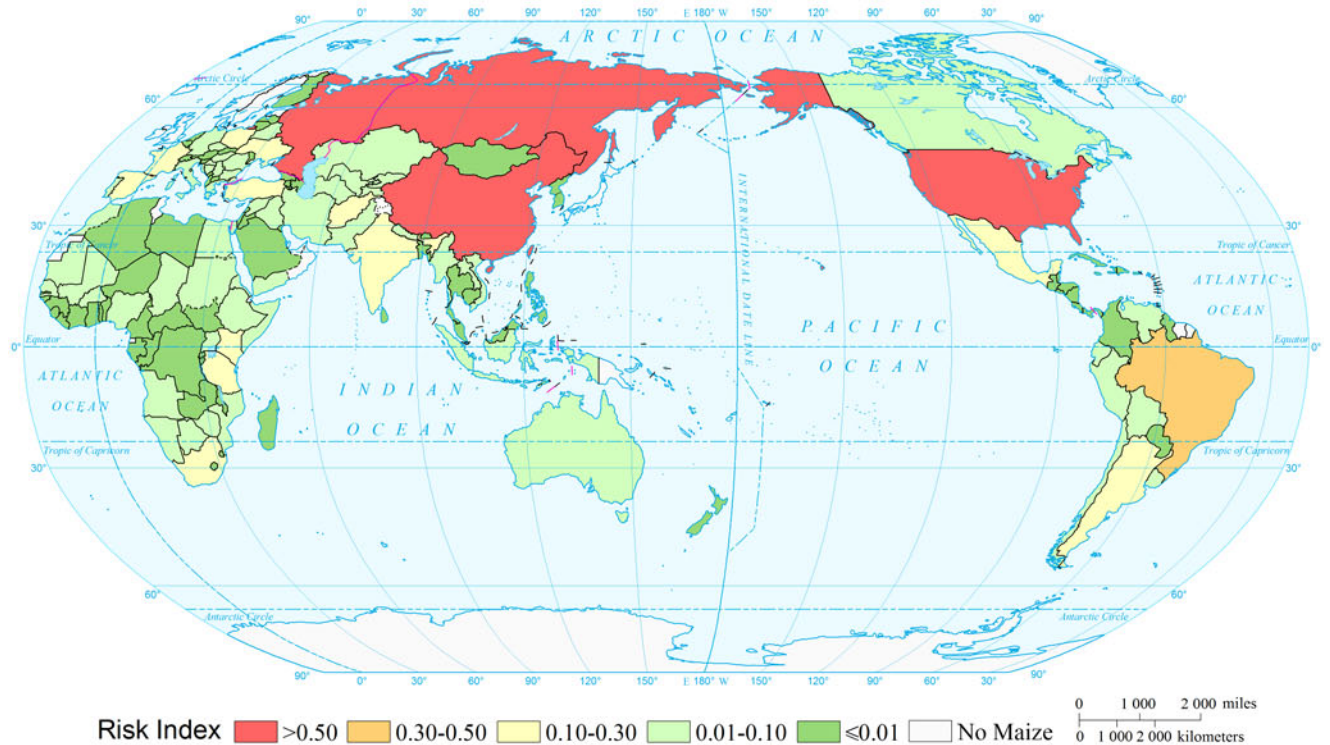
Maize Yield Loss Risk of Drought of the World by Return Period (20a)  
(Country and Region Unit)



Maize Yield Loss Risk of Drought of the World by Return Period (50a)  
(Country and Region Unit)



Maize Yield Loss Risk of Drought of the World by Return Period (100a)  
(Country and Region Unit)



## References

- Intergovernmental Panel on Climate Change (IPCC). 2012. *Managing the risks of extreme events and disasters to advance climate change adaptation*. A special report of working groups I and II of the Intergovernmental panel on climate change. Cambridge and New York: Cambridge University Press.
- Intergovernmental Panel on Climate Change (IPCC). 2013. *Summary for policymakers*. In: Climate change 2013: The physical science basis. Contribution of working group I to the fifth assessment report of the intergovernmental panel on climate change. Cambridge and New York: Cambridge University Press.
- Li, Y.P., W. Ye, M. Wang, et al. 2009. Climate change and drought: A risk assessment of crop-yield impacts. *Climate Research* 39(1): 31–46.
- Moss R.H., M. Babiker, S. Brinkman, et al. 2008. Towards new scenarios for analysis of emissions, climate change, impacts, and response strategies. Technical Summary, Intergovernmental Panel on Climate Change, Geneva.
- United Nations Development Programme (UNDP), Bureau for Crisis Prevention and Recovery. 2004. *Reducing disaster risk: A challenge for development*. New York: UNDP, Bureau for Crisis Prevention and Recovery.
- Yin, Y.Y., X.M. Zhang, D.G. Lin, et al. 2014. GEPIC-V-R model: a GIS-based tool for regional crop drought risk assessment. *Agricultural Water Management* 144: 107–119.

---

# Mapping Drought Risk (Wheat) of the World

Xingming Zhang, Hao Guo, Weixia Yin, Ran Wang, Jian Li, Yaojie Yue,  
and Jing'ai Wang

---

## 1 Background

Drought is one of the disasters that most widely affect and damage agricultural production in the world. Nearly half of the countries in the world bear severe drought (UNDP 2004; Moss et al. 2008). There is very serious drought in North America, Mexico, central and southern part of Africa, part of South America, and in northern part of China (IPCC 2012). Research shows that under the background of climate warming many regions in the world have an increasing risk of future drought because of the reduced precipitation and aggravating evaporation (IPCC 2012, 2013).

Agricultural drought risk, which is defined as the possible yield loss of crops exposed to drought, can be considered as the probability of the occurrence of agricultural drought and the negative impact on agricultural production (Yin et al. 2014). The drought risk of food production was assessed based on drought frequency and intensity, production levels, and adaptability at global scale (Li et al. 2009). Assessing and mapping maize drought risk of the world were made based on GEPIC-Vulnerability-Risk (GEPIC-V-R) model (Yin et al. 2014).

---

**Mapping Editors:** Jing'ai Wang (Key Laboratory of Regional Geography, Beijing Normal University, Beijing 100875, China), Chunqin Zhang (School of Geography, Beijing Normal University, Beijing 100875, China) and Shujuan Cui (School of Geography, Beijing Normal University, Beijing 100875, China).

**Language Editor:** Wei Xu (Key Laboratory of Environmental Change and Natural Disaster, Ministry of Education, Beijing Normal University, Beijing 100875, China).

X. Zhang · W. Yin · R. Wang · J. Li  
School of Geography, Beijing Normal University, Beijing 100875,  
China

H. Guo · Y. Yue · J. Wang (✉)  
Key Laboratory of Regional Geography, Beijing Normal  
University, Beijing 100875, China  
e-mail: jwang@bnu.edu.cn

In this study, the wheat yield loss risk of drought at global scale is assessed and mapped based on the GEPIC-V-R model developed by Yin et al. (2014). The vulnerability of wheat to drought is simulated at grid level ( $0.5^\circ \times 0.5^\circ$ ), which improved the spatial resolution compared with the work of Yin et al. (2014).

---

## 2 Method

Figure 1 shows the technical flowchart for mapping wheat yield loss risk of drought of the world.

### 2.1 Model

In the GEPIC-V-R model (Yin et al. 2014), drought risk is treated as the function of hazard, vulnerability of exposure, and environment (Eq. 1).

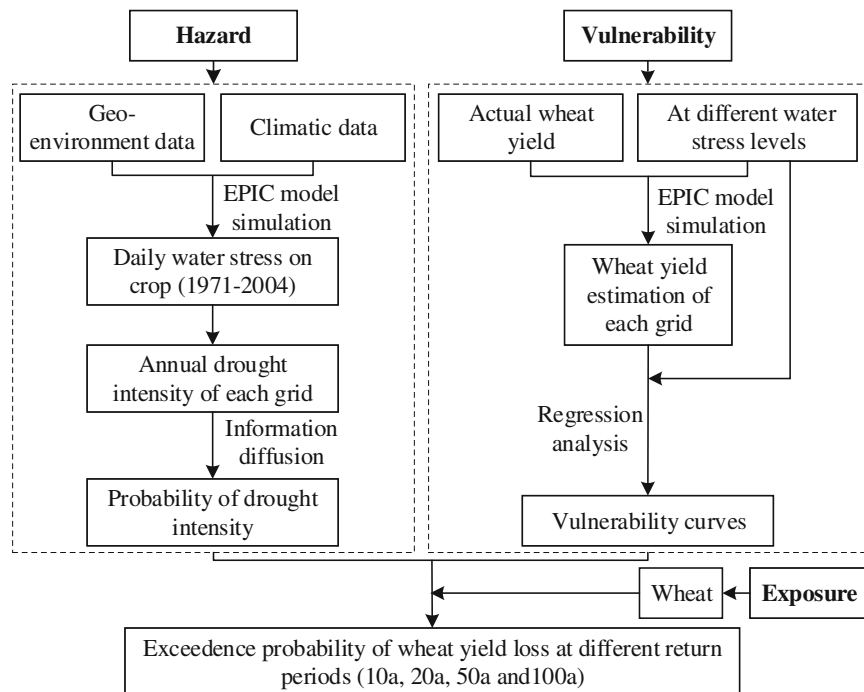
$$R = f(E, H, V) = H\{P, h_E\} \times V\{l_E, h_E\} \quad (1)$$

where  $E$  is the sensitivity of environment;  $H$  is the drought;  $V$  is vulnerability;  $P$  is the occurrence probability of drought;  $h_E$  is the drought intensity index; and  $l_E$  is the loss rate.  $H\{P, h_E\}$  is the drought intensity under a certain probability.  $V\{l_E, h_E\}$  determines the relationship between  $h_E$  and  $l_E$ .

GEPIC-V-R model is a crop risk assessment model for large scale (i.e., regional, national, continental, and global) with functions to fit vulnerability curves and calculate risk. In this model, there are four modules: model calibration module, hazard module, vulnerability module, and risk calculation module (Yin et al. 2014).

Data for assessing the wheat yield loss risk by drought of the world consist of crop growth environment data (Appendix III, Environments data 2.1, 2.2, and 2.7, Appendix III, Hazards data 4.15), crop management data

**Fig. 1** The technical flowchart for mapping wheat yield loss risk of drought of the world



(Appendix III, Environments data 3.13–3.16), crop species attribute data (Appendix III, Environments data 3.18), and actual yield data (Appendix III, Environments data 3.17).

## 2.2 Spatial Resolution

Compared with the work of Yin et al. (2014), the vulnerability of wheat to drought is simulated at grid level ( $0.5^\circ \times 0.5^\circ$ ) instead of the regional level which greatly improves the spatial resolution. Furthermore, the wheat exposure is calculated and mapped at  $5' \times 5'$  grid level in this study, instead of  $0.5^\circ \times 0.5^\circ$  grid level done by Yin et al. (2014).

## 3 Results

### 3.1 Intensity

Areas with high value of drought intensity on spring wheat is mainly distributed in Mongolian Plateau, Indian River plains in Asia, Mexican plateau in North America and Andes

Mountains in South America, Mediterranean coast, the Great Rift Valley, and Orange River Basin in Africa. Areas with high value of drought intensity on winter wheat is mainly distributed in the hemisphere of  $30^\circ\text{N}$ – $60^\circ\text{N}$ , including the Hindu Kush Mountains in Central Asia, Great Britain, Paris Basin and North European Plain in Europe, and the Rocky Mountains in America.

### 3.2 Vulnerability

Based on the GEPIC-V-R model, vulnerability curves of wheat to drought for each grid ( $0.5^\circ \times 0.5^\circ$ ) are fitted (Fig. 2).

### 3.3 Risk

By zonal statistics of the expected risk result, the expected annual wheat yield loss risk of drought of the world at national level is derived and ranked (Fig. 3). The top 1 % country with the highest expected annual wheat yield loss

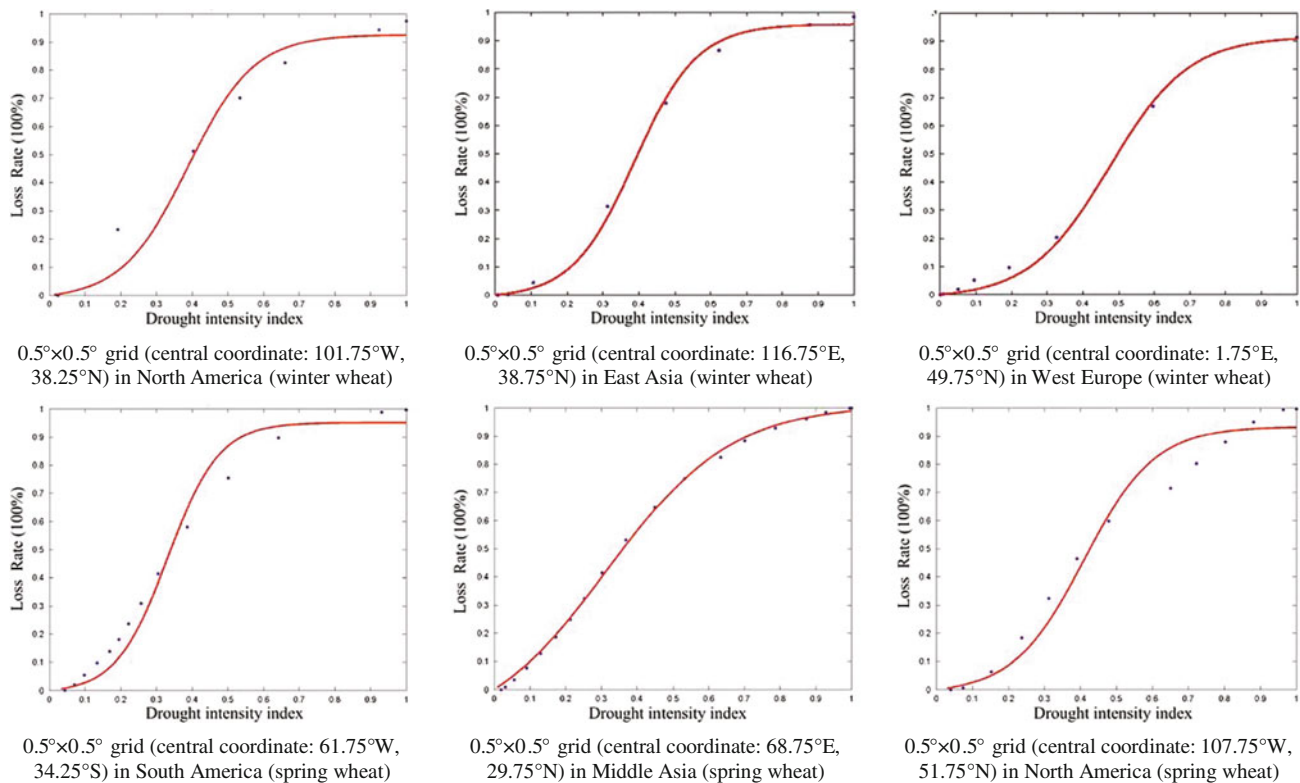


**Fig. 2** Examples of vulnerability curve of wheat to drought



**Fig. 3** Expected annual wheat yield loss risk of drought of the world. 1 (0, 10 %]. China, Russia, USA, Kazakhstan, Canada, Kenya, Mongolia, Pakistan, Mexico, Chile, South Africa, and Afghanistan. 2 (10, 35 %]. Argentina, Spain, Peru, Bolivia, Australia, India, Turkey, Morocco, Iraq, Ethiopia, Kyrgyzstan, Turkmenistan, Germany, Algeria, Saudi Arabia, Syria, Uzbekistan, Italy, Egypt, Iran, Zimbabwe, United Kingdom, Yemen, Portugal, Tajikistan, Brazil, Sudan, Greece, and Poland. 3 (35, 65 %]. Finland, Uruguay, France, Tanzania, Jordan, New Zealand, Ukraine, Lebanon, Burma, North Korea, Eritrea, Libya, Israel, the Netherlands, Gaza Strip, Sweden, Tunisia, Denmark, Nepal,

Lesotho, Norway, Belarus, Paraguay, Ireland, Oman, Nigeria, Lithuania, Niger, Belgium, Azerbaijan, Uganda, Ecuador, Latvia, Estonia, and South Sudan. 4 (65, 90 %]. Malawi, Bosnia and Herzegovina, Armenia, Czech Republic, Serbia, Japan, Georgia, Zambia, Montenegro, Romania, Macedonia, Kuwait, Bhutan, Bulgaria, Croatia, Botswana, Mali, Guatemala, Honduras, Hungary, Luxembourg, South Korea, Slovenia, Madagascar, Thailand, Albania, Vietnam, Somalia, and Swaziland. 5 (90, 100 %]. Slovakia, Austria, Laos, Bangladesh, Switzerland, Cameroon, San Marino, Mozambique, Moldova, El Salvador, Colombia, and Burundi

risk of drought is China, and the top 10 % countries are China, Russia, USA, Kazakhstan, Canada, Kenya, Mongolia, Pakistan, Mexico, Chile, South Africa, and Afghanistan.

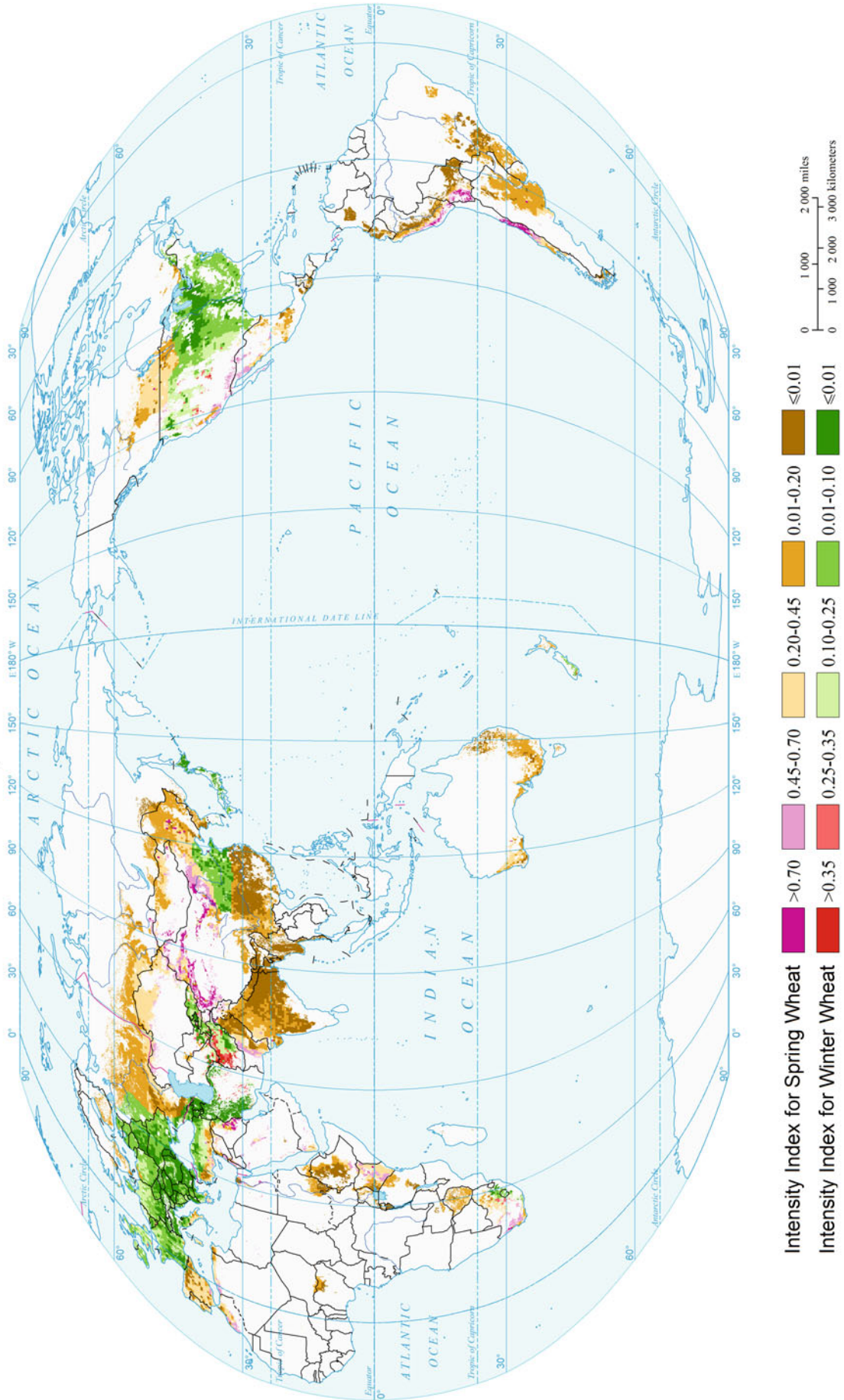
**4 Maps**



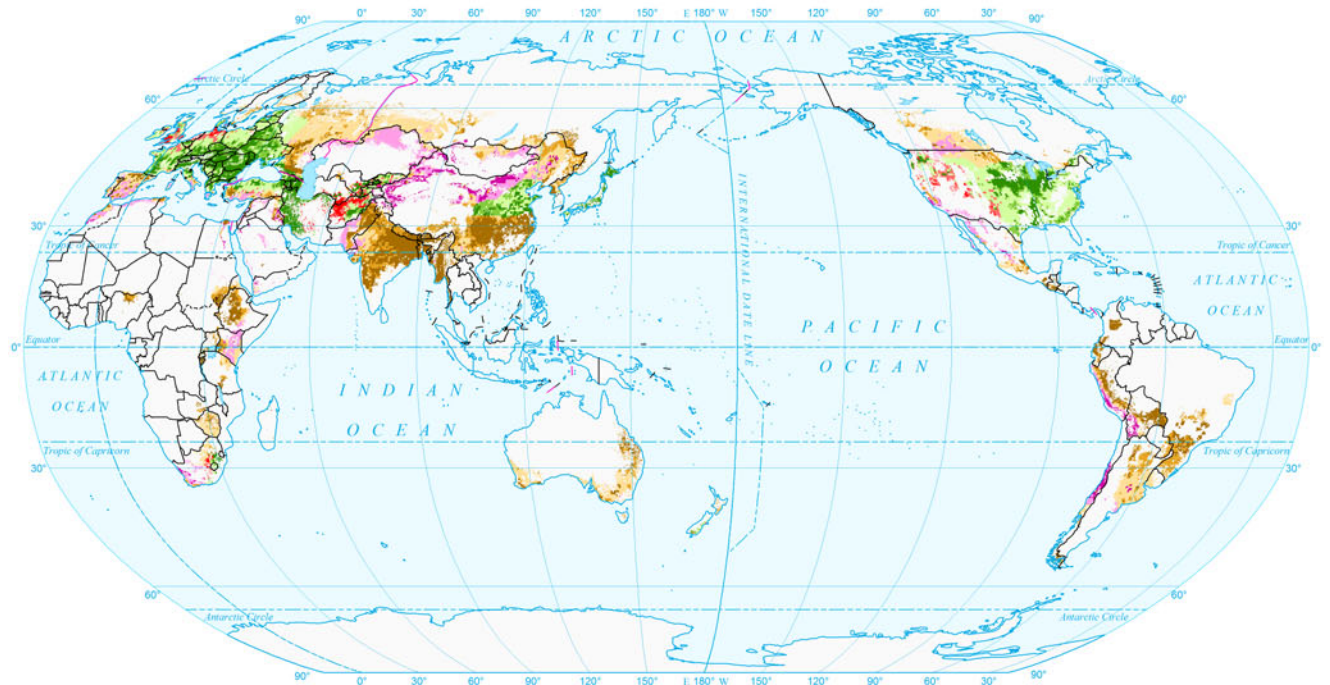
Wheat

Drought Disasters

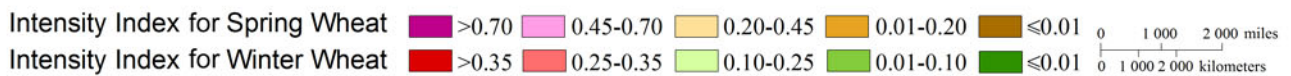
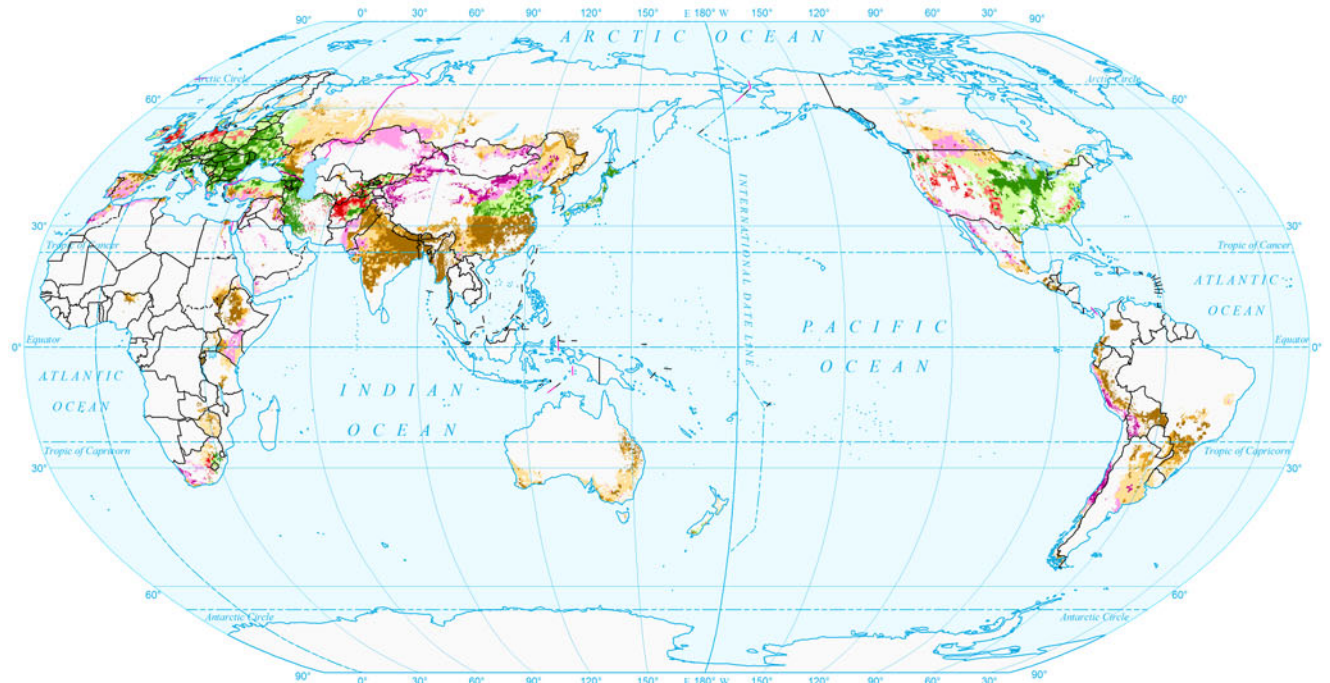
Global Expected Annual Drought Intensity for Wheat (0.5°x0.5°)



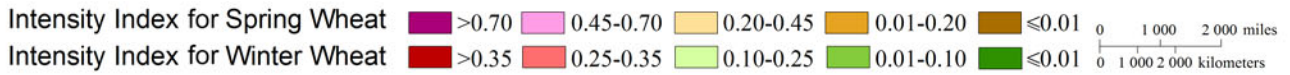
Global Drought Intensity for Wheat by Return Period (10a)  
(0.5°×0.5°)



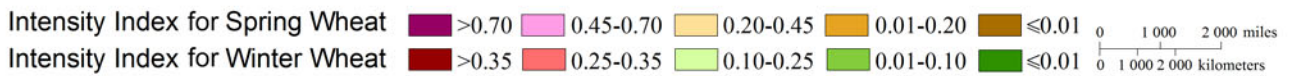
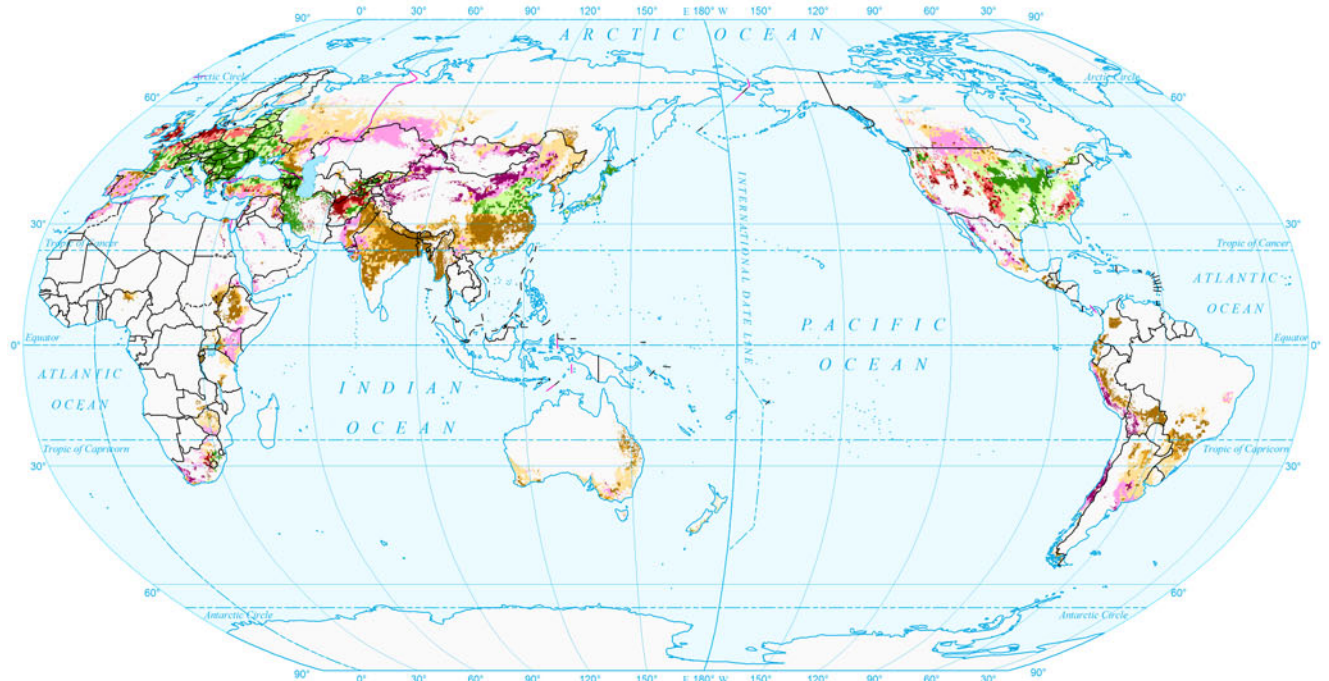
Global Drought Intensity for Wheat by Return Period (20a)  
(0.5°×0.5°)



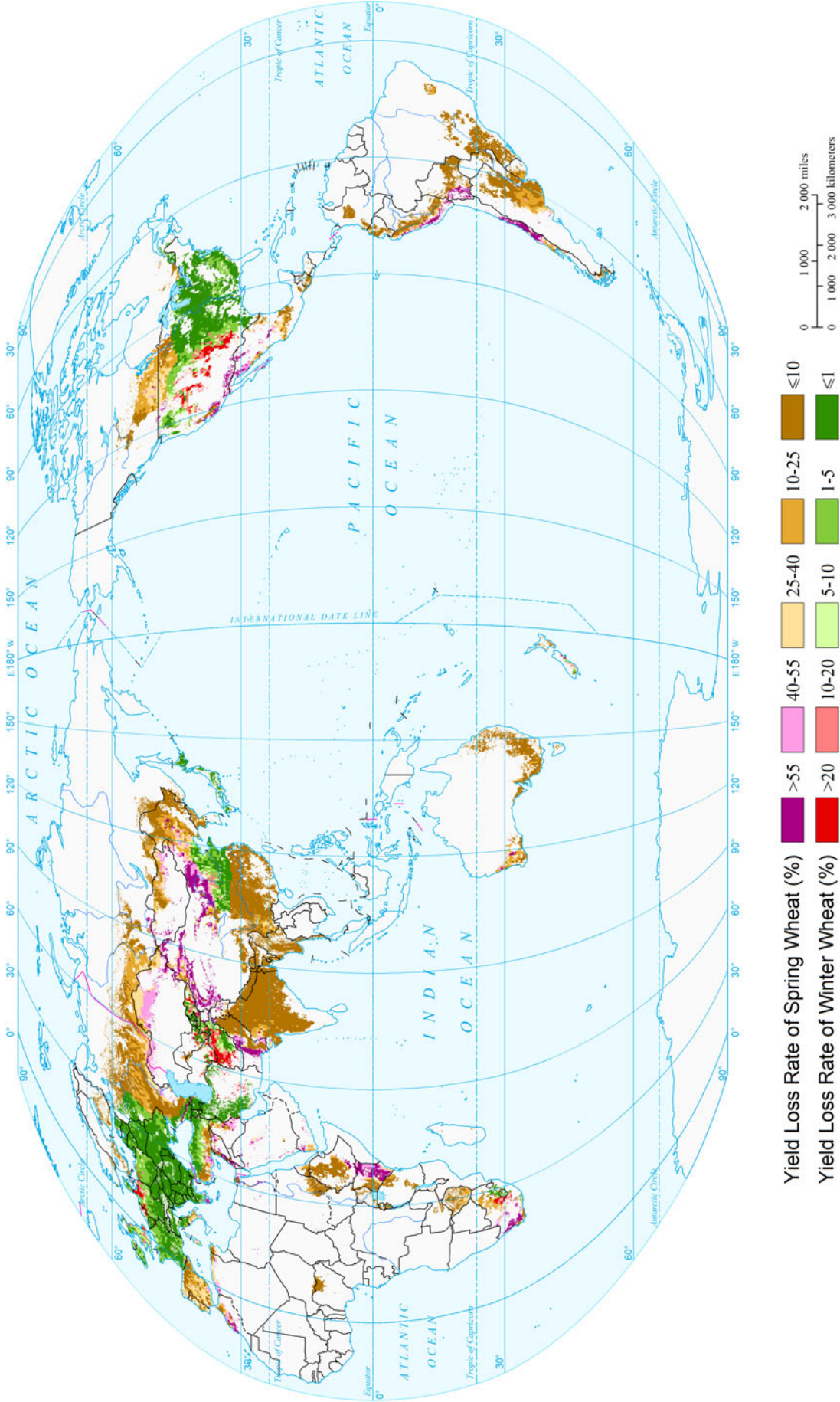
### Global Drought Intensity for Wheat by Return Period (50a) (0.5°×0.5°)



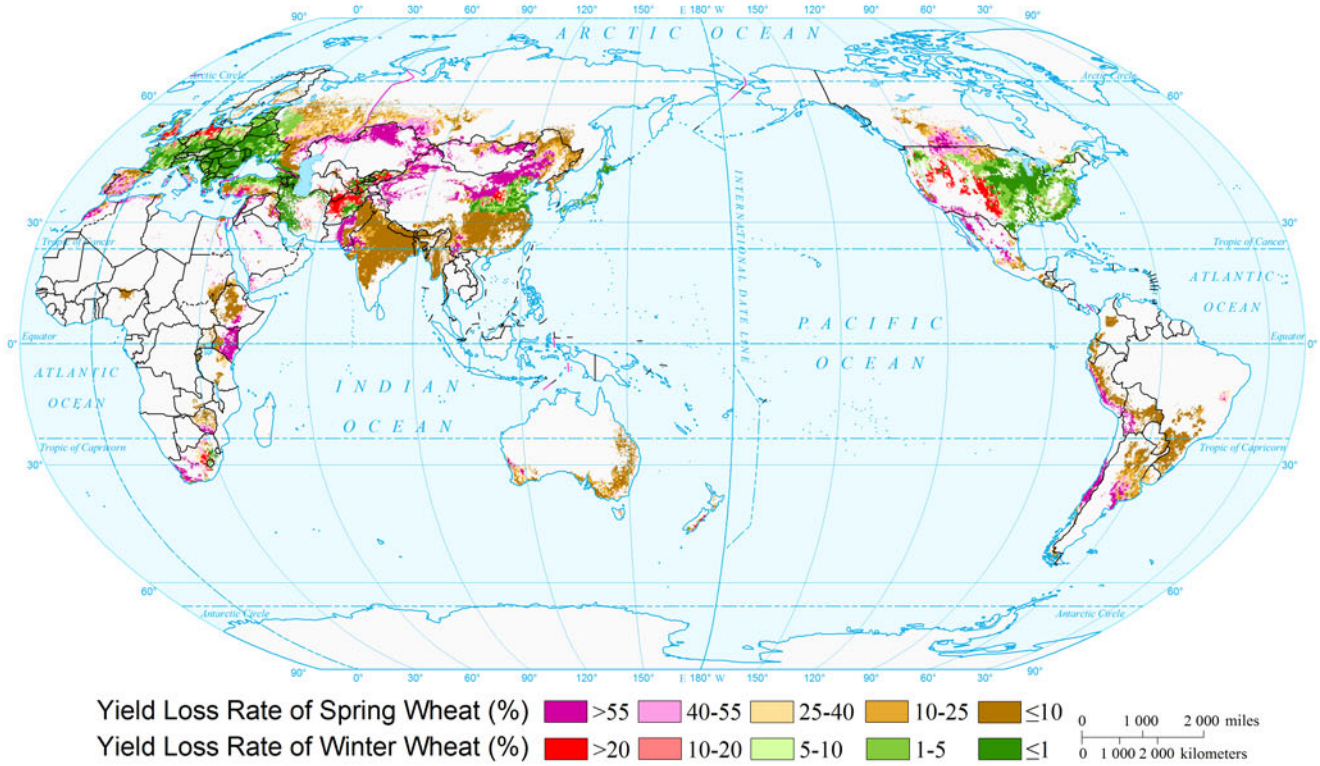
### Global Drought Intensity for Wheat by Return Period (100a) (0.5°×0.5°)



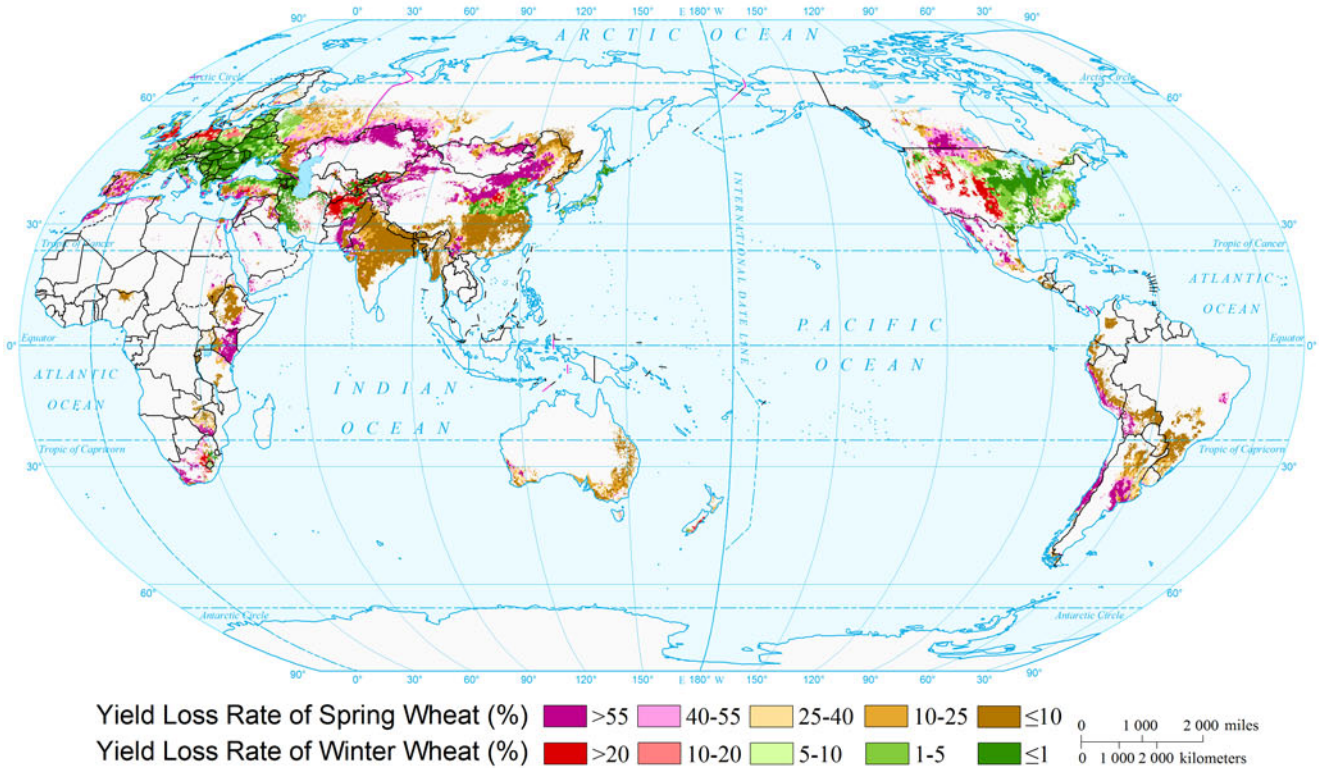
Expected Annual Wheat Yield Loss Risk of Drought of the World (0.5°x0.5°)



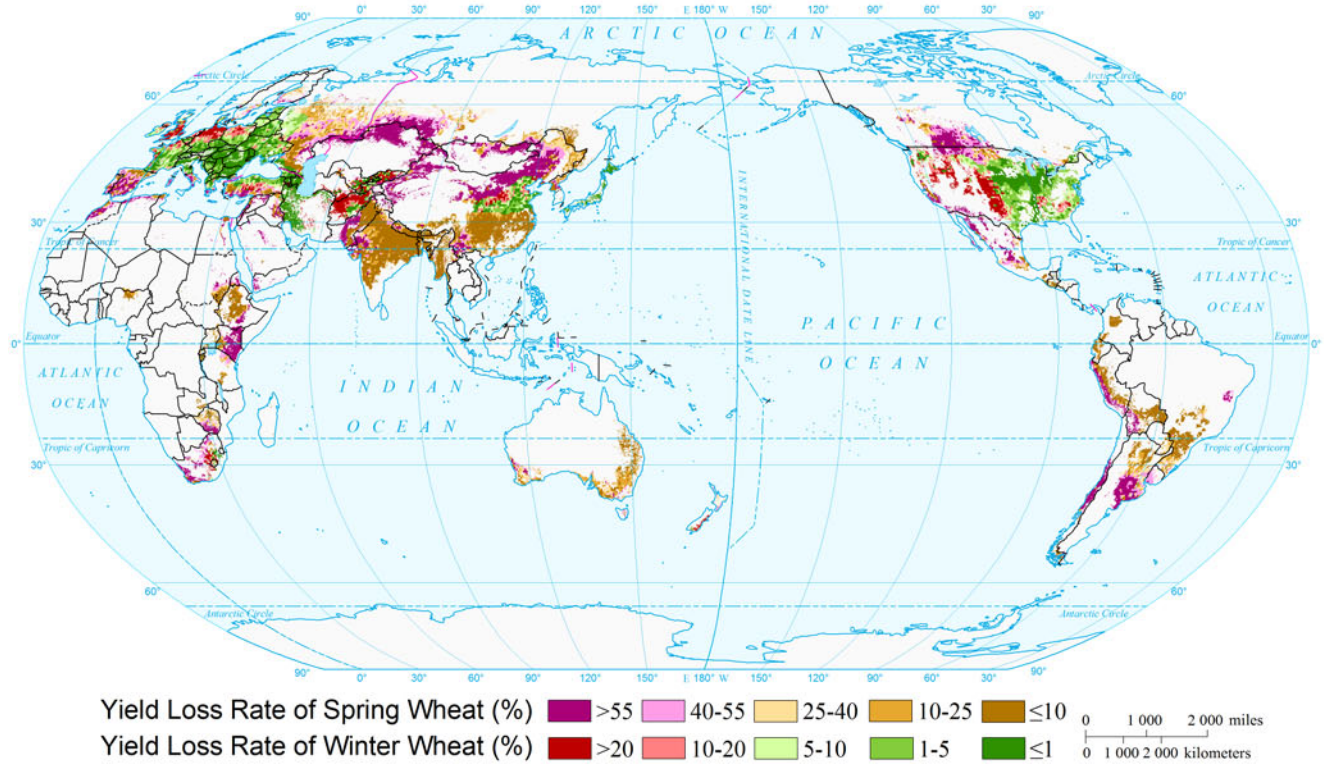
Wheat Yield Loss Risk of Drought of the World by Return Period (10a)  
(0.5°×0.5°)



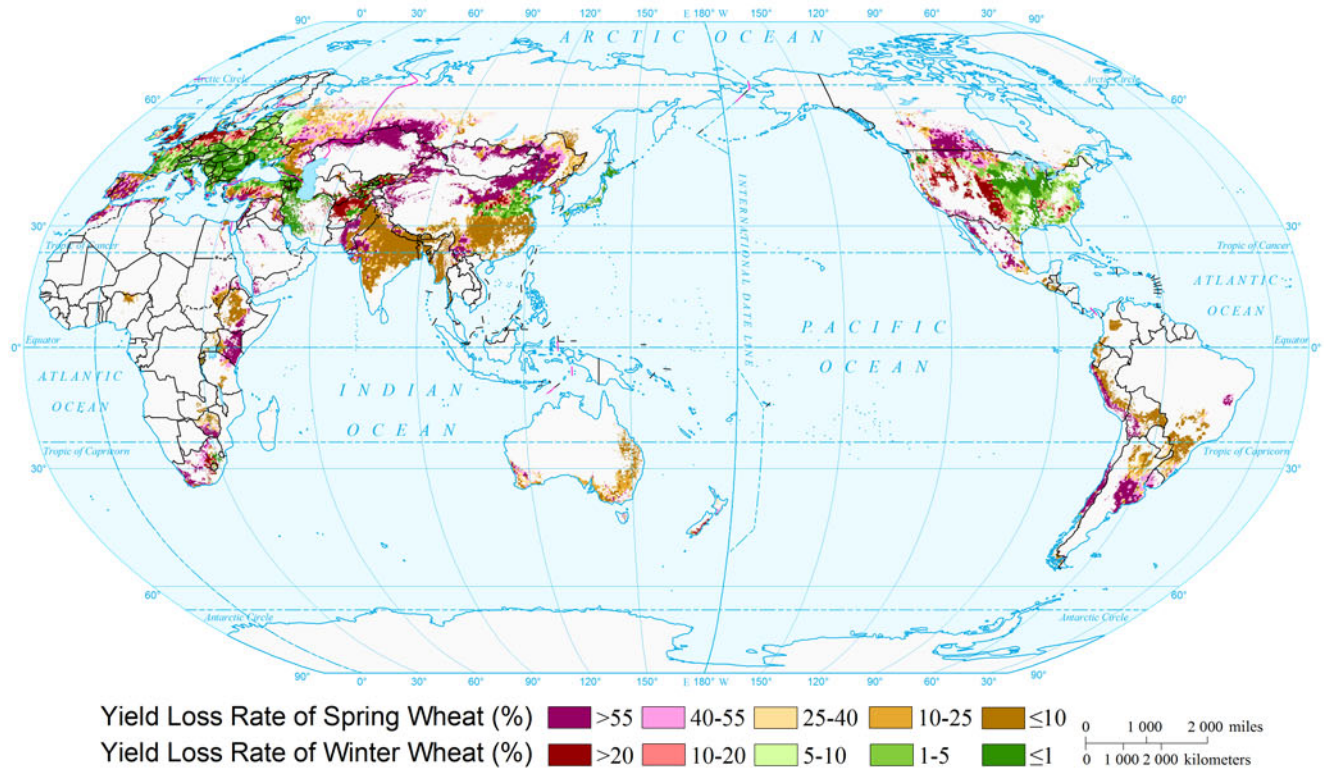
Wheat Yield Loss Risk of Drought of the World by Return Period (20a)  
(0.5°×0.5°)



Wheat Yield Loss Risk of Drought of the World by Return Period (50a)  
(0.5°×0.5°)



Wheat Yield Loss Risk of Drought of the World by Return Period (100a)  
(0.5°×0.5°)

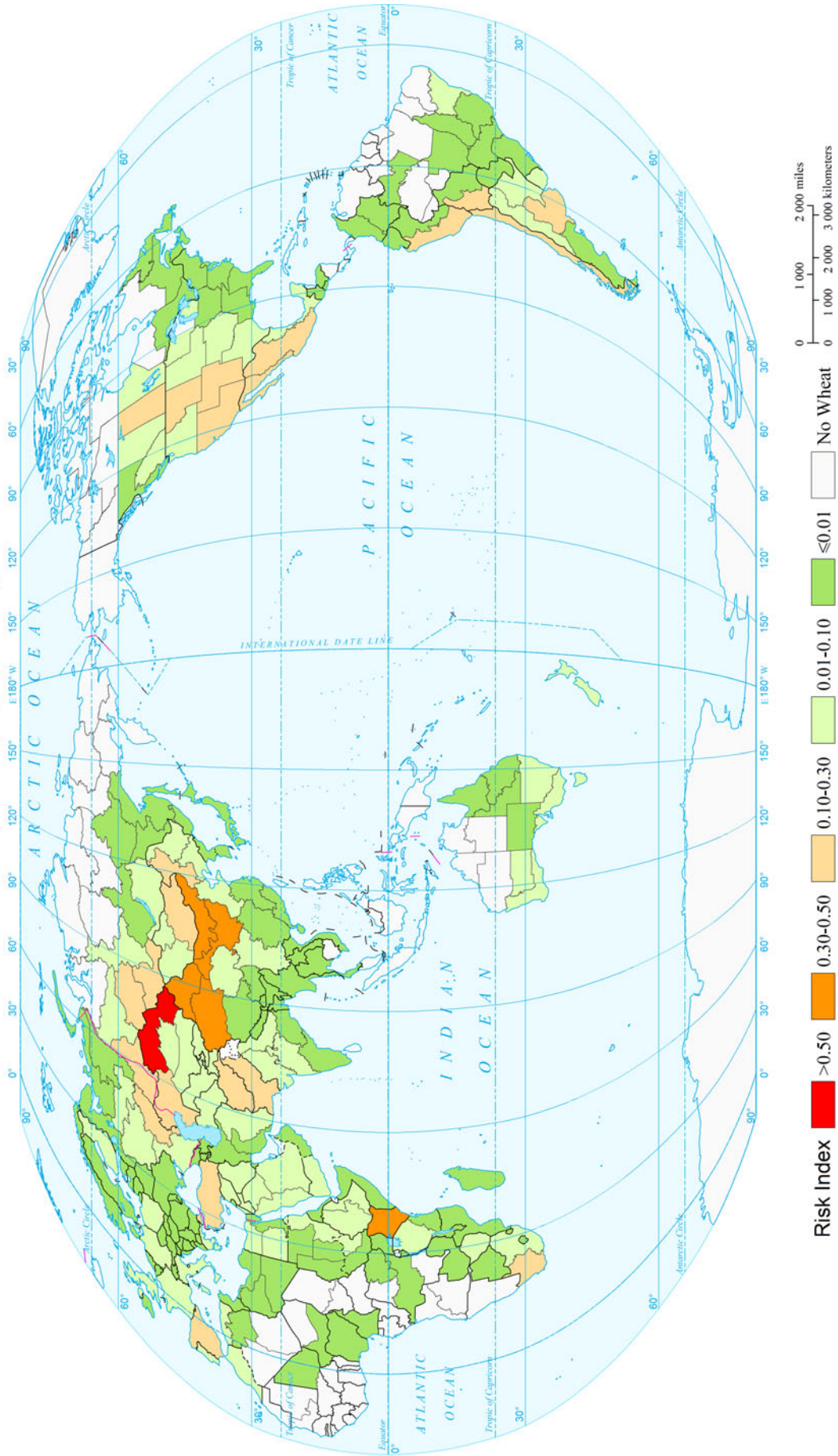




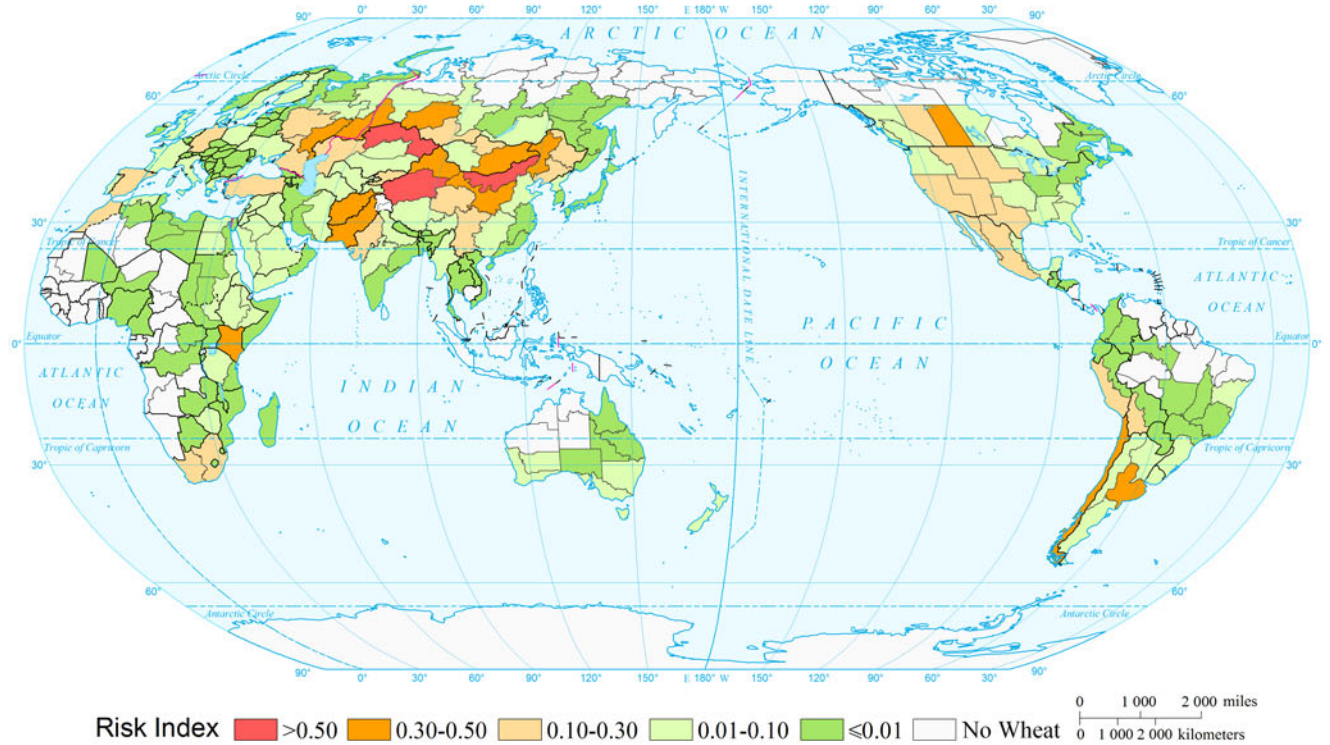
Wheat

Drought Disasters

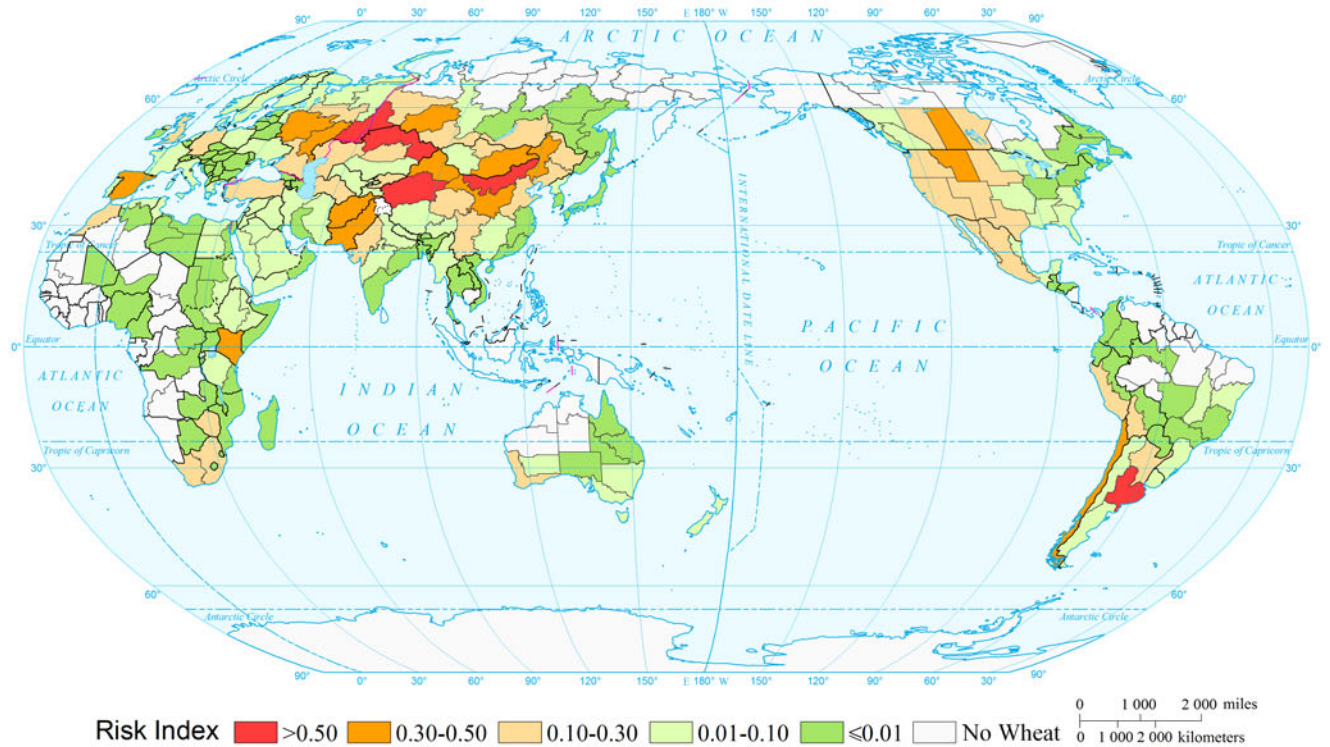
Expected Annual Wheat Yield Loss Risk of Drought of the World  
(Comparable-geographic Unit)



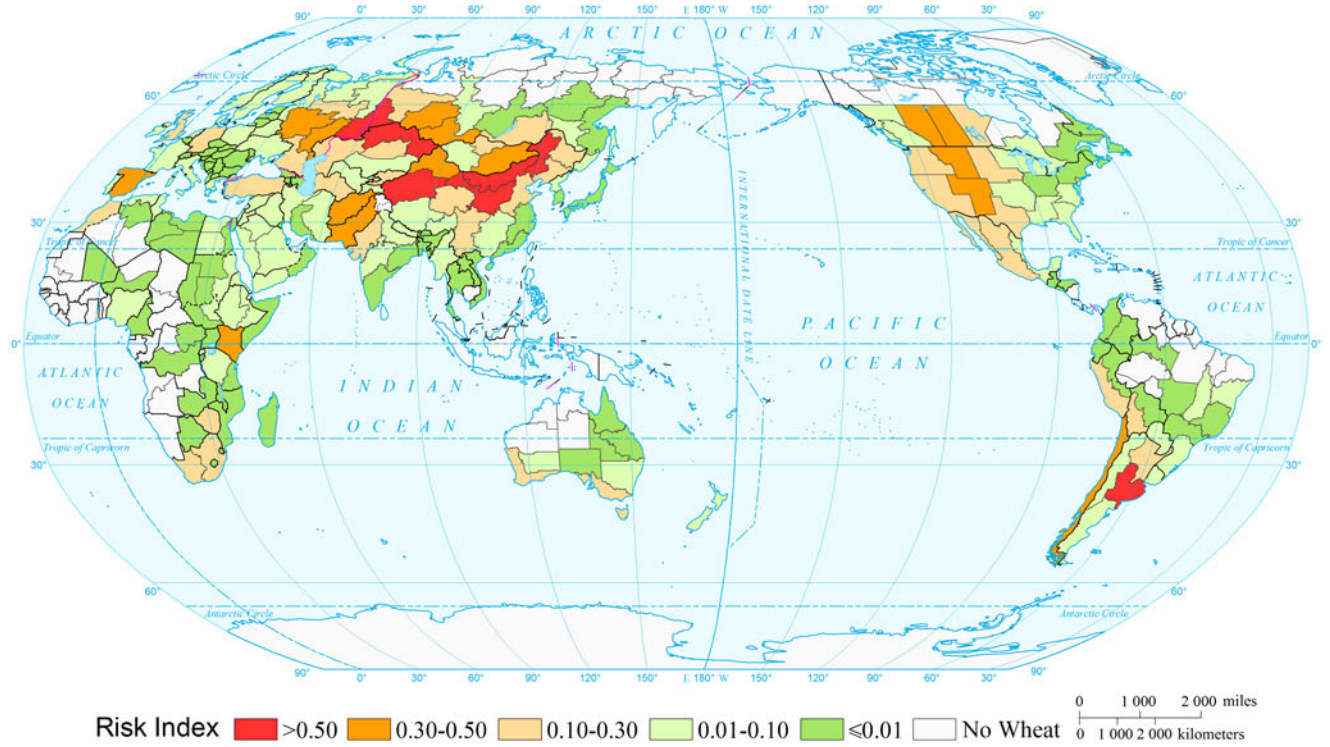
Wheat Yield Loss Risk of Drought of the World by Return Period (10a)  
(Comparable-geographic Unit)



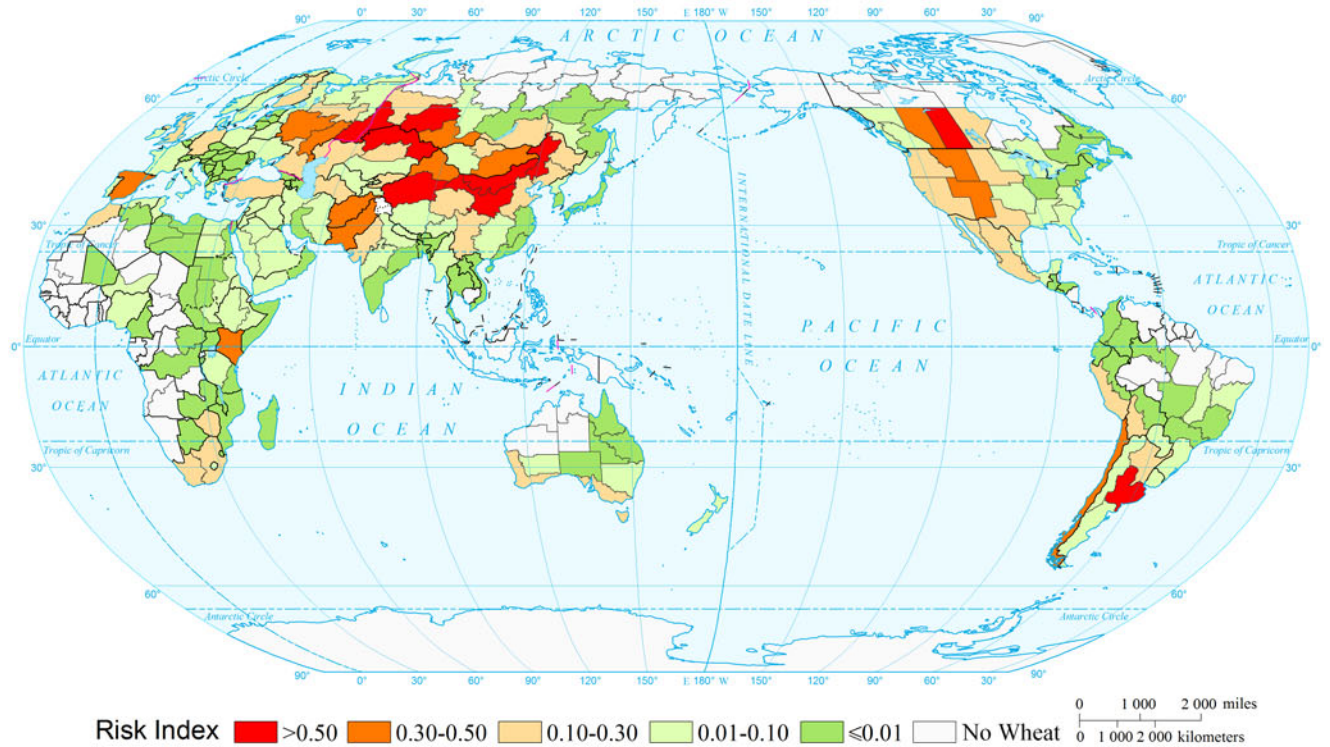
Wheat Yield Loss Risk of Drought of the World by Return Period (20a)  
(Comparable-geographic Unit)



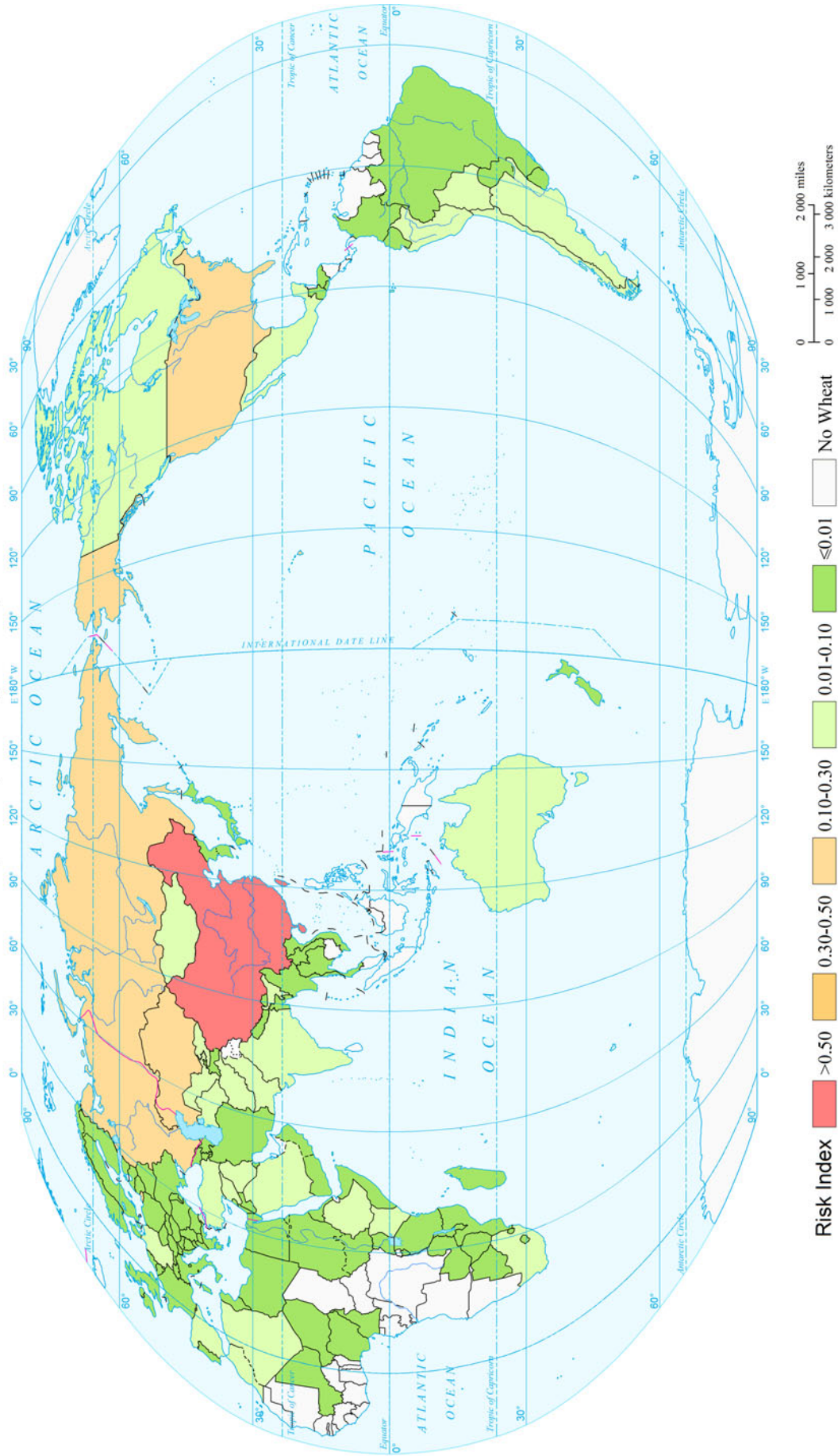
### Wheat Yield Loss Risk of Drought of the World by Return Period (50a) (Comparable-geographic Unit)



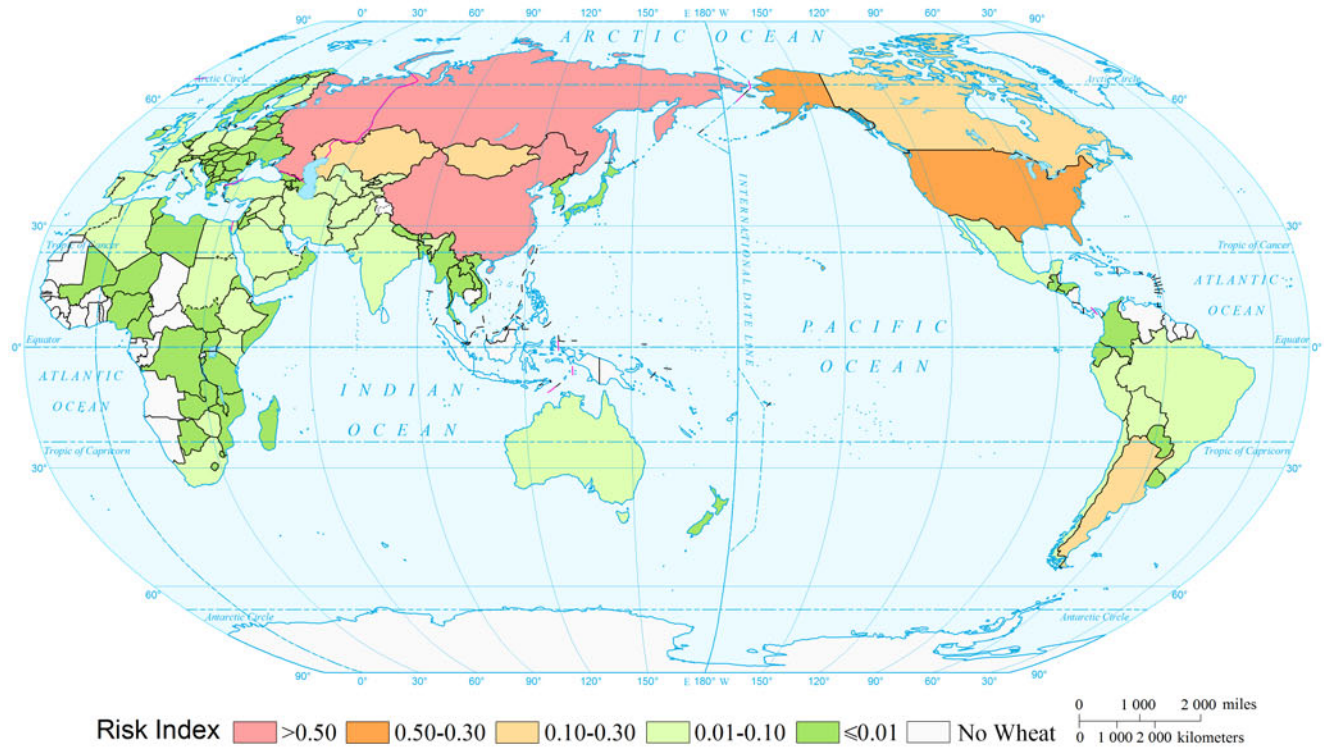
### Wheat Yield Loss Risk of Drought of the World by Return Period (100a) (Comparable-geographic Unit)



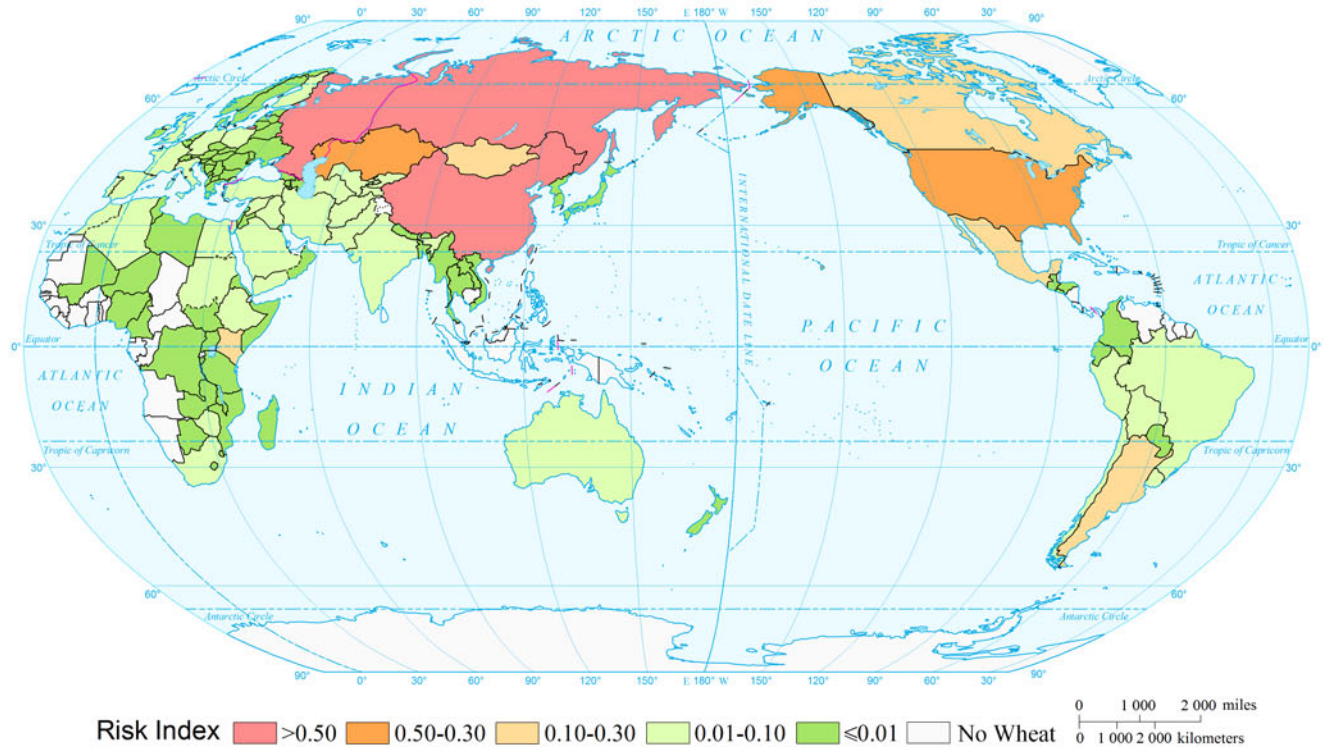
### Expected Annual Wheat Yield Loss Risk of Drought of the World (Country and Region Unit)



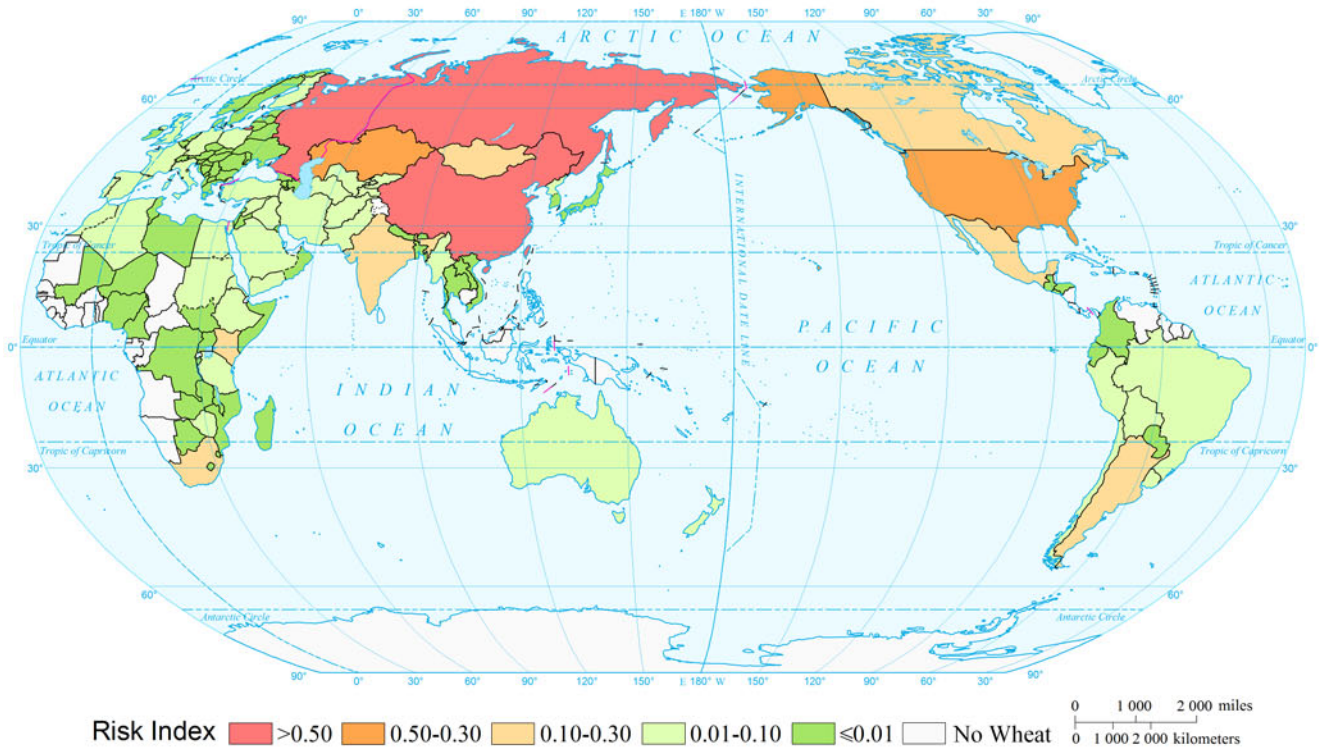
Wheat Yield Loss Risk of Drought of the World by Return Period (10a)  
(Country and Region Unit)



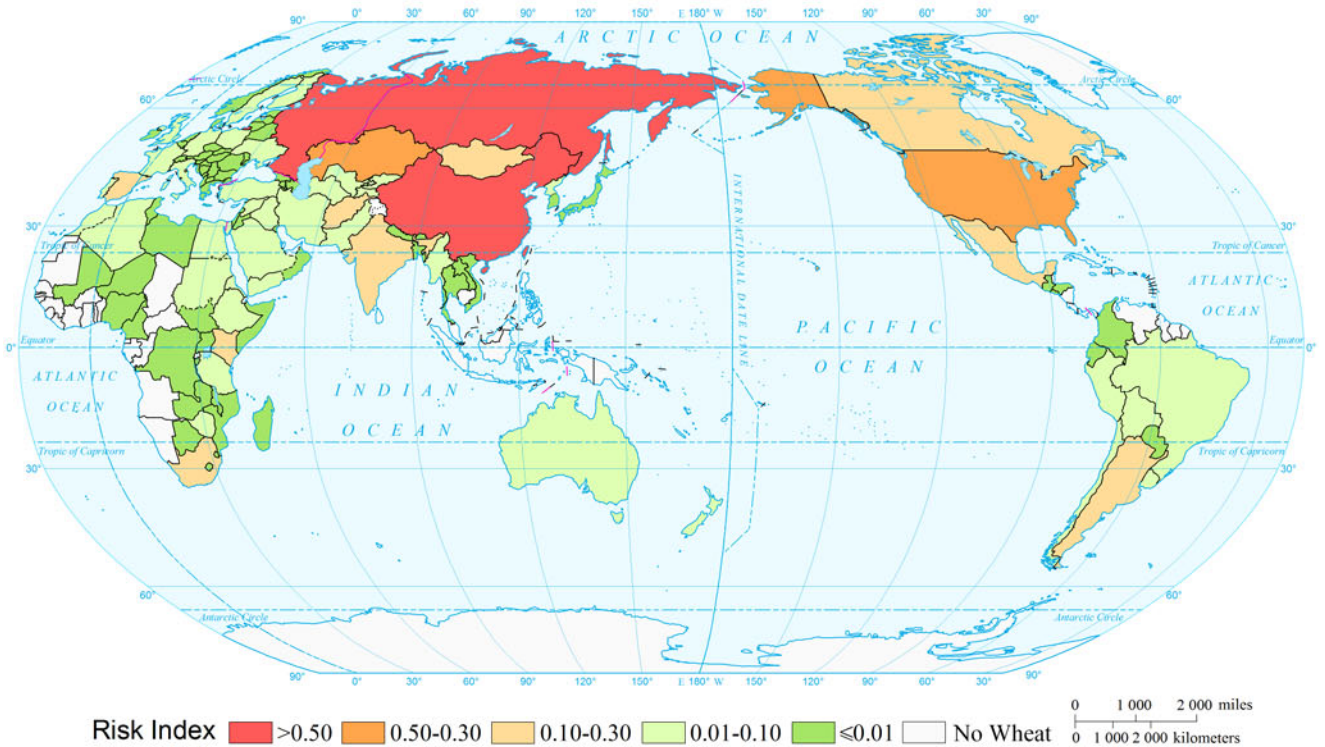
Wheat Yield Loss Risk of Drought of the World by Return Period (20a)  
(Country and Region Unit)



Wheat Yield Loss Risk of Drought of the World by Return Period (50a)  
(Country and Region Unit)



Wheat Yield Loss Risk of Drought of the World by Return Period (100a)  
(Country and Region Unit)



## References

- Intergovernmental Panel on Climate Change (IPCC). 2012. *Managing the risks of extreme events and disasters to advance climate change adaptation*. A special report of working groups I and II of the intergovernmental panel on climate change. Cambridge and New York: Cambridge University Press.
- Intergovernmental Panel on Climate Change (IPCC). 2013. *Summary for policymakers*. In: Climate change 2013: The physical science basis. Contribution of working group I to the fifth assessment report of the intergovernmental panel on climate change. Cambridge and New York: Cambridge University Press.
- Li, Y.P., W. Ye, M. Wang, et al. 2009. Climate change and drought: a risk assessment of crop-yield impacts. *Climate Research* 39(1): 31–46.
- Moss R.H., M. Babiker, S. Brinkman, et al. 2008. Towards new scenarios for analysis of emissions, climate change, impacts, and response strategies. Technical Summary, Intergovernmental Panel on Climate Change, Geneva.
- United Nations Development Programme (UNDP), Bureau for Crisis Prevention and Recovery. 2004. *Reducing disaster risk: a challenge for development*. New York: UNDP, Bureau for Crisis Prevention and Recovery.
- Yin, Y.Y., X.M. Zhang, D.G. Lin, et al. 2014. GEPIC-V-R model: a GIS-based tool for regional crop drought risk assessment. *Agricultural Water Management* 144: 107–119.

---

# Mapping Drought Risk (Rice) of the World

Xingming Zhang, Degen Lin, Hao Guo, Yaoyao Wu, and Jing'ai Wang

---

## 1 Background

Drought is one of the disasters that most widely affect and damage agricultural production in the world. Nearly half of the countries in the world bear severe drought (UNDP 2004; Moss et al. 2008). There is very serious drought in North America, Mexico, central and southern part of Africa, part of South America, and in northern part of China (IPCC 2012). Research shows that under the background of climate warming many regions in the world have an increasing risk of future drought because of the reduced precipitation and aggravating evaporation (IPCC 2012, 2013).

Agricultural drought risk, which is defined as the possible yield loss of crops exposed to drought, can be considered as the probability of the occurrence of agricultural drought and the negative impact on agricultural production (Yin et al. 2014). The drought risk of food production was assessed based on drought frequency and intensity, production levels, and adaptability at global scale (Li et al. 2009). Assessing and mapping rice yield loss risk of drought of the world were made based on GEPIC-Vulnerability-Risk (GEPIC-V-R) model (Yin et al. 2014).

---

**Mapping Editors:** Jing'ai Wang (Key Laboratory of Regional Geography, Beijing Normal University, Beijing 100875, China), Chunqin Zhang (School of Geography, Beijing Normal University, Beijing 100875, China), Shujuan Cui (School of Geography, Beijing Normal University, Beijing 100875, China) and Fang Chen (School of Geography, Beijing Normal University, Beijing 100875, China).  
**Language Editor:** Wei Xu (Key Laboratory of Environmental Change and Natural Disaster, Ministry of Education, Beijing Normal University, Beijing 100875, China).

X. Zhang · D. Lin · Y. Wu  
School of Geography, Beijing Normal University, Beijing 100875,  
China

H. Guo · J. Wang (✉)  
Key Laboratory of Regional Geography, Beijing Normal  
University, Beijing 100875, China  
e-mail: jwang@bnu.edu.cn

In this study, the rice yield loss risk of drought at global scale is assessed and mapped based on the GEPIC-V-R model developed by Yin et al. (2014). The vulnerability of rice to drought is simulated at grid level ( $0.5^\circ \times 0.5^\circ$ ), which improved the spatial resolution compared with the work of Yin et al. (2014).

---

## 2 Method

Figure 1 shows the technical flowchart for mapping rice yield loss risk of drought of the world.

### 2.1 Model

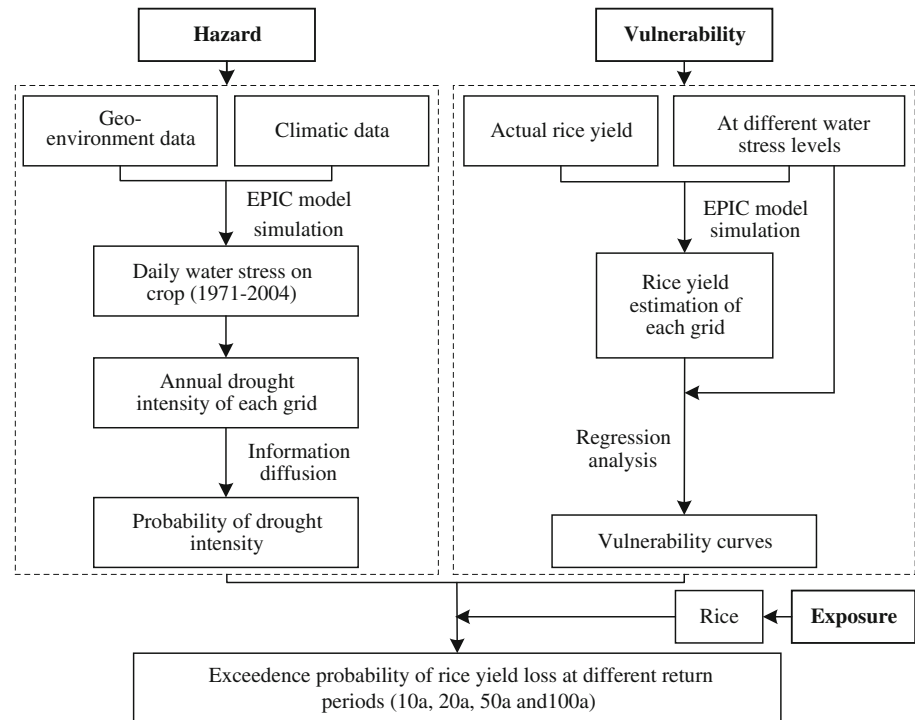
In the GEPIC-V-R model (Yin et al. 2014), drought risk is treated as the function of hazard, vulnerability of exposure, and environment (Eq. 1).

$$R = f(E, H, V) = H\{P, h_E\} \times V\{l_E, h_E\} \quad (1)$$

Where  $E$  is the sensitivity of environment;  $H$  is the drought;  $V$  is the vulnerability;  $P$  is the occurrence probability of drought;  $h_E$  is the drought intensity index; and  $l_E$  is the loss rate.  $H\{P, h_E\}$  is the drought intensity under a certain probability.  $V\{l_E, h_E\}$  determines the relationship between  $h_E$  and  $l_E$ .

GEPIC-V-R model is a crop risk assessment model for large scale (i.e., regional, national, continental, and global) with functions to fit vulnerability curves and calculate risk. In this model, there are four modules: model calibration module, hazard module, vulnerability module, and risk calculation module (Yin et al. 2014).

**Fig. 1** The technical flowchart for mapping rice yield loss risk by drought of the world



Data for assessing the rice yield loss risk by drought of the world consist of crop growth environment data (Appendix III, Environments data 2.1, 2.2 and 2.7, Appendix III, Hazards data 4.15), crop management data (Appendix III, Environments data 3.13–3.16), crop species attribute data (Appendix III, Environments data 3.18), and actual yield data (Appendix III, Environments data 3.17).

## 2.2 Spatial Resolution

Compared with the work of Yin et al. (2014), the vulnerability of rice to drought is simulated at grid level ( $0.5^\circ \times 0.5^\circ$ ) instead of the regional level which greatly improves the spatial resolution. Furthermore, the rice exposure is calculated and mapped at  $5' \times 5'$  grid level in this study, instead of  $0.5^\circ \times 0.5^\circ$  grid level done by Yin et al. (2014).

## 3 Results

### 3.1 Intensity

Areas with high value of drought intensity on rice mainly distribute in the Hindu Kush Mountains and the Deccan plateau of Asia, Niger Basin of western Africa and Great Rift Valley of East Africa, Iberian Peninsula and Don river basin of Europe, Darling Basin at east of Australia and northeast of Brazil Plateau, and Pampas plains in America.

### 3.2 Vulnerability

Based on the GEPIC-V-R model, vulnerability curves of rice to drought for each grid ( $0.5^\circ \times 0.5^\circ$ ) are fitted. Figure 2 shows the vulnerability curves of some selected grids.

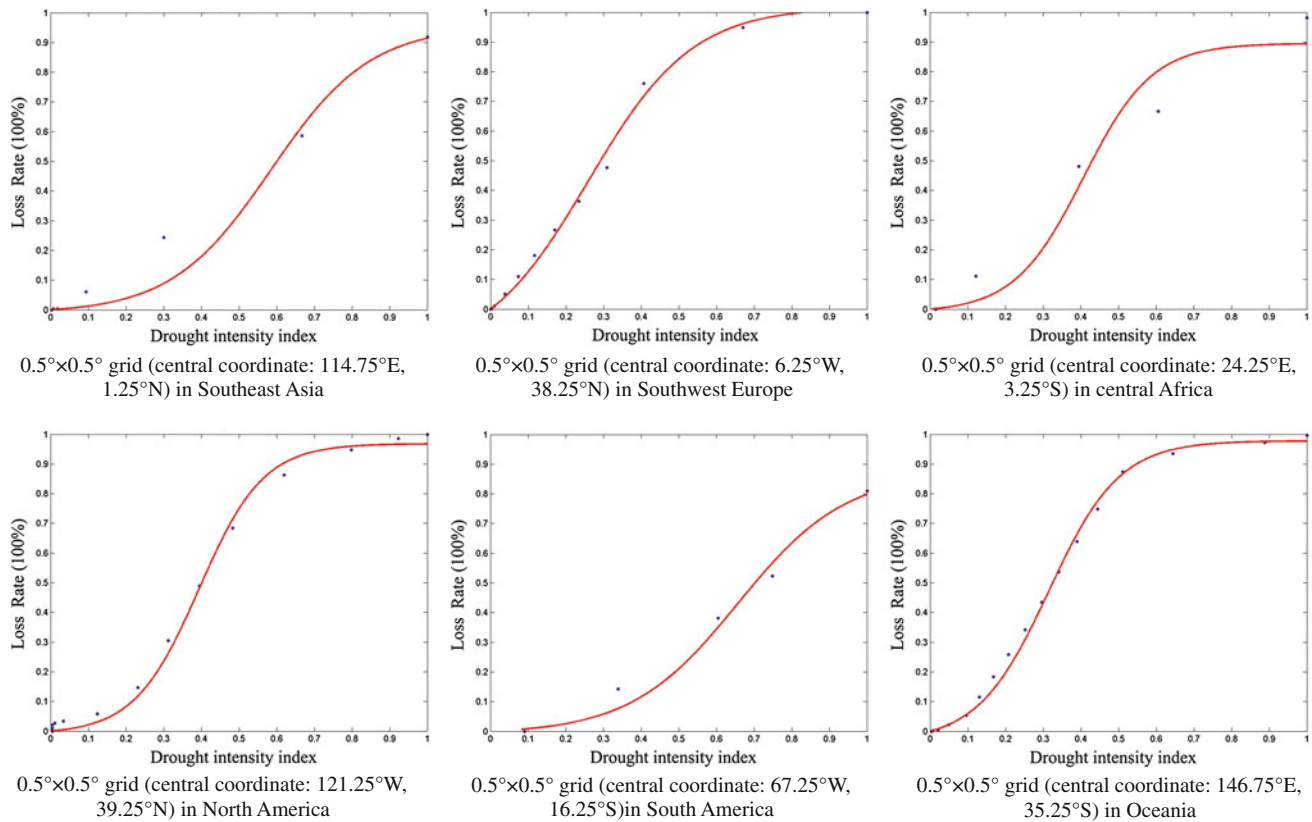


**Fig. 2** Examples of vulnerability curve of rice to drought



**Fig. 3** Expected annual rice yield loss risk of drought of the world. 1 (0, 10 %]. Afghanistan, China, Spain, Pakistan, Tanzania, India, Russia, Brazil, Burkina Faso, Australia, and Kazakhstan. 2 (10, 35 %]. Uzbekistan, Turkmenistan, Portugal, Iran, Iraq, Nigeria, USA, Chile, Peru, Turkey, Senegal, Mali, Tajikistan, Madagascar, Morocco, Ukraine, Uruguay, Indonesia, France, Egypt, Italy, Argentina, Mexico, Niger, Mauritania, Mozambique, and Japan. 3 (35, 65 %]. Kenya, Paraguay, Cuba, Vietnam, French Guiana, Bolivia, South Korea, Greece, Kyrgyzstan, Sri Lanka, Dominican Republic, Haiti, Laos, Uganda, Philippines, Azerbaijan, Honduras, Nicaragua, Gambia,

Nepal, Colombia, Zambia, the Republic of Côte d’Ivoire, Guinea-Bissau, North Korea, Cambodia, Burma, Guatemala, Thailand, Congo (Democratic Republic), Guyana, and El Salvador. 4 (65, 90 %]. Benin, Ecuador, Timor-Leste, Venezuela, Ghana, Malawi, Macedonia, Belize, Togo, Cameroon, Bulgaria, Bangladesh, Bhutan, Burundi, Malaysia, Suriname, Trinidad and Tobago, Hungary, Costa Rica, Romania, Central African Republic, Angola, Chad, Armenia, and Congo. 5 (90, 100 %]. San Marino, Zimbabwe, Rwanda, Albania, South Sudan, Mongolia, Sierra Leone, Panama, Liberia, Gabon, and Brunei Darussalam

**3.3 Risk**

By zonal statistics of the expected risk result, the expected annual rice yield loss risk of drought of the world at national level is derived and ranked (Fig. 3). The top 1 % country with the highest expected annual rice yield loss risk of drought is

Afghanistan, and the top 10 % countries are Afghanistan, China, Spain, Pakistan, Tanzania, India, Russia, Brazil, Burkina Faso, Australia, and Kazakhstan.

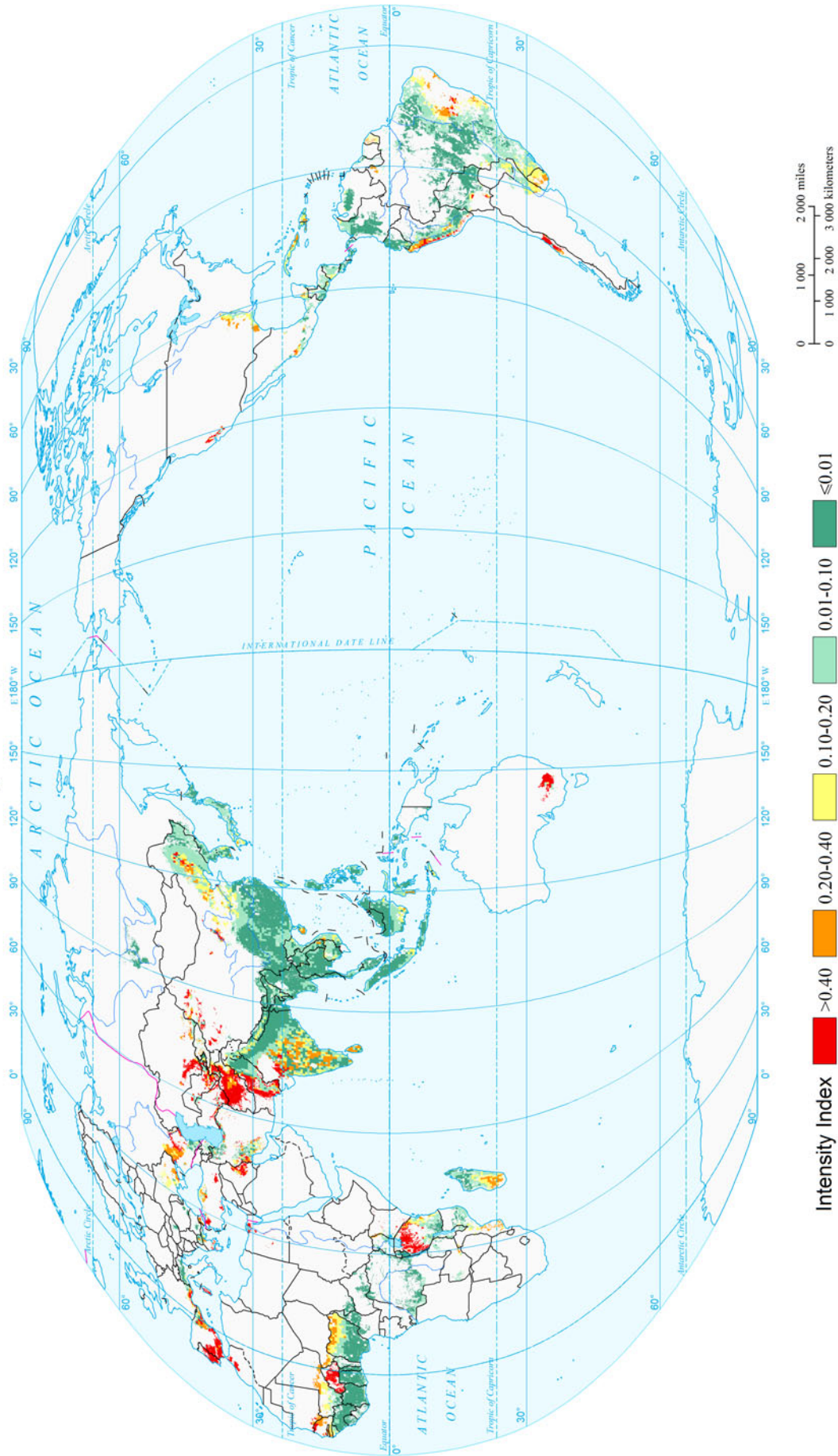
**4 Maps**



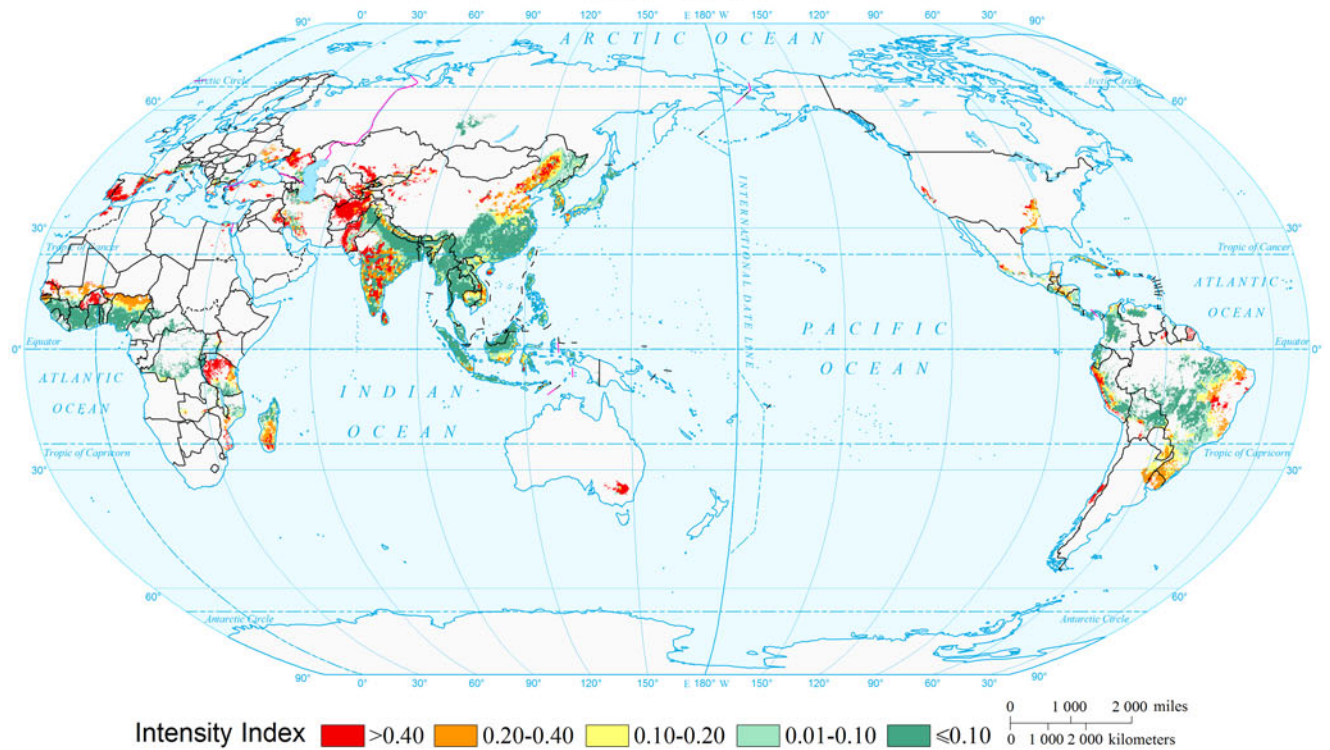
Rice

Drought Disasters

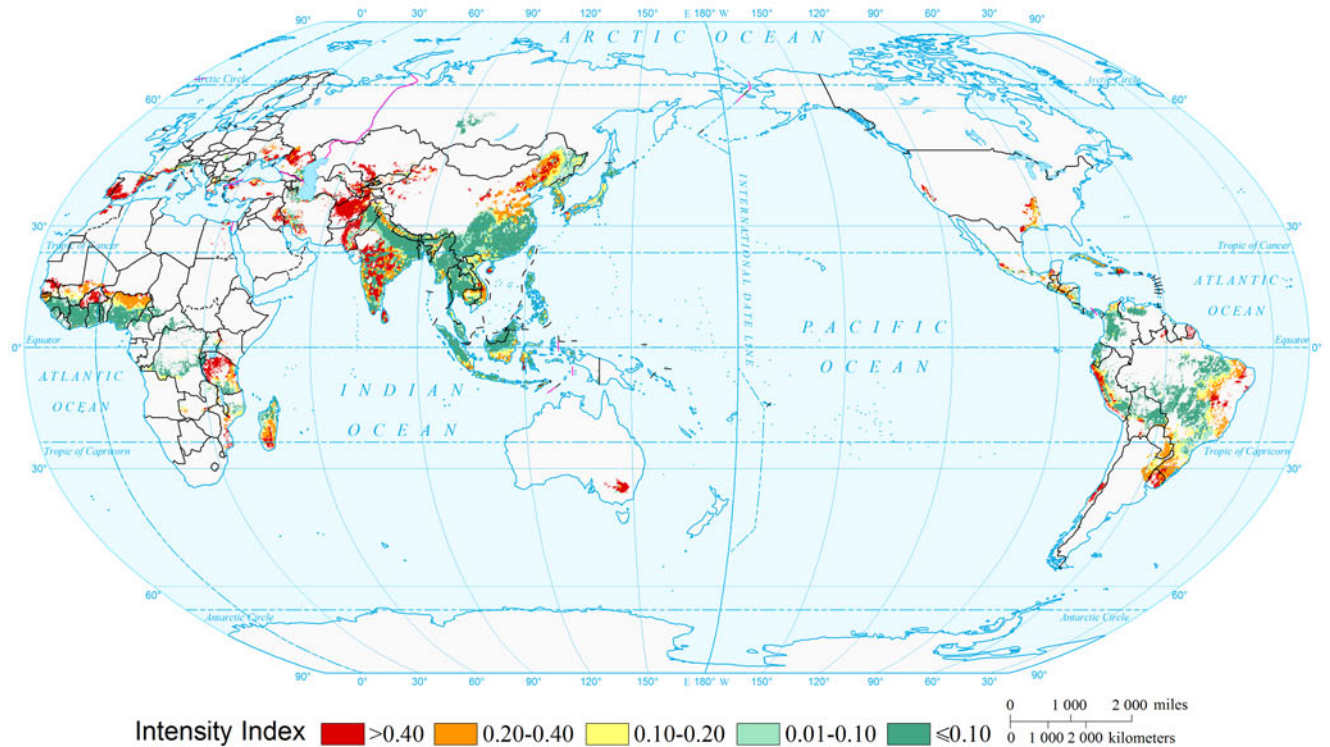
Global Expected Annual Drought Intensity for Rice  
( $0.5^\circ \times 0.5^\circ$ )



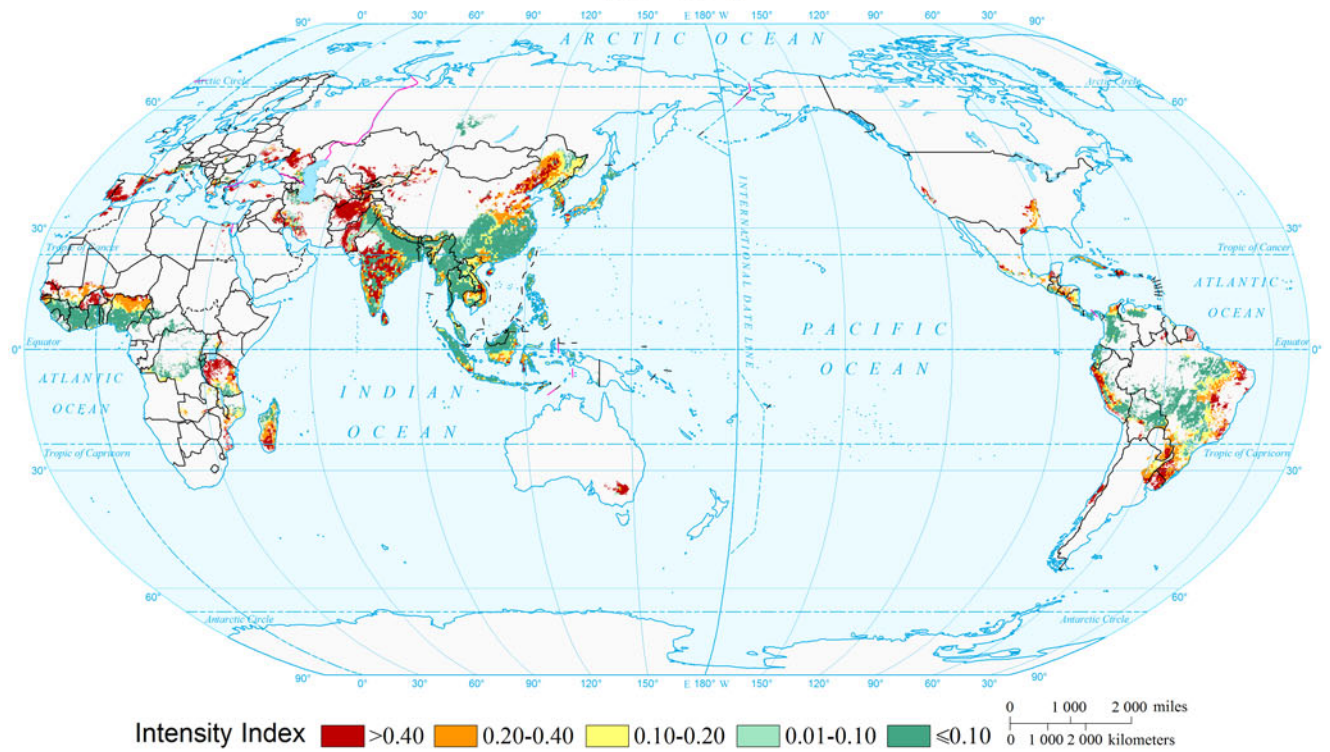
Global Drought Intensity for Rice by Return Period (10a)  
(0.5°×0.5°)



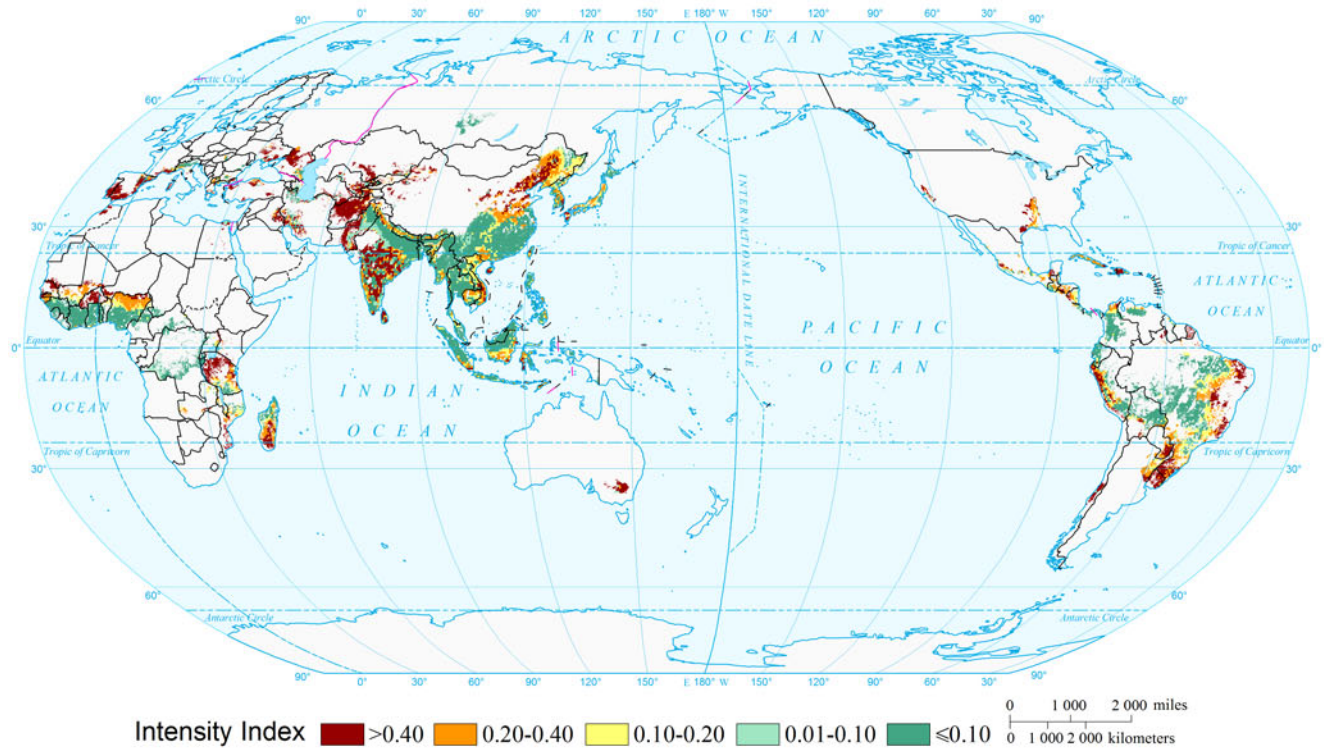
Global Drought Intensity for Rice by Return Period (20a)  
(0.5°×0.5°)



Global Drought Intensity for Rice by Return Period (50a)  
(0.5°×0.5°)



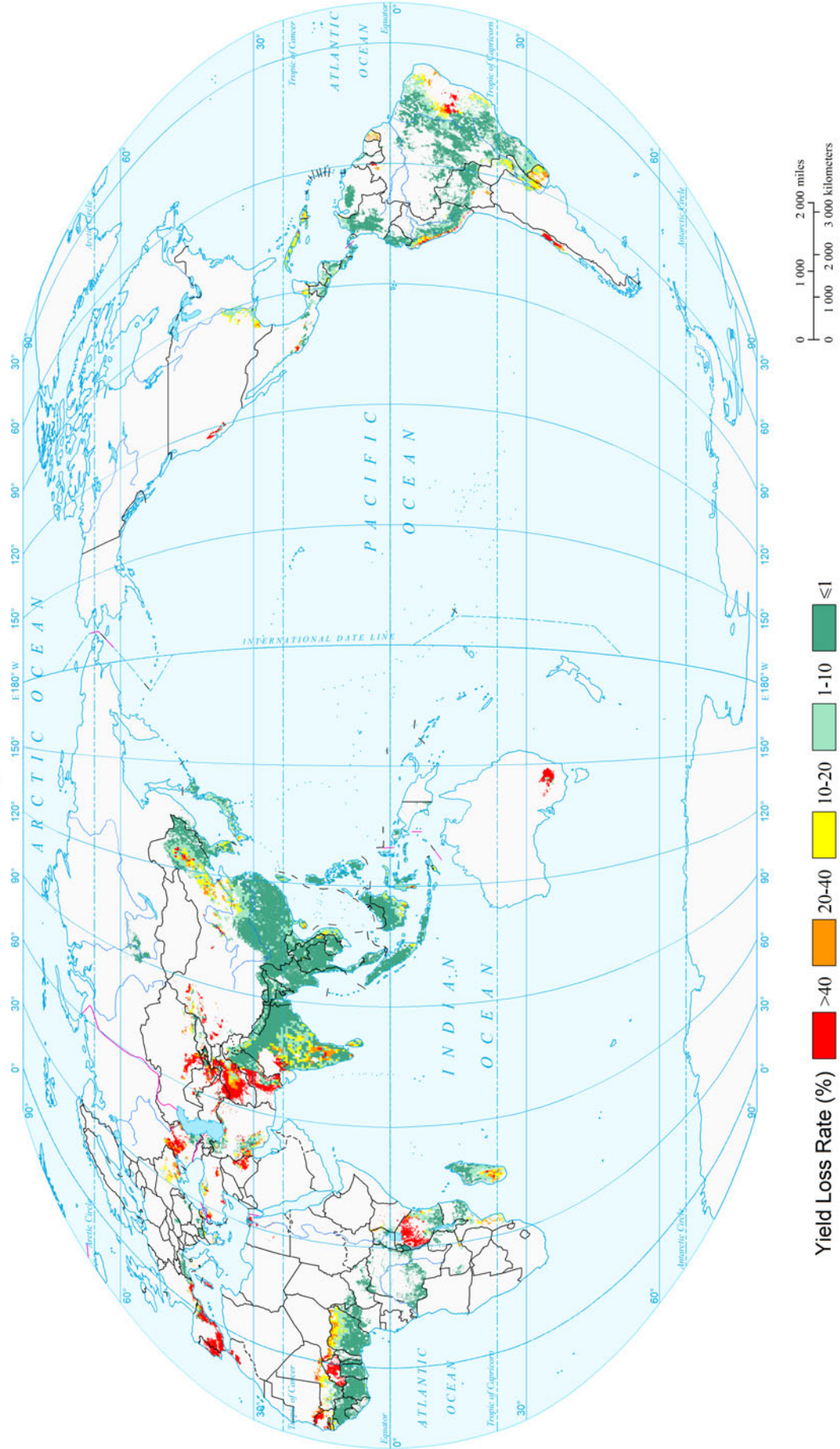
Global Drought Intensity for Rice by Return Period (100a)  
(0.5°×0.5°)



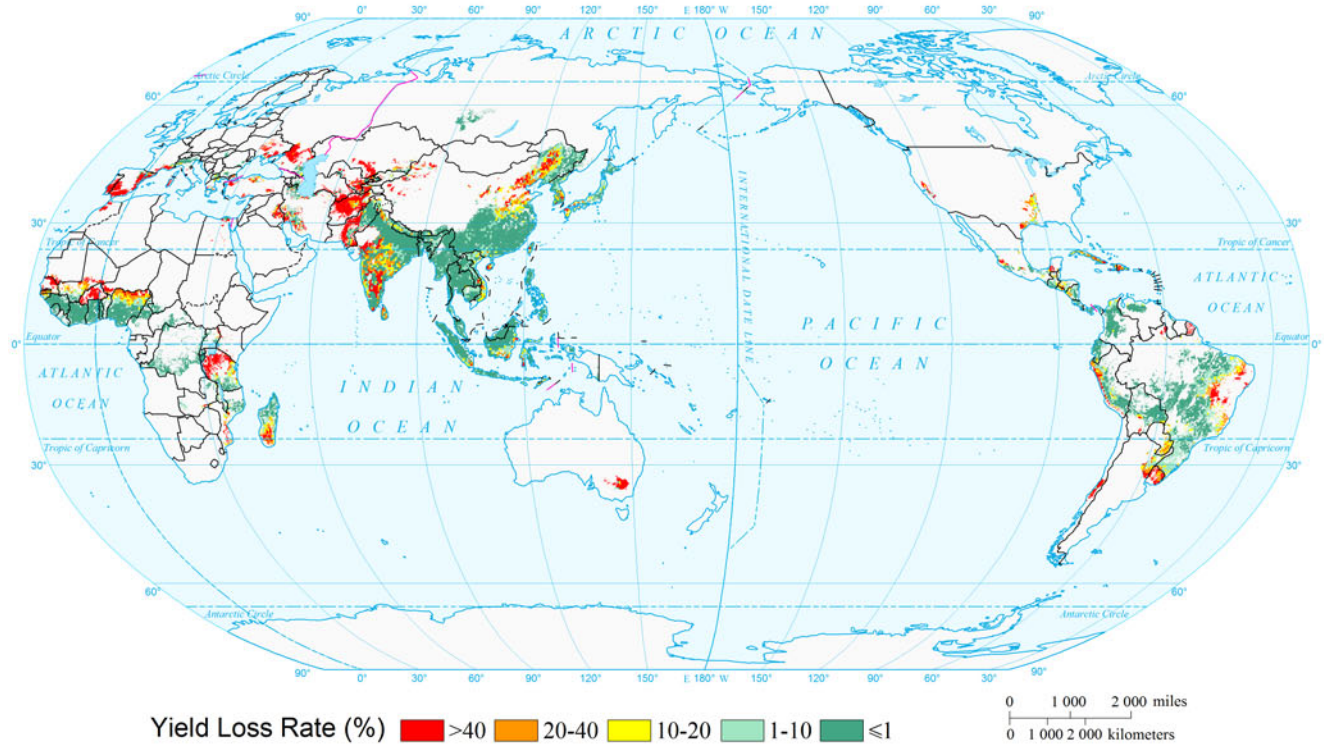


Drought Disasters

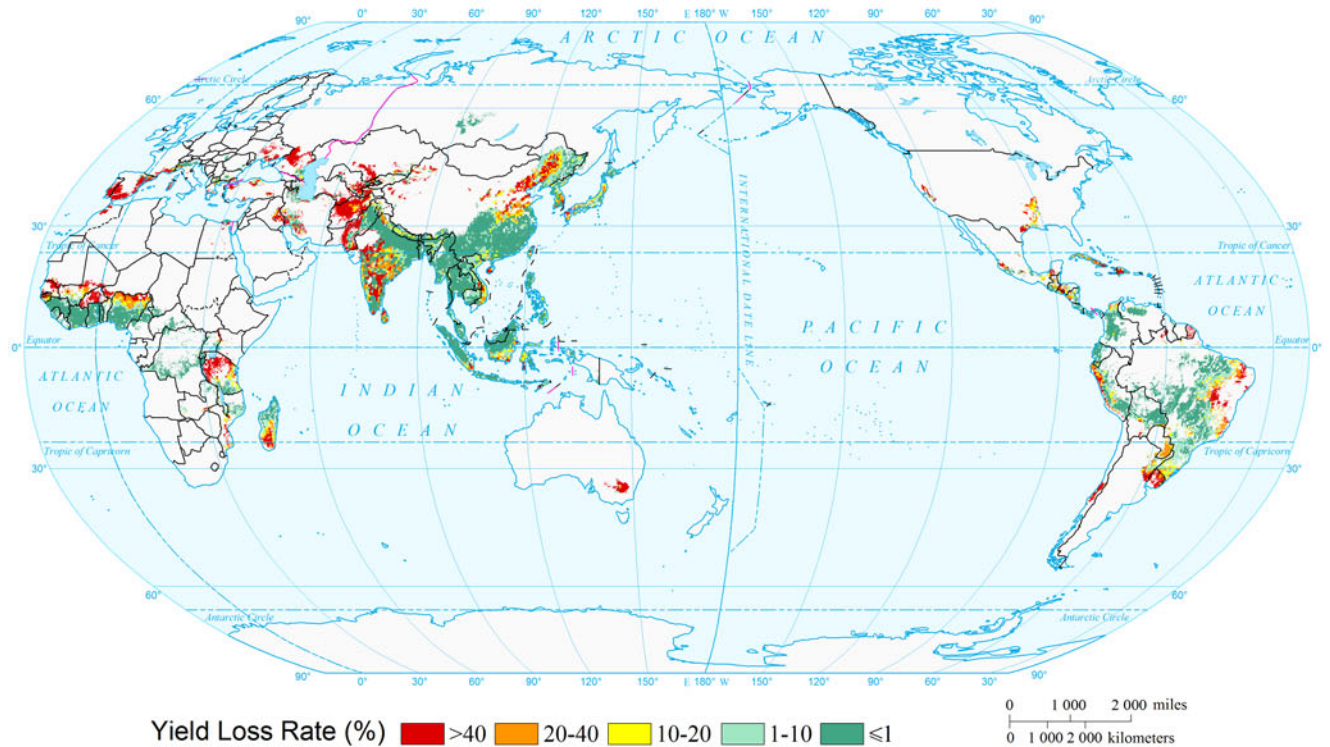
Expected Annual Rice Yield Loss Risk of Drought of the World  
( $0.5^\circ \times 0.5^\circ$ )



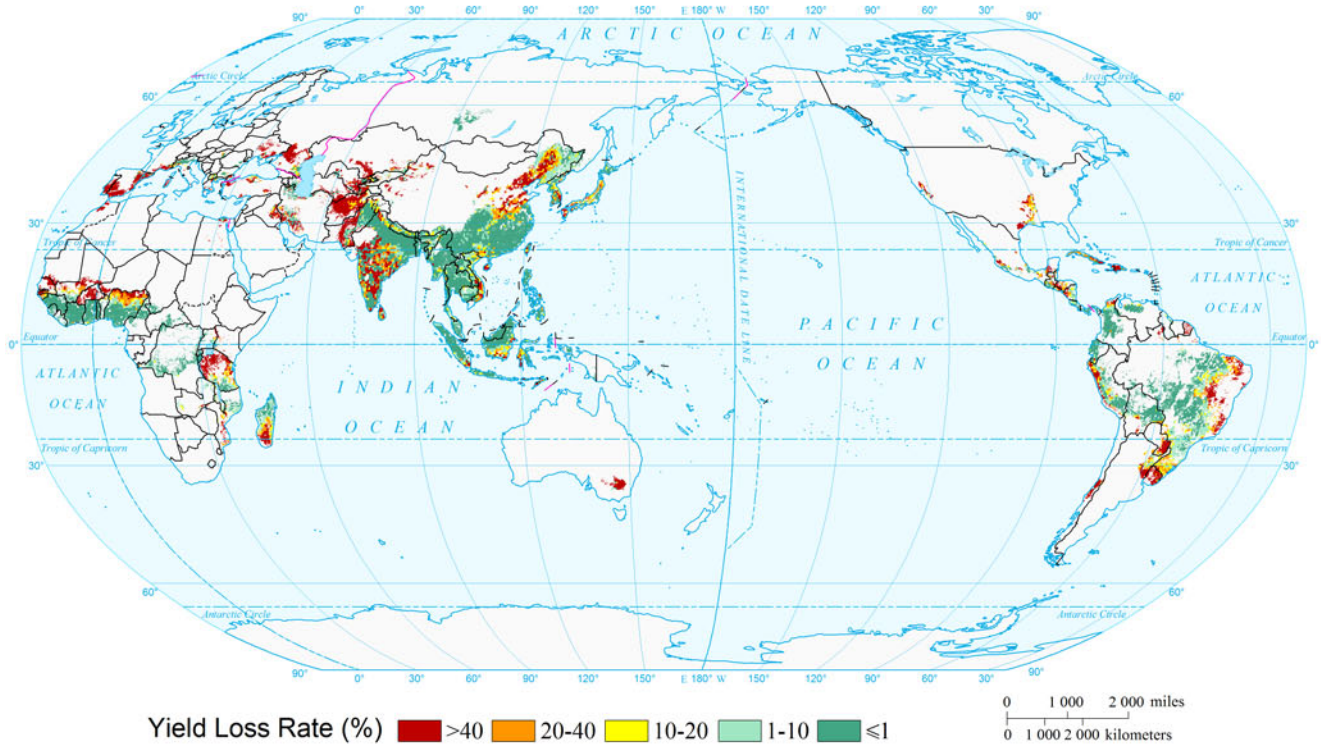
Rice Yield Loss Risk of Drought of the World by Return Period (10a)  
(0.5°×0.5°)



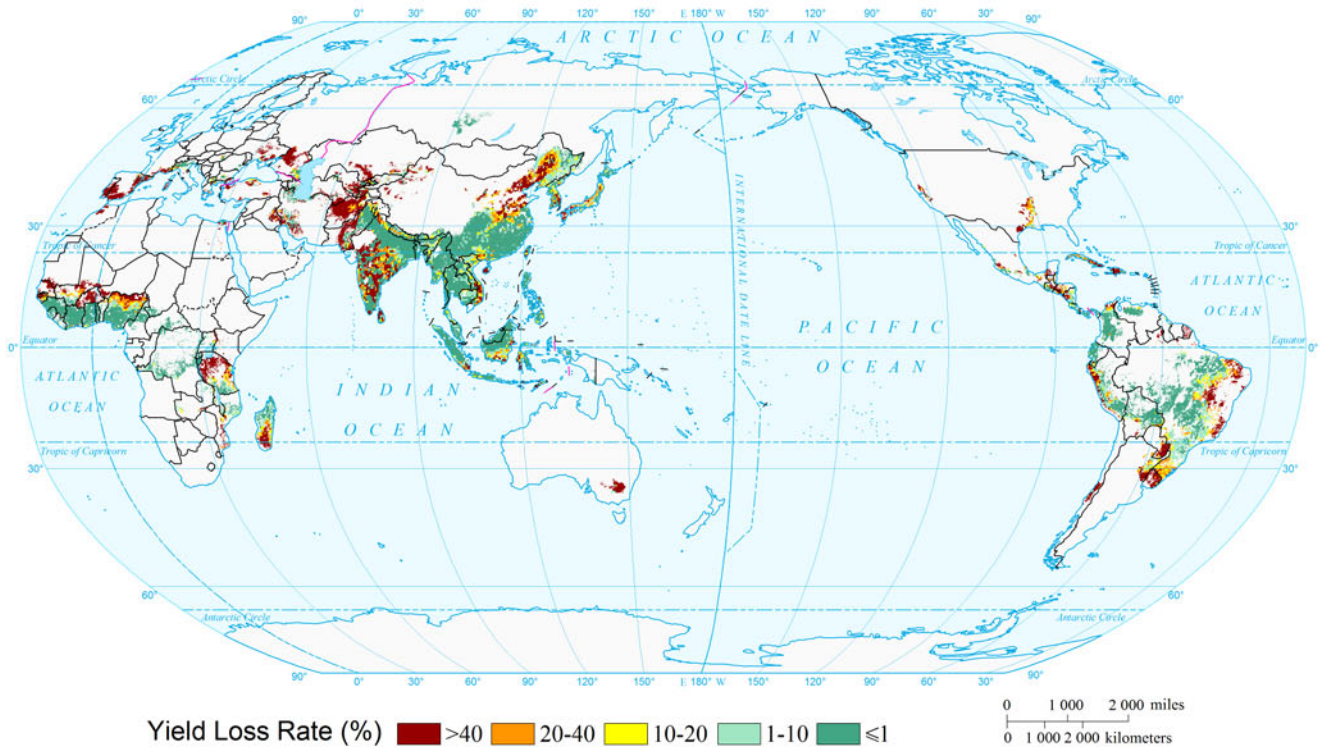
Rice Yield Loss Risk of Drought of the World by Return Period (20a)  
(0.5°×0.5°)



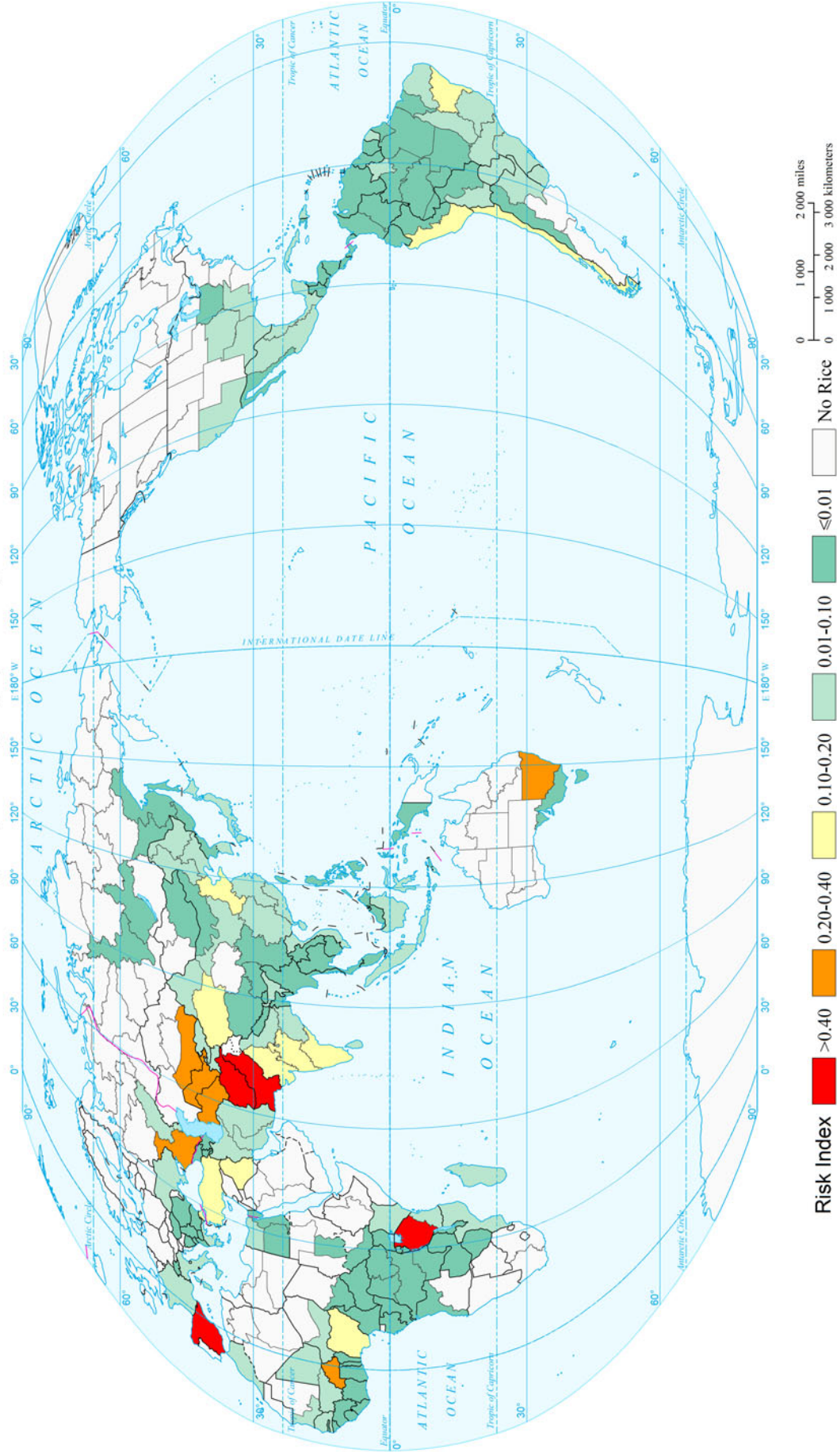
Rice Yield Loss Risk of Drought of the World by Return Period (50a)  
(0.5°×0.5°)



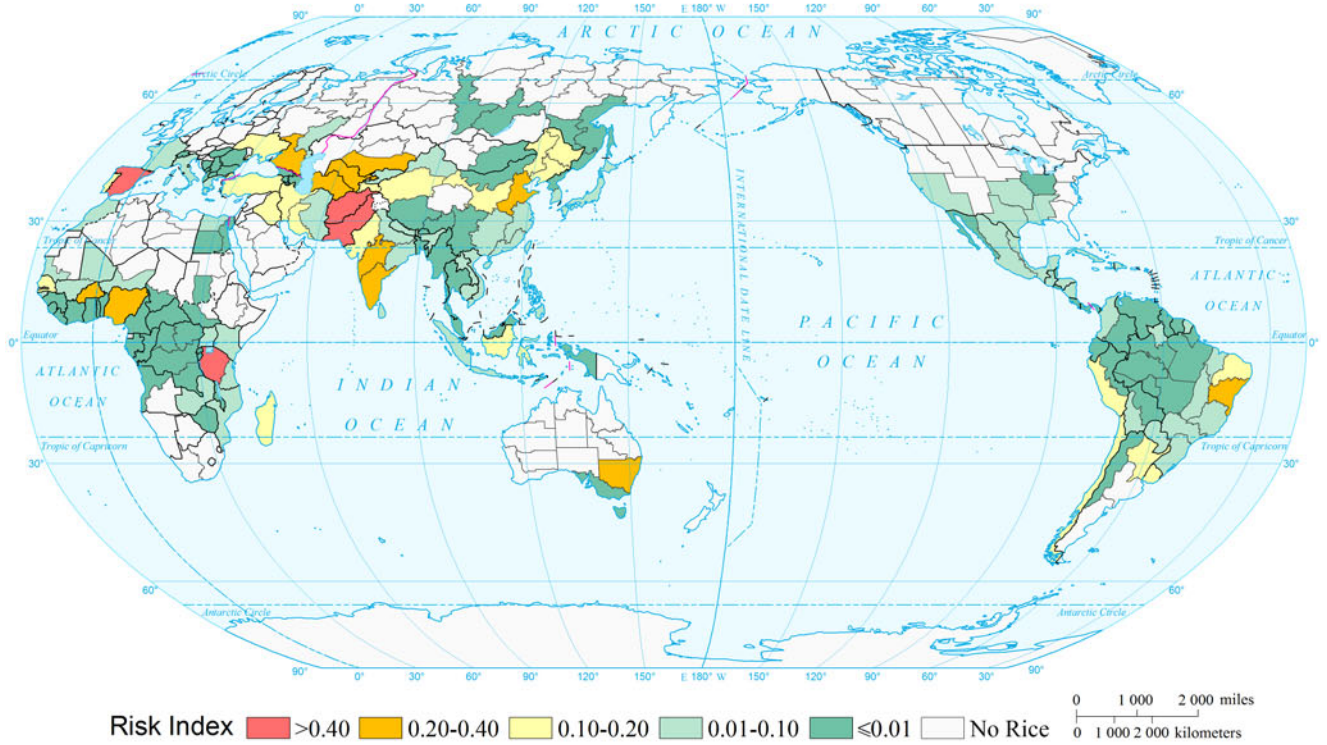
Rice Yield Loss Risk of Drought of the World by Return Period (100a)  
(0.5°×0.5°)



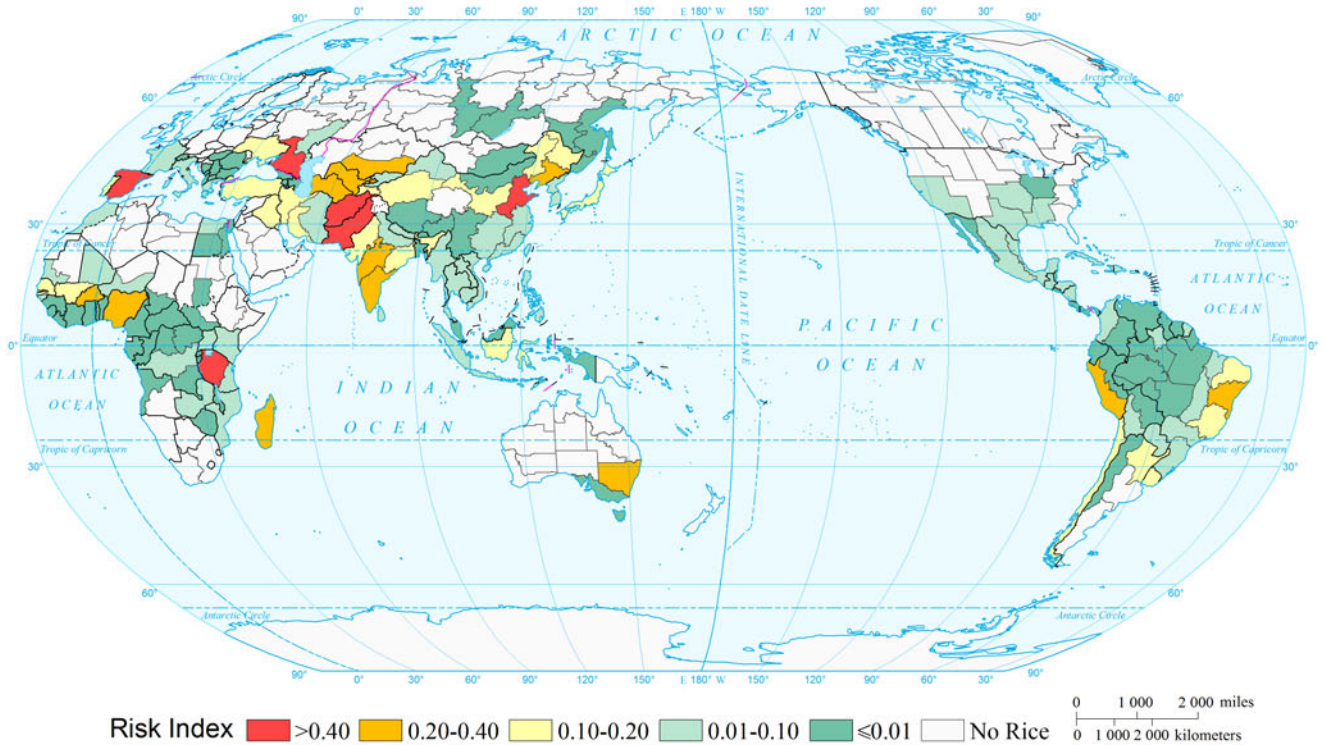
Expected Annual Rice Yield Loss Risk of Drought of the World  
(Comparable-geographic Unit)



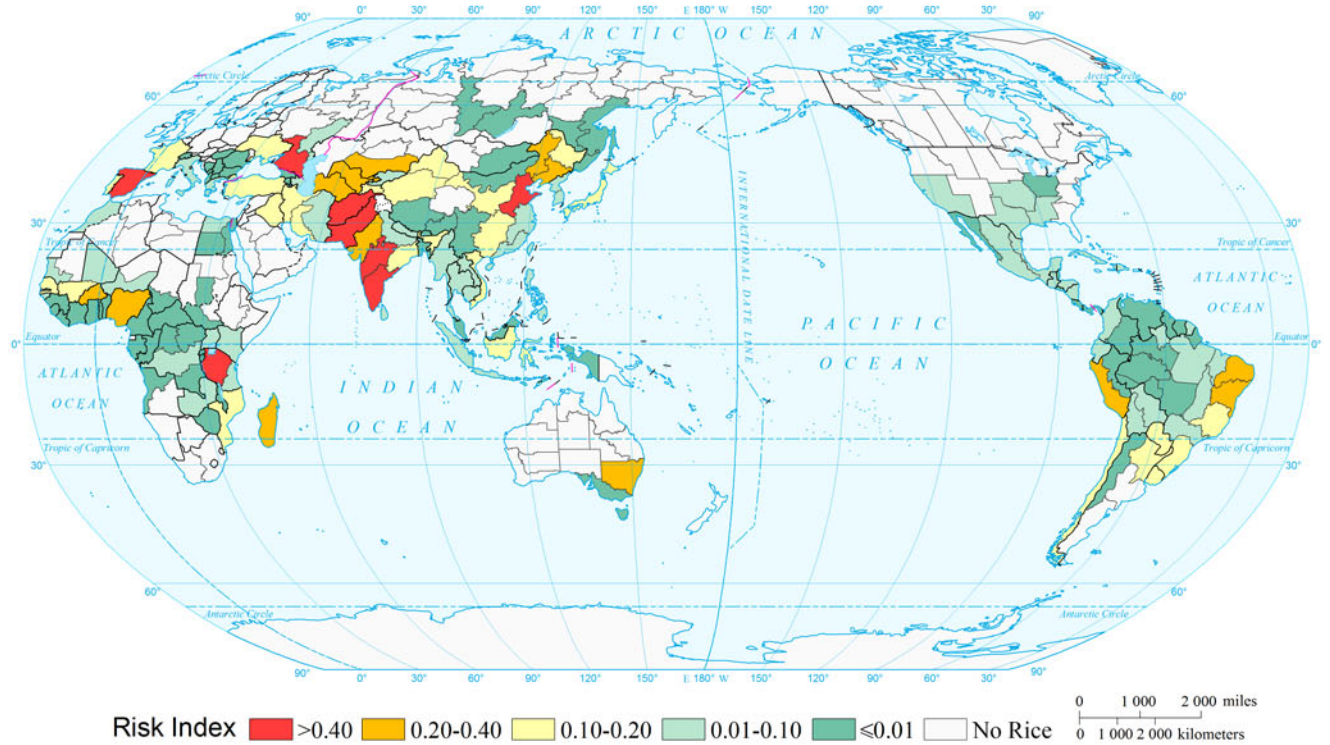
Rice Yield Loss Risk of Drought of the World by Return Period (10a)  
(Comparable-geographic Unit)



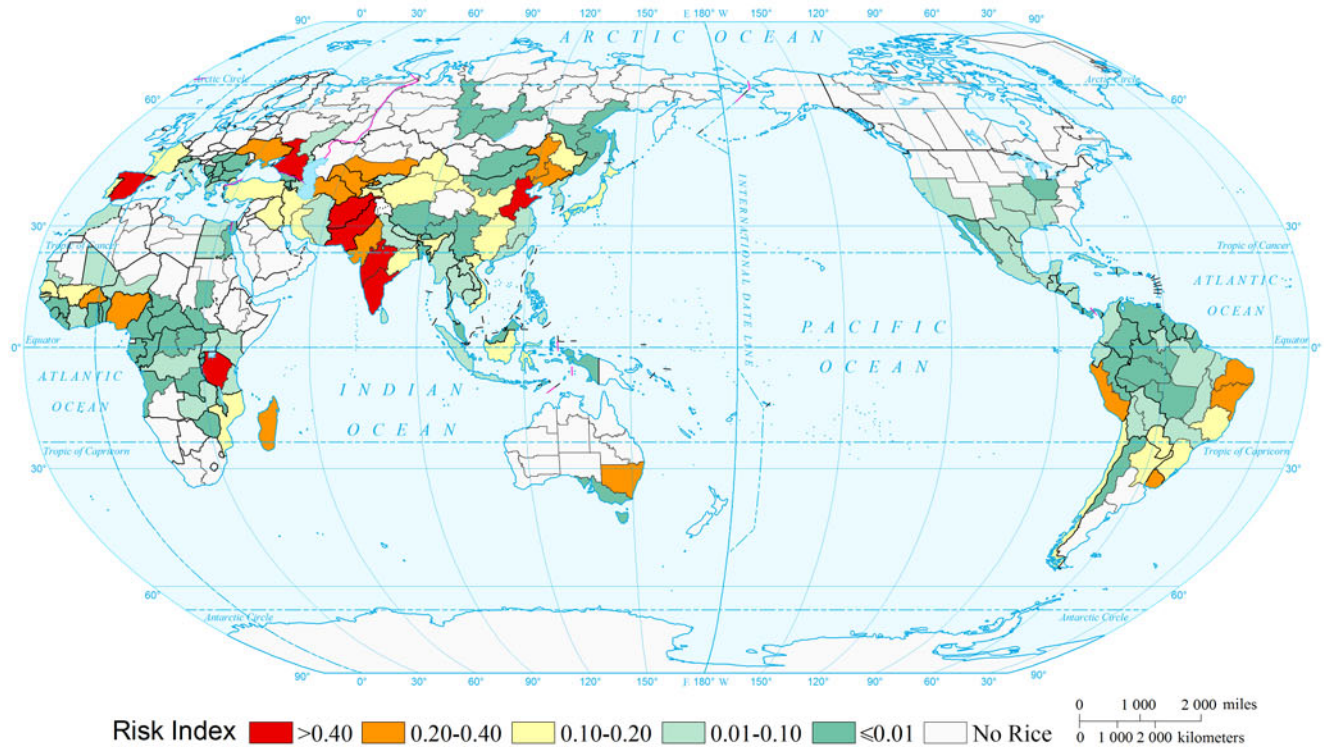
Rice Yield Loss Risk of Drought of the World by Return Period (20a)  
(Comparable-geographic Unit)



Rice Yield Loss Risk of Drought of the World by Return Period (50a)  
(Comparable-geographic Unit)



Rice Yield Loss Risk of Drought of the World by Return Period (100a)  
(Comparable-geographic Unit)

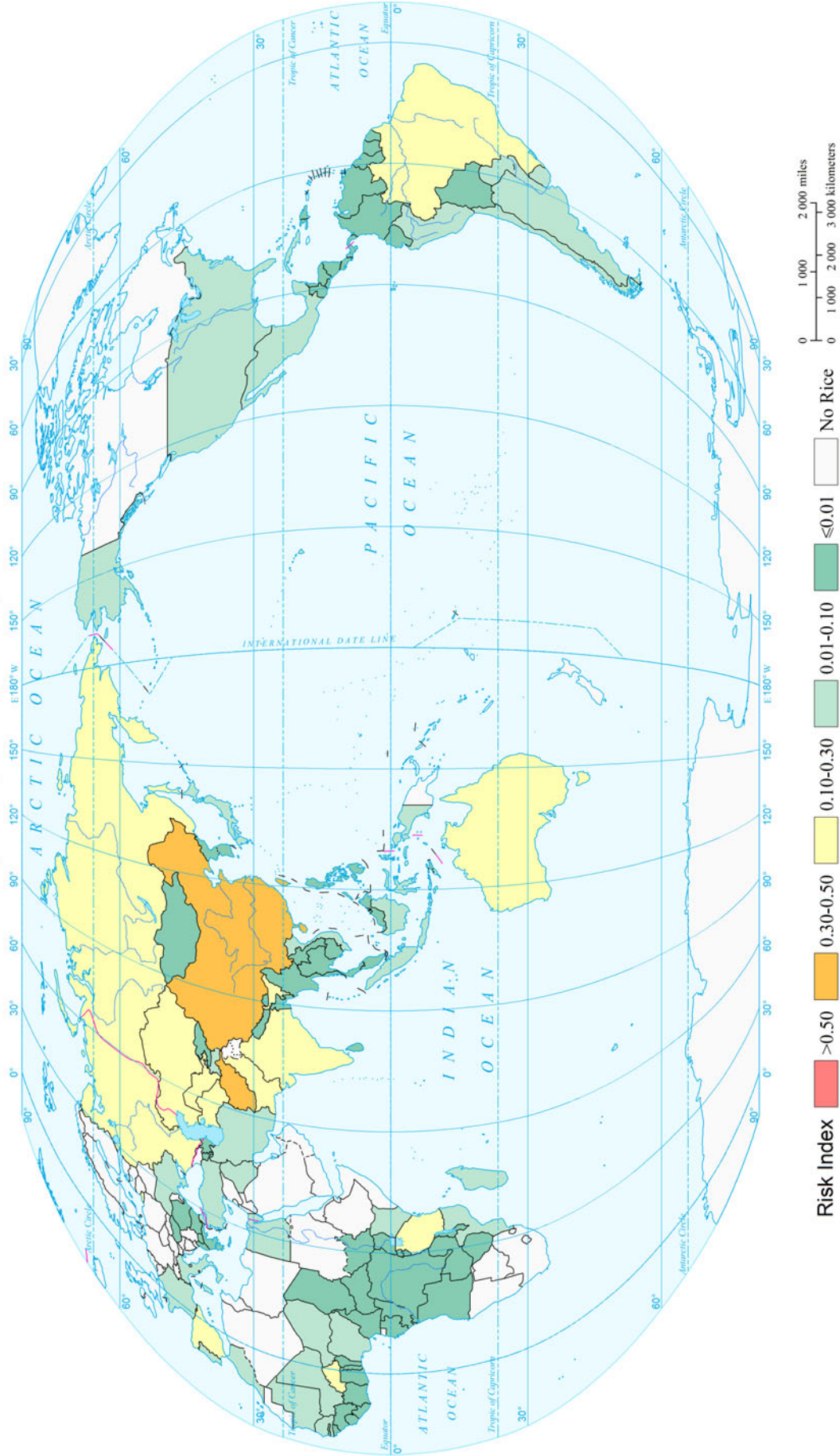




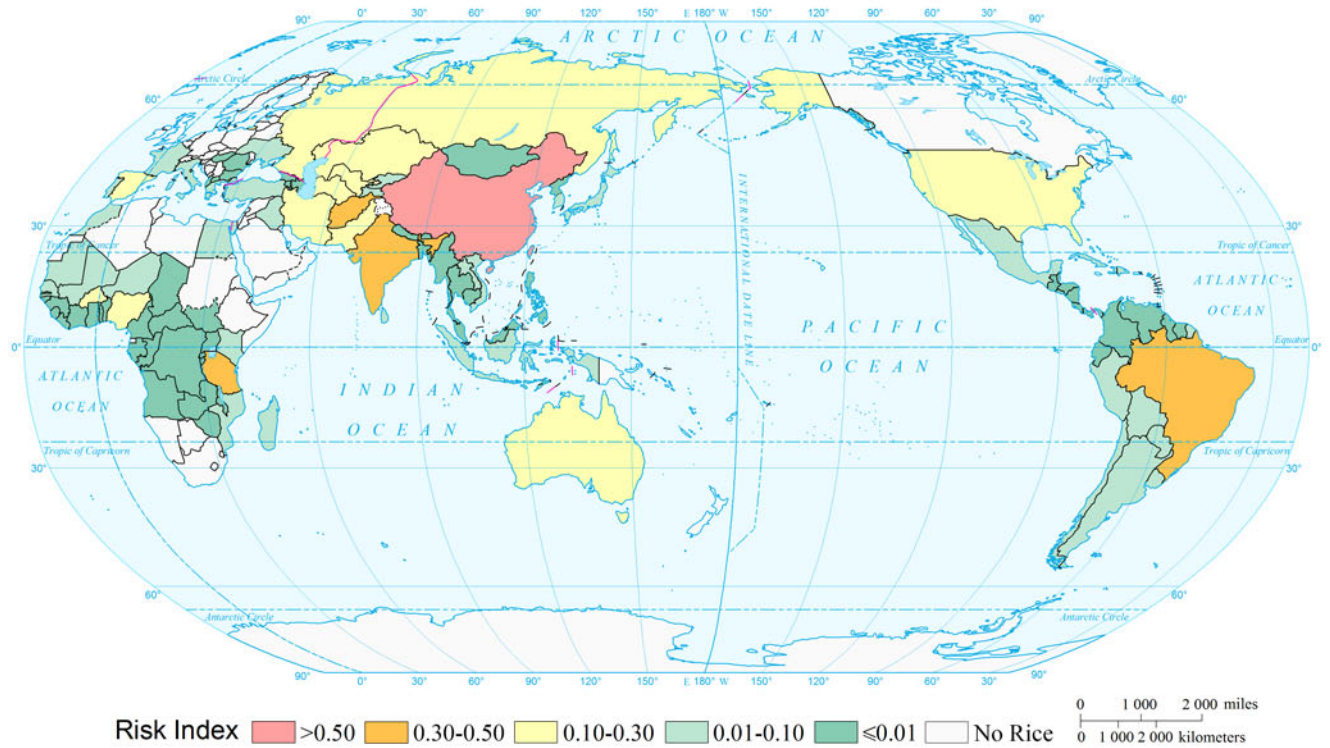
Rice

Drought Disasters

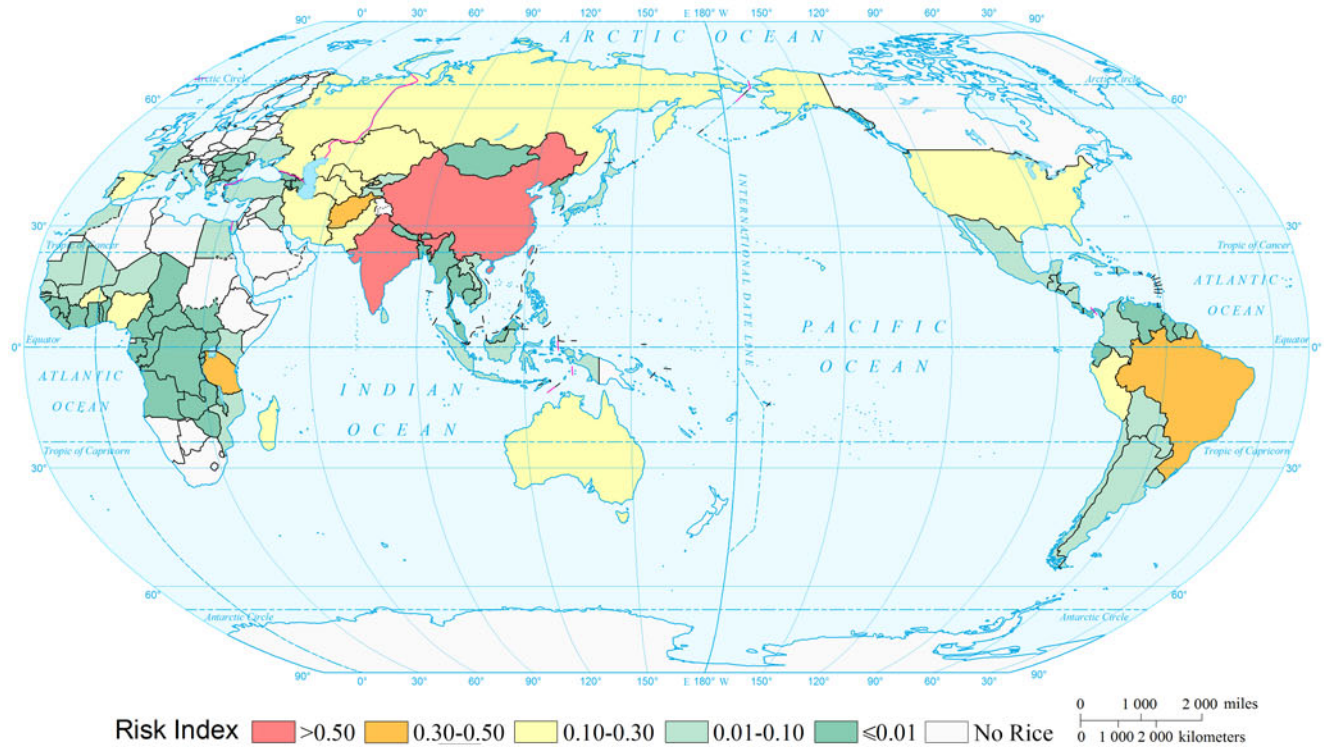
### Expected Annual Rice Yield Loss Risk of Drought of the World (Country and Region Unit)



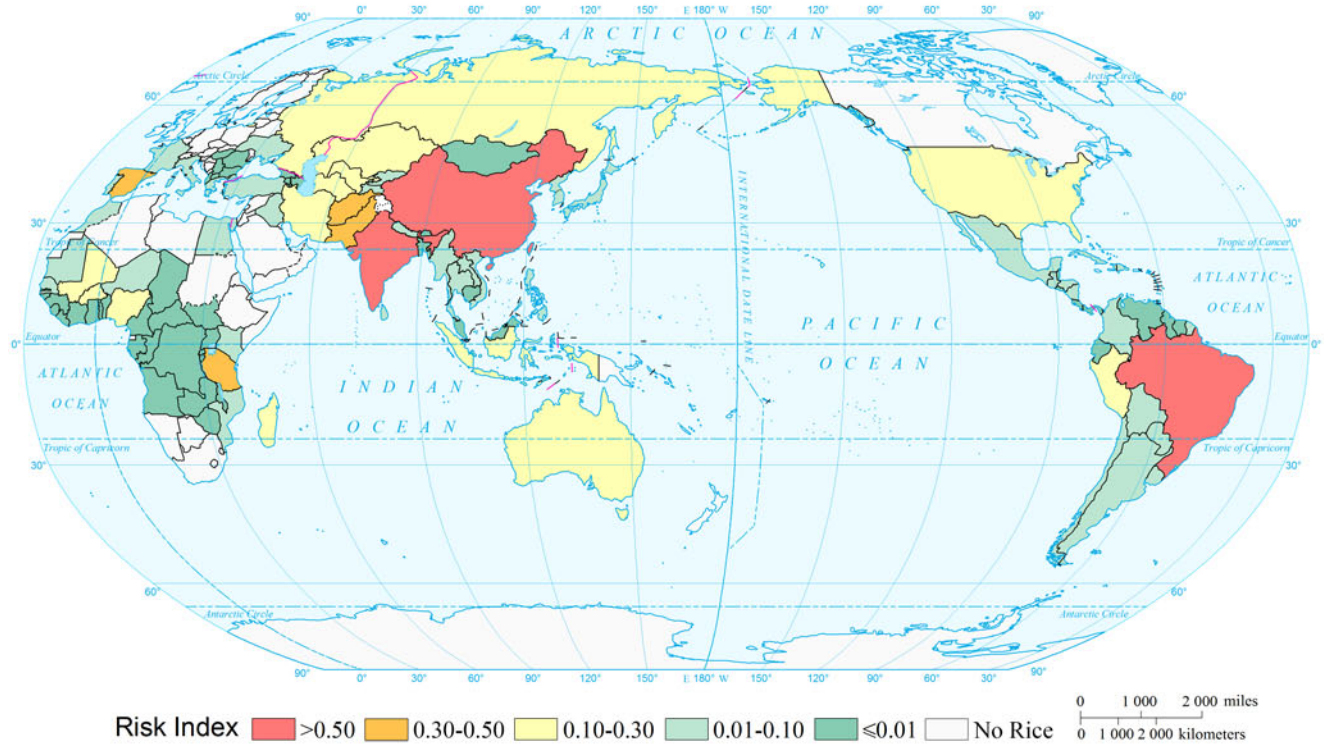
Rice Yield Loss Risk of Drought of the World by Return Period (10a)  
(Country and Region Unit)



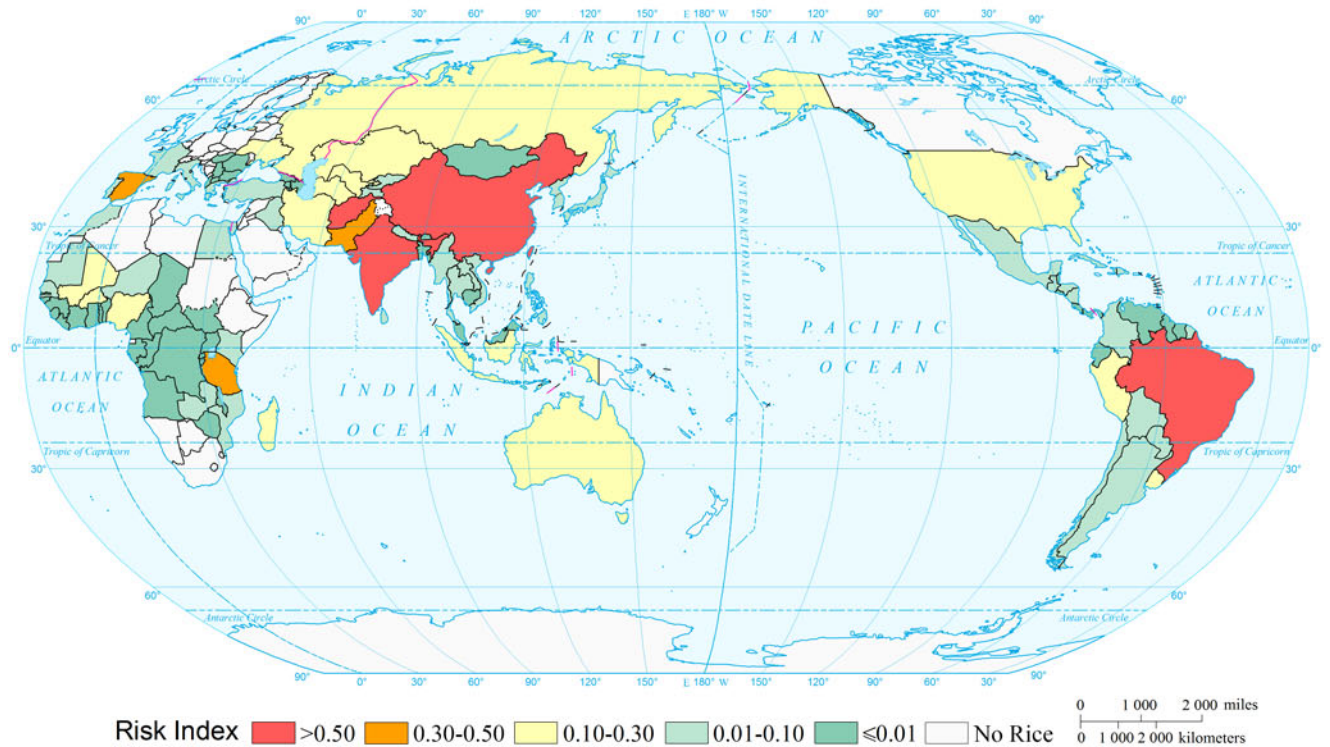
Rice Yield Loss Risk of Drought of the World by Return Period (20a)  
(Country and Region Unit)



Rice Yield Loss Risk of Drought of the World by Return Period (50a)  
(Country and Region Unit)



Rice Yield Loss Risk of Drought of the World by Return Period (100a)  
(Country and Region Unit)



## References

- Intergovernmental Panel on Climate Change (IPCC). 2012. *Managing the risks of extreme events and disasters to advance climate change adaptation*. A special report of working groups I and II of the intergovernmental panel on climate change. Cambridge and New York: Cambridge University Press.
- Intergovernmental Panel on Climate Change (IPCC). 2013. *Summary for policymakers*. In: Climate change 2013: The physical science basis. Contribution of working group I to the fifth assessment report of the intergovernmental panel on climate change. Cambridge and New York: Cambridge University Press.
- Li, Y.P., W. Ye, M. Wang, et al. 2009. Climate change and drought: A risk assessment of crop-yield impacts. *Climate Research* 39(1): 31–46.
- Moss R.H., M. Babiker, S. Brinkman, et al. 2008. Towards new scenarios for analysis of emissions, climate change, impacts, and response strategies. Technical Summary, Intergovernmental Panel on Climate Change, Geneva.
- United Nations Development Programme (UNDP), Bureau for Crisis Prevention and Recovery. 2004. *Reducing disaster risk: A challenge for development*. New York: UNDP, Bureau for Crisis Prevention and Recovery.
- Yin, Y.Y., X.M. Zhang, D.G. Lin, et al. 2014. GEPIC-V-R model: A GIS-based tool for regional crop drought risk assessment. *Agricultural Water Management* 144: 107–119.

---

**Part VII**

**Wildfire Disasters**

---

# Mapping Forest Wildfire Risk of the World

Yongchang Meng, Ying Deng, and Peijun Shi

---

## 1 Background

Forest wildfire is one of the most severe natural hazards. It can start and spread quickly in an uncontrollable way and cause extensive losses and damages. Currently, the occurrence of forest wildfires around the world is over 200 thousand per year, with burned areas of 3.5–4.5 million km<sup>2</sup>, which is approximately equal to the sum of the land areas of India and Pakistan and is greater than half of the land area of Australia (ISDR 2009). Forest wildfire is a hazard that causes the second-largest affected area over the world, following drought (ISDR 2009). Thus, forest wildfire poses a serious threat to national economic development, global ecological system, and personnel safety.

The simulation of forest wildfire propagation dynamically investigates the mechanism of fire spreading under different environmental conditions (topography, weather conditions, etc.) to forecast the fire spread direction and the final burned areas. Some models, such as the Rothermel model (Rothermel 1972) (USA) and the McArthur model (Noble et al. 1980) (Australia), are developed based on wildfire burning experiments and computer stimulations. These models exhibit good simulation results in specific areas but cannot

be applied globally. In addition, these models focus on the dynamic process in certain scenarios after a fire breaks out but unable to predict whether fires will occur in the future and assess its risk level.

The analysis of the causing factors of forest wildfire attempts to establish the correlation between fire features (probability of burning and burned area), natural factors (lightning, temperature, wind speed, topography, etc.), and socioeconomic factors (GDP, population, transportation, etc.), which can not only detect the drivers of forest wildfires in different regions but also can be used to assess the fire risk in different regions. Cruz et al. (2002) studied the relationship between natural factors (canopy height, wind speed, fuel moisture content etc.) and crown fire occurrences by using logistic regression analysis; Viegas et al. (2000) classified fuel types based on the measurements of plant moisture and discussed its relationship with the drought coefficient; Chuvieco et al. (2008) determined the relationship between the interannual variability of the unit area GDP and fire density on a global scale.

Satellite remote sensing and the monitoring of forest wildfires based on 3S techniques has been applied to identify active fire, predict fire propagation potential, and monitor burned area. Remote sensing has unique advantages in forest wildfire monitoring owing to its large spatial scale and temporal continuity of the images. Riano et al. (2007) used years of remote sensing data at 8-km-spatial resolution from the advanced very high resolution radiometer (AVHRR) to map the burned area at a global scale but unable to adequately monitor small-scale, lower-intensity fires due to the low saturation of the AVHRR images. Simon et al. (2004) compiled a global burned area map at a 1-km-spatial resolution by the interpretation of the along track scanning radiometer (ATSR-2) images. The ATSR images, however, underestimated the actual fire intensity, as they contain many forms of noise, such as high land temperature, gas combustions, and city lights. Moderate resolution imaging

---

**Mapping Editors:** Jing'ai Wang (Key Laboratory of Regional Geography, Beijing Normal University, Beijing 100875, China) and Fang Lian (School of Geography, Beijing Normal University, Beijing 100875, China).

**Language Editor:** Kai Liu (Key Laboratory of Environmental Change and Natural Disaster, Ministry of Education, Beijing Normal University, Beijing 100875, China).

Y. Meng · Y. Deng  
Academy of Disaster Reduction and Emergency Management,  
Ministry of Civil Affairs and Ministry of Education,  
Beijing Normal University, Beijing 100875, China

P. Shi (✉)  
State Key Laboratory of Earth Surface Processes and Resource  
Ecology, Beijing Normal University, Beijing 100875, China  
e-mail: spj@bnu.edu.cn

spectroradiometer (MODIS) fire products mark a milestone in the development of fire remote sensing monitoring, with their high spectral resolution, spatial resolution, and middle- and long-wave infrared bands designed specifically for the observation of actively burning fires, which greatly enhance the reliability of the MODIS fire products (Kaufman et al. 1998). Giglio et al. (2006) revealed the spatial pattern of global fire density by compiling MODIS fire products. Based on MODIS, the spatial resolution of the visible infrared imaging radiometer suit (VIIRS) images has increased to 750 m even 375 m, which is more favorable for fire monitoring and identification; however, the time series of the images is too short for further analysis since it was launched in 2011.

Previous studies mainly focus on the identification of active fire, the extraction of the burned area and the spatial-temporal patterns of fire density (van der Werf et al. 2006, 2010; Giglio et al. 2013), lacking of in-depth research studies on forest wildfire risk assessment of different regions in the future. Thus, this study performs a quantitative assessment and mapping of forest wildfire risk at the global scale by compiling relatively long time series data acquired from MODIS products.

## 2 Method

Figure 1 shows the technical flowchart for mapping forest wildfire risk of the world.

### 2.1 Disaster System Theory of Forest Wildfire

According to natural disaster system theory, disasters are integrations of environments, exposures, and hazards (Shi 1991, 1996, 2002). The hazard of forest wildfire disaster is fire, including both man-made and natural fires. The hazard intensity can be measured by the fire occurrence, fire intensity, burned area, flame height, and so on. This study selects annual frequencies of fire occurrence as the hazard intensity indicator. Exposures are the potential objects affected by forest wildfire hazards, such as vegetation, population, infrastructure, and agriculture. The susceptibility of exposures to forest wildfire is related to vulnerability, that is, more vulnerable corresponds to more probable to be damaged. The averaged burned area in a single fire is chosen as the vulnerability index. The hazard-formative environment denotes the particular topography and weather conditions that nurture and affect the occurrences and propagation of forest wildfire disasters. Therefore, a comprehensive understanding and investigation of the interactions of all three components are required to get a better understanding of global forest wildfire risk distribution.

### 2.2 Forest Wildfire Risk

The forest wildfire risk is assessed with a  $0.1^\circ \times 0.1^\circ$  grid cell which contains the land cover types of forest (Appendix III, Exposures data 3.19). In this study, six types of land

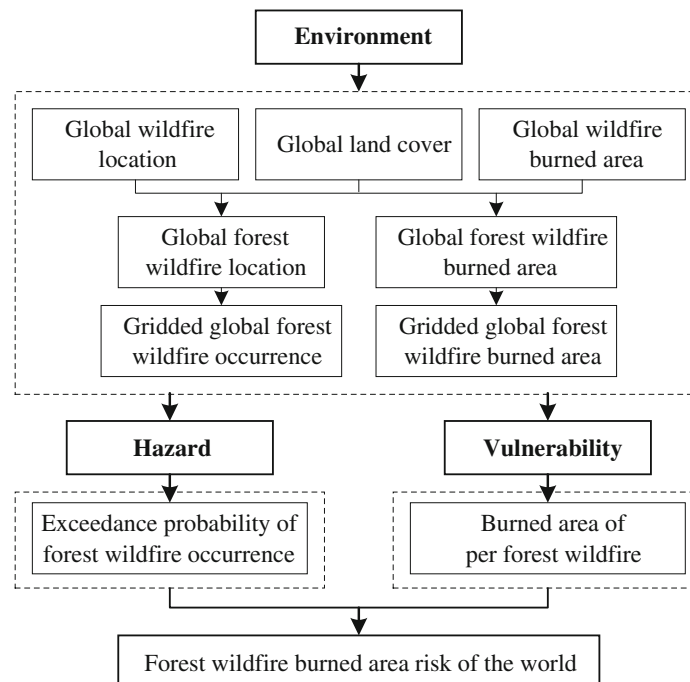


**Fig. 1** Technical flowchart for mapping forest wildfire risk of the world

cover were selected as forest: evergreen needle leaf forest, evergreen broadleaf forest, deciduous needle leaf forest, deciduous broadleaf forest, mixed forests, and closed shrub lands.

### 2.2.1 Intensity

This study assumes that the forest wildfire is a stochastic Markov Process, and its state changes according to a transition rule that only depends on the known past  $N$  years' state.

As aforementioned, this study uses the annual forest wildfire occurrence as the indicator of hazard intensity and uses the historical forest wildfire occurrence to conduct the assessment. The time series of grid global forest wildfire occurrence dataset acquired from MODIS (Appendix III, Hazards data 4.16) is too short ( $N = 12$ ) to analyze using the traditional extreme value fitting theories. The information diffusion theory is therefore introduced to cope with this problem. Information diffusion theory is a fuzzy mathematic method that makes the dataset elements set valued by taking advantage of the fuzzy information optimally (Huang 1997). This study applies normal information diffusion model—one of the most widely used models for calculating the return periods of hazards with different intensities developed by Huang (2012)—to the assessment of forest wildfire hazard.

### 2.2.2 Vulnerability

We calculated the fire occurrence and the corresponding burned area (Appendix III, Disasters data 5.8) of each cell to obtain the average burned area per fire as the vulnerability indicator. Here, the vulnerability reflects the sensitivity of the forest in different regions to fires: high vulnerability indicates that one or a few fires can easily cause large-scale forest wildfires, while in areas of low vulnerability, even a high fire occurrence may not lead to large-scale forest wildfires.

### 2.2.3 Risk

The assessment of hazard and vulnerability is based on the historical recorded data which has already taken the amplification or reduction effect of environments into account. Therefore, in the further assessment of forest wildfire risk, we can use Eq. (1) to obtain the approximate forest wildfire risk as follows:

$$R = H \times V \times E \approx H' \times V' \quad (1)$$

where  $H$  denotes the hazard,  $V$  denotes the vulnerability,  $E$  denotes the environments, and  $H'$  and  $V'$  denote the hazard and the vulnerability impacted by environments, respectively.

## 3 Results

### 3.1 Hazard Intensity

The global forest wildfire occurrence distribution of different return periods is generated in this study. The high-occurrence regions are mainly distributed in central South America, southwest of the Gulf of Mexico, northwest of Southeast Asia, and the central and western regions of Africa. The fire occurrence in these areas is almost over 100 times per year, even more than 1,000 times per year for some regions such as central South America, southern edge of rainforest located in Brazil and Bolivia, as well as Sierra Leone in West Africa. High fire occurrence in forest areas is scattered in the eastern and western coastal areas of Mexico, the northwestern area of the USA, the central part of Canada, the Russian Far East and eastern China, and southeastern Australia. Low forest wildfire occurrence areas are mainly found in northwestern Europe, northern Siberia, southwest China, northern and eastern areas of Canada, and inaccessible regions near the equatorial rainforest areas.

### 3.2 Vulnerability

The world forest areas with a relatively high vulnerability to forest wildfire are mainly concentrated in the regions of central Africa, southwestern Europe, southcentral and eastern areas of Siberia, midwest Canada, and central South America. In specific, the vulnerability of midwest Canada, northern Bolivia, and northeast China into Russia as well as the border of the Democratic Republic of Congo with Angola is particularly high, with a burned area per fire of 25 km<sup>2</sup> (2,500 ha) or more.

### 3.3 Risk

World forest wildfire risk maps were generated under different return periods. The high risk of forest wildfires mainly concentrated in central Africa, central South America, northwestern Southeast Asia, mid-eastern Siberia, and the northern regions of North America. The junction regions of the three African countries of the Democratic Republic of Congo, Republic of Angola, and the Republic of Zambia, along with Myanmar, Thailand, Laos, Cambodia, Bangladesh, Russia Far East, and the eastern coastal areas of Australia, North America, Mexico, Canada, Brazil, Bolivia, and Argentina, are high-risk areas for forest wildfires. The forest wildfire risk of Sierra Leone in West Africa is low although it has a high forest wildfire occurrence, since it is

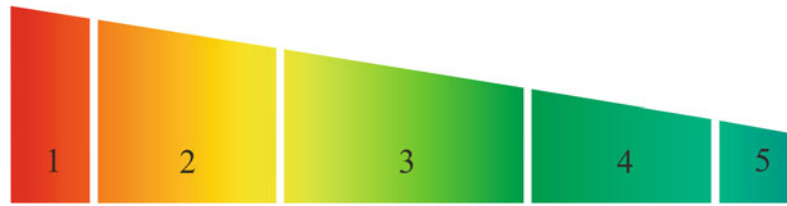


**Fig. 2** Expected annual burned forest area risk of wildfire of the world. 1 (0, 10 %] Russia, Canada, Angola, Brazil, Congo (Democratic Republic of the), USA, Argentina, Burma, Bolivia, China, and Australia. 2 (10, 35 %] Mexico, South Sudan, Chad, India, Mongolia, Thailand, Laos, Vietnam, Zambia, Nigeria, Portugal, Cambodia, Indonesia, Spain, Paraguay, Guatemala, South Africa, Congo, Ethiopia, Cameroon, Nepal, Mali, North Korea, Central African Republic, Uganda, Sudan, and Venezuela. 3 (35, 65 %] Benin, Greece, Kazakhstan, Chile, Papua New Guinea, Romania, Madagascar, Japan, Honduras, Bangladesh, Mozambique, Colombia, France, Belarus,

Cuba, Tanzania, Guinea, Ukraine, Gambia, Peru, Zimbabwe, Senegal, Sierra Leone, Malawi, Belize, Philippines, The Republic of Côte d'Ivoire, Albania, Italy, Nicaragua, Bhutan, and Rwanda. 4 (65, 90 %] Costa Rica, Burkina Faso, Botswana, Lesotho, Syria, Liberia, Sweden, Norway, Dominican Republic, Guyana, UK, Croatia, Bosnia and Herzegovina, Swaziland, Sri Lanka, Algeria, Kenya, Uruguay, Bahamas, Slovenia, Serbia, Timor-Leste, Latvia, Malaysia, Ireland, and Montenegro. 5 (90, 100 %] Suriname, Guinea-Bissau, Iran, South Korea, Ghana, Pakistan, Hungary, Estonia, and Comoros, Macedonia

located in a tropical rainforest climate region with numerous thunderstorms, which contributes to the high forest wildfire occurrence, but simultaneously, the abundant rainfall helps to keep the forest wildfire spread under control.

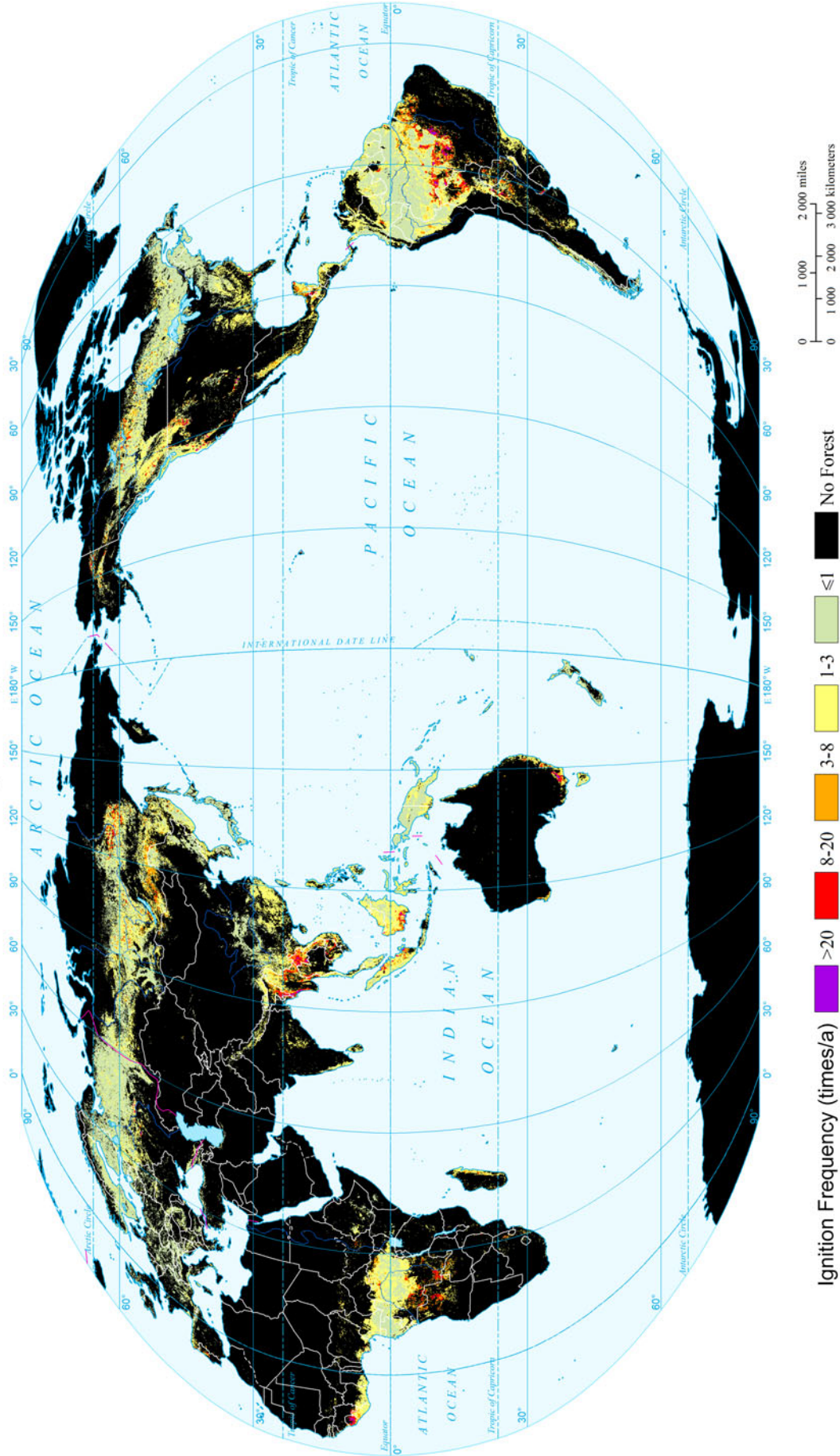
By zonal statistics of the expected risk result, the expected annual burned forest area risk of wildfire of the world at national level is derived and ranked (Fig. 2). The top 1 % country with the highest expected annual burned

forest area risk of wildfire is Russia, and the top 10 % countries are Russia, Canada, Angola, Brazil, the Democratic Republic of Congo, the USA, Argentina, Burma, Bolivia, China, and Australia.

---

#### 4 Maps

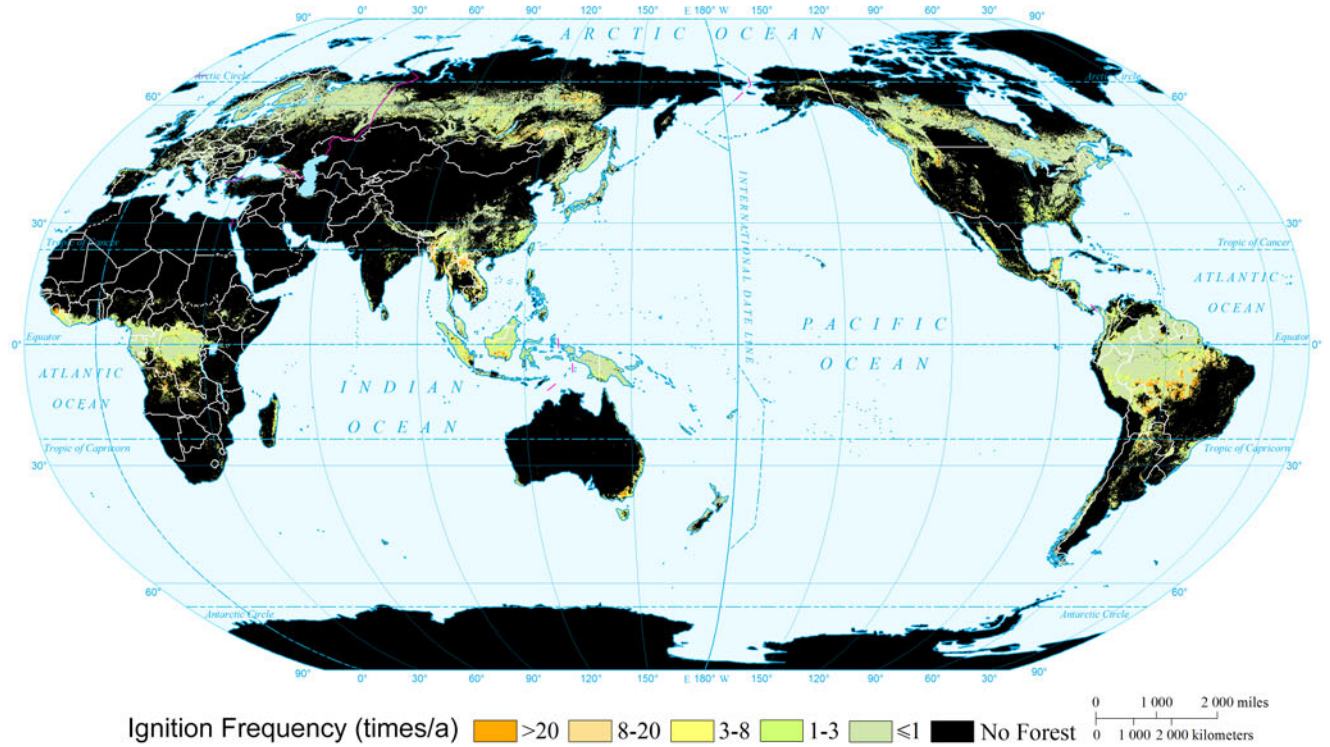
### Expected Annual Intensity of Global Forest Wildfire ( $0.1^\circ \times 0.1^\circ$ )



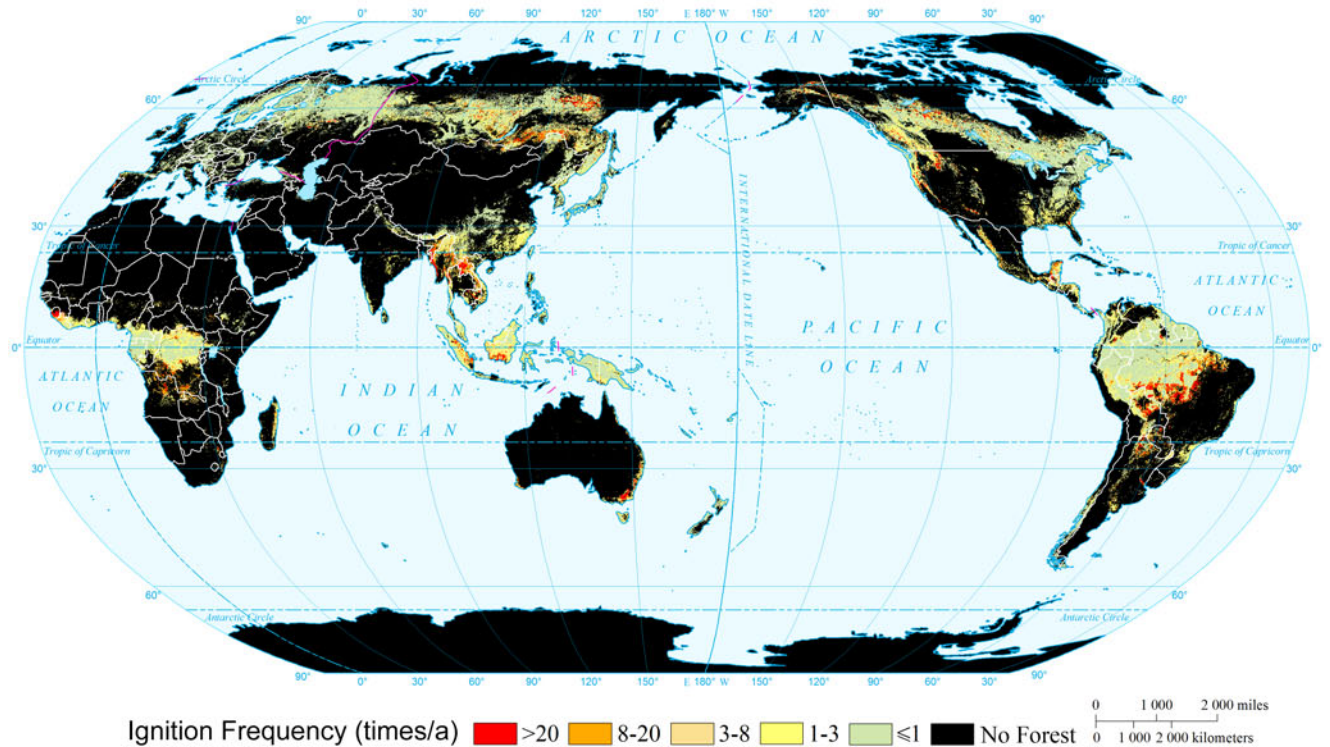
0 1 000 2 000 miles  
0 1 000 2 000 3 000 kilometers

Ignition Frequency (times/a) ■ No Forest ■  $\leq 1$  ■ 1-3 ■ 3-8 ■ 8-20 ■ >20

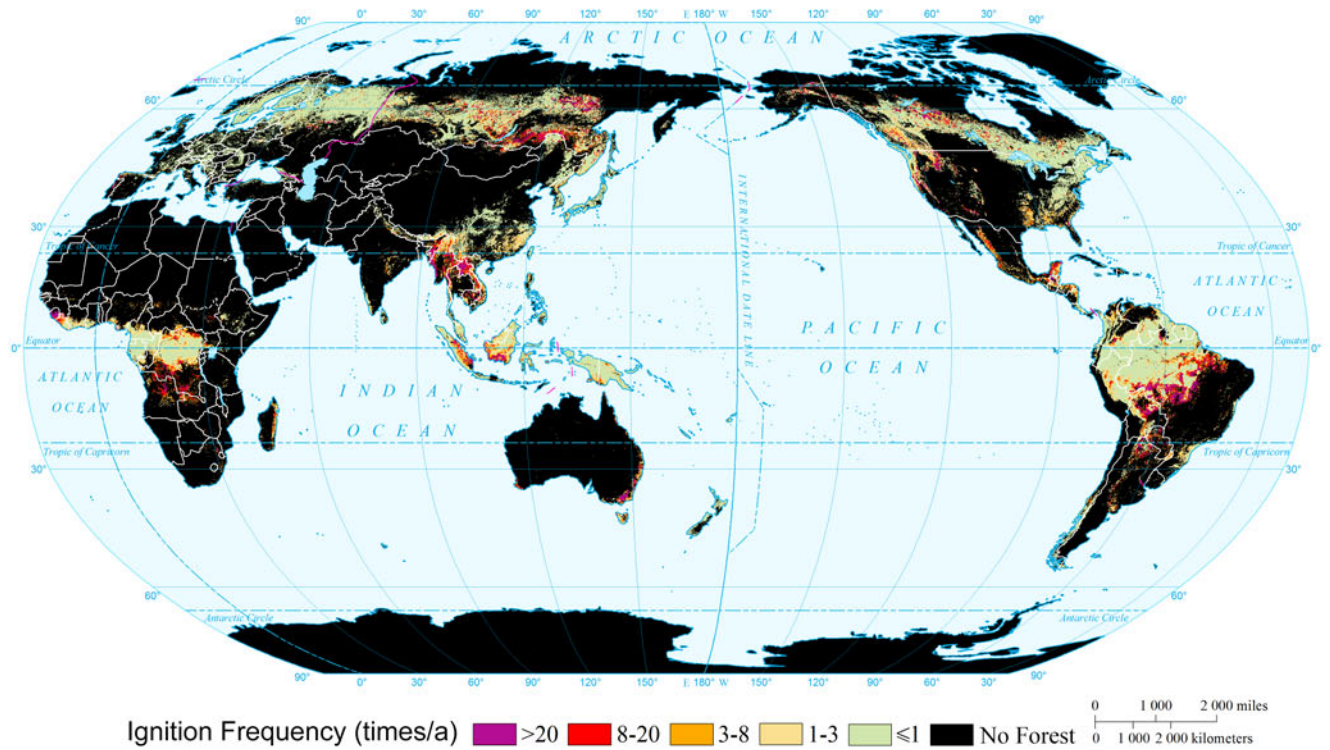
### Global Intensity of Forest Wildfire by Return Period (10a) (0.1°×0.1°)



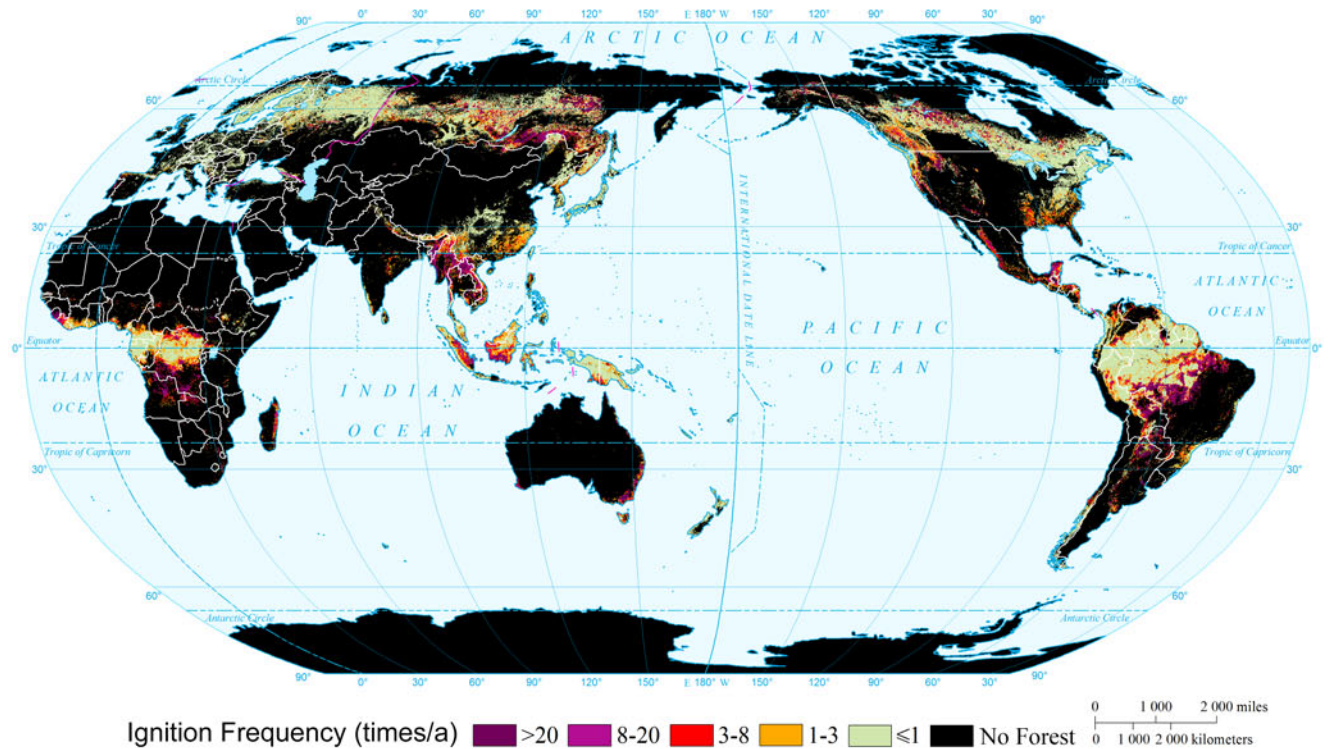
### Global Intensity of Forest Wildfire by Return Period (20a) (0.1°×0.1°)



Global Intensity of Forest Wildfire by Return Period (50a)  
(0.1°×0.1°)



Global Intensity of Forest Wildfire by Return Period (100a)  
(0.1°×0.1°)

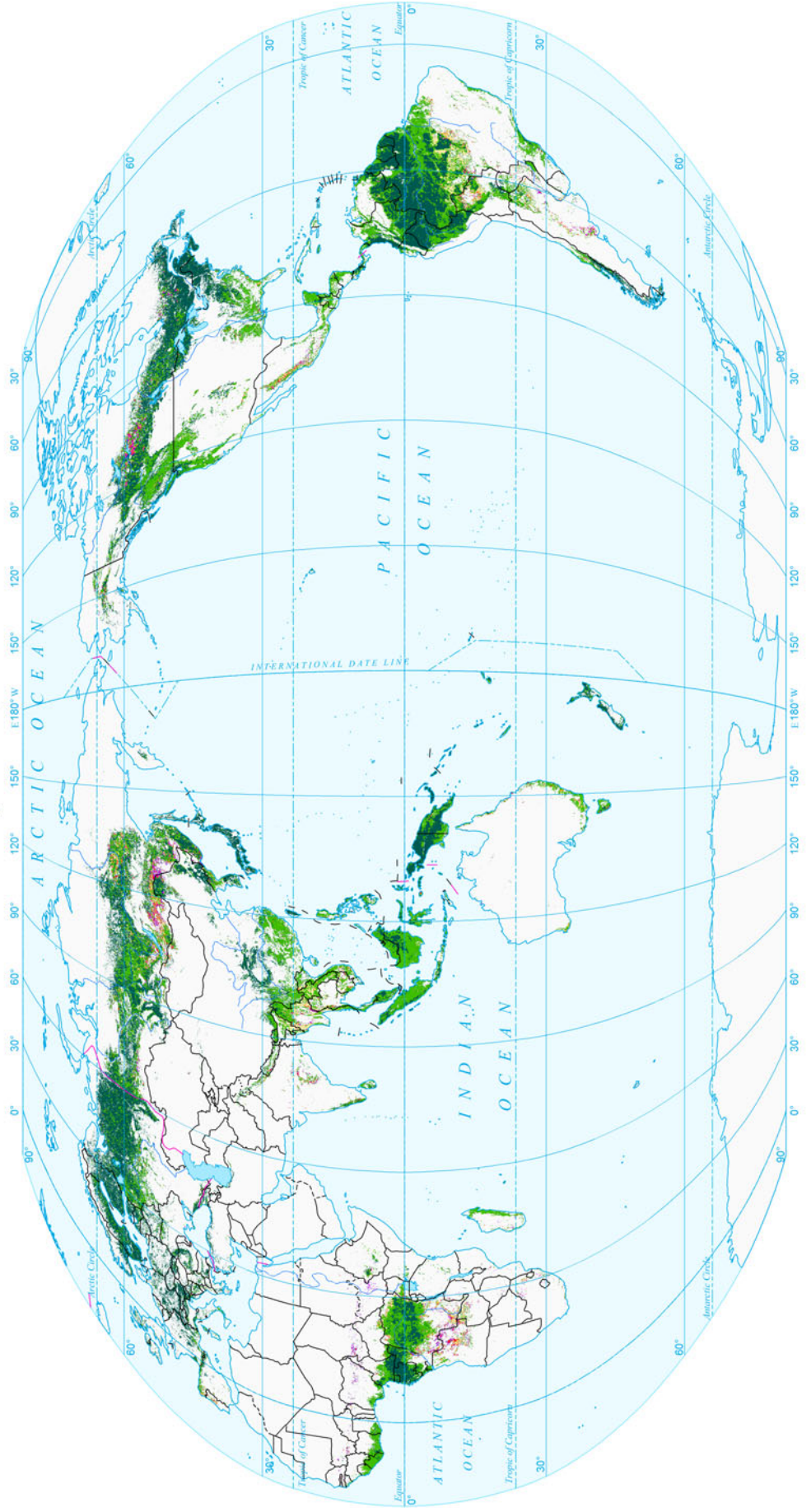




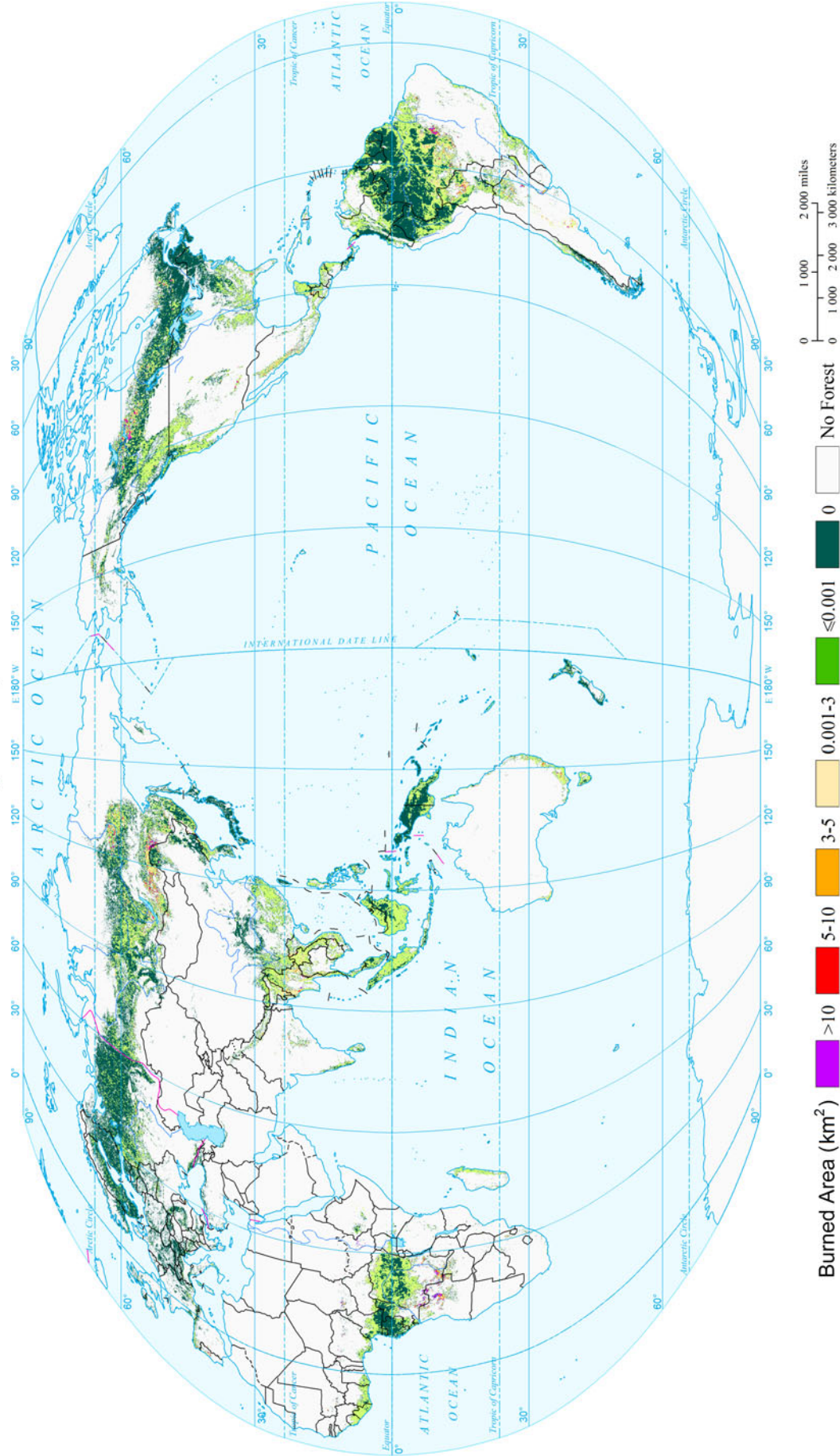
Forest

Wildfire Disasters

Average Annual Burned Area of Global Forest Wildfire (2001-2012)  
(0.1°x0.1°)



### Expected Annual Burned Area Risk of Forest Wildfire of the World ( $0.1^\circ \times 0.1^\circ$ )

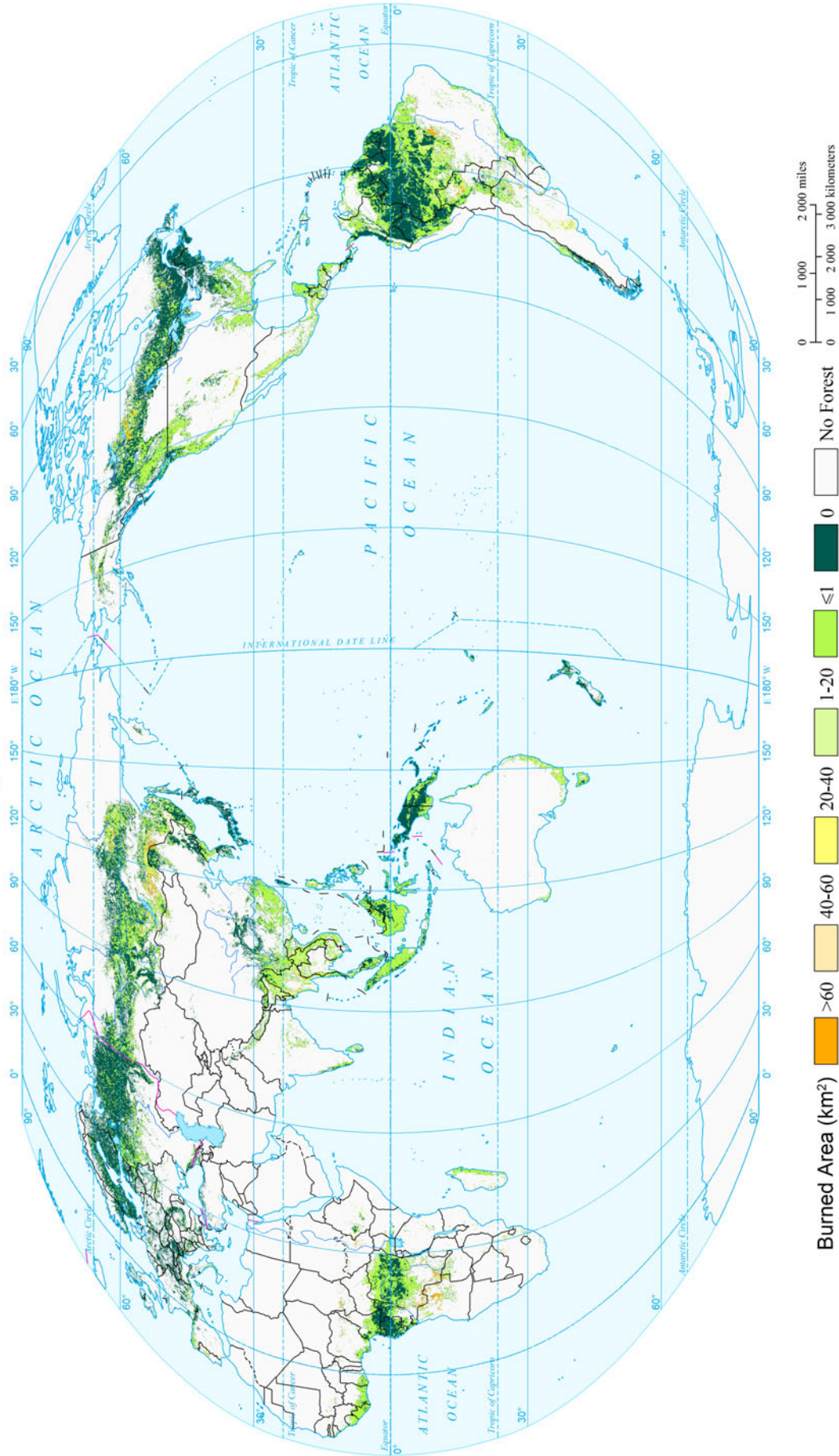




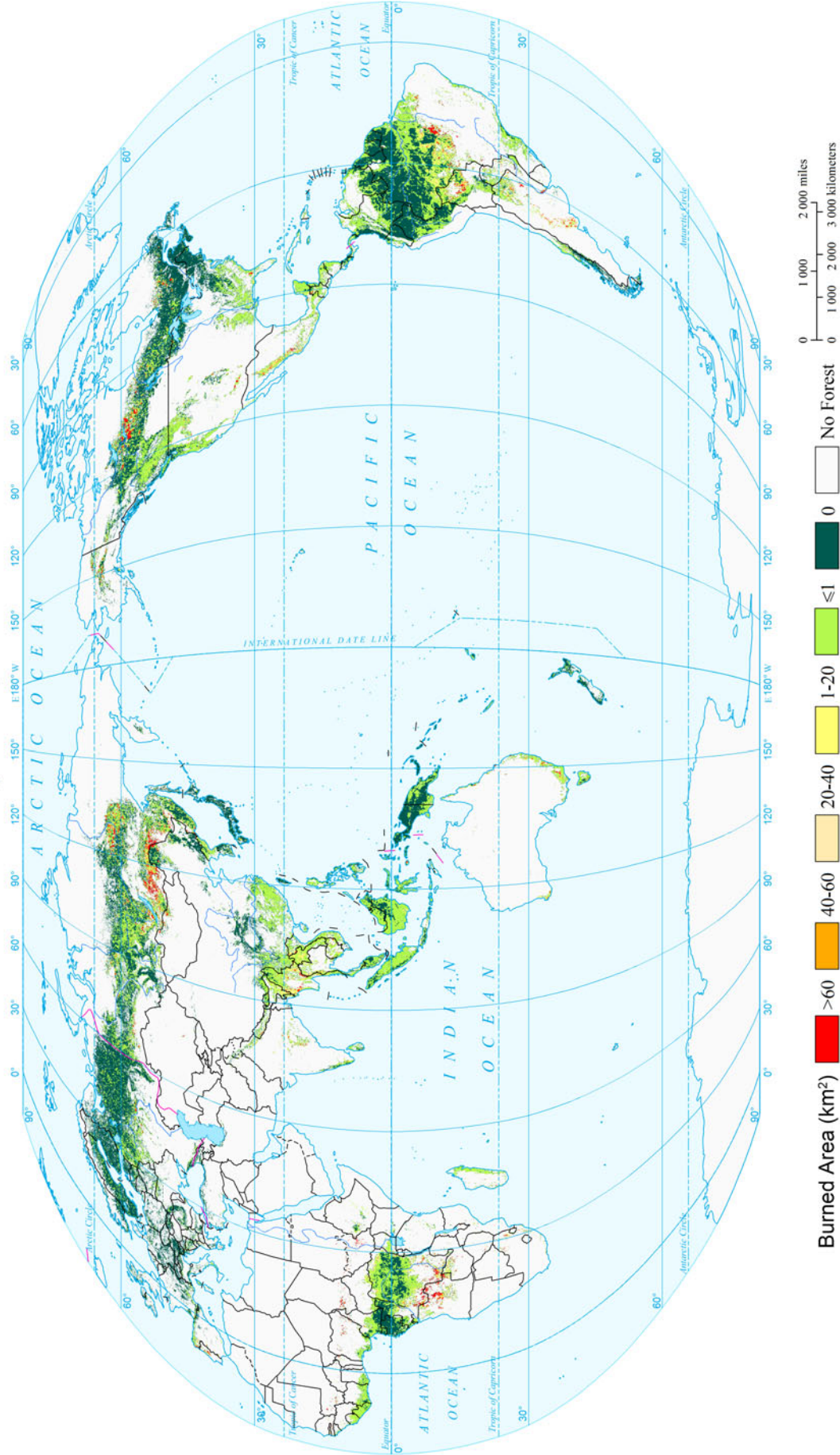
Forest

Wildfire Disasters

Burned Area Risk of Forest Wildfire of the World by Return Period (10a)  
( $0.1^\circ \times 0.1^\circ$ )



Burned Area Risk of Forest Wildfire of the World by Return Period (20a)  
( $0.1^\circ \times 0.1^\circ$ )

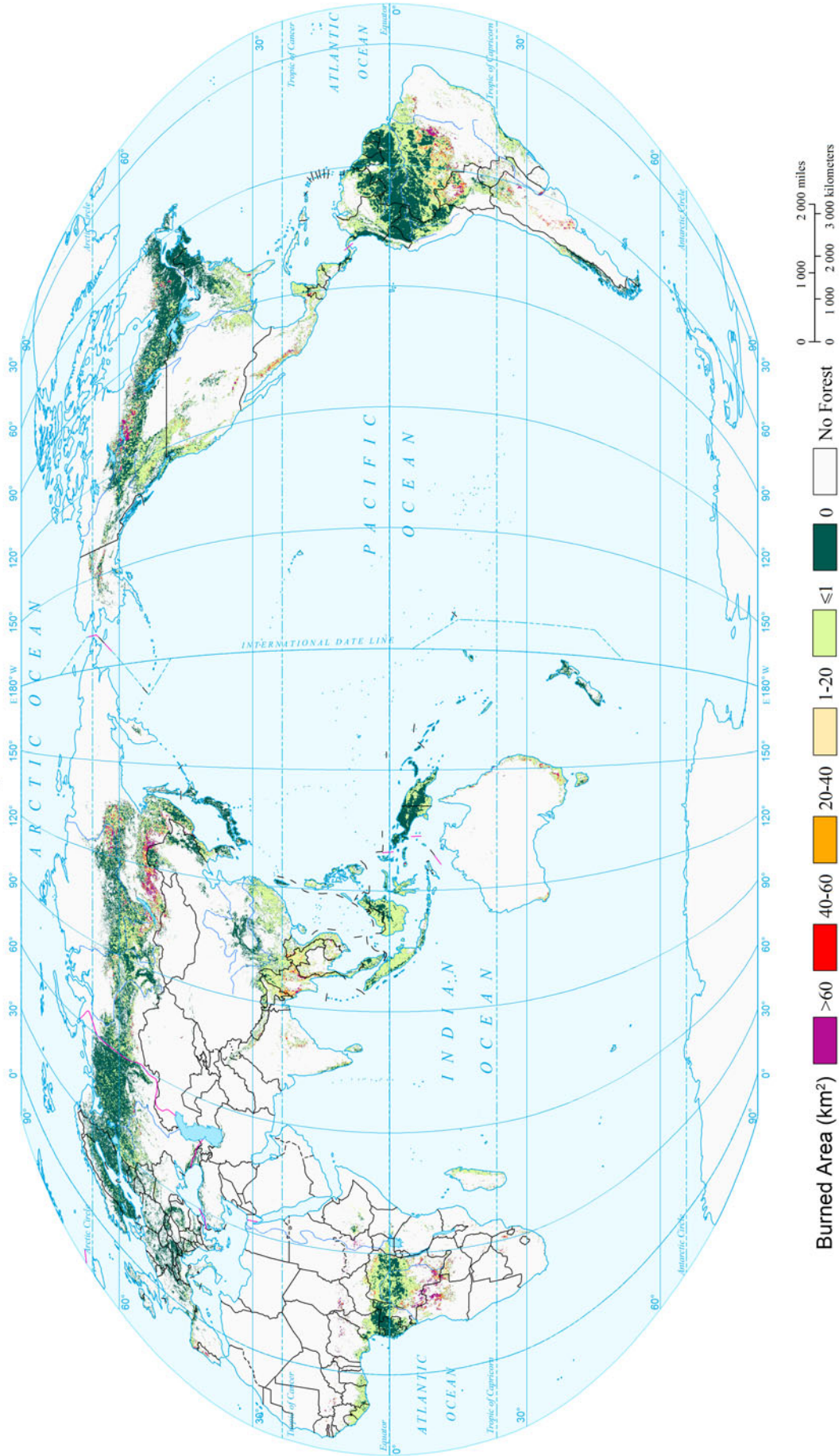




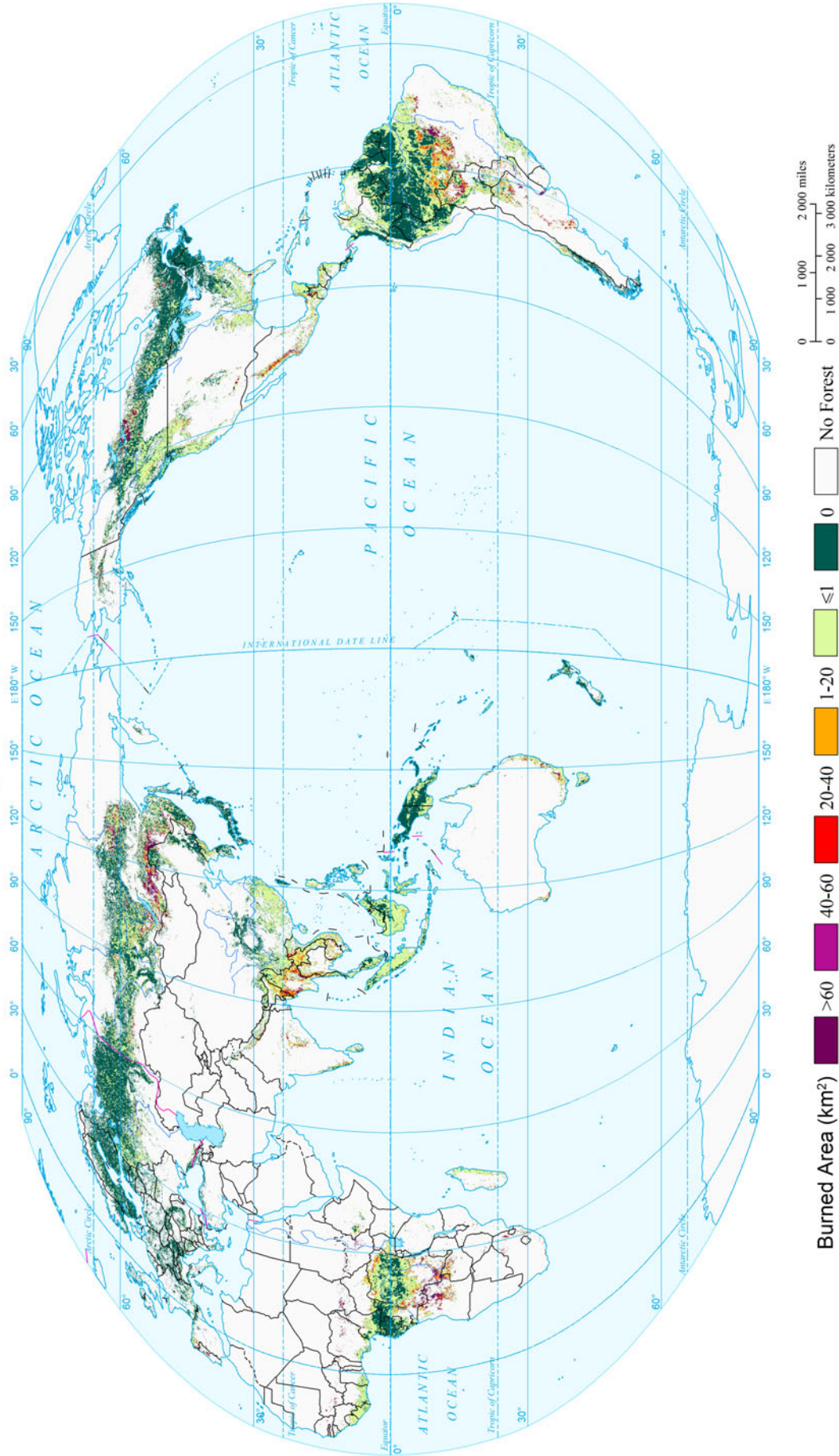
Forest

Wildfire Disasters

Burned Area Risk of Forest Wildfire of the World by Return Period (50a)  
(0.1°x0.1°)

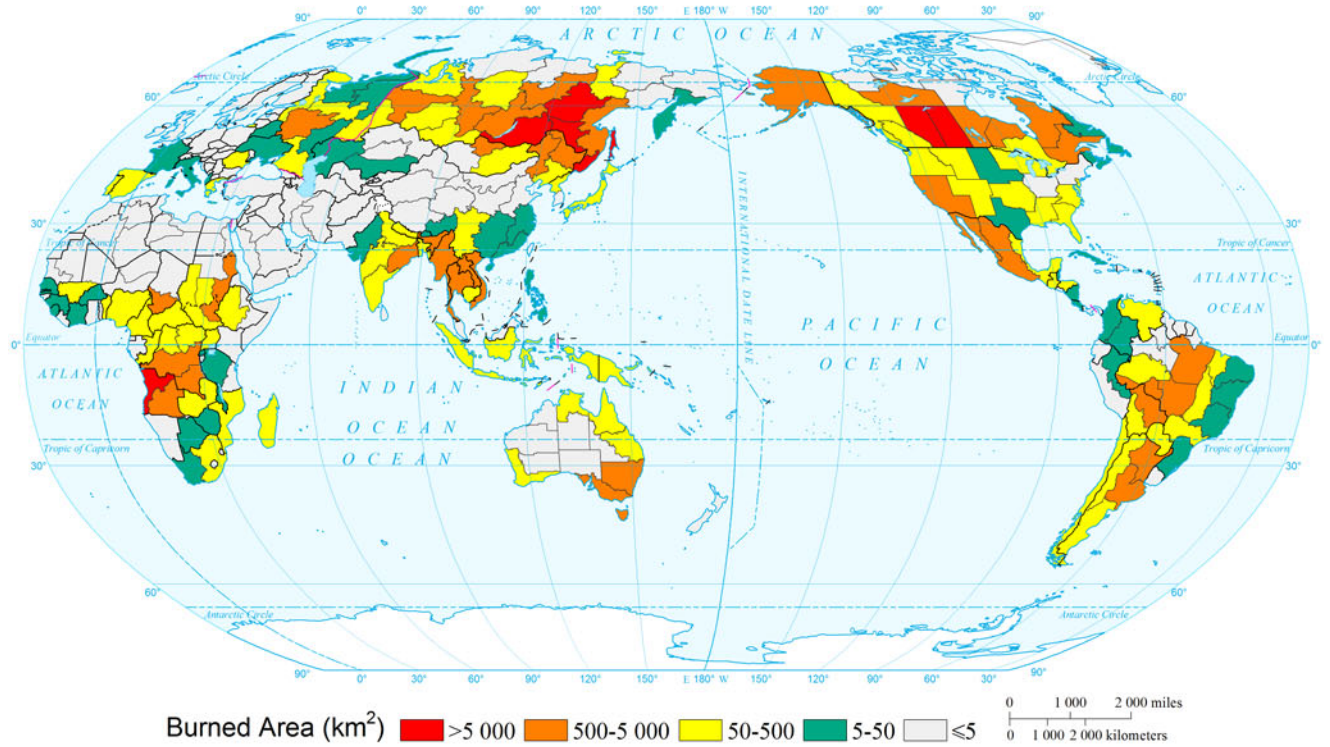


Burned Area Risk of Forest Wildfire of the World by Return Period (100a)  
( $0.1^\circ \times 0.1^\circ$ )

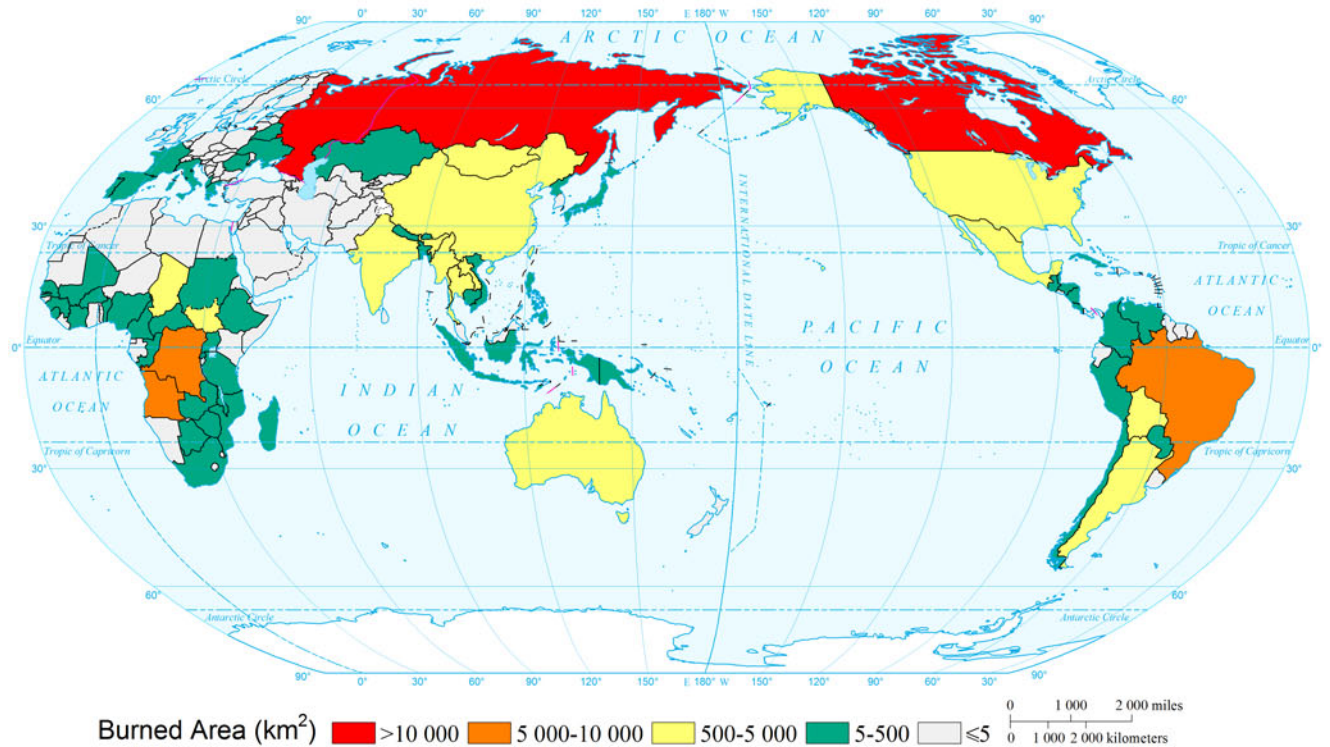


Burned Area ( $\text{km}^2$ )

Expected Annual Burned Area Risk of Forest Wildfire of the World  
(Comparable-geographic Unit)



Expected Annual Burned Area Risk of Forest Wildfire of the World  
(Country and Region Unit)



## References

- Chuvieco, E., L. Giglioand, and C. Justice. 2008. Global characterization of fire activity: Toward defining fire regimes from earth observation data. *Global Change Biology* 14: 1488–1502.
- Cruz, M.G., M.E. Alexander and R.H. Wakimoto. 2002. Predicting crown fire behavior to support forest fire management decision-making. In *Forest fire research and wildland fire safety*, ed. D.X. Viegas, 1–11. Rotterdam: Millpress.
- Giglio, L., I. Csizsarand and C.O. Justice. 2006. Global distribution and seasonality of active fires as observed with the terra and aqua moderate resolution imaging spectroradiometer (MODIS) sensors. *Journal of Geophysical Research: Biogeosciences (2005–2012)*, 111(G2). doi:10.1029/2005JG000142.
- Giglio, L., J.T. Randersonand, and G.R. Werf. 2013. Analysis of daily, monthly, and annual burned area using the fourth-generation global fire emissions database (GFED4). *Journal of Geophysical Research: Biogeosciences* 118: 317–328.
- Huang, C.F. 1997. Principle of information diffusion. *Fuzzy Sets and Systems* 91: 69–90.
- Huang, C.F. 2012. *Natural disaster risk analysis and management*. Beijing: Science Press. (in Chinese).
- International Strategy for Disaster Reduction (ISDR). 2009. *Global assessment report on disaster risk reduction*. Geneva, Switzerland: United Nations.
- Kaufman, Y.J., C.O. Justiceand, L.P. Flynn, et al. 1998. Potential global fire monitoring from EOS-MODIS. *Journal of Geophysical Research: Atmospheres (1984–2012)* 103: 32215–32238.
- Noble, I.R., A.M. Gilland, and G.A.V. Bary. 1980. McArthur's fire-danger meters expressed as equations. *Australian Journal of Ecology* 5: 201–203.
- Riano, D., J.A. Moreno Ruizand, D. Isidoro, et al. 2007. Global spatial patterns and temporal trends of burned area between 1981 and 2000 using NOAA-NASA Pathfinder. *Global Change Biology* 13: 40–50.
- Rothermel, R.C. 1972. A mathematical model for predicting fire spread in wildland fuels: USDA Forest Service.
- Shi, P.J. 1991. Study on the theory of disaster research and its practice. *Journal of Nanjing University (Natural Sciences)* 11(Supplement): 37–42. (in Chinese).
- Shi, P.J. 1996. Theory and practice of disaster study. *Journal of Natural Disasters* 5(4): 6–17. (in Chinese).
- Shi, P.J. 2002. Theory on disaster science and disaster dynamics. *Journal of Natural Disasters* 11(3): 1–9. (in Chinese).
- Simon, M., S. Plummerand, F. Fierens, et al. 2004. Burnt area detection at global scale using ATSR-2: The GLOBSCAR products and their qualification. *Journal of Geophysical Research: Atmospheres (1984–2012)* 109(D14). doi:10.1029/2003JD003622.
- van der Werf, G.R., J.T. Randersonand, L. Giglio, et al. 2006. Interannual variability in global biomass burning emissions from 1997 to 2004. *Atmospheric Chemistry and Physics* 6: 3423–3441.
- van der Werf, G.R., J.T. Randersonand, L. Giglio, et al. 2010. Global fire emissions and the contribution of deforestation, savanna, forest, agricultural, and peat fires (1997–2009). *Atmospheric Chemistry and Physics* 10: 11707–11735.
- Viegas, D.X., G. Bovioand, A. Ferreira, et al. 2000. Comparative study of various methods of fire danger evaluation in southern Europe. *International Journal of Wildland Fire* 9: 235–246.

---

# Mapping Grassland Wildfire Risk of the World

Xin Cao, Yongchang Meng, and Jin Chen

---

## 1 Background

Recent researches indicated an increasing frequency and intensity of grassland wildfire (Running 2006; Balshi et al. 2009), which arose the debate whether grassland wildfire can accelerate global warming (Randerson et al. 2006). Fluctuations of weather and fuel due to climate change will enhance the spatio-temporal uncertainty of grassland wildfire. Therefore, analyzing fire ignition probability, assessing fire propagation damage, and modeling grassland wildfire risk are of great importance with the climate change context.

Existing methods for grassland wildfire risk assessment focus on fire danger monitoring and assessment of fire potential damage and can be classified as fire danger index methods (Gonzalez-Alonso et al. 1997; Burgan et al. 1998; Lopez et al. 2002; Peng et al. 2007), fire causing factors

(Jaiswal et al. 2002; Xu et al. 2005), fire spread model using historic fire database (Mbow et al. 2004; Carmel et al. 2009), and integrated wildfire risk assessment (Tong et al. 2009; Chuvieco et al. 2010). Various fire danger rating systems (FDRSs) have been developed based on the fuel-burning model and climate factors, such as fire behavior prediction and fuel modeling system (BEHAVE) (Burgan and Rothermel 1984), National Fire Danger Rating System (NFDRS) (Bradshaw et al. 1983), Canadian Forest Fire Danger Rating System (CFFDRS) (Canadian Forest Service 1992), Fire Area Simulator (FARSITE) (Finney 2004), etc.

This study performs a quantitative assessment and mapping of grassland wildfire risk at the global scale by multivariate logistic regression based on the long time-series data acquired from MODIS products.

---

## 2 Method

Figure 1 shows the technical flowchart for mapping grassland wildfire risk of the world. The grassland wildfire risk is assessed with a 1 km × 1 km grid cell which contains the land cover types of grassland (Appendix III, Exposures data 3.19). In this study, three types of land cover were selected as grassland: woody savannas, savannas, and grasslands.

### 2.1 Intensity

A multivariate logistic regression model was used to predict grassland burning probability (Cao et al. 2013). Logistic regression is used in the condition of the dichotomous (i.e., binary) response variable. The specific form of the multivariate logistic regression model is as follows:

---

**Mapping Editors:** Jing'ai Wang (Key Laboratory of Regional Geography, Beijing Normal University, Beijing 100875, China) and Fang Lian (School of Geography, Beijing Normal University, Beijing 100875, China).

**Language Editor:** Kai Liu (Key Laboratory of Environmental Change and Natural Disaster, Ministry of Education, Beijing Normal University, Beijing 100875, China).

X. Cao

State Key Laboratory of Earth Surface Processes and Resource Ecology, Beijing Normal University, Beijing 100875, China

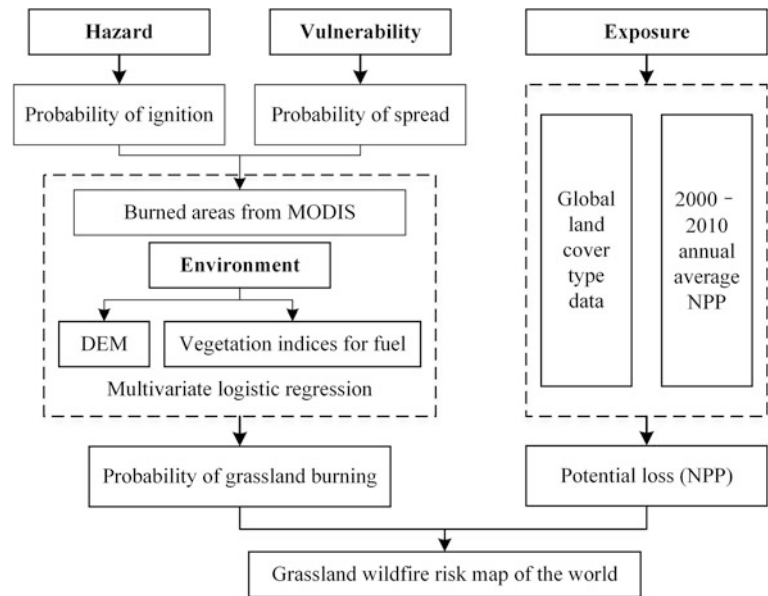
Y. Meng

Academy of Disaster Reduction and Emergency Management, Ministry of Civil Affairs and Ministry of Education, Beijing Normal University, Beijing 100875, China

J. Chen (✉)

College of Global Change and Earth System Science, Beijing Normal University, Beijing 100875, China  
e-mail: chenjin@bnu.edu.cn

**Fig. 1** Technical flowchart for mapping grassland wildfire risk of the world



Assume response variable  $y$  has a binomial distribution (Eq. 1):

$$y = \begin{cases} 1 \\ 0 \end{cases} \quad (1)$$

where  $y = 1$  indicates burned grasslands,  $y = 0$  indicates randomly selected unburned areas. The logistic regression model is defined in Eq. (2):

$$P_{y=1} = \frac{1}{1 + e^{-(\beta_0 + \sum \beta_i X_i)}} \quad (2)$$

where  $P_{y=1}$  represents the burning probability,  $\beta_0$  is the constant value of the logistic regression model, and  $\beta_i$  is the coefficient for variable  $X_i$ .  $X_i$  takes into account the properties of fuels and topography. The following factors were selected or calculated from MODIS 1-km reflectance product (Appendix III, Environments data 2.14) and DEM data (Appendix III, Environments data 2.1) and then used as the explanatory variables for burning probability. It should be noted that the properties of fuels were represented by VIs (vegetation indices) calculated from MODIS data rather than the specific physical indicators of fuel properties.

- Live fuel load: Normalized Difference Vegetation Index (NDVI) and Optimized Soil-Adjusted Vegetation Index (OSAVI)
- Live fuel moisture content: Global Vegetation Moisture Index (GVMI) and Moisture Stress Index (MSI)
- Dead fuel (coverage): Dead Fuel Index (DFI)
- Topography: Digital Elevation Model (DEM), slope, and aspect

Based on the historical burned areas database acquired from MODIS (Appendix III, Hazards data 4.17), we built up the grassland burning probability model by using 2000–2010 historical burned areas as the response variable, while the information of fuels in grassland together with topographic factors is taken as the explanatory variables.

## 2.2 Vulnerability

Considering the main potential loss of grassland fire is the stockbreeding industry, and the stock capacity is directly dependent on the biomass of grassland. Net primary product (NPP) was then used as a surrogate to represent the potential loss of grassland fire. The average NPP distribution was calculated based on the data from 2000 to 2010 (Appendix III, Exposures data 3.20).

## 2.3 Risk

Under the framework of disaster risk assessment, the grassland fire risk model is constructed in Eq. (3):

$$R = H \times V \times E \quad (3)$$

where  $R$  is the risk of grassland fire;  $H$  is the grassland fire, i.e., the probability of fire ignition;  $V$  is the vulnerability, i.e., the probability of fire propagation;  $E$  is the exposure, i.e., the potential loss or NPP. In this model, both fire ignition and propagation information are considered, the probability of



**Fig. 2** Expected annual grassland NPP loss risk of wildfire of the world. 1 (0, 10 %] Brazil, United States, Australia, Russia, Kazakhstan, Mozambique, Madagascar, China, Tanzania, Canada, Angola, South Africa, Venezuela, Argentina, Nigeria, Sudan, Colombia. 2 (10, 35 %] Mexico, Zimbabwe, Zambia, Democratic Republic of the Congo, Botswana, Mongolia, Bolivia, Kenya, India, Namibia, The Republic of Côte d'Ivoire, Central African Republic, Turkey, Burma, Paraguay, Ethiopia, Uruguay, Ghana, Spain, Thailand, Congo, Indonesia, Chad, Somalia, Mali, Burkina Faso, Vietnam, Cameroon, Guinea, Portugal, France, Ecuador, Benin, Malawi, Chile, Italy, Cambodia, Peru, Senegal, New Zealand, Nicaragua, Niger, Togo, Laos. 3 (35, 65 %] Honduras, Uganda, Gabon, Guyana, Romania, Iran, Germany, Kyrgyzstan, Morocco, Japan, Papua New Guinea, Belarus, United Kingdom, Greece, Georgia, Swaziland, Ukraine, Croatia, Guatemala, Sweden, Cuba, Mauritania, Norway, Bosnia and Herzegovina, Dominican

Republic, Finland, Sierra Leone, Nepal, Serbia, Afghanistan, Uzbekistan, Poland, Azerbaijan, Philippines, Bangladesh, South Korea, Turkmenistan, Sri Lanka, Tajikistan, Iceland, Guinea-Bissau, El Salvador, Panama, Czech Republic, North Korea, Costa Rica, Timor-Leste, Bulgaria, Armenia, Haiti, Ireland, Algeria. 4 (65, 90 %] Latvia, Austria, Slovakia, Malaysia, Hungary, Lesotho, Burundi, Lithuania, Switzerland, Tunisia, Slovenia, Rwanda, Gambia, Bahamas, Bhutan, Albania, Pakistan, Estonia, Macedonia, Belize, Montenegro, Eritrea, Iraq, Suriname, Cyprus, Denmark, Trinidad and Tobago, Liberia, Jamaica, Fiji, the Netherlands, Belgium, Mauritius, Israel, Syria, Egypt, Lebanon, Oman, Cape Verde, Libya, Moldova, Yemen, Comoros, Luxembourg. 5 (90, 100 %] Palestine, Barbados, Equatorial Guinea, Saudi Arabia, Gaza Strip, Antigua and Barbuda, Jordan, San Marino, Singapore, Andorra, Baker Island, Saint Lucia, Liechtenstein, Djibouti, United Arab Emirates, Solomon Islands, Western Sahara, Kuwait

grassland burning is therefore taken as a combination of the probability of ignition and propagation.

### 3 Results

Based on the grassland fire risk assessment model, we firstly calculated the grassland burning probability at 8-day scale and then calculated the annually averaged grassland burning probability. The yearly grassland fire 'risk' was then modeled by the product of yearly grassland burning probability and NPP. The final global grassland burning probability map and risk map were obtained by averaging the above results during 2000–2010.

#### 3.1 Hazard Intensity

The intensity of grassland fire was represented by the grassland burning probability. A higher probability of grassland burning means the higher intensity of hazard. Grasslands with high burning probabilities concentrate in the central part of Asia, western Europe, western Africa, northern Oceania, central part of North America and eastern part of South America. The grassland in Kazakhstan, western Russia, eastern Mongolia, Ukraine, Somalia, Kenya, Madagascar, northwestern Australia, northern United States, southern Canada, and eastern Brazil is prone to be affected by grassland fire.

#### 3.2 The NPP Loss Risk

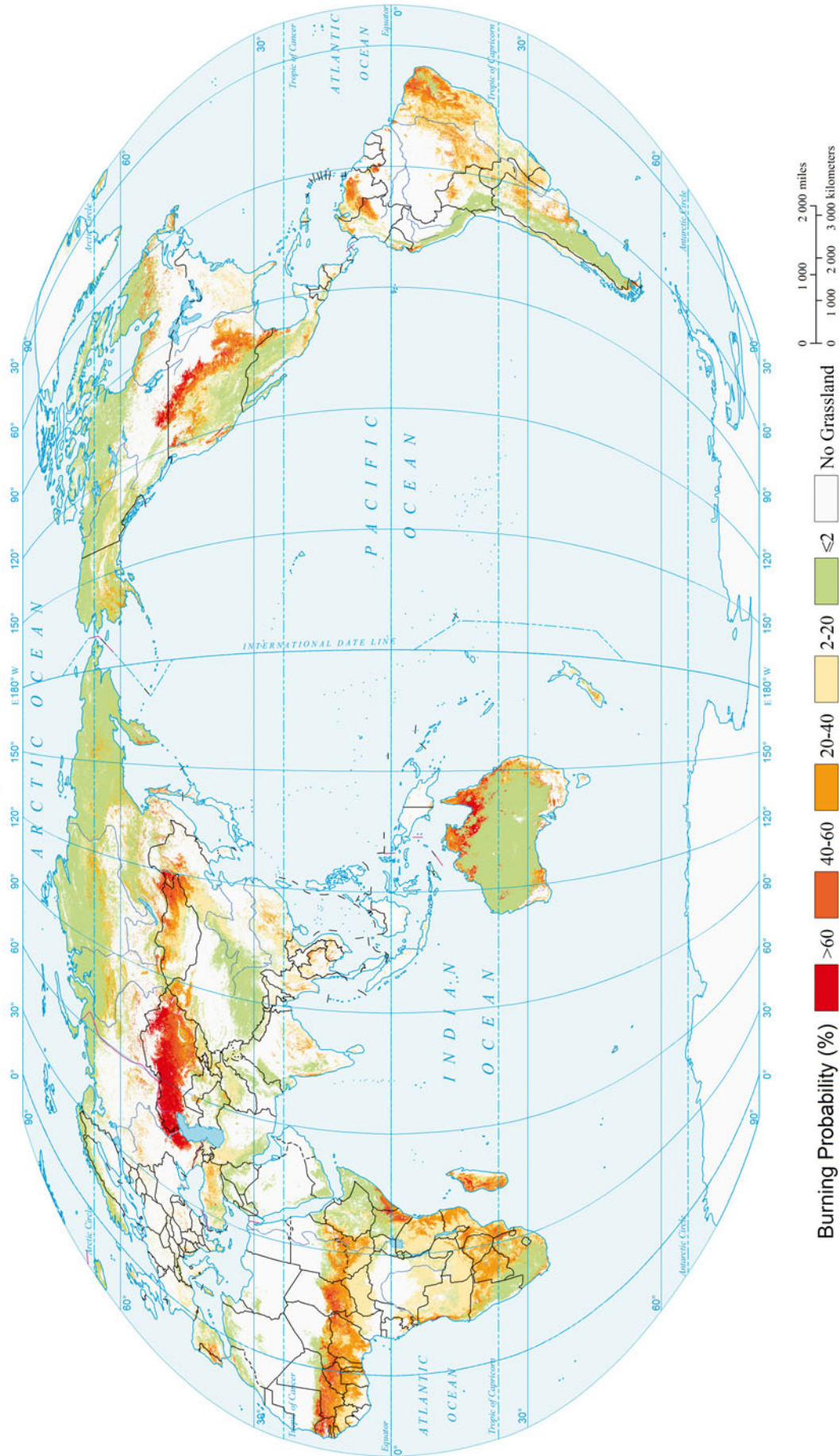
The risk of grassland fire is represented by the product of the grassland burning probability and NPP. The higher average potential loss of NPP means the higher risk of grassland fire. It can be observed that the high-grassland-fire-risk regions are concentrated in the central part of Asia, western Europe, southwestern Africa, northern Oceania, central part of North America, and northeastern South America, including Kazakhstan, western Russia, eastern Mongolia, Ukraine, Somalia, Kenya, Mozambique, Tanzania, Madagascar, northwestern Australia, central part of United States, southern Canada, Columbia, Venezuela, and eastern Brazil.

By zonal statistics of the expected risk result, the expected annual grassland NPP loss risk of wildfire of the world at national level is derived and ranked (Fig. 2). The top 1 % countries with highest expected annual grassland NPP loss risk of wildfire are Brazil and United States, and the top 10 % countries are Brazil, United States, Australia, Russia, Kazakhstan, Mozambique, Madagascar, China, Tanzania, Canada, Angola, South Africa, Venezuela, Argentina, Nigeria, Sudan and Colombia.

### 4 Maps



Average Annual Burning Probability of Global Grassland Wildfire (2000-2010)  
(1kmx1km)

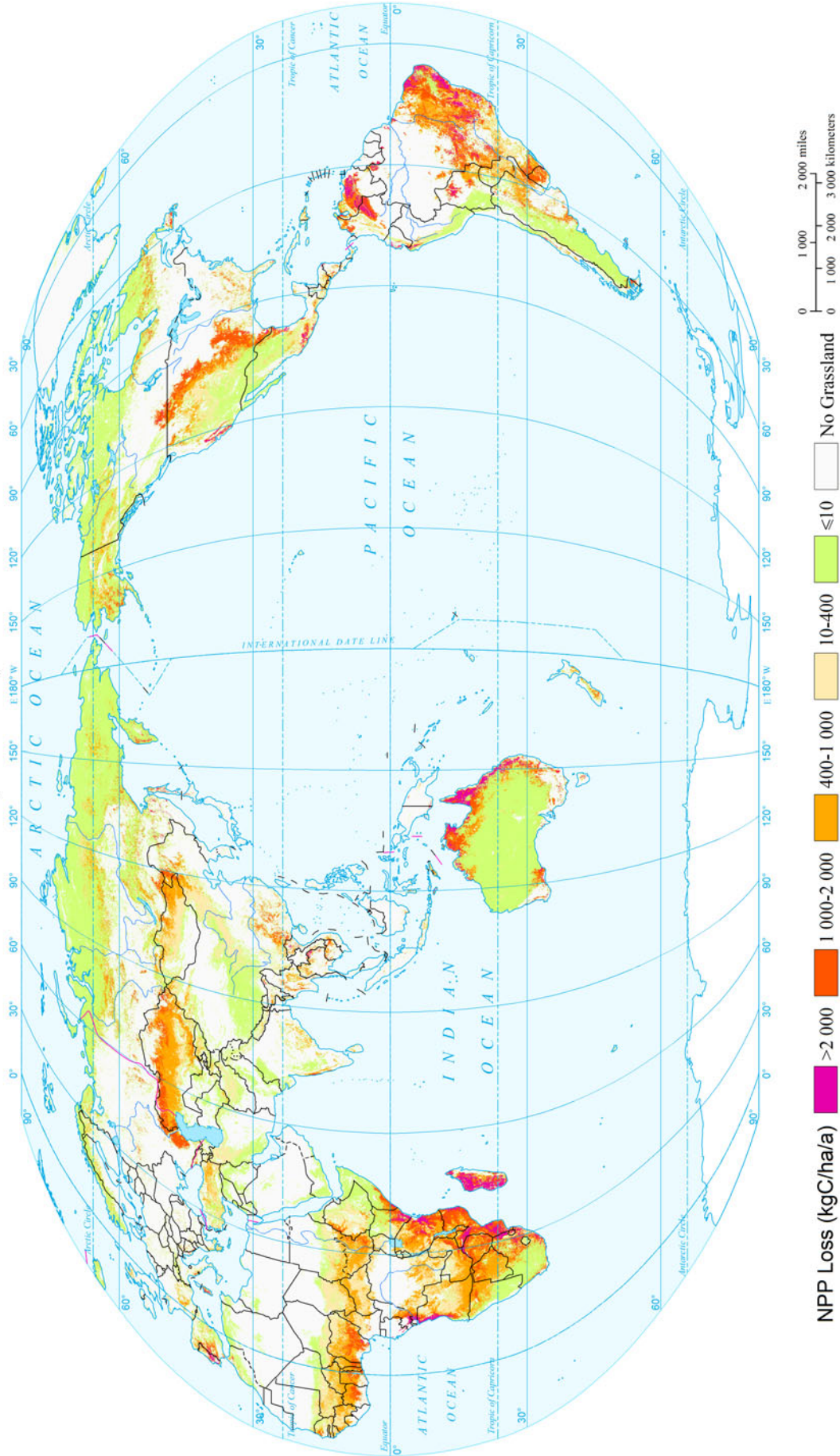




Grassland

Wildfire Disasters

### Expected Annual NPP Loss Risk of Grassland Wildfire of the World (1km x 1km)

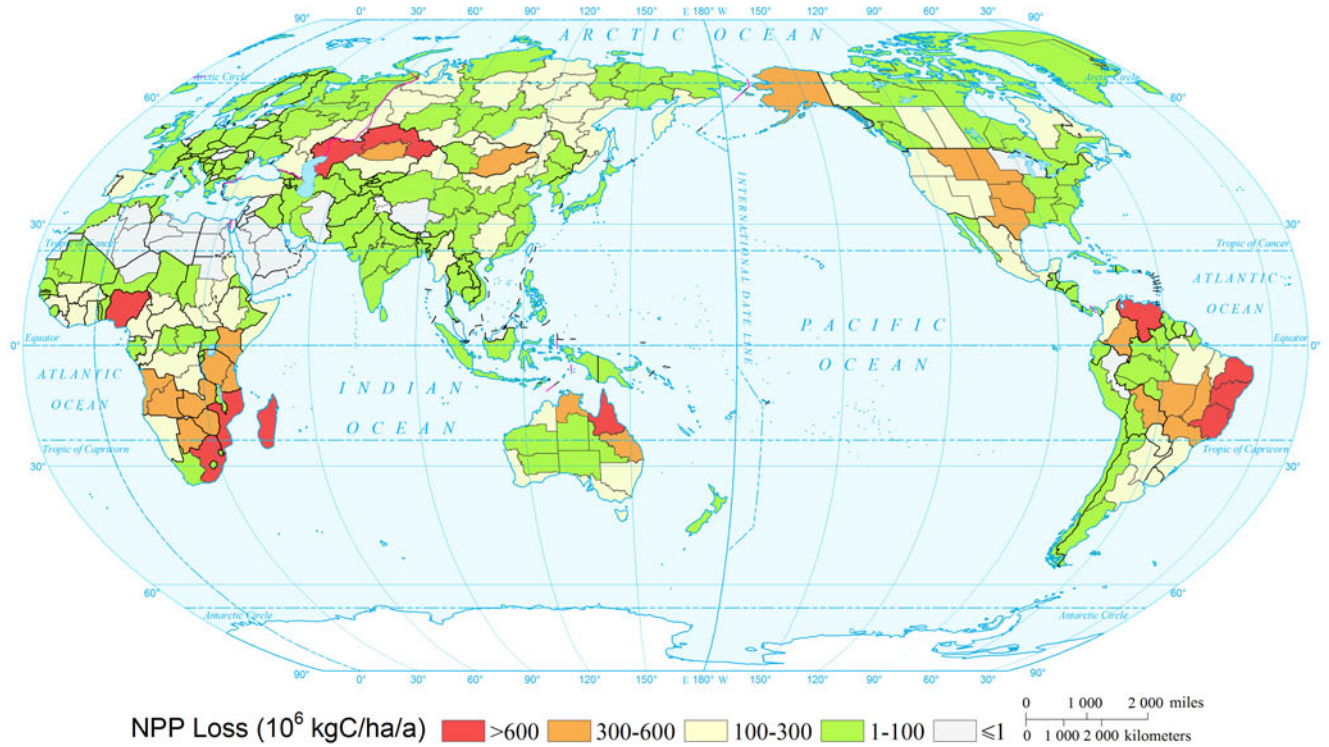


NPP Loss (kgC/ha/a)

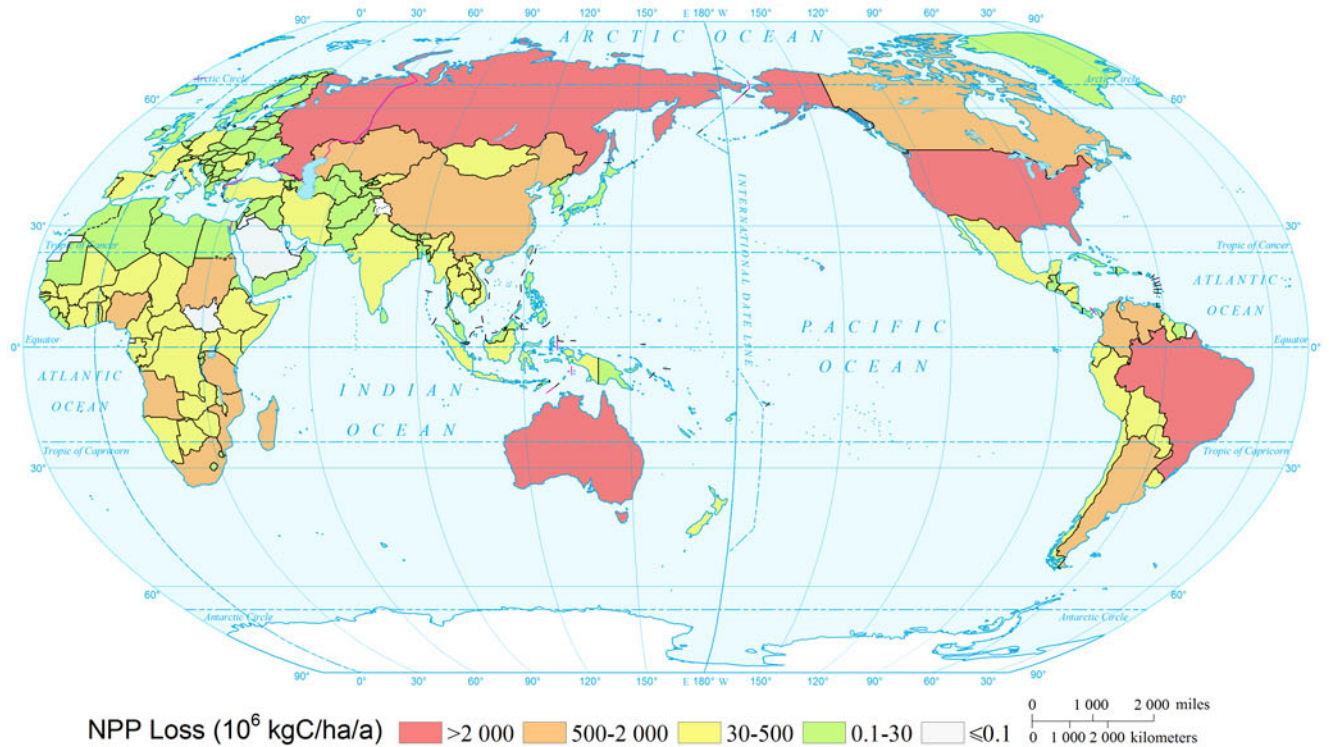
- >2 000
- 1 000-2 000
- 400-1 000
- 10-400
- ≤10
- No Grassland

0 1 000 2 000 miles  
0 1 000 2 000 3 000 kilometers

Expected Annual NPP Loss Risk of Grassland Wildfire of the World  
(Comparable-geographic Unit)



Expected Annual NPP Loss Risk of Grassland Wildfire of the World  
(Country and Region Unit)



## References

- Balshi, M.S., A.D. McGuire, P. Duffy, et al. 2009. Assessing the response of area burned to changing climate in western boreal North America using a multivariate adaptive regression splines (MARS) approach. *Global Change Biology* 15: 578–600.
- Bradshaw, L.S., J.E. Deeming, R.E. Burgan, et al. 1983. *The 1978 national fire-danger rating system: Technical documentation*. General Technical Report INT-169. Ogden, UT: US Department of Agriculture, Forest Service, Intermountain Forest and Range Experiment Station.
- Burgan, R.E. and R.C. Rothermel. 1984. *BEHAVE: Fire behavior prediction and fuel modeling system—FUEL subsystem*. General Technical Report INT-167, Ogden, UT: US Department of Agriculture, Forest Service, Intermountain Forest and Range Experiment Station.
- Burgan, R.E., R.W. Klaver, and J.M. Klaver. 1998. Fuel models and fire potential from satellite and surface observation. *International Journal of Wildland Fire* 8: 159–170.
- Canadian Forest Service. 1992. *Development and structure of the Canadian forest fire danger rating system*. Canadian Forest Service, Information Report ST-X-3, Ottawa, Ontario, Canada. <http://fire.cfs.nrcan.gc.ca/research/>. Accessed in July 2013.
- Cao, X., X.H. Cui, M. Yue, et al. 2013. Evaluation of wildfire propagation susceptibility in grasslands using burned areas and multivariate logistic regression. *International Journal of Remote Sensing* 34(19): 6679–6700.
- Carmel, Y., S. Paz, F. Jahashan, et al. 2009. Assessing fire risk using monte carlo simulations of fire spread. *Forest Ecology and Management* 257: 370–377.
- Chuvieco, E., I. Aguadoa, M. Yebra, et al. 2010. Development of a geographic information system technologies. *Ecological Modelling* 221(1): 46–58.
- Finney, M.A. 2004. *FARSITE: Fire area simulator—Model development and evaluation*. General Technical Report, RMRS-RM-4 revised. Ogden, UT: US Department of Agriculture, Forest Service.
- Gonzalez-Alonso, F., J.M. Cuevas, J.L. Casanova, et al. 1997. A forest fire risk assessment using NOAA AVHRR images in the Valencia area, eastern Spain. *International Journal of Remote Sensing* 18 (10): 2201–2207.
- Jaiswal, R.K., S. Mukherjee, K.D. Raju, et al. 2002. Forest fire risk zone mapping from satellite imagery and GIS. *International Journal of Applied Earth Observation and Geoinformation* 4: 1–10.
- Lopez, A.S., J. San-Miguel-Ayanz, and R.E. Burgan. 2002. Integration of satellite sensor data, fuel type maps and meteorological observations for evaluation of forest fire risk at the pan-European scale. *International Journal of Remote Sensing* 23(13): 2713–2719.
- Mbow, C., K. Goita, and G. Benie. 2004. Spectral indices and fire behavior simulation for fire risk assessment in savanna ecosystems. *Remote Sensing of Environment* 91: 1–13.
- Peng, G.X., J. Li, Y.H. Chen, et al. 2007. A forest fire risk assessment using ASTER images in Peninsular Malaysia. *Journal of China University of Mining & Technology* 17(2): 232–237.
- Randerson, J.T., H. Liu, M.G. Flanner, et al. 2006. The impact of boreal forest fire on climate warming. *Science* 314: 1130–1132.
- Running, S.W. 2006. Is global warming causing more, larger wildfires? *Science* 313: 927–928.
- Tong, Z.J., J.Q. Zhang, and X.P. Liu. 2009. GIS-based risk assessment of grassland fire disaster in western Jilin Province, China. *Stochastic Environmental Research and Risk Assessment* 23(4): 463–471.
- Xu, D., L.M. Dai, G.F. Shao, et al. 2005. Forest fire risk zone mapping from satellite images and GIS for Baihe Forestry Bureau, Jilin, China. *Journal of Forestry Research* 16(3): 169–173.

---

**Part VIII**

**Multi-natural Disasters**

---

# Mapping Multi-hazard Risk of the World

Peijun Shi, Xu Yang, Fan Liu, Man Li, Hongmei Pan, Wentao Yang, Jian Fang, Shao Sun, Chenyan Tan, Huimin Yang, Yuanyuan Yin, Xingming Zhang, Lili Lu, Mengyang Li, Xin Cao, and Yongchang Meng

---

## 1 Introduction

Multi-hazard risk assessment aims at assessing the total risk of various types of hazards happened in an area in a certain period of time (Shi 2009). Since the 1980s, many organizations around the world have carried out in-depth research on multi-hazard risk assessment and attempted risk mapping at regional and global scales.

In 2004, the United Nations Development Programme (UNDP) developed the Disaster Risk Index (DRI) to assess the worldwide mortality risk caused by multi-hazard including earthquake, cyclone, flood, and drought at national level (UNDP 2004). The DRI is estimated by combining exposure with historical human vulnerability acquired from EM-DAT database. Specific hazard risk is calculated and further combined in a multiple DRI allowing for a classification of countries. This index, however, only considers 4 types of hazards in a specific time period, which cannot

reflect total hazard risk of the world. Meanwhile, the DRI cannot be used in a predictive way to estimate potential casualties in the future.

To overcome deficiencies of DRI, the World Bank and Columbia University introduced the Hotspots index. The Hotspots index mainly takes into account mortality-related risks and economic risk caused by six types of natural hazards—earthquake, volcano, landside, flood, drought, and cyclone. The vulnerability indicator is obtained by calculating the loss rates for each hazard from historical losses over 20 years (1981–2000) obtained from EM-DAT database (Dilley et al. 2005). Compared to DRI, the economic losses are considered in Hotspots index and the spatial resolution has been improved. A drawback of Hotspots index is that it uses the fitted vulnerability curve of death toll and economic losses at national level, which leads to an inadequate accuracy of the assessment result for counties with large area and significant geographic differences.

---

**Mapping Editors:** Jing'ai Wang (Key Laboratory of Regional Geography, Beijing Normal University, Beijing 100875, China), Fang Lian (School of Geography, Beijing Normal University, Beijing 100875, China) and Chunqin Zhang (School of Geography, Beijing Normal University, Beijing 100875, China).

**Language Editors:** Wei Xu (Key Laboratory of Environmental Change and Natural Disaster, Ministry of Education, Beijing Normal University, Beijing 100875, China) and Kai Liu (Key Laboratory of Environmental Change and Natural Disaster, Ministry of Education, Beijing Normal University, Beijing 100875, China).

P. Shi (✉) · X. Cao  
State Key Laboratory of Earth Surface Processes and Resource Ecology, Beijing Normal University, Beijing 100875, China  
e-mail: spj@bnu.edu.cn

---

X. Yang · F. Liu · M. Li · H. Pan · W. Yang · J. Fang · S. Sun  
C. Tan · L. Lu · M. Li · Y. Meng  
Academy of Disaster Reduction and Emergency Management,  
Ministry of Civil Affairs and Ministry of Education, Beijing  
Normal University, Beijing 100875, China

H. Yang · X. Zhang  
School of Geography, Beijing Normal University,  
Beijing 100875, China

H. Yang · Y. Yin  
Key Laboratory of Regional Geography, Beijing Normal  
University, Beijing 100875, China

The United Nations University (UNU-EHS) proposed a World Risk Index (WRI) for multi-hazard risk assessment at national level. The WRI is the product of exposure and vulnerability combined with the coping capacity and adaptation. Based on this approach, the multi-hazard risk of 173 countries was assessed and ranked in the World Risk Report in 2013 (UNU-EHS 2013). Although WRI considers comprehensive factors, it lacks consideration of the different levels of various hazard types. Furthermore, judgment weights are used when combining the risk factors which may cause an inaccurate prediction.

In this study, two methods are adopted for mapping the multiple risks for population and property. In the first method, a Total Risk Index (TRI) is proposed to calculate the world multiple risks by weighting the world risk maps of each individual hazard. The TRI takes into account mortality (including affected population) risk, economic loss (including affected GDP) risk, crop yield loss risk, burned area risk caused by eleven types of natural hazards, that is, earthquake, volcano, landside, flood, storm surge, tropical cyclone, sand-dust storm, drought, heat wave, cold wave, and wildfire. Based on the risk results within different return periods and expected annual loss or damage (affected) risk assessment of individual hazard, the multi-hazard risk of eleven hazards of the world is assessed at grid level ( $0.5^\circ \times 0.5^\circ$ ) using the methods of Hotspots index (Dilley et al. 2005) and Multi-Risk Index (Shi 2011). In the second method, a Multi-hazard Risk Index (MhRI) is proposed to calculate the world multiple risks by weighting the expected annual intensity of each individual hazard. The MhRI takes into account affected population and GDP caused by eleven types of natural hazards at grid level ( $0.5^\circ \times 0.5^\circ$ ). The world

risk results at comparable-geographic unit and national level are calculated and mapped based on the grid level ( $0.5^\circ \times 0.5^\circ$ ) risk maps by GIS.

## 2 Methodology

Figure 1 shows the technical flowchart for mapping population and property risk of the world by TRI.

Figure 2 shows the technical flowchart for mapping population and property risk of the world by MhRI.

### 2.1 Data

In this study, the TRI assessment is performed based on the risk assessment results within different return periods and expected annual loss or damage (affected) risk of eleven hazards. The MhRI assessment is performed based on the expected annual intensity of each individual hazard. Table 1 shows the data used for the assessments.

### 2.2 Data Processing

#### 2.2.1 Spatial Resolution

An important step before calculating the TRI and MhRI is to unify the spatial resolution of all hazards. Earthquake contributes significantly to the world mortality risk and social-wealth loss or GDP loss risk, thus the spatial resolution of the world earthquake risk assessment map is taken as the standard ( $0.5^\circ \times 0.5^\circ$ ) when calculating the multi-hazard risk.

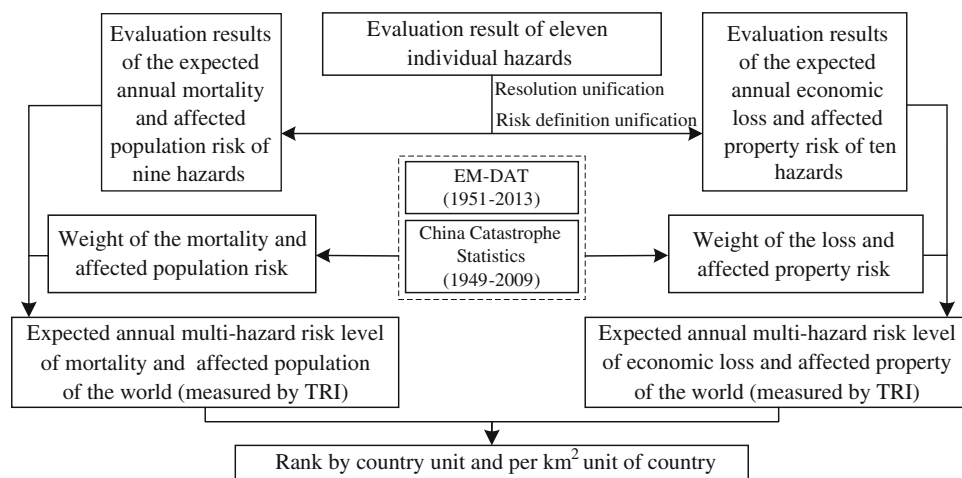


**Fig. 1** Technical flowchart for mapping population and property risk of the world by TRI

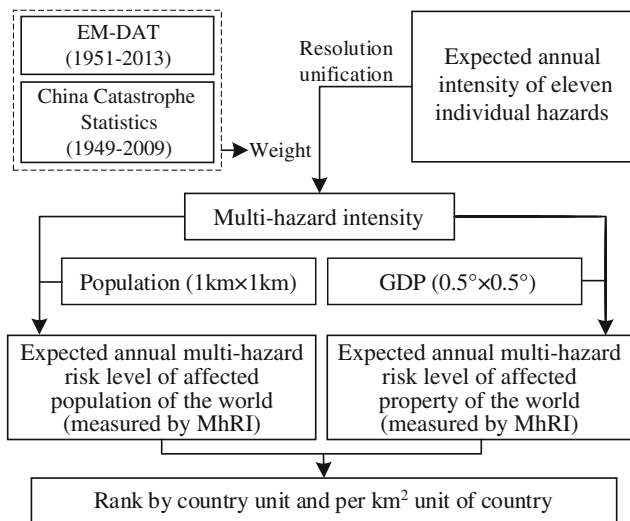


**Fig. 2** Technical flowchart for mapping population and property risk of the world by MhRI

For hazards with higher spatial resolution than earthquake (e.g., 1 km × 1 km), raster polymerization method, which is the sum of the initial values of the pixels in the  $0.5^\circ \times 0.5^\circ$  grid, is used for unifying the spatial resolution so as to keep the risk value of the grids unchanged. For those with lower spatial resolution than earthquake (e.g.,  $0.75^\circ \times 0.75^\circ$ ), equally allocated resampling method is used to keep the risk value unchanged in the sample pixel of the grid.

### 2.2.2 Normalization of the Risks of Individual Hazards

An important step for the TRI is to unify the results of individual hazard risk on which the multiple risks are calculated. For comparison, the loss or damage risk is first changed to the risk of loss ratio or damage ratio, then normalized to [0, 1]. The risk results of wildfire, drought, and flood are loss ratio of their exposure. For others, the expected annual mortality loss risk and expected annual affected population risk are divided by the total population, and the expected annual GDP loss risk and expected annual social-wealth loss risk are divided by the total GDP to obtain the ratio, respectively.

### 2.2.3 Weights of Individual Disaster Risks and Multi-hazard

The TRI of the world is calculated based on the weighting schemes of Hotspots index (Dilley et al. 2005) and MhRI (Shi 2011). The weights of total risk are calculated based on the historical loss and damage data caused by individual

disaster from 1951 to 2013 of the world recorded in the EM-DAT database (EM-DAT 2014) and from 1949 to 2009 of China Catastrophe Statistic (CCS) (Zheng et al. 2009).

The weight of MhRI is obtained based on the frequency of individual hazard from 1951 to 2013 of the world recorded in the EM-DAT database and from 1949 to 2009 of China recorded in the database of CCS.

### 2.2.4 Weights for TRI

*Weights for Expected Annual Mortality and Affected Population Risk.* For expected annual mortality and affected population risk, nine disasters—earthquake, volcano, landslide, flood, storm surge, tropical cyclone, sand-dust storm, heat wave, and cold wave—are considered. The average values of the mortality rate in the two databases are used as the weights (Table 2). Drought is not considered in this assessment because the EM-DAT database considers secondary hazards losses of drought, leading to a mortality ratio of 45 % which cannot be used as the weight for calculating the direct losses by drought. While based on the CCS, the mortality ratio directly caused by drought is only 1.15 %, which can be neglected when calculating the multi-hazard risk of mortality and affected population risk.

*Weights for Expected Annual Loss and Affected Properties Risk.* For expected annual loss and affected properties risk, seven disasters—earthquake, flood, storm surge, tropical cyclone, sand-dust storm, drought, and wild fire—are considered.

In the EM-DAT database, there is no record for sand-dust storm; the weight for sand-dust storm is therefore calculated according to the CCS database. The weights for drought risk of maize, wheat, and rice are calculated according to the proportion of global yield of the three crops in 2012, that is, 48.25 %, 11.92 %, and 39.82 %, respectively. For other types of disasters, the weights are used according to the economic loss rates in the EM-DAT database (Table 3).

### 2.2.5 Weights for MhRI

*Weights for Expected Annual Multi-hazard Intensity.* For expected annual multi-hazard intensity, it denotes the total intensity of all the natural disasters. Therefore, eleven disasters—earthquake, volcano, landslide, flood, storm surge, tropical cyclone, sand-dust storm, heat wave, cold wave, drought, and wildfire—are all considered.

The weight for sand-dust storm is also calculated according to the CCS database. While in the CCS database, there are no records for volcano, cold wave, heat wave, wildfire (grassland), and storm surge; thus, the weights for these disasters are calculated according to the EM-DAT database. For other disasters, the average values of the

**Table 1** Data used for TRI and MhRI

Disaster	Hazard			Exposure			Risk			
	Intensity	Spatial resolution	Return periods	Expected annual intensity	Spatial resolution of expected annual intensity	Economic	Population	Spatial resolution	Spatial resolution of population risk	Spatial resolution of economic risk
Earthquake	Peak ground acceleration (PGA) ( $\text{m/s}^2$ )	0.5°	475a	Peak ground acceleration	0.5°	Economic-social wealth loss	Mortality	1 km	Sampled at 0.5°	0.5°
Volcano	Volcanic explosively index (VEI)	1 km	10a, 20a, 50a, 100a	Expected annual volcanic explosively index (VEI)	1 km	–	Mortality	1 km	1 km	–
Landslide	(Between 50°N and 50°S) TRMM 3B42 3 h precipitation data (mm)	0.25°	–	Expected annual landslide hazard index	Sampled at 0.25°	–	Mortality	1 km	Sampled at 0.25°	–
	(Out of 50°N–50°S) NCEP/NCAR 6 h precipitation data (mm)	2.5°	–	–	–	–	–	–	–	–
Flood	Global 3-day precipitation (mm)	1°	10a, 20a, 50a, 100a	Expected annual 3-day precipitation	1°	Affected GDP	Affected population	0.5°	Sampled at 1°	Sampled at 1°
Storm surge	Maximum inundation area ( $\text{km}^2$ )	1 km	–	Expected annual maximum inundation area	1 km	Affected GDP	Affected population	1 km	1 km	1 km
Sand-dust storm	Energy of sand-dust storm ( $\text{J/m}^3$ )	0.5°	10a, 20a, 50a, 100a	Expected annual energy of sand-dust storm	0.5°	Affected GDP	Affected population	0.5°	1 km	Sampled at 0.5°
Tropical cyclone	The intensity-frequency of 3 s gust wind and 10 min sustained wind	1 km	10a, 20a, 50a, 100a	Expected annual intensity-frequency of 3 s gust wind	1 km	Affected GDP	Affected population	0.5°	1 km	Sampled at 0.5°
Heat wave	Max temperature (°C)	0.75°	10a, 20a, 50a, 100a	Expected annual max temperature (°C)	0.75°	–	Mortality	1 km	0.75°	–
Cold wave	Largest temperature drop of the cold wave (°C)	0.75°	10a, 20a, 50a, 100a	Expected annual global temperature drop (°C)	0.75°	–	Affected population	1 km	0.75°	–
Drought	Normalized cumulative water stress during the crop's growing season	1 km	10a, 20a, 50a, 100a	Expected annual normalized cumulative water stress during the crop's growing season	1 km	Crop yield loss ratio	–	1 km	–	1 km
Wildfire	Ignition probability of forest wildfire	0.1°	10a, 20a, 50a, 100a	Expected annual ignition probability of forest wildfire	0.1°	Forest area loss ratio	–	500 m	–	Sampled at 0.1°
	Ignition probability of grassland wildfire	1 km	–	Annual average ignition probability of grassland wildfire	1 km	Net primary productivity loss ratio	–	1 km	–	1 km

**Table 2** Weights of mortality and affected population risk for each disaster

Disaster	Weight calculated according to EM-DAT database	Weight calculated according to EM-DAT database (without considering drought)	Weight calculated according to the CCS database	Adjusted weight
Earthquake	28.23	50.67	66.20	58.43
Tropical cyclone	19.75	35.45	4.13	19.79
Flood	2.42	4.34	26.43	15.39
Heat wave	3.08	5.53	–	2.77
Landslide	0.82	1.48	0.49	0.98
Cold wave	0.33	0.60	–	0.64
Volcano	0.64	1.15	–	0.58
Storm Surge	0.43	0.78	–	0.39
Sand-dust storm	–	–	0.02	0.01
Total	55.72	100	97.27	98.98

**Table 3** Weights of expected annual loss and affected property risk for each disaster

Disaster	Weight calculated according to EM-DAT database	Weight calculated according to CCS database	Adjusted weight
Tropical cyclone	39.36	15.79	39.36
Earthquake	31.89	38.75	31.89
Flood	19.28	36.58	19.28
Drought (maize)	5.68	5.01	5.68
Drought (wheat)			2.74
Drought (rice)			0.68
			2.26
Wildfire(forest)	1.77	0.02	1.77
Storm Surge	0.43	–	0.43
Sand-dust storm	–	0.40	0.40
Wildfire(grassland)	0.19	–	0.19
Total		96.55	99.01

frequency ratio in the two databases are used as the weights. As for drought, weights for multi-hazard intensity of maize, wheat, and rice are calculated according to the proportion of global yield of the three crops in 2012 (Table 4).

## 2.3 TRI and MhRI

### 2.3.1 TRI

The TRI for expected annual mortality and affected population risk of the world is calculated according to Eq. (1):

$$R_{pL} = \sum_{i=1}^n r_{iL} \times w_{ip}, \quad i = 1, 2, \dots, n \quad (1)$$

where  $R_{pL}$  is the level of total mortality or affected population risk;  $r_{iL}$  is the risk level of  $i$ th disaster,  $w_{ip}$  is weight of the  $i$ th disaster,  $n$  is total number of natural disasters evaluated (Table 2).

The TRI for expected annual loss and affected property risk of the world is calculated according to Eq. (2):

$$R_{eL} = \sum_{i=1}^n r_{iL} \times w_{ie}, \quad i = 1, 2, \dots, n \quad (2)$$

where  $R_{eL}$  is the level of total economic loss or affected property risk;  $r_{iL}$  is the risk level of the  $i$ th disaster,  $w_{ie}$  is weight of the  $i$ th disaster,  $n$  is the number of natural disasters evaluated (Table 3).

**Table 4** Weights of MRI for each hazard

Disaster	Weight calculated according to EM-DAT database	Weight calculated according to CCS database	Adjusted weight
Flood	25.93	45.80	35.86
Tropical cyclone	37.85	22.60	30.23
Earthquake	11.86	6.20	9.03
Landslide	5.99	5.30	5.65
Drought (maize)	6.73	2.00	4.36
Drought (wheat)			2.10
Drought (rice)			0.52
			1.73
Cold wave	2.99	–	2.99
Volcano	2.21	–	2.21
Heat wave	1.77	–	1.77
Wildfire (forest)	2.76	0.002	1.38
Storm surge	1.04	–	1.04
Sand-dust storm	0.88	–	0.88
Wildfire (grassland)	–	0.31	0.31
Total	100.00	82.21	94.66

### 2.3.2 MhRI

The multi-hazard intensity index for expected annual multi-hazard of the world is calculated according to Eq. (3):

$$Mh_L = \sum_{i=1}^n h_{iL} \times w_{ih}, \quad i = 1, 2, \dots, n \quad (3)$$

where  $Mh_L$  is the level of expected annual multi-hazard intensity;  $h_{iL}$  is the expected annual intensity level of the  $i$ th hazard,  $w_{ih}$  is weight of the  $i$ th intensity,  $n$  is the number of natural hazards evaluated (Table 4).

The MhRI for expected annual affected population risk of the world is calculated according to Eq. (4):

$$MhRI_{pL} = Mh_L \times E_{pL}, \quad i = 1, 2, \dots, n \quad (4)$$

where  $MhRI_{pL}$  is the level of affected population risk;  $E_{pL}$  is the population exposed to multi-hazard.

The MhRI for expected annual affected property risk of the world is calculated according to Eq. (5):

$$MhRI_{eL} = Mh_L \times E_{eL}, \quad i = 1, 2, \dots, n \quad (5)$$

where  $MhRI_{eL}$  is the level of affected property risk;  $E_{eL}$  is the property exposed to multi-hazard.

## 3 Results

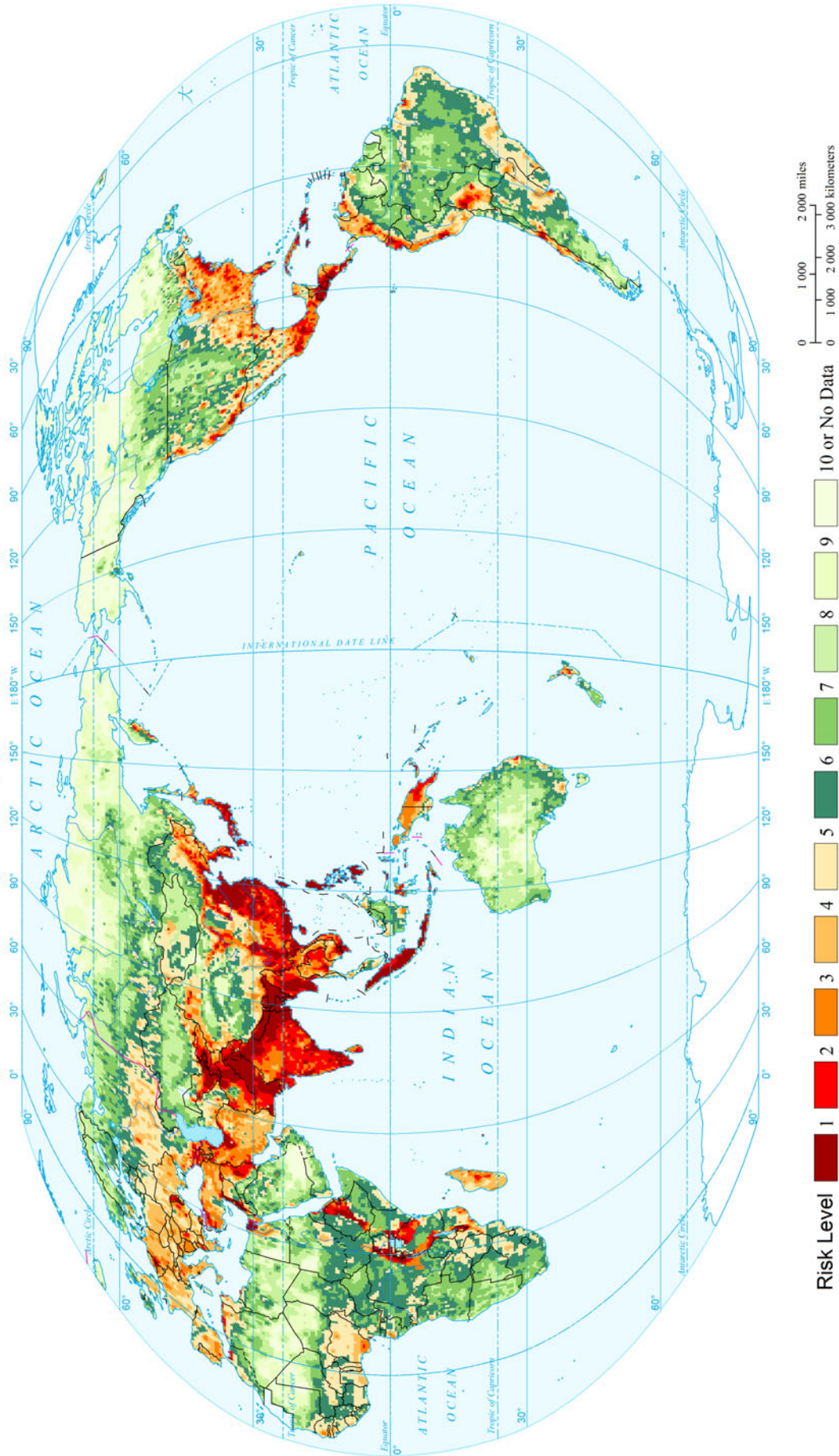
By zonal statistics, the Mh, TRI, and MhRI values of 197 countries of the world are ranked in descending order. For comparison, the Mh, TRI, and MhRI values by dividing the area of the country are also calculated and ranked. The Mh, TRI, and MhRI values of all 197 countries of the world are calculated and ranked in descending order at country and per unit area, respectively (Appendix IV, Tables 1, 2, and 3).

## 4 Maps



Multi-natural Disasters

Expected Annual Multi-hazard Risk Level of Mortality and Affected Population of the World (Measured by TRI)  
(0.5°x0.5°)



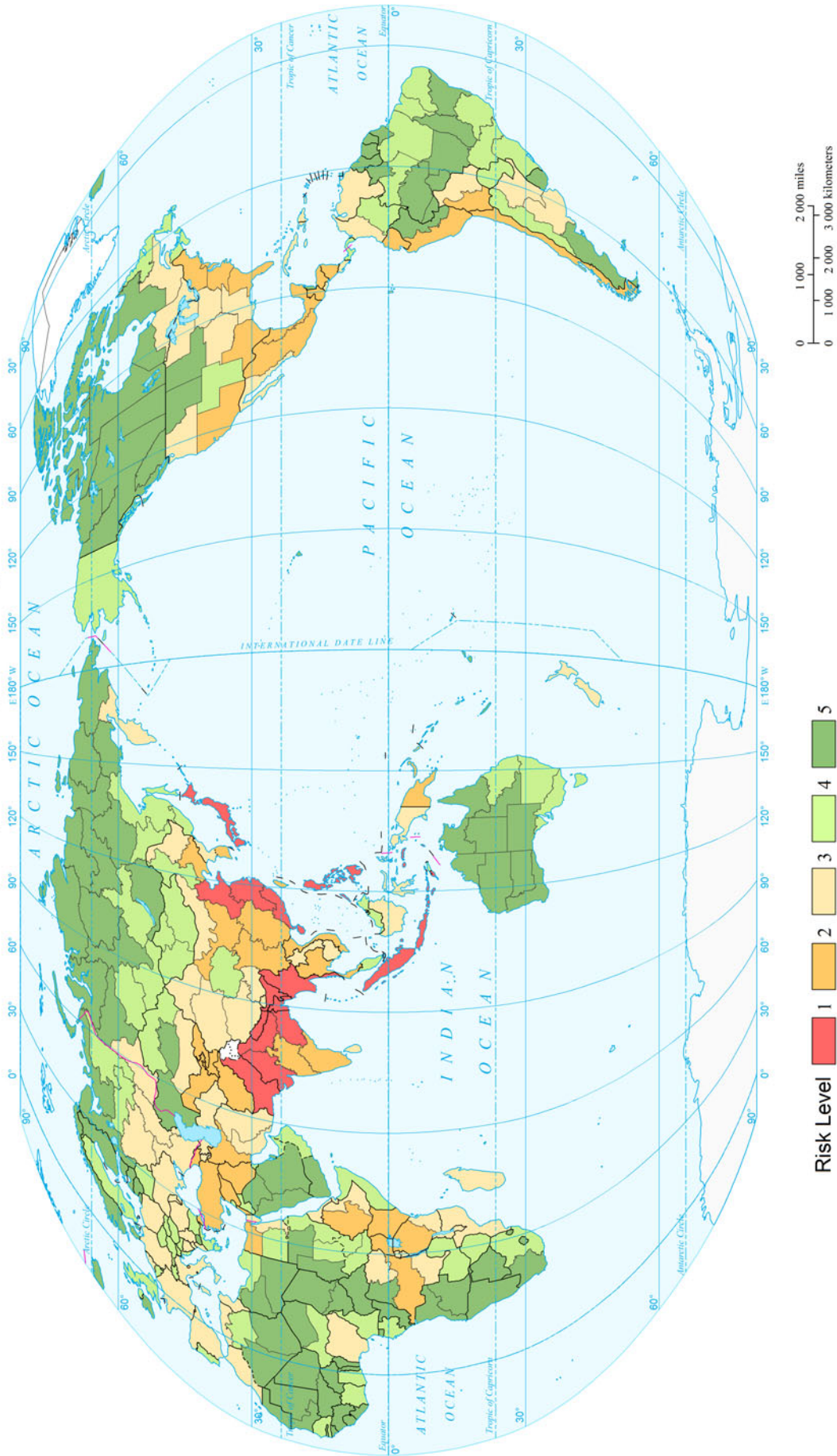
Risk Level 1 2 3 4 5 6 7 8 9 10 or No Data

0 1 000 2 000 miles  
0 1 000 2 000 3 000 kilometers



Multi-natural Disasters

Expected Annual Multi-hazard Risk Level of Mortality and Affected Population of the World (Measured by TRI)  
(Comparable-geographic Unit)



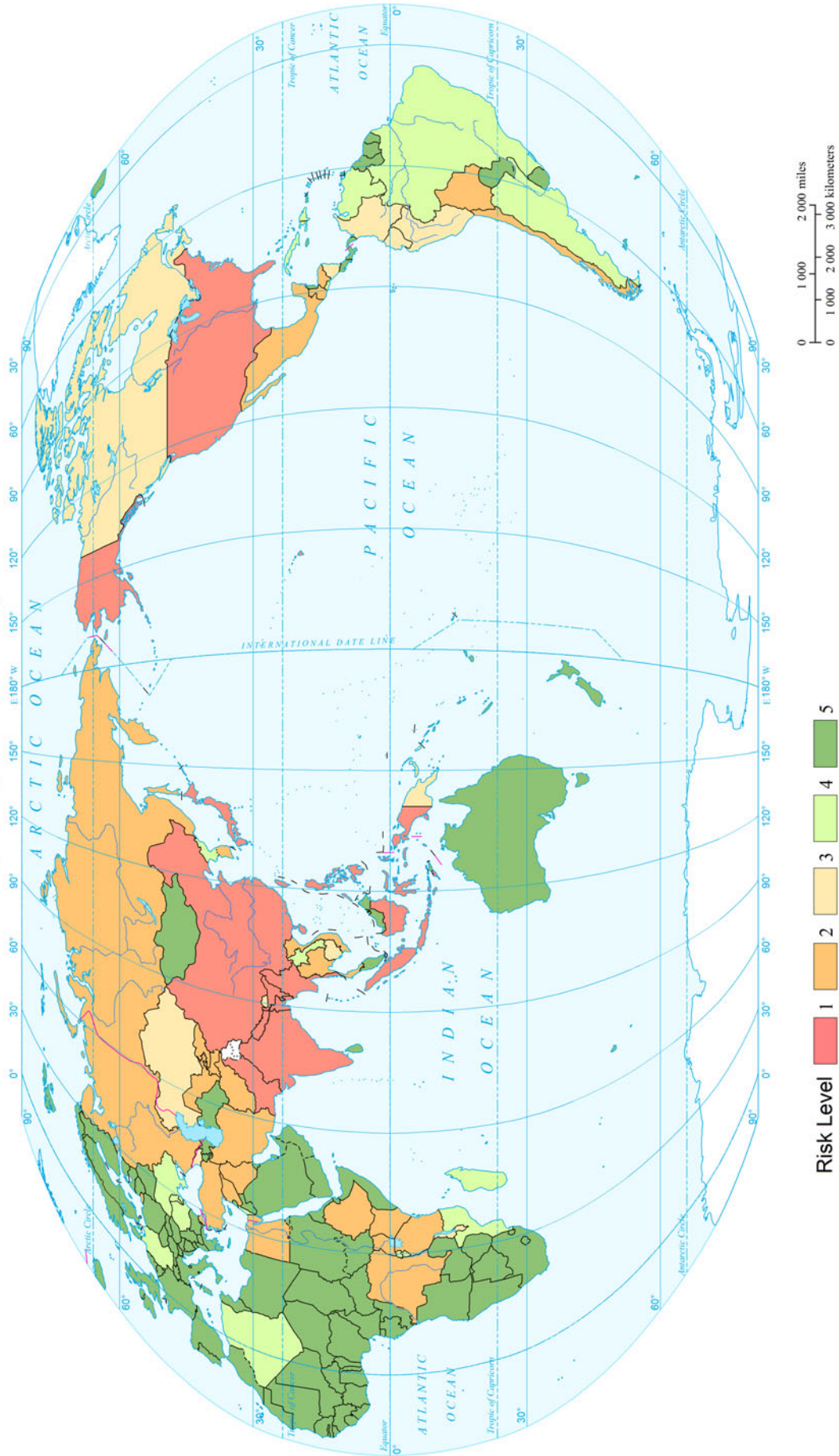
0 1 000 2 000 miles  
0 1 000 2 000 3 000 kilometers

Risk Level 1 2 3 4 5



Multi-natural Disasters

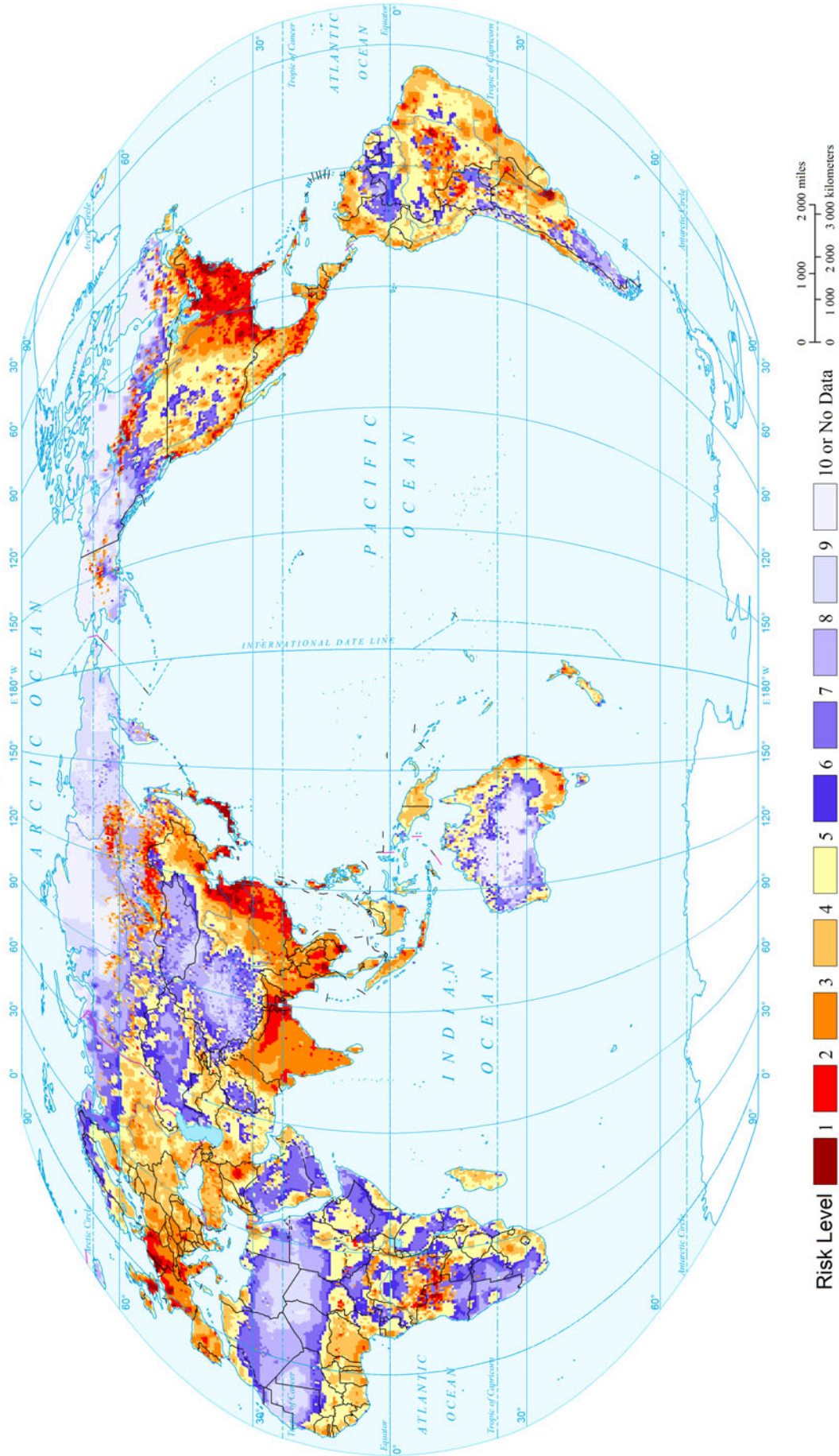
Expected Annual Multi-hazard Risk Level of Mortality and Affected Population of the World (Measured by TRI)  
(Country and Region Unit)





Multi-natural Disasters

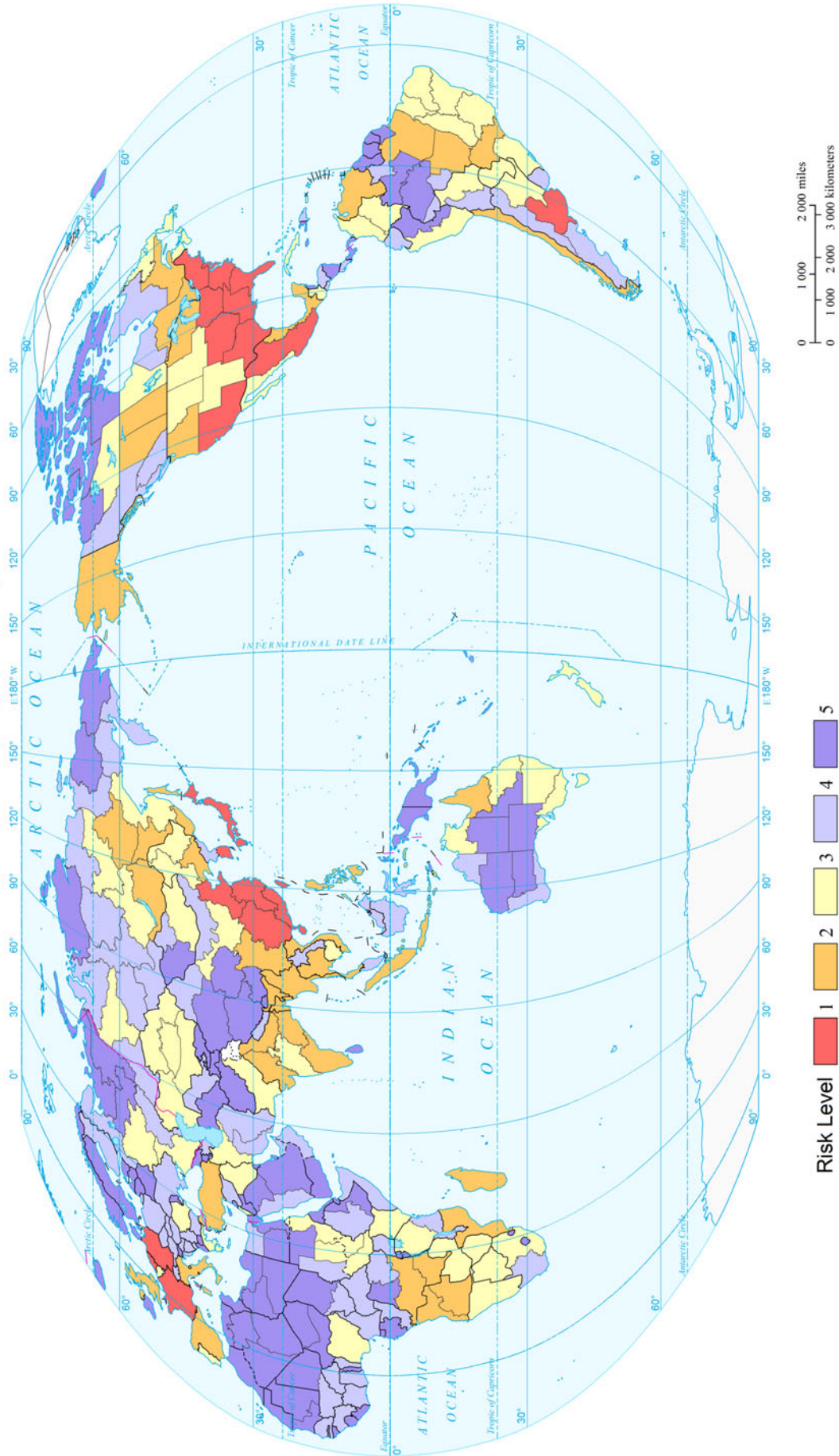
Expected Annual Multi-hazard Risk Level of Economic Loss and Affected Property of the World (Measured by TRI) (0.5°x0.5°)





Multi-natural Disasters

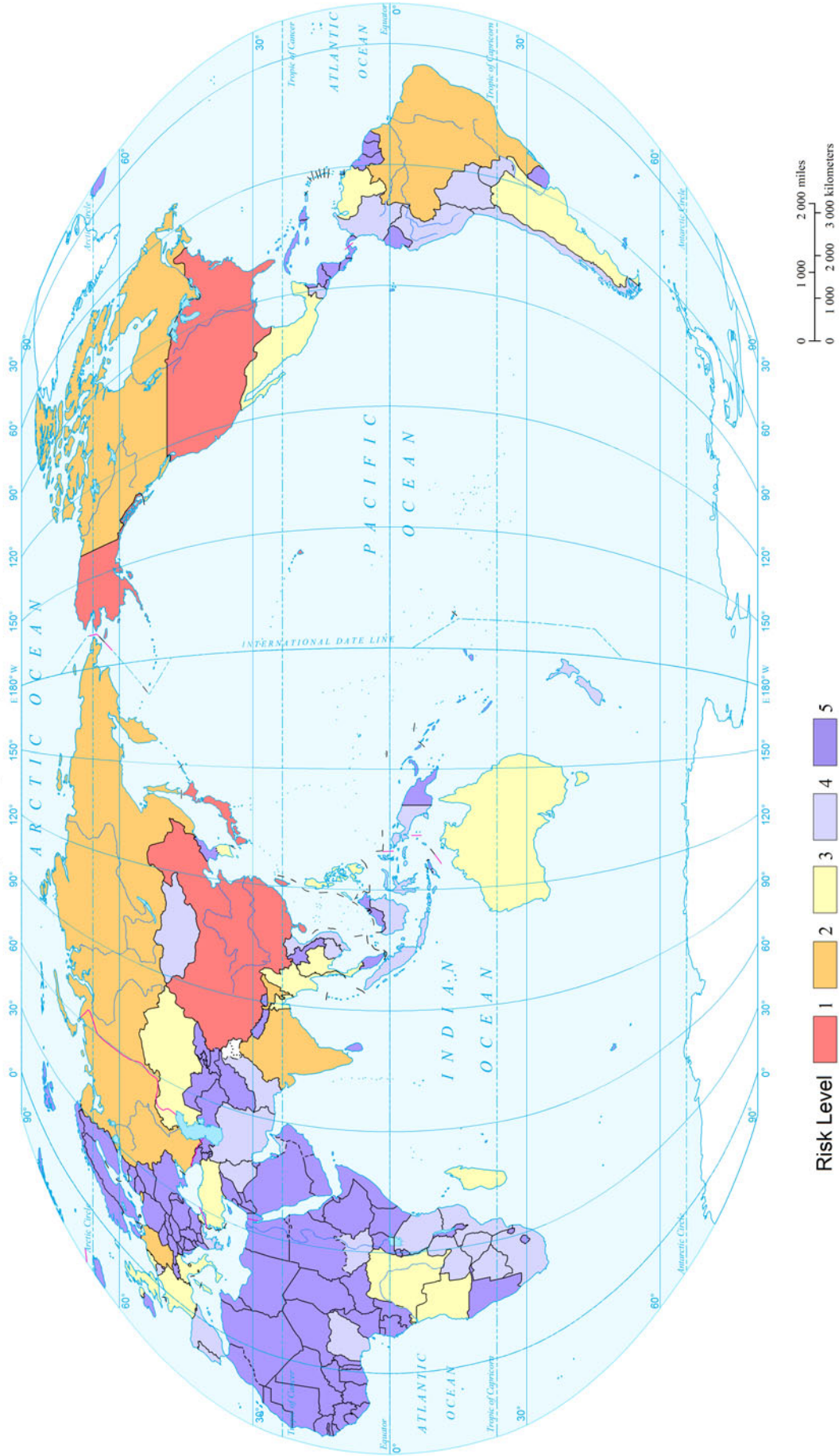
Expected Annual Multi-hazard Risk Level of Economic Loss and Affected Property of the World (Measured by TRI)  
(Comparable-geographic Unit)





Multi-natural Disasters

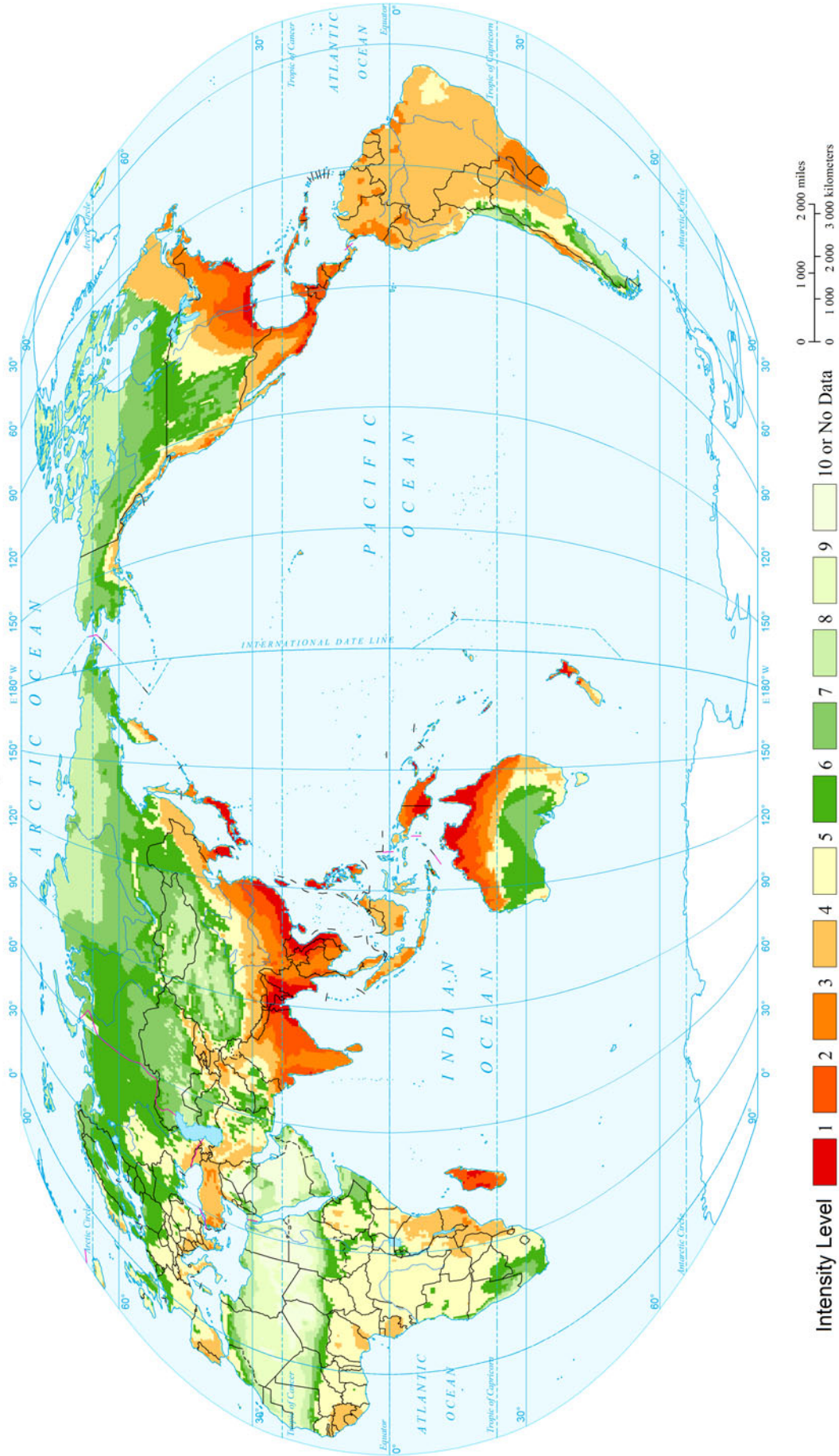
Expected Annual Multi-hazard Risk Level of Economic Loss and Affected Property of the World (Measured by TRI)  
(Country and Region Unit)





Multi-natural Disasters

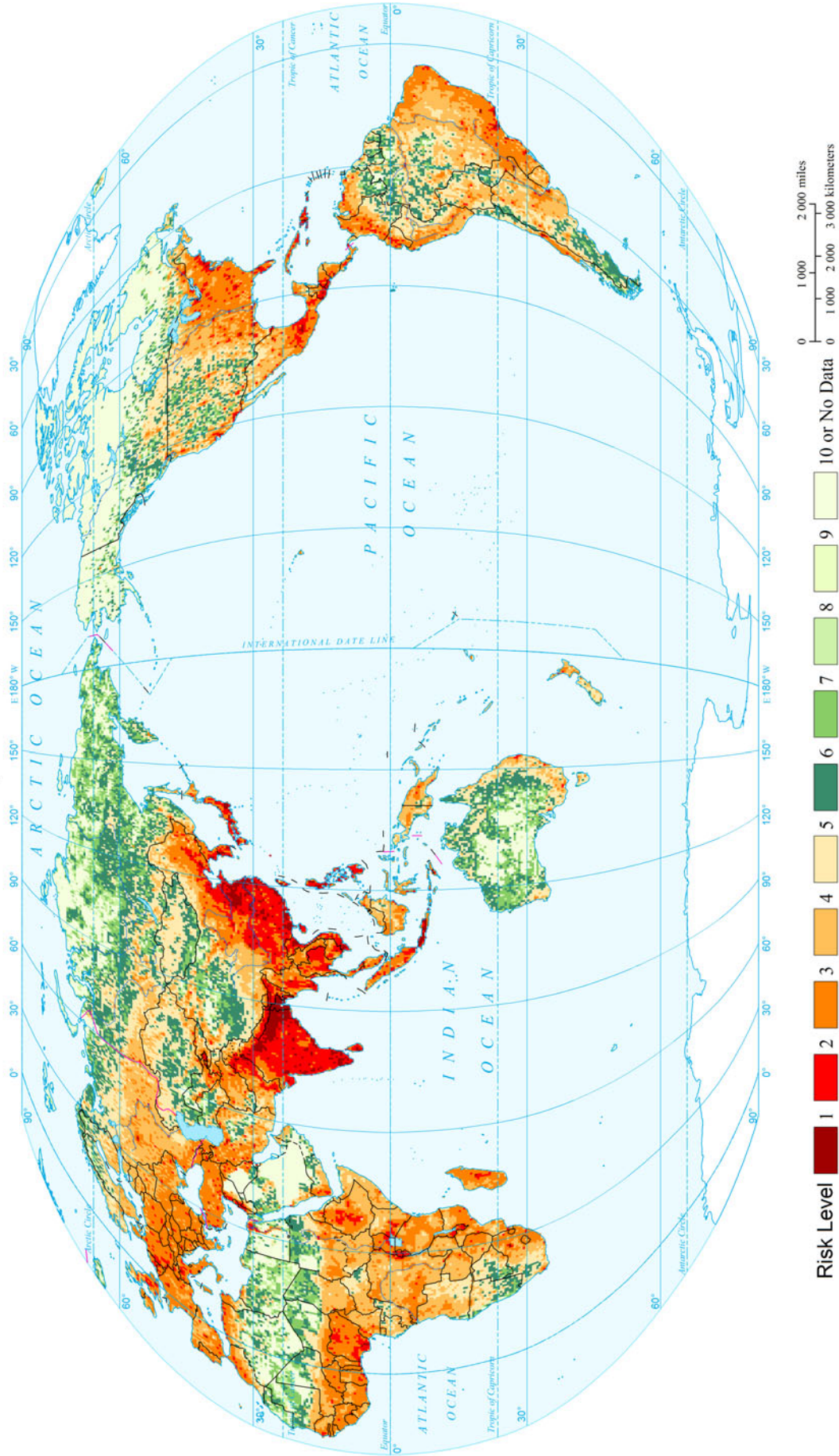
Global Expected Annual Multi-hazard Intensity  
(0.5°x0.5°)





Multi-natural Disasters

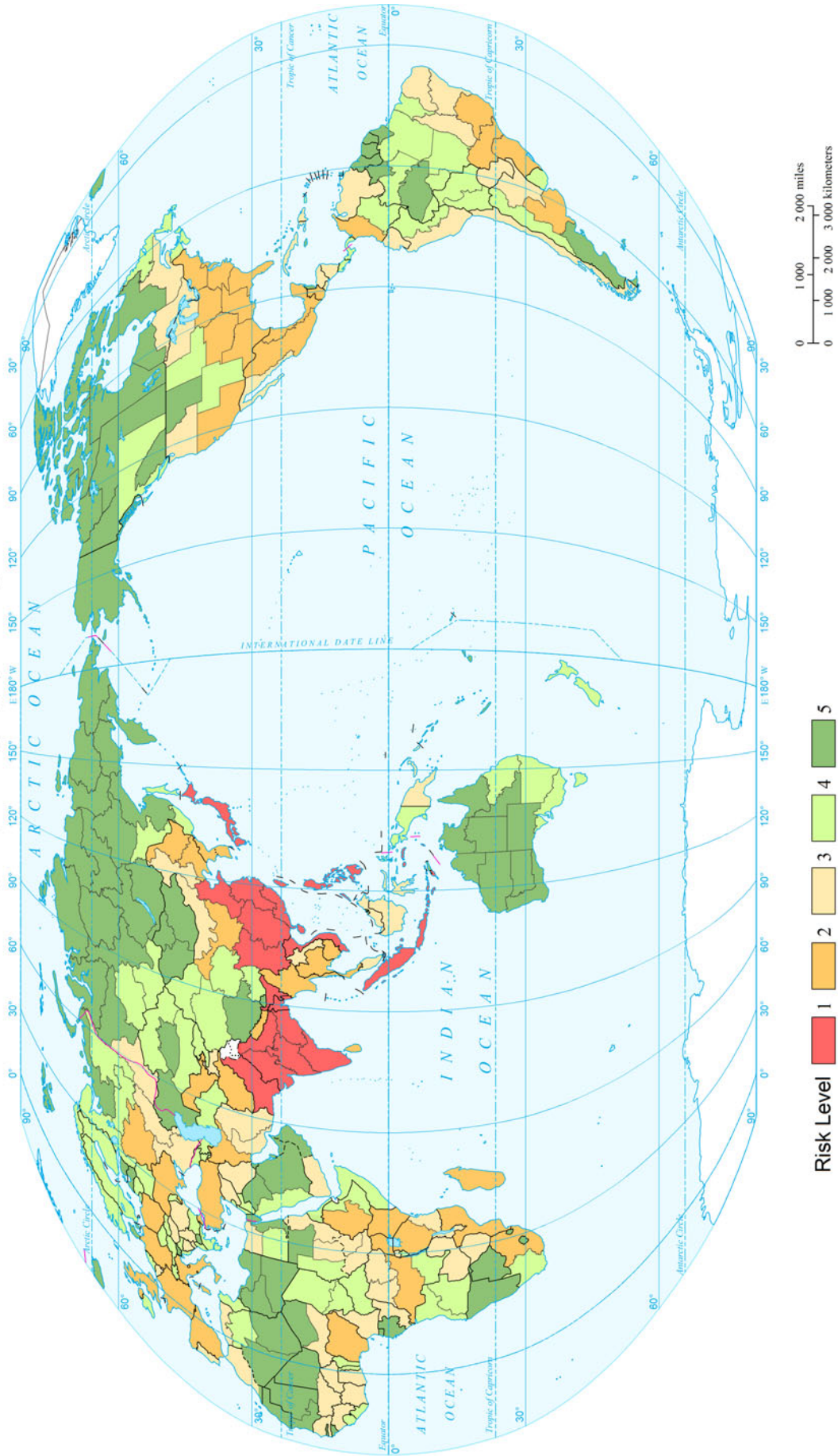
Expected Annual Multi-hazard Risk Level of Affected Population of the World (Measured by MhRI) (0.5°x0.5°)





Multi-natural Disasters

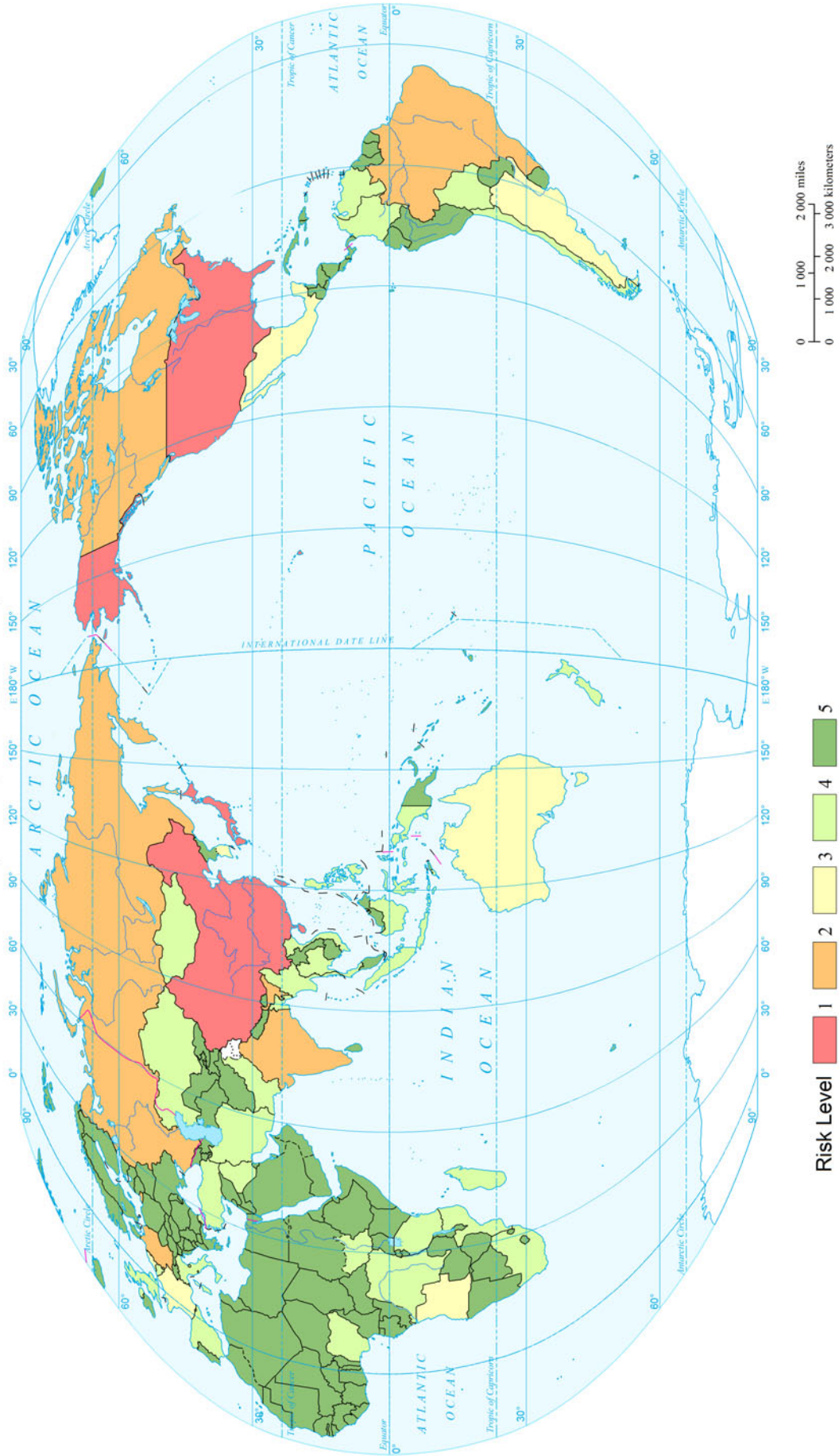
Expected Annual Multi-hazard Risk Level of Affected Population of the World (Measured by MhRI)  
(Comparable-geographic Unit)





Multi-natural Disasters

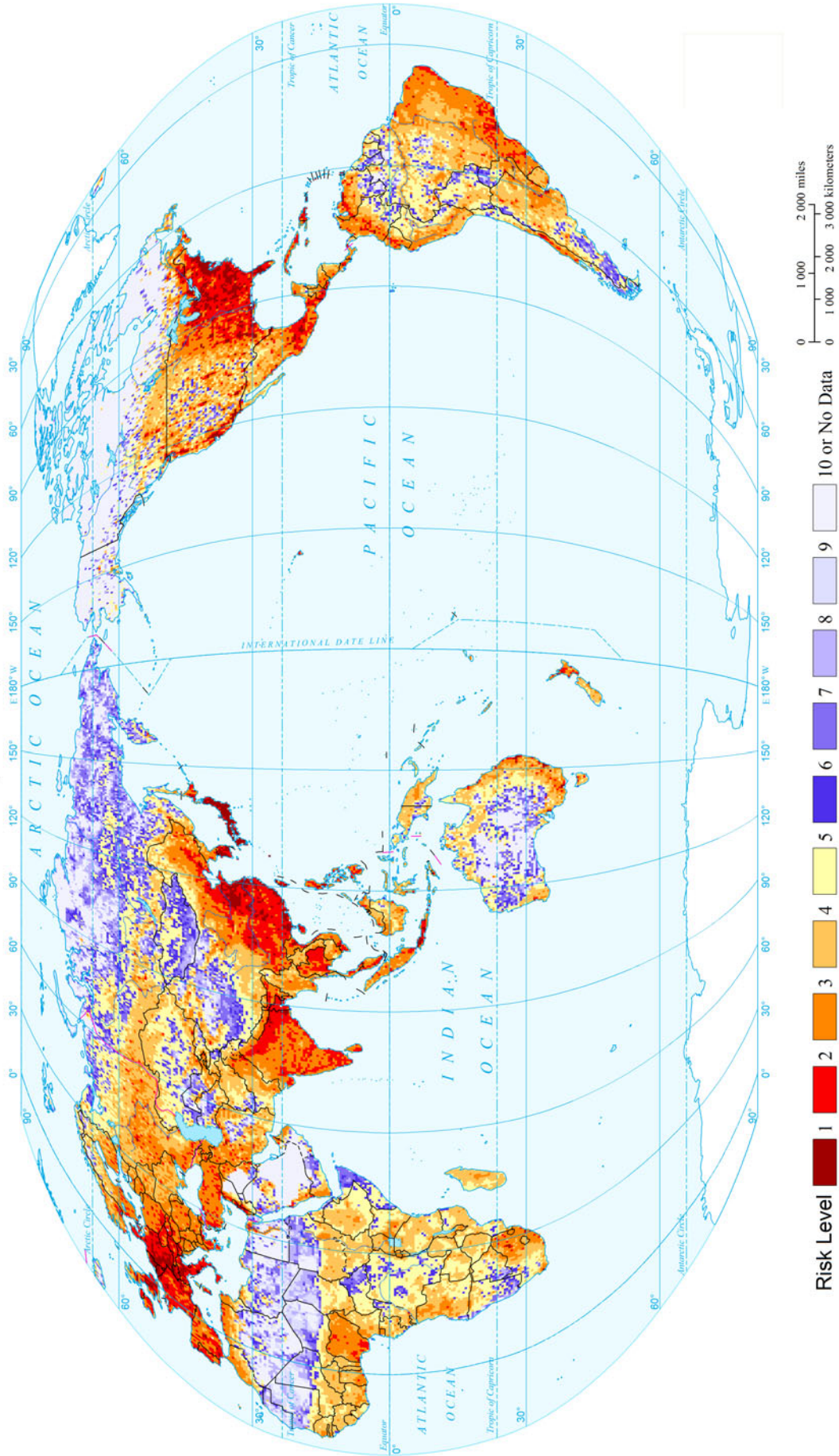
Expected Annual Multi-hazard Risk Level of Affected Population of the World (Measured by MhRI)  
(Country and Region Unit)





Multi-natural Disasters

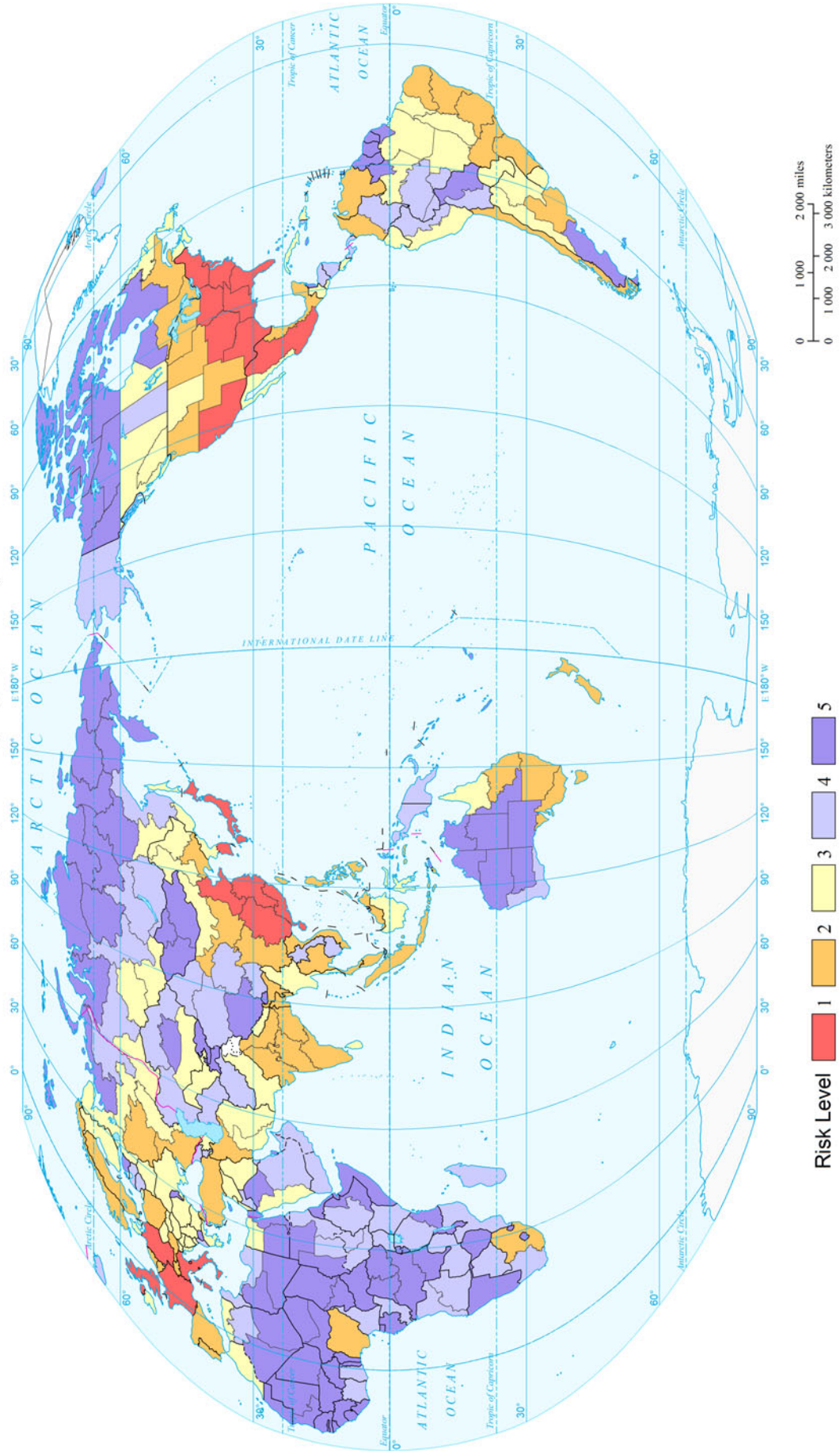
Expected Annual Multi-hazard Risk Level of Affected Property of the World (Measured by MhRI) (0.5°x0.5°)





Multi-natural Disasters

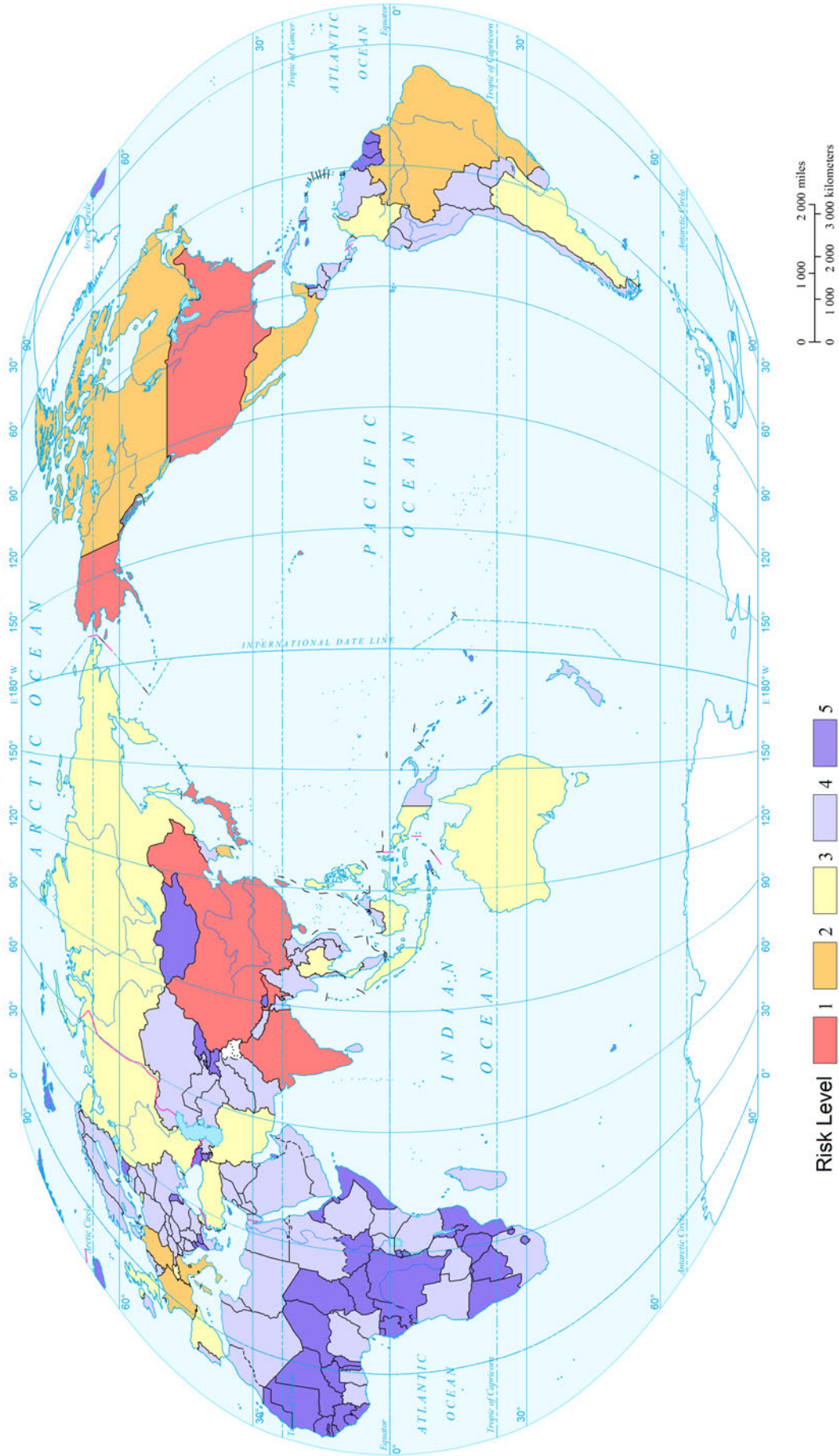
Expected Annual Multi-hazard Risk Level of Affected Property of the World (Measured by MhRI)  
(Comparable-geographic Unit)





Multi-natural Disasters

Expected Annual Multi-hazard Risk Level of Affected Property of the World (Measured by MhRI)  
(Country and Region Unit)



## References

- Dilley, M., U. Deichmann, and R.S. Chen. 2005. *Natural disaster hotspots: A global risk analysis*. Washington, DC: World Bank Publications.
- Emergency Events Database (EM-DAT). 2014. Natural disaster database. <http://www.emdat.be/>. Accessed in July 2013.
- Shi, P.J. 2009. Theory and practice on disaster system research—The fifth discussion. *Journal of Natural Disasters* 18(5): 1–9. (in Chinese).
- Shi, P.J. 2011. *Atlas of natural disaster risk of China*. Beijing: Science Press.
- United Nations Development Programme (UNDP), Bureau for Crisis Prevention and Recovery. 2004. *Reducing disaster risk: A challenge for development*. New York: UNDP, Bureau for Crisis Prevention and Recovery.
- United Nations University Institute for Environment and Human Security (UNU-EHS). 2013. *World Risk Report (2013)*.
- Zheng G.C. 2009. *Significant historical epic for disaster prevention and reduction in sixty-year of China*. Changsha: Hunan People's Publishing House. (in Chinese).

---

Part IX

**Understanding the Spatial Patterns  
of Global Natural Disaster Risk**

---

# World Atlas of Natural Disaster Risk

## Understanding the Spatial Patterns of Global Natural Disaster Risk

Peijun Shi, Jing'ai Wang, Wei Xu, Tao Ye, Saini Yang, Lianyou Liu, Weihua Fang, Kai Liu, Ning Li, and Ming Wang

---

### 1 Background

#### 1.1 International Initiatives in Disaster Risk Reduction

The year 2015 is the 25th annum of the international disaster and risk reduction proposed by the United Nations. Disaster risk reduction (DRR) has achieved significant progress worldwide. The goals of disaster risk reduction, climate change adaptation, and sustainable development have become the joint responsibility of all countries in their economic, societal, cultural, political, and ecological construction activities. In the past 25 years, UNISDR together with national governments, scientific community, NGOs, entrepreneur groups, media and various relevant regional organizations is gaining effective results in alleviating human being's casualties, property losses, and damages to resources and environment caused by natural hazards on the world and is earning a great reputation at every stratum of society as well. Nevertheless, data released by related UN organizations indicate that natural disaster and disaster risk are still on the rise globally. Some nations and regions are still extremely vulnerable to large-scale disasters, although significant progress has been made in DRR actions. Natural disaster risk reduction is still a long haul ahead.

---

P. Shi (✉) · T. Ye · S. Yang · M. Wang  
State Key Laboratory of Earth Surface Processes and Resource Ecology, Beijing Normal University, Beijing 100875, China  
e-mail: spj@bnu.edu.cn

J. Wang  
Key Laboratory of Regional Geography, Beijing Normal University, Beijing 100875, China

W. Xu · L. Liu · W. Fang · K. Liu · N. Li  
Key Laboratory of Environmental Change and Natural Disaster, Ministry of Education, Beijing Normal University, Beijing 100875, China

### 1.2 Foundations

The global hot spots project jointly finished by the World Bank and Columbia University (the USA) is the first ever cartography of major natural disaster risks at the global scale (Dilley et al. 2005). The UNISDR Global Assessment Report on Disaster Risk Reduction (GAR) inspired this Atlas (UNISDR 2009, 2011, 2013). The Institute for Environment and Human Security of the United Nations University has ranked world risk at national level (UNU-EHS 2013). Compared to existing work, this Atlas improves in multiple aspects, including disaster types, assessment methodology and accuracy, latest data, spatial comparability, spatial and temporal resolution, and validation of results. Assessment results derived are appropriate and broadly applicable. Sharing service for global-scale datasets is critical in compiling this Atlas, while Internet open-access datasets such as EM-DAT provides substantial convenience.

Funded by Chinese government, a series of scientific projects have attained enormous results and valuable references which laid solid foundation for the compilation of this atlas. Ongoing programs/projects include the "Relationship Between Global Change and Environmental Risks and Its Adaptation Paradigm" (No. 2012CB955400), "Hazard and Risk Science Base at Beijing Normal University" (111 Project) (No. B08008), "Model and Simulation of Earth Surface Process" (No. 41321001), the "Research on the Regional Agriculture Drought Adaptation Assessment Model and Risk Reduction Paradigm" (No. 41171402), "the Land-use and Integrated Erosion of Soil by Wind and Water in the Eastern Ecotone of Agriculture and Animal Husbandry in North China" (No. 41271286), "Comparative Study on Integrated Risk Governance Techniques and Paradigms of Typically Vulnerable Regions" (No. 2012DFG20710), "Cooperative Research on Severe Drought Disaster Monitoring Techniques" (No. 2013DFG21010), and "Study on the Disaster-chain and Integrated Risk Assessment of Major Earthquake-geological Disasters" (No. 2012BAK10B03). Finished programs/projects include "the Geographic Transaction Zone Study on Interaction

Mechanism of Human-earth System on Earth Surface” (No. 40425008), “Integrated Natural Disaster Risk Evaluation and Disaster Reduction Paradigm Study in Rapid Urbanization Regions” (No. 40535024), “Integrated Risk Governance—Case Study of IHDP—IRG Core Science Plan” (No. 40821140354), “Global Climate Change and Large-scale Disaster Governance” (No. 2008DFA20640), “Integrated Risk Governance: Models and Modeling” (No. 2010DFB20880), “the Key Technology Study and Demonstration of Integrated Risk Prevention” (No. 2006BAD20B00), and the “Technology for Evaluating Natural Disaster Risk in the Yangtze River Delta” (No. 2008BAK50B07).

All faculties and students of BNU on the disaster risk science and the international experts who participated in the IHDP/Future Earth-Integrated Risk Governance and “111 Project”, as well as all the personnel involved in these two projects, throughout ten years of preparation, planning, and action, were organized to compile this atlas, aiming to reflect the spatial patterns of the main natural disaster risk all around the world. This atlas provides scientific evidence for taking effective measures of world natural disaster risk reduction by demonstrating the spatial variation from the following three spatial scales for the main natural disaster risk on the world: the grid unit ( $1^\circ \times 1^\circ$ ,  $0.75^\circ \times 0.75^\circ$ ,  $0.5^\circ \times 0.5^\circ$ ,  $0.25^\circ \times 0.25^\circ$ ,  $0.1^\circ \times 0.1^\circ$  or  $1 \text{ km} \times 1 \text{ km}$ ), the comparable geographic unit (about  $448,334 \text{ km}^2$  per unit), and the national or regional unit (245 nations and regions).

### 1.3 International Scientific and Technological Cooperation

Close cooperation with worldwide scientific institutions lays the scientific foundation of this Atlas. These institutions include Disaster Research Institute of Kyoto University (Japan), International Institute for Applied System Analysis (Austria), Sweden Environment Institute (Sweden), Clark University (USA), School of Sustainability of Arizona State University (USA), and Potsdam Institute for Climate Impact Research (Germany). There are many institutions provided considerable data and methodological support, including University of Maryland (USA), Nanyang Technological University (Singapore), University of Vienna (Austria), Oxford University (UK), the University of Stuttgart (Germany), University of California—Berkeley (USA), Risk Management Solutions Inc. (USA), Swiss Re (Switzerland), Munich Re (Germany), Aon Benfield (UK), etc. UNISDR provides solid support and guidance to this Atlas. Star Map Press (Beijing) has provided great supports in editing the maps, and Beijing Normal University Press and Springer-Verlag enable the fluent publication process. All institutions mentioned above are highly appreciated.

Three generations of natural disaster atlas of China were compiled under the guidance of regional disaster system theory and published by Science Press of China, namely *Atlas of Natural Disaster of China* (Chinese and English Version) (Zhang and Liu 1992), *Atlas of Natural Disaster System of China* (Chinese and English Version) (Shi 2003), and *Atlas of Natural Disaster Risk of China* (Chinese and English Version) (Shi 2011). The compiling and publication of the World Atlas of Natural Disaster Risk was based on the earlier practice in those atlases.

## 2 Scientific Basis

The *World Atlas of Natural Disaster Risk* attempts to reveal the spatial pattern of the risks of natural disaster which are mainly caused by physical hazards in the world with multiple perspectives of natural environment, exposure, disaster loss, and disaster risk with the framework of Regional Disaster System Theory (Shi 1991, 1996, 2002, 2005, 2009). It emphasizes the spatial-temporal pattern of worldwide natural disasters from the perspective of individual disasters and integrated disasters, including earthquake, volcano, landslide, flood, storm surge, sand-dust storm, tropical cyclone, heat wave, cold wave, and wild fire. In the Atlas, natural disaster risks of the world are assessed objectively by integrating the stability of natural environment, hazard intensity and probability, and the vulnerability of the exposure, based on Regional Disaster System Theory and Disaster Risk Science. Meanwhile, factors like the concurrent coping capacity of reducing hazard severity and vulnerability, social and economic development level, as well as data incompleteness at the global scale are also considered during risk assessment. The goals of this atlas are to support national/regional integrated disaster risk reduction planning, integrated risk governance strategic planning, sustainable development planning of the world, and so on.

### 2.1 Disaster Risk Science

The demand of regional disaster risk governance spurred the development of disaster risk science, which has becoming transdisciplinary field of disaster mechanism, process, and risk dynamics. Disaster risk science could be further divided into three fields as disaster science, emergency technology, and risk management.

#### 2.1.1 Disaster Science

Disaster science studies the physical process, mechanism, and temporal-spatial pattern of natural environment, natural hazards, physical and social vulnerability of exposure, and

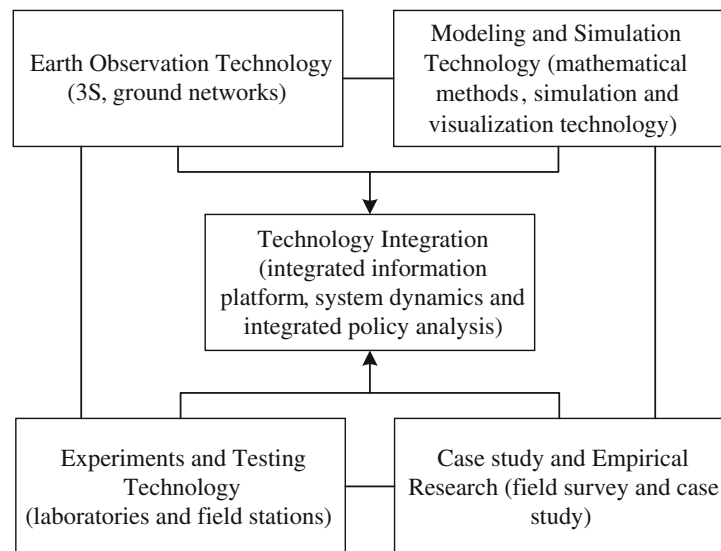


**Fig. 1** Methodology and technical system of integrated disaster science

how loss is caused. Disaster science is the foundation for DRR, and it can be categorized as basic disaster science, applied disaster science, and regional disaster science.

### 2.1.2 Emergency Technology

Emergency technology develops technique and equipment related to disaster prevention, resistance, relief, and emergency response. The technological systems for disaster monitoring, forecasting, early warning, coping capacity building, emergency response, population evacuation and resettlement, recovery and reconstruction, system optimization, and system integration are all the essentials of this field. Emergency technology can be further divided into emergency response technology, disaster reduction technology, and recovery and reconstruction technology.

### 2.1.3 Risk Management

Risk management is to establish standard, institution, planning, and policy systems of disaster risk governance, develop and optimize systems of assessment indices, standards, and models of disaster and risk assessment, and improve application of laws, rules and regulations of disaster, and risk management. It also compiles and modifies emergency plan, strategy, and plan of regional DRR, compiles all related policies for integrated disaster risk governance, and develops information platform and network service system for integrated disaster risk governance which offers regulations and service for integrated disaster reduction. Risk management can be further classified as disaster management, emergency management, and risk transfer and governance.

The general methodology and techniques for disaster risk science study are shown in Fig. 1.

## 2.2 Vulnerability, Resilience, and Adaptation

Vulnerability is the severity of disasters caused by hazards. It is interpreted by a curve or function reflecting disaster loss or damage ratio to hazard intensity (Fig. 2).

Disaster loss increases as hazards get severer under the constant coping capacity, which means the lower the frequency or the higher the intensity of hazard, the larger is the loss of disaster, and vice versa. Therefore, vulnerability reflects the interaction between hazard and property or population at risk. On the other hand, disaster loss decreases as the coping capacity increases, while hazard intensity remains constant. Quantitative description vulnerability

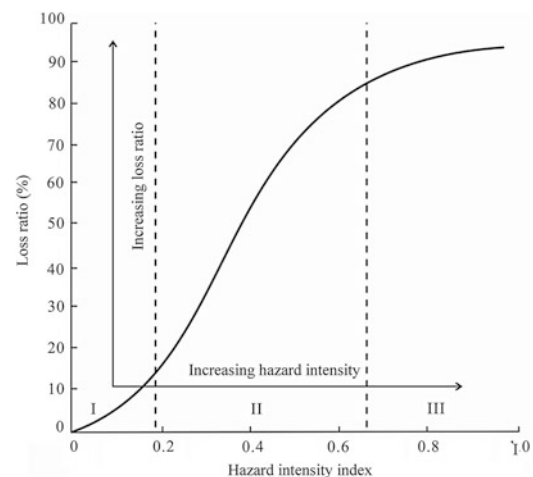


**Fig. 2** Vulnerability curve of the exposure

(with a curve or function) is the necessary condition for assessing and mapping natural disaster risk.

Resilience is generally the reciprocal of social vulnerability. The resilience of a society or region increases as its social vulnerability decreases, and vice versa. Resilience can be regarded as the collective representation of disaster-coping capacity, or the combining capacity of disaster preparedness, prevention, emergency response, disaster relief, rehabilitation, and reconstruction. The concept of resilience greatly enriched the risk theory, and hence, it is a great complementary to the concept of vulnerability. In addition, resilience is also a reflection of the soundness of integrated risk governance at national or regional level. Risk transfer mechanism can play an essential role in resilience even if the region is highly vulnerable. For countries or regions with well-designed natural disaster insurance system, their resilience to natural disasters can be improved even though they may have high physical vulnerability. For instance, insurance indemnity contributed nearly 40 % of the reconstruction cost in hurricane Katrina of the USA, while for countries like China with a strong top-down system, risks can be transferred among different administrative areas through financial transfer payment under the coordination of the central government. For example, post-5.12 Wenchuan Earthquake reconstruction was completed less than 3 years under the support of central government and local governments. Quantification of resilience is also a key factor for mapping disaster risk (Shi et al. 2012).

Adaptation is a strategy for living with risk, which is complement to disaster-coping capacity, and improvement to resilience. Adaptation has become a mainstream instrument for climate change and ecological risk governance. The higher the adaptation capacity is, the lower the vulnerability and vice versa. Adaptation is a developing mode through dynamically optimizing industrial structure, land use/land cover structure, development scale and speed. For instance, risks to sustainable development from global warming, especially disaster risks due to extreme climate events, can be mitigated by decreasing greenhouse gases concentration through reducing carbon emission, increasing carbon sink, and saving resources.

Therefore, resilience and adaptation are two concepts which enriched and deepened the concept of vulnerability in the field of risk assessment and the three concepts are used.

### 2.3 Risk, Risk Grade, and Risk Level

Three types of risk maps are developed according to data availability and modeling accuracy, namely quantitative risk maps in the form of absolute expected loss, semi-quantitative maps categorized from quantitative risk maps due to less

accurate modeling result, and non-quantitative risk ranking. The above three types of maps are noted as risk, risk grade, and risk level, for the convenience of explanation.

Risk of a disaster or multiple disasters ( $R$ ) in a region or grid is defined as loss expectation calculated based on hazard intensity–probability distribution ( $H_p$ ), vulnerability curve or matrix ( $V_e$ ), and exposure ( $E_m$ ) as follows:

$$R = H_p \times V_e \times E_m \quad (1)$$

Risk grade in a region or grid of a disaster or multiple disasters is the ranking of disaster loss expectation ( $v$ ) through quantitative risk assessment ( $h$ ) and then risk categorization as shown below (Fig. 3):

$$R_g = H_p \times V_m \times E_m \quad (2)$$

where  $R_g$  is risk grade,  $H_p$  is hazard intensity–probability,  $V_m$  is vulnerability, and  $E_m$  is exposure magnitude.

Risk level of regional natural disaster is the level of disaster loss expectation developed through integrating hazard grade ( $H_g$ ), vulnerability magnitude (or matrix of hazard severity and exposure loss grade,  $V_m$ ), and magnitude of exposure ( $E_m$ ) (Fig. 4), as below:

$$R_l = H_g \times V_m \times E_m \quad (3)$$

where  $R_l$  is risk level;  $H_g$  is hazard grade;  $V_m$  is vulnerability matrix; and  $E_m$  is exposure magnitude.

Risk is the quantitative estimation of loss or damage expectation with a hazard intensity–probability function, and the accuracy of results is statistically significant. Risk grade is the semi-quantitative ranking of expected loss with medium accuracy after quantitative estimation. For risk level, it is qualitative estimation of expected loss with least accuracy level.

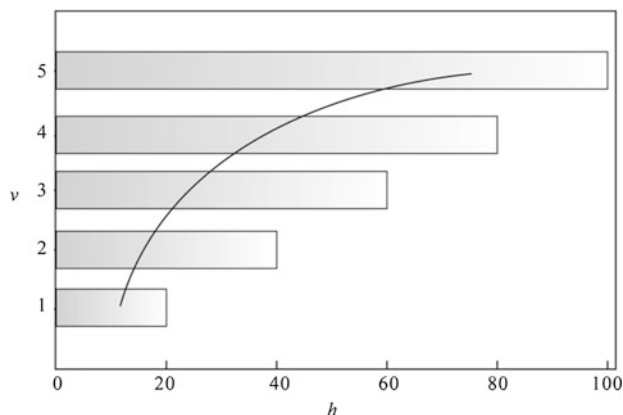


Fig. 3 Risk grade

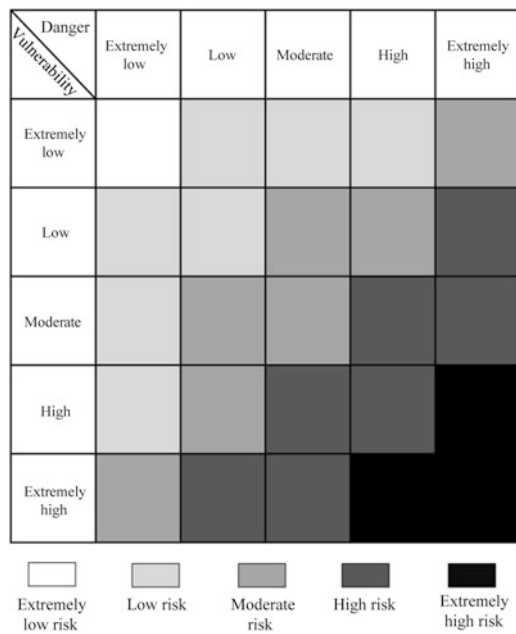


Fig. 4 Risk level

## 2.4 Natural Disaster Risk Assessment

Risk assessment of natural disaster is the estimation of casualty, property loss, and environmental damage in a region to certain physical hazards.

Risk assessment of major natural disaster is the estimation of loss or damage caused by the major disasters in a specific region. In the Atlas, the risk for major natural disasters of the world are assessed including earthquake, volcano, landslide, typhoon, flood, storm surge, drought, sand–dust storm, wild fire, heat wave, and cold wave. Exposures taken into consideration include population, livestock, property (house, family property, equipment, and infrastructure), crop (maize, wheat, and rice), Gross Domestic Product (GDP), Net Primary Production (NPP), and forest areas.

Risk assessment of multi-hazard is an overall risk assessment or integration of the aforementioned 11 types of natural disasters of the world through the weighted mean of each individual disaster risk. The weights for each disaster risk are derived from the frequency and total loss claimed by major and severe natural disasters recorded globally during the last 60 years. According to the statistics of frequency, flood has the highest weight among all disasters, followed by typhoon, hail (hail storm and hailstone), and earthquake. In terms of casualty and direct economic loss, the top three disasters are earthquake, flood, and typhoon. For the quantity of collapsed building and displaced population, flood, earthquake, and typhoon topped the list.

In the Atlas, risk, risk grade, and risk level for individual natural disasters, and risk grade for multi-hazards are derived

according to data availability, data accuracy (especially for vulnerability), modeling methodology, and result reliability. The process lays on the latest progress in disaster risk science, with the support of a variety of information technology like remote sensing, geographic information system (GIS), and database.

The providers of the shared data online have made a great scientific contribution to global natural disaster risk reduction, which does not only inspire us to make joint efforts to develop disaster risk science and compile this atlas, but also will save numerous lives, huge properties, and the service capacity of earth ecological system from the damage of disasters. Hence, we express our heartfelt appreciation and respect to those institutions and Web sites who provided related global data, and to those scientific personnel who devoted themselves to this grand cause.

## 3 Data Source and Methodology

In the past three decades, disaster risk research group at Beijing Normal University cumulated considerable regional natural disaster datasets in and outside China with the development of disaster risk science. In the meanwhile, international cooperation with scientific research institutions outside of China also helps produce/collect natural disaster data of other regions in the world. Global/regional natural disaster datasets with open access provided by data-sharing institutions on the Internet were also used. Besides, a part of global and regional natural disaster system datasets were purchased from data production institutions.

### 3.1 Data Source

Natural Disaster System Datasets of China used in this Atlas mainly came from *Atlas of Natural Disaster of China* (Chinese and English Version) (Zhang and Liu 1992), *Atlas of Natural Disaster System of China* (Chinese and English Version) (Shi 2003), and *Atlas of Natural Disaster Risk of China* (Chinese and English Version) (Shi 2011) published by Science Press of China. State Key Laboratory of Earth Surface Processes and Resources Ecology of China at Beijing Normal University, Key Laboratory of Environmental Change and Natural Disaster of Ministry of Education of China at Beijing Normal University, and Key Laboratory of Regional Geography of Beijing Normal University contributed to database construction.

Natural Disaster System Datasets of the rest of the world came from a variety of sources. Appendix III lists detailed information about datasets on environments, hazards, exposure, and disasters.

### 3.2 Assessment Methodology

This Atlas employs the assessment methodology used in *Atlas of Natural Disaster Risk of China* (Chinese and English Version) (Shi 2011), including regional natural disaster risk assessment, risk grade assessment, and risk level assessment as described earlier. The object of assessment include world major natural disasters and multi-hazard, considering loss of, damage to, or impact on population, property (house, family property, equipment, and infrastructure), crop (maize, wheat, and rice), GDP, NPP, and forest areas. Detailed methodologies have been elaborated by disaster type and map series.

## 4 Thematic Map Development

### 4.1 Design Concept

The natural disaster risk maps are designed to express the regions of spatial–temporal attributes. The core contents are regional differences of disaster risk. By transfer of disaster risk map information, readers and users are able to directly realize “Where is the highest risk zone?” and “Where is the higher risk zone under certain return period of loss?”, which will help understand the spatial disaster system and time variation process, and making decision. Every disaster risk map contains three-dimensional information of space (including mapping region scale and unit precision), time (including type of time interval and return period), and risk (different grades). The Atlas is supported by the three-

dimensional structure (Fig. 5) to finish the contents, expression methods, color and layout designs.

The disaster risk assessment results are expressed as symbols in each page of the Atlas (Fig. 6), which is reflected in the disaster risk assessment model  $Risk (R) = Hazard (H) \times Vulnerability (V) \times Exposure (E)$ .

### 4.2 Cartographic Units

There are three basic cartographic units used in this Atlas:

Grid Unit is the fundamental units for risk assessment as well as cartography of the 11 natural disasters. Unit sizes are applied by disaster type, including  $1 \text{ km} \times 1 \text{ km}$  grid,  $0.1^\circ \times 0.1^\circ$  grid,  $0.25^\circ \times 0.25^\circ$  grid,  $0.5^\circ \times 0.5^\circ$  grid,  $0.75^\circ \times 0.75^\circ$  grid, or  $1^\circ \times 1^\circ$  grid.

Comparable geographic unit is a new assessment and cartographic unit introduced in this atlas, which divides national and regional boundaries into subregions according to their areas (Fig. 7). The base map of this unit contains 349 comparable geographic units worldwide (Fig. 8, Appendix II). Due to the substantial area difference among regions and countries, large area could conceal inner-regional disparity, exaggerate visual feeling, and even lead to wrong perception. Therefore, the comparable geographic unit system was introduced.

Country and region unit uses the base map of national (regional) administrative divisions provided by the Star Map Press (China). National (regional) risks can be derived by zonal statistics applied to assessment results in grid units with the national (regional) boundary base map. Cartography based on national (regional) units can directly present

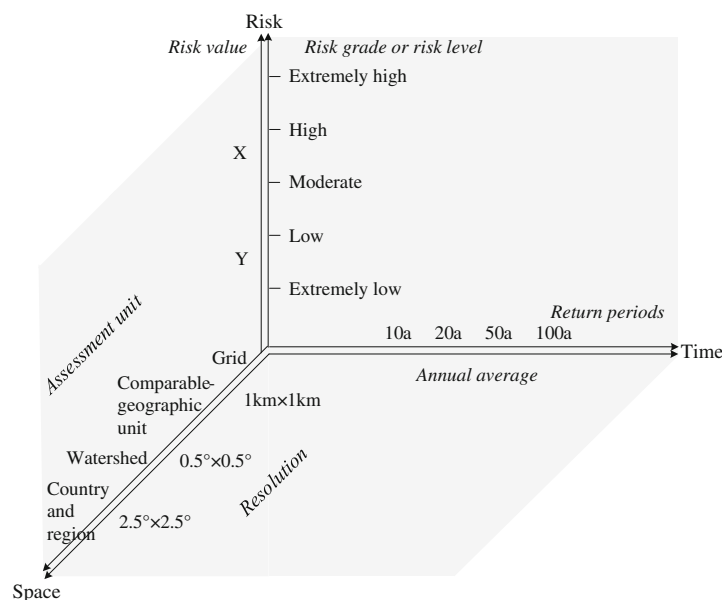
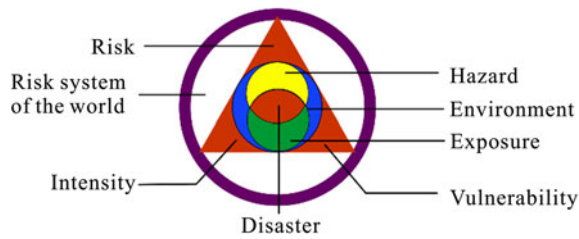


Fig. 5 Methodology and technical system of integrated disaster science



**Fig. 6** The symbol of integrated disaster risk

disaster risk difference among countries. The base map of national (regional) units contains all 245 countries and regions listed in world development index used by the World Bank (Appendix I.A and I.B).

Watershed unit is the best spatial unit for assessing flood risk and revealing flood risk process. It also eases integrated flood risk management by means of watershed management. In this Atlas, the watershed unit base map containing global 254 major watershed units was provided by World Resources Institute, within which 106 watersheds were involved in flood risk assessment and cartography.

### 4.3 Technical Flowchart

The mapping and compilation of this atlas contains four steps: preparedness and design, mapping, map review, and computer to plate. The editing technical flowchart is shown in Fig. 9.

### 4.4 Cartographic Presentation

A variety of conventional cartographic presentation methods are used in this Atlas to describe natural disaster risk (Table 1), such as the ratio classification, area method, quality-based method, dot method, line method, quantity-based mapping, and isopleths.

Disaster risk map-group method can express the maps of complicated disaster processes with a group of risk maps through an intuitive and visual way. It makes use of visual expression to identify the complex and abstract contents of risk maps. In maps series of each type of disaster in this atlas, there are map groups by return period, mapping units, and exposures. Return period map-group refers to the risk metric maps with annual average loss, 10a, 20a, 50a, and 100a loss maps. Mapping unit map-group refers to a series of maps derived on grid units, comparable geographic units, national/regional units, and watershed units. Exposure map-group refers to a series of map with identical hazard but different exposure and measures of loss. Examples of the map-group method are provided in Tables 2, 3, and 4.

### 4.5 Map Color Design

Symbol color design for disaster risk map is based on three basic modes: (1) C-H mode: direct color feeling mode in which the color (C) will directly be associated with certain hazard (H); (2) C-F-H mode: indirect color feeling mode in which certain hazard (H) and color can bring people similar feeling (F); and (3) C-S-H mode: indirect color feeling mode in which feeling of the landscape (S) associated with hazard (H) is similar as the color. The color experience of certain hazard (H) may be caused by more than one mode.

This atlas includes 11 types of hazards, i.e., earthquake, volcano, landslide, flood, storm surge, tropical cyclone and sand-dust storm, heat wave, cold wave, drought and wildfire. The final color system for each hazard type was listed in Table 5.

In this atlas, the color design is difficult, but it is also the highlight. The presentation of risks in the Atlas adopts the 5-grade classification system. The color design principles are as follows: (1) Emphasize the areas at high disaster risk, using red at grades 1 and 2 (grade 3 for some disaster types), as the top level of risk for warning. Gray or canary yellow is used at regions of no data or no risk. (2) Keep the

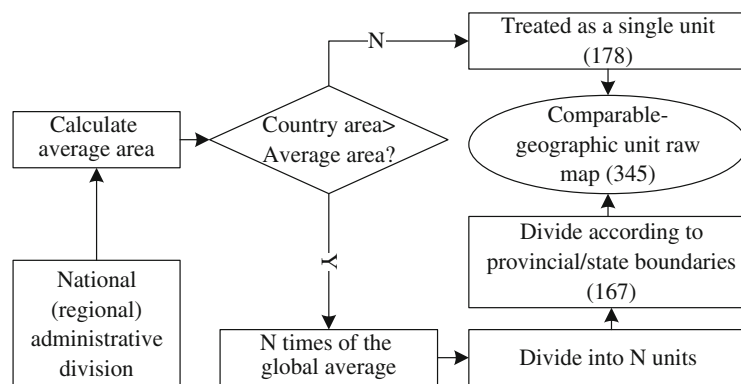


**Fig. 7** Technical flowchart for developing comparable geographic base map based on national (regional) administrative divisions

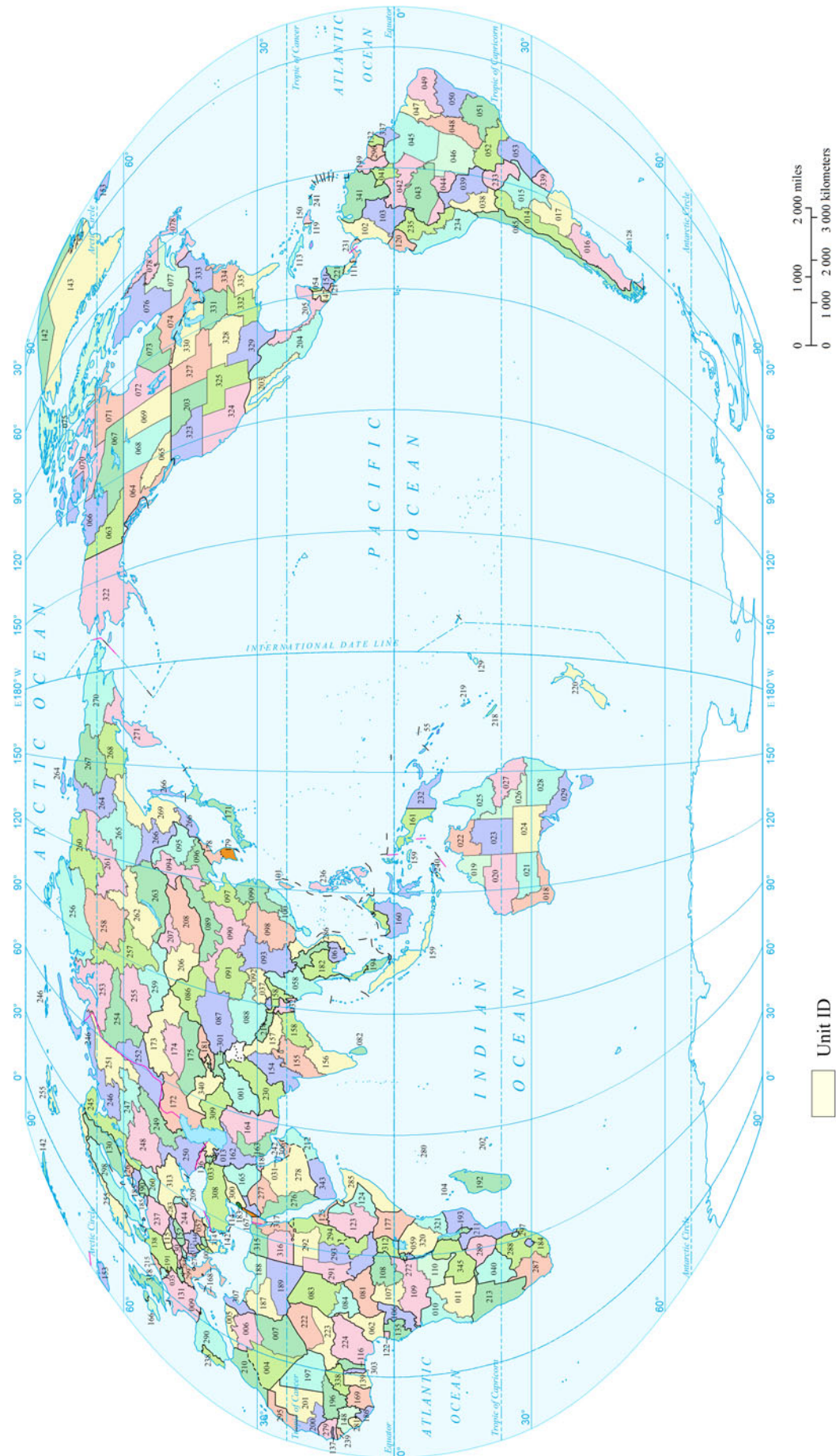
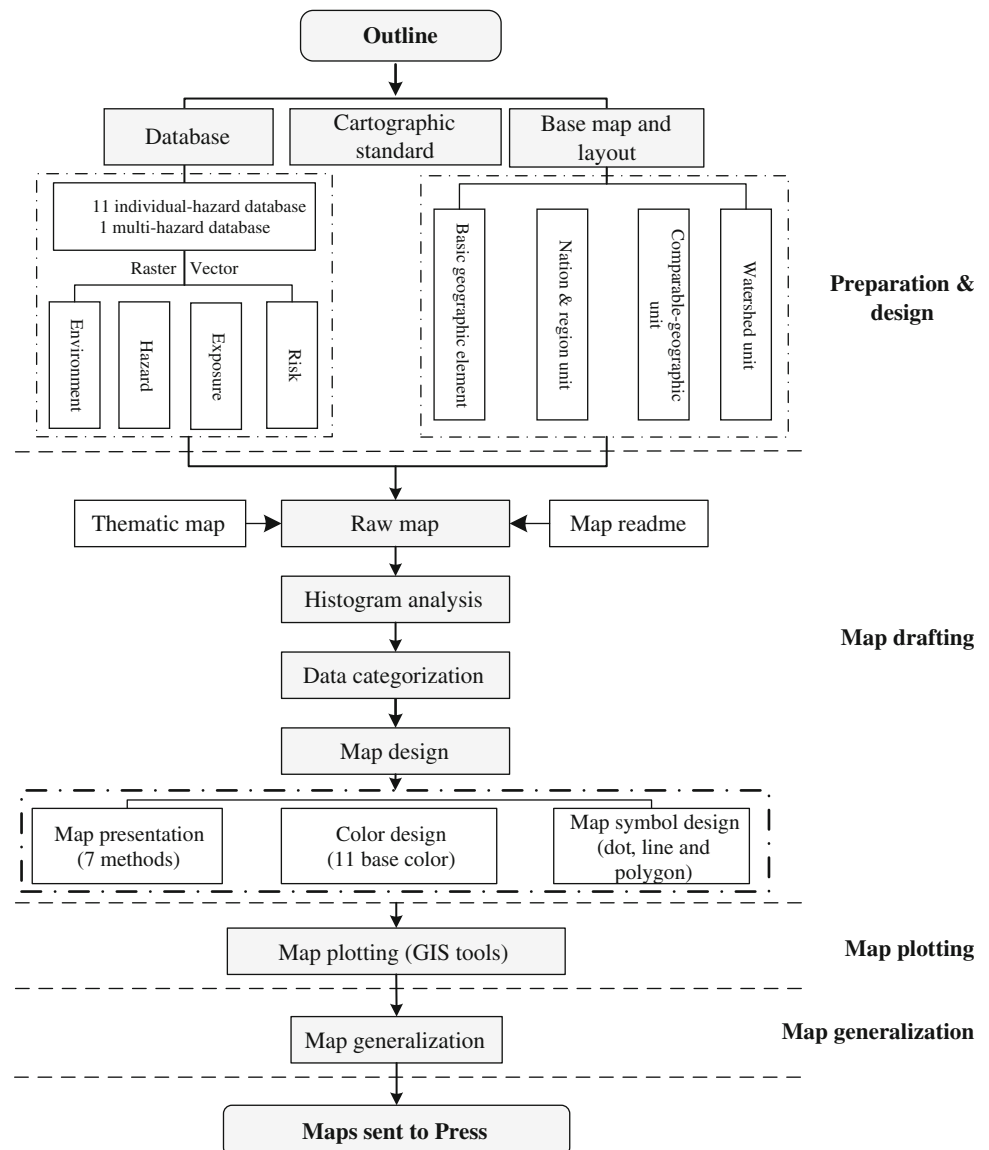


Fig. 8 Comparable geographic unit (The Unit ID is the last three numbers of the unit coding in Appendix II)

**Fig. 9** The editing technical flowchart of *World Atlas of Natural Disaster Risk*



discernment and continuity of each grade. For the legend design of 10-grade risk level, usually gradient among 3–5 or 4–5 colors are used, and there are two arrangement forms according the color shade: from dark to light [i.e., annual expected rainstorm flood population risk of the world (grid units)] and from light to dark [i.e., expected cold wave population risk (grid unit)]. The former is commonly used at monochrome hypsometric layer mapping based on grid units, average area units, basin units, and country units, and the latter is used at double-color or multi-color hypsometric layer mapping based on grid cell, average area units, basin units, and country units. (3) Weaken the color presentation in regions with no data or no risk. Generally, light gray or light yellow are adopted.

In this atlas, disaster risk maps in grid units are classified into 5 or 10 levels. Risk maps in comparable geographic

units or nation units are classified into 5 levels. The color design referred to the plan used in *Atlas of Natural Disaster System of China* (Chinese and English Version) (Shi 2003) and *Atlas of Natural Disaster Risk of China* (Chinese and English Version) (Shi 2011).

A part of the maps enhances the contrast of color to better deliver map information. There are three color-enhancing methods used. (1) Continents are set as black, while keeping the basic color of oceans. This method is applied to grid-based earthquake disaster risk maps, landslide disaster risk maps, sand–dust storm disaster risk maps, and forest/grassland fire disaster risk maps. (2) Oceans are set as dark blue, while continents remain in its base color. This method is applied to volcanic hazard intensity maps. (3) Dark gray continents and dark blue oceans are applied to storm surge disaster risk maps.

**Table 1** Map presentation methods

Map group	Presentation methods	Thematic map examples
Introduction maps	Quality-based method	Political Map of the World (2014)
	Satellite image	Global Satellite Image (2012)
Environments and exposures	Ratio classification	Population of the World (2010) (1 km × 1 km)
	Quality-based method	Global Lithology (2012) (0.5° × 0.5°)
	Line symbols	Global River Systems (2010)
	Quantity-based method	Land Use System of the World (2010) (10 km × 10 km)
	Isopleth	Global Permafrost Zones (1997)
Earthquake, volcano, and landslides disasters	Ratio classification	Mortality Rate of Earthquake Disaster (Intensity = VII) of the World
	Area method	Expected Annual Mortality Risk of Earthquake of the World (0.5° × 0.5°)
	Dot symbols	Historical Eruption Locations of Global Volcano (4360B.C–2012A.D)
Flood and storm surge disasters	Ratio classification	Annual Mortality in Historical Flood Disaster of the World (1950–2012)
	Area method	Global Flood Inundation Area by Return Period (100a)
	Line symbols	Global Coastal Geomorphology
Sand–dust storm and tropical cyclone disasters	Area method	Susceptibility of Global Sand-dust Storm (0.5° × 0.5°)
	Point symbols	Global Tropical Cyclone Paths
Heat wave and cold wave disasters	Ratio classification + Dot symbols	Threshold Temperature (0.75° × 0.75°) and Historical Events Location of Global Heat Wave
	Area method	Expected Annual Affected Population Risk of Cold Wave of the World (0.75° × 0.75°)
Drought disasters (wheat, maize, and rice)	Area method	Global Drought Intensity for Maize by Return Period (10a & 20a) (0.5° × 0.5°)
	Quality-based method	Global Drought Intensity for Wheat by Return Period (10a & 20a) (0.5° × 0.5°)
Wildfire disasters (forest and grassland)	Ratio classification	Expected NPP Loss Risk of Grassland Wildfire of the World (Comparable Geographic Unit & Country and Region Unit)
	Area method	Expected Annual Burned Area Risk of Forest Wildfire of the World (Comparable Geographic Unit)
Multi-natural disasters	Ratio classification	Expected Annual Mortality and Affected Population Risk Level by Total Risk Index of the World (0.5° × 0.5°)

**Table 2** Flood disaster risk map-group by watershed

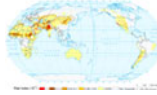
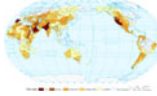
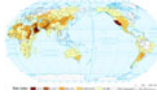
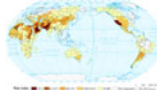
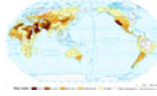
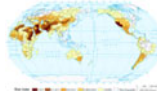
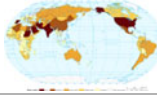
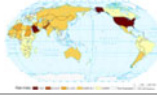
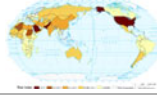
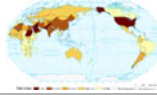
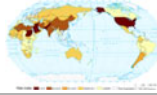
Exposure	Return period				
	Annual average	10a	20a	50a	100a
Population risk					
GDP (property) risk					

In the introduction texts for each disaster risk type, there are disaster risk color ramps designed for results in nation units. Color ramps include five levels. Level 1 and Level 2 use red colors. Level 4 and Level 5 use the base color system listed in Table 5. Level 3 generally uses yellow colors. The widths of color block levels 1–5 represent percentage ranks of (0, 10 %], (10, 35 %], (35, 65 %], (65, 90 %], (90, 100 %], respectively.

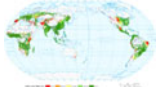
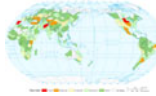
## 4.6 Cartographic Specifications

The world national/regional boundary map in this atlas is provided by the Star Map Press (China) using the 2014 boundary data; the designations employed and the presentation of material on the maps do not imply the expression of any opinion concerning the legal status of any country, territory, city, or area or of its authorities, or concerning the delimitation of its frontiers or

**Table 3** Sand–dust storm affected GDP risk map-group

Mapping unit	Return period				
	Annual average	10a	20a	50a	100a
Grid unit					
Comparable geographic unit					
National/regional unit					

**Table 4** Drought disaster-induced annual average crop yield loss risk map-group

Exposure	Mapping unit		
	Grid unit	Comparable geographic unit	National/Regional unit
Maize			
Wheat			
Rice			

**Table 5** Color system by hazard type

Hazard	Base color	Hazard	Base color	Hazard	Base color
Earthquake	Red	Cold wave	Blue–Purple	Storm surge	Blue–Cyan
Volcano	Red–Purple	Heat wave	Red–Yellow	Flood	Green
Landslide	Brown	Typhoon	Blue	Wildfire	Red–Green
Drought	Orange–Green	Sand–dust storm	Yellow–Orange	Multi-hazard	Red/Purple–Green

boundaries. It uses Equivalent Difference Latitude Parallel Polyconic Projection with central meridian 150 °E. This Atlas adopts the projection transformation from Equivalent Difference Latitude Parallel Polyconic Projection into Robinson Projection and registration before using the boundary.

Most maps in the Atlas adopt Robinson Project with Central Median of 160 °E. Global tropic cyclone maps use central meridian of 160 °W to keep completeness the Pacific, Atlantic, and Indian Ocean. The minimum distances for both latitude and longitude are set at 30°. Tropic of Cancer and Tropic of Capricorn are also presented in maps.

According to the task and purpose of the Atlas, we use the following scales for the full map of the world: 1:140,000,000 (single page) and 1:200,000,000 (1/2 page).

In the Atlas, maps without the annotations of country and region names can be referred to the Political Map of the World (2014). Maps noted with Internet linkage address are directly derived from these shared Internet sources (only slight modification is made for some maps); others are originally developed by the authors. The disaster risks of earthquake, volcano, landslide, flood, tropical cyclone, heat wave, and grassland wildfire for Antarctic are not assessed,

and the disaster risks of storm surge, sand–dust storm, cold wave, forest wildfire, and multi-hazard for Antarctic and Greenland are not assessed due to the lack of available data.

---

## 5 Atlas Structure

In this Atlas, the Political Map and Global Satellite Image are served as opening maps. After introducing Environments and Exposures, there comes Major Natural Disaster Risk Maps, which is the main body of this Atlas. This section consists of earthquake, volcano and landslide disasters, flood and storm surge disasters, sand–dust storm and tropical cyclone disasters, heat wave and cold wave disasters, drought disasters of maize, wheat and rice, and wildfire disasters of forest and grassland. The final section is about total disaster and multi-hazard of the world.

### 5.1 Environments and Exposures

This section is made up of 16 maps; they are Global Lithology, Global Tectonic Faults, Global Land Elevation, Global Terrain Slope, Global Permafrost Zones, Global Land Cover, Global Soil, Global Climate Zone, Global River Systems, Global Annual Average Net Primary Production (NPP), Land Use System of the World, Population of the World, Social Wealth of the World, Gross Domestic Product (GDP) of the World, Livestock Density of the World, and Night Light Index of the World.

### 5.2 Major Natural Disaster Risk Maps

This section includes the maps of hazard, disaster, and risk for 11 types of hazards, i.e., earthquake (15 maps), volcano (18 maps), landslide (6 maps), flood (46 maps), storm surge (6 maps), tropical cyclone (17 maps), sand–dust storm (51 maps), heat wave (26 maps), cold wave (23 maps), drought risk (60 maps), and wildfire (17 maps). These maps present a comprehensive spatial pattern of major natural disaster risks of the world.

### 5.3 Multi-hazard Risk Maps

This section includes mortality and affected population risk level by Total Risk Index (TRI) (3 maps), loss, and affected property risk level by TRI (3 maps), multi-hazard intensity (1 map), mortality and affected population risk level by Multi-hazard Risk Index (MhRI) (3 maps), and loss and affected property risk level by MhRI (3 maps).

## 6 Validation of the Results

We take advantage of EM-DATA and other related data to validate our results. For earthquake mortality risk, volcano mortality risk, landslide mortality risk, flood economic loss and mortality risk, affected population/GDP risk of storm surge, heat wave mortality risk, affected population risk of cold wave, burned forest area, expected annual mortality and affected population risk rank by TRI of country unit and per unit area, expected annual affected population risk rank by MhRI of country unit, expected annual loss and affected property risk rank by TRI of country unit and per unit area, and expected annual affected property risk rank by MRI of country unit, we use Spearman rank correlation to validate the results. For earthquake economic–social wealth loss risk, affected population/GDP risk of flood, affected population/GDP risk of sand–dust storm, maize yield loss risk of drought, wheat yield loss risk of drought and rice yield loss risk of drought, expected annual mortality and affected population risk by TRI of grid unit ( $0.5^\circ \times 0.5^\circ$ ), and expected annual loss and affected property risk by TRI of grid unit ( $0.5^\circ \times 0.5^\circ$ ), we use Pearson correlation to validate the results. The detailed table and significance of the validation results are shown in Appendix IV.

---

## 7 Ranks of Major Natural Disaster Risk Level of the World

According to the assessment results of the country unit based on each disaster risk, Table 6 shows the top 1 % and top 10 % countries of the ranks of earthquake, volcano, landslide, flood, storm surge, tropical cyclone, sand–dust storm, heat wave, cold wave, drought (maize, wheat, and rice), and wildfire (forest wildfire and grassland wildfire) of the world.

According to the assessment results of the country unit based on Total Risk Index (TRI), Table 7 shows the top 1 % and top 10 % countries of the affected population (3 maps) and property (3 maps) risk level of TRI rank of the world. According to the assessment results of the country based on Multi-hazard Risk Index (MhRI), Table 7 shows the top 1 % and top 10 % countries of the MhRI (1 map) rank and affected population (3 maps) and property (3 maps) risk level of MhRI rank of the world.

---

## 8 Conclusion and Discussion

In this Atlas, the world risk of 11 major natural disasters—earthquake, volcano, landslide, flood, storm surge, sand–dust storm, tropical cyclone, heat wave, cold wave, drought, and wildfire—were assessed and mapped initiatively at grid unit,

**Table 6** The top 1 % and top 10 % countries with the highest major natural disaster risk

Hazard	Risk	The top 1 % countries	The top 10 % countries	Assessed countries
Earthquake	Mortality	India	India, Indonesia, Pakistan, Bangladesh, China, Philippines, Burma, Iran, Afghanistan, Uzbekistan, Nepal, Ethiopia	115
	Affected economic-social wealth	Japan, United States	Japan, United States, China, Turkey, Italy, Mexico, Chile, Canada, Indonesia, Venezuela, Iran, Philippines	122
Volcano	Mortality	Indonesia	Indonesia, Japan, Chile, Philippines, Papua New Guinea	54
Landslide	Mortality	China, Congo	China, Congo, Brazil, Iran, Uganda, Philippines, Indonesia, India, Nepal, Paraguay, Bolivia, Burundi, Colombia	126
Flood	Affected population	Bangladesh	Bangladesh, China, India, Cambodia, Pakistan, Brazil, Nepal, Netherlands, Indonesia, United States, Vietnam, Burma, Thailand, Nigeria, Japan	154
	Affected GDP	United States	United States, China, Japan, Nederland, India, Germany, France, Argentina, Bangladesh, Brazil, United Kingdom, Thailand, Myanmar, Cambodia, Canada	150
Storm surge	Affected population	Bangladesh	Bangladesh, India, China, Viet Nam, United States, Sri Lanka	57
	Affected GDP	United States	United States, China, Japan, Australia, Ireland, Bangladesh	57
Tropical cyclone	Affected population	China	China, Philippines, Japan, United States, Viet Nam, South Korea, India, Cuba	83
Sand-dust storm	Affected population	Pakistan	Pakistan, Georgia, Burkina Faso, Yemen, India, Tunisia, Azerbaijan, Ghana, Ethiopia, Ecuador, Eritrea	106
	Affected GDP	Kuwait	Kuwait, Georgia, Israel, United States, Spain, Slovakia, Pakistan, Colombia, Saudi, Arabia, Greece, Syria	106
	Affected livestock	Pakistan	Pakistan, Burkina Faso, Syria, Mali, Sudan, India, Jordan, Azerbaijan, Mongolia, Afghanistan, Georgia	109
Heat wave	Mortality	India	India, Pakistan, United States, Iraq, Russia, Ukraine, Spain, China, Germany, Turkey, France, Iran, Poland	129
Cold wave	Affected population	China, India	China, India, United States, Russia, Pakistan, Bangladesh, Brazil, Mexico, Germany, Egypt, Japan, South Korea, Iran, United Kingdom, Turkey, Ukraine	161
Drought	Yield loss (Maize)	United States	United States, China, Russia, Brazil, Spain, Afghanistan, Kenya, Argentina, Mexico, Turkey, Ukraine, Kazakhstan, South Africa, Tanzania, Iraq, Australia	146
	Yield loss (Wheat)	China	China, Russia, United States, Kazakhstan, Canada, Kenya, Mongolia, Pakistan, Mexico, Chile, South Africa, Afghanistan	119
	Yield loss (Rice)	Afghanistan	Afghanistan, China, Spain, Pakistan, India, Tanzania, Brazil, Russia, Burkina Faso, Australia, Kazakhstan	109
Wildfire	Burned forest area	Russia	Russia, Canada, Angola, Brazil, Democratic Republic of the Congo, United States, Argentina, Burma, Bolivia, China, Australia	113
	Grassland NPP loss	Brazil, United States	Brazil, United States, Australia, Russia, Kazakhstan, Mozambique, Madagascar, China, Tanzania, Canada, Angola, South Africa, Venezuela, Argentina, Nigeria, Sudan, Colombia, Mexico, Zimbabwe, Zambia	194

**Table 7** The top top 1 % and 10 % countries with the highest multi-hazard risk

Index	Intensity or risk	The top 1 % countries	The top 10 % countries	Assessed countries
Mh	Multi-hazard intensity at country unit	Russia, United States	Russia, United States, China, Canada, Australia, Brazil, India, Mexico, Argentina, Indonesia, Kazakhstan, Congo (Democratic Republic of the), Iran, Colombia, Burma, Peru, Madagascar, Bolivia, Turkey, Venezuela	197
	Multi-hazard intensity per unit area	Bangladesh, South Korea	Bangladesh, South Korea, Japan, Vietnam, Laos, Belize, Burma, Guatemala, Madagascar Dominican Republic, North Korea, Philippines, Bhutan, El Salvador, Honduras, Papua New Guinea, Cambodia, India, New Zealand, Thailand	197
TRI	Mortality and affected population at country unit	India, China	India, China, Indonesia, Pakistan, Bangladesh, Philippines, Burma, United States, Japan, Iran, Afghanistan, Nepal, Egypt, Uzbekistan, Mexico, Vietnam, Ethiopia, Guatemala, Kyrgyzstan, Turkey	195
	Mortality and affected population per unit area	Bangladesh, Gaza Strip	Bangladesh, Gaza Strip, Philippines, Nepal, Pakistan, Guatemala, Bhutan, Israel, Haiti, Burundi, El Salvador, India, Japan, Indonesia, Rwanda, South Korea, Moldova, Uzbekistan, Georgia, Burma	195
	Loss and affected property of country unit	United States, Japan	United States, Japan, China, Russia, Canada, Germany, Brazil, India, Netherlands, Mexico, Australia, Argentina, France, South Korea, Angola, Congo (Democratic Republic of the), Burma, Italy, Turkey, Thailand	196
	Loss and affected property per unit area	Netherlands, Japan	Netherlands, Japan, South Korea, Germany, Belgium, Singapore, Gaza Strip, Israel, Bangladesh, Liechtenstein, Trinidad and Tobago, Monaco, United Kingdom, San Marino, Luxembourg, Italy, France, United States, Switzerland, Mauritius	196
MhRI	Affected population of country unit	China, India	China, India, United States, Bangladesh, Japan, Indonesia, Brazil, Philippines, Vietnam, Mexico, Pakistan, Nigeria, Thailand, Burma, South Korea, Russia, Turkey, Ethiopia, Iran, Germany	197
	Affected population per unit area	Bangladesh, Singapore	Bangladesh, Singapore, South Korea, Philippines, Japan, India, Vietnam, Haiti, El Salvador, San Marino, Gaza Strip, Dominican Republic, Sri Lanka, Nepal, North Korea, Lebanon, Rwanda, Guatemala, Burundi, Monaco	197
	Affected property at country unit	United States, Japan	United States, Japan, China, India, Germany, Brazil, South Korea, France, Mexico, Canada, Italy, United Kingdom, Russia, Spain, Australia, Indonesia, Turkey, Netherlands, Thailand, Switzerland	196
	Affected property per unit area	Netherlands, Japan	Japan, South Korea, San Marino, Netherlands, Liechtenstein, Monaco, Luxembourg, Switzerland, Belgium, Germany, Andorra, United Kingdom, Singapore, Italy, Austria, Israel, France, Gaza Strip, Lebanon, Denmark	196

comparable geographic unit, and national unit. The multi-hazard risk of above 11 hazards was also assessed, mapped, and ranked initiatively with the Total Risk Index (TRI) and Multi-hazard Risk Index (MhRI) at grid unit and national unit. By zonal statistics of the expected risk result, the expected annual mortality and/or affected population risks and expected annual economic loss and/or affected property risks of 11 hazards and multi-hazard of the world at national level are initiatively derived and ranked.

The Atlas proposed the comparative geographic unit to map the major natural disaster risks of the world, which can better present the spatial patterns of the mortality and economic loss risks of those hazard. The Atlas derived the top 1 and 10 % countries with highest risk value for 11 types of hazards, and the top 50 counties with the highest multi-hazard risk both at national level and per unit area level.

This is the first world atlas for systematically mapping the major natural disaster risks with the framework of Regional Disaster System Theory. However, due to the limitation of data availability, the vulnerability curves are not fitted at grid or comparable geographic unit level or even at national level for some types of disaster, and affected population and GDP risks are assessed instead of the risks for mortality and property loss. Besides, weighting methods are used to assess the multi-hazard risk by EM-DAT and China Catastrophe Statistics (CCS), but the weights for some types of hazards were not obtained due to the limited available data. Thus, the result reasonability was limited. Thirdly, only the top 50 countries with the highest multi-hazard risks at higher confidence level were ranked; other countries were listed by 4 groups from top 51 to top 100, from top 101 to top 150, and from top 151 to the lowest. Finally, due to the limitation of data spatial resolution, maps for some types of hazards were only developed at relatively lower spatial resolution, such as  $0.75^\circ \times 0.75^\circ$  for heat wave and cold wave, and  $1^\circ \times 1^\circ$  for flood.

The authors greatly appreciate the institutes, organizations, companies, and official departments who provided data, models, publications, and related documents for this atlas.

We look forward to more contributions to improve data resolution, methods, and models related to map world disaster risks at different spatial-temporal levels for disaster risk reduction of the world.

## References

- Dilley, M., U. Deichmann, and R.S. Chen. 2005. *Natural disaster hotspots: A global risk analysis*. Washington, DC: World Bank Publications.
- Institute for Environment and Human Security, United Nations University (UNU-EHS). 2013. *World risk report 2013*. Berlin: Bündnis Entwicklung Hilft, Alliance Development Works.
- Shi, P.J., ed. 2003. *Atlas of natural disaster system of China (Chinese-English Version)*. Beijing: Science Press.
- Shi, P.J., ed. 2011. *Atlas of natural disaster risk of China (Chinese-English Version)*. Beijing: Science Press.
- Shi, P.J. 1991. Study on the theory of disaster research and its practice. *Journal of Nanjing University (Natural Sciences)* 11(Supplement): 37–42. (in Chinese).
- Shi, P.J. 1996. Theory and practice of disaster study. *Journal of Natural Disasters* 5(4): 6–17. (in Chinese).
- Shi, P.J. 2002. Theory on disaster science and disaster dynamics. *Journal of Natural Disasters* 11(3): 1–9. (in Chinese).
- Shi, P.J. 2005. Theory and practice on disaster system research—The fourth discussion. *Journal of Natural Disasters* 14(6): 1–7. (in Chinese).
- Shi, P.J. 2009. Theory and practice on disaster system research—The fifth discussion. *Journal of Natural Disasters* 18(5): 1–9. (in Chinese).
- Shi, P.J. Qian Ye, Guoyi Han, et al. 2012. Living with global climate diversity—Suggestions on international governance for coping with climate change risk. *International Journal of Disaster Risk Science* 3(4): 177–183.
- United Nations International Strategy for Disaster Reduction (UNISDR). 2009. *Global assessment report on disaster risk reduction 2009*. Geneva, Switzerland: United Nations.
- United Nations International Strategy for Disaster Reduction (UNISDR). 2011. *Global assessment report on disaster risk reduction 2011*. Geneva, Switzerland: United Nations.
- United Nations International Strategy for Disaster Reduction (UNISDR). 2013. *Global assessment report on disaster risk reduction 2013*. Geneva, Switzerland: United Nations.
- Zhang, L.S. and E.Z. Liu, eds. 1992. *Atlas of natural disaster of China (Chinese and English Version)*. Beijing, China: Science Press.

## Appendix I Name and Abbreviation of Countries and Regions

### I.A Name and Abbreviation of Countries (Alphabetical Order of the Initial of the Short Name)<sup>1</sup>

Full name	Short name	Abbreviation
The Islamic Republic of Afghanistan	Afghanistan	AFG
The Republic of Albania	Albania	ALB
The People's Democratic Republic of Algeria	Algeria	DZA
The Principality of Andorra	Andorra	AND
The Republic of Angola	Angola	AGO
Antigua and Barbuda	Antigua and Barbuda	ATG
The Argentine Republic	Argentina	ARG
The Republic of Armenia	Armenia	ARM
Australia	Australia	AUS
The Republic of Austria	Austria	AUT
The Republic of Azerbaijan	Azerbaijan	AZE
The Commonwealth of the Bahamas	Bahamas	BHS
The Kingdom of Bahrain	Bahrain	BHR
Brunei Darussalam	Baker Island	BRN
The People's Republic of Bangladesh	Bangladesh	BGD
Barbados	Barbados	BRB
The Republic of Belarus	Belarus	BLR
The Kingdom of Belgium	Belgium	BEL
Belize	Belize	BLZ
The Republic of Benin	Benin	BEN
The Kingdom of Bhutan	Bhutan	BTN

(continued)

(continued)

Full name	Short name	Abbreviation
The Plurinational State of Bolivia	Bolivia	BOL
Bosnia and Herzegovina	Bosnia and Herzegovina	BIH
The Republic of Botswana	Botswana	BWA
The Federative Republic of Brazil	Brazil	BRA
The Republic of Bulgaria	Bulgaria	BGR
Burkina Faso	Burkina Faso	BFA
The Republic of the Union of Myanmar	Burma	MMR
The Republic of Burundi	Burundi	BDI
The Kingdom of Cambodia	Cambodia	KHM
The Republic of Cameroon	Cameroon	CMR
Canada	Canada	CAN
The Republic of Cabo Verde	Cape Verde	CPV
The Central African Republic	Central African Republic	CAF
The Republic of Chad	Chad	TCD
The Republic of Chile	Chile	CHL
The People's Republic of China	China	CHN
The Republic of Colombia	Colombia	COL
The Union of the Comoros	Comoros	COM
The Republic of the Congo	Congo	COG
The Democratic Republic of the Congo	Congo (Democratic Republic of the)	COD
The Cook Islands	Cook Islands	COK

(continued)

<sup>1</sup> <http://unterm.un.org>

(continued)		
Full name	Short name	Abbreviation
The Republic of Costa Rica	Costa Rica	CRI
The Republic of Croatia	Croatia	HRV
The Republic of Cuba	Cuba	CUB
The Republic of Cyprus	Cyprus	CYP
The Czech Republic	Czech Republic	CZE
The Kingdom of Denmark	Denmark	DNK
The Republic of Djibouti	Djibouti	DJI
The Commonwealth of Dominica	Dominica	DMA
The Dominican Republic	Dominican Republic	DOM
The Republic of Ecuador	Ecuador	ECU
The Arab Republic of Egypt	Egypt	EGY
The Republic of El Salvador	El Salvador	SLV
The Republic of Equatorial Guinea	Equatorial Guinea	GNQ
The State of Eritrea	Eritrea	ERI
The Republic of Estonia	Estonia	EST
The Federal Democratic Republic of Ethiopia	Ethiopia	ETH
The Federated States of Micronesia	Federated States of Micronesia	FSM
The Republic of Fiji	Fiji	FJI
The Republic of Finland	Finland	FIN
The French Republic	France	FRA
The Gabonese Republic	Gabon	GAB
The Republic of the Gambia	Gambia	GMB
State of Palestine	Gaza Strip	PSE
Georgia	Georgia	GEO
The Federal Republic of Germany	Germany	DEU
The Republic of Ghana	Ghana	GHA
The Hellenic Republic	Greece	GRC
Grenada	Grenada	GRD
The Republic of Guatemala	Guatemala	GTM
The Republic of Guinea	Guinea	GIN
The Republic of Guinea-Bissau	Guinea-Bissau	GNB
The Republic of Guyana	Guyana	GUY
The Republic of Haiti	Haiti	HTI
The Republic of Honduras	Honduras	HND
Hungary	Hungary	HUN
The Republic of Iceland	Iceland	ISL
The Republic of India	India	IND
The Republic of Indonesia	Indonesia	IDN
The Islamic Republic of Iran	Iran	IRN
The Republic of Iraq	Iraq	IRQ

(continued)

(continued)		
Full name	Short name	Abbreviation
Ireland	Ireland	IRL
The State of Israel	Israel	ISR
The Republic of Italy	Italy	ITA
Jamaica	Jamaica	JAM
Japan	Japan	JPN
The Hashemite Kingdom of Jordan	Jordan	JOR
The Republic of Kazakhstan	Kazakhstan	KAZ
The Republic of Kenya	Kenya	KEN
The Republic of Kiribati	Kiribati	KIR
The State of Kuwait	Kuwait	KWT
The Kyrgyz Republic	Kyrgyzstan	KGZ
The Lao People's Democratic Republic	Laos	LAO
The Republic of Latvia	Latvia	LVA
The Lebanese Republic	Lebanon	LBN
The Kingdom of Lesotho	Lesotho	LSO
The Republic of Liberia	Liberia	LBR
Libya	Libya	LBY
The Principality of Liechtenstein	Liechtenstein	LIE
The Republic of Lithuania	Lithuania	LTU
The Grand Duchy of Luxembourg	Luxembourg	LUX
The former Yugoslav Republic of Macedonia	Macedonia	MKD
The Republic of Madagascar	Madagascar	MDG
The Republic of Malawi	Malawi	MWI
Malaysia	Malaysia	MYS
The Republic of Maldives	Maldives	MDV
The Republic of Mali	Mali	MLI
The Republic of Malta	Malta	MLT
The Republic of the Marshall Islands	Marshall Islands	MHL
The Islamic Republic of Mauritania	Mauritania	MRT
The Republic of Mauritius	Mauritius	MUS
The United Mexican States	Mexico	MEX
The Republic of Moldova	Moldova	MDA
The Principality of Monaco	Monaco	MCO
Mongolia	Mongolia	MNG
Montenegro	Montenegro	MNE
The Kingdom of Morocco	Morocco	MAR
The Republic of Mozambique	Mozambique	MOZ
The Republic of Namibia	Namibia	NAM
The Republic of Nauru	Nauru	NRU
The Federal Democratic Republic of Nepal	Nepal	NPL

(continued)

(continued)		
Full name	Short name	Abbreviation
The Kingdom of the Netherlands	Netherlands	NLD
New Zealand	New Zealand	NZL
The Republic of Nicaragua	Nicaragua	NIC
The Republic of the Niger	Niger	NER
The Federal Republic of Nigeria	Nigeria	NGA
Niue	Niue	NIU
The Democratic People's Republic of Korea	North Korea	PRK
The Kingdom of Norway	Norway	NOR
The Sultanate of Oman	Oman	OMN
The Islamic Republic of Pakistan	Pakistan	PAK
The Republic of Palau	Palau	PLW
The Republic of Vanuatu	Palestine	VUT
The Republic of Panama	Panama	PAN
Independent State of Papua New Guinea	Papua New Guinea	PNG
The Republic of Paraguay	Paraguay	PRY
The Republic of Peru	Peru	PER
The Republic of the Philippines	Philippines	PHL
The Republic of Poland	Poland	POL
The Portuguese Republic	Portugal	PRT
The State of Qatar	Qatar	QAT
Romania	Romania	ROU
The Russian Federation	Russia	RUS
The Republic of Rwanda	Rwanda	RWA
Saint Kitts and Nevis	Saint Kitts and Nevis	KNA
Saint Lucia	Saint Lucia	LCA
Saint Vincent and the Grenadines	Saint Vincent and the Grenadines	VCT
The Independent State of Samoa	Samoa	WSM
The Republic of San Marino	San Marino	SMR
The Democratic Republic of Sao Tome and Principe	Sao Tome and Principe	STP
The Kingdom of Saudi Arabia	Saudi Arabia	SAU
The Republic of Senegal	Senegal	SEN
The Republic of Serbia	Serbia	SRB
The Republic of Seychelles	Seychelles	SYC
The Republic of Sierra Leone	Sierra Leone	SLE
The Republic of Singapore	Singapore	SGP
The Slovak Republic	Slovakia	SVK
The Republic of Slovenia	Slovenia	SVN
Solomon islands	Solomon Islands	SLB

(continued)

(continued)		
Full name	Short name	Abbreviation
The Federal Republic of Somalia	Somalia	SOM
The Republic of South Africa	South Africa	ZAF
The Republic of Korea	South Korea	KOR
The Republic of South Sudan	South Sudan	SSD
The Kingdom of Spain	Spain	ESP
The Democratic Socialist Republic of Sri Lanka	Sri Lanka	LKA
The Republic of the Sudan	Sudan	SDN
The Republic of Suriname	Suriname	SUR
The Kingdom of Swaziland	Swaziland	SWZ
The Kingdom of Sweden	Sweden	SWE
The Swiss Confederation	Switzerland	CHE
The Syrian Arab Republic	Syria	SYR
The Republic of Tajikistan	Tajikistan	TJK
The United Republic of Tanzania	Tanzania	TZA
The Kingdom of Thailand	Thailand	THA
The Republic of Côte d'Ivoire	The Republic of Côte d'Ivoire	CIV
The Democratic Republic of Timor-Leste	Timor-Leste	TLS
The Togolese Republic	Togo	TGO
The Kingdom of Tonga	Tonga	TON
The Republic of Trinidad and Tobago	Trinidad and Tobago	TTO
The Republic of Tunisia	Tunisia	TUN
The Republic of Turkey	Turkey	TUR
Turkmenistan	Turkmenistan	TKM
Tuvalu	Tuvalu	TUV
The Republic of Uganda	Uganda	UGA
Ukraine	Ukraine	UKR
The United Arab Emirates	United Arab Emirates	ARE
The United Kingdom of Great Britain and Northern Ireland	United Kingdom	GBR
The United States of America	United States	USA
The Eastern Republic of Uruguay	Uruguay	URY
The Republic of Uzbekistan	Uzbekistan	UZB
The Holy See	Vatican City	VAT
The Bolivarian Republic of Venezuela	Venezuela	VEN
The Socialist Republic of Viet Nam	Vietnam	VNM
The Republic of Yemen	Yemen	YEM
The Republic of Zambia	Zambia	ZMB
The Republic of Zimbabwe	Zimbabwe	ZWE

### I.B Name, Dependency Country and Abbreviation of Regions (Alphabetical Order of the Initial of the Name)<sup>2</sup>

Name	Dependency of	Abbreviation
Anguilla	United Kingdom	AIA
Bermuda	United Kingdom	BMU
British Virgin Islands	United Kingdom	VGB
Cayman Islands	United Kingdom	CYM
Christmas Island	Australia	CXR
Cocos Islands	Australia	CCK
Faroe Islands	Denmark	FRO
French Guiana	France	GUF
French Polynesia	France	PYF
Gibraltar	United Kingdom	GIB
Greenland	Denmark	GRL
Guadeloupe	France	GLP
Guam	United States	GUM
Islas Malvinas	United Kingdom	FLK
Martinique	France	MTQ

(continued)

(continued)

Name	Dependency of	Abbreviation
Montserrat	United Kingdom	MSR
New Caledonia	France	NCL
Norfolk Island	Australia	NFK
Northern Mariana Islands	United States	MNP
Pitcairn Islands	United Kingdom	PCN
Puerto Rico	United States	PRI
Reunion	France	REU
Saint Barthelemy	France	BLM
Saint Helena	United Kingdom	SHN
Saint Martin	France	MAF
Saint Pierre and Miquelon	France	SPM
Saint Maarten	Netherlands	TCA
Tokelau	New Zealand	TKL
Virgin Islands	United States	VIR
Wallis et Futuna	France	WLF

<sup>2</sup> Fan, J. and M. Zhou (eds.) 2010. Atlas of the World. Beijing: Sino Maps Press. (in Chinese)

## Appendix II

### Name and Coding System of the Comparable-Geographic Unit in the Atlas (Alphabetical Order of the Initial of the Country Name)<sup>3</sup>

Code	Country	Continent
004001	Afghanistan	Asia
008002	Albania	Europe
012004	Algeria	Africa
012005	Algeria	Africa
012006	Algeria	Africa
012007	Algeria	Africa
016008	American Samoa	Oceania
020009	Andorra	Europe
024010	Angola	Africa
024011	Angola	Africa
010003	Antarctica	Antarctica
028012	Antigua and Barbuda	South America
032014	Argentina	South America
032015	Argentina	South America
032016	Argentina	South America
032017	Argentina	South America
051033	Armenia	Asia
533216	Aruba	South America
036018	Australia	Oceania
036019	Australia	Oceania
036020	Australia	Oceania
036021	Australia	Oceania
036022	Australia	Oceania
036023	Australia	Oceania
036024	Australia	Oceania
036025	Australia	Oceania
036026	Australia	Oceania
036027	Australia	Oceania
036028	Australia	Oceania

(continued)

(continued)

Code	Country	Continent
036029	Australia	Oceania
040030	Austria	Europe
031013	Azerbaijan	Asia
048031	Bahrain	Asia
050032	Bangladesh	Asia
052034	Barbados	South America
112060	Belarus	Europe
056035	Belgium	Europe
084054	Belize	South America
204116	Benin	Africa
060036	Bermuda	South America
064037	Bhutan	Asia
068038	Bolivia	South America
068039	Bolivia	South America
072040	Botswana	Africa
076041	Brazil	South America
076042	Brazil	South America
076043	Brazil	South America
076044	Brazil	South America
076045	Brazil	South America
076046	Brazil	South America
076047	Brazil	South America
076048	Brazil	South America
076049	Brazil	South America
076050	Brazil	South America
076051	Brazil	South America
076052	Brazil	South America
076053	Brazil	South America

(continued)

<sup>3</sup> The generation method of the Comparable-geographic unit is shown in Fig. 7 in “World Atlas of Natural Disaster Risk—Understanding the spatial patterns of global natural disaster risk”

(continued)

Code	Country	Continent
850337	Brazil	South America
096056	Brunei	Asia
100057	Bulgaria	Europe
854338	Burkina Faso	Africa
108059	Burundi	Africa
116061	Cambodia	Asia
120062	Cameroon	Africa
124063	Canada	North America
124064	Canada	North America
124065	Canada	North America
124066	Canada	North America
124067	Canada	North America
124068	Canada	North America
124069	Canada	North America
124070	Canada	North America
124071	Canada	North America
124072	Canada	North America
124073	Canada	North America
124074	Canada	North America
124075	Canada	North America
124076	Canada	North America
124077	Canada	North America
124078	Canada	North America
132079	Cape Verde	Africa
136080	Cayman Islands	South America
140081	Central African Republic	Africa
148083	Chad	Africa
148084	Chad	Africa
152085	Chile	South America
156086	China	Asia
156087	China	Asia
156088	China	Asia
156089	China	Asia
156090	China	Asia
156091	China	Asia
156092	China	Asia
156093	China	Asia
156094	China	Asia
156095	China	Asia
156096	China	Asia
156097	China	Asia
156098	China	Asia
156099	China	Asia
156100	China	Asia

(continued)

(continued)

Code	Country	Continent
158101	China	Asia
170102	Colombia	South America
170103	Colombia	South America
174104	Comoros	Africa
188111	Costa Rica	South America
384169	Côte d'Ivoire	Africa
191112	Croatia	Europe
192113	Cuba	South America
620238	Cuba	South America
196114	Cyprus	Asia
203115	Czech Republic	Europe
180107	Democratic Republic of the Congo	Africa
180108	Democratic Republic of the Congo	Africa
180109	Democratic Republic of the Congo	Africa
180110	Democratic Republic of the Congo	Africa
208117	Denmark	Europe
262134	Djibouti	Africa
212118	Dominica	South America
214119	Dominican Republic	South America
626240	East Timor	Asia
218120	Ecuador	South America
818315	Egypt	Africa
818316	Egypt	Africa
818317	Egypt	Africa
222121	El Salvador	South America
226122	Equatorial Guinea	Africa
232125	Eritrea	Africa
233126	Estonia	Europe
231123	Ethiopia	Africa
231124	Ethiopia	Africa
234127	Faeroe Islands	Europe
238128	Falkland Islands (Malvinas)	South American
242129	Fiji	Oceania
246130	Finland	Europe
250131	France	Europe
254132	French Guiana	South America
258133	French Polynesia	Oceania
266135	Gabon	Africa
270137	Gambia	Africa
268136	Georgia	Asia
276138	Germany	Europe
288139	Ghana	Africa
292140	Gibraltar	Europe
300142	Greece	Europe

(continued)

(continued)

Code	Country	Continent
304143	Greenland	North America
308144	Grenada	South America
312145	Guadeloupe	Africa
316146	Guam	Oceania
320147	Guatemala	South America
324148	Guinea	Africa
624239	Guinea-Bissau	Africa
328149	Guyana	South America
332150	Haiti	South America
340151	Honduras	South America
348152	Hungary	Europe
352153	Iceland	Europe
356154	India	Asia
356155	India	Asia
356156	India	Asia
356157	India	Asia
356158	India	Asia
360159	Indonesia	Asia
360160	Indonesia	Asia
360161	Indonesia	Asia
364162	Iran	Africa
364163	Iran	Africa
364164	Iran	Africa
368165	Iraq	Asia
372166	Ireland	Europe
833319	Isle of Man	Europe
376167	Israel	Asia
380168	Italy	Europe
388170	Jamaica	South America
392171	Japan	Asia
400176	Jordan	Asia
398172	Kazakhstan	Asia
398173	Kazakhstan	Asia
398174	Kazakhstan	Asia
398175	Kazakhstan	Asia
404177	Kenya	Africa
296141	Kiribati	Oceania
414180	Kuwait	Asia
417181	Kyrgyzstan	Asia
418182	Laos	Asia
428185	Latvia	Europe
422183	Lebanon	Asia
426184	Lesotho	Africa
430186	Liberia	Africa

(continued)

(continued)

Code	Country	Continent
434187	Libya	Africa
434188	Libya	Africa
434189	Libya	Africa
440190	Lithuania	Europe
442191	Luxembourg	Europe
807314	Macedonia	Europe
450192	Madagascar	Africa
454193	Malawi	Africa
458194	Malaysia	Asia
462195	Maldives	Asia
466196	Mali	Africa
466197	Mali	Africa
470198	Malta	Europe
584228	Marshall Islands	Oceania
474199	Martinique	South America
478200	Mauritania	Africa
478201	Mauritania	Africa
480202	Mauritius	Africa
175105	Mayotte	Africa
484203	Mexico	North America
484204	Mexico	North America
484205	Mexico	North America
538217	Micronesia (Federated States of)	Asian
498209	Moldova	Europe
496206	Mongolia	Asia
496207	Mongolia	Asia
496208	Mongolia	Asia
504210	Morocco	Africa
508211	Mozambique	Africa
104058	Myanmar	Asia
516213	Namibia	Africa
524214	Nepal	Asia
528215	Netherlands	Europe
540218	New Caledonia	Oceania
554220	New Zealand	Oceania
558221	Nicaragua	South America
562222	Niger	Africa
562223	Niger	Africa
566224	Nigeria	Africa
408178	North Korea	Asia
580226	Northern Mariana Islands	Oceania
578225	Norway	Europe
512212	Oman	Asia
586230	Pakistan	Asia

(continued)

(continued)

Code	Country	Continent
585229	Palau	Oceania
591231	Panama	South America
598232	Papua New Guinea	Oceania
600233	Paraguay	South America
604234	Peru	South America
604235	Peru	South America
608236	Philippines	Asia
616237	Poland	Europe
630241	Puerto Rico	South America
634242	Qatar	Asia
178106	Republic of Congo	Africa
638243	Reunion	Africa
642244	Romania	Europe
643245	Russia	Asia
643246	Russia	Asia
643247	Russia	Asia
643248	Russia	Asia
643249	Russia	Asia
643250	Russia	Asia
643251	Russia	Asia
643252	Russia	Asia
643253	Russia	Asia
643254	Russia	Asia
643255	Russia	Asia
643256	Russia	Asia
643257	Russia	Asia
643258	Russia	Asia
643259	Russia	Asia
643260	Russia	Asia
643261	Russia	Asia
643262	Russia	Asia
643263	Russia	Asia
643264	Russia	Asia
643265	Russia	Asia
643266	Russia	Asia
643267	Russia	Asia
643268	Russia	Asia
643269	Russia	Asia
643270	Russia	Asia
643271	Russia	Asia
646272	Rwanda	Africa
706285	Rwanda	Africa
662273	Saint Lucia	North America
882342	Samoa	Oceania

(continued)

(continued)

Code	Country	Continent
674274	San Marino	Europe
678275	Sao Tome and Principe	Africa
682276	Saudi Arabia	Africa
682277	Saudi Arabia	Africa
682278	Saudi Arabia	Africa
686279	Senegal	Africa
690280	Seychelles	Africa
694281	Sierra Leone	Africa
702282	Singapore	Asia
703283	Slovakia	Europe
705284	Slovenia	Europe
090055	Solomon Islands	Oceania
710287	South Africa	Africa
710288	South Africa	Africa
410179	South Korea	Asia
724290	Spain	Europe
144082	Sri Lanka	Asia
729291	Sudan	Africa
729292	Sudan	Africa
729293	Sudan	Africa
729294	Sudan	Africa
740296	Suriname	South America
748297	Swaziland	Africa
752298	Sweden	Europe
756299	Switzerland	Europe
760300	Syria	Asia
762301	Tajikistan	Asia
834320	Tanzania	Africa
834321	Tanzania	Africa
764302	Thailand	Asia
768303	Togo	Africa
776304	Tonga	Oceania
780305	Trinidad and Tobago	South America
788307	Tunisia	Africa
792308	Turkey	Asia
795309	Turkmenistan	Asia
796310	Turks and Caicos Islands	South America
798311	Tuvalu	Oceania
800312	Uganda	Africa
804313	Ukraine	Europe
784306	United Arab Emirates	Asia
826318	United Kingdom	Europe
840322	United States	North America
840323	United States	North America

(continued)

(continued)

Code	Country	Continent
840324	United States	North America
840325	United States	North America
840326	United States	North America
840327	United States	North America
840328	United States	North America
840329	United States	North America
840330	United States	North America
840331	United States	North America
840332	United States	North America
840333	United States	North America
840334	United States	North America
840335	United States	North America

(continued)

(continued)

Code	Country	Continent
840336	United States	North America
858339	Uruguay	South America
860340	Uzbekistan	Asia
548219	Vanuatu	Oceania
862341	Venezuela	South America
706286	Vietnam	Asia
581227	Virgin Islands, U.S.	South America
732295	Western Sahara	Africa
887343	Yemen	Asia
891344	Yugoslavia	Europe
894345	Zambia	Africa
716289	Zimbabwe	Africa

---

## Appendix III

### Data Source and Database for *World Atlas of Natural Disaster Risk*<sup>4</sup>

---

<sup>4</sup> *Note* There are four kinds of data sources: A refers to free data of open access, B refers to data quoted from other documents, C refers to purchased data, and D refers to data provided from cooperation institutions

No.	Name	Data description	Period	Resolution/scale	Data access	Data sources	Data usage
<i>Basic data</i>							
1.1	Base map	Continent boundaries, national boundaries, coastlines, rivers, and lakes	2014	1:150,000,000; 1:200,000,000	D	Star Map Press, Beijing, China	All of the maps
<i>Environments data</i>							
2.1	Global digital elevation model (DEM)	GTOPO30 is a global digital elevation model (DEM) resulting from a collaborative effort led by the staff at the U.S. Geological Survey's EROS Data Center in Sioux Falls, South Dakota. Elevations in GTOPO30 are regularly spaced at 30-arc s (approximately 1 km)	1997	1 km × 1 km	A	United States Geological Survey (USGS) <a href="ftp://edcftp.cr.usgs.gov">ftp://edcftp.cr.usgs.gov</a>	Environments and exposures, landslide, flood, tropical cyclone, drought, and grassland wildfire
2.2	Distribution of terrain slopes	The global terrain slope and aspect database has been compiled using elevation data from the Shuttle Radar Topography Mission (SRTM). The SRTM data are publicly available as 3 arc-s (approximately 90 m resolution at the equator) DEMs (CGIAR-CSI 2006). The SRTM data cover the globe for areas up to 60° latitude. For the areas north of 60° latitude, 30 arc-s elevation data and derived slope class information were compiled from GTOPO30 (USGS-GTOPO30 2002)	2002, 2006	10 km × 10 km	A	International Institute for Applied Systems Analysis-Global Agro-ecological Zones (GAEZ) <a href="http://www.gaez.iiasa.ac.at">http://www.gaez.iiasa.ac.at</a>	Environments and exposures, landslide, storm surge, and drought
2.3	Global lithological map database v1.0	The lithological classification consists of three levels: the first level contains 16 lithological classes, and the additional two levels contain 12 and 14 subclasses	2012	0.5° × 0.5°	B	<a href="http://doi.pangaea.de">http://doi.pangaea.de</a>	Environments and exposures
2.4	Global geological map (third edition)	Geological map including data on fault distribution shows the distribution of the main chronostratigraphic units and the main structural features that make up the mosaic of the present-day surface of our planet	2010	1: 25,000,000	C	Commission for the Geological Map of the World (CGMW) <a href="http://cgmw.org">http://cgmw.org</a>	Environments and exposures, landslide
2.5	World land system (version 1.1)	Soil data, climate zones data, livestock density data, and land use system data	2010	10 km × 10 km	A	Food and Agriculture Organization (FAO) <a href="http://www.fao.org/geonetwork/srv/en">http://www.fao.org/geonetwork/srv/en</a>	Environments and exposures
2.6	Global land cover characteristics data (version 2)	Global land cover types with USGS land use/land cover classification system, such as urban and built-up land, grassland, water bodies, snow or ice, et al.	2000	1 km × 1 km	A	USGS <a href="http://edc2.usgs.gov">http://edc2.usgs.gov</a>	Tropical cyclone
2.7	Global soil physicochemical property data	Global soil physico-chemical property data, such as bulk density, electrical conductivity, PH, total nitrogen, content of coarse fragments	2012	1 km × 1 km	A	International Soil Reference and Information Centre (ISRIC) <a href="http://www.isric.org">http://www.isric.org</a>	Drought
2.8	MODIS land cover classification map	The MODIS land cover products describe the geographic distribution of the 17 IGBP land cover types based on an annual time series of observations	2012	5.6 km × 5.6 km	A	USGS <a href="https://lpdaac.usgs.gov">https://lpdaac.usgs.gov</a>	Landslide
2.9	Circum-Arctic map of permafrost and ground-ice conditions	The data set includes continuous, discontinuous, sporadic, or isolated permafrost	1997	–	A	National Snow and Ice Data Center (NSIDC), USA <a href="http://nsidc.org">http://nsidc.org</a>	Environments and exposures; sand-dust storm

(continued)

No.	Name	Data description	Period	Resolution/scale	Data access	Data sources	Data usage
2.10	Global river network	The world is divided into eight parts. This data adopts Strahler river classification system: there are seven classes of all river streams	2010	–	A	FAO <a href="http://www.fao.org/geonetwork/srv/en">http://www.fao.org/geonetwork/srv/en</a>	Environments and exposures, flood
2.11	Global watersheds	Watersheds	2006	–	A	FAO <a href="http://www.fao.org/geonetwork/srv/en">http://www.fao.org/geonetwork/srv/en</a>	Flood
2.12	Global coastal typology	The coastal typology is divided into eight types	2011	0.5° × 0.5°	A	<a href="http://geotypes.net">http://geotypes.net</a>	Storm surge
2.13	Global aridity index	The Global-Aridity is modeled using the data available from the WorldClim Global Climate Data (Hijmans et al. 2005) as input parameters (including precipitation, mean, minimum, and maximum temperature)	1950–2000	1 km × 1 km	A	CGIAR Consortium for Spatial Information (CGIAR-CSI) <a href="http://www.cgiar.org">http://www.cgiar.org</a>	Sand-dust storm
2.14	Global surface reflectance products	MODIS 8-day gridded level-3 surface reflectance product	2000–2010	500 m × 500 m	A	National Aeronautics and Space Administration (NASA) <a href="https://wist.echo.nasa.gov">https://wist.echo.nasa.gov</a>	Grassland wildfire
<i>Exposures data</i>							
3.1	World population density data	Global population density calculated using an innovative approach with Geographic Information System and Remote Sensing	2010	1 km × 1 km	C	Oak Ridge National Laboratory (ORNL) <a href="http://web.ornl.gov/sci/landscan/">http://web.ornl.gov/sci/landscan/</a>	Earthquake, volcano, landslide, flood, storm surge, tropical cyclone, sand-dust storm, heat wave, and cold wave
3.2	Total population	Total population is based on the de facto definition of population, which counts all residents regardless of legal status or citizenship—except for refugees not permanently settled in the country of asylum, who are generally considered part of the population of their country of origin	1960–2012	National level	A	World Bank <a href="http://data.worldbank.org">http://data.worldbank.org</a>	Flood
3.3	GDP (at market exchange rate)	GGI (Greenhouse Gas Initiative) scenario database	2010	0.5° × 0.5°	A	Greenhouse Gas Initiative (GGI) Program of the International Institute for Applied Systems Analysis (IIASA) <a href="http://www.iiasa.ac.at">http://www.iiasa.ac.at</a>	Flood and sand-dust storm
3.4	An estimate of gross domestic product (GDP) Derived from satellite data	A model has been developed for creating a disaggregated map of estimated total (formal plus informal) economic activity for countries and states of the world	2006	1 km × 1 km	A	NOAA, National Geophysical Data Center (NGDC) <a href="http://ngdc.noaa.gov">http://ngdc.noaa.gov</a>	Storm surge
3.5	GDP of countries	GDP at purchaser's price are in current U.S. dollars. Dollar figures for GDP are converted from domestic currencies using single-year official exchange rates	2010	National level	A	World bank <a href="http://data.worldbank.org">http://data.worldbank.org</a>	Earthquake and flood
3.6	Building construction vulnerability and inventory	Experts in a number of countries provided estimates of the vulnerability of major construction types in their countries, as well as rough estimates of inventory and occupancy	2007	National level	A	World Housing Encyclopedia (WHE) project <a href="http://www.world-housing.net">http://www.world-housing.net</a>	Earthquake

(continued)

(continued)	No.	Name	Data description	Period	Resolution/scale	Data access	Data sources	Data usage
	3.7	Probability of casualties due to collapse of buildings	The PAGER fatality estimates are mainly deduced from modeling the collapse fragilities of different structure types. Eight types of common buildings including Adobe buildings, Mud wall buildings, Nonductile concrete moment frame, Precast framed buildings, Block or dressed stone masonry, Rubble or field stone masonry, Brick masonry with lime/cement mortar, and Steel moment frame with concrete infill wall are considered. The fatality ratios caused by collapse of these eight types of buildings are 0.06, 0.06, 0.15, 0.10, 0.08, 0.06, 0.06, and 0.14, respectively	2009	-	B	Earthquake Casualty Models within the USGS Prompt Assessment of Global Earthquakes for Response (PAGER) System (Jaiswal et al. 2009)	Earthquake
	3.8	Investment ratio	Investment ratio (% of GDP) data are based on individual countries' national accounts statistics	2010	National level	A	Economy Watch <a href="http://www.economywatch.com">http://www.economywatch.com</a>	Earthquake
	3.9	Urbanization rate	Percentage of the urban population accounted for total population	2010	National level	A	World Bank <a href="http://databank.worldbank.org">http://databank.worldbank.org</a>	Earthquake
	3.10	Live animals	Stocks of live animals are given in Heads except for: poultry/birds/rabbits in 1,000 heads and beehives in number. Aggregates are the sum of available data	2011	National level	A	FAO <a href="http://faostat.fao.org.sixxs.org">http://faostat.fao.org.sixxs.org</a>	Sand-dust storm
	3.11	Night lights 2012—flat map	This new image of the Earth at night is a composite assembled from data acquired by the Suomi National Polar-orbiting Partnership (Suomi NPP) satellite over 9 days in April 2012 and 13 days in October 2012	2012	1 km × 1 km	A	NASA <a href="http://www.earthobservatory.nasa.gov">http://www.earthobservatory.nasa.gov</a>	Environments and exposures
	3.12	Global land use data	The Land Cover Type Yearly Climate Modeling Grid (CMG) is a lower spatial resolution (0.05°) product, which provides the dominant land cover type and also the sub-grid frequency distribution of land cover classes. The CMG product (Short name: MCD12C1) is derived using the same algorithm that produces the Y051 Global 500 m Land Cover Type product (MCD12Q1).	2012	0.05° × 0.05°	A	USGS <a href="https://pdaac.usgs.gov">https://pdaac.usgs.gov</a>	Flood
	3.13	Crop calendar dataset	Gridded maps of planting dates, harvesting dates, etc., for 19 crops. These maps are available at two different resolutions (5 min and 0.5°), and in two different formats	2010	0.5° × 0.5°	A	University of Wisconsin-Madison Sustainability and the Global Environment (SAGE) <a href="http://www.sage.wisc.edu">http://www.sage.wisc.edu</a>	Drought
	3.14	Planting area data	The data are provided in NetCDF and ArcGIS ASCII format at 5-min resolution in latitude by longitude	2008	1 km × 1 km	A	Land Use and the Global Environment (LUGE) <a href="http://www.luge.geog.mcgill.ca">http://www.luge.geog.mcgill.ca</a>	Drought
	3.15	Irrigation data	The irrigation water withdrawal of each year	2010	0.5° × 0.5°	A	The University of Tokyo (OKI Laboratory) <a href="http://hydro.iis.u-tokyo.ac.jp">http://hydro.iis.u-tokyo.ac.jp</a>	Drought
	3.16	Fertilizer data	Global Fertilizer and Manure, Version 1: Nitrogen Fertilizer Application	2011	0.5° × 0.5°	A	NASA <a href="http://dx.doi.org/10.7927/H4Q81B0R">http://dx.doi.org/10.7927/H4Q81B0R</a>	Drought

(continued)

No.	Name	Data description	Period	Resolution/scale	Data access	Data sources	Data usage
3.17	Yield data	Most crops (including maize, wheat, rice) yield data that come from FAO national unit, USA, China, India, and Australia using the data of provincial (state) level	2000–2004	National or provincial (state) level	A	FAO <a href="http://faostat.fao.org">http://faostat.fao.org</a> Chinese Ministry of Agriculture (CMA) <a href="http://lzys.agri.gov.cn">http://lzys.agri.gov.cn</a> United States Department of Agriculture (USDA) <a href="http://quickstats.nass.usda.gov">http://quickstats.nass.usda.gov</a> Australian Bureau of Statistics (ABS) <a href="http://www.abs.gov.au">http://www.abs.gov.au</a> Directorate of Economics and Statistics (DES) <a href="http://eands.dacnet.nic.in">http://eands.dacnet.nic.in</a>	Drought
3.18	Crop parameter data	The default parameter to describe the attributes of the crop, which is provided by Texas A&M Agriculture and Life Sciences	–	–	A	Texas A&M University (A&M) <a href="http://www.tamu.edu">http://www.tamu.edu</a>	Drought
3.19	Land cover type product	The MODIS land cover type product provides data characterizing five global land cover classification systems. In addition, it also provides a land cover type assessment, and quality control information	2005	500 m × 500 m	A	USGS <a href="https://pdaac.usgs.gov">https://pdaac.usgs.gov</a>	Forest wildfire and grassland wildfire
3.20	Net primary production	This FTP fold contains MODIS 8-day GPP, PsnNet, monthly GPP, PsnNet (MOD17A2), and annual GPP and NPP (MOD17A3)	2001–2012	1 km × 1 km	A	Numerical Terradynamic Simulation Group (NTSG), University of Montana <a href="http://www.netsg.umt.edu">http://www.netsg.umt.edu</a>	Environments and exposures, grassland wildfire
<i>Hazards data</i>							
4.1	Peak ground acceleration (PGA)	The GSHAP Global Seismic Hazard Map depicts the global seismic hazard as Peak Ground Acceleration (PGA) with grid format with a 10 % chance of exceedance in 50 years, corresponding to a return period of 475 years	1999	0.1° × 0.1°	A	Global Seismic Hazard Assessment Program (GSHAP) <a href="http://www.seismo.ethz.ch">http://www.seismo.ethz.ch</a>	Earthquake and landslide
4.2	Global volcanism program—volcanoes of the world	<i>Volcanoes of the World</i> is a database describing the physical characteristics (primary volcano type, last eruption year, minor rock, etc.) of Holocene volcanoes and their eruptions	9950 B.C.–2012 A.D.	–	A	Smithsonian Institution National Museum of Natural History, Global Volcanism Program <a href="http://www.volcano.si.edu">http://www.volcano.si.edu</a>	Volcano
4.3	Large magnitude explosive volcanic eruptions	Historical large magnitude explosive volcanic eruptions, including volcano type, eruption date, tephra fall deposit volume, maximum column height, VEI, and data quality	9490 B.C.–2010 A.D.	–	A	British Geological Survey/VOGRIPA (Volcanic Global Risk Identification and Analysis Project) <a href="http://www.bgs.ac.uk/vogrpa">http://www.bgs.ac.uk/vogrpa</a>	Volcano
4.4	TRMM-based precipitation estimates	TRMM 3B42 has a spatial resolution of 0.25° and a temporal resolution of 3 h. It covers between 30°S and 50°N.	1998.1.1–2012.12.31	0.25° × 0.25°	A	NASA/Goddard Space Flight Center Tropical Rainfall Measuring Mission (TRMM) <a href="http://trmm.gsfc.nasa.gov">http://trmm.gsfc.nasa.gov</a>	Landslide

(continued)

No.	Name	Data description	Period	Resolution/scale	Data access	Data sources	Data usage
4.5	NCEP/NCAR reanalysis precipitation data	NCEP/NCAR Reanalysis has a spatial resolution of 2.5° and a temporal resolution of 6 h. It covers between 90°S and 90°N. This dataset is used as ancillary data for continents beyond 50°S and 50°N to make up for the TRMM 3B42 data	1998.1.1–2012.12.31	2.5° × 2.5°	A	The Weather Prediction Center (WPC) NCEP <a href="http://www.esrl.noaa.gov">http://www.esrl.noaa.gov</a>	Landslide
4.6	Global flood inundation extent	The data are available as a raster GIS layer of horizontal flood extents for return periods up to 100 years	Point Data	2.5' × 2.5'	A	UNEP/UNISDR PREVIEW Global Risk Data Platform <a href="http://preview.grid.unep.ch">http://preview.grid.unep.ch</a>	Flood
4.7	Global daily precipitation data	Precipitation estimates on a 1° grid over the entire globe at 1-day (daily) for the period October 1996–present	1996–2012	1° × 1°	A	NASA Goddard Space Flight Center <a href="ftp://rsd.gsfc.nasa.gov">ftp://rsd.gsfc.nasa.gov</a> <a href="http://precip.gsfc.nasa.gov">http://precip.gsfc.nasa.gov</a>	Flood
4.8	Global monthly river discharge	Monthly averaged discharge measurements for 1,018 stations located throughout the world. The period of record varies widely from station to station with a mean of 21.5 years	1807–1991	–	A	ORNL Distributed Active Archive Center <a href="http://daac.ornl.gov">http://daac.ornl.gov</a>	Flood
4.9	Global hourly sea level data	The dataset contains 596 stations along the seaside of the world, monitoring sea level data hourly. The longest period is from 1846 to 2009, while the shortest period is 1 year	Different time scales	Point data	A	The University of Hawaii Sea Level Center <a href="http://hikai.soest.hawaii.edu">http://hikai.soest.hawaii.edu</a>	Storm surge
4.10	CMA best-track dataset	Ocean: Northwestern Pacific; main parameters include: tropical cyclone ID, name, time (year, month, date, and hour), location (longitude, latitude), central minimum pressure (hPa), maximum wind speed, and radius of the maximum wind speed	2013	6 h	A	CMA <a href="http://cdata.typhoon.gov.cn">http://cdata.typhoon.gov.cn</a>	Tropical cyclone
4.11	HURDAT V2 (The North Atlantic Hurricane Database)	Ocean: Northwestern Pacific, Central Pacific, North Atlantic; main parameters include: tropical cyclone ID, name, time (year, month, date and hour), location (longitude, latitude), central minimum pressure, maximum wind speed, and radius of the maximum wind speed, etc.	2013	6 h	A	NOAA <a href="http://www.aoml.noaa.gov">http://www.aoml.noaa.gov</a>	Tropical cyclone
4.12	IBTrACSS	Global; main parameters include: tropical cyclone ID, name, time (year, month, date, and hour), location (longitude, latitude), central minimum pressure, maximum wind speed, and radius of the maximum wind speed	2013	6 h	A	NOAA <a href="http://www.ncdc.noaa.gov">http://www.ncdc.noaa.gov</a>	Tropical cyclone
4.13	Global surface synoptic timing dataset	Each record has 65 elements. The main elements include station ID, latitude (0.01°), longitude (0.01°), station height (0.1 m), station type, temperature (0.1 °C), precipitation (0.1 mm), visibility (m), special weather phenomena, etc.	1982–2011	Point data	A	CMA <a href="http://cdc.cma.gov.cn/home.do">http://cdc.cma.gov.cn/home.do</a>	Sand-dust storm
4.14	Global 6 h temperature	The raster data provide the global 6 h temperature data which are at 0:00, 06:00, 12:00, and 18:00 h	1979–2013	0.75 * 0.75	A	European Centre for Medium-Range Weather Forecasts (ECMWF) <a href="http://data-portal.ecmwf.int">http://data-portal.ecmwf.int</a>	Heat wave and cold wave

(continued)

(continued)

No.	Name	Data description	Period	Resolution/scale	Data access	Data sources	Data usage
4.15	Global meteorological data	Daily precipitation, temperature, solar radiation, and other information in different regions of the world	1971–2099	0.5° × 0.5°	D	German Federal Ministry of Education and Research (BMBWF)-The ISIMIP Fast Track project	Drought
4.16	Global monthly fire location product (MCD14ML)	The monthly fire location product contains the geographic location, date, and some additional information for each fire pixel detected by the Terra and Aqua MODIS sensors on a monthly basis	2000–2010	Point data	A	University of Maryland (UMD) <a href="http://fioco.geog.umd.edu">http://fioco.geog.umd.edu</a>	Forest wildfire
4.17	Global active fire product (MOD14A2)	MODIS 8-day gridded level-3 summary active fire product	2000–2010	1 km × 1 km	A	NASA <a href="https://wist.echo.nasa.gov">https://wist.echo.nasa.gov</a>	Grassland wildfire
<i>Disasters data</i>							
5.1	Significant volcanic eruption database	Latitude, longitude, elevation, eruption date, VEI, volcano effects (death number, injures number, damage houses, etc.)	4360 B.C.–2012 A.D.	–	A	NOAA <a href="http://www.ngdc.noaa.gov">http://www.ngdc.noaa.gov</a>	Volcano
5.2	Global landslide inventory	Landslide catalog for rainfall triggered events for several years, drawing upon news reports, scholarly articles, and other hazard databases to provide a landslide catalog at the global scale	2003, 2007–2011	Point data	A	NASA and Columbia University <a href="http://trmm.gsfc.nasa.gov">http://trmm.gsfc.nasa.gov</a>	Landslide
5.3	World large flood events inventory	The listing is comprehensive and global in scope. Deaths and damage estimates for tropical storms are totals from all causes, but tropical storms without significant river flooding are not included	1985–2013	–	A	Dartmouth Flood Observatory (DFO) <a href="http://floodobservatory.colorado.edu">http://floodobservatory.colorado.edu</a>	Flood
5.4	The international disaster database (EM-DAT)	EM-DAT contains essential core data on the occurrence and effects of over 18,000 mass disasters in the world from 1900 to present. It includes geographical, temporal, human, and economic information on disasters at the country level	1900–2013	–	A	Emergency Events Database, EM-DAT (EM-DAT) of the Centre for Research on the Epidemiology of Disasters (CRED) <a href="http://www.emdat.be/database">http://www.emdat.be/database</a>	Flood, storm surge, tropical cyclone, heat wave, and cold wave
5.5	Tracks of the past 150 years of tropical cyclones	The tracks of the past 150 years of tropical cyclones weave across the globe	2006	–	A	NASA <a href="http://earthobservatory.nasa.gov">http://earthobservatory.nasa.gov</a>	Storm surge
5.6	Tropical cyclones surges 1975–2007	This dataset includes a compilation of estimated storm surges triggered by tropical cyclones 1975–2007, which contains information about the place, time, population effected, GDP effected, et al.	1975–2007	Point data	A	Global Risk Data Platform (GRDP) <a href="http://preview.grid.unep.ch">http://preview.grid.unep.ch</a>	Storm surge
5.7	Global IDEntifier number	The cold wave disaster database, includes occurrence time, place, casualty, affected population, etc.	2000.1–2004.5	National level	A	Global IDEntifier Number <a href="http://www.gldentifier.net">http://www.gldentifier.net</a> Asian Disaster Reduction Centre (ADRC)	Cold wave
5.8	Global monthly burned area product	The MCD45A1 Burned Area Product is a monthly Level 3 product containing per-pixel burning and quality information, and tile-level metadata	2000–2012	500 m × 500 m	A	NASA <a href="https://wist.echo.nasa.gov">https://wist.echo.nasa.gov</a>	Forest wildfire

## Further Readings

- Boschetti, L., D. Roy and A.A. Hoffmann. 2009. MODIS Collection 5 Burned Area Product-MCD45. User's Guide. Ver 2.0.
- Brakenridge, G.R. 2013. Global active archive of large flood events 1985–2012. Dartmouth Flood Observatory, University of Colorado. <http://floodobservatory.colorado.edu/Archives/index.html>. Accessed in July 2013.
- Bright, E.A., P.R. Coleman, A.N. Rose, et al. 2011. *LandScan 2010*. Oak Ridge National Laboratory: Oak Ridge, TN.
- Brown, J., O.J. Ferrians, J.A. Heginbottom, et al. 1998. Revised February 2001. *Circum-arctic map of permafrost and ground ice conditions*. Boulder, CO: National Snow and Ice Data Center. Digital media.
- Commission for the Geological Map of the World (CGMW). 2010. World tectonic map, lithological map of the world. <http://ccgm.org/en/>. Accessed in May 2013.
- Dürr, H.H., G.G. Laruelle, C.M. van Kempen, et al. 2011. Worldwide typology of nearshore coastal systems: Defining the estuarine filter of river inputs to the Oceans. *Estuaries and Coasts* 34(3): 441–458.
- Earth Resources Observation and Science (EROS) Data Center, U.S. Geological Survey. 1997. Global digital elevation model (DEM) 1996. Sioux Falls, South Dakota. <ftp://edcftp.cr.usgs.gov/data/gtopo30/global/>. Accessed in July 2013.
- European Center for Medium-Range Weather Forecasts (ECMWF). 2014. ERA Interim data (1979–2014). [http://data-portal.ecmwf.int/data/d/interim\\_full\\_daily/](http://data-portal.ecmwf.int/data/d/interim_full_daily/). Accessed in April 2014.
- Giglio, L. 2010. MODIS Collection 5 Active Fire Product User's Guide Version 2.4. University of Maryland: College Park, MD.
- GLIDENumber. 2014. Cold wave disaster database (2004–2014). <http://www.glidenumber.net/glide/public/search/search.jsp>. Accessed in April 2014.
- Global Risk Data Platform (GRDP). 2009. Tropical cyclones surges 1975–2007. <http://preview.grid.unep.ch/index.php?preview=data&events=surges&lang=eng>. Accessed in July 2013.
- Goddard Earth Sciences (GES) Data and information services center (DISC), NASA. 2013. TRMM 3B42. <http://trmm.gsfc.nasa.gov>. Accessed in July 2013.
- Grübler, A., B. O'Neill, K. Riahi, et al. 2007. Regional, national, and spatially explicit scenarios of demographic and economic change based on SRES. *Technological Forecasting and Social Change* 74(7): 980–1029.
- Hartmann, J., and N. Moosdorf. 2012. The new global lithological map database GLiM: A representation of rock properties at the earth surface. *Geochemistry, Geophysics, Geosystems* 13: Q12004. doi:10.1029/2012GC004370.
- Herold, C., and F. Mouton. 2011. Global flood hazard mapping using statistical peak flow estimates. *Hydrology and Earth System Sciences* 8(1): 305–363.
- Huffman, G.J., R.F. Adler, M.M. Morrissey, et al. 2001. Global precipitation at one-degree daily resolution from multi-satellite observations. *Journal of Hydrometeorology* 2: 36–50.
- IIASA/FAO. 2012. Global agro-ecological zones (GAEZ v3.0). IIASA, Laxenburg, Austria and FAO, Rome, Italy.
- Jaiswal, K.S., D.J. Wald, P.S. Earle, et al. 2009. Earthquake casualty models within the USGS prompt assessment of global earthquakes for response (PAGER) system. In *Second international workshop on disaster casualties*. Cambridge: University of Cambridge.
- Jenness, J., J. Dooley, J. Aguilar-Manjarrez, et al. 2007a. *African water resource database. GIS-based tools for inland aquatic resource management. 1. Concepts and application case studies*. CIFA Technical Paper. No.33, Part 1. Food and Agriculture Organization of the United Nations. Rome.
- Jenness, J., J. Dooley, J. Aguilar-Manjarrez, et al. 2007b. *African water resource database. GIS-based tools for inland aquatic resource management. 2. Technical manual and workbook*. CIFA Technical Paper. No. 33, Part 2. Food and Agriculture Organization of the United Nations. Rome.
- Kalnay, E., M. Kanamitsu, R. Kistler, et al. 1996. The NCEP/NCAR 40-year reanalysis project. *Bulletin of the American Meteorological Society* 77(3): 437–471.
- Kirschbaum, D.B., R. Adler, Y. Hong, et al. 2010. A global landslide catalog for hazard applications: Method, results, and limitations. *Natural Hazards* 52(3): 561–575.
- Knapp, K.R., M.C. Kruk, D.H. Levinson, et al. 2010. The international best track archive for climate stewardship (IBTrACS): Unifying tropical cyclone best track data. *Bulletin of the American Meteorological Society* 91: 363–376.
- Land Processes Distributed Active Archive Center (LP DAAC), USGS. 2010. Surface Reflectance 8-Day L3 Global 500 m (MOD09A1). USGS/Earth Resources Observation and Science (EROS) Center, Sioux Falls, South Dakota.

- Land Processes Distributed Active Archive Center (LP DAAC), USGS. 2013. Land Cover Type Yearly L3 Global 0.05Deg (MCD12Q1) 2001–2012. USGS/Earth Resources Observation and Science (EROS) Center, Sioux Falls, South Dakota.
- Landsea, C.W., and J.L. Franklin. 2013. Atlantic hurricane database uncertainty and presentation of a new database format. *Monthly Weather Review* 141: 3576–3592.
- Loveland, T.R., B.C. Reed, J.F. Brown, et al. 2000. Development of a global land cover characteristics database and IGBP DIS cover from 1-km AVHRR Data. *International Journal of Remote Sensing* 21(6/7): 1303–1330.
- Ming, Y., W. Zhang, H. Yu, et al. 2014. An overview of the China meteorological administration tropical cyclone database. *Journal of Atmospheric and Oceanic Technology* 31(2): 287–301.
- Monfreda, C., N. Ramankutty and J.A. Foley. 2008. Farming the planet: 2. Geographic distribution of crop areas, yields, physiological types, and net primary production in the year 2000, *Global Biogeochemical Cycles* 22(GB1022). doi:10.1029/2007GB002947.
- National Aeronautics and Space Administration (NASA). 2006. Tracks of the past 150 years of tropical cyclones. <http://earthobservatory.nasa.gov/IOTD/view.php?id=7079>. Accessed in July 2013.
- National Oceanic and Atmospheric Administration (NOAA). 2011. An estimate of gross domestic product (GDP) derived from satellite data. [http://ngdc.noaa.gov/eog/dmsp/download\\_gdp.html](http://ngdc.noaa.gov/eog/dmsp/download_gdp.html). Accessed in April 2013.
- Potter, P., N. Ramankutty, E.M. Bennett, and S.D. Donner. 2011. Global fertilizer and manure, version 1: Nitrogen in manure production. Palisades, NY: NASA Socioeconomic Data and Applications Center (SEDAC). <http://dx.doi.org/10.7927/H4KH0K81>. Accessed in April 2014.
- Sacks, W.J., D. Deryng, J.A. Foley, et al. 2010. Crop planting dates: An analysis of global patterns. *Global Ecology and Biogeography* 19: 607–620.
- Smithsonian Institution. 2013. Global volcanism program (GVP). Volcanoes of the world. [http://volcano.si.edu/search\\_volcano\\_results.cfm](http://volcano.si.edu/search_volcano_results.cfm). Accessed in July 2013.
- The University of Tokyo. 2010. Annual water withdrawal (1995, 2050). <http://hydro.iis.u-tokyo.ac.jp/GW/result/global/annual/withdrawal/index.html>. Accessed in May 2013.
- Trabucco, A. and R.J. Zomer. 2009. Global aridity index (Global-Aridity) and global potential evapo-transpiration (Global-PET) geospatial database. CGIAR Consortium for Spatial Information. Published online, available from the CGIAR-CSI GeoPortal. <http://www.csi.cgiar.org>. Accessed in May 2013.
- U.S. Geol. Survery. 1996. Global 30-Arc Second Elevation Data Set. Eris Data Center, Dept. Interior, Sioux Falls, SD.
- University of Hawaii Sea Level Center. 2013. Global hourly sea level data. <http://ilikai.soest.hawaii.edu>. Accessed in July 2013.
- Vorosmarty, C.J., B.M. Fekete and B.A. Tucker. 1998. Global river discharge, 1807–1991, V1.1 (RivDIS). Oak Ridge National Laboratory Distributed Active Archive Center, Oak Ridge, Tennessee, U.S.A. <http://www.daac.ornl.gov>. Accessed in May 2013.
- World Bank. 2013. Total population (1980–2013). <http://data.worldbank.org/indicator/SP.POP.TOTL>. Accessed in September 2013.

## Appendix IV Validation

### Validation for Major Natural Disaster Risk

Risk type	Validation data	Sample size	Validation results
Earthquake mortality risk	The earthquake mortality risk ranking for each country was derived from 2009 Global Risk Assessment Report and used as reference for validation	84	The Spearman rank correlation coefficient is 0.731, significant at $p < 0.01$ level (two-tailed)
Earthquake economic-social wealth loss risk	The earthquake economic loss data for each country was derived from EM-DAT historical earthquake event records from 1900 to 2012 and used as reference for validation	58	The Pearson correlation coefficient is 0.834, significant at $p < 0.01$ level (two-tailed)
Volcano mortality risk	The ranks of volcano mortality risk for each country derived from <i>Natural Disaster Hotspots: A Global Risk Analysis</i>	30	The Spearman rank correlation coefficient is 0.763, significant at $p < 0.01$ level (two-tailed)
Landslide mortality risk	Country level: Country level landslide hazard index is calculated using global landslide hotspot program based from Norwegian Geotechnical Institute's work (Nadim et al. 2006)	76	The Spearman rank correlation coefficient is 0.847, significant at $p < 0.01$ level
Flood economic loss and mortality risk	Country level: The flood economic loss and motility data for each country were derived from EM-DAT historical flood event records from 1900 to 2012 and used as reference for validation	100	The Spearman rank correlation coefficients for economic loss and motility risk are 0.706 and 0.836 respectively, significant at $p < 0.01$ level (two-tailed)
	Watershed level: The flood economic loss and motility data for each watershed were derived from the global large flood events archive of DFO and used as reference for validation	106	The Spearman rank correlation coefficients for economic loss and motility risk are 0.813 and 0.786 respectively, significant at $p < 0.01$ level (two-tailed)
Affected population/GDP risk of flood	Grid level: The global natural disaster risk hotspots report published by the World Bank was used as reference and the correlation between flood risk grade in this study and the results of the World Bank's report were analyzed	All grids	The Pearson correlation coefficients for affected economy and population risk are 0.614 and 0.564 respectively, significant at $p < 0.01$ level (two-tailed)

(continued)

(continued)

Risk type	Validation data	Sample size	Validation results
Affected population/GDP risk of storm surge	Dataset includes a compilation of estimated storm surges triggered by tropical cyclones from 1975 to 2007 provided by GRDP	57	The Spearman rank correlation coefficients for inundated area, affected population and affected GDP are 0.72, 0.47, and 0.57, respectively, significant at $p < 0.01$ level (two-tailed)
Affected population/GDP risk of sand-dust storm	Based on sand and dust storm frequency supplied by provincial newspapers database of China, correlation analysis of expected annual kinetic energy of sand and dust storm and the frequency was made	254	The Pearson correlation analysis shows that the dependency is observable, with correlation coefficient of 0.471, significant at $p < 0.01$ level (two-tailed)
Heat wave mortality risk	The heat wave mortality data for each country was derived from EM-DAT historical heat wave event records from 1900 to 2013	48	The Spearman rank correlation coefficient is 0.462, significant at $p < 0.01$ level (two-tailed)
Affected population risk of cold wave	Cold wave loss data of frequency, affected population, and mortality etc. from the Global IDentifier Number database	49	The spearman correlation coefficient is 0.602, significant at $p < 0.01$ level (two-tailed)
Maize yield loss risk of drought	The crop yield loss rate of provinces in China derived from statistical data of slightly, moderately, and severely damaged areas caused by drought disasters and sowing area from 1997 to 2005	22	The Pearson correlation coefficient for 100a return period loss is 0.62, significant at $p < 0.01$ level (two-tailed)
Wheat yield loss risk of drought		22	The Pearson correlation coefficient for 100a return period loss is 0.55, significant at $p < 0.01$ level (two-tailed)
Rice yield loss risk of drought		20	The Pearson correlation coefficient for 100a return period loss is 0.60, significant at $p < 0.01$ level (two-tailed)
Burned forest area risk	The Global Risk Data Platform built by UNEP and UNISDR provides a density of fires dataset, including an estimation of the density of fires over the period from 1997 to 2010	100	The Spearman rank correlation coefficient for is 0.767, significant at $p < 0.01$ level (two-tailed)
Grassland NPP loss risk	Grid level: Evaluation of wildfire propagation susceptibility in grasslands using burned areas and multivariate logistic regression (Cao et al. 2013)	194	Based on the reviewer reports

## Validation for Multi-hazard Risk

Risk type	Validation data	Sample size	Validation results
Expected annual mortality and affected population risk rank by TRI (country)	The rank of total affected population and property damage data for each country was derived from EM-DAT historical natural disaster event records from 1951 to 2013.	177	The Spearman rank correlation coefficient is 0.662, significant at $p < 0.01$ level (two-tailed)
Expected annual affected population risk rank by MhRI (country)		177	The Spearman rank correlation coefficient is 0.744, significant at $p < 0.01$ level (two-tailed)
Expected annual loss and affected property risk rank by TRI (country)		165	The Spearman rank correlation coefficient is 0.596, significant at $p < 0.01$ level (two-tailed)
Expected annual affected property risk rank by MRI (country)		165	The Spearman rank correlation coefficient is 0.740, significant at $p < 0.01$ level (two-tailed)
Expected annual mortality and affected population risk rank by TRI (country)	Expected annual affected population risk rank by MhRI (country)	197	The Spearman rank correlation coefficient is 0.852, significant at $p < 0.01$ level (two-tailed)
Expected annual mortality and affected population risk rank by TRI (per unit area)	Expected annual affected population risk rank by MhRI (per unit area)	197	The Spearman rank correlation coefficient is 0.672, significant at $p < 0.01$ level (two-tailed)
Expected annual loss and affected property risk rank by TRI (country)	Expected annual affected property risk rank by MhRI (country)	196	The Spearman rank correlation coefficient is 0.843, significant at $p < 0.01$ level (two-tailed)
Expected annual loss and affected property risk rank by TRI (per unit area)	Expected annual affected property risk rank by MhRI (per unit area)	196	The Spearman rank correlation coefficient is 0.763, significant at $p < 0.01$ level (two-tailed)
Expected annual mortality and affected population risk by TRI ( $0.5^\circ \times 0.5^\circ$ )	Expected annual affected population risk by MhRI ( $0.5^\circ \times 0.5^\circ$ )	85,789 grids	The Pearson correlation coefficient is 0.618, significant at $p < 0.01$ level (two-tailed)
Expected annual loss and affected property risk by TRI ( $0.5^\circ \times 0.5^\circ$ )	Expected annual affected property risk by MhRI ( $0.5^\circ \times 0.5^\circ$ )	58,605 grids	The Pearson correlation coefficient is 0.873, significant at $p < 0.01$ level (two-tailed)

## The Significance of the Validation Results

Risk type	Correlation coefficient type	Significance of results
Earthquake mortality risk	Spearman rank correlation	Likely
Earthquake economic-social wealth loss risk	Pearson correlation	Very likely
Volcano mortality risk	Spearman rank correlation	Likely
Landslide mortality risk	Spearman rank correlation	Likely
Flood Economic loss and mortality risk	Spearman rank correlation	Likely
	Spearman rank correlation	Likely
Affected population/GDP risk of flood	Pearson correlation	Likely
Affected population/GDP risk of storm surge	Spearman rank correlation	Likely
Affected population/GDP risk of sand-dust storm	Pearson correlation	Likely
Heat wave mortality risk	Spearman rank correlation	Likely
Affected population risk of cold wave	Spearman rank correlation	Likely
Maize yield loss risk of drought	Pearson correlation	Very likely
Wheat yield loss risk of drought	Pearson correlation	Very likely

(continued)

(continued)

Risk type	Correlation coefficient type	Significance of results
Rice yield loss risk of drought	Pearson correlation	Very likely
Burned forest area	Spearman rank correlation	Likely
Grassland NPP loss <sup>a</sup>	–	Very likely
Expected annual mortality and affected population risk rank by TRI (country)	Spearman rank correlation	Likely
Expected annual affected population risk rank by MhRI (country)	Spearman rank correlation	Likely
Expected annual loss and affected property risk rank by TRI (country)	Spearman rank correlation	Likely
Expected annual affected property risk rank by MRI (country)	Spearman rank correlation	Likely
Expected annual mortality and affected population risk rank by TRI (country)	Spearman rank correlation	Likely
Expected annual mortality and affected population risk rank by TRI (per unit area)	Spearman rank correlation	Likely
Expected annual loss and affected property risk rank by TRI (country)	Spearman rank correlation	Likely
Expected annual loss and affected property risk rank by TRI (per unit area)	Spearman rank correlation	Likely
Expected annual mortality and affected population risk by TRI (0.5° × 0.5°)	Pearson correlation	Very likely
Expected annual loss and affected property risk by TRI (0.5° × 0.5°)	Pearson correlation	Very likely

<sup>a</sup> The method of calculating grassland NPP loss risk has been published

## Validation Data<sup>5</sup>

Disaster type	Validation data description	Data access	Data sources
Earthquake	Earthquake mortality risk provided by UNISDR	A	UNISDR. (2009) Global assessment report on disaster risk reduction <a href="http://www.preventionweb.net">http://www.preventionweb.net</a>
	Historical economic loss caused by earthquake provided by EM-DAT		EM-DAT, CRED <a href="http://www.emdat.be">http://www.emdat.be</a>
Volcano	Volcano mortality risk map provided by <i>Natural Disaster Hotspots: A Global Risk Analysis</i>	A	Socioeconomic Data and Applications Center (SEDAC), NASA <a href="http://sedac.ciesin.columbia.edu">http://sedac.ciesin.columbia.edu</a>
Landslide	Global landslide hazard hotspot produced by the collaboration between NGI and Columbia University	A	Socioeconomic Data and Applications Center (SEDAC), NASA <a href="http://sedac.ciesin.columbia.edu/data/set/ndh-landslide-hazard-distribution">http://sedac.ciesin.columbia.edu/data/set/ndh-landslide-hazard-distribution</a>
Flood	EM-DAT historical flood event records from 1900 to 2012	A	EM-DAT <a href="http://www.emdat.be">http://www.emdat.be</a>
	Global large flood events archive from Dartmouth Flood Observatory (DFO)	A	Dartmouth Flood Observatory <a href="http://www.dartmouth.edu/~floods/Archives/index.html">http://www.dartmouth.edu/~floods/Archives/index.html</a>
	Global flood economic and mortality risk maps provided by <i>Natural Disaster Hotspots: A Global Risk Analysis</i>	A	Socioeconomic Data and Applications Center (SEDAC), NASA <a href="http://sedac.ciesin.columbia.edu">http://sedac.ciesin.columbia.edu</a>

(continued)

<sup>5</sup> Note there are four kinds of data sources, A refers to free data of open access, B refers to data quoted from other documents, C refers to bought data, and D refers to data provided from cooperation.

(continued)

Disaster type	Validation data description	Data access	Data sources
Storm surge	This dataset includes a compilation of estimated storm surges triggered by tropical cyclones from 1975 to 2007, which contains information about the place, time, population effected, GDP effected, etc.	A	GRDP <a href="http://preview.grid.unep.ch">http://preview.grid.unep.ch</a>
Sand-dust storm	Natural disasters newspaper database of China from 1992 to 2010	D	Beijing Normal University (BNU), the database based on provincial newspapers of China (1992–2005) and internet reports (2006–2010) was supplied by BNU
Heat wave	Heat wave mortality data at the country level is provided by the International Disaster Database (EM-DAT) from 1900 to 2013	A	EM-DAT, CRED <a href="http://www.emdat.be/database">http://www.emdat.be/database</a>
Cold wave	Global IDentifier Number Database The cold wave disaster database, include occurrence time, place, casualty, affected population, etc., from 2000 to 2014	A	Global IDentifier Number <a href="http://www.glidenumber.net/glide/public/search/search.jsp">http://www.glidenumber.net/glide/public/search/search.jsp</a>
Drought	Drought data released by China's Ministry of Agriculture including the slightly, moderately, and severely damaged crop area by drought from 1997 to 2005 The crop sown area published by the National Bureau of Statistics of China, in provincial units	A	China's Ministry of Agriculture <a href="http://www.zzys.moa.gov.cn/">http://www.zzys.moa.gov.cn/</a> National Bureau of Statistics of China <a href="http://www.stats.gov.cn/">http://www.stats.gov.cn/</a>
Forest wildfire	The Global Risk Data Platform built by UNEP and UNISDR provides a density of fires dataset, including an estimation of the density of fires over the period from 1997 to 2010	A	Global Risk Data Platform <a href="http://preview.grid.unep.ch/index.php?preview=data&amp;events=fires&amp;lang=eng">http://preview.grid.unep.ch/index.php?preview=data&amp;events=fires&amp;lang=eng</a>
Multi-hazard	The rank of total affected population and property damage data for each country was derived from EM-DAT historical natural disaster event records from 1951 to 2013	A	EM-DAT, CRED <a href="http://www.emdat.be">http://www.emdat.be</a>

## Appendix V

### Ranks of Multi-hazard Risk of the World

See Tables 1, 2 and 3

**Table 1** Rank in descending order by multi-hazard (Mh) intensity

Rank at country unit (top 50)			Rank at per unit area (top 50)		
Rank	Country	Ratio to the maximum Mh value (%)	Rank	Country	Ratio to the maximum Mh value (%)
1	Russia	100.00	1	Bangladesh	100.00
2	United States	72.15	2	South Korea	90.05
3	China	61.92	3	Japan	84.22
4	Canada	55.86	4	Vietnam	82.80
5	Australia	54.31	5	Laos	80.42
6	Brazil	53.57	6	Belize	75.71
7	India	29.89	7	Burma	74.36
8	Mexico	17.46	8	Guatemala	73.60
9	Argentina	15.80	9	Madagascar	70.15
10	Indonesia	11.52	10	Dominican Republic	69.56
11	Kazakhstan	11.15	11	North Korea	68.86
12	Congo (Democratic Republic of the)	9.79	12	Philippines	68.44
13	Iran	8.47	13	Bhutan	67.89
14	Colombia	7.99	14	El Salvador	64.69
15	Burma	7.84	15	Honduras	64.16
16	Peru	7.76	16	Papua New Guinea	63.27
17	Madagascar	6.55	17	Cambodia	62.54
18	Bolivia	6.25	18	India	61.40
19	Turkey	6.06	19	New Zealand	60.96
20	Venezuela	5.63	20	Thailand	59.22
21	Mongolia	5.48	21	Nicaragua	58.85
22	Mozambique	5.15	22	Nepal	58.52
23	Angola	5.07	23	Uruguay	57.46
24	South Africa	5.07	24	Haiti	57.34

(continued)

**Table 1** (continued)

Rank at country unit (top 50)			Rank at per unit area (top 50)		
Rank	Country	Ratio to the maximum Mh value (%)	Rank	Country	Ratio to the maximum Mh value (%)
25	Japan	4.97	25	Mexico	56.53
26	Thailand	4.81	26	Cuba	56.47
27	Pakistan	4.64	27	Iceland	54.32
28	Tanzania	4.63	28	Montenegro	53.26
29	Papua New Guinea	4.61	29	Portugal	51.75
30	Ethiopia	4.51	30	Norway	49.40
31	Vietnam	4.28	31	Turkey	49.16
32	Nigeria	4.17	32	United States	49.02
33	Sudan	3.81	33	Sri Lanka	48.73
34	Chile	3.75	34	Kyrgyzstan	48.73
35	Zambia	3.60	35	Bosnia and Herzegovina	48.10
36	Algeria	3.44	36	Costa Rica	47.95
37	Afghanistan	3.40	37	Albania	47.65
38	Ukraine	3.25	38	Tajikistan	46.74
39	Philippines	3.20	39	Singapore	46.14
40	Mali	3.19	40	Armenia	45.94
41	France	3.06	41	Australia	44.77
42	Chad	3.02	42	Georgia	44.76
43	Spain	3.00	43	Paraguay	44.66
44	Laos	2.92	44	Colombia	44.49
45	Sweden	2.87	45	Finland	44.27
46	Paraguay	2.81	46	Macedonia	44.14
47	Namibia	2.81	47	Liechtenstein	43.55
48	New Zealand	2.60	48	Switzerland	43.34
49	Central African Republic	2.54	49	Ecuador	42.97
50	Norway	2.53	50	Suriname	41.80

(continued)

**Table 1** (continued)

Rank at country unit (51–197)		Rank at per unit area (51–197)	
Rank	Country	Rank	Country
51–100	Kenya	51–100	Mozambique
	South Sudan		Malaysia
	Botswana		China
	Finland		Baker Island
	Malaysia		Slovenia
	Bangladesh		Serbia
	Cameroon		Guyana
	Turkmenistan		Sierra Leone
	Zimbabwe		Sweden
	Uzbekistan		Brazil
	Germany		Austria
	Niger		Venezuela
	Somalia		Indonesia
	Libya		Azerbaijan
	Cambodia		Croatia
	Italy		Peru
	Ecuador		Belarus
	Mauritania		Malawi
	Poland		Spain
	Uruguay		Russia
	Kyrgyzstan		Latvia
	Congo		Guinea
	Guinea		San Marino
	Morocco		Romania
	South Korea		Italy
	Romania		Bolivia
	Guyana		Panama
	Nepal		Samoa
	The Republic of Côte d'Ivoire		Germany
	North Korea		Lithuania
	Gabon		Slovakia
	Guatemala		Argentina
	Saudi Arabia		Hungary
	Belarus		Czech Republic
	Burkina Faso		Luxembourg
	Nicaragua		Canada
	United Kingdom		Bulgaria
	Iraq		France
	Honduras		Andorra
	Tajikistan		Moldova
	Ghana		Swaziland
	Cuba		Ukraine
	Uganda		Belgium

(continued)

**Table 1** (continued)

Rank at country unit (51–197)		Rank at per unit area (51–197)	
Rank	Country	Rank	Country
	Suriname		Greece
	Egypt		Poland
	Senegal		Afghanistan
	Iceland		Pakistan
	Yemen		Zimbabwe
	Portugal		Iran
	Greece		Lebanon
101–150	Malawi	101–150	Ireland
	Bulgaria		Gambia
	Serbia		Estonia
	Syria		Gabon
	Oman		Chile
	Dominican Republic		Lesotho
	Hungary		Liberia
	Austria		Tanzania
	Azerbaijan		Timor-Leste
	Sri Lanka		United Kingdom
	Georgia		Jamaica
	Benin		Zambia
	Liberia		Uzbekistan
	Sierra Leone		Denmark
	Tunisia		Fiji
	Czech Republic		Nigeria
	Panama		Senegal
	Bhutan		Guinea-Bissau
	Costa Rica		Burkina Faso
	Bosnia and Herzegovina		Cameroon
	Latvia		Congo
	Lithuania		Kenya
	Ireland		Togo
	Croatia		Netherlands
	Eritrea		Turkmenistan
	Switzerland		The Republic of Côte d'Ivoire
	Slovakia		Benin
	Belize		Gaza Strip
	Haiti		Congo (Democratic Republic of the)
	Togo		Ghana
	Estonia		South Africa
	Jordan		Kazakhstan
	Armenia		Central African Republic
	Albania		Uganda
	El Salvador		Botswana
	Denmark		Angola

(continued)

**Table 1** (continued)

Rank at country unit (51–197)		Rank at per unit area (51–197)	
Rank	Country	Rank	Country
	Moldova		Ethiopia
	Macedonia		South Sudan
	Belgium		Burundi
	Guinea-Bissau		Rwanda
	Lesotho		Equatorial Guinea
	Netherlands		Mongolia
	Slovenia		Morocco
	Montenegro		Israel
	Burundi		Namibia
	Equatorial Guinea		Syria
	Swaziland		Tunisia
	Rwanda		Somalia
	United Arab Emirates		Eritrea
	Fiji		Palestine
151–197	Israel	151–197	Iraq
	Timor-Leste		Djibouti
	Djibouti		Mali
	Gambia		Jordan
	Jamaica		Trinidad and Tobago
	Lebanon		Chad
	Solomon Islands		Sudan
	Baker Island		Kuwait
	Kuwait		Oman
	Palestine		Yemen
	Gaza Strip		Niger
	Samoa		Mauritania
	Luxembourg		Algeria
	Trinidad and Tobago		Solomon Islands
	Bahamas		Mauritius
	Singapore		United Arab Emirates
	Cyprus		Libya
	Andorra		Monaco
	Mauritius		Bahamas
	Liechtenstein		Egypt
	San Marino		Saint Vincent and the Grenadines
	Saint Vincent and the Grenadines		Saudi Arabia
	Qatar		Cyprus
	Comoros		Niue
	Niue		Comoros

(continued)

**Table 1** (continued)

Rank at country unit (51–197)		Rank at per unit area (51–197)	
Rank	Country	Rank	Country
	Cape Verde		Qatar
	Monaco		Dominica
	Dominica		Tonga
	Tonga		Marshall Islands
	Palau		Cape Verde
	Antigua and Barbuda		Saint Kitts and Nevis
	Federated States of Micronesia		Palau
	Saint Kitts and Nevis		Antigua and Barbuda
	Marshall Islands		Maldives
	Maldives		Federated States of Micronesia
	Cook Islands		Vatican City
	Vatican City		Cook Islands
	Tuvalu		Tuvalu
	Seychelles		Nauru
	Malta		Malta
	Bahrain		Seychelles
	Saint Lucia		Bahrain
	Nauru		Saint Lucia
	Kiribati		Barbados
	Barbados		Kiribati
	Grenada		Grenada
	Sao Tome and Principe		Sao Tome and Principe

*Note* (1) The Mh value of all 197 countries of the world is calculated and ranked in descending order at county and per unit area respectively.  
(2) The top 50 countries with the highest Mh values (about 35 % of all) are listed with their rank order, and other countries with lower Mh value are listed by groups with the order from the 51th to the 100th, from the 101th to the 150th, and from the 151th to the lowest

**Table 2** Rank in descending order by total risk index (TRI)

Expected annual mortality and affected population risk						Expected annual loss and affected property risk					
Rank at country unit (top 50)			Rank at per unit area (top 50)			Rank at country unit (top 50)			Rank at per unit area (top 50)		
Rank	Country	Ratio to the maximum TRI value (%)	Rank	Country	Ratio to the maximum TRI value (%)	Rank	Country	Ratio to the maximum TRI value (%)	Rank	Country	Ratio to the maximum TRI value (%)
1	India	100.00	1	Bangladesh	100.00	1	United States	100.00	1	Netherlands	100.00
2	China	78.56	2	Gaza Strip	47.59	2	Japan	80.70	2	Japan	83.90
3	Indonesia	54.28	3	Philippines	34.45	3	China	50.49	3	South Korea	21.91
4	Pakistan	47.97	4	Nepal	26.64	4	Russia	18.37	4	Germany	16.54
5	Bangladesh	40.63	5	Pakistan	18.39	5	Canada	15.69	5	Belgium	15.94
6	Philippines	30.35	6	Guatemala	16.84	6	Germany	15.21	6	Singapore	15.27
7	Burma	15.06	7	Bhutan	14.17	7	Brazil	12.73	7	Gaza Strip	10.05
8	United States	13.97	8	Israel	13.92	8	India	12.52	8	Israel	7.69
9	Japan	11.91	9	Haiti	11.86	9	Netherlands	9.00	9	Bangladesh	7.67
10	Nepal	11.66	10	Burundi	11.44	10	Mexico	8.75	10	Liechtenstein	7.55
11	Iran	9.98	11	El Salvador	10.96	11	Australia	7.00	11	Trinidad and Tobago	7.48
12	Uzbekistan	9.86	12	India	10.89	12	Argentina	6.59	12	Monaco	6.03
13	Afghanistan	9.62	13	Japan	10.70	13	France	6.33	13	United Kingdom	4.86
14	Mexico	7.09	14	Indonesia	9.65	14	South Korea	5.59	14	San Marino	4.82
15	Vietnam	7.03	15	Rwanda	8.99	15	Angola	4.84	15	Luxembourg	4.70
16	Egypt	5.64	16	South Korea	8.89	16	Congo (Democratic Republic of the)	4.12	16	Italy	4.67
17	Ethiopia	5.55	17	Moldova	8.51	17	Burma	3.68	17	France	4.48
18	Guatemala	5.48	18	Uzbekistan	7.65	18	Italy	3.63	18	United States	4.17
19	Tanzania	3.55	19	Georgia	7.59	19	Turkey	3.27	19	Switzerland	4.06
20	Turkey	3.33	20	Burma	7.58	20	Thailand	3.22	20	Mauritius	3.96
21	Kyrgyzstan	2.95	21	Honduras	7.35	21	United Kingdom	3.06	21	El Salvador	3.94
22	Congo (Democratic Republic of the)	2.87	22	Vietnam	7.21	22	Kazakhstan	3.00	22	Costa Rica	3.17
23	Bolivia	2.85	23	Tajikistan	6.72	23	Bangladesh	2.70	23	United Arab Emirates	3.15
24	Tajikistan	2.84	24	Mauritius	5.34	24	Venezuela	2.41	24	Philippines	3.10
25	Syria	2.74	25	Jamaica	5.26	25	Philippines	2.36	25	Greece	2.83
26	Russia	2.66	26	Dominican Republic	5.18	26	Madagascar	2.15	26	Dominican Republic	2.79
27	Kenya	2.63	27	Afghanistan	5.04	27	Indonesia	2.10	27	Portugal	2.62
28	South Korea	2.62	28	Kyrgyzstan	4.98	28	Mozambique	2.10	28	Guatemala	2.44
29	Honduras	2.47	29	Syria	4.96	29	Chile	2.00	29	Thailand	2.43
30	Uganda	2.40	30	Nicaragua	4.02	30	Colombia	1.84	30	Burma	2.14
31	Iraq	2.21	31	Lebanon	3.78	31	Bolivia	1.75	31	China	2.07
32	Thailand	2.12	32	Netherlands	3.63	32	Spain	1.70	32	Cambodia	1.97
33	Chile	2.01	33	Djibouti	3.36	33	Vietnam	1.60	33	Vietnam	1.90
34	Peru	1.97	34	Uganda	3.34	34	South Africa	1.58	34	Kuwait	1.77
35	Ecuador	1.81	35	Malawi	3.09	35	Nigeria	1.41	35	Slovenia	1.76

(continued)

**Table 2** (continued)

Expected annual mortality and affected population risk						Expected annual loss and affected property risk					
Rank at country unit (top 50)			Rank at per unit area (top 50)			Rank at country unit (top 50)			Rank at per unit area (top 50)		
Rank	Country	Ratio to the maximum TRI value (%)	Rank	Country	Ratio to the maximum TRI value (%)	Rank	Country	Ratio to the maximum TRI value (%)	Rank	Country	Ratio to the maximum TRI value (%)
36	Papua New Guinea	1.77	36	Albania	2.86	36	Iran	1.39	36	Mexico	1.74
37	Bhutan	1.68	37	China	2.78	37	Pakistan	1.39	37	Cuba	1.72
38	Georgia	1.58	38	Costa Rica	2.62	38	Iraq	1.38	38	New Zealand	1.68
39	Nicaragua	1.54	39	North Korea	2.52	39	Tanzania	1.26	39	Turkey	1.62
40	Colombia	1.43	40	Ecuador	2.38	40	Belgium	1.26	40	Austria	1.61
41	Cambodia	1.20	41	Cambodia	2.22	41	New Zealand	1.17	41	India	1.58
42	Kazakhstan	1.10	42	Armenia	2.22	42	Mongolia	1.16	42	Angola	1.51
43	Malawi	1.09	43	Sri Lanka	2.12	43	South Sudan	1.15	43	North Korea	1.46
44	Canada	1.03	44	Cuba	2.11	44	Zambia	1.05	44	Jamaica	1.46
45	Haiti	0.96	45	Iran	2.07	45	Greece	0.96	45	Madagascar	1.41
46	North Korea	0.92	46	Egypt	1.93	46	Zimbabwe	0.92	46	Hungary	1.41
47	Burundi	0.92	47	Azerbaijan	1.92	47	Cambodia	0.92	47	Serbia	1.35
48	Israel	0.91	48	Saint Vincent and the Grenadines	1.72	48	Botswana	0.86	48	Andorra	1.34
49	Germany	0.90	49	Iraq	1.70	49	Peru	0.75	49	Croatia	1.33
50	Gaza Strip	0.88	50	Ethiopia	1.65	50	Paraguay	0.73	50	Spain	1.30

(continued)

**Table 2** (continued)

Rank at country unit (51–195)		Rank at per unit area (51–195)		Rank at country unit (51–196)		Rank at per unit area (51–196)	
Rank	Country	Rank	Country	Rank	Country	Rank	Country
51–100	Madagascar	51–100	Trinidad and Tobago	51–100	Guatemala	51–100	Iraq
	Moldova		Barbados		Portugal		Bhutan
	Brazil		Kenya		United Arab Emirates		Cyprus
	Laos		Turkey		Romania		Lebanon
	Mozambique		Thailand		Kenya		Azerbaijan
	Dominican Republic		Papua New Guinea		Chad		Nepal
	Algeria		Tanzania		Namibia		Swaziland
	Venezuela		Mexico		Cuba		Mozambique
	Cuba		Bosnia and Herzegovina		North Korea		Chile
	Rwanda		Laos		Ecuador		Venezuela
	El Salvador		Comoros		Israel		Saint Vincent and the Grenadines
	Ukraine		Kuwait		Switzerland		Argentina
	Romania		Timor-Leste		Costa Rica		Zimbabwe
	Argentina		Chile		Central African Republic		Slovakia
	Azerbaijan		Bolivia		Nepal		Barbados
	Italy		Slovenia		Poland		Romania
	Nigeria		Romania		Laos		Uruguay
	France		Germany		Sudan		Czech Republic
	Spain		Belgium		Austria		South Sudan
	Sri Lanka		Serbia		Dominican Republic		Bosnia and Herzegovina
	Turkmenistan		Palestine		Uzbekistan		Paraguay
	Costa Rica		Fiji		Hungary		Antigua and Barbuda
	Netherlands		Jordan		Uruguay		Congo (Democratic Republic of the)
	Morocco		Grenada		Egypt		Ecuador
	Australia		Croatia		Ethiopia		Laos
	Poland		Switzerland		Finland		Ireland
	Mongolia		Singapore		Serbia		Colombia
	New Zealand		Italy		Ghana		Bolivia
	Albania		Peru		The Republic of Côte d'Ivoire		Honduras
	Djibouti		Hungary		Malaysia		Bulgaria
	Serbia		United States		Mali		Pakistan
	Armenia		Madagascar		Cameroon		Canada
	Jordan		Eritrea		Azerbaijan		Nigeria
	Bosnia and Herzegovina		Liechtenstein		Burkina Faso		Albania
	Eritrea		Samoa		Somalia		Sri Lanka
	Jamaica		Vatican City		El Salvador		Benin
	Greece		Belize		Guinea		Brazil
	Tunisia		San Marino		Croatia		Botswana
	South Sudan		Slovakia		Saudi Arabia		Malawi
	Hungary		Dominica		Ukraine		Togo
	United Kingdom		Macedonia		Honduras		Gambia

(continued)

**Table 2** (continued)

Rank at country unit (51–195)		Rank at per unit area (51–195)		Rank at country unit (51–196)		Rank at per unit area (51–196)	
Rank	Country	Rank	Country	Rank	Country	Rank	Country
	Lebanon		Colombia		Bulgaria		Zambia
	Libya		Greece		Benin		Baker Island
	Croatia		Saint Lucia		Malawi		Tanzania
	Portugal		Antigua and Barbuda		Syria		South Africa
	Paraguay		Congo (Democratic Republic of the)		Gaza Strip		Poland
	South Africa		Tonga		Oman		Macedonia
	Somalia		Ukraine		Senegal		Ghana
	Bulgaria		Portugal		Czech Republic		Saint Kitts and Nevis
	Senegal		Mozambique		Congo		Georgia
101–150	Sudan	101–150	Tunisia	101–150	Uganda	101–150	Grenada
	Malaysia		New Zealand		Niger		Indonesia
	Belgium		Poland		Bhutan		Kazakhstan
	Switzerland		Spain		Sweden		Russia
	Zambia		Czech Republic		Papua New Guinea		Belize
	Gabon		Turkmenistan		Afghanistan		Finland
	Cameroon		Morocco		Slovakia		Australia
	Czech Republic		France		Ireland		Haiti
	Slovakia		Venezuela		Norway		The Republic of Côte d'Ivoire
	Austria		Panama		Sri Lanka		Syria
	Ghana		Luxembourg		Trinidad and Tobago		Dominica
	Panama		Austria		Belarus		Kenya
	Belarus		Bulgaria		Slovenia		Malaysia
	Saudi Arabia		Montenegro		Bosnia and Herzegovina		Iran
	Kuwait		Saint Kitts and Nevis		Algeria		Guinea
	Slovenia		United Arab Emirates		Nicaragua		Timor-Leste
	United Arab Emirates		Andorra		Georgia		Armenia
	Niger		Qatar		Togo		Burkina Faso
	Timor-Leste		Gambia		Kyrgyzstan		Montenegro
	Oman		Nigeria		Kuwait		Uzbekistan
	Sweden		United Kingdom		Morocco		Panama
	Fiji		Kazakhstan		Gabon		Senegal
	Zimbabwe		Senegal		Iceland		Fiji
	Mali		Solomon Islands		Turkmenistan		Mongolia
	Iceland		Bahrain		Libya		Iceland
	The Republic of Côte d'Ivoire		Iceland		Panama		Nicaragua
	Angola		Algeria		Jordan		Guinea-Bissau
	Macedonia		Guinea-Bissau		Tunisia		Central African Republic
	Mauritius		Belarus		Mauritania		Moldova
	Burkina Faso		Gabon		Guyana		Jordan
	Belize		Togo		Swaziland		Saint Lucia
	Chad		Ghana		Albania		Denmark
	Uruguay		Malaysia		Jamaica		Bahrain

(continued)

**Table 2** (continued)

Rank at country unit (51–195)		Rank at per unit area (51–195)		Rank at country unit (51–196)		Rank at per unit area (51–196)	
Rank	Country	Rank	Country	Rank	Country	Rank	Country
	Palestine		Sierra Leone		Tajikistan		Namibia
	Trinidad and Tobago		South Sudan		Sierra Leone		Peru
	Guinea		Paraguay		Macedonia		Malta
	Mauritania		Latvia		Luxembourg		Lesotho
	Sierra Leone		Argentina		Lithuania		Rwanda
	Togo		Bahamas		Lebanon		Cameroon
	Latvia		Lithuania		Denmark		Uganda
	Finland		Mongolia		Cyprus		Oman
	Benin		Russia		Yemen		Belarus
	Liberia		Uruguay		Armenia		Sierra Leone
	Lithuania		Cameroon		Haiti		Lithuania
	Congo		Somalia		Singapore		Samoa
	Central African Republic		Liberia		Guinea-Bissau		Congo
	Yemen		Oman		Moldova		Kyrgyzstan
	Solomon Islands		Denmark		Latvia		Chad
	Guinea-Bissau		Benin		Belize		Burundi
	Botswana		Burkina Faso		Mauritius		Somalia
151–195	Montenegro	151–195	Baker Island	151–196	Lesotho	151–196	Tunisia
	Norway		The Republic of Côte d'Ivoire		Gambia		Latvia
	Qatar		Canada		Rwanda		Egypt
	Namibia		Brazil		Fiji		Qatar
	Denmark		Zimbabwe		Timor-Leste		Ukraine
	Comoros		Estonia		Montenegro		Norway
	Gambia		Swaziland		Burundi		Ethiopia
	Ireland		Zambia		Baker Island		Gabon
	Estonia		Guinea		Estonia		Sweden
	Samoa		Sweden		Eritrea		Papua New Guinea
	Guyana		Cyprus		Liberia		Tajikistan
	Bahamas		South Africa		Suriname		Guyana
	Saint Vincent and the Grenadines		Ireland		Qatar		Mali
	Luxembourg		Libya		Liechtenstein		Sudan
	Barbados		Lesotho		Bahamas		Morocco
	Swaziland		Finland		Djibouti		Afghanistan
	Lesotho		Sudan		Palestine		Estonia
	Singapore		Australia		Equatorial Guinea		Bahamas
	Suriname		Congo		Andorra		Palestine
	Dominica		Niger		Solomon Islands		Turkmenistan
	Tonga		Cook Islands		Samoa		Niger
	Saint Lucia		Mali		Saint Vincent and the Grenadines		Saudi Arabia
	Cyprus		Saudi Arabia		Barbados		Tonga
	Grenada		Angola		Antigua and Barbuda		Djibouti
	Baker Island		Norway		San Marino		Yemen

(continued)

**Table 2** (continued)

Rank at country unit (51–195)		Rank at per unit area (51–195)		Rank at country unit (51–196)		Rank at per unit area (51–196)	
Rank	Country	Rank	Country	Rank	Country	Rank	Country
	Equatorial Guinea		Yemen		Dominica		Equatorial Guinea
	Antigua and Barbuda		Niue		Grenada		Cook Islands
	Andorra		Chad		Bahrain		Liberia
	Bahrain		Palau		Saint Lucia		Solomon Islands
	Liechtenstein		Equatorial Guinea		Saint Kitts and Nevis		Cape Verde
	Saint Kitts and Nevis		Maldives		Cape Verde		Comoros
	San Marino		Mauritania		Malta		Eritrea
	Palau		Central African Republic		Monaco		Mauritania
	Cook Islands		Botswana		Comoros		Federated States of Micronesia
	Cape Verde		Guyana		Tonga		Nauru
	Niue		Marshall Islands		Federated States of Micronesia		Algeria
	Maldives		Suriname		Cook Islands		Libya
	Kiribati		Namibia		Palau		Suriname
	Seychelles		Kiribati		Kiribati		Palau
	Marshall Islands		Seychelles		Marshall Islands		Marshall Islands
	Vatican City		Tuvalu		Nauru		Tuvalu
	Federated States of Micronesia		Cape Verde		Maldives		Maldives
	Tuvalu		Federated States of Micronesia		Seychelles		Kiribati
	Malta		Malta		Tuvalu		Seychelles
	Monaco		Monaco		Niue		Niue
					Sao Tome and Principe		Sao Tome and Principe

*Note* (1) The TRI assesses the expected annual multi-hazard risk level of mortality and affected population of 195 countries (lack of mortality and affected population data to individual hazard of Nauru and Sao Tome and Principe) of the world and the expected annual multi-hazard risk level of loss and affected property of 196 countries (lack of GDP data of Vatican City) of the world. (2) The TRI value is calculated and ranked in descending order at country unit and per unit area respectively. (3) The top 50 countries with the highest TRI values (about 35 % of all) are listed with their rank order, and other countries with lower TRI value are listed by groups with the order from the 51th to the 100th, from the 101th to the 150th, and from the 151th to the lowest

**Table 3** Rank in descending order by multi-hazard risk index (MhRI)

Expected annual affected population risk						Expected annual affected property risk					
Rank at country unit (top 50)			Rank at per unit area (top 50)			Rank at country unit (top 50)			Rank at per unit area (top 50)		
Rank	Country	Ratio to the maximum MhRI value (%)	Rank	Country	Ratio to the maximum MhRI value (%)	Rank	Country	Ratio to the maximum MhRI value (%)	Rank	Country	Ratio to the maximum MhRI value (%)
1	China	100.00	1	Bangladesh	100.00	1	United States	100.00	1	Japan	100.00
2	India	95.91	2	Singapore	36.04	2	Japan	53.18	2	South Korea	69.77
3	United States	21.56	3	South Korea	33.98	3	China	47.76	3	San Marino	59.06
4	Bangladesh	20.23	4	Philippines	24.06	4	India	13.53	4	Netherlands	55.73
5	Japan	13.30	5	Japan	24.02	5	Germany	10.96	5	Liechtenstein	45.80
6	Indonesia	11.58	6	India	20.98	6	Brazil	10.84	6	Monaco	43.35
7	Brazil	10.64	7	Vietnam	19.64	7	South Korea	9.84	7	Luxembourg	41.81
8	Philippines	10.55	8	Haiti	19.41	8	France	8.32	8	Switzerland	37.07
9	Vietnam	9.54	9	El Salvador	18.48	9	Mexico	7.75	9	Belgium	32.64
10	Mexico	8.59	10	San Marino	12.93	10	Canada	7.21	10	Germany	21.55
11	Pakistan	7.91	11	Gaza Strip	12.25	11	Italy	6.29	11	Andorra	17.39
12	Nigeria	6.45	12	Dominican Republic	12.24	12	United Kingdom	5.25	12	United Kingdom	15.09
13	Thailand	5.39	13	Sri Lanka	11.90	13	Russia	4.84	13	Singapore	14.95
14	Burma	5.14	14	Nepal	10.73	14	Spain	4.20	14	Italy	14.66
15	South Korea	4.99	15	North Korea	9.70	15	Australia	4.09	15	Austria	11.83
16	Russia	4.58	16	Lebanon	9.63	16	Indonesia	3.16	16	Israel	11.09
17	Turkey	3.48	17	Rwanda	9.58	17	Turkey	3.09	17	France	10.65
18	Ethiopia	3.43	18	Guatemala	8.52	18	Netherlands	2.77	18	Gaza Strip	8.68
19	Iran	3.29	19	Burundi	8.22	19	Thailand	2.46	19	Lebanon	8.20
20	Germany	2.80	20	Monaco	7.76	20	Switzerland	2.18	20	Denmark	8.00
21	Congo (Democratic Republic of the)	2.75	21	Netherlands	7.23	21	Philippines	1.89	21	United States	7.53
22	Colombia	2.74	22	China	7.12	22	Argentina	1.88	22	Portugal	7.43
23	Nepal	2.34	23	Thailand	7.06	23	Iran	1.75	23	El Salvador	6.51
24	Argentina	2.22	24	Belgium	7.03	24	Colombia	1.72	24	Bangladesh	6.46
25	France	2.11	25	Liechtenstein	6.43	25	Venezuela	1.53	25	Baker Island	6.44
26	Madagascar	1.98	26	Pakistan	6.09	26	Nigeria	1.50	26	Slovenia	6.31
27	Italy	1.88	27	Mauritius	6.05	27	Belgium	1.43	27	Dominican Republic	6.01
28	North Korea	1.76	28	Germany	5.30	28	Austria	1.41	28	Czech Republic	5.84
29	South Africa	1.76	29	Switzerland	5.29	29	Poland	1.40	29	Spain	5.84
30	Canada	1.64	30	Jamaica	5.23	30	Bangladesh	1.25	30	Ireland	5.69
31	Tanzania	1.63	31	Burma	5.20	31	South Africa	1.25	31	Trinidad and Tobago	4.65
32	Kenya	1.58	32	Gambia	4.90	32	Vietnam	1.18	32	Kuwait	4.54
33	United Kingdom	1.52	33	Malawi	4.83	33	Malaysia	1.15	33	Philippines	4.47
34	Spain	1.51	34	Nigeria	4.79	34	Chile	1.11	34	Slovakia	4.15
35	Ukraine	1.48	35	Cambodia	4.60	35	Portugal	0.97	35	Greece	3.99
36	Malaysia	1.38	36	Cuba	4.60	36	Sweden	0.93	36	Mauritius	3.79

(continued)

**Table 3** (continued)

Expected annual affected population risk						Expected annual affected property risk					
Rank at country unit (top 50)			Rank at per unit area (top 50)			Rank at country unit (top 50)			Rank at per unit area (top 50)		
Rank	Country	Ratio to the maximum MhRI value (%)	Rank	Country	Ratio to the maximum MhRI value (%)	Rank	Country	Ratio to the maximum MhRI value (%)	Rank	Country	Ratio to the maximum MhRI value (%)
37	Guatemala	1.38	37	Andorra	4.53	37	Norway	0.86	37	China	3.54
38	Uzbekistan	1.33	38	Israel	4.46	38	New Zealand	0.85	38	Thailand	3.36
39	Mozambique	1.28	39	Luxembourg	4.34	39	Greece	0.75	39	Hungary	3.35
40	Afghanistan	1.27	40	Honduras	4.27	40	Pakistan	0.74	40	Poland	3.16
41	Uganda	1.25	41	Italy	4.20	41	Czech Republic	0.66	41	India	3.08
42	Cambodia	1.24	42	United Kingdom	4.18	42	Romania	0.61	42	Mexico	2.78
43	Egypt	1.21	43	Indonesia	4.14	43	Finland	0.60	43	Turkey	2.78
44	Sri Lanka	1.17	44	Portugal	3.62	44	Ireland	0.57	44	Sri Lanka	2.68
45	Poland	1.17	45	Uganda	3.50	45	Peru	0.51	45	Croatia	2.67
46	Algeria	1.10	46	Armenia	3.42	46	Denmark	0.51	46	Guatemala	2.65
47	Venezuela	1.10	47	Costa Rica	3.24	47	Algeria	0.48	47	Costa Rica	2.63
48	Morocco	1.02	48	Albania	3.02	48	Kazakhstan	0.45	48	Cuba	2.58
49	Peru	1.00	49	Bosnia and Herzegovina	3.02	49	Hungary	0.44	49	Vietnam	2.54
50	Sudan	0.94	50	Turkey	3.01	50	Ukraine	0.43	50	Malaysia	2.45

(continued)

**Table 3** (continued)

Rank at country unit (51–197)		Rank at per unit area (51–197)		Rank at country unit (51–196)		Rank at per unit area (51–196)	
Rank	Country	Rank	Country	Rank	Country	Rank	Country
51–100	Ecuador	51–100	Serbia	51–100	Burma	51–100	Jamaica
	Ghana		Togo		Guatemala		New Zealand
	Chile		Mexico		Dominican Republic		Norway
	Dominican Republic		Trinidad and Tobago		Cuba		Romania
	Malawi		Syria		Ecuador		Azerbaijan
	Australia		Moldova		Saudi Arabia		Sweden
	Romania		Czech Republic		Israel		United Arab Emirates
	Syria		Malaysia		Egypt		Serbia
	Cameroon		Slovenia		Iraq		Finland
	The Republic of Côte d'Ivoire		Baker Island		Slovakia		Haiti
	Haiti		Macedonia		Morocco		Macedonia
	Cuba		France		Angola		Albania
	Honduras		Slovakia		Sri Lanka		Venezuela
	Laos		Ghana		Syria		Indonesia
	Iraq		Hungary		Uruguay		Nigeria
	Burkina Faso		Poland		Croatia		Bosnia and Herzegovina
	Zambia		Nicaragua		North Korea		Panama
	El Salvador		Austria		Uzbekistan		North Korea
	Guinea		Azerbaijan		Costa Rica		Lithuania
	Yemen		Ecuador		El Salvador		Bulgaria
	Zimbabwe		Swaziland		Slovenia		Armenia
	Mali		Romania		Azerbaijan		Ecuador
	Niger		Sierra Leone		Serbia		Montenegro
	Portugal		Madagascar		Bulgaria		Colombia
	Kazakhstan		Croatia		Belarus		Chile
	Papua New Guinea		Timor-Leste		Luxembourg		Brazil
	Nicaragua		Uzbekistan		United Arab Emirates		Uruguay
	Bolivia		Ethiopia		Paraguay		Honduras
	Angola		Spain		Nepal		Syria
	Paraguay		Benin		Honduras		Iran
	Serbia		Laos		Sudan		Latvia
	Netherlands		Georgia		Kenya		South Africa
	Senegal		Kenya		Panama		Swaziland
	Chad		Montenegro		Lebanon		Saint Vincent and the Grenadines
	Tajikistan		Tajikistan		Ghana		Nepal
	Rwanda		Morocco		Kuwait		Jordan
	Hungary		Ukraine		Tunisia		Equatorial Guinea
	Benin		Bulgaria		Libya		Belarus
	Czech Republic		Burkina Faso		Lithuania		Pakistan
	Burundi		The Republic of Côte d'Ivoire		Ethiopia		Iraq
	Switzerland		Colombia		Cambodia		Canada
	South Sudan		Lesotho		Bolivia		Ukraine
	Belgium		United States		Cameroon		Georgia
	Azerbaijan		Guinea		Oman		Tunisia
	Austria		Greece		Tanzania		Rwanda
	Belarus		Panama		Laos		Morocco

(continued)

**Table 3** (continued)

Rank at country unit (51–197)		Rank at per unit area (51–197)		Rank at country unit (51–196)		Rank at per unit area (51–196)	
Rank	Country	Rank	Country	Rank	Country	Rank	Country
	Kyrgyzstan		Denmark		Bosnia and Herzegovina		Argentina
	Greece		Jordan		The Republic of Côte d'Ivoire		Burma
	Tunisia		Iran		Madagascar		Estonia
	New Zealand		Afghanistan		Jordan		Moldova
101–150	Somalia	101–150	Ireland	101–150	Gaza Strip	101–150	Cambodia
	Bulgaria		Senegal		Turkmenistan		Australia
	Togo		Tunisia		Papua New Guinea		Belize
	Sierra Leone		Liberia		Yemen		Nicaragua
	Costa Rica		Kuwait		Afghanistan		Ghana
	Bosnia and Herzegovina		Bhutan		Zambia		Uzbekistan
	Uruguay		Tanzania		Latvia		Cyprus
	Georgia		Cameroon		Nicaragua		Peru
	Jordan		Mozambique		Uganda		Bhutan
	Sweden		Lithuania		Baker Island		Fiji
	Saudi Arabia		Kyrgyzstan		Congo (Democratic Republic of the)		Laos
	Slovakia		Iraq		Mozambique		Paraguay
	Central African Republic		Belarus		Georgia		Gambia
	Croatia		Saint Vincent and the Grenadines		Gabon		Egypt
	Turkmenistan		South Africa		Albania		Oman
	Liberia		Zimbabwe		Botswana		Russia
	Panama		Eritrea		Armenia		Iceland
	Eritrea		Belize		Haiti		Lesotho
	Armenia		Guinea-Bissau		South Sudan		Samoa
	Moldova		Yemen		Macedonia		The Republic of Côte d'Ivoire
	Israel		Samoa		Congo		Burundi
	Lebanon		Brazil		Namibia		Malawi
	Finland		Egypt		Senegal		Uganda
	Congo		Uruguay		Burkina Faso		Timor-Leste
	Ireland		Venezuela		Chad		Angola
	Albania		Chile		Jamaica		Kenya
	Gaza Strip		Congo (Democratic Republic of the)		Mali		Togo
	Norway		Fiji		Trinidad and Tobago		Algeria
	Libya		Paraguay		Zimbabwe		Benin
	Lithuania		Papua New Guinea		Malawi		Cameroon
	Denmark		New Zealand		Kyrgyzstan		Senegal
	Macedonia		Latvia		Iceland		Gabon
	Jamaica		Argentina		Estonia		Saudi Arabia
	Slovenia		Zambia		Tajikistan		Tajikistan
	Mauritania		Peru		Suriname		Kazakhstan
	Gambia		Equatorial Guinea		Equatorial Guinea		Suriname
	Namibia		South Sudan		Benin		Yemen
	Lesotho		Sudan		Guinea		Sierra Leone
	Botswana		Algeria		Montenegro		Turkmenistan
	Mongolia		Estonia		Niger		Papua New Guinea

(continued)

**Table 3** (continued)

Rank at country unit (51–197)		Rank at per unit area (51–197)		Rank at country unit (51–196)		Rank at per unit area (51–196)	
Rank	Country	Rank	Country	Rank	Country	Rank	Country
	Bhutan		Bolivia		Moldova		Kyrgyzstan
	Gabon		United Arab Emirates		Rwanda		Burkina Faso
	Latvia		Somalia		Swaziland		Madagascar
	Swaziland		Niger		Bhutan		Congo
	Oman		Sweden		Mongolia		Afghanistan
	Timor-Leste		Mali		Singapore		Guinea
	Guinea-Bissau		Finland		Togo		Tanzania
	Guyana		Congo		Sierra Leone		Zambia
	Montenegro		Angola		Andorra		Ethiopia
	Singapore		Turkmenistan		Belize		Bolivia
151–197	United Arab Emirates	151–197	Djibouti	151–196	Mauritius	151–196	Zimbabwe
	Kuwait		Norway		Liechtenstein		Botswana
	Belize		Cyprus		Mauritania		Guinea-Bissau
	Suriname		Central African Republic		Lesotho		South Sudan
	Baker Island		Chad		Guyana		Sudan
	Trinidad and Tobago		Russia		Central African Republic		Mozambique
	Estonia		Gabon		Fiji		Libya
	Fiji		Suriname		Burundi		Liberia
	Mauritius		Comoros		Eritrea		Eritrea
	Luxembourg		Kazakhstan		Liberia		Namibia
	Equatorial Guinea		Guyana		San Marino		Djibouti
	Iceland		Oman		Cyprus		Palestine
	Djibouti		Canada		Gambia		Guyana
	Solomon Islands		Solomon Islands		Timor-Leste		Bahamas
	Samoa		Palestine		Somalia		Chad
	Andorra		Botswana		Guinea-Bissau		Mali
	Cyprus		Australia		Djibouti		Congo (Democratic Republic of the)
	Palestine		Saudi Arabia		Samoa		Niger
	Liechtenstein		Iceland		Monaco		Solomon Islands
	San Marino		Namibia		Palestine		Central African Republic
	Saint Vincent and the Grenadines		Mauritania		Solomon Islands		Comoros
	Comoros		Libya		Bahamas		Mongolia
	Bahamas		Mongolia		Saint Vincent and the Grenadines		Mauritania
	Monaco		Bahamas		Qatar		Qatar
	Qatar		Tonga		Comoros		Somalia
	Tonga		Saint Kitts and Nevis		Antigua and Barbuda		Antigua and Barbuda
	Federated States of Micronesia		Federated States of Micronesia		Dominica		Saint Kitts and Nevis
	Dominica		Antigua and Barbuda		Tonga		Dominica
	Antigua and Barbuda		Dominica		Saint Kitts and Nevis		Tonga
	Saint Kitts and Nevis		Marshall Islands		Federated States of Micronesia		Niue
	Cape Verde		Niue		Niue		Federated States of Micronesia
	Niue		Vatican City		Cape Verde		Maldives

(continued)

**Table 3** (continued)

Rank at country unit (51–197)		Rank at per unit area (51–197)		Rank at country unit (51–196)		Rank at per unit area (51–196)	
Rank	Country	Rank	Country	Rank	Country	Rank	Country
	Marshall Islands		Qatar		Palau		Palau
	Palau		Palau		Maldives		Marshall Islands
	Maldives		Cape Verde		Marshall Islands		Cape Verde
	Cook Islands		Maldives		Cook Islands		Cook Islands
	Vatican City		Cook Islands		Barbados		Barbados
	Saint Lucia		Nauru		Kiribati		Tuvalu
	Kiribati		Tuvalu		Bahrain		Nauru
	Tuvalu		Grenada		Saint Lucia		Kiribati
	Grenada		Saint Lucia		Malta		Malta
	Nauru		Seychelles		Grenada		Grenada
	Seychelles		Malta		Tuvalu		Bahrain
	Bahrain		Kiribati		Seychelles		Saint Lucia
	Malta		Bahrain		Nauru		Seychelles
	Barbados		Barbados		Sao Tome and Principe		Sao Tome and Principe
	Sao Tome and Principe		Sao Tome and Principe				

*Note* (1) The MhRI assesses the expected annual multi-hazard risk level of affected population of 197 countries of the world and the expected annual multi-hazard risk level of affected property of 196 countries (lack of GDP data of Vatican City) of the world. (2) The MhRI value is calculated and ranked in descending order at country unit and per unit area respectively. (3) The top 50 countries with the highest MhRI values (about 35 % of all) are listed with their rank order, and other countries with lower MhRI value are listed by groups with the order from the 51th to the 100th, from the 101th to the 150th, and from the 151th to the lowest